BULLETIN OF THE EARTHQUAKE RESEARCH INSTITUTE,
TOKYO UNIVERSITY. Vol. XXXII, Part 1. March, 1954.

東京大學
地震研究所彙報

第 32 號　第 1 册

昭和 29 年 3 月

目　次

論文及報告

			頁
1.	固体液体の境の面の S-波 (独文)	松沢武雄	1
2.	表面波の研究 X. 流体中の音波と SH-波のつくる表面波の対応性 (英文)	佐藤泰夫	7
3.	三原山の地球磁気学的研究 第4報 (一連の伏角測量と偏角変化の連続観測) (英文)	横山泉	17
4.	伊豆大島三原山昭和 25 年及び 26 年の噴火 その 1 昭和 25 年の噴火 (英文)	津屋弘達 森本良平 小坂丈予	35
5.	弾性波の発生機構に関する実験 (第4報) (英文)	笠原慶一	67
6.	東北日本における第4回爆破地震動観測 (英文)	爆破地震動研究グループ	79
7.	エデン平行薄片の理論と地震計への応用 (英文)	西村源六郎 鈴木正治 古川英一	87
8.	自然風及び起振機等による木造二階建住宅の振動 (英文)	西村源六郎 鈴木正治	113

(The titles in occidental languages are given on the back cover.)

本彙報ハ年4回（但シ第1號ヨリ第6號マデハ不定期ニ，第7號ハ3冊トシテ發行セリ），彙報別冊ハ不定期ニ發行ス．

本彙報掲載ノ論文及ビ報告ノ内容ニ關シテハ著者ノミニ其責任アルモノトス．

本彙報ニ關スル照會通信ハ東京大學地震研究所長ヘ宛テラレタシ．

The Bulletin is published quarterly. (Vols. I–VI were published at irregular intervals and Vol. VII consisted of three parts.)
Supplementary Volume is published at irregular interval.

The authors of the papers alone are responsible for the statements and opinions contained in their respective papers.

All communications relating to this Bulletin should be addressed to the Director of the Earthquake Research Institute, Tokyo University.

1. *S-Wellen an der fest-flüssigen Schichtgrenze. I.*

Von Takeo MATUZAWA,

Institut für Erdbebenforschung.

(Vorgelegt den 22. Dez. 1953.-Eingegangen den 7. Jan. 1954.)

1. Problemstellung.

Nach meiner thermodynamischen Überlegung[1] ist die Phasentransformation zwischen festen und flüssigen Zuständen sehr wahrscheinlich bei der Entstehung der Grossbeben. Auch bei der grossen vulkanischen Ausbrüchen wird irgend eine Änderung im Magmareservoir erwartet.

Wegen der kleinen Schichtdicke des betreffenden Gebietes muss es ziemlich schwer sein, durch die Laufzeit der seismischen Wellen die Zustandsänderung klar zu machen.

Andererseits haben wir kennengelernt, dass die reflexionsseismische Beobachtung aus grossen Tiefen möglich ist[2]. Auch bei uns in Japan konnte die Forschungsgruppe der Sprengseismik die Reflexionswellen aus grossen Tiefen bei der zweiten Kamaisi-Sprengung deutlich beobachten[3]. Bei diesen Beobachtungen brauchte man natürlich Reflexionen der P-Wellen wie gewöhnlich.

Wenn die Zustandsänderung zwischen den festen und flüssigen Phasen der Fall ist, können wir die Veränderung durch das Reflexionsverfahren ziemlich leicht klar machen.

Dabei kann man lieber die S-Wellen brauchen, weil diese Wellen sich stärker als die P-Wellen bei der Phasenänderung ändern müssen. Für diesen Zweck kann man die Sprengung oder auch die natürlichen Beben brauchen. Wir haben kennengelernt, dass auch bei grossen Sprengungen die S-Wellen sehr deutlich erzeugt werden können[4].

Um die Möglichkeit des Reflexionsaufschlusses mit S-Wellen klar zu machen, ist es nötig, das Verhalten der S-Wellen an der Schichtgrenze zu schätzen. Dabei kommt hauptsächlich die Reflexion der SH-Wellen in

1) T. MATUZAWA, *Bull. Earthq. Res. Inst.*, **31** (1953), 180.

2) A. Junger, *Geophysics*, **16** (1951), 499; H. Reich, *Bull. Inform. U.G.G.I., I.U. G.G. News Letter*, No. 2 (1953) 229.

3) Veröffentlicht an der Tagung der seismologischen Gesellschaft, Japan, am 30. Okt. 1953.

4) *Z.B.* O. FÖRTSCH und G.A. SCHULZE, *Naturforschung und Medizin in Deutschland 1939-1946*, **18** (1948), Geophysik II. 44–53. Unsere Forschungsgruppe der Sprengseismik hat auch oft diese Tatsache bestätigt.

Frage, vorausgesetzt dass die Epizentralentfernung kleiner als die Schichttiefe ist.

2. Verhalten der SH-Wellen an der Schichtgrenze zwischen der Zähflüssigkeit und dem festen Körper.

Es sei die (xy)-Ebene an der Schichtgrenze genommen, und die z-Achse in die Zähflüssigkeit gerichtet.

Die Bewegungsgleichung lautet wie gewöhnlich

$$\rho' \frac{\partial^2 v'}{\partial t^2} = \nu \frac{\partial}{\partial t}\left(\frac{\partial^2 v'}{\partial x^2} + \frac{\partial^2 v'}{\partial z^2}\right),$$

$$\rho \frac{\partial^2 v}{\partial t^2} = \mu\left(\frac{\partial^2 v}{\partial x^2} + \frac{\partial^2 v}{\partial z^2}\right),$$

wo, ρ' die Dichte der Flüssigkeit ist,
ρ die Dichte des festen Körpers,
ν die Viskosität der Flüssigkeit,
μ der Gestaltsmodul des festen Teils,
v' die y Komponente der Verschiebung in der Flüssigkeit,
v die y Komponente der Verschiebung in dem festen Teil.

Setze man

$$v' = Ae^{-nz} e^{ik'x + ipt},$$

dann

$$n^2 = k'^2 + i\frac{\rho' p}{\nu} = \sqrt{(k'^2)^2 + \left(\frac{\rho' p}{\nu}\right)^2}\, e^{i\theta},$$

wo,

$$\tan\theta = \frac{\rho' p}{\nu k'^2}.$$

Also

$$n = \sqrt[4]{(k'^2)^2 + \left(\frac{\rho' p}{\nu}\right)^2}\, e^{i\frac{\theta}{2}} = \alpha + i\beta.$$

Setze man im festen Teil,

$$v = B\, e^{ik(lx+mz)+ipt},$$

$$v_r = B_r\, e^{ik(lx-mz)+ipt},$$

dann

$$\frac{\rho p^2}{\mu} = k^2(l^2+m^2) = k^2, \quad l^2+m^2 = 1.$$

Die Grenzbedingungen an der Schichtgrenze, nämlich $z=0$, sind

$$v'=v+v_r,$$

und

$$\nu\frac{\partial}{\partial z}\left(\frac{\partial v'}{\partial t}\right)=\mu\frac{\partial}{\partial z}(v+v_r).$$

Daraus bekommt man

$$k'=kl,$$

$$A=B+B_r,$$

und

$$-ip\nu(\alpha+i\beta)A=ikm\,\mu(B-B_r).$$

Dann,

$$A=\frac{2\,km\mu}{km\mu-\alpha p\nu-i\beta p\nu}B,$$

$$B_r=\frac{km\mu+\alpha p\nu+i\beta p\nu}{km\mu-\alpha p\nu-i\beta p\nu}B.$$

Nun, für den Fall $|l|\ll 1$ wollen wir die Approximation machen.

$$|n^2|=\frac{\rho p^2}{\mu}\sqrt{l^4+\left(\frac{\rho'\mu}{\rho\nu p}\right)^2}\doteqdot\frac{\rho' p^2}{\nu p},$$

$$\tan\theta=\frac{\rho'\mu}{l^2\rho\nu p}.$$

Setzt man $\theta=(\pi/2)-\delta$, dann ist δ bis l^2,

$$\delta=l^2\frac{\rho(\nu p)}{\rho'\mu}.$$

Nun,

$$\cos\frac{\theta}{2}\doteqdot\frac{1}{\sqrt{2}}\left(1+\frac{\delta}{2}\right),\quad \sin\theta\doteqdot\frac{1}{\sqrt{2}}\left(1-\frac{\delta}{2}\right).$$

Also

$$\alpha\doteqdot\frac{1}{\sqrt{2}}\sqrt{\frac{\rho' p}{\nu}}\left(1+\frac{\delta}{2}\right),\quad \beta\doteqdot\frac{1}{\sqrt{2}}\sqrt{\frac{\rho' p}{\nu}}\left(1-\frac{\delta}{2}\right).$$

$$B_r\doteqdot\frac{\sqrt{\left\{1+\left(\frac{\rho' p\nu}{\rho\mu}\right)^2\right\}-2l^2\left\{1+\left(\frac{p\nu}{\mu}\right)^2\right\}}}{\left\{\left(1-\sqrt{\frac{\rho' p\nu}{\rho\mu}}\right)^2+(2-\sqrt{2})\sqrt{\frac{\rho' p\nu}{\rho\mu}}\right\}-l^2\left\{1+\frac{1}{\sqrt{2}}\sqrt{\frac{\rho'\nu p}{\rho\mu}}\left(\frac{\rho\nu p}{\rho^2\mu}-1\right)\right\}}e^{i\varphi}B,$$

wo,

$$\tan\varphi \doteqdot \sqrt{2}\sqrt{\frac{\rho'\nu p}{\rho\mu}}\frac{\left(1-\frac{l^2}{2}-\frac{\delta}{2}\right)}{1-\frac{\rho' p\nu}{\rho\mu}-l^2}.$$

$$A \doteqdot \frac{2\sqrt{1-l^2}}{\left\{\left(1-\sqrt{\frac{\rho' p\nu}{\rho\mu}}\right)^2+(2-\sqrt{2})\sqrt{\frac{\rho' p\nu}{\rho\mu}}\right\}-l^2\left\{1+\frac{1}{\sqrt{2}}\sqrt{\frac{\rho'\nu p}{\rho'\mu}}\left(\frac{\rho\nu p}{\rho'\mu}-1\right)\right\}}e^{i\psi}B,$$

wo,

$$\tan\psi \doteqdot \frac{1}{\sqrt{2}}\sqrt{\frac{\rho' p\nu}{\rho\mu}}\frac{\left(1-\frac{\delta}{2}\right)}{1-\frac{1}{\sqrt{2}}\sqrt{\frac{\rho' p\nu}{\rho\mu}}-\frac{l^2}{2}-\frac{\delta}{2\sqrt{2}}\sqrt{\frac{\rho' p\nu}{\rho\mu}}}.$$

3. Zahlenmässige Schätzung der Reflexion für $l^2=0$.

Wir sehen also, dass B_r für $l^2=0$ nur von $\rho' p\nu/\rho\mu$ abhängt.

Die Viskosität gegen die Temperatur des frischen Lavas bei der Eruption vom 1951 des Oosima wurde von T. Minakami[5] geschätzt zu 5.6×10^3 poises (c.g.s.) für 1125°C, 2.3×10^5 poises für 1038°C u.s.w.

Unter grossem Druck muss die Viskosität natürlich grösser sein als unter kleinem Druck. Aber wir können von diesen Materialien die Idee der Grössenordnung der Viskosität des Magmas bekommen.

Tabelle 1.

$\frac{\rho' p\nu}{\rho\mu}$	0	10^{-4}	10^{-2}	1	10^2	10^4	∞
$\frac{\lvert B_r\rvert}{B}$	1	1	1.16	2.41	1.15	1	1
$\tan\varphi$	0	0	.142	$+\infty$ $-\infty$	$-.142$	0	0
φ	0	0	.141	$\frac{\pi}{2}$	$\pi-.141$	π	π
$\frac{\lvert A\rvert}{B}$	2	2.02	2.15	2.61	.215	.02	0
$\tan\psi$	0	.007	.076	2.41	-1.16	-1.01	-1
ψ	0	.007	.076	1.18	$\pi-.86$	$\pi-.79$	$\frac{3}{4}\pi$

5) T. MINAKAMI, *Bull. Earthq. Res. Inst.*, **29** (1951), 487–498.

Was $p=2\pi/T$ betrifft, wählen wir gewöhnlich im Reflexionsverfahren bequemlicherweise die Spektren für T etwa 1/20 Sek.

Darum mag es zweckmässig sein, B_r im Bereich zwischen etwa 10^{-4} und 10^{4} von $\rho' p\nu/\rho\mu$ zu zeigen. Das Rechenresultat ergibt sich in Tabelle I. (Tabelle 1)

Es mag etwas paradox scheinen, dass $|B_r|$ grösser als B sein kann. Das kommt aber natürlich von der Phasenverschiebung in A und B_r.

Von diesem Resultat kann man hoffnungsvoll erwarten, dass man mit dem Reflexionsverfahren der S-Wellen die Phasenänderung in der Erdkruste entdecken kann.

1. Kotai Ekitai no Sakai no Men no S-Nami.

Zisin Kenkyûsyo, MATUZAWA-Takeo.

Oozisin ya Kazan no Katudô no Toki niwa Kotai-Ekitai no Sakai no Men no iroiro na Henka ga yosô sareru.

Sono Henka wa P-Nami no Hansya demo wakaru Hazu de aruga, S-Nami wo tukaeba motto hakkiri suru Koto ga yosô dekiru.

Sono Tame ni Nensei-Ekitai to Kotai tono Sakai no Men no S-Mami no Hansya no Keisan wo okonatta.

2. *Study on Surface Waves X. Equivalency of SH-waves and Sound Waves in a Liquid.*

By Yasuo SATÔ,

Earthquake Research Institute.

(Read Dec. 16, 1952.—Received Jan. 4, 1954.)

1. Introduction.

The existence of two sorts of elastic waves in a homogeneous isotropic solid body has been a well-known fact ever since the late 19th century[1]. They are named as P- and S-waves, and their nature was investigated by many authors. It was found out By K. Sezawa[2] that the S-waves can be separated into two kinds, and in a two-dimensional problem with one or several parallel plane boundaries, it is classified in SV- and SH-waves. Although the former alone cannot satisfy boundary conditions, the latter can exist by itself. If we denote the displacement of SH-waves by v, it is the solution of a differential equation of the type

$$\frac{\partial^2 v}{\partial t^2} = V_s^2\left(\frac{\partial^2 v}{\partial x^2} + \frac{\partial^2 v}{\partial z^2}\right), \qquad \ldots\ldots(1.1)$$

where

$V_s = \sqrt{(\mu/\rho)}$ is the propagation velocity of S-waves,
x, y, z are the Cartesian coordinates,
v is the displacement in y-direction.

On the other hand, the sound waves in an elastic liquid also satisfies the equation

$$\frac{\partial^2 \Delta}{\partial t^2} = V^{*2}\left(\frac{\partial^2 \Delta^*}{\partial x^2} + \frac{\partial^2 \Delta^*}{\partial z^2}\right) \quad ..(1.2)$$

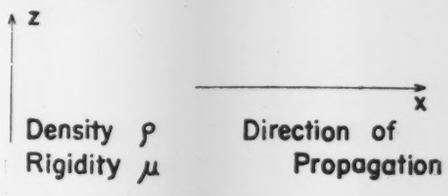

Fig. 1.

1) A historical sketch of our knowledge in this field of seismology is admirably given in H. KAWASUMI's elaborate review entitled "An Historical Sketch of the Development of Knowledge concerning the Initial Motion of an Earthquake," *Publication du Bureau central seismologique international, serie A: Travaux scientifiques, fascicule* **15** (1937).

2) K. SEZAWA, "Dilatational and Distorsional Waves generated from a Cylindrical or a Spherical Origin," *Bull. Earthq. Res. Inst.*, **2** (1927), 13. *Sindôron*, p. 652 (in Japanese.)

where $V^*=\sqrt{(k^*/\rho^*)}$ is the propagation velocity of sound waves, and Δ^* is the volume dilatation.

The two equations (1.1) and (1.2) have the same form, while the SH-waves in a layered medium forms the surface waves now called as Love-waves. Thus a doubt naturally occurs whether sound waves in a liquid might form a similar or same type of surface waves with Love-waves[3].

In this paper, however, we will try a more general way of treatment and examine the equivalency of surface waves constituted by SH-waves and sound waves in an elastic liquid.

2. Boundary conditions.

Boundary conditions required at the plane of contact of different media or at the free surface are;

SH-waves;

$$v_n=v_{n+1}\,, \qquad \text{.....(2.1a)}$$

$$\widehat{yz}_n=\widehat{yz}_{n+1}\,, \qquad \text{.....(2.1b)}$$

where v_n implies a displacement of y-component in the n-th medium and the latter condition is modified to the next form

$$\mu_n\frac{\partial v_n}{\partial z}=\mu_{n+1}\frac{\partial v_{n+1}}{\partial z}\,. \qquad \text{.....(2.1b)'}$$

Sound waves;

$$w_n^*=w_{n+1}^*\,, \qquad \text{.....(2.2a)}$$

$$\widehat{zz}_n^*=\widehat{zz}_{n+1}^*\,, \qquad \text{.....(2.2b)}$$

where w_n implies a displacement of z-component in the n-th medium. If the conditions (2.2a) and (2.2b) are expressed in terms of Δ^*, they are modified, using the relation

$$\rho_n^*\frac{\partial^2 w_n^*}{\partial t^2}=k_n^*\frac{\partial \Delta_n^*}{\partial z}\,,$$

$$\widehat{zz}_n=k_n^*\Delta_n^*\,,$$

(where k_n^* is a bulk modulus) as

3) Relation between the velocity equation of the gravity wave in the water and that of Love-waves was pointed out more than ten years ago. K. SEZAWA and K. KANAI, "On Shallow Water Waves Transmitted in the Direction Parallel to a Sea Coast, with Special Reference to Love-waves in a Heterogeneous Media," *Bull. Earthq. Res. Inst.*, **17** (1939), 685.

$$\begin{cases} -\dfrac{1}{p^2} V_n^{*2} \dfrac{\partial \Delta_n^*}{\partial z} = -\dfrac{1}{p^2} V_{n+1}^{*2} \dfrac{\partial \Delta_{n+1}^*}{\partial z} & \cdots\cdots(2.3a) \\ k_n^* \Delta_n^* = k_{n+1}^* \Delta_{n+1}^* & \cdots\cdots(2.3b) \end{cases}$$

where Δ_n^* is assumed to be proportional to $\exp(ipt)$.

If the solutions of the type in the elastic body;

$$v_n = \{A_n \exp(\beta_n z) + B_n \exp(-\beta_n z)\} \exp(ifx + ipt),$$
$$\beta_n = \sqrt{(f^2 - k_n^2)},$$
$$k_n = p/V_{Sn}, \qquad \cdots\cdots(2.4)$$

and in the liquid;

$$\Delta_n^* = \{C_n \exp(\alpha_n^* z) + D_n \exp(-\alpha_n^* z)\} \exp(ifx + ipt),$$
$$\alpha_n^* = \sqrt{(f^2 - h_n^{*2})},$$
$$h_n^* = p/V_n^*, \qquad \cdots\cdots(2.5)$$

are employed, the above conditions become

for SH-waves;

$$A_n \exp(\beta_n z_n) + B_n \exp(-\beta_n z_n) = A_{n+1} \exp(\beta_{n+1} z_n) + B_{n+1} \exp(-\beta_{n+1} z_n), \quad \cdots\cdots(2.6a)$$

$$\mu_n \beta_n \{A_n \exp(\beta_n z_n) - B_n \exp(-\beta_n z_n)\} = \mu_{n+1} \beta_{n+1} \{A_{n+1} \exp(\beta_{n+1} z_n) - B_{n+1} \exp(-\beta_{n+1} z_n)\}, \quad \cdots\cdots(2.6b)$$

for Sound waves;

$$-V_n^{*2} \alpha_n^* \{C_n \exp(\alpha_n^* z_n) - D_n \exp(-\alpha_n^* z_n)\} = -V_{n+1}^{*2} \alpha_{n+1}^* \{C_{n+1} \exp(\alpha_{n+1}^* z_n) - D_{n+1} \exp(-\alpha_{n+1}^* z_n)\}, \quad \cdots\cdots(2.7a)$$

$$k_n^* \{C_n \exp(\alpha_n^* z_n) + D_n \exp(-\alpha_n^* z_n)\} = k_{n+1}^* \{C_{n+1} \exp(\alpha_{n+1}^* z_n) + D_{n+1} \exp(-\alpha_{n+1}^* z_n)\}, \quad \cdots\cdots(2.7b)$$

where $z = z_n$ implies the boundary surface of two media "n" and "$n+1$".

If we put

$$k_n^* C_n \equiv C_n^* \quad \text{and} \quad k_n^* D_n \equiv D_n^*, \qquad \cdots\cdots(2.8)$$

we obtain, from the expressions (2.7a) and (2.7b),

$$-\frac{1}{\rho_n^*} \alpha_n^* \{C_n^* \exp(\alpha_n^* z_n) - D_n^* \exp(-\alpha_n^* z_n)\}$$

$$=-\frac{1}{\rho_{n+1}^*}\alpha_{n+1}^*\{C_{n+1}^*\exp(\alpha_{n+1}^* z_n)-D_{n+1}^*\exp(-\alpha_{n+1}^* z_n)\}\,, \qquad \cdots\cdots(2.9a)$$

$$C_n^*\exp(\alpha_n^* z_n)+D_n^*\exp(-\alpha_n^* z_n) = C_{n+1}^*\exp(\alpha_{n+1}^* z_n)+D_{n+1}^*\exp(-\alpha_{n+1}^* z_n)\,, \qquad \cdots\cdots(2.9b)$$

Comparing the boundary conditions of SH-waves (2.6a) and (2.6b) with those of sound waves in liquid (2.9a) and (2.9b), we shall at once notice that (2.6a) and (2.9b) are quite similar in the from of expressions. For, if the frequeney, wave-length and the velocity of bodily waves are respectively equal in both problems,

$$\alpha_n^*=\beta_n\,. \qquad \cdots\cdots(2.10)$$

Thus the expression (2.9b) becomes

$$C_n^*\exp(\beta_n z_n)+D_n^*\exp(-\beta_n z_n) = C_{n+1}^*\exp(\beta_{n+1} z_n)+D_{n+1}^*\exp(-\beta_{n+1} z_n)\,, \qquad \cdots\cdots(2.11)$$

which is identical with (2.6a), only the constants A_n and B_n are replaced by C_n^* and D_n^* respectively.

On the other hand, introducing (2.10) into the expression (2.9a), we have at once

$$\frac{1}{\rho_n^*}\beta_n\{C_n^*\exp(\beta_n z_n)-D_n^*\exp(-\beta_n z_n)\} =\frac{1}{\rho_{n+1}^*}\beta_{n+1}\{C_{n+1}^*\exp(\beta_{n+1} z_n)-D_{n+1}^*\exp(-\beta_{n+1} z_n)\}\,, \qquad \cdots\cdots(2.12)$$

which becomes identical with (2.6b) if we may put

$$1/\rho_n^*=K\mu_n\,, \qquad \cdots\cdots(2.13)$$

using a common constant K independent upon n.

Summarizing the above discussion, we can conclude as follows:

"The elastic surface waves constituted by SH-waves and sound waves in a liquid are equivalent if

1) the frequency, wave-length and the velocity of bodily waves are respectively equal in both problems,

and 2) ρ_n^* is inversely proportional to μ_n."

However, it must be added that the displacement in one problem corresponds to the stress in the other, hence the condition of the continuity of displacement of SH-waves corresponds to the continuity of

stress of sound waves in a liquid, while the continuity of stress of the former corresponds to that of the displacement of the latter.

Therefore, if a free surface exists (in the case of an elastic plate two free surfaces exist), the two kinds of problems are not quite equivalent. For the condition of the free surface of SH-waves corresponds to that of the fixed surface of sound waves in a liquid, and *vice versa*. Thus the phenomenon of the reflection of SH-waves at the free boundary corresponds to that of the reflection of sound waves at a rigid wall. We will explain the details by employing some appropriate examples in the following sections.

The next table briefly shows the correspondency of the various elements in both problems.

Table I. Correspondency of the elements in the problems of SH-waves and sound waves in a liquid.

SH-waves.	Sound waves in a liquid.
H_n (Thickness of the layer.)	H_n (Thickness of the layer.)
$z=z_n$ (Boundary surface.)	$z=z_n$ (Boundary surface.)
V_{sn} (Velocity of S-waves.)	V_n^* (Velocity of sound waves.)
$k_n=p/V_{sn}$	$h_n^*=p/V_n^*$
$\beta_n=\sqrt{(f^2-k_n^2)}$	$\alpha_n^*=\sqrt{(f^2-h_n^{*2})}$
μ_n (Rigidity.)	$1/\rho_n^*$ (Density.)
$\chi\ (=\mu'/\mu)$	$1/\Gamma^*\ \left(=1\Big/\left(\frac{\rho^{*\prime}}{\rho^*}\right).\right)$
v_n (Horizontal displacement.)	$\widehat{zz}_n^*$ (Stress component.)
$\widehat{yz}_n$ (Stress component.)	$-w_n^*$ (Vertical displacement.)
Condition of free surface.	Condition of fixed surface.
Condition of fixed surface.	Condition of free surface.

3. Elastic liquid surface waves corresponding to Love-waves.

As is well-known, Love-waves are a very conspicuous type of surface waves constituted by SH-waves, and an example of the above theory may readily be given. We will obtain a corresponding one in the field of elastic liquid waves.

Let us suppose an elastic solid medium specified by Fig. 2, in which the Love-type of waves can naturally exist and propagate. If the condition

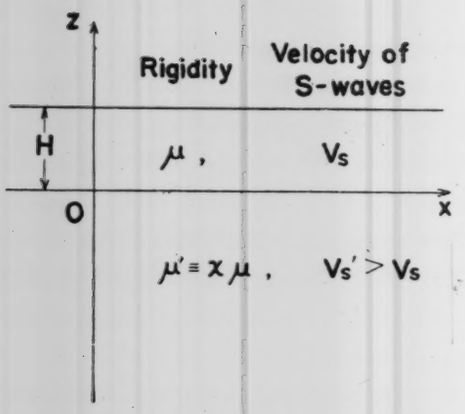

Fig. 2. Elastic media in which Love-waves can exist.

$$V_s < V_s' \qquad \ldots\ldots(3.1)$$

is satisfied, the distribution of amplitude of v and $\widehat{yz}$ becomes as illustrated in Figs. 3a and 3b.

The corresponding liquid medium is shown in Fig. 4. If the condition $\rho^{*\prime}=\rho^*/\chi$ holds, as is in the figure,

$$\mu : \mu' = \frac{1}{\rho^*} : \frac{1}{\rho^{*\prime}} , \qquad \ldots\ldots(3.2)$$

and the correspondency explained in the previous section comes into existence. In this case the distribution of the amplitude of displacement and stress becomes as are shown in the Figs. 5a and 5b. Fig. 3a corresponds to Fig. 5b and Fig. 3b to Fig. 5a.

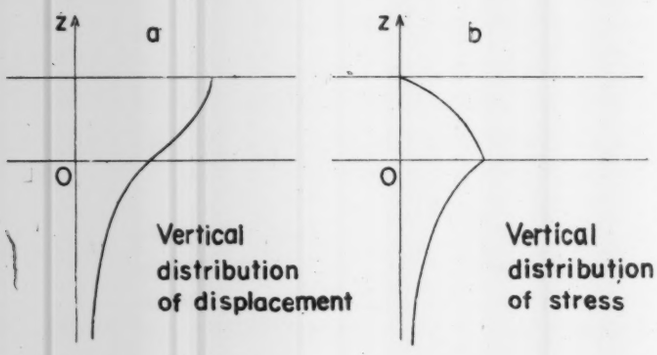

Fig. 3. Vertical distribution of displacement and stress in Love-waves. (not to scale)

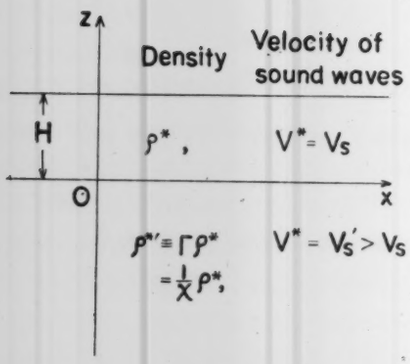

Fig. 4. Elastic liquid media in which surface waves of Love-type can exist. Correspondency of elements in this and Love-type of waves is shown in Table I.

Therefore, if we solve some problem of Love-waves, giving some material constants, the solution at once will be applicable to the prob-

lem of elastic surface waves in a layered liquid medium[4]. Since, in ordinary cases, the rigidity of the surface layer is smaller than that

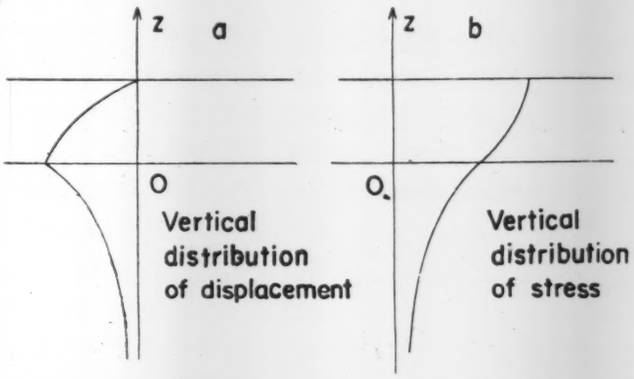

Fig. 5. Elastic liquid media in which surface waves of Love-type can exist. Correspondency of elements in this and Love-type of waves is shown in Table I. In this case upper surface is a fixed boundary. (not to scale)

of the substratum, we must naturally assume that the density of the upper liquid is larger than that of the lower. However, if we put the distribution of the substance upside down, the new arrangement of the medium has a rigid bottom (free boundary of Love-waves corresponds to the fixed boundary, cf. Table I.), and the heavy liquid layer lies between this rigid bottom and the other light liquid medium. This structure of medium is not unlike to that of oceans suggested by a number of authors.[5]

4. Love-waves with a fixed boundary. Elastic liquid surface waves with a free surface.

In the previous section we have treated the ordinary Love-waves and the corresponding ones existent in an elastic liquid medium. As a matter of course, ordinary Love-waves have a free surface, consequently the corresponding liquid waves assume a fixed boundary. On the other hand, in this section, we will solve the problem of Love-waves with a fixed boundary. Or one may suppose a layered elastic liquid medium with a free surface, which may be more natural than the above model.

Assuming (cf. Fig. 2)

$$v=\{A\exp(\beta z)+B\exp(-\beta z)\}\exp(ifx+ipt)$$

in the part of the surface layer, and

4) *cf.*, T. SAKAI, SINDÔ, **1** (1947), 124, (in Japanese.).
5) *e.g.*, M. EWING and F. PRESS, *Bull. Seism. Soc. Amer.*, **40** (1950), 271.

$$v'=A'\exp(\beta' z)\cdot\exp(ifx+ipt) \qquad \ldots\ldots(4.1)$$

in the subjacent medium, we put the boundary conditions

$$\text{at} \quad z=H\,; \quad v=0\,, \qquad \ldots\ldots(4.2)$$

$$\text{and at} \quad z=0\,; \quad v=v'\,,$$

$$\widehat{yz}=\widehat{yz'}\,, \qquad \ldots\ldots(4.3)$$

we thus obtain the expressions

$$\begin{cases} A\exp(\beta H)+B\exp(-\beta H)=0\,, \\ A\quad\quad +B\quad\quad =A'\,, \\ A\,\mu\,\beta\quad -B\,\mu\,\beta\quad =A'\mu'\beta'\,, \end{cases} \qquad \ldots\ldots(4.4)$$

from which we have

$$\beta\cosh\beta H+\chi\beta'\sinh\beta H=0\,, \qquad \ldots\ldots(4.5)$$

and by somewhat modifying it

$$\tilde{\beta}H=\operatorname{Arctan}\left(\chi\frac{\beta'}{\tilde{\beta}}\right)+\frac{\pi}{2}\,. \qquad \ldots\ldots(4.6)$$

In the above expressions we have employed ordinary notations, viz.,

$$\begin{cases} \beta=i\tilde{\beta}=\sqrt{(f^2-k^2)}\,, \\ \beta' \quad\quad =\sqrt{(f^2-k'^2)}\,, \\ k \quad\quad =p/V_s\,, \\ k' \quad\quad =p/V_s'\,, \\ \chi \quad\quad =\mu'/\mu\,. \end{cases} \qquad \ldots\ldots(4.7)$$

(4.6) is a formula with which we can calculate the velocity of this case, while the corresponding velocity equation of liquid medium is at once obtained from Table I.

$$\tilde{\alpha}^*H=\operatorname{Arctan}\left(\frac{1}{\Gamma^*}\frac{\alpha^{*\prime}}{\tilde{\alpha}^*}\right)+\frac{\pi}{2}\,, \qquad \ldots\ldots(4.8)$$

where

$$\begin{cases} \alpha^*=i\tilde{\alpha}^*=\sqrt{(f^2-h^{*2})}\,, \\ \alpha^{*\prime} \quad\quad =\sqrt{(f^2-h^{*\prime 2})}\,, \\ h^* \quad\quad =p/V^*\,, \\ h^{*\prime} \quad\quad =p/V^{*\prime}\,, \\ \Gamma^* \quad\quad =\rho^{*\prime}/\rho^*\,. \end{cases} \qquad \ldots\ldots(4.9)$$

6) *e.g.*, Y. SATÔ, *Bull. Earthq. Res. Inst.*, **29** (1951), 1.

When remember the characteristic equation of Love-waves[6], the phase velocity of the case without node in the layer is expressed by

$$\tilde{\beta}H=\mathrm{Arctan}\left(\chi\frac{\beta'}{\tilde{\beta}}\right), \qquad \cdots\cdots(4.10)$$

while that with a node is

$$\tilde{\beta}H=\mathrm{Arctan}\left(\chi\frac{\beta'}{\tilde{\beta}}\right)+\pi\,. \qquad \cdots\cdots(4.11)$$

(4.6) is just the arithmetic mean of the above two expressions, and may be described as the Love-waves with half a node. This is a somewhat interesting property for us.

5. Conclusion.

Correspondency of the surface waves formed by SH-waves propagated in an elastic solid medium and that in an elastic liquid medium was discussed and the following results were obtained.

If some kind of surface waves can exist in an elastic solid medium, then also the corresponding type of waves can exist always in an elastic liquid medium. In this case, the correspondency of the elements in both problems becomes as shown in Table I. The remarkable fact is that the condition of a free surface in one problem corresponds to that of a fixed surface in the other problem, and the displacement corresponds to the stress compoment. This condition was explained in § 2 and in the later sections some examples were given.

---

2. 表面波の研究 X.

流体中の音波と SH-波のつくる表面波の対応性

地震研究所 佐 藤 泰 夫

流体中の音波が満たす運動方程式と SH- 波のそれとは全く同じ形を持つてゐる．従つて，それらが作る表面波の間にも或る対応が存在し，一方の解は又他方の問題に於いても意味を持つた内容を表現する事が期待される（§ 1）．本文においては，この点を明らかにする事を目標とし，あはせて一二の例をも示した．

基礎をなす波動方程式が同形であることは上述の通りであるが，境界条件について見る時，両者は完全に同形とはならない．即ち一方の問題で変位について与へられる条件は，他方の問題では応力

に課せられる条件と同じであるし，又その逆の関係も成立つて居る．従つて一方の問題について得られた解を他方にあてはめようとする時には，一方の変位は他方の応力を，応力は逆に変位を表現して居る事になる．従つて又，一方の問題の自由表面は他方の固定表面と対応する事になる．この間の事情を第1表に要約して示してある（§ 2）．

上に述べた如くであるから，SH-波の作る代表的な表面波である Love 波を表はす解を求めれば，これは，その各種の要素が表はす内容に関して，第1表に示したやうな適当な解釈を与へるならば，流体中の音波が作る表面波をも表現する事になる．それは，剛体の底の上に密度が大きく音波速度のおそい流体の層が横たはり，その上に十分に深い流体が存在する時に，主として層内を伝はつてゆく所の表面波である（§ 3）．

一方では又，表面が自由との条件にかへて，表面で変位 0 との条件を課したところの，Love 波類似の表面波も存在するわけであるが，これは，流体中の波におきかへて考へるならば，表面が自由な一つの流体層があり，その下に音波速度のはやい流体が存在する場合の問題に相当する事になる．その速度方程式を求めてみると，層内に一つの節を持つた Love 波と，節を持たない Love 波の丁度中間の性質をもつたものである事がわかる．

3. *Geomagnetic Studies of Volcano Mihara. The 4th paper.* (*A Series of Geomagnetic Dip-Surveys and Continuous Observation of Changes in Geomagnetic Declination.*)

By Izumi YOKOYAMA,

Earthquake Research Institute.

(Read June 22 and Oct. 27, 1953.—Received Dec. 31, 1953.)

1. Introduction.

Since the 1950 eruption of Volcano Mihara in Ooshima Island, the writer has been carrying on geomagnetic studies there. As has been already reported in a series of papers[1)2)3)], the remarkable changes in geomagnetic dip that accompanied the earlier stage of the eruptions as well as some plausible changes in geomagnetic declination associated with the volcanic activities were observed. The former was detected by a series of dip-surveys with a miniature earth-inductor[4)] and the latter by continuous recording of declination at a temporary station situated on the western foot of the volcano.

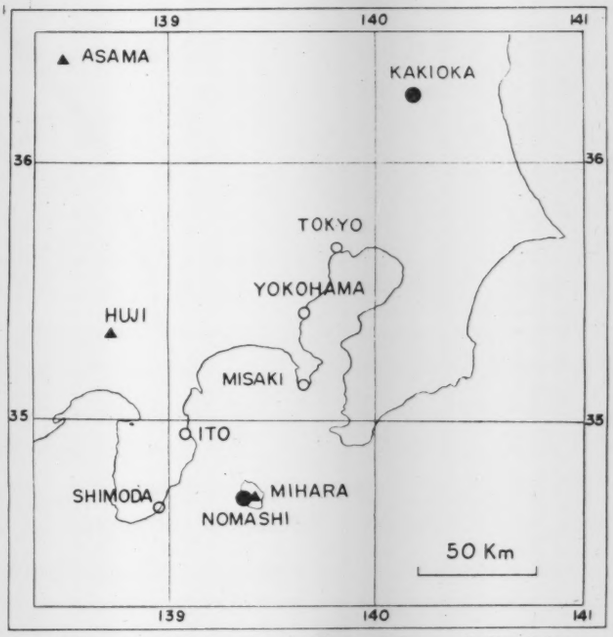

Fig. 1. Geographical position of Ooshima Island.

It has become evident that, as far as volcanoes composed of basaltic rocks are concerned, some anomalous changes in the earth's magnetic field occur in relation to volcanic

1) T. RIKITAKE, *Bull, Earthq. Res. Inst.*, **29** (1951), 161.
2) T. RIKITAKE, *Bull. Earthq. Res. Inst.*, **29** (1951), 499.
3) T. RIKITAKE, I. YOKOYAMA, A. OKADA and Y. HISHIYAMA, *Bull. Earthq. Res. Inst.*, **29** (1951), 583.
4) T. RIKITAKE, *Bull. Earthq. Res. Inst.*, **29** (1951), 147.

eruptions as proved by the studies on the 1950 eruption of Volcano Mihara. Although the each result slightly differed one another, we have another similar evidence in the case of the 1940 eruption of Volcano Miyake-Shima[5)6)7)8)]. In order to bring out geomagnetic changes of this kind more clearly, the writer had been trying to carry out geomagnetic surveys and observations as accurately as possible. As a result, we could accumlate the geomagnetic data in regard to the various periods of the activities of Volcano Mihara. On the basis of these data, the writer would like to discuss the relation between changes in geomagnetic field and volcanic activities in this paper. The interpretations conjectured by analyzing the results will be discussed in the next report.

2. The activities of Volcano Mihara and geomagnetic surveys by Oct. 1953.

The activities of Volcano Mihara from July 1950 to Oct. 1953 are briefly summarized in Table I.

The magnetic dip-surveys I, II, III and V were carried out with a miniature dip-inductor. The surveys IV, VI and VII and the absolute measurements of three geomagnetic elements in order to check the base-line value of the declination-variometer at the temporary station at Nomashi Village were made with G.S.I. type magnetometers. The sensibilities of these instruments are standardized to the Kakioka Magnetic Observatory and tabulated in Table II.

The results of the dip surveys I, II and III were already shown and fully discussed in the preceding reports[9)10)] by T. Rikitake. As some stations were buried under the newly overflowed lava and some have suffered from artificial changes in the surroundings, the number of the stations available for the present study has decreased in these three years. The observed values of dip-angle in all surveys in Ooshima from July 1950, are shown in Table III, where the differences between the values of dip at Ooshima and Kakioka are also shown in order to eliminate the influences of the geomagnetic disturbances and daily

5) R. TAKAHASHI and K. HIRANO, *Bull. Earthq. Res. Inst.*, **19** (1941), 82 and 373.
6) T. MINAKAMI, *Bull. Earthq. Res. Inst.*, **19** (1941), 356.
7) T. NAGATA, *Bull. Earthq. Res. Inst.*, **19** (1941), 335.
8) Y. KATO, *Proc. Imp. Acad. Japan*, **16** (1940), 440.
9) I. TSUBOKAWA, General Discription of a New Type Magnetometer (1949).
10) I. YOKOYAMA, *Bull. Earthq. Res. Inst.*, **31** (1953), 211.

Table I. The activities of Volcano Mihara from July 1950 to Oct. 1953.

Date		Activities	Magnetic surveys
1950			
July	16	Eruption commenced.	
	25	Depth of ejected lava in the old pit reached to 30m.	I (Dip survey)
Aug.	15	Lava filled up the old pit.	
Sept.	12	Lava filled up the inner somma.	
	23	Eruption stopped.	II (Dip survey)
The mass of the ejected lava amounted to about 4×10^7 *metric tons.*			
1951			
Feb.	4	Eruption relapsed.	
	28	Lava overflowed the inner somma.	
Mar.	17	Lava-flow reached to the outer somma.	
	24	Lava-fountain appeared.	III (Dip survey)
Apr.	1	Eruption stopped.	Continuous observation of geomagnetic declination was begun.
Apr.	16 ~ 29		
May	1 ~ 7	Pyroxysmal eruption.	IV (Survey of three geomagnetic elements)
June	9 ~ 27		
June	30	Eruption ended.	
The mass of the ejected lava totaled to about 7×10^7 *metric tons.*			
July	10		Absolute measurement of declination.
Nov.	9		〃
1952			
Jan.	19		〃
May	9		〃
1953			
Feb.	27		〃
Mar.	27		V (Dip survey)
August			VI (Surevy of three geomagnetic elements)
Oct.	5	Minor eruption commenced.	
Oct.	8		VII (〃)

Table II. Sensibilities of the instruments.

	Declination	Horizontal Intensity	Inclination
Miniature Dip-inductor[4] (I, II, III, V)	—	—	1′
G.S.I. First Order Magnetometer[9] — Trial Machine — (IV)	0′.14	2.3γ	0′.21
G.S.I. Second Order Magnetometer[10] (VI, VII)	0′.20	1.5γ	0′.15

variation. In Table III, the station No. 5 (bench mark point for the leveling survey on the central cone) which lies within a distance of about 5 *meters* from the front of the 1951 lava showed a remarkable change in dip-angle as much as 4 *degrees* during the period from II to V. On the station No. 33 (the Nomashi pass on the first somma), the change amounted to about 20 *minutes* of arc. This may be presumably ascribed

Table III.

Dip-angle (Ooshima)

Dip-surveys / Nos. of station	I 1950 July	II 1950 Sept.	III 1951 March	IV 1951 May	V 1953 March	VI 1953 August	VII 1953 Oct.
4	51° 33.3	51° 18.6	51° 16.4		51° 28.5		
5	56 26.6	56 07.0			52 07.2		51° 59.4
7	53 57.0	53 34.2	53 30.4		53 39.4		
14	48 34.6	48 24.4	48 23.8	48° 22.5	48 17.8	48° 19.0	
16	48 36.9	48 37.1	48 36.0	48 37.7	48 32.0	48 33.2	
19	48 13.8	48 10.3	48 08.8	48 13.7	48 03.2	48 07.6	
24	47 40.3	47 28.6	47 25.4	47 18.6	47 20.0	47 21.1	
26	47 02.3	46 59.5	46 57.5	46 57.0	46 57.0	46 53.4	
28	48 26.5	48 22.5	48 18.9		48 26.0		
33	51 44.4	51 27.2	51 23.9		51 41.2		
37			47 19.1	47 22.0	47 21.2	47 22.0	47 19.3
38				49 28.4	49 22.3	49 21.7	
39				52 16.2	52 13.5	52 11.4	52 10.0
40				50 40.8	50 40.0	50 41.0	
41				48 23.7	48 26.0	48 19.6	
42						47 29.8	47 28.4

Differences in Dip-angle (Ooshima–Kakioka)

Dip-surveys / Nos. of station	I 1950 July	II 1950 Sept.	III 1951 March	IV 1951 May	V 1953 March	VI 1953 August	VII 1953 Oct.
4	2° 08.1	1° 52.6	1° 50.0		2° 06.1		
5	7 00.1	4 41.5			2 43.9		2° 39.4
7	4 28.6	4 08.5	4 06.3		4 16.2		
14	− 51.2	−1 01.2	−1 01.1	−1° 02.7	−1 03.4	−1° 03.2	
16	− 48.7	− 48.7	− 48.3	− 48.0	− 49.2	− 48.7	
19	−1 10.7	−1 16.6	−1 15.6	−1 12.8	−1 19.5	−1 13.9	
24	−1 44.5	−1 58.3	−1 58.4	−2 05.0	−2 02.5	−2 03.3	
26	−2 21.3	−1 25.4	−2 26.5	−2 27.3	−2 24.1	−2 27.9	
28	− 56.8	−1 02.6	−1 04.8		− 57.0		
33	2 20.3	2 00.6	1 59.2		2 18.2		
37			−2 05.0	−2 00.6	−2 02.3	−1 59.9	−2 02.1
38				04.0	− 0.2	0.6	
39				2 52.0	2 50.8	2 52.7	2 49.5
40				1 14.9	1 16.6	1 15.3	
41				−1 01.2	− 57.0	−1 00.9	
42						−1 51.8	−1 53.5

to the stone-wall which was constructed to stop the lava-flow[11].

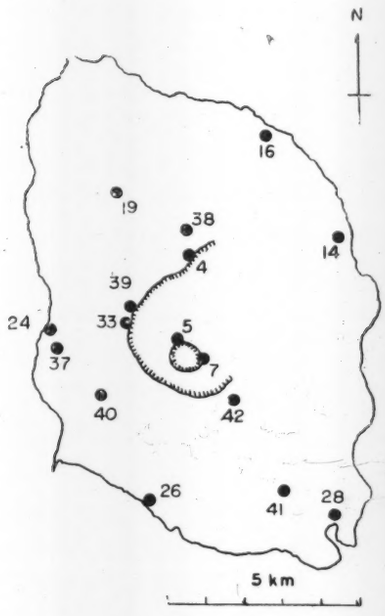

Fig. 2. Positions of the geomagnetic stations.

Nos. of station	Locality	
4	岡田登山道十合目	First somma
5	内輪山水準点	Central cone
7	内輪山最高点	Highest point of central cone
14	動物園	Zoo
16	泉津小学校	Senzu primary school
19	大島測候所	Ooshima Meteorol. Station
24	野増村緑地	Nomashi village
26	間伏	Mabushi
28	波浮港小学校	Habukō primary school
33	野増口峠	Nomashi pass
37	眞坂邸	Mr. Masaka's garden
38	湯場	Yuba
39	御神火茶屋	Gojinka-chaya
40	滑り台	Suberidai
41	差木地，余川	Sashikiji, Yokawa
42	白石山南方	Shiraishi-yama

3. The effects of the ejected lava-flow upon the geomagnetic field.

Since the cooled lava have intense magnetization, it is important to eliminate the magnetic field caused by the lava-flows in order to presume the interior of the volcano from the changes in geomagnetic field. Following the outbreak of the activity in July 16, 1950, lava filled up the central pit by Aug. 15 and then flowed down the slope to the caldera. The amount of the lava which welled up during the period of activity in 1950 totaled to about 4×10^7 *metric tons*. On Feb. 4, next year, the volcano recovered its activity in a large scale and the overflowed lava reached the inside wall of the first somma on Mar. 17. The total amount of the lava which welled up in these two years was estimated as much as 7×10^7 *metric tons*.

If we assume an uniform magnetization, Poisson's theorem gives

$$V=\frac{J}{G\sigma}\frac{\partial U}{\partial i},$$

11) A. C. Mason and H. L. Foster, *American Journal of Science*, **25** (1953), 249.

where V is the magnetic potential, J the intensity of remanent magnetization, G the gravitational constant, σ density, U the gravity potential, and i the direction of magnetization. With the aid of this relation, the effects of the ejected lava-flow upon the geomagnetic field at the respective stations are roughly estimated assuming that $J=5\times10^{-2}$ *e.m.u.* per *cubic centimeter*[12] and $i=53$ *degrees* (geomagnetic dip-angle in

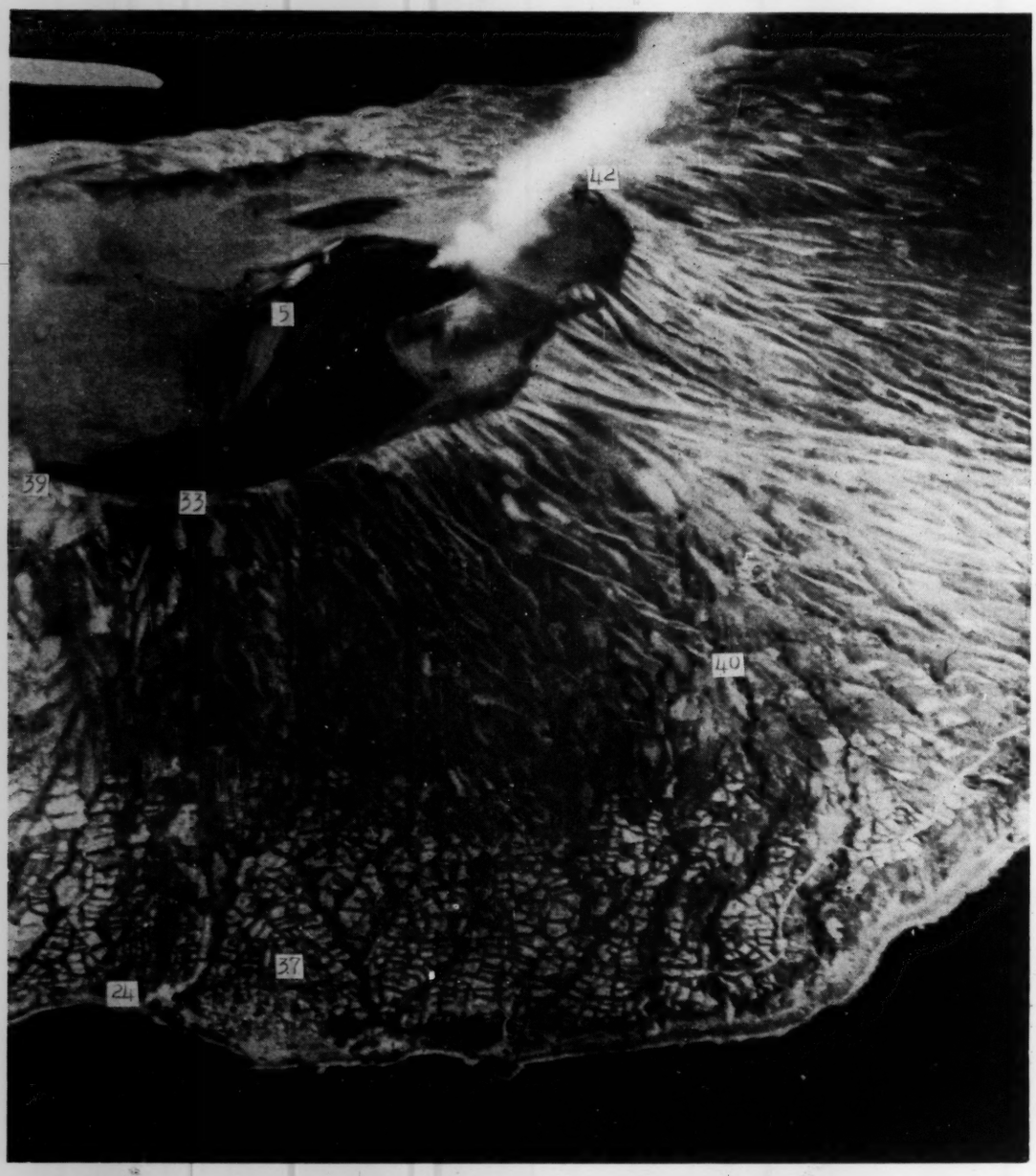

Fig. 3. Scene of the overflowed lava on Mar. 23, 1951 and distribution of geomagnetic stations. Photographed by T. YOSHIDA, Yomiuri Shimbun.

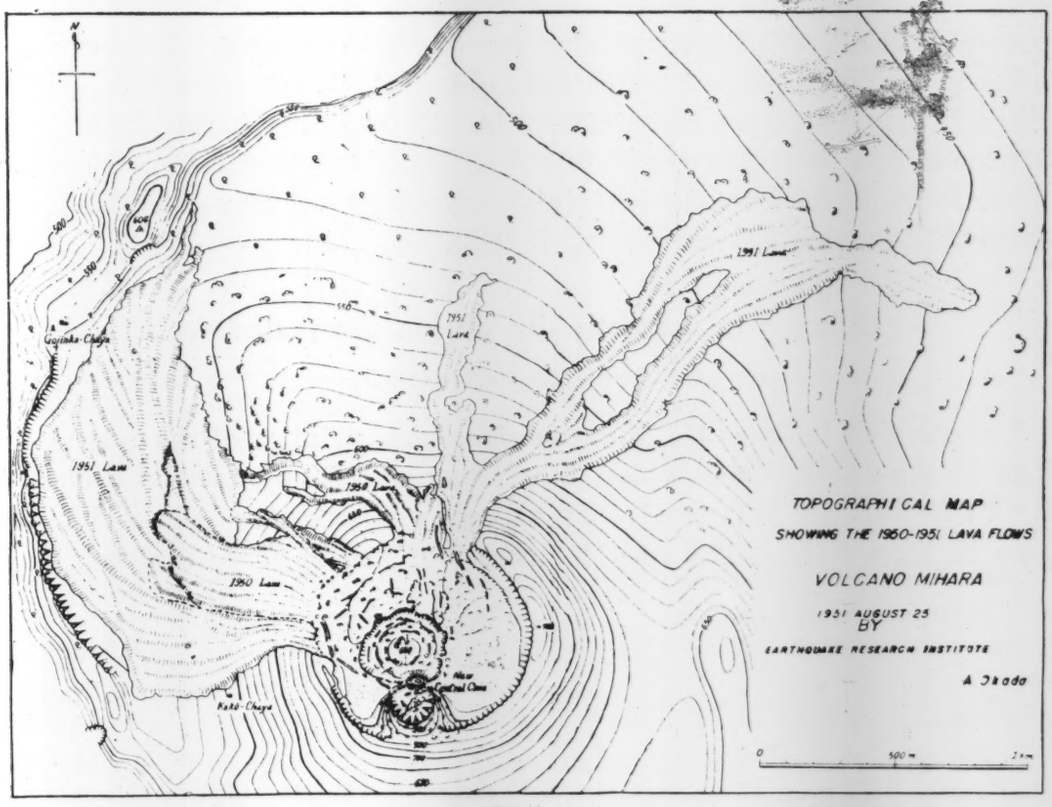

Fig. 4.

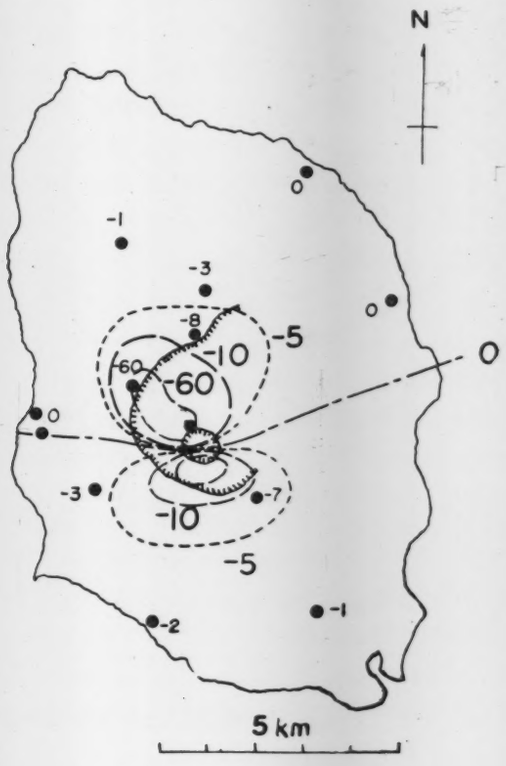

Fig. 5.
The effects of the ejected lava in dip-angle. The unit is *minute* of arc.

the neighborhood of the central cone of the volcano). The gravity gradients and curvature values are obtained by the usual graphical method in Fig. 4 where the station No. 39 (Gojinka-chaya) is so close to the lava-flow that the result is only a rough estimation. The effects of the ejected lava-flow at each station are thus roughly estimated and converted into dip-angle as shown in Fig. 5.

4. Changes in magnetic dip during the period from July 1950 to Oct. 1953.

By referring to Table III, the succesive time-variation of the difference-values in dip-angle, from which the influences of magnetic storms and daily variations are corrected with the aid of the values at Kakioka, are shown in Figs. 6–11. The unit is *minute* of arc in these figures.

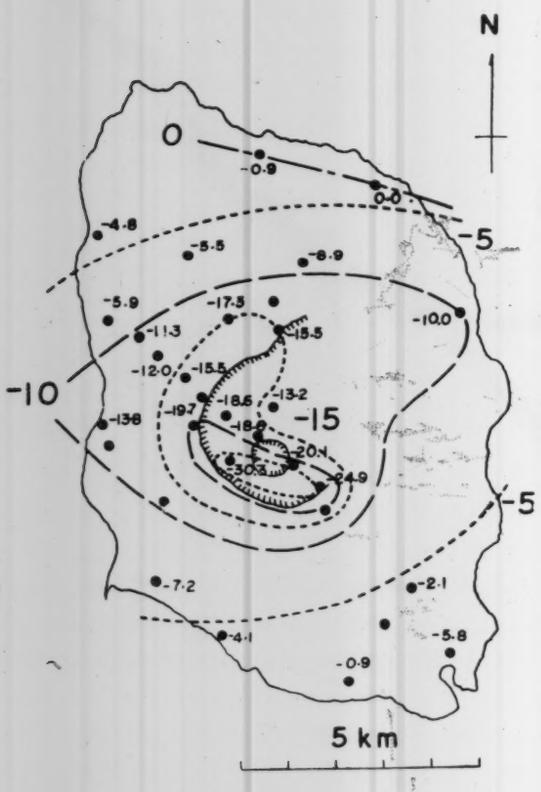

Fig. 6. Changes in geomagnetic dip II Sept. 1950—I July 1950.

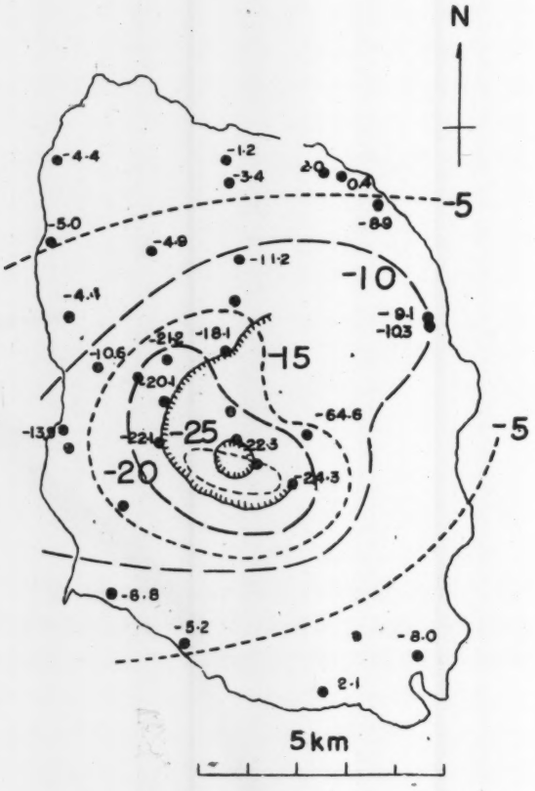

Fig. 7. Changes in geomagnetic dip III Mar. 1951—I July 1950.

12) T. NAGATA, *Journal of Geography (Tokyo)*, **60** (1951), 44.

Since the difference of general secular changes of dip-angle between Ooshima and Kakioka amounts to about 0.22 *minute* of arc per year for 1950.0, the corrections for this difference are taken into account in the case of (VI Aug. 1953–IV May 1951) where the accuracies of both observations were very high and the time interval was more than two years. Moreover, the effect of the ejected lava-flow is eliminated in the cases of (V Mar. 1953–I July 1950), (VI Aug. 1953–I July 1950) and (V Mar. 1953–III Mar. 1951).

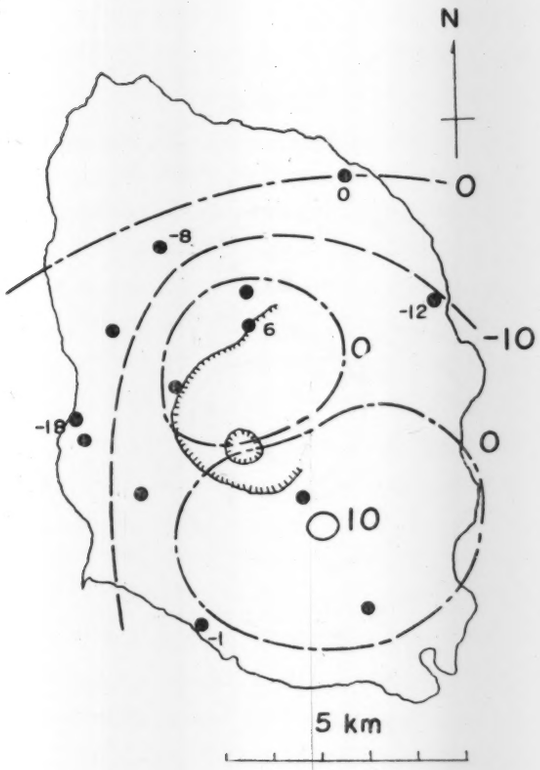

Fig. 8. Changes in geomagnetic dip V Mar. 1953—I July 1950 (the effects of ejected lava are corrected).

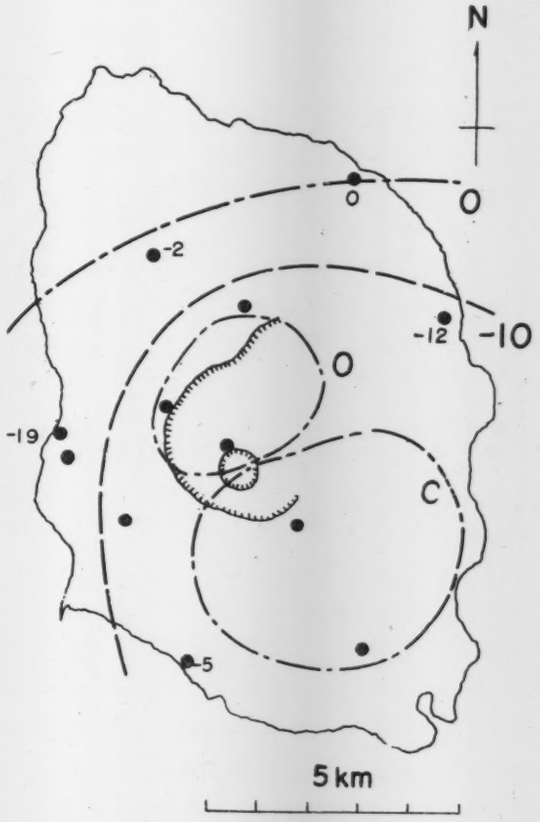

Fig. 9. Changes in geomagnetic dip VI Aug. 1953—I July 1950 (the effects of ejected lava are corrected).

The anomalous changes accompanying (II Sept. 1950–I July 1950) were fully discussed in the 2nd paper by Rikitake who concluded that the changes seem to be explained by the apparent demagnetization of a roughly spherical region of which the centre is situated at a depth of about 5 *km* and the mean radius is about 2 *km*. In other words, it was interpreted that the above-mentioned region may be presumed to have

lost its magnetic property owing to the rise in temperature associated with the eruption.

Comparing Figs. 8 (V–I) and 9 (VI–I) to Figs. 6 (II–I) or 7 (III–I), anomalous changes in dip-angle that accompanied the eruption in 1950 seem to have been almost recovered by 1953. Although the distribution of changes in geomagnetic field in the central region is not clear owing to the magnetic disturbances due to the overflowed lava, it seems likely that the recovering changes exceed the earlier ones at some stations.

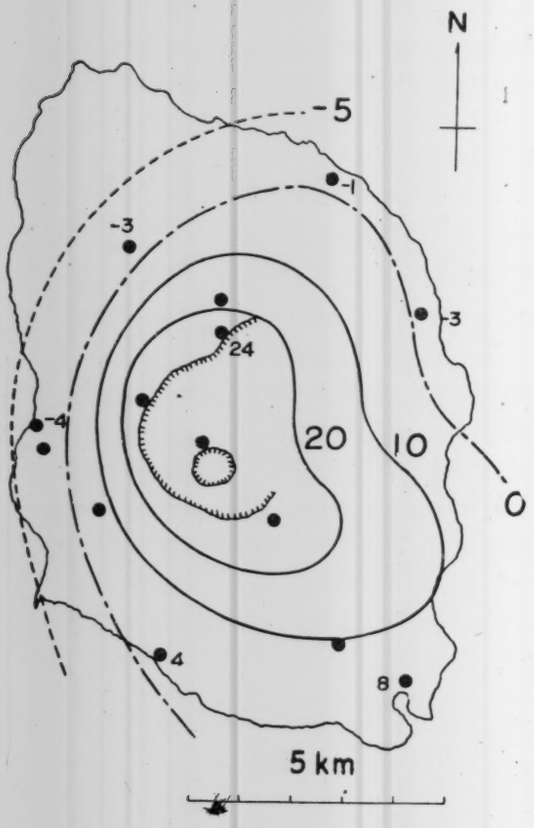

Fig. 10. Changes in geomagnetic dip V Mar. 1953—III Mar. 1951 (the effects of ejected lava are corrected).

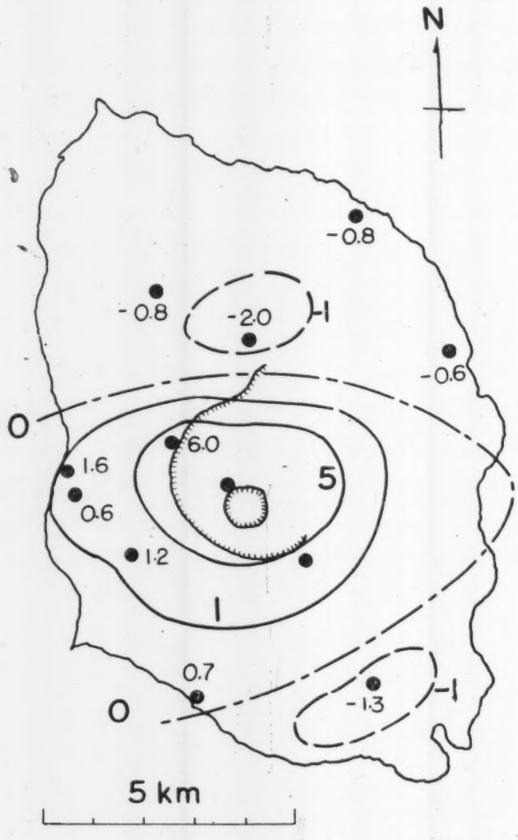

Fig. 11. Changes in geomagnetic dip VI Aug. 1953—IV May 1951 (secular variation and the effects of ejected lava are corrected.)

Survey VII was carried out on Oct. 8 and 9, 1953 for the purpose of detecting the change accompanying the minor activity that abruptly occurred on Oct. 5 after about two years' quiescence. The survey was made on the stations near the central cone with G.S.I. type magnetometer, the accuracy of the measurements being 0.1 *minute* of arc. As shown in Fig. 12, concentric distribution of decrease in dip-angle

amounted to more than 3 *minutes* of arc during the period from August to October. This decrease may be ascribed to the minor activity of the volcano. Since the new activity is intermittent pyroxysmal eruption in

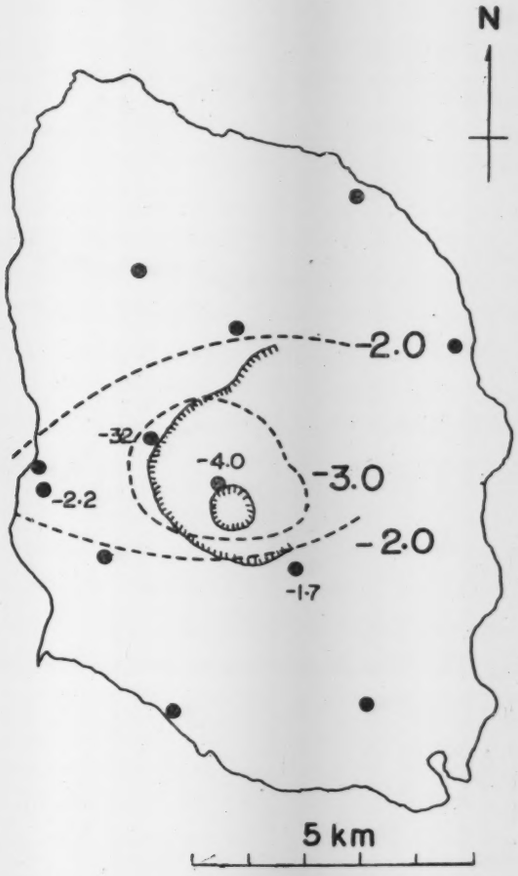

Fig. 12.

Changes in geomagnetic dip accompanied by the minor eruption in Oct. 1953 (VII Oct. 1953 —VI Aug. 1953). The unit is *minute* of arc.

a minor scale, it seems natural that we got smaller changes in geomagnetic field than those of the earlier and more violent stage of the 1950 eruption.

5. Some results of the continuous observation of changes in geomagnetic declination at the temporary station.

As already reported in the 3rd paper, since April 1951, the writer has continuously recorded the changes in geomagnetic declination with a variometer at the temporary station (No. 37) on the western foot of the volcano, about 4 *km* distant from the crater.

The 15-day means of the westerly declination at Ooshima and Kakioka are shown in Fig. 13. For the purpose of showing the gradual

time-variation of the declination, the 15-day means are convenient. The mean values are calculated from daily means obtained by averaging hourly values. In order to check the base-line value of the variometer,

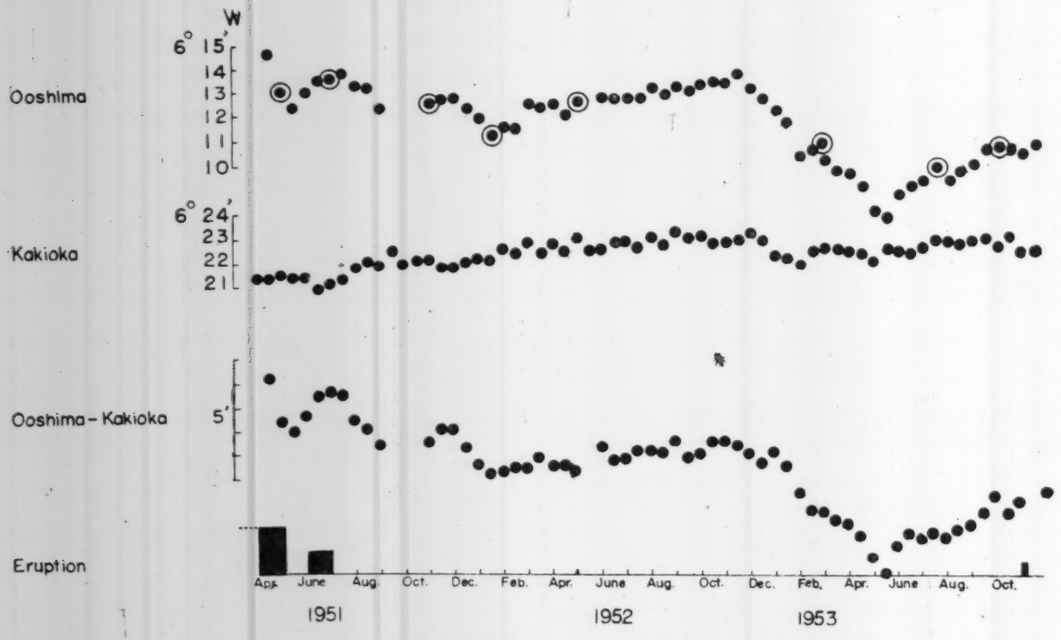

Fig. 13. The 15-day means of the westerly declination at Ooshima and Kakioka.

a series of absolute measurements of declination has been carried out in front of the variometer-room, the results of which are shown in Fig. 13 with large hollow circles and in Table IV including the other elements. In order to express the changes which may be presumed to be related with activities of the volcano more clearly, the differences between the values of the declination at Ooshima and Kakioka are also plotted together with the period during which the eruption continued. As already stated in the 3rd paper, an increase in the westerly declination was observed just before the active period in June 1951, which was the finale of the 1951 eruption. Meanwhile the westerly declination showed again a decrease which followed the said maximum and another maximum was observed in December 1951. Although no active eruption took place at that time, some topographical change occurred at the bottom of the new pit and micro-tremors of large amplitude were observed by seismometers. As may be seen in the figure, the differences between both stations increased gradually in 1952 in spite of the gradient of opposite sign in the differences of geomagnetic secular variations which amount to respectively 2.00 and 2.27 *minutes*

Table IV. Results of absolute measurements at the station No. 37, Nomashi Village.

Time (J.S.T.)	D	I
1951 Nov. 8		
14*h* 36*m*	6° 16′.7	47° 30′.9
15 54	15.5	29.5
18 04	13.0	26.0
Nov. 9		
09 08	11.3	26.7
10 08	12.0	25.9
11 06	12.1	24.2
11 50	14.1	24.4
Mean	6° 13′.5	47° 26′.8

Time (J.S.T.)	H
1951 Nov. 9	
10*h* 21*m*	30010γ
11 18	30020
Mean	30015γ

Time	D	I
1952 Jan. 19		
12*h* 08*m*	6° 11′.8	47° 24′.2
13 07	12.4	24.6
14 08	12.0	24.5
15 06	11.6	24.1
16 18	10.9	24.5
17 10	11.0	24.4
18 00	10.4	24.4
19 26	11.1	24.3
21 08	10.7	24.2
Jan. 20		
01 20	10.5	24.5
04 10	11.3	24.0
08 10	10.0	23.5
09 20	8.7	23.4
10 48	8.9	24.2
Mean	6° 10′.8	47° 24′.3

Time	H
1952 Jan. 19	
11*h* 30*m*	29991γ
13 22	30016
14 08	30026
16 20	30016
21 08	30001
Jan. 20	
10 08	30008
Mean	30010γ

Time	D	I
1952 May 8		
16*h* 29*m*	6° 14′.4	47° 25′.4
17 58	14.9	25.2
18 38	13.9	25.2
20 35	12.6	25.0
22 38	12.0	24.7
23 34	10.8	24.8
May 9		
01 08	7.9	24.5
01 52	7.5	25.2
02 35	7.9	25.2
10 34	14.3	25.0
11 06	14.8	24.4
11 34	15.5	24.7
12 06	16.0	24.0
12 36	16.2	23.9
Mean	6° 12′.8	47° 24′.8

Time	H
1952 May 8	
16*h* 44*m*	29987γ
18 06	29991
18 48	30019
20 46	30003
23 48	30012
May 9	
01 20	30007
02 08	30002
Mean	30003γ

(to be continued.)

Table IV. (Continued.)

Time (J.S.T.)	D	I
1953 Feb. 27		
09h 13m	6° 10′.4	47° 23′.0
10 31	11.6	22.0
11 34	14.0	20.2
12 14	13.9	21.6
13 18	14.3	22.1
14 28	13.0	20.9
15 31	12.0	22.4
18 51	9.6	22.9
20 50	6.8	23.0
22 02	10.2	23.0
23 32	9.6	22.1
Feb. 28		
04 46	8.9	23.0
06 55	10.5	23.2
10 05	8.1	23.9
Mean	6° 10′.9	47° 23′.2

Time (J.S.T.)	H
1953 Feb. 27	
10h 46m	30006γ
17 59	30012
Mean	30009γ

Time	D	H	I
1953 July 30~31			
08h 56m	6° 10′.5		47° 21′.2
10 12	9.9		21.4
12 42	14.2		20.6
14 12	14.7		25.9
16 10	13.2		23.4
17 46	11.3		23.6
18 30	10.4		23.3
21 04	6.9		21.4
21 34	9.7		21.7
07 05	7.8		21.7
07 53	8.8	29995γ	22.7
09 18	9.9	29996	21.9
10 10	—	29991	21.5
10 52	10.2	29991	20.7
11 36	11.4	29987	22.0
Mean	6° 10′.6	29992γ	47° 22′.0

Time	D	H	I
1953 Oct. 8			
21h 14m	6° 11′.4	30044γ	47° 20′.0
22 04	11.1	30041	19.9
22 24	10.8	30045	19.7
22 44	10.6	30045	19.5
Oct. 9			
08 55	7.9		
10 05			19.8
10 53	10.7		19.3
11 05	11.6		19.3
12 11	13.1		19.0
12 32	13.7		19.0
14 59	11.3		18.6
15 08	11.8		18.5
16 15	9.9	30048	19.2
Mean	6° 11′.2	30045γ	47° 19′.3

of arc westerly per year. According to the reports of the Ooshima Meteorological Station, on Sept. 18, 1952 a fissure appeared at the

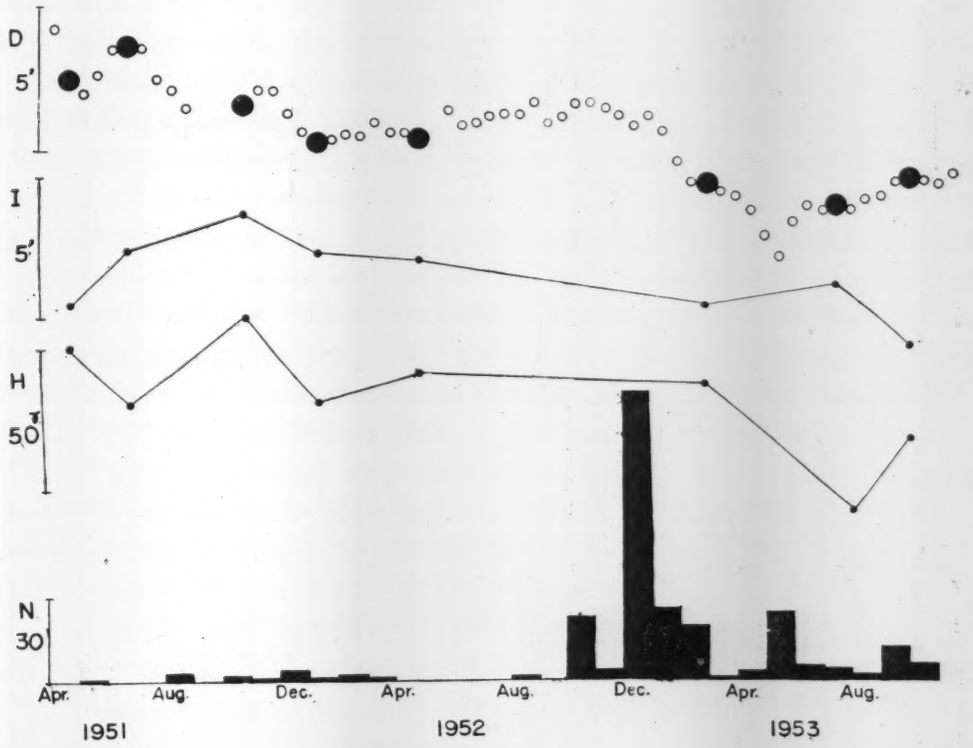

Fig. 14. Changes in three geomagnetic components (Ooshima-Kakioka) at the Nomashi Station (No. 37). Lowest column shows the number of the earthquake observed by the Ooshima Meteorological Station of which PS-time is shorter than 5 *seconds*.

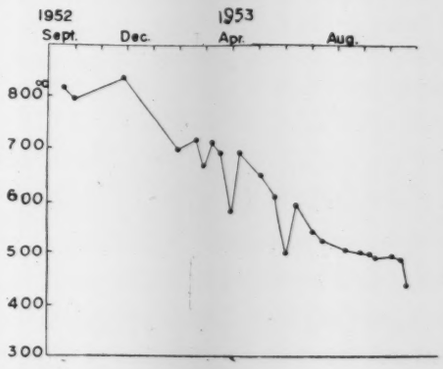

Fig. 15. Cooling curve of a fissure in the inner somma. (After Ooshima Meteorological Station)

1951 lava-flow in the inner somma and its temperature was measured at 817°C. This temperature reached the highest 840°C in December and then began to decrease as shown in Fig. 15. The westerly declination showed a remarkable minimum in May 1953, and recovery towards October, while the crater of the volcano continued to emit only water vapour of small amount after the last eruption in June 1951. It is noticeable that the increase of the westerly declination coincides with the abrupt minor eruption on Oct. 5. Fig. 14 shows the changes in the differences between

both stations in horizontal intensity and inclination obtained by a series of absolute measurements and the number of the earthquakes observed by the Ooshima Meteorological Station of which PS-time is shorter than 5 *seconds*.

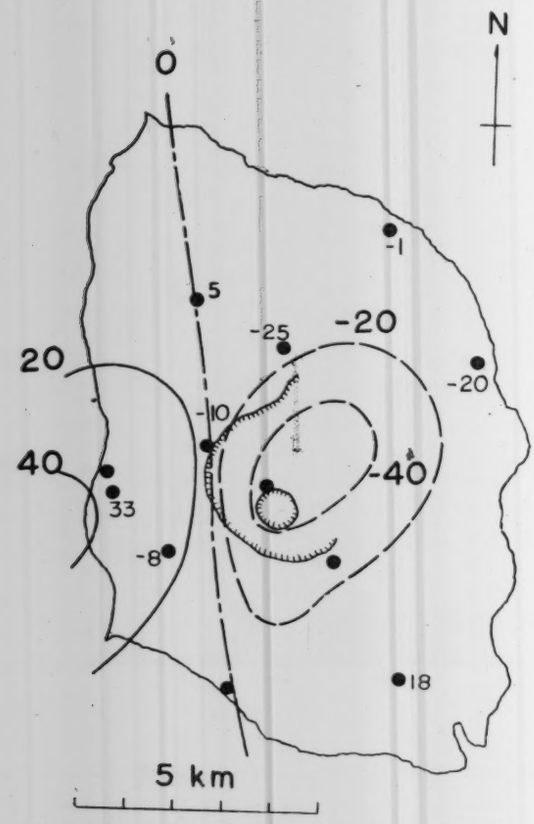

Fig. 16. The changes in geomagnetic east-component from May 1951 to Aug. 1953 (secular variation and the effects of ejected lava are corrected). The unit is *gamma*.

To examine the general tendency in the changes of declination all over the island, the differences of values in declination at the stations where the three-elements survey IV was carried out in May 1951, are obtained by repeating similar measurements VI in Aug. 1953, as shown in Fig. 16 (refer to the next report). Comparing this chart with the distribution of the declination shown in Fig. 4 of the 3rd paper, it seems likely that the decrease in the westerly declination may correspond to the increase of the magnetization of the under-ground mass and *vice versa*. However, much more data should be accumlated in order to infer the internal condition of the volcano from geomagnetic changes observed on it.

6. Summary and conclusion.

Succeeding to the 3rd paper, the writer reported the results obtained by the subsequent surveys and observations in this paper. By a series of dip-surveys, the recovery of the local anomalous changes which accompanied the 1950 eruption was detected. According to the results obtained by the continuous observation of declination at the temporary station, it was observed that there were decreases and increases of declination relating to the volcanic activities. This change is compatible with those of declination observed at various stations during the period from May 1951 to Aug. 1953 as shown in Fig. 16. The characteristic changes in both declination and dip were also confirmed

on the occasion of the minor eruption in Oct. 1953. Detailed interpretations conjectured by analyzing the results will be given in the future reports.

In concluding, the writer wishes to express his hearty thanks to Dr. T. Rikitake for his helpful advices, who initiated this study and is now staying in England. To Prof. T. Nagata for his helpful criticism and encouragement, the writer's cordial thanks are also due. The writer's hearty thanks are also due to Mr. T. Yoshimatsu of the Kakioka Magnetic Observatory and Mr. T. Yokoyama of the Ooshima Meteorological Station who placed valuable data at the writer's disposal. Mr. A. Okada assisted the writer in field works, to whom the writer's cordial thanks are also due. The writer wishes to express his sincere thanks to Messrs. T. Masaka, T. Yanai and S. Saito and Miss Y. Hishiyama who assisted the writer in the course of study.

---

3. 三原山の地球磁気学的研究
第4報
(一連の伏角測量と偏角変化の連続観測)

地震研究所　横山　泉

三原山の1950年の噴火以来，地球磁場の変動を出来る限りの高い精度で，しかも長期にわたつて観測し，その資料を集めるよう努力してきたが，第3報に続いて，1953年10月までに行われた一連の伏角測量と偏角変化の連続観測との結果をとりまとめて報告した．地磁気変化と火山活動との関係を吟味すると，推論は当然，地下の状態に及ぶのであるが，そのためには火口から溢出した熔岩の磁気的効果を考慮せねばならぬ．4回にわたる全島伏角測量を比較すると，1950年の噴火に際して生じた著しい伏角の減少はある程度回復したように思われる．又，1953年10月の小噴火に際しても，僅かではあるが，伏角の減少が確認された．

野増村に設けられた偏角変化計の記録から，15日平均を求め，柿岡地磁気観測所の値を基準として，その変化の模様を調べると，火山活動と偏角変化との間に有意な関係があるように見える．又島全体としての偏角変化の傾向を調べるために，1951年5月の観測結果と，1953年8月のそれとを比較すると，地下にあらたに帯磁が生じたような変化を示している．この量的な吟味は次報で行う予定である．

4. *The 1950-1951 Eruptions of Mt. Mihara, Oshima Volcano, Seven Izu Islands, Japan. Part I. The 1950 eruption.**

By Hiromichi TSUYA, Ryōhei MORIMOTO and Joyo OSSAKA,

Earthquake Research Institute.

(Read Sept. 19, 1950, June 19, 1951, and March 18, 1952.
Received Jan. 4, 1954)

I. Introduction.

After 10 years' repose, Mt. Mihara, the central cone of Oshima volcano, one of the Seven Izu Islands, about 110 km southwest of Tokyo, began an eruptive activity at the summit crater in the morning of July 16, 1950. The activity was exhibited as a continuous and progressive eruption of the Strombolian type, lasting for ten weeks until September 23, 1950, when it suddenly stopped. During the next year, from February 4 to June 28, the volcano displayed again eruptions on a larger scale, with more extensive lava outflows. This paper includes the results of our investigations of the eruptions, such as observation of the events, topographic survey of the active crater, measurement of temperature and specific heat of the new lavas, and estimation of the quantity of the lavas, besides petrography and chemistry of the lavas, incrustations, and sublimates, already reported in the previous papers[1].

The Seven Izu Islands consist of several Quaternary insular volcanoes that rest upon a submarine ridge elongating in NNW.-SSE. direction from Izu region through Southern Islands toward Marianas (Fig. 1). Oshima, the largest of the Islands is composed almost entirely of oversaturated basalts. It comprises a truncated central cone Miharayama (Mt. Mihara. "Mihara" means hole.) and a somma dotted with several parasitic knobs and explosion-hollows, besides the ruins of older volcanic bodies underlying the northwestern skirt of the somma. According

* Dedicated to Prof. Seitarô TSUBOI in celebration of his 61st birthday.

1) H. TSUYA & R. MORIMOTO, "Petrography of the 1950-lavas of Oshima volcano, Seven Izu Islands, Japan." *Bull. Earthq. Res. Inst.*, **29** (1951), 563-570.

H. TSUYA, R. MORIMOTO & Joyo OSSAKA, "Chemical composition of the 1951-lavas of Oshima volcano, Seven Izu Islands, Japan," *Bull. Earthq. Res. Inst.*, **30** (1952), 231-236.

R. MORIMOTO, & Joyo OSSAKA, "On the Miharayama lavas," *Jour. Geography*, **60** (1951), 136-140 (in Japanese).

to S. Tsuboi[2] who studied the geology of the island after the 1912–1914 eruption, the Oshima volcano came into being at a late date, probably in the late Diluvium. Mt. Mihara was born in a pre-historic age at the southern portion of the summit caldera by the volcanic activity rejuvenated after the cauldron subsidence of the somma volcano. The Quaternary Oshima volcano rests on the deeply dissected volcanic ruins represented by the basalts exposed along the seashore near Okata (Fig. 2). Sawamura[3] pointed out that the Okata basalts may be of the Pliocene age, seeing that they are accompanied with a tuff breccia containing fragments of altered andesites and gabbro, probably one of Miocene volcanics correlative to the Yugashima series on the adjoining Izu peninsula.

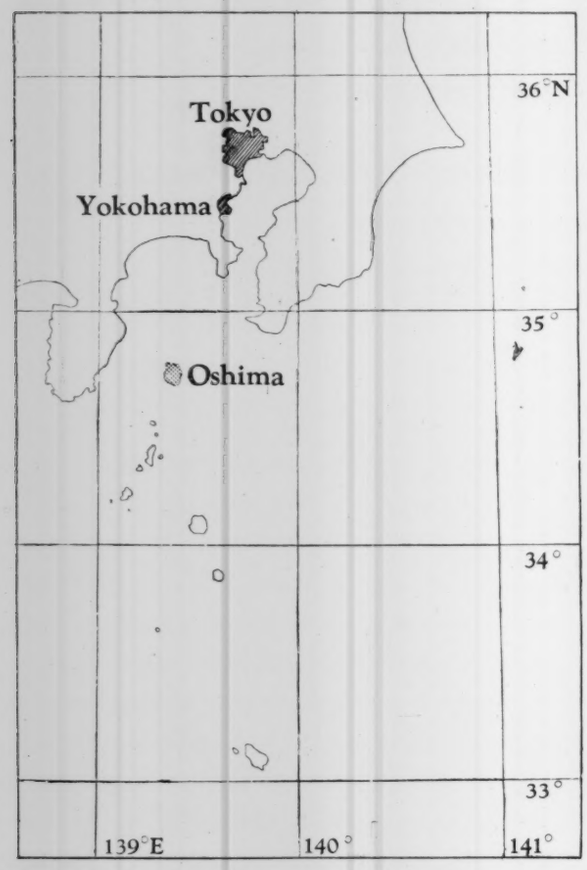

Fig. 1. An index map of Oshima volcano with Seven Izu Islands.

Mt. Mihara is one of the most active crater in Japan and has repeated many activities in historic times as shown in the following table (Table I). Among them, the 1684–1690 and 1777–1778 eruptions are most remarkable in having poured out lavas from the crater over the flanks of the somma and further down into the sea. The present eruptions may be comparable in scale to these historic eruptions. In the 1912–1914 eruptions, the most remarkable of the recent activities prior to the present ones, the lava filled the crater almost to its lowest brim but did not run over the crater rim. Since the end of the eruptions, the volcano had kept a considerable quiescence for about 25 years, its activities being represented only by occasional

2) S. TSUBOI, "Volcano Oshima, Idzu," *Jour. Coll. Sci.*, **43** (1920), **vi** 1–146.

3) K. SAWAMURA, "Development of the Oshima Island," *Jour. Geography*, **60** (1951), 104–106 (in Japanese).

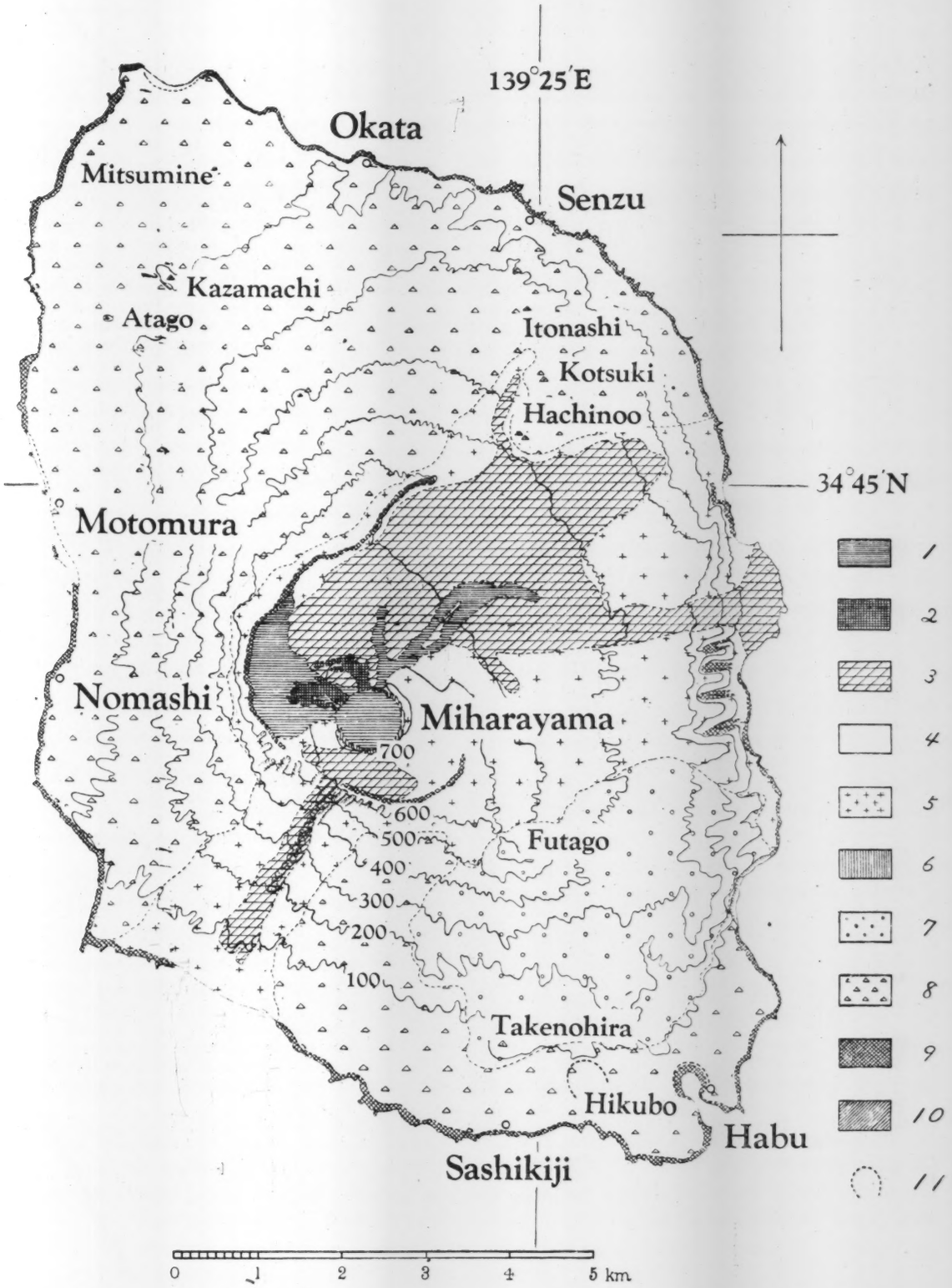

Fig. 2. Distribution of 1950 and 1951 lavas plotted on the geologic map after S. Tsuboi (1916–1918). The 1912–1914 lava was covered by the 1950–1951 lavas. 1: 1951-lava, 2: 1950-lava, 3: 1778-lava, 4: Beach deposits, 5: Central cone ejecta, 6: Central cone lava, 7: Scoriae from flank openings, 8: Somma ejecta, 9: Somma lavas, 10: Rocks of northwestern demolished igneous bodies, 11: Phreatic explosion-crater.

Table I. Recorded volcanic activities of Oshima in historic times.

684:	Nov. 29. It is said that the land increased on the western and northern sides of the island.
1112:	From Nov. 18 till the end of the next month, detonations were heard repeatedly in Kyoto.
1416:	Sept. 2. An eruption took place.
1421:	May 14. An eruption occurred, noises were heard in Kamakura. Sea water became hot.
1600–1601:	Minor eruption.
1612–1613:	Minor eruption.
1636–1637:	Minor eruption.
1684–1690:	On March 31, a violent eruption began and continued for 7 years. It is said that a crater, ca. 1 km in dia., was formed on the summit of Mt. Mihara. On Apr. 22, lava flowed down toward NE. and poured into the sea.
1777–1778:	Most violent eruption ever recorded in the history of the volcano. (Fig. 2)
1803:	On Nov. 14, eruption took place, and ashes fell in Tokyo on the next day.
1822:	Ashes fell in Tokyo.
1846:	Eruption.
1870:	Minor activity.
1876–1877:	From the end of Dec. 1876 to Feb. 6, 1877. Lava poured out in the crater of Mihara but it did not run over the brim of the crater. A minor spatter cone was formed at the bottom of the crater.
1912–1914:	March-June 10 in 1912, welling out of lava at the bottom of the crater. July 27–29, depression of solid lava due to its own weight accompanied with breaking up of spatter cone and squeezing out of lava. Sept. 16–Oct. 29, 1912, extrusion of lava at the crater bottom and formation of a spatter cone. Jan. 14, 1913, depression of lava layer accompanied with extrusion of lava. Lava emission lasted for 12 days. During May 15–21, 1914, paroxysmal lava extrusion occurred, followed by intermittent emission of lava for a few days.
1915:	Minor activity from Oct. 10 to the end of the month. Roarings and air-quakes were felt and ash fell in the southwestern part of the island. No lava poured out.
1938:	Aug. 11, the bottom of the pit turned into an incandescent lava pool and scoria fell around the mouth of the pit.
1939:	Minor activities in Sept. 2–3, and Sept. 16. Incandescent lava appeared at the bottom of the crater. Quantities of bombs and scoria were thrown up, though they did not reach above the rim of the pit.
1940:	Minor activity in Aug. 18–19. Ejection of incandescent bombs and emission of gas from the fissure opened in the solidified lava at the bottom of the pit on Apr. 18. Incandescent bombs and lapilli were ejected in quantity up to 500 m in height above the summit of the central cone, and were deposited thickly on the 1912–1914 lava field on Apr. 19.

Remarks on the eruptions from 684 to 1915 are compiled from S. Tsuboi's paper (*Ibid.* pp. 53–59), and those of 1938–1940 from T. Nagata's ("A geomagnetic study of the minor activities of Volcano Mihara, Oosima Island, August 1940", *Bull. Earthq. Res. Inst.*, **19** (1941), 402–410.)

volcanic rumblings and earth tremors, vapour emissions, ejections of a little volcanic ashes, etc. But the crater-floor covered with the 1912–1914 lavas had changed its topographical features in that period. Thus,

after the end of 1912–1914 eruptions, the central portion of the crater floor had been depressed in the form of a circular pit, although it is not clear when the central pit was formed. The central pit had increased its mean diameter linearly with time due to collapses of the wall[4], while the pit had decreased its depth linearly with time till the beginning of the 1940 eruption[5]. A small mass of red-hot lava could be seen from time to time on the floor of the pit. The crater had been quiet for ten years since the minor explosive activity in August of 1940. Just before the beginning of the present eruptions, July 16, 1950, the crater was virtually identical in topography with that shown in the map prepared by Takahasi and Nagata in 1936[6]. But the pit had become a little shallower being about 170 m[7] in depth and about 310 m in mean diameter. The surface of the 1912–1914 lava-field was more or less flat, being veneered with the 1940 ash and scoria. Relief of the crater immediately before the eruptions is also inferred to have differed not greatly in topography from that observed by two of the writers a few days after the beginning of the activity (Fig. 20), though the pit wall had already been destroyed by outbursts and the bottom of the pit had been filled by a new lava.

Our works on the volcano were assisted by many eyewitnesses of the eruptions, especially, Messrs. S. Watanabe, K. Mase, Y. Fujita, and T. Yoshinari, inhabitants of Motomura village, to whom our thanks are due. The daily sketches and photographs of the eruptions taken by Mr. Watanabe were useful to complement our observations of the eruptions. Our thanks are also due to Mr. T. Kizawa, Chief of the Meteorological Observatory, for his kind information on the state of the crater before the eruptions. We express our cordial thanks to Dr. R. Takahasi and Mr. D. Shimozuru of the Earthquake Research Institute, who kindly allowed us to publish one of the crater maps prepared by them. Our cordial thanks are also due to Dr. T. Yamanouchi and Dr.

4) R. TAKAHASI and T. NAGATA, "Geophysical Studies of Volcano Mihara, Oosima Island: The general aspect of physical conditions in the crater," *Bull. Earthq. Res. Inst.* **15** (1937), 1047.

5) T. NAGATA, "Mihara-yama, Oosima, Izu," *Bull. Volc. Soc. Japan.* **4** (1940), 196 (in Japanese).

6) R. TAKAHASI and T. NAGATA, "Geophysical Studies of Volcano Mihara, Oosima Island: Topographic survey of the Crater of Mihara and the magnetic survey of Oosima," *Bull. Earthq. Res. Inst.* **15** (1937), 441–462.

7) Oral communication from Mr. T. Kizawa, Chief of the Meteorological Observatory of the island. Data from the expedition of the pit by Mainichi Press, May 13, 1950.

Y. Shiraki, and to Mr. H. Suzuki of the Tokyo Institute of Technology for their kind instructions on some of our laboratory works. We are indebted to Messrs. T. Aoki, T. Sakamoto, and Y. Shimazaki, students of the Mineralogical Institute of our University, for helping us in measuring temperatures of the flowing lavas. We are also indebted to Messrs. T. Watanabe and A. Okata, Miss F. Toraiwa and T. Fukuda, for their assistance in the field and in the laboratory.

A part of the expense necessary for the investigations was defrayed from the Grant in Aid for Scientific Research from the Department of Education.

II. History of the 1950 eruption.

Premonitory symptoms were not reported before the present eruptions.[8]

(1) *Opening of the first vent and collapse of the pit wall*:

The 1950 eruption began at 09h15 m (Japanese Standard Time), July 16, with sudden explosions on an arcuate and almost vertical fissure (Fig. 3) which had already been formed along the southern periphery of the central pit.[9]

Owing to the explosions, the pit wall adjacent to the fissure scaled off several meters in thickness, and collapsed on the bottom of the pit, making a pile there in the form of a talus. These explosions were heard at the crater floor like noises of a diving aeroplane, and fine pieces of the broken wall were seen to rise as dark ash clouds blown away by the wind northeastward. Explosions were repeated in like manner at intervals of about 4 to 10 minutes. In the intervals of two successive explosions, vapours continuously rising from the exploded portion of the pit wall were visible through the misty air, but red-hot lava was not found at that time[10].

Just after noon of the same day, according to Mr. H. Yamazaki of Motomura village, a narrow stream of incandescent lava could be recognized hanging over the slope of the above-mentioned talus, from a crack on the collapsed pit wall, about 20 m below the southern rim

8) In this connection, it must be taken into consideration that seismographical observations of the volcano by sensitive seismometers had long been interrupted during and after World War II.

9) A seismograph of the Meteorological Observatory of the island began to record the volcanic tremors on 09h07m23s (Japanese Standard Time).

10) After Mr. B. Hirata of Okata village, the first eyewitness of the eruption.

of the pit, toward the pit floor (A in Figs. 4, 5, and 7). It is remarkable that the fluidal basalt lava rose halfway up the fissure in the pit wall, the upper part of which had already been destroyed by the forerunning gas explosions, instead of welling out of the bottom of the pit. It is said that another smaller stream of red-hot lava was hanging down from the point on the side of the previously formed crack designated as A in Figs. 4, 5 and 7. The collapses of the pit wall continued for hours; they became most remarkable in the afternoon, from 13h to 16h, July 16. The lava streams hanging on the pit wall had disappeared before the noon of July 18, owing to the accumulation of ash and rock debris of the collapsed wall[11-12].

Ash clouds, about 300–500 m in height above the crater, were sometimes observable even from the skirt of the somma.

(2) *Enlargement of the explosive vent*:

Dense misty weather often interrupted the observations by eyewitnesses at the beginning stage of the present eruptions. Thus, on July 17 and 19, the crater was put out of sight by dense clouds day and night.

In the morning of July 20, the crater took off her misty veil. Then, at last, one of the writers (R. M.) caught his first opportunity to observe the actual scene of the activity.

The upper portion of the southern wall, about 30 m in length, 20 m in height, and several meters in width, of the central pit had collapsed down to form a talus beneath. Fumarolic activity continued along the cracks on the destructed wall behind the talus and along the fissure between the talus and the wall. Two red-hot points were visible on the wall near A and B respectively (Figs. 4 and 5), through the rising vapour like a fenestella of a furnace. At 10h30m, an explosion took place at the east end of the fissure (B in Figs. 5, 7, and 9), about 20 m below the rim of the pit; gas was jetted vertically, dark ash clouds were thrusted to the sky every two minutes, the rocks around the new explosion opening were gradually heated into a red-hot state. Outpouring of fluidal lava began at the southwestern corner of the bottom of the pit. At 12h27m, a severe explosion occurred on the same fissure at a point designated as C in Figs. 5, 7, and 9. Explosions

11) An informal report from the Meteorological Observatory of Oshima.

12) Vapours and ash clouds rose from the crack on the pit wall; lava was hanging down; wall was crumbling down with rising columns of dense dusty smoke; earth-rumblings were felt in the crater; extrusion of lava from the bottom of the pit was not observed (10h15m, July 18, after B. Hirata).

at C repeated at intervals from 20 to 30 seconds, with ejections of dark grey smokes of fine ashes. At 14h00m, red-hot fume became observable at C with brown ash-clouds. At that time, activity at A had already subsided, exhibiting a gentle vapour emission.

In the evening of July 20, the explosions at B appeared to be more active and stationary: Noises like surfs on seashore were heard at intervals from 10 to 15 seconds; with every roar, a jet of red-hot fume was seen; ejected red-hot rock fragments fell to crumble on the slope of the talus; collapses of the pit wall near the explosion-openings continued; and incandescent lava was squeezed out through clefts on the already solidified crust of lava at the southwestern corner of the bottom of the pit. These activities must have continued through the next day, but they could not be observed because of bad weather.

On July 22, the explosion-opening at B was enlarged up to 10 m in width along the fissure, and the talus grew larger owing to the collapse of the pit wall. At 12h55m, activity at B declined comparatively, and lava poured out from the bottom of the pit (Fig. 6), while the opening at C was awakened again to be active from a relative calmness in the preceding several hours. In the afternoon, violent explosions often took places. Ejections of ashes, which were brought about by the explosive emissions of gas through different openings, were followed every time by stationary ejections of lava-blocks and scoria, lasting for about 10 to 20 minutes. Repeating these explosions, and sometimes being accompanied with temporary squeezing-out of lava from the bottom of the pit, the eruption became gradually larger in scale.

On July 23, the activities became so violent that explosions were heard frequently even on the skirt of the somma. Explosions at B and C occurred either alternately or simultaneously (Fig. 9). Frequently, the centre of explosive action moved along the fissure step by step from B toward C, or from C toward B.

On July 24, at 06h30m, B and C were united with each other to form a large opening (the 1st vent) by explosions accompanying heavy ash-falls. Thereafter, the first vent repeated explosions without interruption, until the end of the same month, resulting in the formation of a cinder cone, about 20 m in height above the crater floor (Figs. 11 and 15).

During July 31—Aug. 1, the explosions occurred at the 1st vent; the vent was enlarged; and two bowl-shaped openings were formed

within it (Fig. 32).

(*3*) *Welling out of lava from the pit-bottom*:

It was reported that, on July 16, an incandescent lava began to well out from two spots near the southwestern corner of the bottom of the central pit at 21 h[13]. Spreading over the pit-bottom, the lava flow was soon covered with a dark solidified crust, although the underlying still fluidal lava was visible through clefts in the crust. Lava fountains were being displayed on a small scale temporarily, but always at the southwestern corner of the pit-bottom (Figs. 6, 8, 10, 16, 18, and 19).

The lava fountains in the pit-bottom seemed to have some connection in activity with the explosion-openings along the fissure. Thus, their activities, as observed during 13 h 59 m–18 h on Jnly 30, were as follows: the stationary explosive activity at the openings along the fissure was disturbed by the lava fountainings on the pit-bottom, in such a manner that the former decreased its violence as the latter increased. Lava-outpouring at the fountains was continual, although a sudden engulfment of the fountaining lava into the feeding channel below was temporarily observed at 15 h 10 m. At 16 h 55 m, the lava-outpouring gradually declined, while the explosions at the openings became violent. At 17 h 30 m, simultaneously with the subsidence of activity of the latter, the former became vigorous again, being supplemented later at 17 h 40 m by a "boiling" action at the lava fountains. Toward 18 h, the lava-outpouring became stationary and rather weak, while the explosive activity at the opening recovered from its declining activity, coming back to its stationary state of repeating explosions. Then, both the lava fountains and explosive openings continued their activities side by side. The following is a fuller account of the feature of the lava fountainings observed by one of the writers (R. M.) on July 30.

An incandescent lava wells out like water pouring forth from a big pipe. The force of splashing of the lava in the fountain is not so strong as that observed in the Hawaiian eruptions[14] and also as that observed in the 1951 eruption of the present volcano. But at the climax of fountainings, the lava is splashed like water around its source (Fig.

13) T. KIZAWA, "Geophysical phenomena in volcanic activity (1)", *Journal of Meteorological Research from the Central Meteorological Observatory*, **3** (1951), No. 7, 249 (in Japanese).

2) G. A. MACDONALD & J. B. ORR, "The 1949 summit eruption of Mauna Loa, Hawaii," *Bull. Geol. Surv. U.S.A.*, 974–A (1950).

19). The lava flows with a speed of about 18 m every minute from its source to the lower portions in the pit-bottom (Figs. 10, 16, and 18). Temperatures at the surface of the lava in and about the fountains are high, sometimes attaining up to 1200°C, as measured with an optical pyrometer on the spots illuminated in orange-yellow. Viscosity of the lava may be small as inferred from the appearance of the lava splashes.

The head of lava column in the central pit was rising continually with or without outpouring of an incandescent lava to the surface, probably owing to the continuous feeding of liquid lava from below to the bottom of new lava pool in the pit. Thus, the level of the new lava in the pit became higher day by day, its depths from the rim of the pit (C in Fig. 20) being 140 m, 125 m, 123 m, 99 m, and 60 m, on July 21, 24, 25, 28, and 30, respectively, and 52 m on Aug. 1.

From midnight of Aug. 1 to dawn of the next day, a new lava began to appear beneath the talus, which was described in a foregoing section, with tremendous earth-trembles amid heavy rain-falls. On Aug. 2, at 11 h 00 m, extrusion of the lava took place vigorously, thrusting up northward on the already-solidified surface of the lava column in the central pit. Such extrusions of the lava further occurred in the following Aug. 3, to form a mound at the foot of the talus.[15] Cinders were piled on the mound and its topography, thus formed, remains even after the cease of the present activity (Figs. 31, 61).

(*4*) *Ejecta at the initial stage of the eruption*:

The materials ejected by explosions were different in certain respects, as the initial provisional explosion-openings were enlarged to a definite explosion-vent (1st vent) on the new cinder cone, and as the head of lava column in the central pit upheaved at the initial stage of the eruption. Thus at the initial stage of the eruption, volcanic ashes were blown out, forming dense ash-clouds in the air. They were deposited on the southern half of the crater-floor, especially on its southernmost corner where old fumaroles[16] were still active. They consist mainly of old rock fragments, probably derived from the pit-wall smashed by the explosions.

15) K. SAWAMURA, "On the volcanic activity of Mt. Mihara, Izu Oshima Is. in 1950," *Bull. Geol. Surv. Japan*, **4** (1953), 175.
T. KIZAWA, *Ibid.* 253.

16) Almost constant in temperature, about 50°C before and after the beginning of the 1950 eruption. (Oral communication from Mr. T. Kizawa).

Juvenile volcanic bombs and scoriae are comparatively rare in the ejecta at the beginning of the eruption. Some of the bombs, so far found, carry an angular fragment of old rocks as their central cores. Ash-clouds were usually blown out whenever an explosive activity began after a time of repose, particularly when an explosion began at a new opening. Juvenile volcanic bombs and scoriae were ejected when the explosive activity entered in a stationary state, with a succession of explosions showing a volcanic eruption of the Strombolian type.

(5) *Shifting of the explosive vent (1st vent)*:

For ten days from Aug. 1, the eruptions were recurrent without any long repose, as suggested by frequent detonations, but nothing important of the activity could be seen, for the mountain was shrouded for most of the time with a dense cloud accompanying heavy rain-falls.

In the morning of Aug. 5, the top of the cinder pile on the northern side of the explosive vent had reached to the rim of the central pit, and the cinder pile on the southern side of the vent had grown into a cone, about 50 m in height above the old crater-floor.

On Aug. 7, the vent, situated about 20 m above the rim of the pit, had shifted southward (Figs. 22–23) to be surrounded by a complete cinder cone. The southern side of the cinder cone, which covered the old crater-floor, was connected with adjoining old crater-wall. The cinder pile which was deposited on the talus formed by the debris of collapsed pit-wall, adjoining to the northern side of the cinder cone had been pushed from below by the rising lava column in the pit and moved somewhat to the north. The rising of the lava column in the pit was accelerative; the lava, which was fed through a concealed path at the southern corner of the pit, continued to flow northward on the surface of lava column in the pit. Both the upward movement of the lava column and the northward movement of the overflowing lava caused a northward drift of the cinder pile on the northern side of the cinder cone, bringing the latter to the centre of the central pit. The southward shift of the explosive vent, which resulted in the formation of a separate cinder cone, suggests the shifting in that direction of the underlying feeding channel of a gaseous lava, probably due to a lateral pressure of the rising lava column in the pit. The upward extrusion of the lava column, which brought about the remarkable shifting of the vent and the cinder pile, is inferred to have occurred mainly during Aug. 4–5.[17]

17) Earthquakes were felt 10 times or more in the island on Aug. 5.

On Aug. 9, explosive activity was rather small, both in noise and in force of ejection, compared with that in the preceding two days. The same day, however, rising of the lava column in the central pit and emission of lava from the southern part of the pit became more conspicuous, accompanying remarkable volcanic tremors about every 5 minutes. In the next two days, the explosive activity was violent together with powerful emissions of incandescent lava through clefts in the solidified crust of the lava column. In the evening of Aug. 11, the explosions were heard as severe rumblings even on the skirts of the volcano.

On Aug. 12, at noon, lava welled out from two openings, situated at the southeastern corner of the central pit and adjacent to the east of the active cinder cone, spurting light-bluish fumes. There, lava fountainings were being displayed to a height of several metres, and the southern half of the pit was covered with the incandescent lava, exhibiting something like a sea of flames. The surface of the lava in the pit was about 20 m in average below the edge of the crater-floor (Fig. 34). At that time, the explosive vent was almost in a dormant state. But on the next day, the vent resumed an explosive activity, ejecting cinders and bombs, 200 m or more above the rim of the vent. The cinder cone, which was formed around the explosive vent, attained to a height, only 2 m lower in altitude than the southern crater-wall. Moreover, from an opening adjoining to the cinder cone and corresponding to the site of the explosions at the initial stage of the eruption, lava welled out with an upward jet of about 1 m in height, and ran down with a speed of about 1.5 m/sec, forming ripply streams. Then, these glowing lava streams advanced slowly on the floor of the central pit along its southwestern wall, and transformed before long into a pahoehoe lava.

On Aug. 14, emissions of lava from the same spot as mentioned above, became again conspicuous, their jets attaining to a height of about 3 m or more. The lava filled up the central pit almost completely. The solid crust of the lava near the southwestern edge of the pit became about 1 m higher than the edge of the pit. The cinder cone also became about 1 m higher than the southern wall of the crater.

(6) Outflows of lavas from the central pit to the crater-floor:

On Aug. 15, explosions were rather weak, as in the foregoing two days; lava cinders and bombs were ejected only about 50–60 m above the rim of the vent at intervals of about 2 to 6 seconds. Red-hot lava was emitted from a spot, about 5 m above the crater-floor, on the western

side of the active cinder cone, and flowed down the slope northwestward. Before noon, the lava flow arrived at the margin of the central pit, and early in the afternoon, it ran over the pit-wall to the crater-floor.

On Aug. 16, the head of lava column in the central pit was still rising, accompanied with overflowing of the lava from the pit. Thus, at dawn, the rising lava in the pit attained to a height of about 5 m above the edge of the northern section, about 30 m in length, of the pit-wall. Then, a red-hot lava welled out through clefts in the crust of the lava, and flowed with a speed of several meters every minute. But the lava fronts were advancing in various directions on the crater floor with a speed of about 1 m every 10 minutes. As the lava-flows advanced on the crater-floor, their solidified crusts were broken into plates of various size, from 1 m to 4 m in diameter, sometimes forming chaotic masses of angular lava blocks.

At noon, the same day, the lava, which had filled up the southeastern half of the central pit since Aug. 12, ran over the eastern periphery of the pit at three spots adjoining each other. The red-hot lava, which welled out at those spots through clefts in the already-solidified lava in the pit, advanced on the crater-floor with a speed of several metres every minute, forming three separate flows, about 2 m in width and parallel with each other. About 30 minutes later, they were united to a single lava-flow covering an area of about 100 m^2 of the crater-floor (Fig. 24).

On Aug. 17, red-hot lava poured out from an opening, 30 m in altitude above the crater-floor, on the northwestern slope of the cinder cone. The distribution of the lava-flows on the crater-floor is shown in Figs. 24–26. Thus, the lava-flows covered more than half of the crater-floor on Aug. 18.

In association with these lava-outflows in and around the central pit, depression of the solidified lava-surface occurred here and there, probably due to withdrawal of the underlying liquid lava. Thus, for example, the eastern side of the cinder pile, about 200 m in length and about 10 m in width, was depressed remarkably. The outflowing of lava from the opening on the western slope of the active cinder cone was incessant.

On Aug. 19, at dawn, the liquid lava that continued to outflow from the opening on the western slope of the active cinder cone became stagnant on the southwestern corner of the crater-floor, forming a temporary red-hot lava-pool, 150 m or more in diameter. The lava that ran over the northern rim of the central pit extended to cover the northern

half of the crater-floor.

(7) *Opening of the second explosive vent*:

On Aug. 20, rainy and misty weather closed the view of Mihara crater all day long. On Aug. 21, the crater was seen to be displaying a conspicuous eruption: A red-hot lava-pool was still active in the southwestern corner of the crater-floor; lava flows were spreading over the northern and northeastern lava-fields in the crater; and explosions were taking places in repetition at intervals of about 2 to 3 seconds from the more or less enlarged vent on the cinder cone. In the evening of the same day, a new vent was opened on the eastern slope of the cinder cone, about 30 m in altitude above the crater-floor (Fig. 26). From the new vent, incandescent lava was ejected in pieces up to a height of 200 m or more above the crater, by explosions that occurred in succession together with continuous loud noises like the sound of a drum. Explosions were going on at the 1st and 2nd vents simultaneously (Fig. 36). But the activity of the 2nd new vent differed from that of the first vent in that the former was accompanied by lava-outflowings from the same vent, besides repeated explosions.

Thus, simultaneously with explosions, a red-hot lava, which filled up the second vent, ran over the eastern lowest rim of the vent, and flowed down northeastward on the crater-floor. The lava-pieces that fell on the lava-flow by explosions were carried away from near the rim of the vent by the flow as it advanced. It was principally due to this action that the vent was left breached on its east side, without being closed with a pile of the ejecta, and that the lava-flows from the vent had the appearance of a block lava of the *aa* type.

The activity at the second vent went on with an increasing intensity, while the activity at the first vent, which was represented by about ten explosions every minute at the most active period, gradually declined. Thus, the next morning, the second vent was seen to have developed into an elliptical opening, about 15 m and 7 m in major and minor diameters respectively.

On Aug. 23, the first vent had already stopped its activity, having been transformed into a shallow dish-shaped hollow, about 50 m in diameter, on the cinder cone which was the largest ever observed, having a height of about 80 m above the old crater-floor. The lava-pool at the southwestern corner of the old crater-floor was buried under the ejecta from the first vent, after having survived for about ten days since Aug.

13. But, red-hot lava continued to well out from clefts in the solidified lava-crust. The second vent was active as the day before, both in out-pouring lava and in ejecting lava-pieces by explosions. The lava-flows from the vent were spreading over the 1912–1914 lava in the north-eastern part of the crater-floor, covering the latter 40 m–50 m thick.

In the afternoon of Aug. 24, the lava-pool, about 20 m in diameter, in the second vent was still active. Thus, its surface was very rough, moving several meters up and down in the intervals of successive explosions, and whenever its surface rose above the lowest rim of the vent, the lava ran over the latter to flow away. The explosions at the vent were being displayed in three different ways: (a) just before an explosion, the lava-pool swelled in the form of a dome; then the lava-swell was broken open by the explosion, just like a half-open lotus-flower (Figs. 38 39,); the lava, broken into pieces, spattered in and about the vent, within less than 100 m in radius; and just after the explosion, the surface of the lava-pool was engulfed in a moment, (b) an explosion occurred at a stroke without any forerunning dome-shaped swell of the lava-pool; the lava, broken into pieces by the explosion, was ejected straight upward to a height of about 200 m above the pool; and the ejecta were scattered about the vent, within a range of about 200 m in diameter (Fig. 37), (c) explosions occurred at several spots in the lava-pool, separately but simultaneously; a small mass of lava-pieces was ejected by each explosion, either straight upward or obliquely, to a height of less than 200 m above the pool; and at times only a single lava-piece was projected in the air by such an explosion.

The explosions of the above-mentioned types occurred irregularly at intervals of several seconds, although puffing noises were heard every one or two seconds, together with a sound like the roar of the sea. Bluish gases like a faint smoke issued from the vent at the time of the explosions. Besides, a black ash-cloud was spouted only when the explosion occurred just after the lava-pool was covered temporarily with cinders tumbling down from the surrounding walls, or in case the explosion blew off a part of the walls.

In the evening, the same day, the incandescent lava-pool in the second vent had a temperature ranging between 1040° and 1140°C, and the lava-flow just outside the vent, about 1020°C, as measured with an optical pyrometer.

On Aug. 25, the second vent continued its activity in the same way as the day before, but with a more or less increasing intensity, although

the scene of the activity could not be observed because of the rainy clouds that screened the volcano from view. At times the explosions were felt in the village of Motomura, together with rattlings of doors due to air-concussions. In the afternoon of the same day, cinders and bombs were being ejected from the second vent to a height of a few hundred meters, as viewed from the western top of the old crater-rim through breaks in the rainy clouds. Occasionally, some of the ejecta were seen to fall on the outside of the southeastern old crater-rim, after flying through the air for about 500 m in horizontal distance. The cinder cone, breached on the east side with the second vent, had grown up to a height of about 60 m above the old crater-floor, its top having attained almost to the same level with the crest of the southern old crater-rim, and the southern slope of the cinder cone had abutted midway on the old crater-wall.

The old crater was becoming gradually full of the new lava-flows. Thus, on Aug. 25, at the northwestern corner of the crater, adjacent to the cottage (Kakôjaya or Kakôchaya), the new lava-flows were one or two meters higher in level than the narrow ledge of the 1912–1914 lava that was left uncovered on the adjoining crater-wall; whereas, on the day before, the former was nearly at the same level with the latter. In various places, red-hot lava was being squeezed from under the solidified crust of the new lava-flows.

On Aug. 26, the eruption continued on all day long in the same manner as in the preceeding two days, presenting in the fine weather a magnificent view of repeated explosions and outpourings of lava from the second vent. The explosions were being displayed in three more or less different ways as observed on Aug. 24. But, this day, it was found that an islet of black lava-mass, a few meters in diameter, appeared occasionally in the second vent, and that small explosive jets of gases were liable to occur along the islet.

From Aug. 27 to the end of the month and covering the first two-third of the next month, the second vent displayed explosions intermittently and with rise and fall of intensity.[18] As the activity proceeded, the cinder cone that surrounded the vent became higher with cinders and bombs ejected by the successive explosions. Thus, the top of the cone attained to heights of 730 m, 739 m and 754 m above the sea,

18) Pouring of liquid lava from the 2nd vent into a continued until Sept. 1. and after the cessation of the lava-outpouring, the breached cone grew into a complete form.

respectively on Aug. 31, Sept. 7 and Sept. 23.[19]

(*8*) *Overflowing of lavas from the crater*:

The new lava-flows spread over the old crater-floor, and at the same time their surface level approached to the upper rim of the old crater-wall. In consequence, the northwestern front of the lava-flows reached to a level of about 20 m below the crest of the northwestern crater-wall on Aug. 28, and only about 10 m below the same crest on Aug. 30. On Sept. 13, at 17 h, a lava-front reached to the saddle (Kawajiri) on the northern crater-rim, at the level of about 660 m above the sea and about 200 m northeast of the cottage (Kakôjaya), and at 18h05m, a lava-flow, about 5 m in width, ran over the saddle, extending for a distance of about 7 m on the outer slope of the central cone (Fig. 46). On the next day, at dawn, another lava-front reached to the crest of the northwestern crater-wall, about 670 m in height above the sea and about 100 m southwest of the cottage, and at 16h, it began to flow down in the form of a lava-tongue, 20 m in width, on the outer slope of the cone.

On the morning of Sept. 19, northern front of the lava in the crater overlapped the crater rim about 400 m NNE. of the cottage (Kakôjaya), and several minutes after noon, a lava-tongue, 8 m in width, began to flow out on the northern slope of the central cone. The lava overflowings from the crater occurred successively until Sept. 24, even after the cessation of the explosive activity at the cinder cone on Sept. 23, at night. The lavas did not flow down simultaneously over a wide range of the crater rim, but ran down successively as narrow lava streams, about 5–10 m in width, and 2–3 m in thickness, on the northern and northwestern slopes of the central cone. The central portion of each lava-flow ran down the slope almost as a stationary current[20], piling solidified lava-blocks of *aa* type on both sides (Fig. 47). So the movement of the central portions of these lava-flows appeared like that of escalators or of belt conveyers carrying piles of cokes. These flows that ran down the outer slope of the central cone were always terminated with comparatively thick piles of *aa* lava-blocks (Fig.

19) R. TAKAHASHI, "The activities in 1950 and the accompanying topographic changes of Volcano Mihara-yama," *Geogr. Mag.* **60** (1951) No. 3, 115 (in Japanese).

20) Viscosity of one of these lavas was measured as $(1.3\pm1.1)\times10^5$ poise, where the maximum temperature of the lava surface was 1040°C. I. MURAI, N. NASU, A. SUGIMURA, & T. SAMEZIMA, *Monthly Meeting of the Earthquake Research Institute*, (Oct. 17, 1950), *Jour. Geol. Soc. Japan*, **58** (1952), 73.

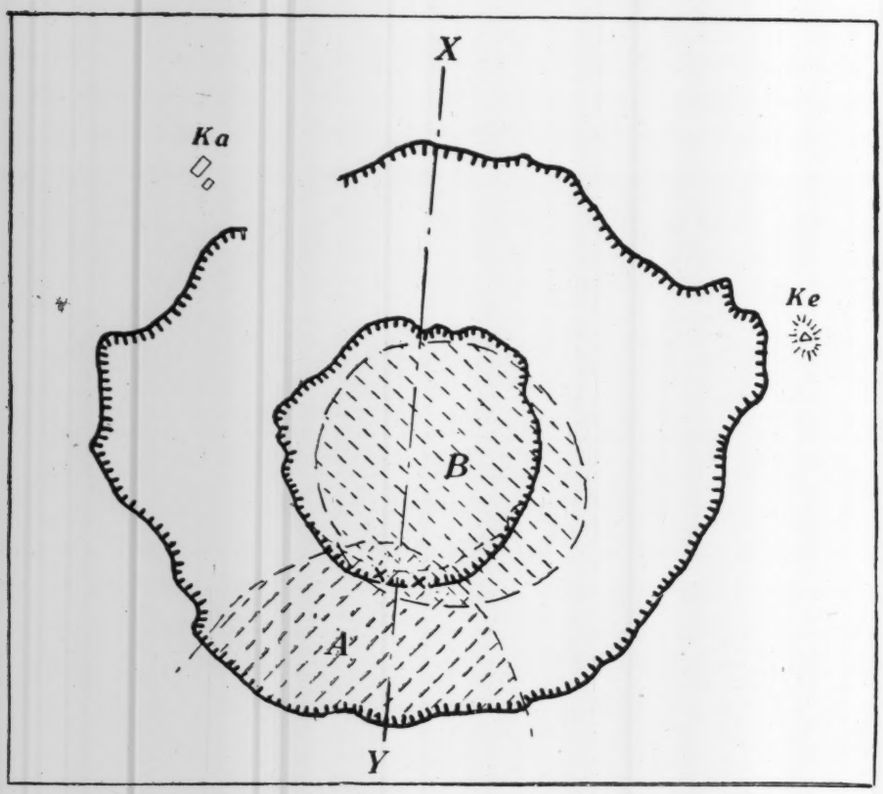

Fig. 21. July 23.

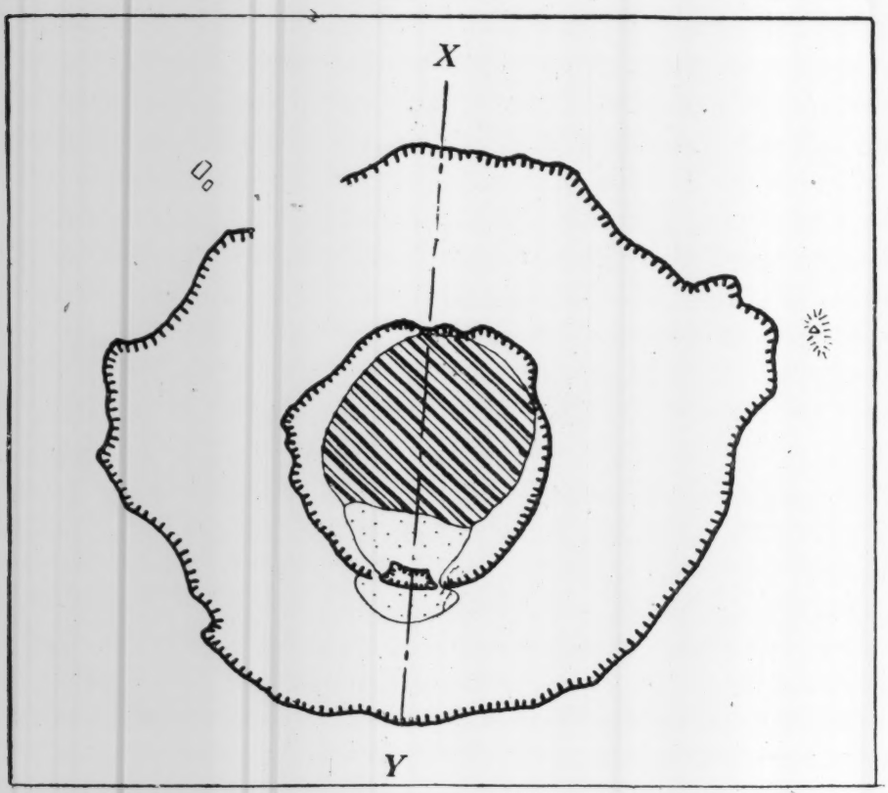

Fig. 22. July 30.

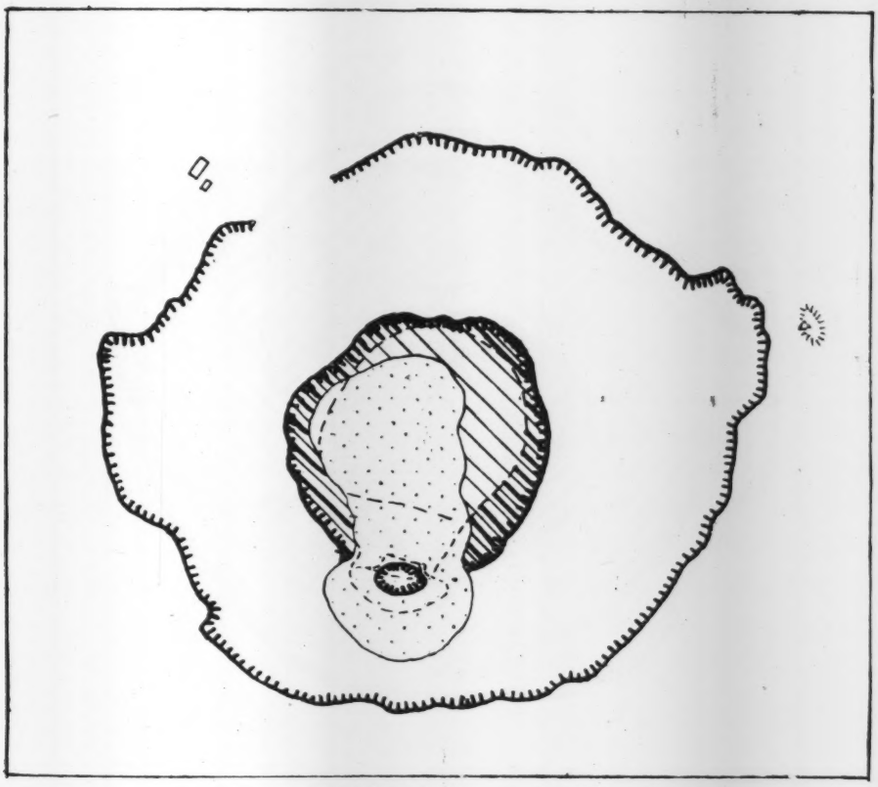

Fig. 23. Aug. 13.

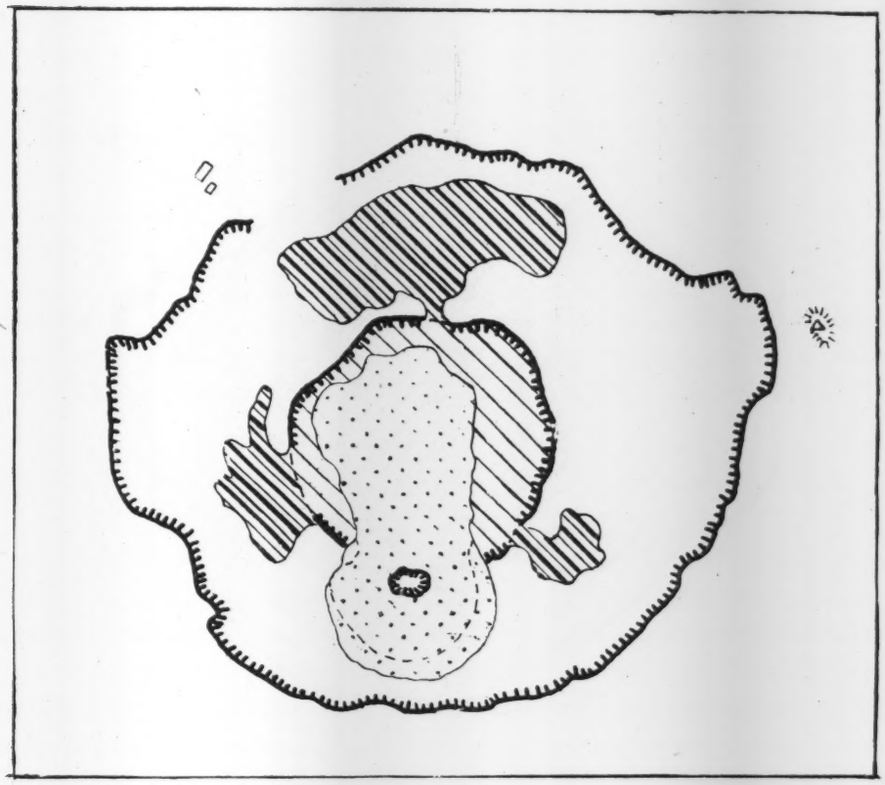

Fig. 24. Aug. 16.

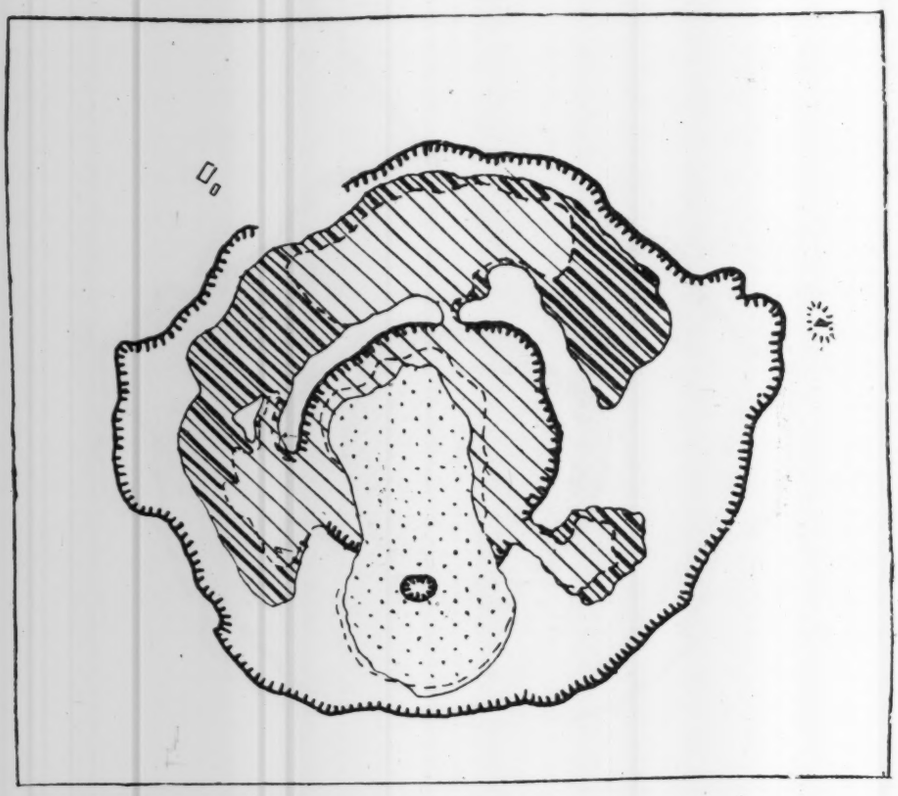

Fig. 25. Aug. 19.

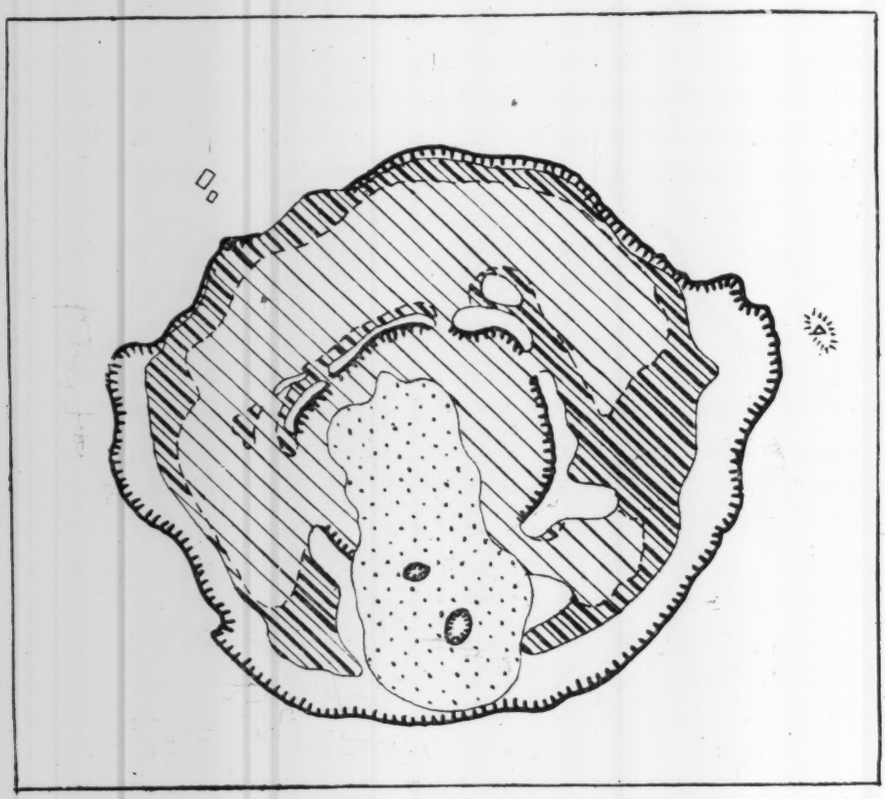

Fig. 26. Aug. 24.

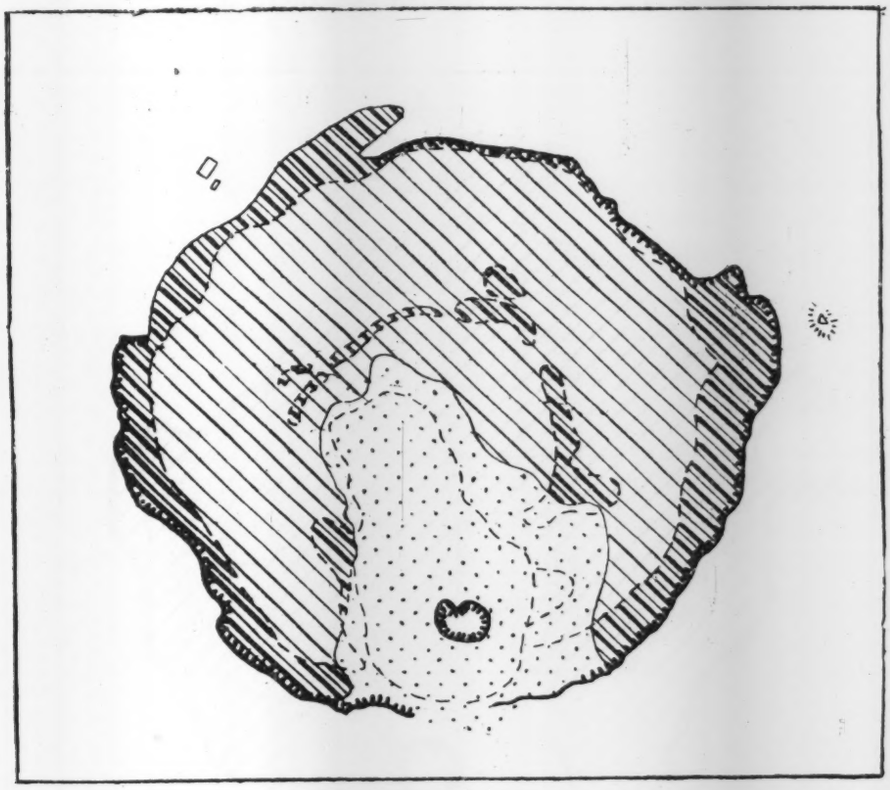

Fig. 27. Sept. 7.

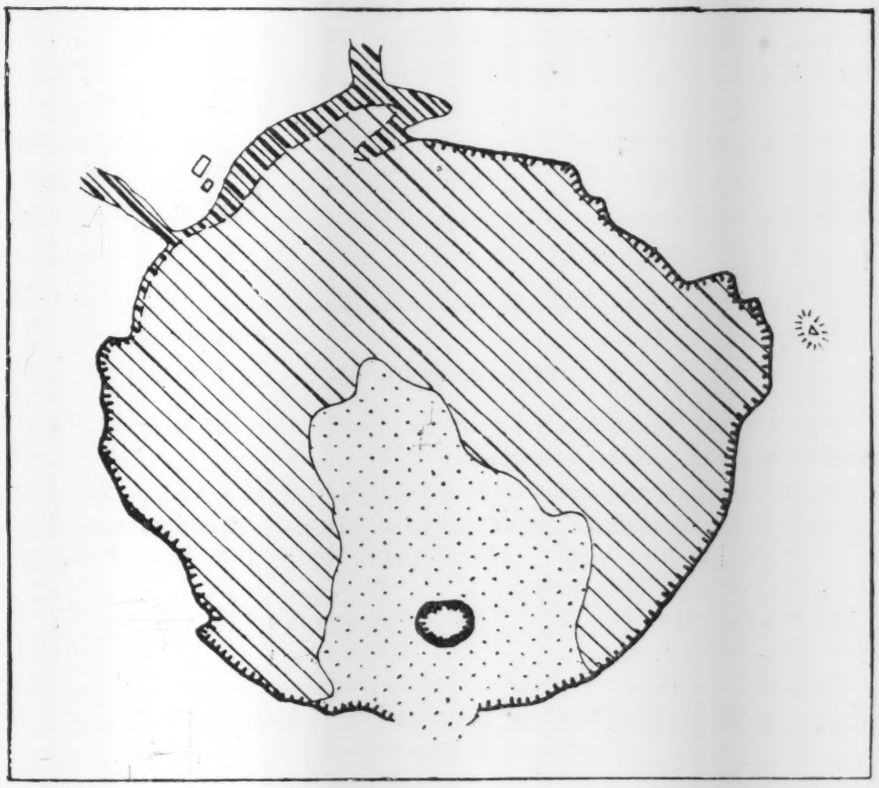

Fig. 28. Sept. 17.

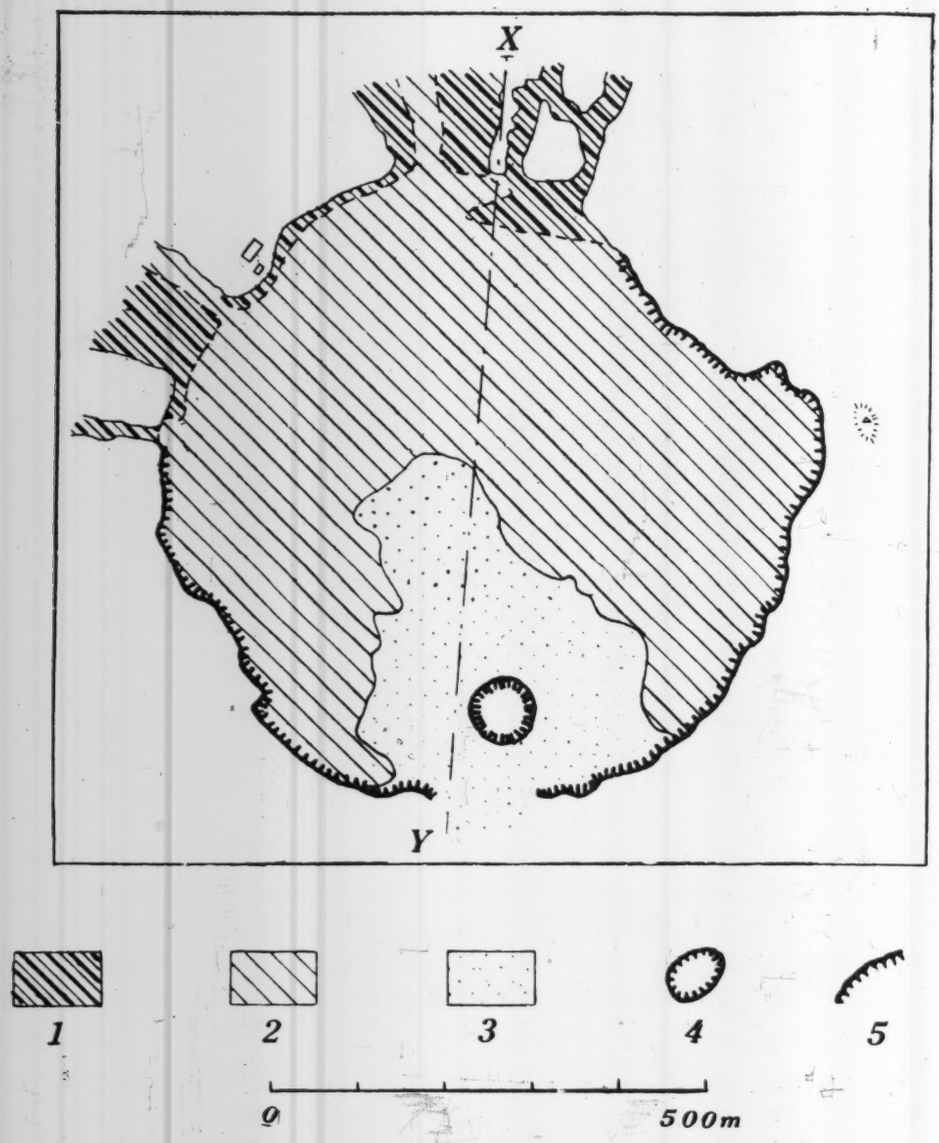

Fig. 29. Sept. 24.

Figs. 21–29. Showing changes in distribution of new ejecta and lavas during the present eruptions.

1. Increase of the area covered with new ejecta and lavas within a period of time between two successive dates of observation.

2. Area covered with lavas already before the first of the two successive dates of observation.

3. Cinder pile
4. Explosive vent
5. Cliff

Ke Kengaminé
Ka Kakôjaya

A, B in Fig. 21 show distribution of ejecta of July 21 and 23 respectively.

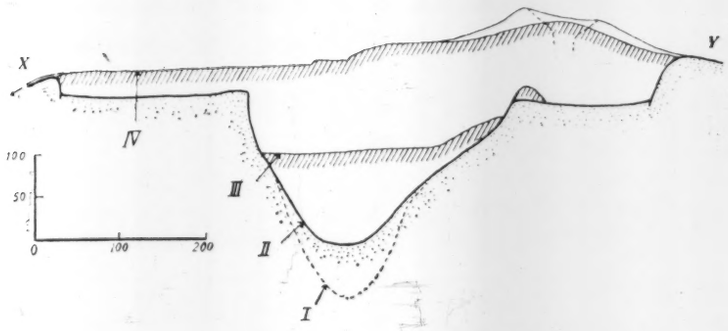

Fig. 30. NW—SE profile of Mihara crater, showing changes in depth by the present eruptions.
I. 1936 III. July 30, 1950
II. May 1950 IV. Sept. 23, 1950.

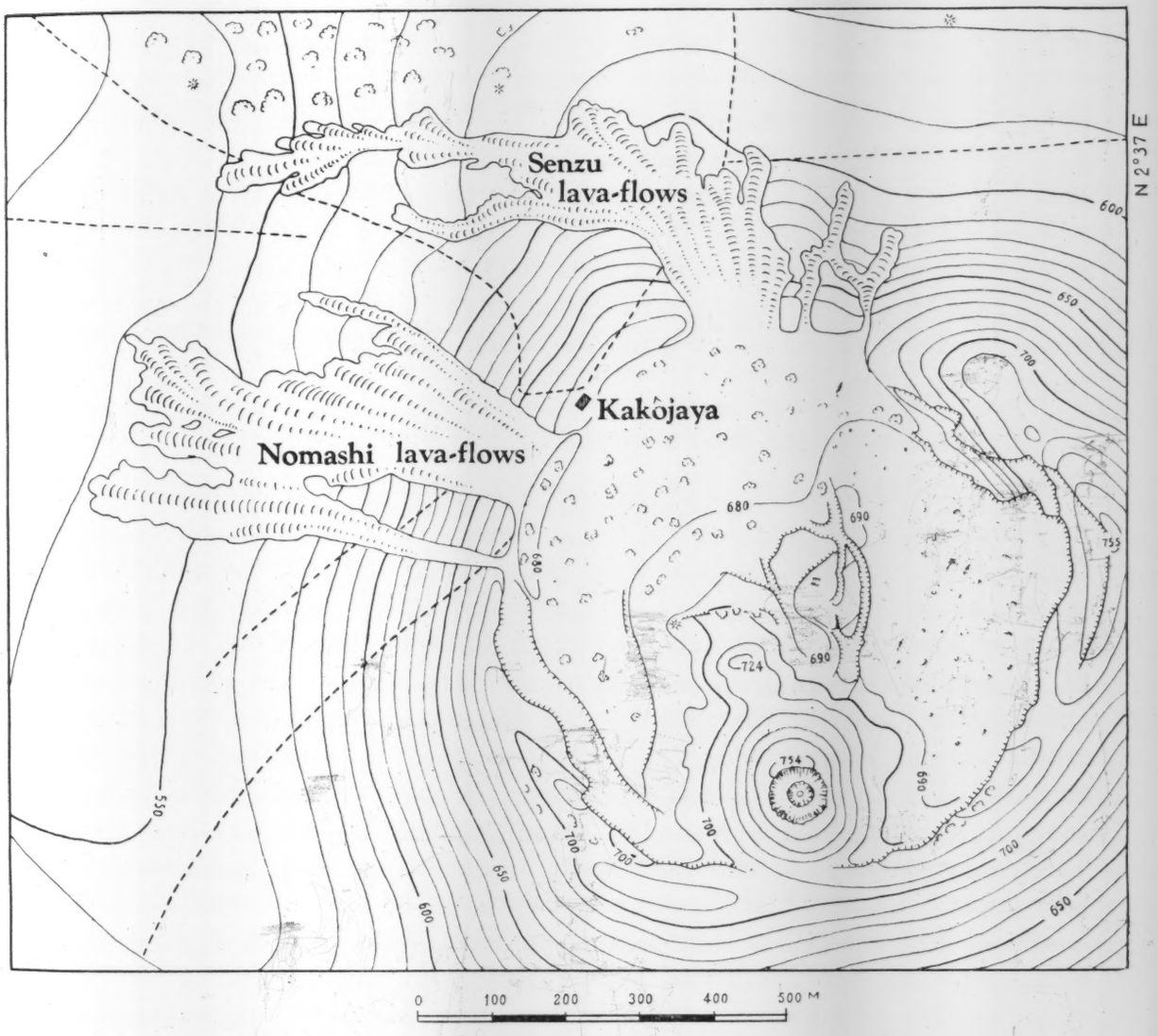

Fig. 31. Topographic map of Mihara crater (Sept. 24, 1950) after R. Takahasi and D. Shimozuru.

48). Velocities of advancing lava-fronts on the slope were measured as shown in the following table (Table II). Figs. 52–60 show the sequence

Table II. Velocities of the fronts of lavas flowing down the slope of central cone on Sept. 17, 1950.

	Inclination of slope	Time for passing through 10 m min.	sec.	Velocity of moving front of lava (cm/sec)
1	29.5°	9	31	1.75 (1050°C)
2	28.0	13	15	1.26
3	26.5	15	15	1.09
4	26.0	18	34	0.896

of the lava outflows from the crater, together with the rise of cinder cone, cinder pile, and lava field in the crater. As shown in Fig. 59, a lava-flow, which ran over the crater rim at about 250 m south of Kakôjaya on Sept. 23 at night, flowed down the northwestern slope of the central cone, forming an extensive new lava field on the next day. Thus, the lavas that flowed out northward (Senzu lava) and those northwestward (Nomashi lava) spread to occuppy the areas of 102,300 m^2 and 123,300 m^2 respectively (Fig. 31).

(9) *Decline of the 1950 eruption*:

On Sept. 18, explosions at the vent became weak: Dark ash columns rose instead of the ejections of incandescent lava pieces; sounds like feeble surfs on the seashore were heard as in the initial stage of the present eruptions. Continuous and stationary activity at the vent became more or less irregular, sometimes violent and sometimes weak. On Sept. 21, depressions of the inner portion of the lava field in the crater along the circular line on the old pit-wall and along the inside wall of the crater became remarkable, though it was said that such depression had already begun in the middle of September. Successive explosive actions at the vent began to be interrupted by timely reposes on these days. On Sept. 22, explosive action at the vent became quite weak, and the times of repose became longer, and vapour emission took the place of explosion. At last, the activity at the vent ceased on Sept. 23, after its 70 days continuation. As was mentioned above, outflowings of lava continued in more or less remarkable extent on the next day, and advancement of the fronts of these outflowing lavas lasted until Sept. 25. Thus, the continuous and progressive eruptions of the crater stopped, and Mt.

Mihara entered into a dormant state until the outburst on February 4, 1951.

III. Temperatures of the new lavas.

Temperatures of the new lavas were measured many times with optical pyrometers at various stages of the 1950 eruption. Besides, after

Table III. Temperatures of the lavas, Mihara crater, Oshima volcano, 1950.

Date	Object	Locality	Temperature (°C)	Instrument
July 30	Incandescent lava (a lava fountain)	Bottom of the pit	1210 1170	Optical pyrometer*
	Flying lava pieces	The 1st explosive vent	1100	Optical pyrometer*
Aug. 24	Incandescent lava	The 2nd vent	1040 1110	Optical pyrometer+
			1050	Optical pyrometer+
Sept. 3	Red-hot lava in crevice of a secondary flow at the lava-front	Lava front approaching to the crater rim, about 200 m east of Kakôjaya.	1080 1090	Optical pyrometer+
Sept. 16	Red-hot lava in the clefts of solidified crust of the lava-front.	Crater rim, about 100 m NE of Kakôjaya.	1020 950	Optical pyrometer+
	Red-hot lava in the clefts of solidified crust of the lava-front.	Crater rim, about 100 m NE of Kakôjaya.	824 820	Thermo-couple Optical pyrometer+
	Secondary red-hot lava outflowing from the clefts on the lava front.	In the crater, 10 m SE of Kakôjaya.	946 836	Calorimeter Calorimeter
Sept. 17	Front of a flowing lava	The western slope of the central cone about 100 m W of Kakôjaya.	1030 970	Optical pyrometer+
	Red-hot lava block tumbling down from the front of flowing lava	Ditto., about 150 m W of Kakôjaya.	806 735	Calorimeter
	Central portion of rapidly flowing lava from crater rim	Crater rim, about 50 m S of Kakôjaya.	1050 1100	Optical pyrometer+

* Optical pyrometer, made by the Yokogawa Electric Works, was used. The instrument was adjusted especially at the Machine Research Institute of the Ministry of International Trade and Industry.

+ Optical pyrometer, made by the Hokushin Electric Works, was used. The Yokogawa-made and Hokushin-made pyrometers were tested and found correct by comparing with each other at the same condition. Red absorption filters were always used in both cases.

the outpouring of the lavas from the central pit, temperatures of some of the accessible lava-flows were measured with a thermoelectric thermometer. The results of these measurements are shown in the foregoing table (Table III), together with temperatures of red-hot lava pieces, obtained by calculating their specific heats after a method we shall describe in a later chapter.

Measurement of lava temperature with a thermo-junction:

Temperature of a red-hot lava was measured by inserting the almel-chromel thermocouple[21] with an iron-tube cover, 30 cm–50 cm deep into the lava through the clefts of its solidified crust. As no ice was available in the field, water in a vacuum flask was used for the cold junction of the electric thermometer. During the experiments, the temperatures of the water in the flask were observed, and they were taken into consideration in correcting the measurements. Thus, in an experiment, the temperature of the water showed a rise of only 0.6°C in 30 minutes,

Table IV. Rising of the temperature, with time, at the hot junction of the thermocouple in one of the temperature measurements of the 1950 lavas of Oshima volcano.

Time (min.)	Temperature (°C)	Time (min.)	Temperature (°C)
1	306	17	818
2	473	18	818
3	588	19	818
4	656	20	819
5	695	21	822
6	720	22	823
7	737	23	828
8	748	24	832
9	761	25	836
10	775	26	837
11	783	27	839
12	790	28	839
13	798	29	841
14	805	30	843
15	808	31	842
16	812	32	840

21) Corrected by comparing with the Standard Siemens's Pt-PtRh thermocouple at the Tokyo Institute of Technology. For this test, the writers are indebted to Prof. T. Yamanouchi and to Mr. H. Suzuki of the Institute.

because the cold junction was kept off by using a 10 m-long compensated wire, in order to minimize as far as possible the effect of heat radiation from the lava. Retardation of the temperature at the thermo-junction in attaining to that of the lava, owing mainly to the heat capacities of the thermocouple itself and of the iron tube, is shown in Fig. 63 and Table IV.

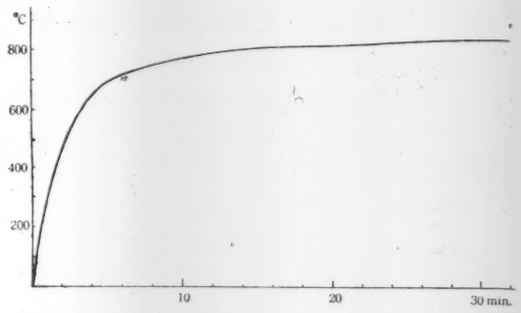

Fig. 63. Rising of temperature with time, at the hot junction of the thermocouple in one of the temperature measurements of the 1950 lavas of Oshima volcano.

IV. Specific heat of the new lava pieces.

In order to know something about the relations between the rate of cooling and the crystallinity of the living lavas, we picked up pieces of the flowing red-hot lavas and quenched them quickly in water (Figs. 49, 50). For the quenching of the lava pieces, a simple portable water calorimeter (Fig. 64) was prepared, so that specific heat of the lavas could be measured at the same time. Inner walls of the calorimeter are made of a thin steel plate (S) whose heat capacity is small. They are covered with saw-dust (C) filled in a wooden box (B). A definite

Table V. Rising of temperature with time of the water in the calorimeter, into which a hot lava-piece was put.

Time (sec.)	Temperature (°C)	Time (sec.)	Temperature (°C)
0	26.4	60	31.3
10	26.4	70	31.3
20	26.4	80	31.4
30	26.4	90	31.4
40	31.2	100	31.4
50	31.2		

quantity, 1200 cc, of water is put in the calorimeter, and while being mixed by stirring with a handle (H), its temperature is read with a thermometer (T) graduated in every 1/10 degree.

A piece of red-hot lava, picked up with a hammer from a flowing lava, was put quickly into the water in the calorimeter. Then the temperature of the water heated by the piece was read with the thermometer every 10 seconds. Two examples of the results

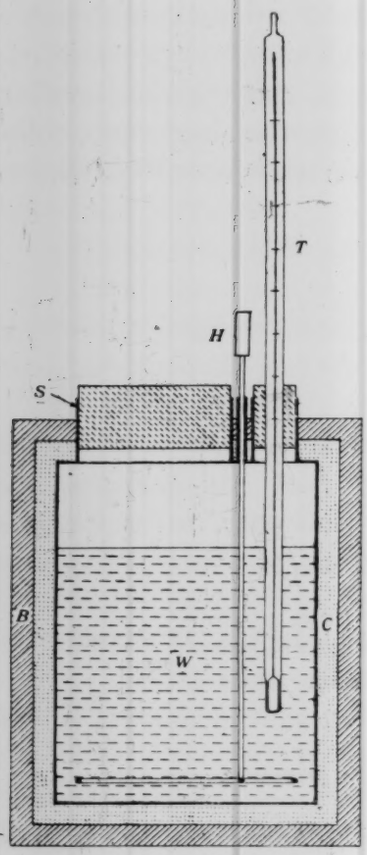

Fig. 64.

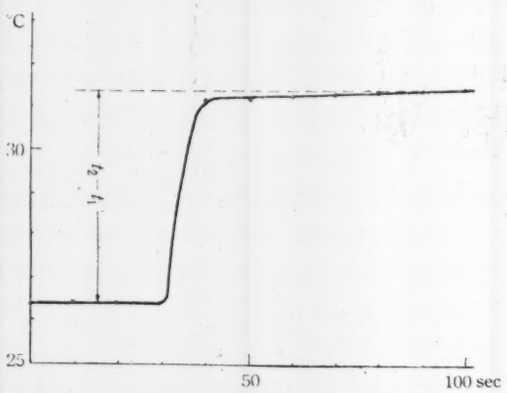

Fig. 65.

Table VI. Rising of the temperature with time of the water in the calorimeter, into which a hot lava piece was put in the field.

Time (sec.)	Temperature (°C)	Time (sec.)	Temperature (°C)
0	31.45	90	48.92
10	31.45	100	49.10
20	31.46	110	49.12
30	31.46	120	49.20
40	31.46	130	49.21
50	42.00	140	49.21
60	47.00	150	49.22
70	47.60	160	49.22
80	48.54		

thus obtained are shown in the above tables (Table V, VI, and Figs. 65, 66). The lava-piece, which was used in the field experiment, was

weighed in the laboratory (Wr). Then, heated at 100°C in the boiling water, it was put into the same calorimeter. The temperatures of the water in the calorimeter, before and after throwing-in of the lava piece, were measured as t_1 and t_2 respectively (Table VII and Fig. 67). The specific heat of the lava piece was calculated as shown in the following table (Table VII).[22] Repeated experiments have shown more or less different values of the specific heat (Table VIII). But $Cr=0.213$ may be taken as the mean value.

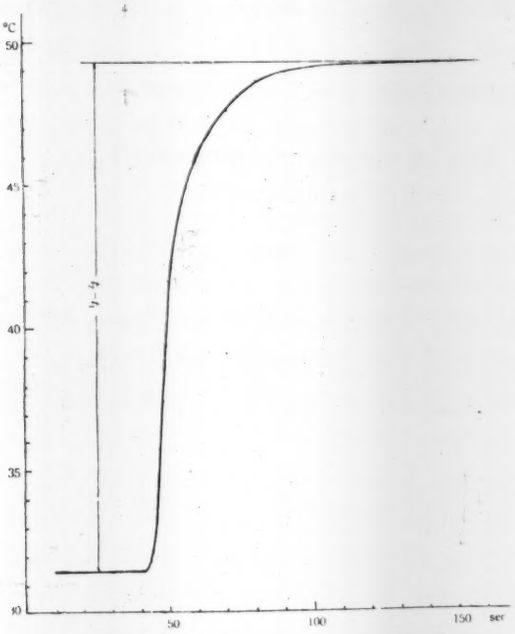

Fig. 66.

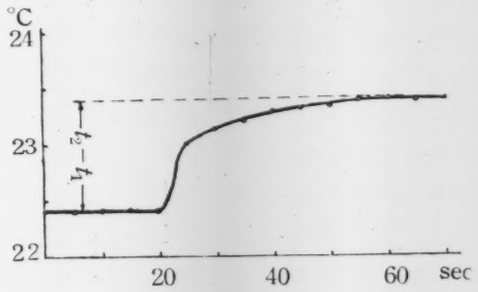

Fig. 67.

Table VII. Rising of the temperature with time of the water in the calorimeter, into which a lava piece heated at 100°C was thrown.

Time (sec.)	Temperature (°C)	Time (sec.)	Temperature (°C)
0	22.41	40	23.31
5	22.41	45	23.32
10	22.41	50	23.33
15	22.41	55	23.40
20	22.41	60	23.41
25	23.00	75	23.38
30	23.16	70	23.40
35	23.22		

22) $Cr=\dfrac{(t_2-t_1)CwWw}{(t_3-t_1)Wr}$ where
Cw : Specific heat of the water.
Ww : 1200 gr.
t_3 : Temperature of the lava-piece (100°C in the laboratory).
Wr : 68.9 gr for an example.

Table VIII. Specific heat of the 1950 lava-pieces, Oshima volcano.

No.	t_1 (°C)	t_2 (°C)	t_2-t_1 (°C)	Cr
1	21.92	22.92	1.00	0.2259
2	23.19	24.00	0.81	0.1856
3	22.41	23.40	0.99	0.2250
4	23.46	24.40	0.94	0.2165

Specimen numbers are the same in Tables X, XI.

Table IX. Temperatures of the lava-pieces, measured by means of a calorimeter, from Oshima, 1950.

No.	t_1 (°C)	t_2 (°C)	t_2-t_1 (°C)	Wr (gr)	t_3 (°C)
1	26.4	31.4	5.0	29.8	946
2	41.5	49.2	7.7	61.2	735
3	38.8	40.9	2.1	38.3	340
4	40.4	41.2	0.8	39.4	152
5	41.2	43.7	2.5	58.1	279
6	41.2	44.1	2.9	25.3	669
7	34.2	44.4	10.2	73.0	806
8	36.5	47.0	10.5	72.5	836
9	42.4	44.4	2.0	41.2	309
10	42.0	42.2	0.1	66.6	55

By assuming that the value of the specific heat of the lava pieces, $Cr=0.213$, is constant even at high temperatures, Table IX shows the results thus calculated.[23] The temperatures of the lavas from which the lava pieces were picked up must have been more or less higher than the temperatures (t_3) shown in the table.

V. Specific gravities of the new lavas.

In order to estimate the quantity of the 1950 lavas and for some other purposes, specific gravities of various portions of the lavas were determined by means of a pycnometer, as shown in the following table (Table X). As a measuring medium, water mixed with a small quantity

23) $t_3=\frac{Cw\cdot Ww\cdot(t_2-t_1)}{Cr\cdot Wr}-t_2=\frac{1200(t_2-t_1)}{0.213Wr}-t_2$, where t_1 and t_2 are the temperatures of the water in the calorimeter before and after the quenching of each lava-piece, measured in the field.

Table X. Specific gravities of the 1950 lavas.

No.	*W* (*gr*)	*R* (*gr*)	*R'* (*gr*)	*d*
1	2.381	69.43	67.84	3.02
2	1.078	68.57	67.84	3.13
3	1.524	68.87	67.84	3.10

Modes of occurrence of the specimens 1, 3 are shown in the next table.
No. 2: One of the bombs that fell on the crater-floor near the northern side of the pit on July 24.
W: Weights of the specimens.
R : Sum of weights of specimen, pycnometer, and water in pycnometer.
R': Weights of pycnometer filled with water.
d : Specific gravities.

Table XI. Apparent specific gravities (*Ga*), bulk specific gravities (*Gb*), apparent porosities (*P*) of the 1950 lavas.

No.	*W* (*gr*)	*Q* (*gr*)	*S* (*gr*)	*V* (*gr*)	*Ga*	*Gb*	*P* (%)
1	35.07	21.25	41.87	20.41	2.54	1.72	33.3
3	28.56	18.82	29.45	10.44	2.93	2.74	8.5
4	3.61	1.93	5.05	3.27	2.16	1.10	38.7
5	37.99	22.40	46.72	22.73	2.44	1.23	38.4
6	25.06	15.63	35.41	18.92	2.66	1.33	54.7
7	58.02	37.86	58.90	20.60	2.88	2.82	4.3
8	20.63	13.62	21.77	8.15	2.94	2.53	14.0

1: One of the lava pieces that fell on the crater-floor near the southern periphery of the pit on July 22.
3: A specimen of the lava that ran over the crater-rim southwest of Kakôjaya on Sept. 18.
4: One of the bombs that fell on the southern slope of the central cone on Sept. 23.
5: Specimen collected from the lava-crust at the front of the Nomashi lava flow.
6: Cinder collected from the cinder cone (2nd vent).
7: Specimen collected at the front of the Senzu lava flow.
8: Specimen collected from the lava field in the crater.

of ethylether was used. Powders of the rock piece were put in a pycnometer filled with the medium, and they were heated on a water bath for about 48 hours to avoid air. The experiments were done always at a constant temperature 70°C.[24] The values of true specific gravity thus obtained are almost constant in each specimen in spite of its different modes of occurrence.

24) For these measurements, we owe much to Dr. Y. Shiraki of the Tokyo Institute of Technology.

As the rocks were various in their porosities, the apparent specific gravities (Ga), bulk specific gravities (Gb), and apparent porosities (P) were determined in several specimens in the laboratory,[25] as shown in the foregoing table (Table XI).

Takahasi and Shimozuru calculated the total volume of the lavas and ejecta produced during the 1950 eruption as $2{,}105\times10^{4}\mathrm{m}^3$.[26] So their total quantity may be estimated to be about 50,000,000 tons.[27]

(To be continued)

---

4. 伊豆大島三原山昭和25年及び26年の噴火

その1　昭和25年の噴火

地震研究所　津屋弘達・森本良平・小坂丈予

伊豆大島三原山は，昭和25年7月16日中央火孔南縁より噴火を開始，漸次その活動規模を増大しつゝ連続的噴火を行い，9月23日噴火を休止，翌26年2月4日噴火を再開，4月1日まで，更に大規模な熔岩流出を伴った活動を継続した．ついで，噴火は，間歇的かつ爆発的になり，6月28日活動を停止した．本篇では，昭和25年の噴火経過の観察を詳細に述べ，地形変化，噴出熔岩の温度，比熱の測定，噴出物の量(大約5千万噸)などについて記載した．

---

25) $Ga=\dfrac{W}{W-Q}$, $Gb=\dfrac{W}{V}$, $P=\dfrac{S-W}{W}\times100$, where
W: Weight of a specimen,
Q: Weight of a specimen in water,
S: Weight of specimen saturated with water, and
V: Volume of water excluded by the water-saturated specimen.

26) They calculated the volumes of
(a) lavas filling up the crater as $1{,}584\times10^{4}\mathrm{m}^3$
(b) cinder cone and cinder pile as 422 〃
(c) lavas flowing out the crater as 99 〃
(R. TAKAHASI, "The activities in 1950 and accompanying topographic changes," *Jour. Geography* **60** (1951) 117 (in Japanese).)

27) If we assume the densities as 2.8, 1.4, and 2.6 for a, b, and c respectively then the quantity may be given as 5,000,000 tons.

Fig. 3. Northeastward view of the central pit in the Mihara crater. The highest point in the background is Kengaminé, 775 m above sea level, highest peak of the island. Fumaroles in the right indicate a part of the arcuate fissure from which the present eruptions began on July 16, 1950. Photo. S. Watanabe, 1933.

Fig. 7. A minor explosive puffing of white vapours from the opening B, July 22.

Fig. 8. The pit-bottom showing welling out of incandescent lava. July 22.

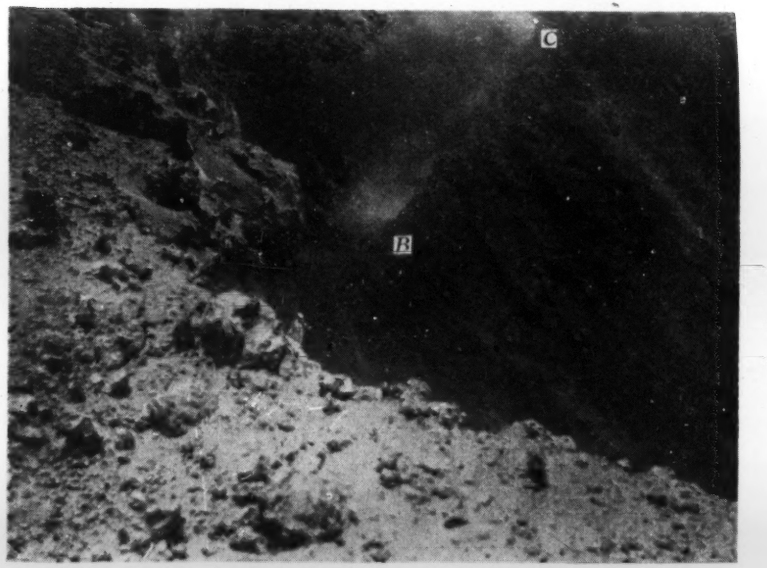

Fig. 9. Ejection of incandescent lava fragments from an explosive vent (corresponding to B in Fig. 7.). July 24.

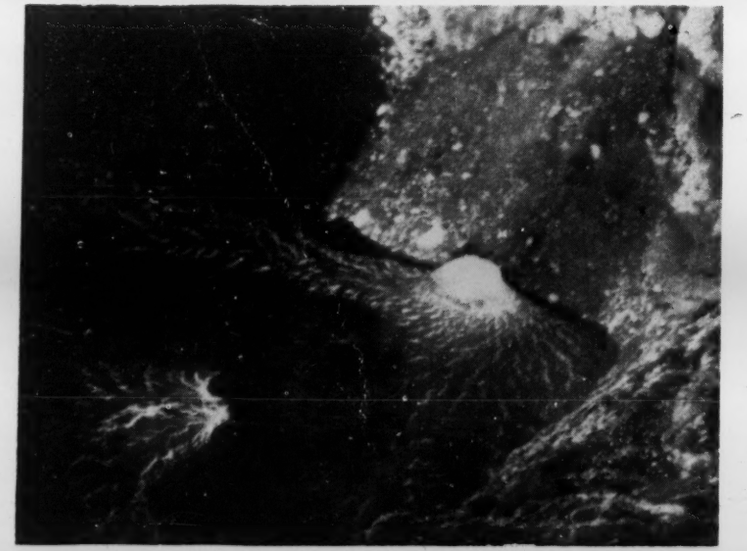

Fig. 10. Lava fountains at the southwestern corner of the pit-bottom July. 24. Photo. S. Watanabe.

Fig. 11. New cinder piles on the talus in front of the explosive vent, and on the crater-floor (outside of the pit) behind the vent. Photo. S. Watanabe, July 25.

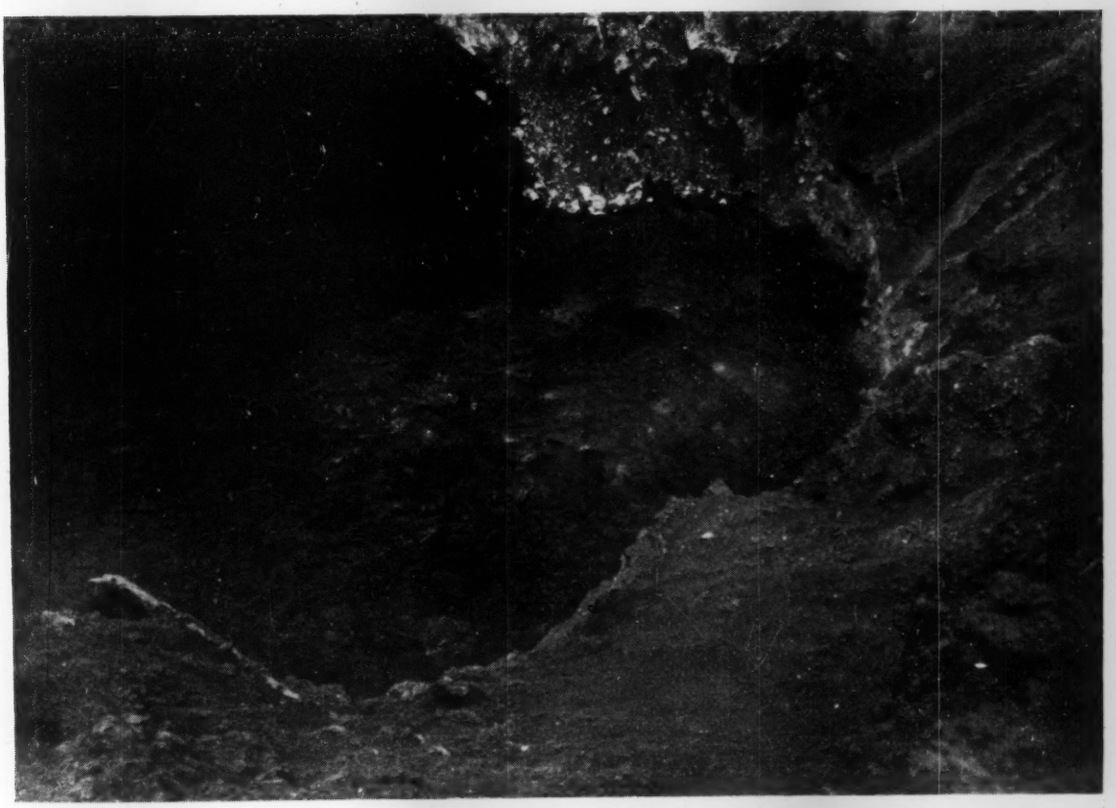

Fig. 12. New lava-pool in the pit, showing red-hot lava visible through many clefts on its solidified surface. Photo. S. Watanabe. July 25.

Fig. 13. Showing ejecta scattered on the crater floor. A picture taken from the crater-floor, south of active vent, July 28.

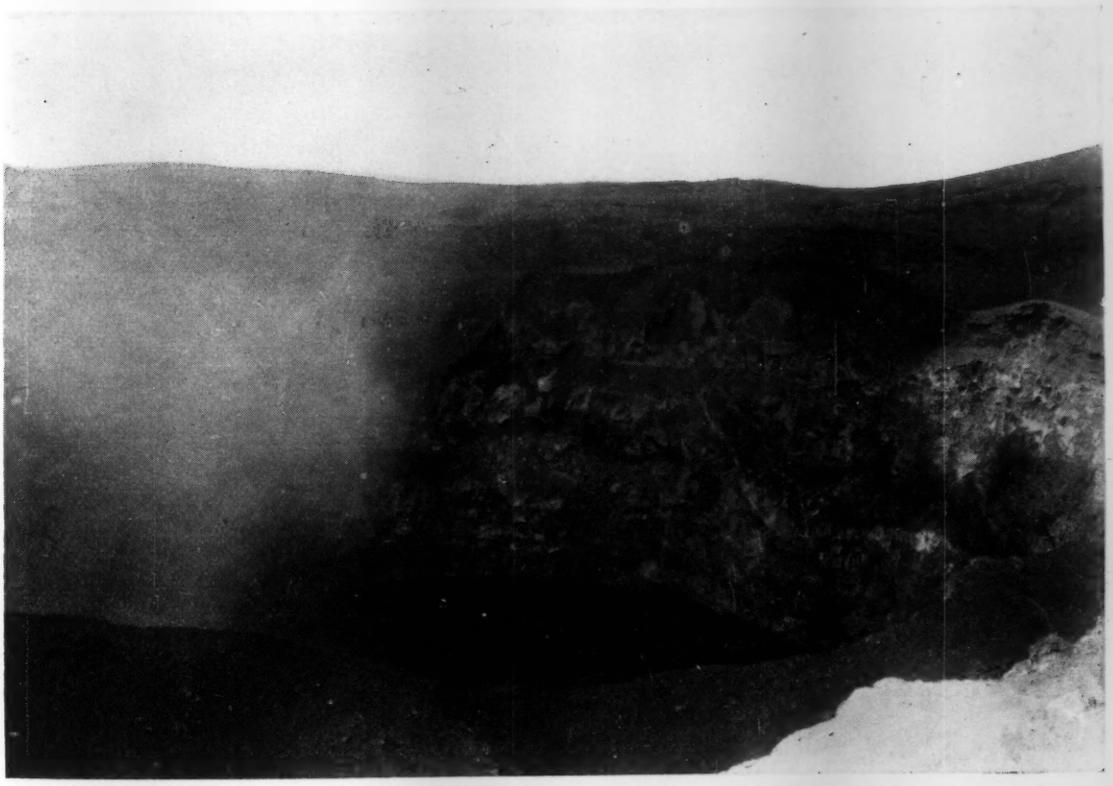

Fig. 14. Head of new lava in the pit. July 26. Photo. S. Watanabe.

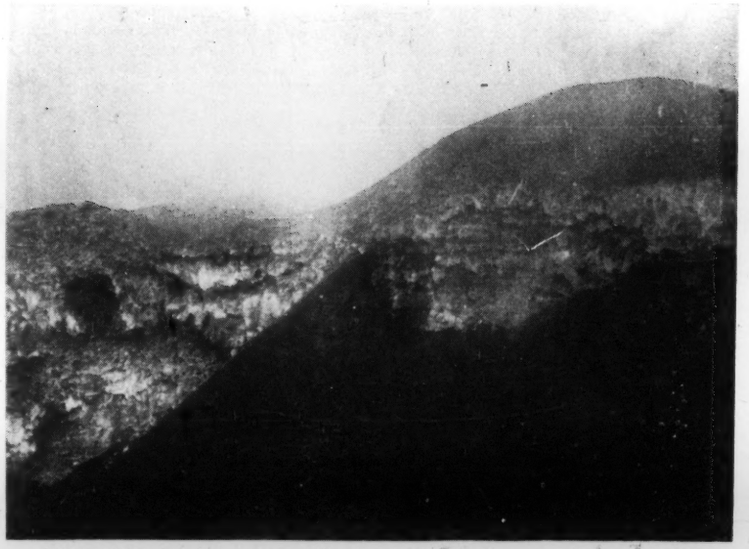

Fig. 15. Development of cinder pile on the talus in front of active vent and on the crater-floor behind the vent. July 30.

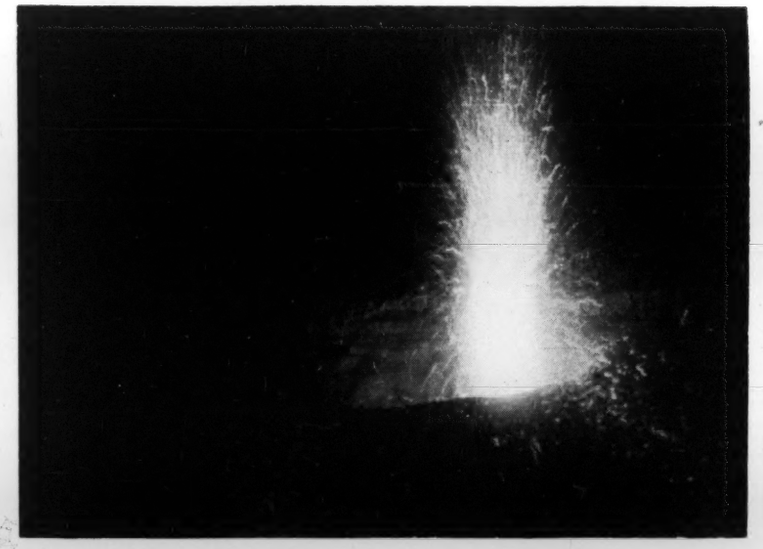

Fig. 17. Night view of the eruption, as seen from the same spot as Fig. 15. July 30.

Fig. 16. Incandescent lava welling out from the pit-bottom. July 30.

Fig. 18. Night view of the same lava flow as that shown in Fig. 16. July 30.

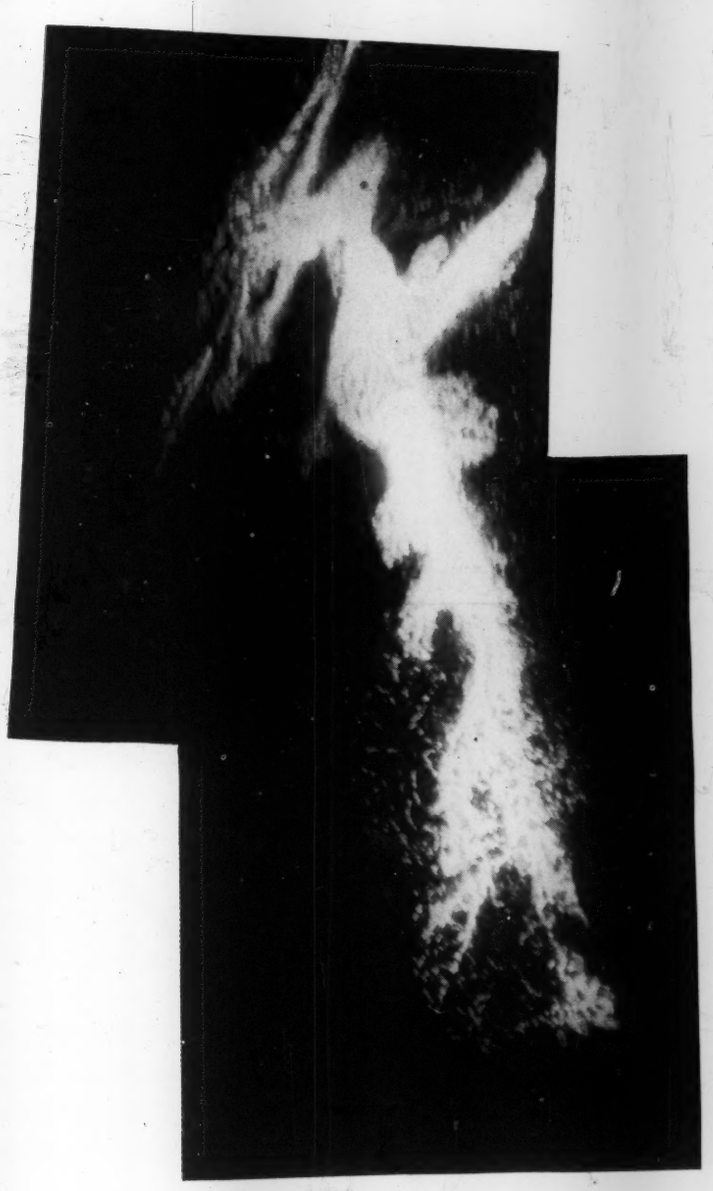

Fig. 19. Night view showing a climax of incandescent lava-fountainings through the solidified crust of lava in the pit-bottom. July 30.

Fig. 32. Cinder pile growing up day by day around the explosive vent. Two bowl-shaped openings are seen in the vent. Aug. 1.

Fig. 33. Incandescent lava-flows outpouring from southwest and northeast sides of the cinder cone. Photo. S. Watanabe, Aug. 13.

Fig. 34. Outpouring of lava at the northern foot of the new cinder cone. Head of lava column in the pit rose nearly to the level of the upper rim (lower right in the picture) of the central pit. Photo. S. Watanabe, Aug. 13.

Fig. 35. Southwestern part of the crater-floor, covered with new lava-flows and cinder cone. Aug. 15.

Fig. 36. Night scene of eruptions displayed simultaneously at two vents (upper right: the 1st vent; lower left: the 2nd vent). The 1st vent was pouring out incandescent lava, besides ejecting lava bombs and cinders. Photo. S. Watanabe. Aug. 21.

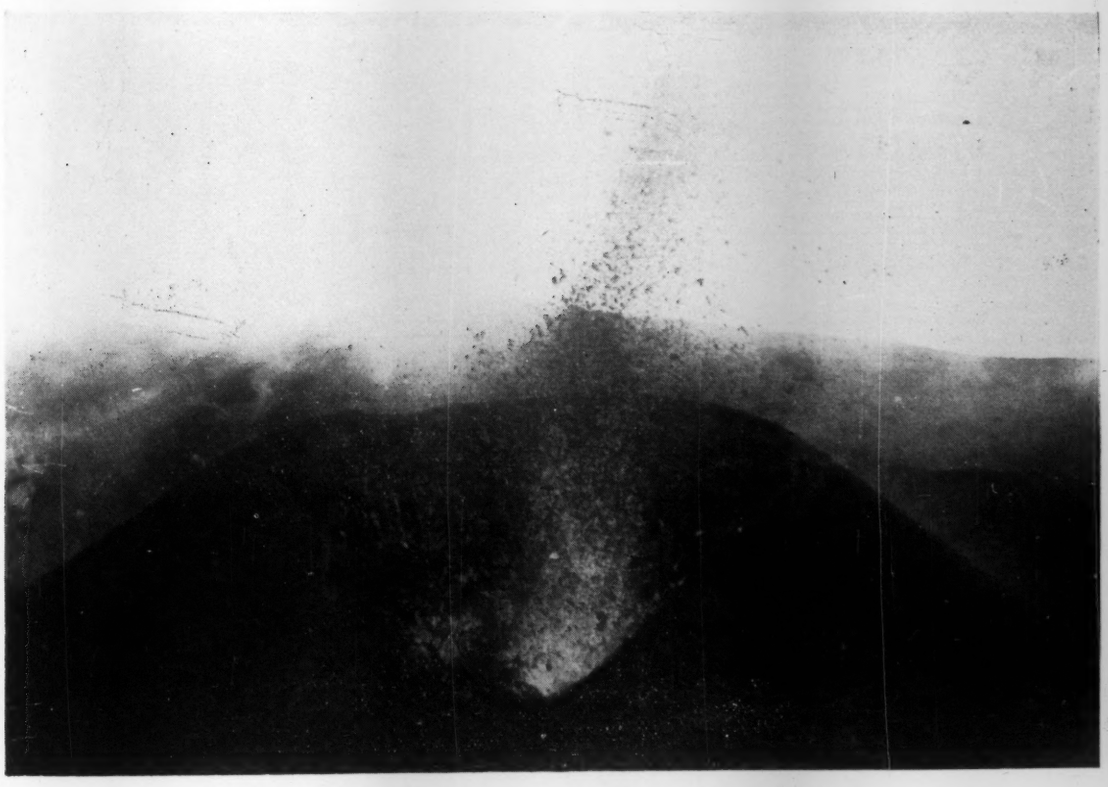

Fig. 37. Explosion at the 2nd vent, Aug. 24.

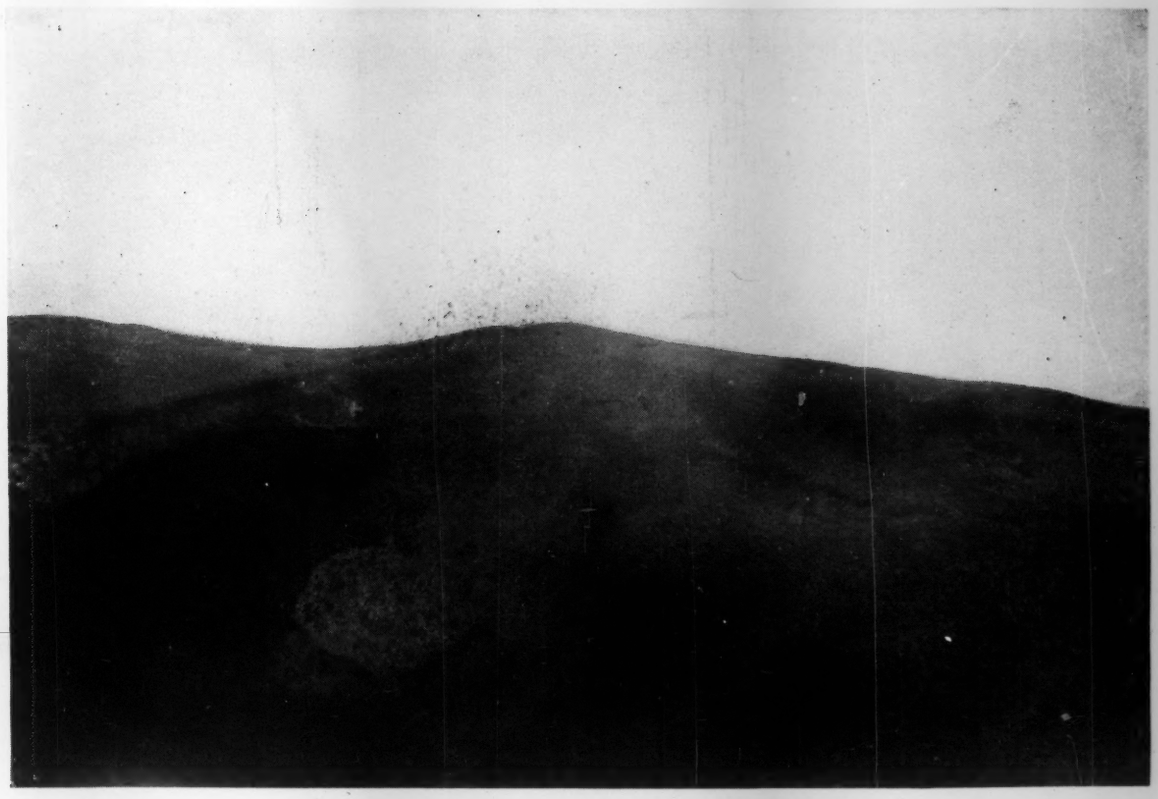

Fig. 38. Explosion at the 2nd vent. Aug. 24.

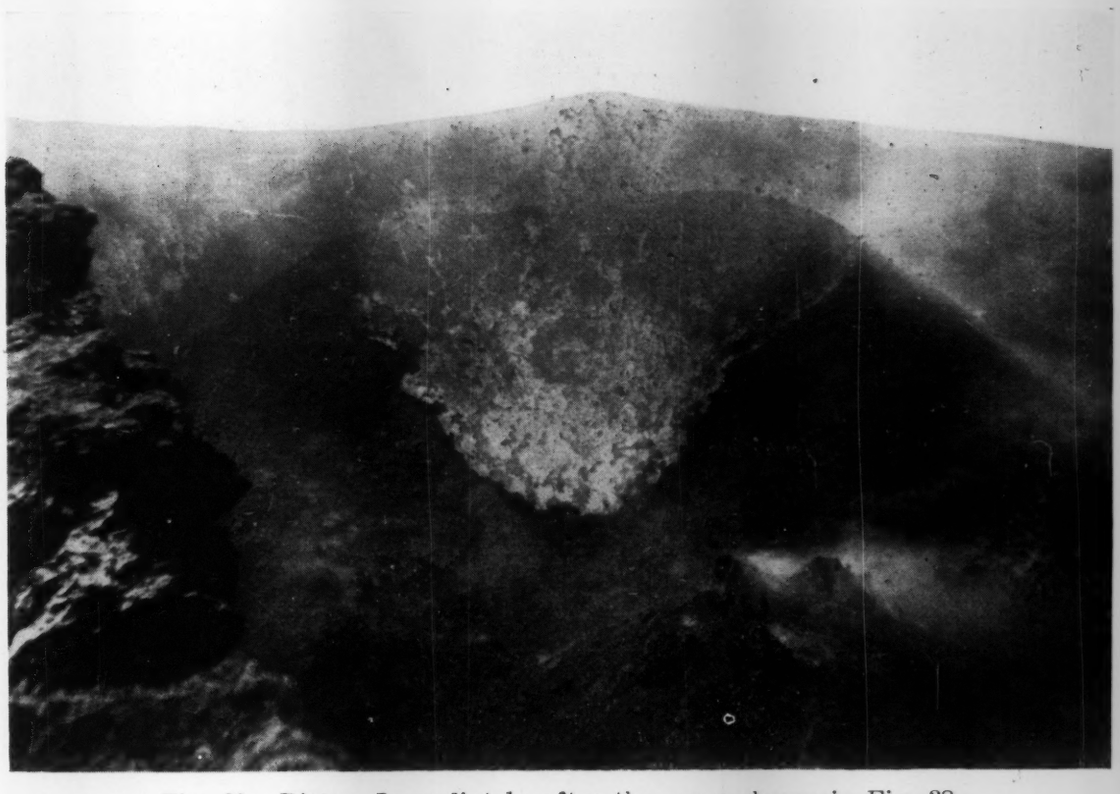

Fig. 39. Ditto. Immediately after the scene shown in Fig. 38.

Fig. 40. A panoramic view of Mihara crater filled with 1950 lavas. Aug. 24.

Fig. 41. Cinder pile around the second vent (centre) overlapping the 1st vent (left). The southern slope of the former was connected with the southern wall of the old crater. Aug. 26. Photo. S. Watanabe.

Fig. 42. Explosive activity at the second vent, 13 h, Aug. 29. Photo. S. Watanabe.

(震研彙報 第三十二号 図版 津屋・森本・小坂)

Fig. 43. Front of lava approaching to the northern rim of the crater. Sept. 3.

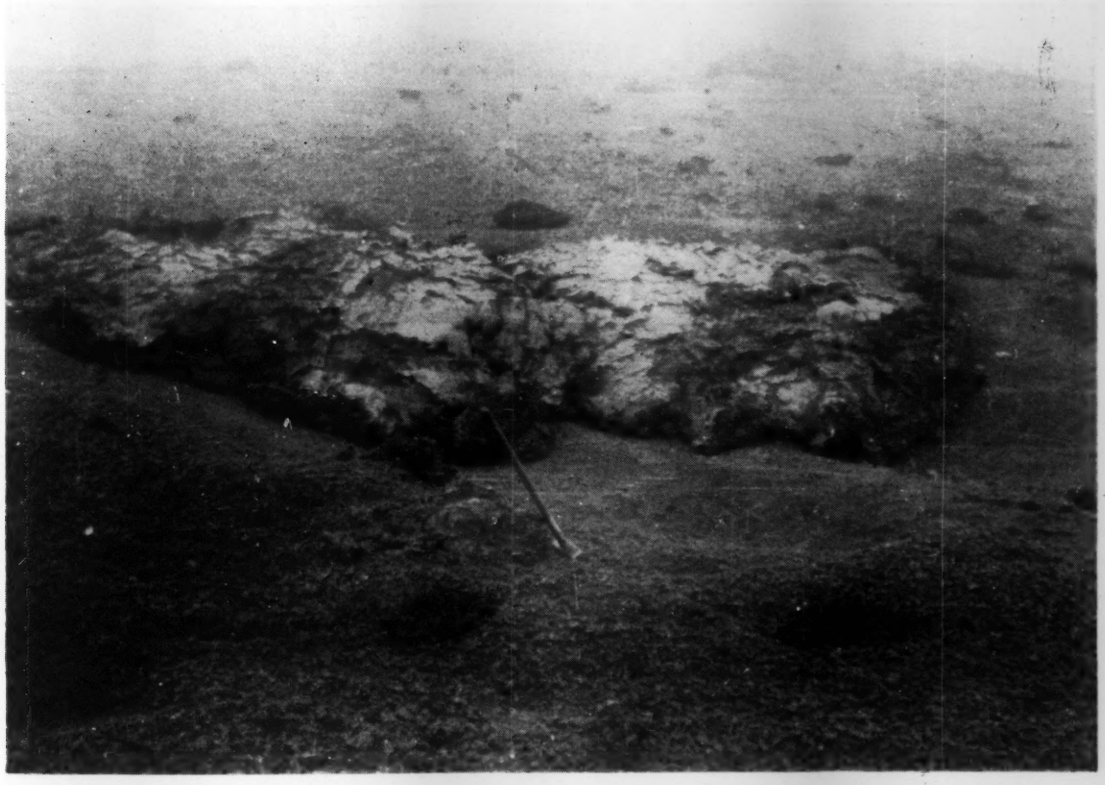

Fig. 44. A huge lava block, 4 m in diameter, ejected from the 2nd vent and flattened upon landing on the crater rim, 200 m SE of the vent, Sept. 3.

(震研彙報 第三十二号 図版 津屋・森本・小坂)

Fig. 45. Front of lava approaching to the crater rim, 80 m south of Kakôjaya. Sept. 11, Photo. S. Watanabe.

Fig. 46. Lava tongue running through the crater rim Sept. 13, 18h05m, Photo. S. Watanabe.

Fig. 47. Lava flow advancing the northwestern slope of the central cone. On both sides of the flow, spinose clinker-like *aa* deposited, forming ridges like a natural levee.

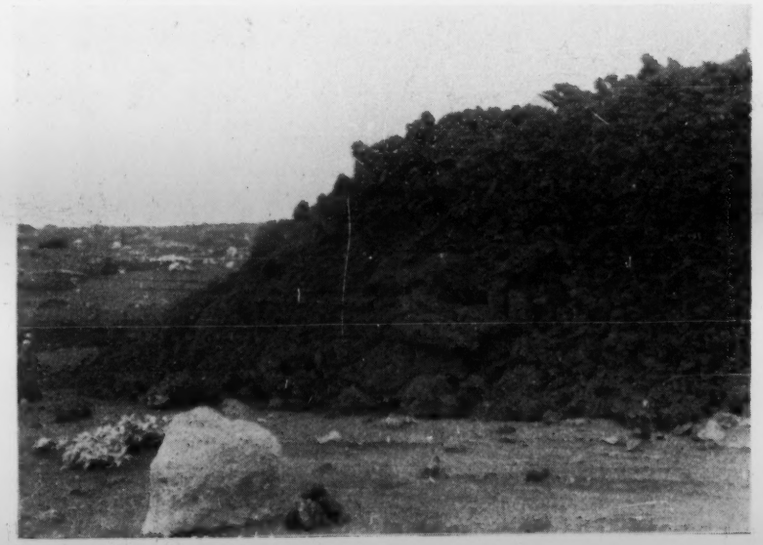

Fig. 48. Side view of the lava front.

Fig. 49. Measurement of temperature of lava approching the crater rim by means of a thermocouple.

Fig. 50. Ditto. Measurement of specific heat of the lava with calorimeter.

Fig. 51. A narrow lava stream running down the southwestern slope of the central cone.
Thickness of the lava flow was about 1 m. or less.

Fig. 52. Sept. 1.

Fig. 53. Sept. 5.

Fig. 54. Sept. 11.

Fig. 55. Sept. 14.

Fig. 56. Sept. 15.

Fig. 57. Sept. 18.

Fig. 58. Sept. 22.

Fig. 59. Sept. 24.

Figs. 52–59. Mt. Mihara, central cone of Oshima volcano viewed southeastward from Goshinkajaya on the western somma, showing successive stages of growth of the new cinder cone and also of advance of the new lava flows during the 1950 eruption.

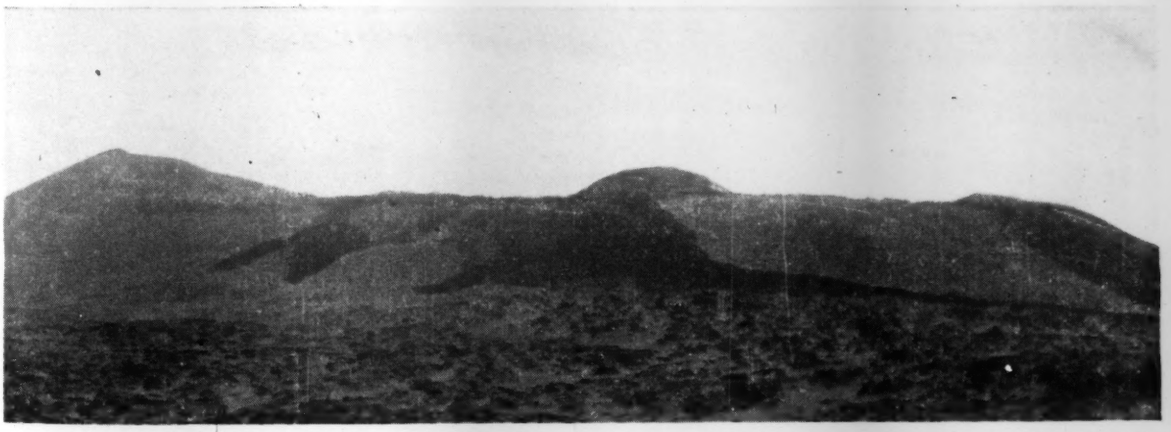

Fig. 60. Southward view of Mt. Mihara. Senzu-lava in the centre. Lava flow left in the figure flowed out from the crater on Sept. 19.

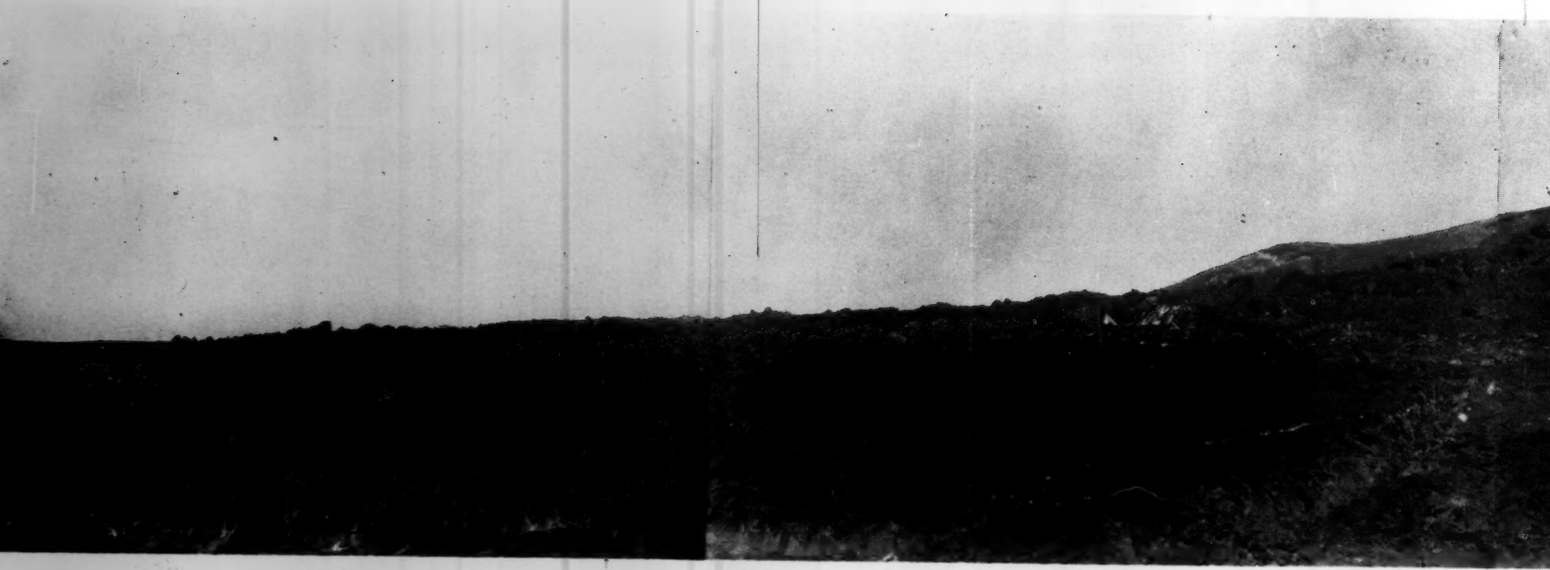

Fig. 61. A panoramic view of Mihara crater after the 1950 eruption ceased. Photo. S. Watanabe 14h, Sept. 26.

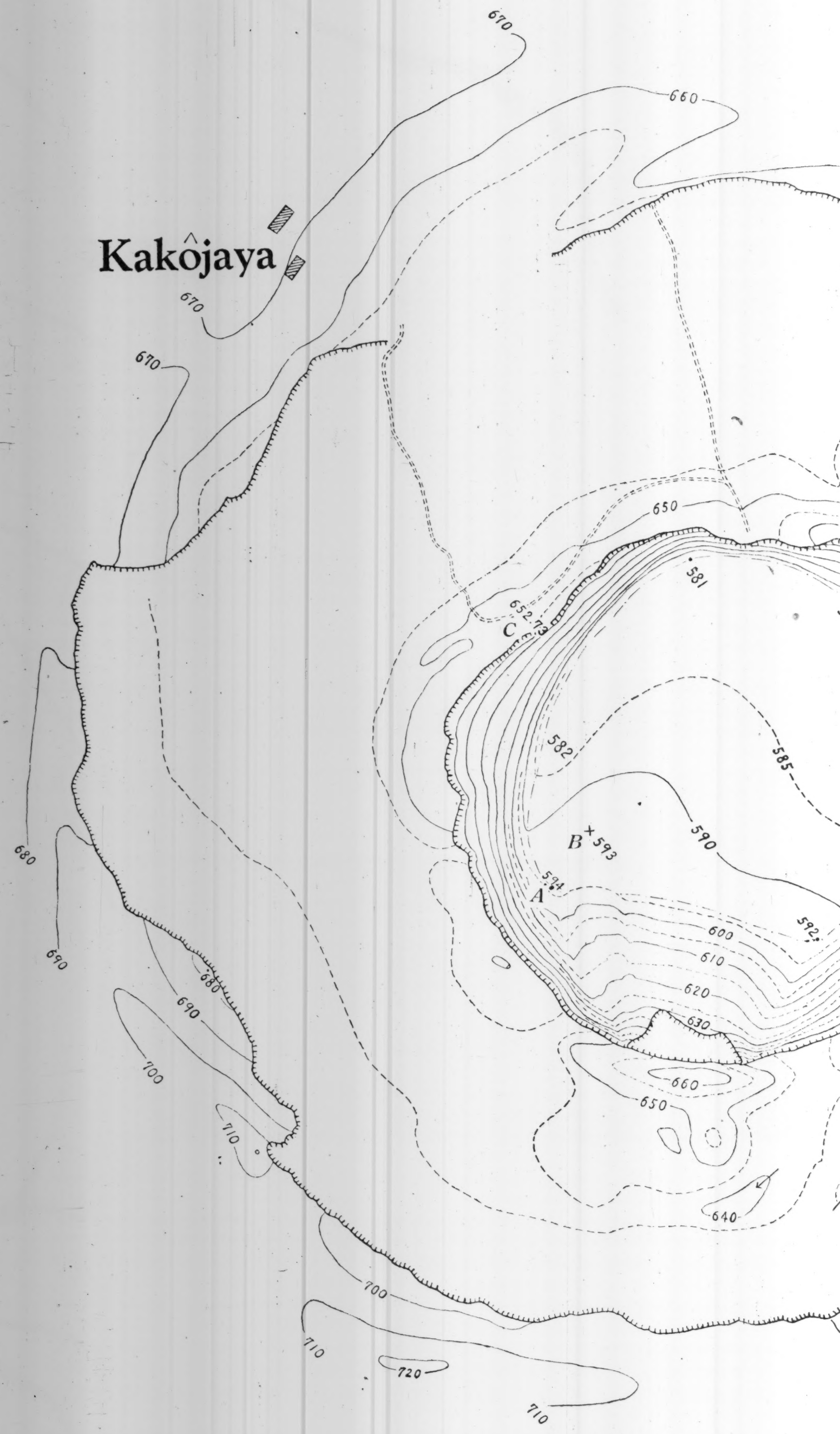

Fig. 20. Topographic map of Mihara crater surveyed by R. Morimoto and
is based on the map prepared by Nagata and Takahasi

and J. Ossaka. General topography of the crater-floor and crater-rim
asi in 1936. (R. Takahasi and T. Nagata, *Ibid.*).

5. *Experimental Studies on the Mechanism of Generation of Elastic Waves IV.*

By Keichi KASAHARA,

Earthquake Research Institute.

(Read December 22, 1953.—Received December 28, 1953.)

1. Introduction.

When we undertake seismic prospectings or other seismological experiments in the field, we have several kinds of energy sources such as explosives, rotating eccentric masses, electrodynamic vibrators[1], and heavy balls dropped to the ground. Since the beginning of seismic prospectings, the last method with falling balls has been employed by many geophysicists as the most simple and convenient energy source in seismic field tests of small scales[2]. However, most of these studies were made to investigate underground structures of the fields or problems of wave propagation, and we have not yet heard about studies which were undertaken to investigate the mechanism of generation of elastic waves by falling bodies. Although the present method of generation is now considered to be unpopular and not so useful as the method with explosives, studies of the mechanism seem still worth trying. Because, in the present method, we can easily control the generation of waves with sufficient accuracy, and these circumstances mean the possibility of obtaining satisfactory explanation on the phenomena which might bring us some valuable suggestions on the problem of generation of earthquake shocks.

Materials reported in the present paper are the results and discussions of a series of field experiments made from such considerations. Of course, the present problem is not so simple as to be explained by a brief experiment, and we shall here so confine ourselves to the problem how the amplitude and the wave form of the initial motion of elastic disturbances depend on the condition of shocking the ground with the falling ball.

1) F.F. EVISON, *Proc. Phys. Soc.*, B, **64** (1951), 311.

2) *f.i.* H. K. MÜLLER, *ZS. f. Geophys.*, **10** (1934), 34.
N. NASU, T. HAGIWARA & S. OMOTE, *Bull. Earthq. Res. Inst.*, **14** (1936), 560, **15** (1937), 87.
K. KISHINOUYE & K. IWAMA, *Bull. Earthq. Res. Inst.*, **22** (1944), 170.
W. INOUYE & H. KIMURA, *Bull. Earthq. Res. Inst.*, **8** (1935), 194.
T. ASADA, *Geophys. Notes*, No. 27 (1947).

2. Instruments and the conditions of the field.

Main instruments employed in the experiment are a special falling ball containing an accelerometer in it, electro-dynamic transducers on the ground, and an electro-dynamic oscillograph recording 12 traces. Besides them a time-marking system and a wooden frame to support the falling ball above the ground were also used.

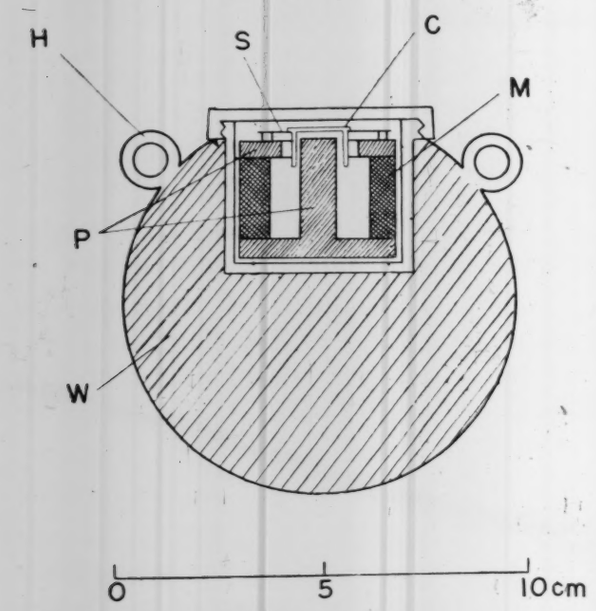

Fig. 1. C: moving coil, H: hooks, M: permanent magnet, P: pole pieces, S: supporter, W: weight.

The falling weight is an iron sphere 9 cm in diameter and 2.7 kg in weight. It contains an electro-dynamic transducer within (Figs. 1 and 9), and can detect the change of the acceleration in the course of its falling and collision with the surface of the ground. Employment of the internal transducer is one of the ideas of the present work and, with this, we can trace directly the effects of conditions of collision. A wooden frame in Fig. 10 was set up to support the falling ball at the given height (0–80 cm) above the earth's surface with a powerful permanent magnet put on the head. When a magnetic shunt works the iron ball becomes free from the magnet and begins falling.

Electro-dynamic transducers for catching and recording the elastic disturbances on the ground possess pendulums of natural frequency of oscillation 3 cps and they behave to the present frequency of ground motion as displacement seismometers of vertical components. The out-

Table I

	Accelerometer	Transducer	Galvanometer
Natural period	1200 c/s	3 c/s	100~120 c/s
Resistance	2.5 Ω	4 Ω	10 Ω
Critical damping	—	7 Ω	4~6 Ω
Sensibility	0.01 V/kine	0.03 V/kine	10 mm/m A

put EMF of transducers (proportional to the velocity of ground motions) were fed to galvanometers in the oscillograph directly but with suitable electric shunt resistances.

Characteristics of these instruments are listed in Table I.

Experiments were made on a tennis court in the Tokyo Astronomical Observatory, Mitaka, on November 21 and 22, 1953. We have had no severe rain during this month there, and the conditions of the ground looked rather dry. Before the beginning of experiments, a simple seismic prospecting was made to clarify the underground structures of the field (Fig. 2). We can consider the field homogeneous

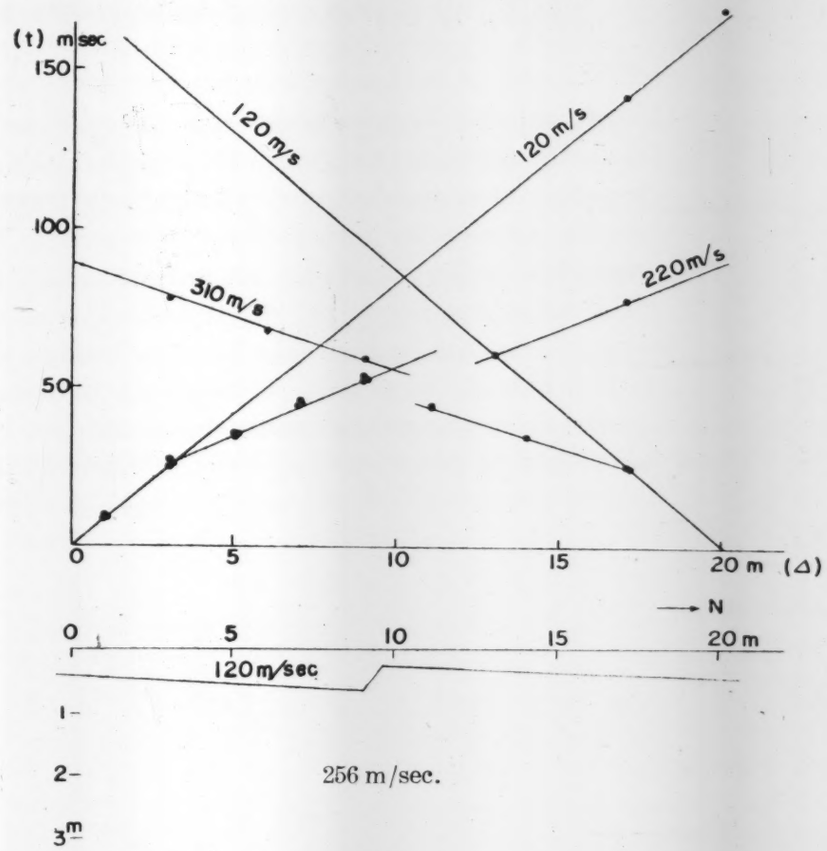

Fig. 2. Travel time curves and underground structures of the field.

(brown soil) to the depth of three or four meters except the thin layer of weathered brown soil lying on the surface.

3. Experimental results and discussions.

In the course of experiments, many kinds of oscillograms were

obtained corresponding to different falling distances, elastic properties of the shocking point, and distances of transducers from the origin. Fig. 11 is an example of these oscillograms, all of which were arranged to find answers to three essential questions. They are:

a) How do the amplitude and the form of the initial motion at a given point on the ground depend on the falling distance of the ball ?

b) How do the amplitude and form of the initial motion at the given point depend on the elastic properties of the shocking point, when the falling distance is kept unchanged ?

c) How does the falling weight move when it falls and collides with the ground, and how is the potential energy of the ball

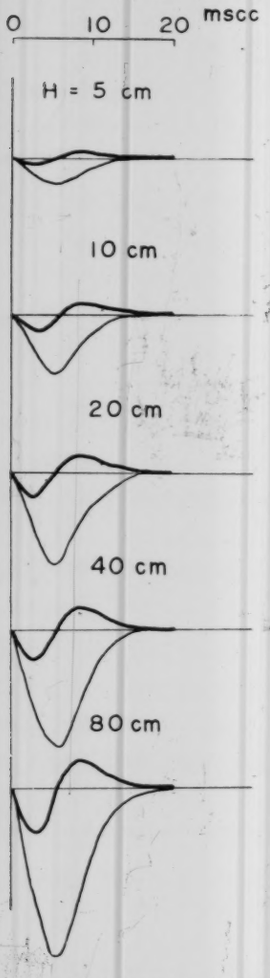

Fig. 3. Oscillograms at the origin (thick, and fine lines show the original and integrated curves, respectively).

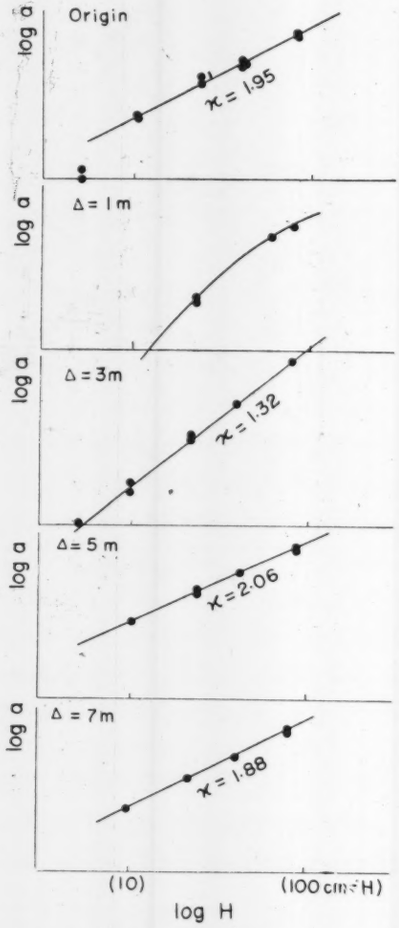

Fig. 4. Amplitudes of initial motions and falling distances. (κ: powers of amplitudes to falling distances.)

transformed to that of elastic waves?

In the following part, we intend to give the experimental results thus arranged and some discussions obtained from them.

a) The initial motion and the falling distance. The potential energy of the ball will increase proportionally to its falling distance and the energy of elastic simple harmonic wave can be estimated by the square roots of the amplitude when the frequency is kept constant. Although the initial motion looks more like a solitary wave than a simple harmonic wave, the above-mentioned fact makes us expect that the amplitude of the initial motion of the present disturbance should also be proportional to the square root of the initial potential energy of the falling ball if the process of energy transformation by the collision is carried on independently of the falling distance of the ball.

According to the experimental results, wave forms (*e.g.* periods) of the initial motions remained unchanged when the falling distance was changed. Fig. 3 shows the wave forms of shocks at the origin corresponding to different falling distances. As to the amplitudes, we find good proportionality to the square root of the falling distance in case of epicentral distances of 0 (origin), 5, and 7 m in Fig. 4. At the point nearer to the origin, however, such proportionality can not be found as shown by $\Delta=3$ m in the same figure.

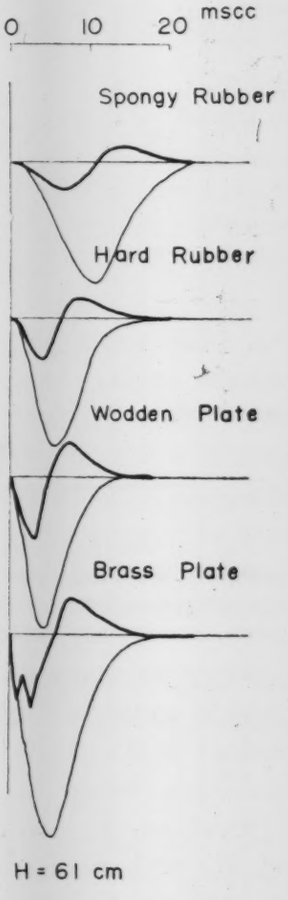

Fig. 5. Oscillograms at the origin.

b) The initial motion and the properties of the shocking point. We can easily expect that the amplitude and wave forms of the initial and the later phase will be affected considerably by the properties of the shocking point, that is to say, if the collision of the ball is made against an elastic soft material, the transformation of the energy of the ball to the elastic disturbances of the ground will take place very gradually, and if it is made against a hard material, the transformation will take place more rapidly. These circumstances will not leave the characters of the initial motion unchanged. For this reason, we have undertaken a series of experiments as will be reported here.

To change the elastic properties of the shocking point, five kinds of material were chosen, that is, brass, hard wood, hard rubber 1 and 2, and spongy rubber. They were placed on the origin point as sheets ($15 \times 20 \times 1$ cm) and the collisions were made on their surface with the falling distance kept constant. We can see the different figures of shocks at the origin in Fig. 5, corresponding to the kinds of sheets. As the original traces of the transducer in the ball show the derivative of the acceleration, we have estimated the forces which affected the ground (finer lines in the same figure). According to the results, the collision lasts as long as 10 msec in case of brass or wooden sheet and with the spongy sheet it lasts more longer (20 msec) and with less maximum acceleration (total amount of forces which comes back to the ball is more than those corresponding to hard materials). Collisions with hard rubber sheets and naked soil show intermediate figures.

Effects of these different figures of shocks to the elastic disturbances propagated can be found clearly in the earlier part of the initial phases as shown in Fig. 6, but, the effects become more faint and unremarkable in the parts following the first peak of recorded traces. This fact seems quite suggestive as to the structures of the initial motions but further considerations will be postponed. Relation between amplitudes of the initial motion and conditions of shocking will be studied in the following section.

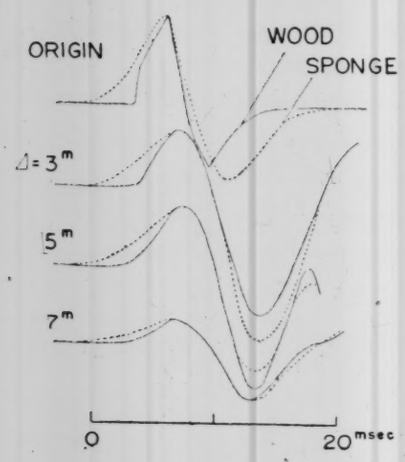

Fig. 6. Oscillograms of initial motions showing the effect of shocking conditions (——: wooden plate, ... spongy rubber).

c) Processes of the transformation of energy of the falling ball to that of elastic waves and others. To give consideration to the problem, we imagine three kinds of energy E_1, E_2 and E_3. E_1 is the kinetic energy accompanying the falling ball at the beginning of the collision and is equal to the decrease of potential energy of the ball in the gravitational field. E_2 is the energy given to the ground in the course of the collision, while E_3, the effective energy of elastic disturbances caused. Therefore, $E_1 - E_2$ is the energy which makes the ball rebound, while E_2/E_1 and E_3/E_2 indicates the first and second kind of efficiency of transformation.

E_2 can easily be estimated from the traces of the accelerometer in

the ball as well as from the maximum height which corresponds to the rebounded ball. In Table II are listed the results from the later method, which show the first kind of efficiency is proper to the elastic characters of the shocking point (from 0.9 for hard mateaials and soil to 0.6 for spongy rubber), and it dose not remarkably change according to the falling distance (in case of the naked surface of soil).

As to the second kind of efficiency, we failed to get evident conclusion, because in order to estimate E_3 we have to know the spatial dis-

Table II. Relative amplitudes of initial motions and the efficiencies of energy transformations.

Shocking point	H	$a_{\Delta=3m}$	$a_{\Delta=5m}$	a_{Origin}	a/a_0	E_2/E_1	n^3	ε	h
	cm								
Brass plate	61	1.15		1.64	0.70	0.93			
Wooden plate	61	1.04		1.60	0.65	0.95			
Soil	61	1.00	1.00	1.00	1.00	0.93	$0{\cdot}10^4$	10^2	0.34
Hard rubber 1	61	0.97		1.02	0.95	0.94			
Hard rubber 2	61	0.91		0.97	0.94	0.91			
Spongy rubber	61	0.66		0.72	0.92	0.67	$4{\cdot}10^4$	$0.3{\cdot}10^2$	0.17
Soil	80		1.29	1.25	1.03	0.01			
〃	40		0.80	0.78	1.02	0.93			
〃	20		0.63	0.65	0.97	0.95			
〃	10		0.41	0.43	0.96	——			

tribution of elastic disturbances quite accurately, which is not easy at the present step. However, we may consider, to some extent, about the quantity by the assumption that the total transmitted energy is given as the determined function of the initial amplitude at a given point on the ground. From this point of view, values of a/E_2 suggest us that the second kind of efficiency E_3/E_2 should also be proper to the properties of shocking point and independent of the falling distance. However, as to the numerical value of the efficiency, we have no bases of estimation.

To understand the above-obtained results more clearly, it may be useful to imagine a model of the present phenomena. As the most simple model which can explain the motion of the falling ball satisfactorily, the mechanical system in Fig. 7 may be used. Here the spring constant E and the mass of a plate m means, respectively, the effective elasticity and the effective mass of the part of the ground responding to the phenomena of collision, while the heat energy which would be absorbed in the dash-pot (k) includes the energy of elastic

disturbances E_3 as well as the miscellaneous energy spent in the process of collision. Transformation of energy of the present system is drawn schematically in Fig. 8. based on the above mentioned model. That is, when the ball becomes free it falls down along the course determined from the equation of motion of a point mass in the gravitational field. When it reaches the surface of the ground (plate m), a new stage begins. The motion of the ball will be known from the equation of motion of the system. viz.,

$$(M+m)\frac{d^2x}{dt^2}+k\frac{dx}{dt}+Ex=0$$

where, at $t=0$ (Commencement of the present stage is considered as the origin of time),

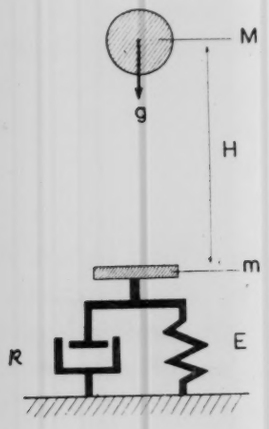

Fig. 7. Mechanical model of the collision.

$$x=0$$

$$\frac{dx}{dt}=\sqrt{\frac{2MgH}{M+m}}.$$

Therefore,

$$x=\frac{\sqrt{\frac{2MgH}{M+m}}}{\sqrt{n^2-\varepsilon^2}}e^{-\varepsilon t}\sin\sqrt{n^2-\varepsilon^2}\,t\,,$$

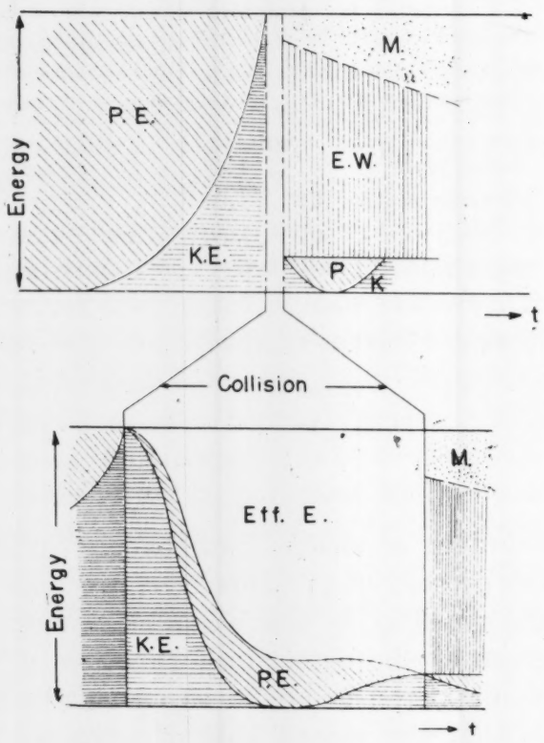

Fig. 8. Diagram of energy participation. P.E. (P) and K.E. (K) means potential and kinetic energy of the ball, respectively. Eff. E.: energy effective in wave generation; E.W: energy accompanied by elastic waves: M: Miscellaneous energy lost in the soil.

$$\frac{dx}{dt}=\frac{\sqrt{\frac{2MgH}{M+m}}}{\sqrt{n^2-\varepsilon^2}}e^{-\varepsilon t}(-\varepsilon\sin\sqrt{n^2-\varepsilon^2}\,t+\sqrt{n^2-\varepsilon^2}\cos\sqrt{n^2-\varepsilon^2}\,t)\,,$$

$$\frac{d^2x}{dt^2}=\frac{\sqrt{\frac{2MgH}{M+m}}}{\sqrt{n^2-\varepsilon^2}}e^{-\varepsilon t}\{(2\varepsilon^2-n^2)\sin\sqrt{n^2-\varepsilon^2}\,t-2\varepsilon\sqrt{n^2-\varepsilon^2}\cos\sqrt{n^2-\varepsilon^2}\,t\}\,,$$

where ;

$$2\varepsilon=\frac{k}{M+m}\,,$$

and

$$n^2=\frac{E}{M+m}\,.$$

As can be seen in the above solutions, the falling height affects only the amplitude of the motion of the ball and the wave form or period (duration time) of collision is kept unchanged. The equation is effective until x becomes 0 again, and at that moment the ball gets off the plate m and rises to its maximum rebounded height (the third stage).

In Fig. 8, the broken line bounding two kinds of energy indicates

Fig. 9. The falling ball.

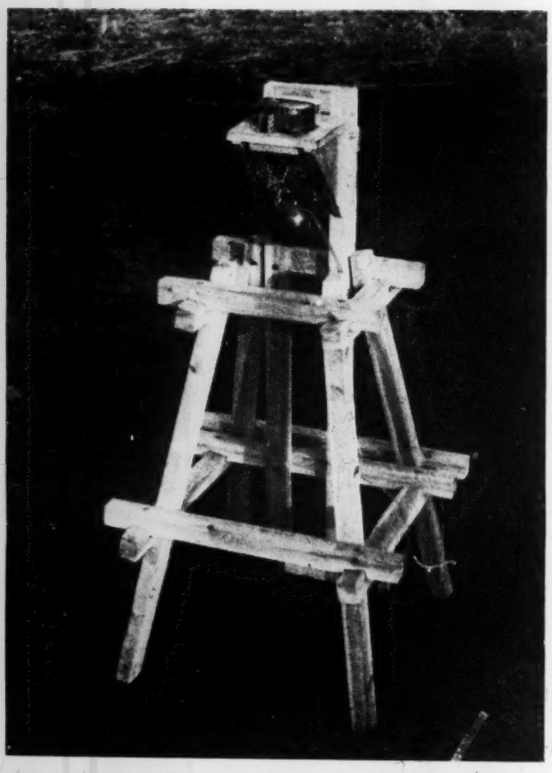

Fig. 10. The supporter of the ball.

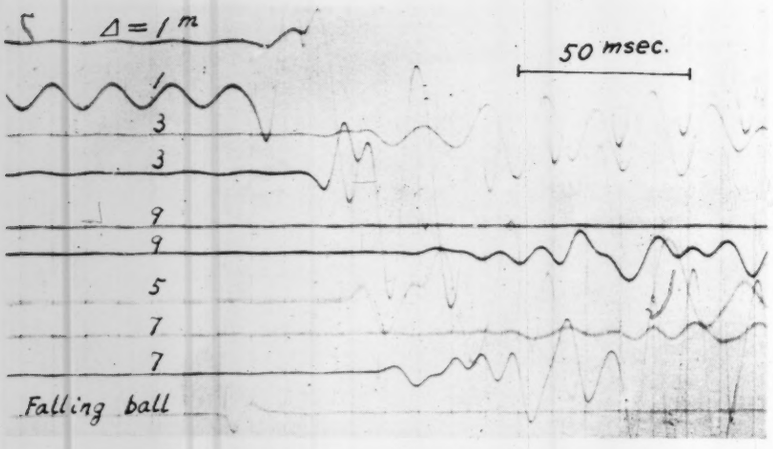

Fig. 11. An example of oscillograms.

unknown boundaries, while the full lines indicate those assumable from the present model. The actual value of E and k can be estimated from the duration time of the collision and the ratio E_2/E_1, some examples of which are listed in Table II.

4. Concluding remarks.

Processes of generation of elastic waves by the collision of a falling ball against the ground were considered and the relation between characters of generated elastic disturbances and the conditions of collisions were investigated experimentally. A simple model of a mechanical system was also proposed to explain the experimental results. Although the present paper may lay claims to some *raison d'etre* for taking the initiative, it failed to offer a satisfactory answer. More perfect one to the present problem will be made another days.

The writer wishes to express his hearty thanks to Prof. T. Hagiwara for his kind encouragement in the course of the study. The writer's thanks are due to Mr. S. Saito who helped him in the field experiments and also to members of the Earthquake Research Institute who gave him valuable suggestions and discussions.

To make the present experiments, the author owes very much to the Grant in Aid of Miscellaneous Scientific Researches from the Department of Education.

---

5. 弾性波の発生機構に関する実験 (第 4 報)

地震研究所 笠 原 慶 一

重錘が地面に落下衝突して弾性波を発生する機構について初歩的考察を実験により行つた．本報に述べてあるのは

1) 重錘の落下距離と，発生する弾性波の初動振巾及び周期との関係
2) 重錘が衝撃を与える局部の弾性的性質と，初動振巾及び周期との関係
3) 最初に重錘が所有するポテンシヤルエネルギーが弾性波のエネルギーに配分されてゆく過程

の考察の三点であり，これらの観測結果を説明する為簡単な模型を提出してある．

6. *The Fourth Explosion-Seismic Observations in North-Eastern Japan.*

By The Research Group for Explosion Seismology.*

(Read Feb. 17, 1953.—Received March 31, 1954.)

1. Preface.

Seismic prospecting on a large scale, using a large amount of explosives, is highly effective in studying the propagation of seismic waves as well as in investigating the crustal structures. In Japan, the first opportunity for such experiments was afforded on October 25th, 1950 when a large amount of explosives was exploded for engineering purpose at the construction site of Isibuti dam in Iwate-ken, and our research group named "The Research Group for Explosion Seismology (R.G.E.S.)" was formed.

After that time, on December 27th, 1951 and on July 25th, 1952, explosions on a similar scale took place at the same spot, and experiments were made on each opportunity, the results of which have already been reported respectively.[1)]

On December 7th 1952, the fourth opportunity was offered when a large amount of explosives, i.e. 29.7 tons of dynamite, were exploded for the purpose of setting down the weakened deposits in the Kamaisi Mine at Sennin-tōge, about 18 km west of the city of Kamaisi, Kamiheigun, Iwate-ken.

Very fortunately the new explosion point was situated exactly on

---

* Members of the group, who participated in the project are as follows (in alphabetic order):

T. AKIMA, S. ASANO, K. KASAHARA, H. KAWASUMI, N. KOBAYASHI, T. MATUMOTO, S. MIYAMURA, S. OMOTE, M. SIBANO, E. SIMA, T. SUZUKI, T. TANAKA, M. TSUJIURA, Y. YAMAZAKI, M. YANAGISAWA (E.R.I.) T. ASADA, N. DEN, T. HASEBA, A. HAYATSU, Naota KOBAYASI, T. MATUZAWA, K. MOGI, R. SATO (Geophys. Inst., Tokyo Univ.) T. OGAWA, O. SAKAI, T. USAMI, T. UTSU (C.M.O.) M. HAYAKAWA, S. HURUYA, T. KANEKO, M. SUZUKI, T. TATEISHI (Geol. Surv.) N. MINE, K. NAKAMURA, K. NORITOMI, A. OSSAKA, T. SIMA, Z. SUZUKI, A. TAKAGI (Geophys. Inst., Tohoku Univ.) T. ASANUMA, S. HONDA, S. MURAUCHI (Nat. Sci. Mus.) K. OKANO, I. TAMAKI (Geophys. Inst., Kyoto Univ.) R. YOSIYAMA (Fac. Sci., Kyushu Univ.) K. TAZIME, S. YAMASITA (Akita Univ.) T. SUGAWA (Mizusawa Lat. Obs.)

1) *Zisin*, [ii], **3** (1951), 77–82. **6** (1953), 7–12. **6** (1953), 84–90. *Bull. Earthq. Res. Inst.* **29** (1951), 97–106, **30** (1952), 279–292. **31** (1953), 281–288.

the eastern profile of the second Isibuti experiment, and it provided a good opportunity for us to reexamine the previous results.

2. Preparation for observation.

Nineteen temporary observation points (14 points on the southern and 5 points on the western profile) were established. Their locations are shown in Fig. 1. The pick-ups used were vertical or horizontal electromagnetic seismographs of 3 c/s, except in a few points, and high-gain amplifiers and oscillographs were prepared as in the previous case.

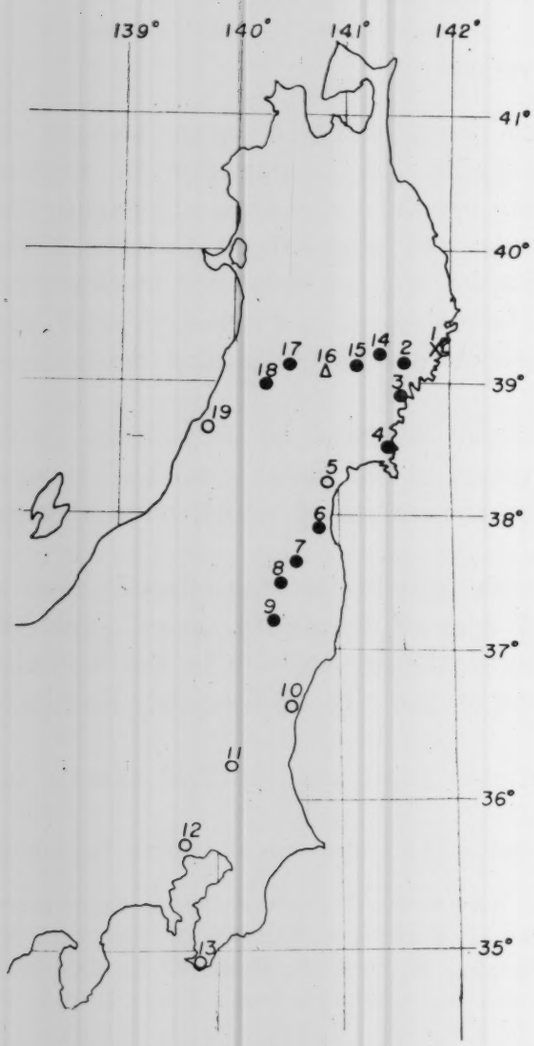

Fig. 1. Seismic stations of the first Kamaisi explosion of Dec. 7, 1952.

As for the time marking system, in addition to the time signals of J.J.Y. in 4 Mc, special cooperation was given by NHK, Nippon Broadcasting Company, who kindly received the time signal of J.J.Y. and broadcast it in its civil broadcasting frequency band of 590 Kc from JOAK, Tokyo, for 20 minutes before and after the explosion time. The special broadcasting from JOAK was also utilized for the communication between the observation points.

The shot-time was calculated as 03 h 34 m 59.91 s from the record obtained at the shot point. The explosives were fired in 7 steps with 25 milli-second delay detonators.

3. Observation and results.

At several distant ones of the nineteen observation points, it

Table I.

	Station	λ	φ	h	Δ	Seismometre	Observers
Southern profile	Shot point	141°41′49″ E	39°17′37″ N	500 m	0 km	20V12	Kaneko, Huruya
	Setamai	32′46″	09′08″	180	20.4	10V1, 10H1	Asano, Sato
	Kesennuma	34′26″	38°53′55″	35	45.5	10V1, 10H1	Matumoto (T), Hayatu
	Onagawa	27′27″	26′15″	20	97.3	3V1, 3H1	Noritomi, Takagi, Ossaka
	Mukaiyama	140°49′07″	14′36″	130	140.0	3V1, 3H1	Yoshiyama, Sima (T), Nakamura
	Kanayama	47′51″	37°53′43″	80	173.7	3V2, 3H1	Murauchi, Honda, Asanuma
	Kawamata	36′47″	40′49″	260	202.3	3V2, 3H1	Kobayashi (Naoyosi), Hagihara
	Siroiwa	28′52″	29′30″	340	226.5	3V1, 3H2	Suzuki (Z), Mine
	Nogizawa	25′18″	10′98″	180	261.1	3V2, 3H1	Yamazaki, Kobayashi (Naota)
	Hitati	36′06″	36°37′33″	374	311.6	3V1	Tanaka, Suzuki (T)
	Tukuba	06′40″	12′36″	280	369.9	3V1	Kasahara, Chujo
	Tokyo	36′53″	35°36′11″	6	445.0	3V1	Tateishi, Suzuki
	Kanbe	139°50′37″	34°56′25″	20	510.0	3V2, 1H1	Den, Mogi, Haseba
Western profile	Ide	141°17′48″ E	39°10′27″ N	140 m	36.9 km	3V1, 3H1	Akima, Tsujiura
	Mizusawa	08′11″	07′57″	61	51.4	10V1, 1H1	Sakai, Sugawa, Usami
	Isibuti	140°54′28″	06′44″	300	70.8	3V1, 3H1	Utsu, Ogawa
	Yuzawa	30′30″	09′36″	120	103.3	15V6, 2H3	Tamaki, Okano
	Mamurogawa	17′13″	38°51′58″	100	130.5	3V2	Sima (E), Sibano, Yanagisawa
	Tagawa	139°38′36″	39′00″	40	195.0	3V1, 3H1	Yamashita, Tazime

N.B. 3V2 means two vertical seismometers of 3 c/s natural frequency.

failed to record the seismic waves generated by the explosion. This regrettable result may have been caused from the fact that the explosion at this time was not effective enough to produce strong seismic waves on account of the following reasons: the first is that the explosion of 29.7 tons of dynamite was performed by delayed blasting: the second is that fairly large amount of blasting energy was probably released into free air due to the condition of blasting chamber. For such reasons, records of only 8 stations in southern and of 3 stations in western profiles were used for the present analysis.

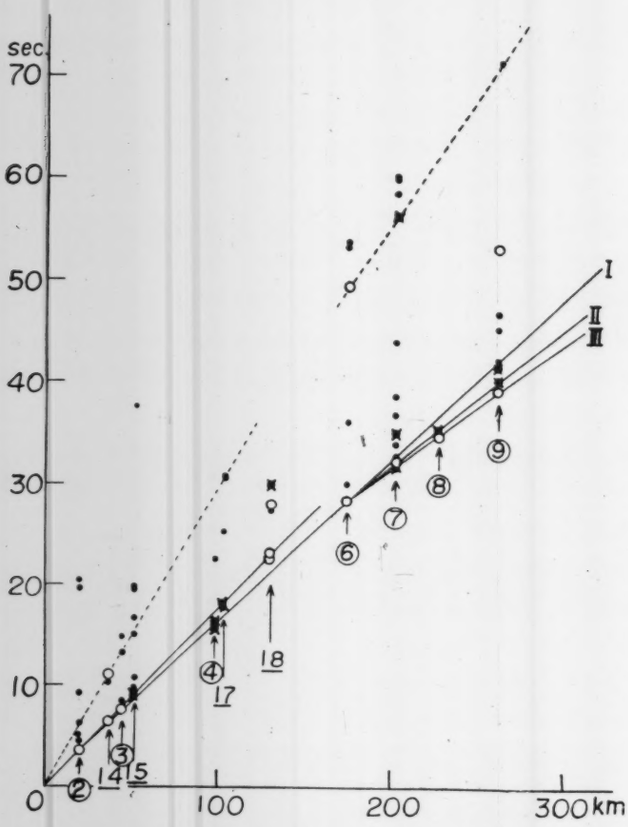

Fig. 2. Time-distance curves in the southern profile of the first Kamaisi explosion seismic observations.

In order to avoid personal error, the arrival times of phases in each record were measured by three members independently of one another. From the data of these results, the travel-time curves are drawn as shown in Fig. 2 and 3, for southern and western profiles respectively. In Fig. 2, the points marked ○, ✖, and ● correspond to the phases

which were recognized by all 3, by 2 and by only one of the 3 persons respectively.

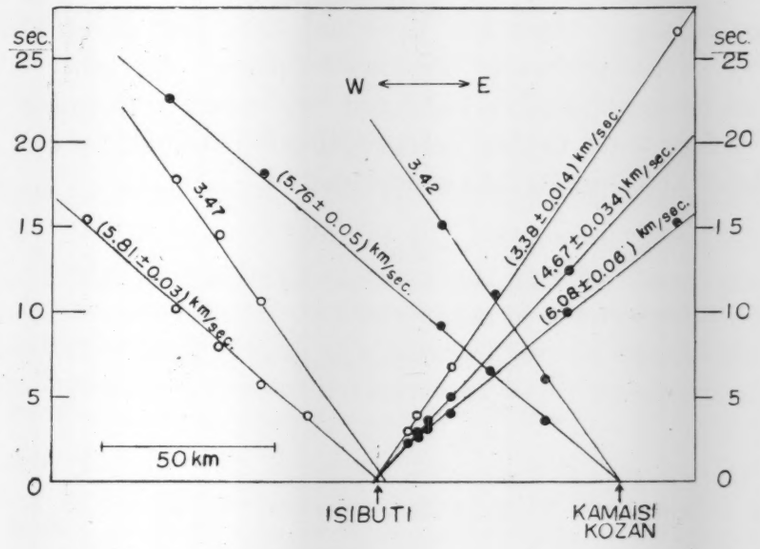

Fig. 3. Time-distance curves of the E-W profile of the first Kamaisi explosion seismic observations.

4. The travel-time curves in southern profile.

Based upon the data concerning the arrival times of identified phases in each record, three travel-time curves are drawn, which are shown by solid straight lines in Fig. 2. By reducing the equations of these lines by the least squares, they are expressed as follows:

$$\text{I} \qquad t=0.21\pm0.07+\frac{\Delta}{6.19\pm0.02}$$

$$\text{II} \qquad t=4.18\pm0.29+\frac{\Delta}{7.37\pm0.06}$$

$$\text{III} \qquad t=7.06\pm0.40+\frac{\Delta}{8.20\pm0.10}$$

The data used for reducing these equations are in Table II.

Equation I means the existence of a layer in which the P-wave travels at an apparent velocity of 6.19 km/sec. This layer seems to correspond to the 3rd layer found in the last three experiments at Isibuti, and the apparent values of P wave velocities obtained in the

layer were (6.13 ± 0.02) km/sec, (5.91 ± 0.02) km/sec and (5.98 ± 0.01) km/sec respectively.

The value of $V_p = (6.19 \pm 0.02)$ km/sec calculated in the present case is significantly larger than the previous ones just given above. This fact deserves investigation in the near future. Anyhow, it cannot be considered as observational errors and we must reexamine our whole process of inferences, taking geographical distributions and geological informations of the profiles into consideration.

Table II.

	Station	P_1	P_2	P_3	S (?)
Southern profile	1	Shot time: $03^h 34^m 59^s.91$			
	2	$35^m 03^s.51$			$06^s.08$
	3	07.63			
	4	15.77			
	6	28.32	$28^s.32$	$28^s.32$	49.45
	7		32.21	31.75	50.40
	8		35.64	34.52	
	9		40.13	39.00	71.38
Western profile	14	$06^s.30$			$10^s.9$
	15	09.00			15.0
	17	18.00			30.79
	18	22.57			

Equation III means the existence of a layer in which P-wave travels at an apparent velocity of 8.20 km/sec. Such a value of velocity has never been observed in Japan, though similar values have been found in other countries. On the other hand, the value of $V_p = 7.37$ km/sec expressed by equation II cannot be disregarded in considering the result of observations in the 3rd Isibuti explosion and values of V_p found in natural earthquakes in Tohoku district.

It remains unsolved which of these two travel-time curves expressed by II and III, is more probable, or whether we may not admit the existence of two layers corresponding to II and III. At present, however, upon the present observations, we will admit the existence of the 2 layers corresponding to I and III, and as to the existence of the layer corresponding to II, we will make sure of it on the next opportunity.

On an assumption that thicknesses of the layers remain the same southward along the profile, they are calculated from the above equations I–II, II–III and I–III as follows:

$$d_{12}=(27.2\pm3.0)\text{ km},$$
$$d_{23}=(\ 5.1\pm3.3)\text{ km},$$
and
$$d_{13}=(32.3\pm1.3)\text{ km}.$$

In these expressions, d_{12}, for instance, means the thickness of the layer corresponding to I overlaying the layer corresponding to II.

As no observation points were spread, at this time, near the shot point, the travel-time curve corresponding to the layer which may probably exist over the layer of $V_p=6.19$ km/sec could not be found. But, considering the intercept time of (0.21 ± 0.07) sec in equation I, it seems to exist.

A dotted line in Fig. 2 shows the velocity of waves 4.1 km/sec, which seems to be slightly larger than that of *S*-waves.

5. The travel-time curves of the western profile.

Fig. 3 shows the travel-time curves of the western profile. By the least square method, the equation of this line becomes as follows:

$$t=(-0.02\pm0.01)^s+\frac{\Delta}{5.76\pm0.05}$$

which shows an apparent *P*-wave velocity of 5.76 km/sec. This value is almost the same as what was found in the same western profile in the last Isibuti experiment (5.78 km/sec), and will confirm our estimation on the crustal structure of the east-west profile of these regions which we have obtained previously.

The dotted line in Fig. 2 shows a velocity of approximately 3.4 km/sec, which seems to correspond to the velocity of *S*-waves.

6. Conclusion.

It is regrettable that sufficient number of records of seismic waves generated by the explosions could not be obtained and that few points remain unsolved. But we may say that the following points in the present investigations are of special interest. (1°) The velocity of the *P*-wave in the 3rd layer in Isibuti case was found to be significantly larger than that in previous cases. (2°) The layer having the value of

8 km/sec was found at a depth of approximately 30 km. (3°) The crustal structure of the east-west profile of these regions estimated in the last Isibuti experiments was confirmed.

7. Acknowledgement.

Finally, we wish to express mach thanks to the agencies and persons to whose helpful cooperation the success of this experiment is due. They are Nittetsu Mining Company, Tohoku District Construction Bureau of Ministry of Construction, Tohoku Electric Company, Japan Government Railway, Technical Department of Nippon Hoso Kyokai (NHK), Telephone Office of Morioka and Kamaisi, Post Office of Kassi, Prefectural and Police Authorities of Morioka.

We also acknowledge the encouragement and instruction given by Prof. T. Matuzawa throughout our study.

---

6. 東北日本における第4回爆破地震動観測

爆破地震動研究グループ

三回にわたる石淵での大爆破による地震動の観測が終了して間もなく，我々は 1952 年 12 月 7 日に，場所も同じ東北地方の，しかも石淵の場合の観測の東西測線上に丁度のる，釜石市から 15 km 程西によつた釜石鉱山における約 30 トンの火薬による大爆破の地震動を観測する機会にめぐまれた．

19 の臨時観測点のすべてがきれいな記録をうることに成功したと云う訳でないので，1，2 その決論を次回にゆづる点を残す結果となつたが，少くとも今度の観測で認められた注意すべき点は，

1. 石淵の場合に見出された第三層に相当すると思われる層の中の P 波の速度が，観測誤差の範囲をかなり外れて大きく出たということ．

2. 今迄日本では見出されなかつた 8 km/sec 程度の P 波の速度をもつ層が，約 30 km 位の深さで見出されたこと．

3. 東方測線による結果は，石淵の場合の東西測線からえられた結果とよく一致し，この辺の東西方向に関する地殻構造は，これでかなりの確実性をおびるに至つたことである．

尚，今回の観測に当つて多大の便宜を与えられた日鉄鉱業釜石鉱山，建設省，国鉄盛岡管理局，NHK技術部，盛岡県庁，東北電力，その他各方面の関係者に対してはここに厚くお礼を申し上げたい．

なお，本研究は，文部省科学研究費によつてなされたものであることを附記して謝意を表する．

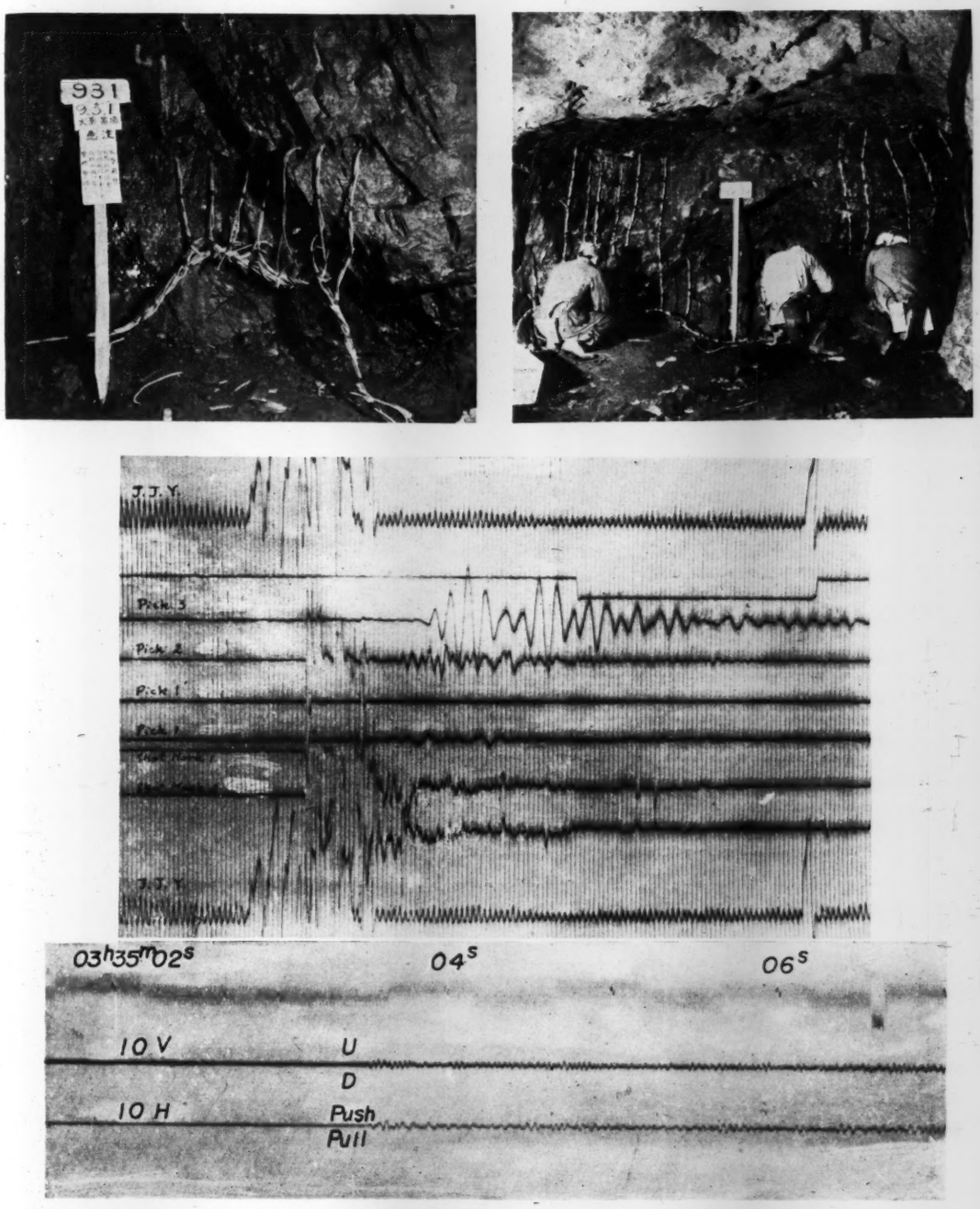

Fig. 4. The first explosion at Kamaisi, Iwate-ken, on December 7th 1952.
Charged walls along the gallery in the mine (*A*). Seismograms on the eastern profile at Shot point (*B*) and Setamai (*C*).

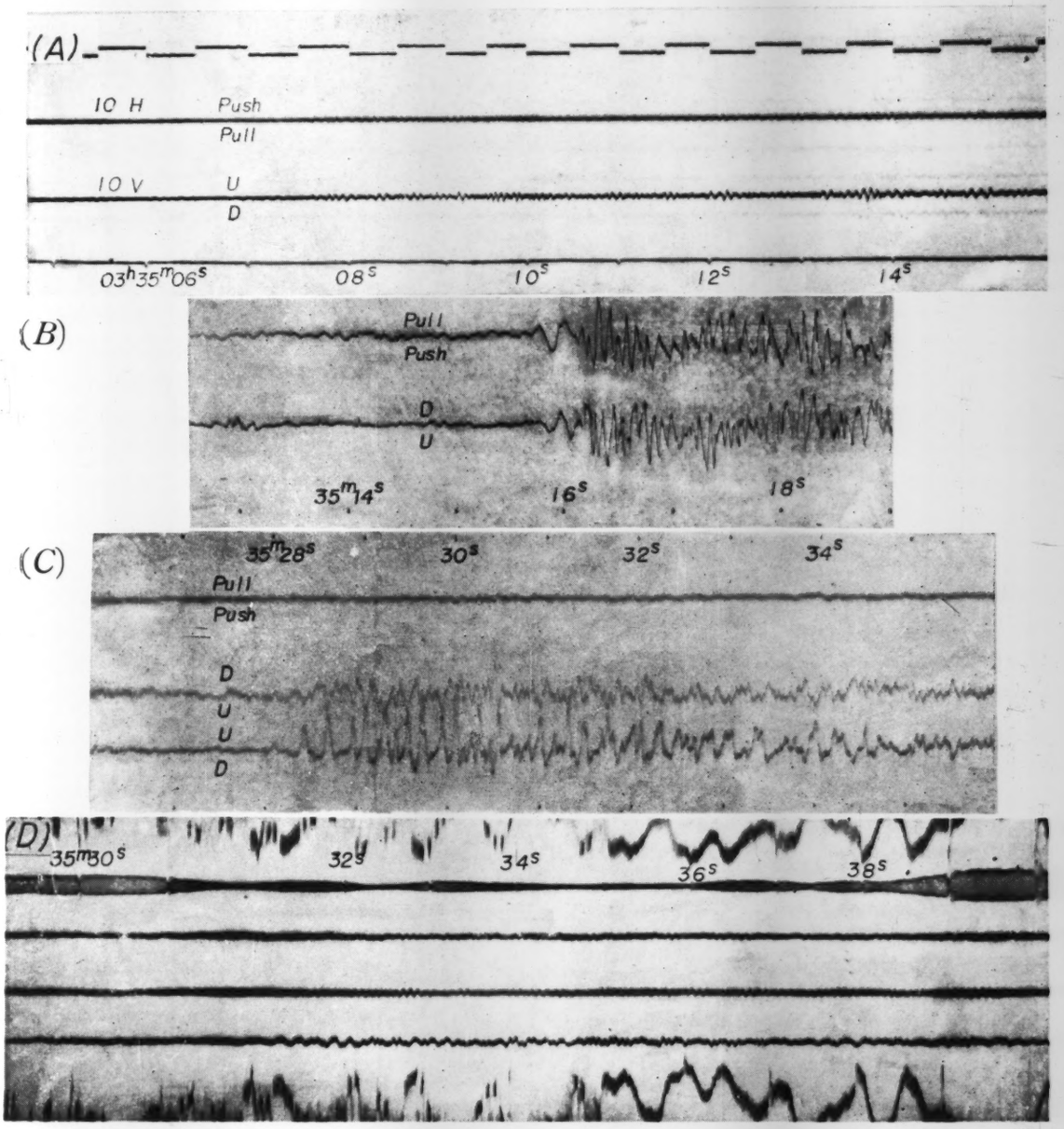

Fig. 5. Seismograms obtained at the first Kamaisi explosion of 1952 on the southern profile at Kesennuma (*A*), Onagawa (*B*), Kanayama (*C*) and Kawamata (*D*).

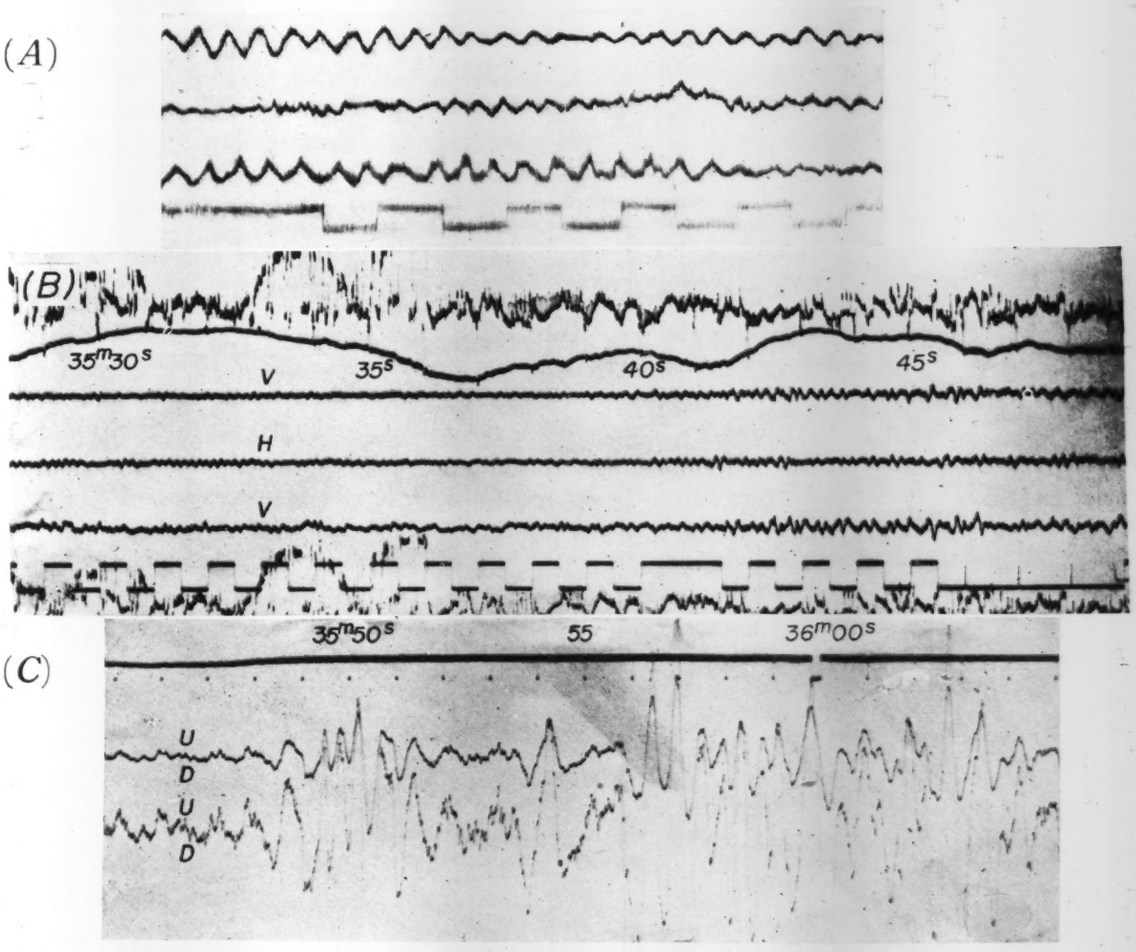

Fig. 6. Seismograms obtained at the first Kamaisi explosion of 1952 on the southern profile at Siroiwa (*A*), Nogizawa (*B*) and Hitati (*C*).

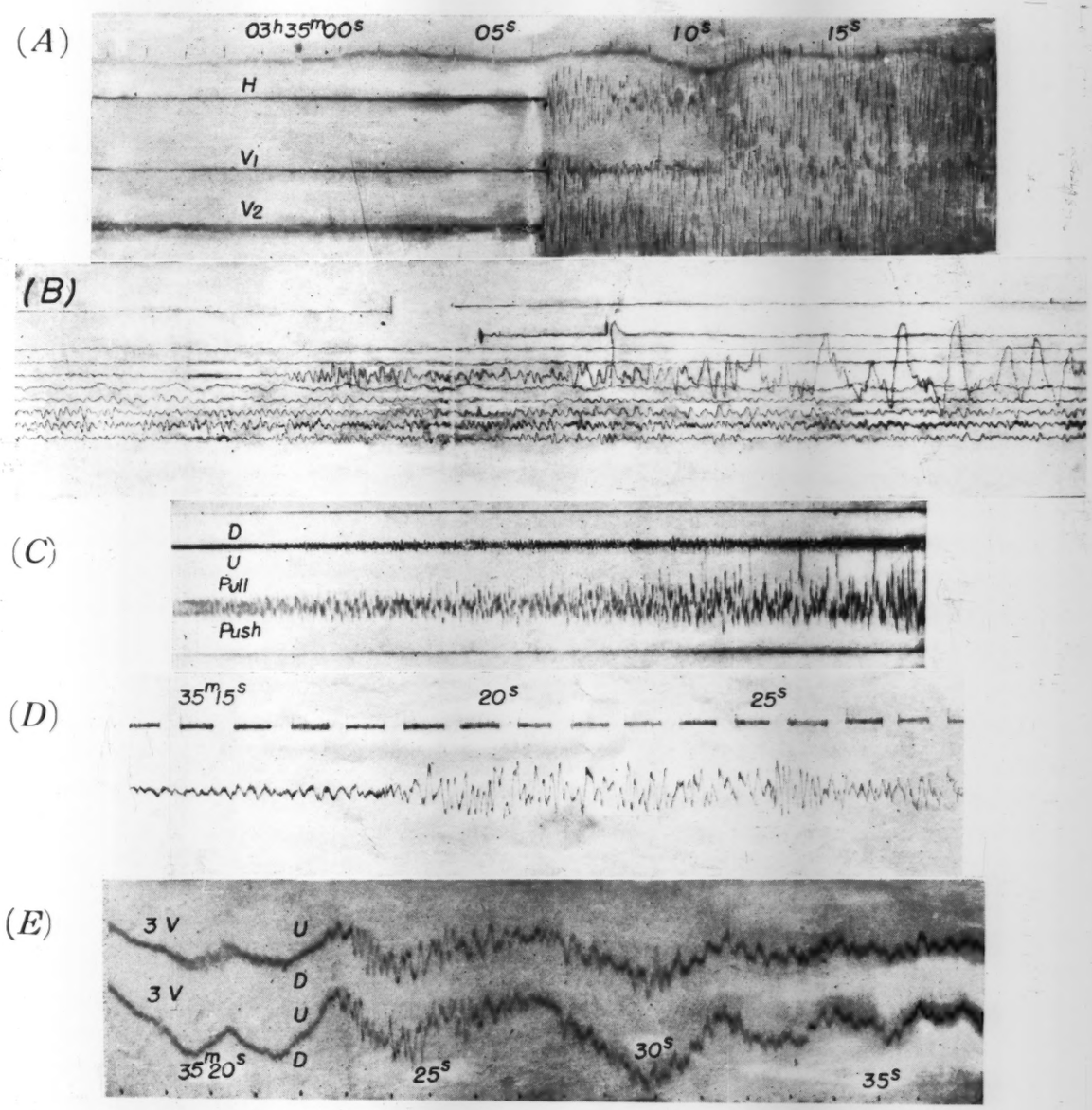

Fig. 7. Seismograms obtained at the first Kamaisi explosion of 1952 on the western profile at Ide (*A*), Mizusawa (*B*), Isibuti (*C*), Yuzawa (*D*) and Mamurogawa (*E*).

7. *Theory of Eden's Twin Strips and Application of It to Magnifying Mechanism of Seismometer.*

By Genrokuro NISHIMURA, Masazi SUZUKI,

Earthquake Research Institute,

and Eiichi FURUKAWA,

Faculty of Engineering, Chuo University, Tokyo.

(Read Oct. 21, 1949 and Sept. 16, 1953.—Received Jan. 8, 1954.)

1. Introduction.

A simple and ingenious magnifying mechanism, known as "Eden's twin strips", has been used chiefly for comparators of high sensitivity such as the Millionth Comparator. So far as we know, it has not been used for the measurements of vibration. However, it is a matter of practical interest to find useful applications to such purpose because of its outstanding advantages which include freedom from backlash and solid friction, high magnification and simple construction. After some preliminary investigations, it was found to be available for such purpose to the best advantage. Hitherto we have found a broad application in the field of the vibration-measuring instruments such as a vibrograph[1], an accelerograph[2], a torsiograph[3], a vibration table[4], and a penmotor[5] and others[6]. It has given satisfactory service in a considerable variety of applications over a period of about five years, and

1) The example is shown in the present paper.

2) G. NISHIMURA, M. SUZUKI & S. KAWAHARA, "Vibration of Machine-Tool.: Horizontal vibration of Grinder," *Soc. Precision Mechanics, Japan*, **18**, No. 10, (1952). G. NISHIMURA & H. KAWASUMI, "Torsional Moment of a Focal Plane Shutter Camera," *Jour. Fac. Eng., Univ. Tokyo*. **24**, No. 2, (1954).

3) G. NISHIMURA & E. FURUKAWA, "Torsiograph and its Application," read on Spring League Meeting of the Soc. of Machine Engineering & the Soc. of Precision Mechanics, Feb. 10, (1951).

G. NISHIMURA & others, "A New-Designed Prospecting Apparatus," *Bull. E.R.I.*, **31**, No. 4, (1954).

4) G. NISHIMURA, M. SUZUKI & S. KAWAHARA, "Measurement of the Reactional Force of Sewing Machine," *Soc. Precision Mechanics, Japan*, **18**, No. 6, (1952).

5) K. KANAI & T. TANAKA, "A Smoked-paper Recorder for High Sensitive Seismometer," *Zisin*, [ii], **5**, No. 3, (1953).

6) G. NISHIMURA & E. FURUKAWA, "Dynamical Measurement of Mesh Error of Gear Trains in Working Condition," read on Spring League Meeting of the Soc. of Mech. Engineering and the Soc. of Precision Mechanics, Feb. 10, (1951).

this fact has encouraged the writers in preparing this paper.

The present paper describes its statical and dynamical characteristics which is determined theoretically and confirmed by the experiments using a vibration table, and furnishes sufficient informations for purposes of designing.

2. Statical Characteristics.

In Fig. 1, suppose that the twin strips are in equilibrium under the action of the known external forces P_0, Q_0 and couple M_0, and the member B_1B_2 is massless and absolutely rigid. Then, the resultant of all external forces acting on a recording pen (or a deflecting mirror) can be completely defined by P_0, Q_0 and M_0. Let P, Q and M denote the longitudinal force (restoring force of the twin strips), the shearing force, and the bending moment at the clamped end A_1, respectively. The signs of these quantities are defined as positive as shown in Fig. 1. Let EI_s denote the flexural rigidity of strips, δ the displacement of the clamped end A_1 from its equilibrium position, θ the slope of strips at the end B_2 ($x_2=l$), Y the deflection at the same point, and l and D the length of strips and the distance between both strips, respectively.

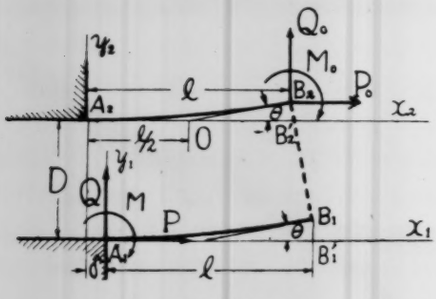

Fig. 1.

Taking coordinate axes, as shown in Fig. 1, and denoting

$$P'=P+P_0\,,\quad Q'=Q+Q_0\,,\quad M'=M+M_0\,,$$

the differential equations for deflection curve of strips may be written in the form

$$\frac{d^2y_1}{dx_1^2}+\frac{P}{EI_s}y_1=\frac{Q}{EI_s}x_1+\frac{M}{EI_s}\,,$$

$$\frac{d^2y_2}{dx_2^2}-\frac{P'}{EI_s}y_2=-\frac{Q'}{EI_s}x_2-\frac{M''}{EI_s}\,,$$

and

$$M''=M'-PD+P_0Y-Q\delta-Q_0l\,.$$

The solutions of these equations satisfying the conditions at the clamped ends are

$$y_1=-\frac{M}{P}\cos\sqrt{\frac{P}{EI_s}}\,x_1-\frac{Q}{P}\sqrt{\frac{EI_s}{P}}\sin\sqrt{\frac{P}{EI_s}}\,x_1+\frac{Q}{P}\,x_1+\frac{M}{P}\,,$$

$$y_2=-\frac{M''}{P'}\cosh\sqrt{\frac{P'}{EI_s}}\,x_2-\frac{Q'}{P'}\sqrt{\frac{EI_s}{P'}}\sinh\sqrt{\frac{P'}{EI_s}}\,x_2+\frac{Q'}{P'}x_2-\frac{M''}{P'},$$

which, for small values of $\sqrt{\frac{P}{EI_s}}\,x_1$, and $\sqrt{\frac{P'}{EI_s}}\,x_2$, become

$$y_1=\frac{M}{EI_s}\frac{x_1^2}{2}\left\{1-\frac{1}{12}\left(\frac{P}{EI_s}\right)x_1^2+\frac{1}{360}\left(\frac{P}{EI_s}\right)^2x_1^4-\cdots.\right\}$$
$$+\frac{Q}{EI_s}\frac{x_1^3}{6}\left\{1-\frac{1}{20}\left(\frac{P}{EI_s}\right)x_1^2+\frac{1}{840}\left(\frac{P}{EI_s}\right)^2x_1^4-\cdots.\right\}, \quad \cdots\cdots\cdots(1.1)$$

$$y_2=-\frac{M''}{EI_s}\frac{x_1^2}{2}\left\{1+\frac{1}{12}\left(\frac{P'}{EI_s}\right)x_2^2+\frac{1}{360}\left(\frac{P'}{EI_s}\right)^2x_2^4+\cdots.\right\}$$
$$-\frac{Q}{EI_s}\frac{x_2^3}{6}\left\{1+\frac{1}{20}\left(\frac{P'}{EI_s}\right)x_2^2+\frac{1}{840}\left(\frac{P'}{EI_s}\right)^2x_2^4+\cdots.\right\}. \quad \cdots\cdots\cdots(1.2)$$

Case (1) $P_0=Q_0=M_0=0$:

Let us begin with a discussion of some particular case in which the problem is simplified. If we put $P_0=Q_0=M_0=0$, i.e., if there are no external forces and couples, the expressions (1.1), (1.2) can be reduced to

$$y_1=\frac{M}{EI_s}\frac{x_1^2}{2}\left\{1-\frac{1}{12}\left(\frac{P}{EI_s}\right)x_1^2+\cdots.\right\}$$
$$+\frac{Q}{EI_s}\frac{x_1^3}{6}\left\{1-\frac{1}{20}\left(\frac{P}{EI_s}\right)x_1^2+\cdots.\right\}, \quad \cdots\cdots\cdots(1.3)$$

$$y_2=\frac{1}{EI_s}\frac{x_2^2}{2}(-M+PD+Q\delta)\left\{1+\frac{1}{12}\left(\frac{P}{EI_s}\right)x_1^2+\cdots.\right\}$$
$$-\frac{Q}{EI_s}\frac{x_2^2}{6}\left\{1+\frac{1}{20}\left(\frac{P}{EI_s}\right)x_2^2+\cdots.\right\}. \quad \cdots\cdots\cdots(1.4)$$

First, keeping only the first term in the expansion, we can readily obtain the following approximate expressions:

$$\left.\begin{aligned} P&=\frac{2EI_s}{lD}\cdot\theta\cdot\left\{1+\frac{3}{2}\left(\frac{D}{l}\right)^2\theta^2\right\},\\ Q&=-\frac{2EI_s}{lD}\cdot\frac{3}{2}\left(\frac{D}{l}\right)^2\cdot\theta^2,\\ M&=\frac{EI_s}{l}\cdot\theta\left\{1+\frac{3}{2}\left(\frac{D}{l}\right)\theta\right\}. \end{aligned}\right\} \quad \cdots\cdots\cdots(1.5)$$

Next, keeping the first two terms in the expansion, the expressions (1.3), (1.4) become

$$y_1=\frac{M}{EI_s}\cdot\frac{x_1^2}{2}\left\{1-\frac{1}{12}\left(\frac{P}{EI_s}\right)x_1^2\right\}+\frac{Q}{EI_s}\cdot\frac{x_1^3}{6}\left\{1-\frac{1}{20}\left(\frac{P}{EI_s}\right)x_1^2\right\}, \qquad \cdots\cdots\cdots(1.6)$$

$$y_2=\frac{1}{EI_s}\cdot\frac{x_2^2}{2}(-M+PD+Q\delta)\left\{1+\frac{1}{12}\left(\frac{P}{EI_s}\right)x_2^2\right\} -\frac{Q}{EI_s}\cdot\frac{x_2^3}{6}\left\{1+\frac{1}{20}\left(\frac{P}{EI_s}\right)x_2^2\right\}. \qquad \cdots\cdots\cdots(1.7)$$

The geometrical relationship at $x_1=x_2=l$

$$\left(\frac{dy_1}{dx_1}\right)=\left(\frac{dy_2}{dx_2}\right)=\tan\theta\approx\theta \qquad \cdots\cdots\cdots(1.8)$$

gives

$$\frac{M}{EI_s}l-\frac{PM}{(EI_s)^2}\cdot\frac{l^3}{6}+\frac{Q}{EI_s}\cdot\frac{l^2}{2}-\frac{PQ}{(EI_s)^2}\cdot\frac{l^2}{24}=\theta,$$

$$\frac{l}{EI_s}(-M+PD+Q\delta)+\frac{P}{(EI_s)^2}\cdot\frac{l^3}{6}(-M+PD+Q\delta) -\frac{Q}{EI_s}\cdot\frac{l^2}{2}-\frac{PQ}{(EI_s)^2}\cdot\frac{l^4}{24}=\theta,$$

from which we obtain

$$Q=\frac{EI_s}{l}\cdot\frac{\left\{2\theta-\frac{PlD}{EI_s}+\frac{P^3D}{(EI_s)^3}\cdot\frac{l^5}{36}\right\}}{\left\{\delta+\frac{P}{EI_s}\cdot\frac{l^3}{12}-\frac{P^2\delta}{(EI_s)^2}\cdot\frac{l^4}{36}\right\}}, \qquad \cdots\cdots\cdots(1.9)$$

$$M=\frac{EI_s}{l}\cdot\frac{\left\{-l\theta+\delta\theta+\frac{Pl^2D}{2EI_s}+\frac{Pl^2\delta\theta}{6EI_s}+\frac{P^2l^4D}{24(EI_s)^2}-\frac{P^3l^6D}{144(EI_s)^2}\right\}}{\left\{\delta+\frac{P}{EI_s}\cdot\frac{l^3}{12}-\frac{P^2\delta}{(EI_s)^2}\cdot\frac{l^4}{36}\right\}} \qquad \cdots\cdots\cdots(1.10)$$

From the geometrical considerations, we con see that

$$\delta+\overline{A_1B_1'}=D\sin\theta+\overline{A_2B_2'},$$

or

$$\delta\approx D\theta, \qquad \cdots\cdots\cdots(1.11)$$

and

$$y_{1_{x_1=l}}+D\cos\theta=D+Y\,,$$

or

$$y_{1_{x_1=l}}-Y\approx\frac{D}{2}\theta^2\,. \qquad \ldots\ldots\ldots(1.12)$$

From the expressions (1.6), (1.7) and (1.8), we obtain

$$\frac{M}{EI_s}l^2+\frac{Q}{EI_s}\cdot\frac{l^3}{3}-\frac{Pl^2D}{2EI_s}-\frac{Ql^2\delta}{2EI_s}-\frac{P^2l^4D}{24(EI_s)^2}-\frac{PQl^4\delta}{24(EI_s)^2}=\frac{D}{2}\theta^2.$$

$$\ldots\ldots\ldots(1.13)$$

Introducing the expressions (1.9), (1.10) into Eq. (1.13) and using the expression (1.11), we obtain the equation from which the restoring force P has to be determined. Thus

$$f(P)=-\frac{l^7D}{864(EI_s)^3}\cdot P^3+\frac{l^4D^2\theta^3}{72(EI_s)^2}\cdot P^2+\frac{l^3D}{6EI_s}\cdot P-\frac{D^2}{2}\cdot\theta^3-\frac{l^2}{3}\theta=0\,.$$

Let the approximate solution of $f(P)=0$ be $\left(\frac{2EI_s}{lD}\theta+u\right)$, in which we know that u is small. Therefore the equation $f(P)=0$ becomes, on neglecting powers of u beyond the first,

$$f\left(\frac{2EI_s}{lD}\theta\right)+uf'\left(\frac{2EI_s}{lD}\theta\right)=0\,,$$

whence an approximate value of u is

$$u=-\frac{f\left(\frac{2EI_s}{lD}\theta\right)}{f'\left(\frac{2EI_s}{lD}\theta\right)}=\frac{2EI_s}{lD}\cdot\theta\cdot\frac{\left\{\frac{3}{2}\left(\frac{D}{l}\right)^2\theta^2+\frac{1}{36}\left(\frac{l}{D}\right)^2\theta^2\right\}}{\left\{1-\frac{1}{12}\left(\frac{l}{D}\right)^2\theta^2\right\}}\,.$$

Consequently, the approximate expression for P becomes

$$P=\frac{2EI_s}{lD}\cdot\theta\cdot\left[1+\frac{\left\{\frac{3}{2}\left(\frac{D}{l}\right)^2+\frac{1}{36}\left(\frac{l}{D}\right)^2\right\}}{\left\{1-\frac{1}{12}\left(\frac{l}{D}\right)^2\theta^2\right\}}\cdot\theta^2\right]=\frac{2EI_s}{lD}\theta\cdot(1+\alpha\theta^2)\,,$$

$$\ldots\ldots\ldots(1.14)$$

and introducing this into Eq. (1.9), (1.10) we obtain

$$Q=\frac{2EI_s}{lD}\cdot\theta^2\cdot\frac{\left\{-\frac{3}{2}\left(\frac{D}{l}\right)^2+\frac{1}{12}\left(\frac{l}{D}\right)^2\right\}}{\left\{1+\frac{1}{6}\left(\frac{l}{D}\right)^2\right\}}=\frac{2EI_s}{lD}\cdot\theta^2\cdot\beta\,,$$

$$\ldots\ldots\ldots(1.15)$$

and

$$M=\frac{EI_s}{l}\cdot\theta\cdot\left[1+\frac{\left\{\frac{3}{2}\left(\frac{D}{l}\right)+\frac{1}{3}\left(\frac{l}{D}\right)\right\}}{\left\{1+\frac{1}{6}\left(\frac{l}{D}\right)^2\right\}}\cdot\theta\right]=\frac{EI_s}{l}\cdot\theta\cdot(1+\gamma\theta)\,, \qquad \cdots\cdots\cdots(1.16)$$

in which α, β and γ are factors depending only on the ratio l/D. In Figs. (2), (3) and (4), the values of these factors are plotted against the ratio l/D.

Referring to Fig. (1), we see that the instantaneous center of rotation of the recording pen coincides with the point O where the tangents at the end B_2 and x_2-axis intersect. Then, the geometrical relationship gives

$$\overline{OB_2'}=\frac{Y}{\tan\theta}=\frac{1}{\theta}\left[\frac{l^2}{2EI_s}(-M+PD+Q\delta)\left\{1+\frac{1}{12}\left(\frac{P}{EI_s}\right)l^2\right\}-\frac{Ql^3}{6EI_s}\left\{1+\frac{1}{20}\left(\frac{P}{EI_s}\right)l^2\right\}\right]\doteqdot\frac{l}{2}\quad\text{approximately.}$$

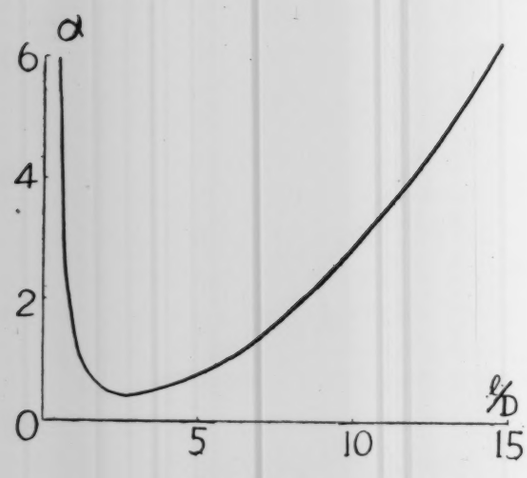

Fig. 2.

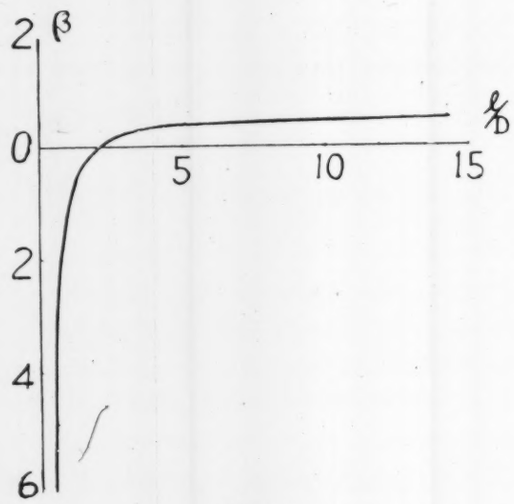

Fig. 3.

Accordingly, the center of rotation of the recording pen remains stationary at the point having the coordinate $x_2=l/2$ and $y_2=0$, i.e., at the mid-point of OB_2'.

In order to determine the validity of these expressions, detailed experiments[7] were carried out, and the experimental results confirmed

7) The results concerning the experiment will be reported in the Journal of the Faculty of Engineering, University of Tokyo, which will be published in the near future.

the validity of these expressions. On comparing these expressions for P, Q and M with the results in the expressions (1.5), we see that, for small value of $l/D(l/D \leqq 1)$, the first approximation differs very little from the second approximation, and that the first approximation differs from the second approximation only by small quantities of second order, so far as the expressions for P and M are concerned.

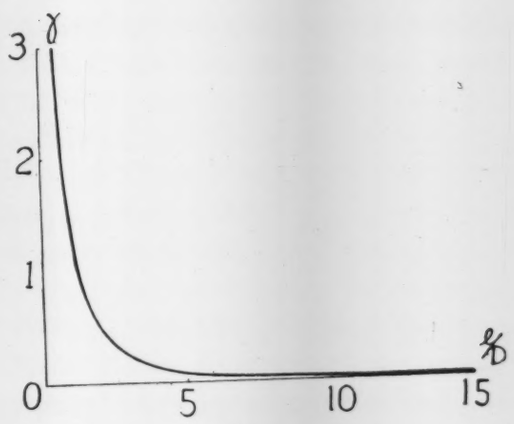

Fig. 4.

Case (2) P_0, Q_0, $M_0 \neq 0$.

In this case, keeping only the first term in the expansions, Eq. (1.1) becomes

$$y_1=\frac{M}{EI_s}\cdot\frac{x_1^2}{2}+\frac{Q}{EI_s}\cdot\frac{x_1^3}{6},$$

$$y_2=\frac{1}{EI_s}\cdot\frac{x_2^2}{6}(-M_0-M+PD-P_0Y+Q_0\delta+Q_0l)$$

$$-\frac{Q_0}{EI_s}\cdot\frac{x_2^3}{2}-\frac{Q}{EI_s}\cdot\frac{x_2^3}{6}.$$

The geometrical relationships (1.5) and (1.8) give

$$\frac{M}{EI_s}l+\frac{Q}{EI_s}\cdot\frac{l^2}{2}=\theta,$$

$$\frac{1}{EI_s}(-M_0l-P_0lY-Ml+PlD+Ql\delta+Q_0l^2)$$

$$-\frac{Q_0}{EI_s}\cdot\frac{l^2}{2}-\frac{Q}{EI_s}\cdot\frac{l^2}{2}=\theta,$$

$$\frac{M}{EI_s}\cdot\frac{l^2}{2}+\frac{Q}{EI_s}\cdot\frac{l^3}{6}-Y=\frac{D}{2}\theta^2,$$

$$Y=\frac{1}{EI_s}\cdot\frac{l^2}{2}(-M_0-M+PD-P_0Y+Q\delta+Q_0l)$$

$$-\frac{Q_0}{EI_s}\cdot\frac{l^3}{6}-\frac{Q}{EI_s}\cdot\frac{l^3}{6}.$$

Solving these equations for P, Q, M and Y algebraically, we obtain the following approximate expressions for P, Q, M and Y:

$$P=\frac{2EI_s}{lD}\left\{1+\frac{3}{2}\left(\frac{D}{l}\right)^2\theta^2\right\}+\frac{M_0}{D}-\frac{Q_0}{2}\cdot\frac{l}{D}\left\{1-\frac{D}{l}\cdot\theta\right\}$$
$$+\frac{P_0Q_0}{D}\cdot\frac{l^3}{24EI_s}+P_0\frac{l}{2D}\theta\left\{1-\frac{1}{2}\left(\frac{D}{l}\right)\theta\right\},$$
$$Q=-\frac{3EI_s}{lD}\cdot\left(\frac{D}{l}\right)^2\cdot\theta^2+\frac{Q_0}{2},$$
$$M=\frac{EI_s}{l}\cdot\theta\cdot\left\{1+\frac{3}{2}\left(\frac{D}{l}\right)\theta\right\}+\frac{Q_0l}{4},$$
$$Y=\frac{l}{2}\theta\left\{1-\frac{1}{2}\left(\frac{D}{l}\right)\theta\right\}+Q_0\frac{l^3}{24EI_s}.$$

For small value of $(D/l)\cdot\theta$, we can neglect the term containing $(D/l)\cdot\theta$ compared with unity. In this way, we obtain the simplified expressions

$$P=\frac{2EI_s}{lD}\theta+\frac{M_0}{D}-\frac{Q_0}{2}\cdot\frac{l}{D}+\frac{P_0Q_0}{D}\cdot\frac{l^3}{24EI_s}+P_0\frac{l}{2D}\theta,$$
$$Q=-\frac{Q_0}{2}-\frac{3EI_s}{lD}\cdot\left(\frac{D}{l}\right)^2\theta^2,$$
$$M=\frac{Q_0}{4}l+\frac{EI_s}{l}\theta,$$
$$Y=\frac{l}{2}\theta+\frac{Q_0l^4}{24EI_s}.$$

In our further discussions, these simplified expressions for P and Y shall be used for the derivation of the equation of motion for the twin strips mechanism.

3. Dynamical Characteristics.

The twin strips have such a wide range of freedom that the rigorous discussion of their dynamical characteristics is a matter of great difficulty. However, from preliminary experiments using a vibration table, it was ascertained that, for an increasing forced frequency, various kinds of resonance, involving a local resonance of strips, occurred successively, and that, under the tacit assumptions that the ratio (l/D)

is relatively small ($l/D<5$) and the center of gravity of the recording pen situated in the vicinity of the center of rotation of the twin strips, the first resonance occurred close to the resonant frequency corresponding to that of the shearing vibration of the twin strips, the mode of which is shown diagrammatically in Fig. 5. Hereafter we will describe this resonant frequency of the shearing vibration as the natural frequency of the twin strips. Accordingly, the working frequency of the twin strips, i.e., the frequency at which the twin strips can be regarded as a perfect magnifying mechanism, should be lower than the natural frequency of the twin strips. From these considerations, when we restrict our discussion to the frequency range smaller than the natural frequency of the twin strips, the following two assumptions may be acceptable: (1) The mass of strips can be neglected, (2) the angle of rotation θ of the recording pen is always proportional to the displacement δ of the movable end ($D\theta=\delta$).

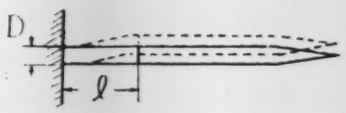

Fig. 5.

Now, in Fig. 6, the general arrangement of the vibrograph with Eden's twin strips is shown schematically. The seismic mass (A) is suspended to the base plate (B) by means of the main springs (C), having the damping apparatus (D). The direction of motion of the seismic mass (A) is restricted to one direction (x-direction) entirely by a suitable guiding device, not shown in the figure. The recording pen (F) attached to the twin strips mechanism (E) gives the trace of vibrations on the recording apparatus (G). The twin strips perform the function as a magnifying mechanism and at the same time produce the additional restoring force, in addition to that of the main springs.

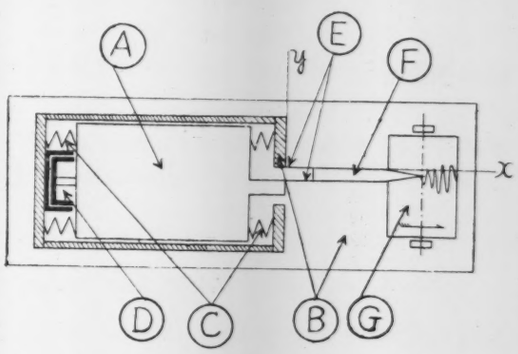

Fig. 6.

Let us take, as shown in Fig. 6, the moving coordinate to be (x, y) fixed to the base plate and assume, for simplicity's sake, that the center of gravity G of the recording pen lies on the tangent at the end B_2 and at a distance r from the end B_2. Then the coordinates of the center of gravity G are

$$x=r\cos\theta, \quad y=l+r\sin\theta+Y.$$

Considering θ and its derivatives with respect to time as small quantities and neglecting terms containing products and powers of small quantities, we obtain

$$\ddot{x}\approx 0, \qquad \ddot{y}\approx r\ddot{\theta}+\ddot{Y}.$$

Let m denote the mass of the recording pen, I the moment of inertia of the recording pen with respect to the center of gravity G, P_0 and Q_0 the component of the reaction force at the end B_2 in x-and y-direction, respectively, M_0 the reaction couple at the same point, P the reaction force at the clamped end A_1 in x-direction, and v_x and v_y the component of the displacement of the forced vibrations in x- and y-direction, respectively. With the arrangement shown in Fig. 6, v_x corresponds to the displacement of the vibration to be measured. Furthermore, let the member B_1B_2 be massless and absolutely rigid, as before. Referring to Fig. 7a, the equations of motion for the recording pen can be written in the form

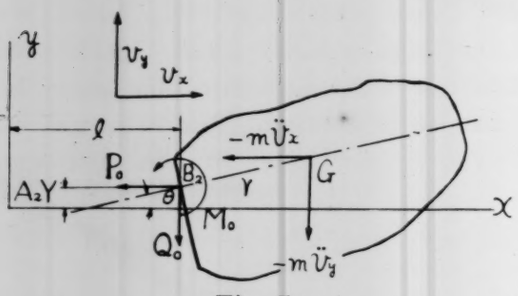

Fig. 7a.

$$m\ddot{x}=-P_0-m\ddot{v}_x=0, \quad \cdots\cdots\cdots\cdots\cdots\cdots \quad (3.1)$$

$$m\ddot{y}=m(r\ddot{\theta}+\ddot{Y})=-Q_0-m\ddot{v}_y, \quad \cdots\cdots\cdots\cdots \quad (3.2)$$

$$I\ddot{\theta}=Q_0r+M_0-P_0r\theta. \quad \cdots\cdots\cdots\cdots\cdots\cdots \quad (3.3)$$

Next, let M denote the mass of the seismic mass, δ its displacement from the equilibrium position, k the spring constant of the main spring, and R the damping constant. Then, referring to Fig. 7c, the equation of motion for the pendulum can be written in the form

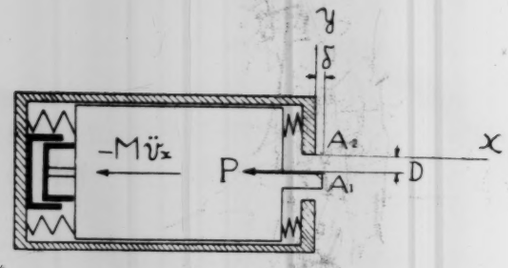

Fig. 7c.

$$M\ddot{\delta}+R\dot{\delta}+k\delta+P=-M\ddot{v}_x.$$

The above assumptions give

$$\delta=D\theta,$$

from which the equation of motion for the pendulum can be reduced to

$$MD\ddot{\theta}+RD\dot{\theta}+kD\theta+P=-M\ddot{v}_x. \quad \cdots\cdots\cdots\cdots \quad (3.4)$$

Referring to Fig. 7b, as derived above, the approximate expressions for P and Y are

$$P=\frac{2EI_s}{lD}\theta+\frac{M_0}{D}-\frac{Q_0 l}{2D}+P_0 Q_0\frac{l^3}{24EI_s}$$
$$+P_0\frac{l}{2D}\theta\,, \quad \cdots\cdots\cdots\cdots \quad (3.5)$$

$$Y=\frac{l}{2}\theta+Q_0\frac{l^3}{24EI_s}\,. \quad \cdots\cdots\cdots\cdots \quad (3.6)$$

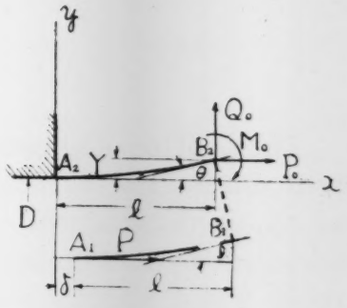

Fig. 7b.

Eliminating P, P_0, Q_0, and M_0 from the equations (3.1), (3.2), (3.3), (3.4), and the expression (3.5), and using the notations

$L=l/2+r$=distance between the center of gravity G and the center of rotation O,

$K=k+2EI_s/(lD^2)$=effective spring constant,

we, after neglecting $\frac{ml^2}{12EI_s}\cdot\ddot{v}_x$ and $\frac{mL}{KD^2}\ddot{v}_y$ compared with unity, obtain

$$\ddot{\theta}\left(MD+\frac{I}{D}+\frac{m}{D}rL\right)+RD\dot{\theta}+\ddot{Y}\frac{m}{D}L+KD\theta=-M\ddot{v}_x-\ddot{v}_y\frac{m}{D}L. \quad (3.7)$$

Eliminating Q_0 from the equation (3.2) and the expression (3.6), we obtain

$$Y=\frac{l}{2}\theta-\frac{ml^3}{24EI_s}\cdot\ddot{v}_y-\frac{ml^3}{24EI_s}r\ddot{\theta}-\frac{ml^3}{24EI_s}\ddot{Y}. \quad \cdots\cdots\cdots \quad (3.8)$$

Eliminating Y and its derivatives with respect to time t from the equation (3.7) and the expression (3.8), and using the notations

$$M_0=M+\frac{I}{D^2}\,, \quad M_e=M_0+m\frac{L^2}{D^2}\,, \quad \rho=\frac{ml^3}{24EI_s}\,,$$

we obtain

$$M_0\dddot{\theta}+R\ddot{\theta}+\ddot{\theta}\left(K+\frac{M_e}{\rho}\right)+\frac{R}{\rho}\dot{\theta}+\frac{K}{\rho}\theta=-\frac{M}{D}\dddot{v}_x-\frac{M}{D\rho}\ddot{v}_x-\frac{m}{D^2}\cdot\frac{L}{\rho}\cdot\ddot{v}_y\,. \quad (3.9)$$

Eliminating θ and its derivatives with respect to time t from the equation (3.7) and the expression (3.8) and neglecting $\frac{\rho}{K}\cdot\frac{mL}{D^2}\cdot\dddot{v}_y$ compared with unity, we obtain

$$M_0\dddot{Y}+R\ddot{Y}+\dot{Y}\left(K+\frac{M_e}{\rho}\right)+\frac{R}{\rho}\dot{Y}+\frac{K}{\rho}Y=-\frac{M}{\rho}\cdot\frac{l}{2D}\cdot\ddot{v}_x$$

$$+\frac{M}{D}r\dddot{v}_x-\left(M_0+\frac{mLr}{D^2}\right)\ddot{v}_y-R\dot{v}_y-K\left(1+\frac{m}{K\rho}\cdot\frac{Ll}{D^2}\right)\cdot\dot{v}_y. \quad \text{.. (3.10)}$$

Thus, after disregarding all non-linearities, we obtain these two linear differential equations from which the dynamical characteristics has to be determined. In analysing these differential equations, it is convenient to distinguish between an acceleration seismograph (accelerograph) and a displacement seismograph (vibrograph). In a displacement seismograph, on account of its low natural frequency, the restoring force is usually limited to within a relatively low limit. Therefore, the additional restoring force of the twin strips also must be small, and this requirement is not consistent with the demand for a wide working frequency range of the twin strips. In an acceleration seismograph, on the other hand, its considerably high natural frequency enables the twin strips to perform their proper function up to the maximum frequency which can be measured without difficulty.

Case (1) Displacement-Seismograph

Now we will consider the forced vibration only and disregard the transient free vibrations and assume that the forced vibration is a harmonic vibration with circular frequency ω. Then we can put

$$v_x=V_xe^{j\omega t},$$
$$v_y=V_ye^{j\omega t},$$
$$\theta=\theta_me^{j\alpha}e^{j\omega t}=\Theta e^{j\omega t},$$
$$y=y_me^{j\beta}e^{j\omega t}=\mathfrak{Y}e^{j\omega t},$$

where α and β are a phase angle, Θ and $\mathfrak{Y}$ being generally complex numbers.

Introducing these expressions and their derivatives with respect to time into the equations (3.9) and (3.10) and introducing the notations

$$f^*=\frac{1}{2\pi}\sqrt{\frac{K}{M_e}}=\text{natural frequency of the pendulum,}$$

$$f_0=\frac{1}{2\pi}\sqrt{\frac{24EI_s}{ml^3}}=\frac{1}{2\pi}\sqrt{\frac{1}{\rho}}=\text{natural frequency of the twin strips,}$$

$$f=\omega/2\pi=\text{frequency of the forced vibration,}$$

$$u=f^*/f=\text{frequency ratio,}$$

$\mu = f/f_0$ = frequency ratio,

and

$$h = \frac{R}{2\sqrt{M_e K}} = \text{damping constant},$$

we obtain

$$\mathfrak{Y} = \frac{\frac{M}{M_e}\cdot\frac{l}{2D}\cdot V_x\cdot\left(1-\frac{2r}{l}\mu^2\right)}{\left\{(1-\mu^2)(u^2-1+j2hu)-\mu^2\left(\frac{M_e-M_0}{M_0}\right)\right\}}$$

$$-\rho V_y\omega^2\cdot\frac{\left[\left\{1+\frac{m}{M_e}\cdot\frac{L}{D^2}\cdot(r-L)\right\}+j2hu+u^2\left(1+\frac{m}{\rho K}\cdot\frac{lL}{2D^2}\right)\right]}{\left\{(1-\mu^2)(u^2-1+j2hu)-\mu^2\left(\frac{M_e-M_0}{M_0}\right)\right\}}, \quad \cdots\cdots\cdots (3.11)$$

$$\Theta = \frac{\frac{M}{M_e}\cdot\frac{1}{D}\cdot V_x(1-\mu^2)}{\left\{(1-\mu^2)(u^2-1+j2hu)-\mu^2\left(\frac{M_e-M_0}{M_0}\right)\right\}}$$

$$-\frac{\frac{m}{M_e}\cdot\frac{L}{D^2}\cdot V_y}{\left\{(1-\mu^2)(u^2-1+j2hu)-\mu^2\left(\frac{M_e-M_0}{M_0}\right)\right\}}. \quad \cdots\cdots (3.12)$$

From these expressions, the amplitude Θ and $\mathfrak{Y}$ of the forced vibration can be calculated for any value of μ or u. In a displacement seismograph, it is essential that the natural frequency f^* of the pendulum should be lower (slower) than the minimum frequency to be measured and the natural frequency f_0 of the twin strips higher than the maximum frequency to be measured. The natural frequency f_0 of the twin strips, therefore, should be very much higher than the natural frequency f^* of the pendulum and μ, for low frequency near or lower than the natural frequency $f^*(u \geqq 1)$, can be considered as small quantity. Consequently, the expressions (3.11), (3.12), for small values of $\frac{M_e-M_0}{M_0}$ and $\frac{2r}{l}$ which we usually have, can be expressed in the approximate form

$$\mathfrak{Y}=\frac{-\frac{M}{M_e}\cdot\frac{l}{2D}V_x}{(u^2-1+j2hu)}$$
$$-\rho V_y\omega^2\cdot\frac{\left[\left\{1+\frac{m}{M_e}\cdot\frac{L}{D^2}(r-L)\right\}+j2hu+u^2\left(1+\frac{m}{\rho K}\cdot\frac{Ll}{2D^2}\right)\right]}{(u^2-1+j2hu)}, \quad \cdots\cdots\cdots (3.13)$$

$$\Theta=\frac{-\frac{M}{M_e}\cdot\frac{1}{D}V_x}{(u^2-1+j2hu)}+\frac{-\frac{m}{M_e}\cdot\frac{L}{D^2}\cdot V_y}{(u^2-1+j2hu)}. \quad \cdots\cdots\cdots\cdots\cdots (3.14)$$

The second terms of these equations represent the undesirable displacement for which the transverse component V_y of the forced vibration is responsible. In order to perform the proper function as a magnifying mechanism, it is neccessary that these undesirable terms should be made negligible compared with the first terms. Fortunately, in most cases, these terms can be made negligible by proper dimensioning. When these requirements are fulfilled, the first terms indicate that the twin strips can be regarded as a perfect magnifying mechanism, i.e., the recording pen rotates about the point O having the coordinates $x=\frac{l}{2}$ and $y=O$ and its short arm is equal to D.

Next, for the frequency range above the natural frequency f^* of the pendulum, i.e., for the working frequency-range of a displacement seismograph ($u<1$), it is well known that

$$(u^2-1+j2h)\approx -1.$$

For such frequency range, introducing the new notations

$$a=\frac{\left(1-\frac{2r}{l}\mu^2\right)}{\left(1-\mu^2\cdot\frac{M_0}{M_e}\right)}, \qquad b=\frac{(1-\mu^2)}{\left(1-\mu^2\cdot\frac{M_0}{M_e}\right)},$$

Eq. (3.11) can be expressed in the approximate form

$$\mathfrak{Y}=-\frac{M}{M_e}\cdot\frac{l}{2D}\cdot V_x\cdot a-\rho\omega^2 V_y\cdot\frac{\left\{1+\frac{m}{M_e}\cdot\frac{L}{D^2}\cdot(r-L)+u^2\frac{m}{\rho K}\cdot\frac{Ll}{2D^2}\right\}}{\left(1-\mu^2\frac{M_0}{M_e}\right)}, \quad \cdots\cdots\cdots (3.15)$$

$$\Theta = -\frac{M}{M_e}\cdot\frac{1}{D}\cdot V_x\cdot b - \frac{m}{M_e}\cdot\frac{L}{D^2}\cdot\frac{1}{\left(1-\mu^2\frac{M_0}{M_e}\right)} \quad \ldots\ldots\ldots\ldots \quad (3.16)$$

When the second terms of these equations can be made negligible compared with the first terms, as before, the first terms define the dynamical characteristics of the twin strips. In Fig. 8, the values of the magnification factor b for various values of M_0/M_e are plotted against the frequency ratio μ, and in Fig. 9, the values of the magnification factor

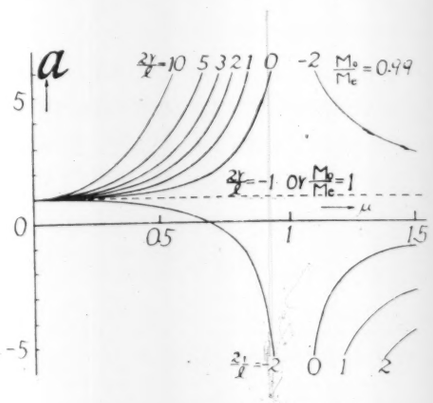

Fig. 8.

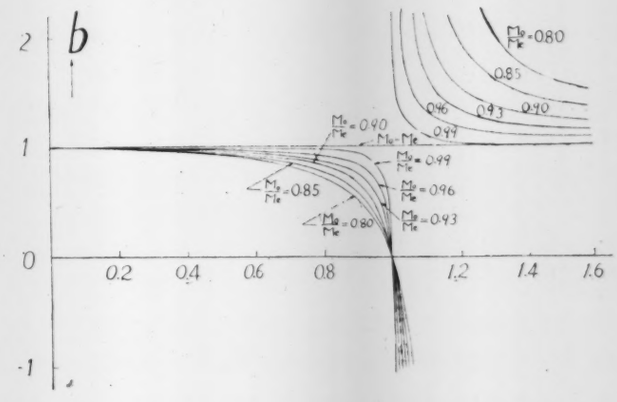

Fig. 9.

a for various values of $2r/l$ are plotted against the frequency ratio μ for a particular case in which $M_0/M_e=0.99$.

In a optical record, the recorded magnitude depends only upon Θ, i.e., for the frequencies at which the magnification factor b differs only slightly from unity, the twin strips can perform their proper function.

In mechanical records, the recorded magnitude depends upon Θ as well as $\mathfrak{y}$. Referring to Fig. 10, the displacement of the tip of the recording pen of length l_0 becomes

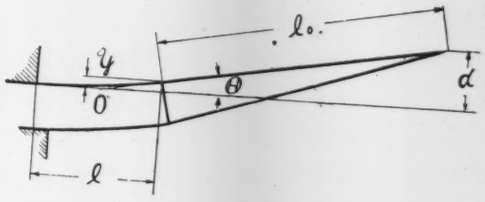

Fig. 10.

$$d=\mathfrak{y}+\Theta\cdot l_0\cdot=\frac{M_0}{M_e}\cdot\frac{V_x}{D}\cdot\left(l_0+\frac{l}{2}\right)\cdot c, \quad \ldots\ldots\ldots \quad (3.17)$$

in which

$$c=\left\{1-\mu^2\cdot\frac{l_0-r}{l_0+l/2}\right\}\Big/\left\{1-\mu^2\cdot\frac{M_0}{M_e}\right\}. \quad \ldots\ldots\ldots \quad (3.18)$$

In this case, for the frequencies at which the magnification factor

c differs only slightly from unity, the twin strips can be regarded as a complete magnifying mechanism, in which the effective length of the recording pen is $(l/2+l_0)$ and the short arm D.

In Fig. 11, the values of the magnification factor c for various values of $(2r/l)$ are plotted against the frequency ratio μ for a particular case in which $l_0=10$ cm, $l=1$ cm, and $M_0/M_e=0.99$. The dotted line corresponds to the particular case in which $M_0/M_e=1$ or $2r/l=-1(L=0)$.

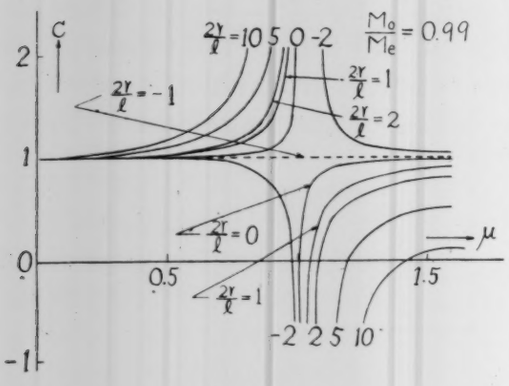

Fig. 11.

By proper dimensioning, we can improve the dynamical characteristics. Now, if we put $L=0$ or $2r/1=-1$, the expression (3.15), (3.16) can be expressed in the more simplified form

$$\Theta=-\frac{M}{M_e}\cdot\frac{1}{D}\cdot V_x, \quad \cdots\cdots\cdots\cdots\cdots\cdots\cdots \quad (3.19)$$

$$\mathfrak{Y}=-\frac{M}{M_e}\cdot\frac{l}{2D}\cdot V_x-\frac{\rho\omega^2 V_y}{(1-\mu^2)}. \quad \cdots\cdots\cdots\cdots\cdots \quad (3.20)$$

In this case, if the transverse component V_y of the forced vibration vanishes, the magnification of the twin strips may be independent of the forced frequency f. The undesirable second term, however, becomes extremely large as the forced frequency f approaches the natural frequency f_0 of the twin strips ($\mu\approx 1$). Therefore the maximum working frequency of the twin strips should be lower than the natural frequency f_0 of the twin strips, but in most cases can be extended to $0.9\ f_0$. Thus, in order to expand the working frequency range of the twin strips, it is effective to make L as small as practicable.

The magnitude of this undesirable term is equivalent to the displacement of the recording pen for a particular case in which the seismic mass is rigidly clamped to the base plate in its equilibrium position, and can be determined experimentally by the use of a vibration table.

Case (2) Acceleration Seismograph

In a acceleration seismograph, after rearranging, the expressions (3.11), (3.12) can be reduced to

$$\mathfrak{Y}=\frac{\omega^2 V_x}{(2\pi f^*)^2}\cdot\frac{M}{M_e}\cdot\frac{l}{2D}\cdot\frac{\left(1-\frac{2r}{l}\mu^2\right)}{\left\{(1-\mu^2)\left(1-\frac{1}{u^2}+j\frac{2h}{u}\right)-\frac{\mu^2}{u^2}\left(\frac{M_e-M_0}{M_0}\right)\right\}}$$
$$+\rho V_y\omega^2\cdot\frac{\left[\left(1+\frac{m}{\rho K}\cdot\frac{Ll}{2D^2}\right)-\frac{1}{u^2}\left\{1+\frac{m}{M_e}\cdot\frac{L}{D^2}(r-L)\right\}+j\frac{2h}{u}\right]}{\left\{(1-\mu^2)\left(1-\frac{1}{u^2}+j\frac{2h}{u}\right)-\frac{\mu^2}{u^2}\left(\frac{M_e-M_0}{M_0}\right)\right\}}, \quad (3.21)$$

$$\Theta=\frac{\omega^2 V_x}{(2\pi f^*)^2}\cdot\frac{M}{M_e}\cdot\frac{1}{D}\cdot\frac{(1-\mu^2)}{\left\{(1-\mu^2)\left(1-\frac{1}{u^2}+j\frac{2h}{u}\right)-\frac{\mu^2}{u^1}\left(\frac{M_e-M_0}{M_0}\right)\right\}}$$
$$+\frac{\omega^2 V_y}{(2\pi f^*)^2}\cdot\frac{m}{M_e}\cdot\frac{L}{D^2}\cdot\frac{1}{\left\{(1-\mu^2)\left(1-\frac{1}{u^2}+j\frac{2h}{u}\right)-\frac{\mu^2}{u^2}\left(\frac{M_e-M_0}{M_0}\right)\right\}}. \quad \ldots\ldots\ldots (3.22)$$

Now, it is desirable that the natural frequency f_0 of the twin strips should be at least several times larger than the natural frequency f^* of the pendulum, and this, on account of high natural frequency of an acceleration seismograph, is always possible. As is well known, for the working frequency of an acceleration seismograph the value of $(1-1/u^2+j2h/u)$ differs only slightly from unity and this occurs when the frequency to be measured is low as compared with the natural frequency f^* of the pendulum. Then, for such frequency range (working frequency range), $1/u^2$ and μ^2 can be neglected compared with unity. Consequently, the expressions (3.21), (3.22) can be expressed in the approximate form

$$\mathfrak{Y}=\frac{\omega^2 V_x}{(2\pi f^*)^2}\cdot\frac{M}{M_e}\cdot\frac{l}{2D}+\rho\omega^2 V_y\left(1-\frac{m}{\rho K}\cdot\frac{Ll}{2D^2}\right), \quad \ldots. (3.23)$$

$$\Theta=\frac{\omega^2 V_x}{(2\pi f^*)}\cdot\frac{M}{M_e}\cdot\frac{1}{D}+\frac{\omega^2 V_y}{(2\pi f^*)^2}\cdot\frac{m}{M_e}\cdot\frac{L}{D^2}. \quad \ldots\ldots\ldots (3.24)$$

When the second terms of these equation can be neglected compared with the first terms, as before, the first term indicates that the twin strips can perform their proper function. Moreover, if we put $L=0$ or $2r/l=-1$, these expressions can be expressed in the more simplified form

$$\mathfrak{Y}=\frac{\omega^2 V_x}{(2\pi f^*)^2}\cdot\frac{M}{M_e}\cdot\frac{l}{2D}+\rho\omega^2 V_y, \quad \ldots\ldots\ldots\ldots (3.25)$$

$$\Theta = \frac{\omega^2 V_x}{(2\pi f^*)} \cdot \frac{M}{M_e} \cdot \frac{1}{D} \quad \cdots\cdots\cdots\cdots\cdots\cdots \quad (3.26)$$

Thus, in an acceleration seismograph, we need only make the natural frequency f_0 of the twin strips at least several times larger than the natural frequency f^* of the pendulum, which is always possible.

Experiment :

1) Vibration table :

We investigated the foregoing theory by an experiment using a vibration table, of which the constructional details are given in Figs. 12

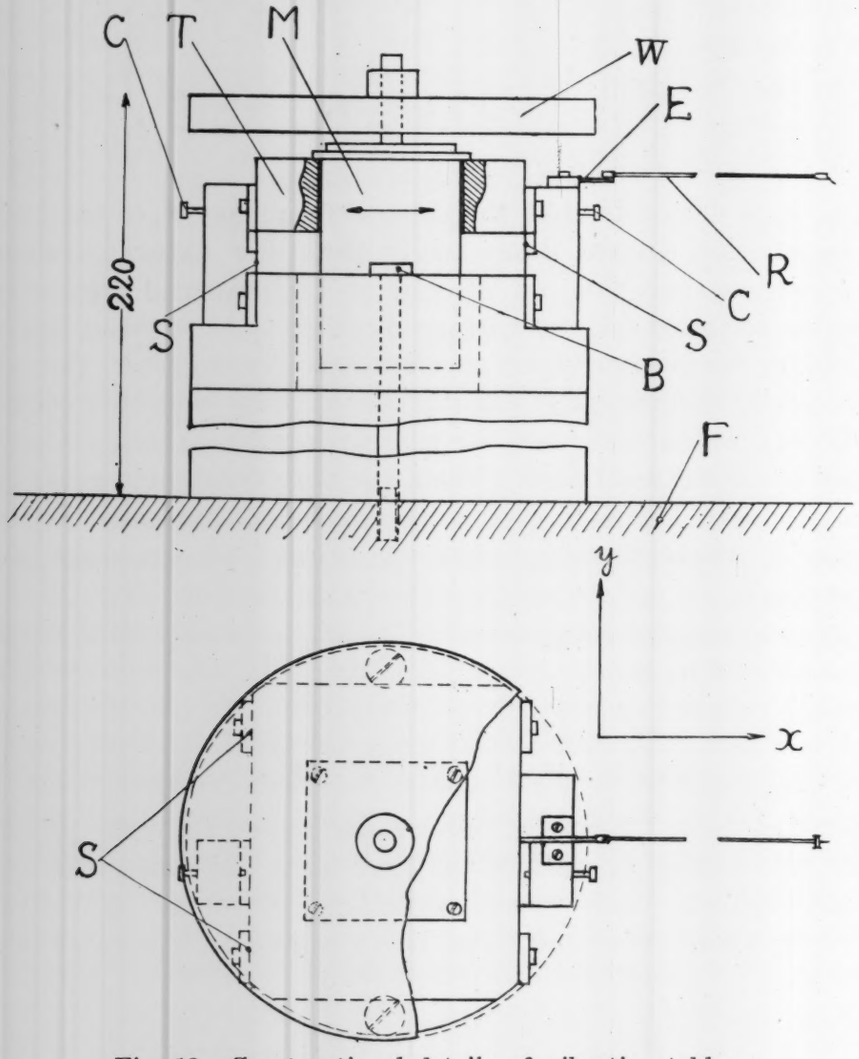

Fig. 12. Constructional details of vibration table.

and 13. The purposely unbalanced fly-wheel W of aluminum-alloy, 15 cm. in diameter and 810 g. in weight, is directly coupled to an axle of a small D.C. motor M fed by 24 V. battery. This motor is firmly bolted to a rigid table T of aluminum-alloy, 12 cm. wide by 10 cm. long by 3 cm. thick. A table T is held between two pairs of flat paralled phosphor-bronze strips S. Eacn strip is 0.025 cm. thick by 0.5 cm. wide by 1.5 cm. long. By means of this simple flat strips suspension the direction of motion of the seismic element is restricted to the x-direction entirely without friction, but some reduction in lateral (y-direction) and torsional stability of the suspension may be involved. However, no appreciable instability (shimmering) was observed concerning this experiment. The natural frequency of the suspension was found to be about 4 c/s. The recording pen R is attached to Eden's twin strips E to be tested, and the movement of the tip of the recording pen is recorded on smoked paper wound upon a drum driven by Warren synchronous motor (6 W). Damping is not intentionally provided ($h=0$), but moderate damping is desirable to reduce the free vibration caused by external vibrations. The seismic element may be clamped by a clamping screw C. The base plate P of aluminum-alloy is rigidly bolted to a massive foundation F of cast-iron by means of two long bolts B. The vibrational frequency of the vibration table can be controlled by varying the rotational speed of a motor M, and the vibrational frequency available in our experiments were of the range 2 c/s to 80 c/s.

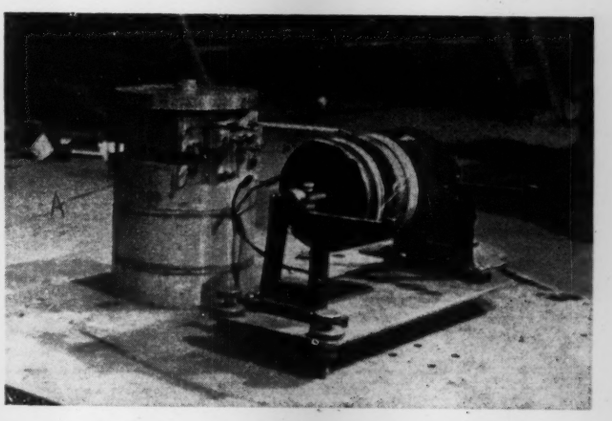

Fig. 13. General view of vibration table.

2) Experiment method and results:

The twin strips used in these experiments were constructed of a main spring of a wrist watch (special steel) by soldering, and had the following dimensions: Length l, 1.9 cm.: width, 0.14 cm.: thickness, 0.009 cm.; distance between both strips D, 0.38 cm.: length ratio l/D, 5. The recording pen was of straw, and its full length l_0 was 10 cm. The magnification of the movements of the seimic element at the tip of the recording pen was about 26 times. Although the experiments were

made for various values of $2r/l$ as shown in Table I, the mass m of the recording pen was kept constant ($m=3.5$ g.) throughout the experiments, and hence the natural frequency f_0 of the twin strips, defined by the formula

$$f_0=\frac{1}{2\pi}\cdot\sqrt{\frac{24EI_s}{ml^3}}\ ,$$

was also kept constant ($f_0=19$ c/s).

Table I.

Case	I	II	III	IV
$2r/l$	+2.1	−0.02	−0.40	−0.65
M_0/M_e	0.99	0.99	0.99	0.99

The original data recorded on smoked papers were generally of the type shown in Fig. 14, which corresponds to Case I.

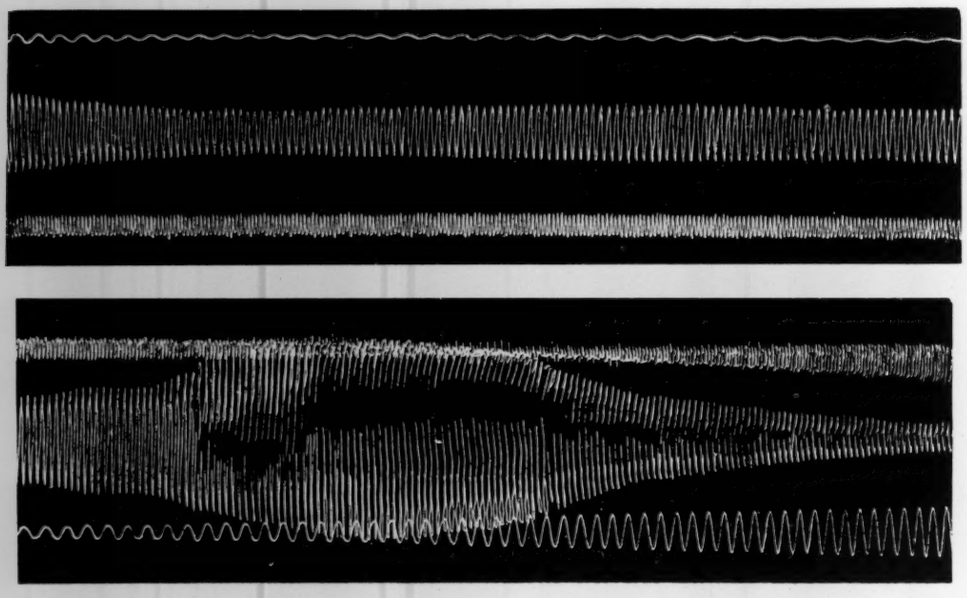

Fig. 14. Forced vibration of Case I at different vibrational frequency.

With the vibration table just mentioned, the expression (3.17), obtained previously for a displacement seismograph, may be readily reduced to

$$d=\mathfrak{Y}+\Theta l_0=\frac{\overline{mr}}{\left(M+\frac{I}{D^2}+m\frac{L^2}{D^2}\right)}\cdot\frac{\left(l_0+\frac{l}{2}\right)}{D}\cdot\frac{1-\left(\frac{f}{f_0}\right)^2\cdot\frac{l_0-r}{\left(l_0+\frac{l}{2}\right)}}{1-\left(\frac{f}{f_0}\right)^2\cdot\frac{\left(M+\frac{I}{D^2}\right)}{\left(M+\frac{I}{D^2}+m\frac{L^2}{D^2}\right)}},$$

$$\mu=f/f_0, \qquad L=l/2+r,$$

in which $\overline{mr}$ denotes the unbalanced moment of the fly-wheel, M the total mass of the seismic element (the table T, a motor M, and the fly-wheel F together), and the other symbols have the same meanings as before. This equation holds, of course, only when the vibrational frequency f is much higher than the natural frequency f^* of the vibration table (suspension). In Figs. 15~18, the absolute values of d calculated from this equation for various values of $2r/l$ are shown by

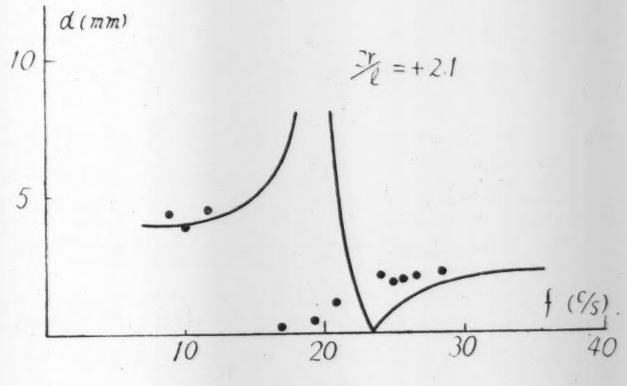

Fig. 15

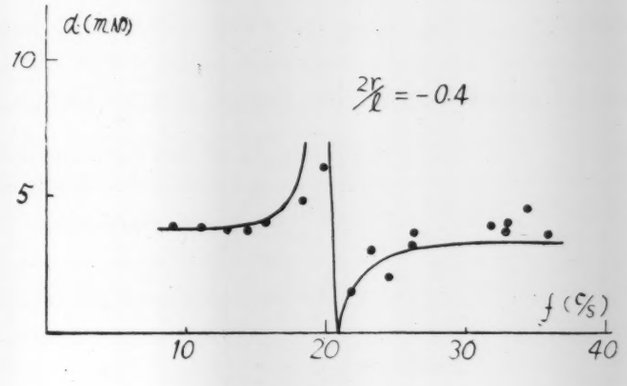

Fig. 16

full lines, while the plottings show the value obtained by experiments.

From Figs. 15~18, it will be seen that the two values, theoretical and experimental, are in fair accord, particularly at the working frequency range of the twin strips.

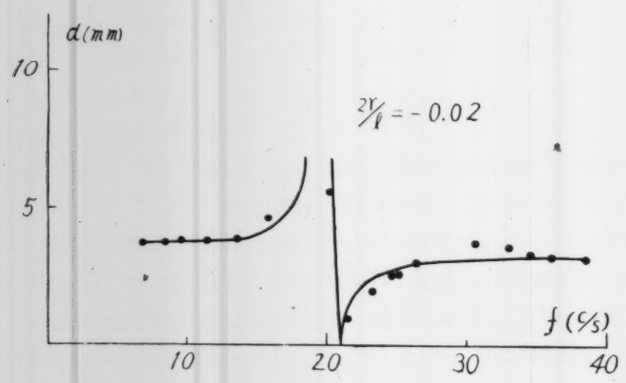

Fig. 17.

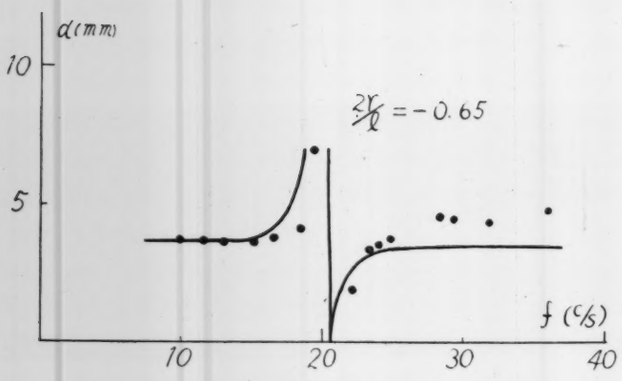

Fig. 18.

Finally, comparison was made between the seismogram of ordinary seismograph and that of the seismograph with twin strips. These two seismographs were installed at the same place (Earthquake Research

Table II. Instrumental Constants of the Seismographs

Kinds \ Constants	Natural Period (sec)	Magnification	Damping ratio
Seismograph with Eden's twin strips	1.0	110	13:1
Seismograph with commonly used magnifying mechanism	1.0	98	10:1

Institute), and had nearly the same instrumental constants as shown in Table II.

The commonly used magnifying mechanism of ordinary inverted pendulum seismograph was replaced by Eden's twin strips mechanism as shown in Figs. 19 and 20, and the supporting spring and twin strips were designed so as to make the natural frequency and the magnification nearly equal to those of the seismograph to be compared.

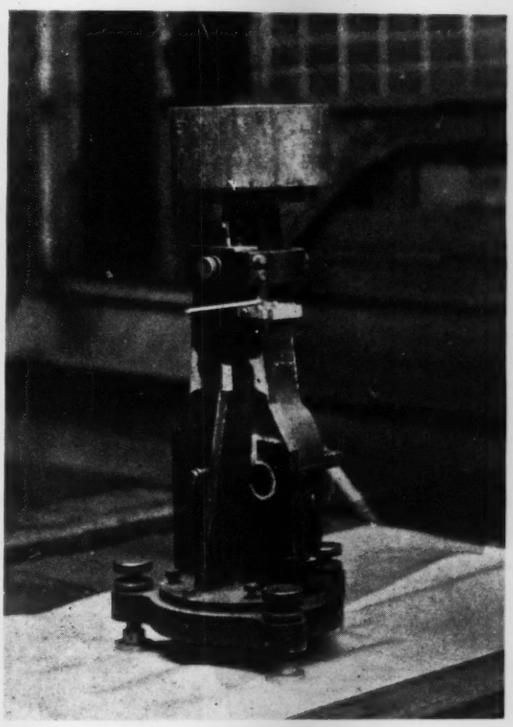

Fig. 19. Inverted Pendulum Seismograph with Eden's Twin Strips Composed of X-ray Photographic Film.

Eden's twin strips attached to this seismograph were of x-ray photographic film in order to minimize the additional restoring force of twin strips, and had the following dimensions: Length l, 1.4 cm.: width, 0.2 cm.: thickness, 0.02 cm.: distance between both strips D, 0.1 cm.: length ratio l/D, 14. The theoretically assumed maximum working frequency of twin strips was about 30 c/s.

In Figs. 21a and 21b, the typical seismograms are shown which were caused by the earthquake of December 7, 1953. Fig. 21a cor-

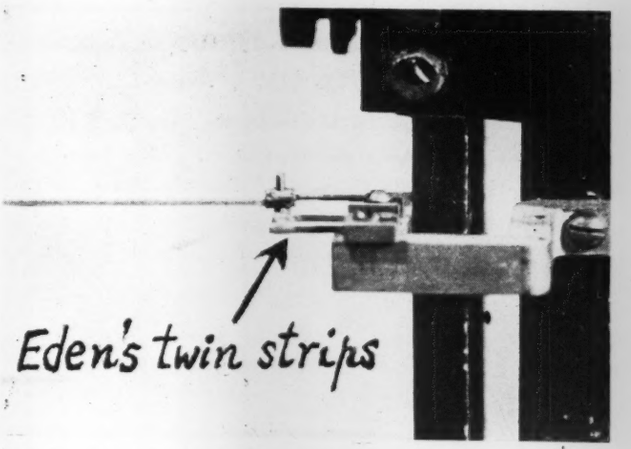

Fig. 20. Enlarged view of Eden's twin strips of the seismograph shown in Fig. 19.

responds to the seismogram of the ordinary seismograph, while Fig. 21b to that of the seismograph with Eden's twin strips composed of X-ray photograpic film. From many seismograms thus obtained, it was ascertained that these seismograms agree closely with each other.

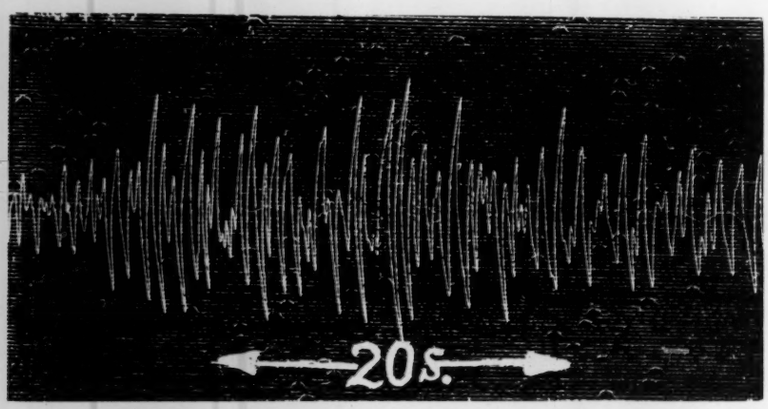

Fig. 21a.

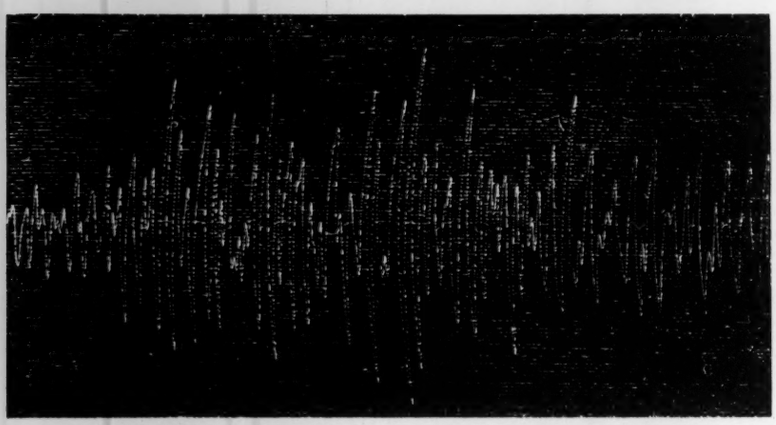

Fig. 21b.

Seismograms recording the earthquake of Dec. 7, 23 h., 12 m., 1953.
Fig. 21a: ordinary seismograph.
Fig. 21b: seismograph with Eden's twin strips.

7. エデン平行薄片の理論と地震計への応用

地震研究所 西村源六郎
鈴木正治
中央大学工学部 古川英一

Eden の twin strips は Millionth の Comparator に用いられている静的拡大機構である．これに関する理論は発表されていない．又その特性の実験的研究もみあたらない．

本研究では Eden の twin strips の静的特性と動特性を理論的に研究し，これが地震計に応用して充分に使用し得る事を述べ，かつ現在用いられている地震計の拡大機構にみられる欠点即ち機構の複雑性，部品間にあるがたや摩擦，製作の容易でない事，かさばる事，製作費のかさむ事その他の欠点を Eden の twin strips を用いる事によつて充分に除却し得る事を述べてある．又簡単に高倍率の地震計も求める事が出来るのであつて，これによる高倍率地震計を製作中である事を述べておく．

尚振動工学方面へ Eden の twin strips を用いた研究に関しては5年位前から著者達によつて行われて来ていて，可なり見るべき研究結果を得ている．例えば，家庭用ミシンの反動力の測定，工作機械特に grinder の加工時の振動研究，又噛合時に於ける歯車の噛合誤差に関する研究，電蓄 record の針先摩擦についての測定，ミシンの始動トルクの測定，その他 focal plane shutter 写真機の torsional moment の測定，或いは shutter の速度特性の研究等に応用している．これ等に関する報告は東京大学工学部記要，精機学会誌等の最近のものに発表し又近い内に出版されるものである．

8. *Horizontal Deformations of a Japanese Two-Storied Frame-House: (1) Vibration due to an Arbitrary Shock, (2) Vibration Caused by a Rotary with Unbalanced Mass, (3) Vibration due to Natural Wind, and (4) Deformation due to the Sun's Radiation Heat.*

By Genrokuro NISHIMURA and Masazi SUZUKI,

Earthquake Research Institute.

(Read Dec. 19, 1940 and July, 3, 1941.—Received Dec. 31, 1953.)

1. Introduction.

For the purpose of making a contribution to the study of a wind-proof construction of Japanese wooden-house, we measured the vibrations of a Japanese two-storied wooden house due to the pressure of natural wind. It is quite reasonable to do concurrently the measurement of natural wind by an anemometer installed at a position near the house of which the vibrations due to wind are measured. As a matter of fact, the vibration problem concerning the dynamical nature[1] of Japanese wooden-house caused by natural wind pressure remains to be treated, not to mention the concurrent observations of both the natural wind and the vibration of the house. The present paper contains not only the dis-

1) Architects are aware that the problem of wind-proof construction of a wooden-house has been hitherto treated only as one of statics, while some of the experimental results of vibration measurement of a steel tower or re-inforced concrete building due to natural wind have already been obtained by some investigators.

F. OMORI, "Measurement of Vibration of the 660 Feet Wireless Telegraph Station Tower at Haranomachi," *Bull. Imp. Earthq. Investi. Comm.*, **9** (1921), 78–99.

F. OMORI, Engineering, **112** (1921), 196.

F. OMORI, "On the Vibration of Reinforced Concrete Chimneys", *Bull. Imp. Earthq. Investi. Comm.*, **9** (1918), 1-29.

T. SAITA, "Vibration of a Framed Structure House," *Rep. of the 14th Sub-Committee (Earthquake Proof Construction), Japan Committee for Promoting Science and Engineering, 1934.*

T. SAITA, "Earthquake Proof Properties of the Castle-Tower (Tenshukaku) of the Nagoya Castle," *Bull. Earthq. Res. Inst.*, **16**, (1941), 145–154.

cussions about the results of these concurrent observations,[2] but also the treatment of both the problem of the horizontal free vibrations due to an arbitrary shock and that of the horizontal forced vibrations excited by a rotary with unbalanced mass. In the last article of this paper, moreover, we studied a special problem concerning the natural horizontal deformation of a Japanese wooden-house due to thermal stresses caused by the radiation heat of the sun.

2. Measuring Apparatus for House Deformation.

The house treated by us is a kind of two-storied wooden house in

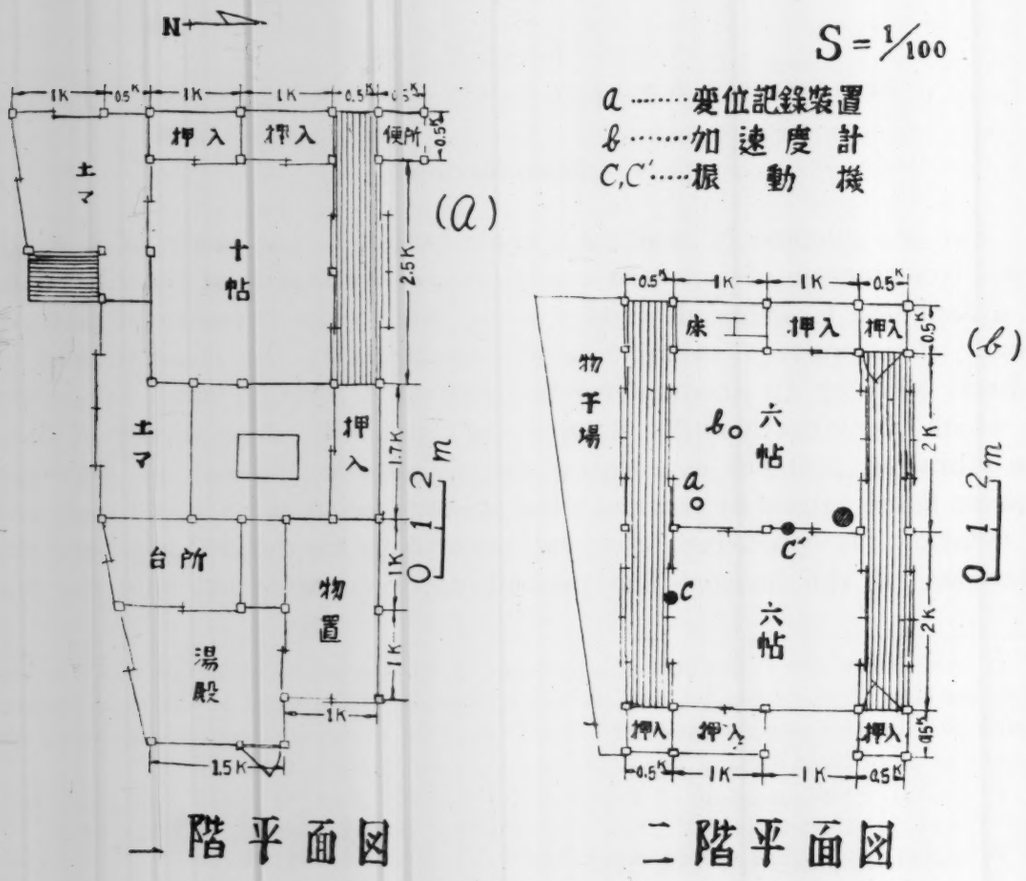

Fig. 1. Plan views of two-storied wooden house at 1st and 2nd floors.
(*a*): 1st floor, (*b*): 2nd floor.

2) In the present study, the anemometer we used was the same with the one we used in the study of natural winds, which will be shown in the next but one Bull. Earthq. Res. Inst.
G. NISHIMURA and M. SUZUKI, "Anemometer of Inverted Pendulum Type and Wind Construction Studied with It," *Bull. Earthq. Res. Inst.*, **32** (1954), Part 3.

Japan, and the plan views of its 1st and 2nd floors are respectively shown in Fig. 1, the total area of the two floors being about 80 m². The respective heights of the two floors become about 0.5 m for the 1st floor and 2.0 m for the 2nd floor from the ground. The environment of the house is as follows. There are many Japanese one- or two-storied houses around the house, and on the east side of it there is an empty space of about 80 m², across which there is a one-storied work house at about one meter's distance from the house. On the west side, there is a small house of one story across a narrow street of about one meter's width, and a common Japanese wooden house of one-story is situated on the north side of the house. On the south side, there is a two-storied house at eight meters' distance from the house. The topographical map is shown in Fig. 2, and it contains the two stations

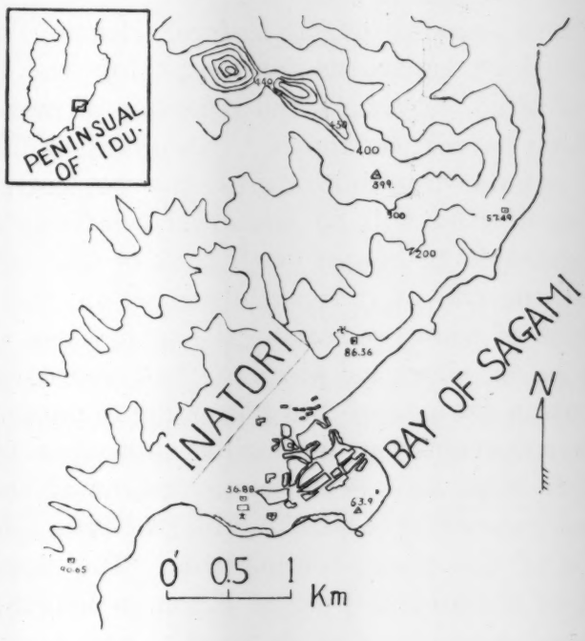

Fig. 2.

where the observations of natural wind and house vibration were carried out respectively and also their environment. The distance between the two observation stations should have been made as short as possible, but it turned out to be about 50 meters, for the reason that no other house was available for installing in it the measuring apparatus for house deformation as will be shown in this section.

For measuring the dynamical displacement of a house, it is gener-

ally convenient to use a displacement vibrograph when the vibration periods of it become comparatively short. As a matter of fact, however, the periods of house vibrations caused by natural winds, in some occasions, will become comparatively long, for the reason that the natural winds contain long periodic variations as may be seen in the characters of natural winds.[3] It is well known that a displacement vibrograph having a comparatively long period pendulum becomes generally unstable. For these reasons, the vibrograph of long period is not favourable for measuring the house vibrations caused by natural wind. Hereupon, if we want to use a short period vibrograph such as an acceleration- or a velocity-vibrograph, we are obliged to do some tedious works of integration and other treatments for obtaining the house displacement-vibrations due to natural wind. The two vibrographic methods mentioned above, in brief, become naturally unfavourable for the present study. From a new standpoint, therefore, clearing the vibrographic method, we obtained an apparatus for measuring the house vibrations excited by natural wind, of which the principle of measurement is very simple and primitive as will be shown. Assuming a long pipe uninfluenced by natural winds, the motions of the respective floors of the house due to natural wind will be measured relatively to this pipe ; the pipe becomes comparable in height with that of the house to be under measurement, and one end of it is rigidly fixed in the ground. From the dynamical point of view, of course, the transversal vibration periods of the pipe must be as short as possible, and moreover shorter than the effective vibration periods of the house due to natural winds. Upon this principle, we constructed a measuring apparatus for house deformation as shown in Fig. 3a. Because the height of the ceiling of the house under measurement is about 5.5 m, we take 6.5 m as the total length of the pipe of the present apparatus. The upper part of the pipe is composed of aluminium pipe of 3.5 m in length, and the lower part of it is of steel pipe of 3.0 m in length, and they are connected by screw and flange at their connection point. The outer and inner diameters of the aluminium pipe are respectively 50 mm and 40 mm, and also the respective outer and inner diameters of the steel pipe become 90 mm and 80 mm. The lower part of the steel pipe just 0.5 m in length is concreted in the ground as shown in Fig. 3. The pipe is set, of course, through the 1st, 2nd floors and the ceiling of the house. To prevent contact between the pipe and any element of the house,

3) *loc. cit.*

there are empty spaces of a few centimeters between the pipe and the floors and also between the pipe and the ceiling of the house as may be seen in Fig. 3a. To cut off the effect of the wind, the pipe is tightly covered with a suitable box such as wooden-made long pipe of square section of which the area is larger than that of the steel pipe.

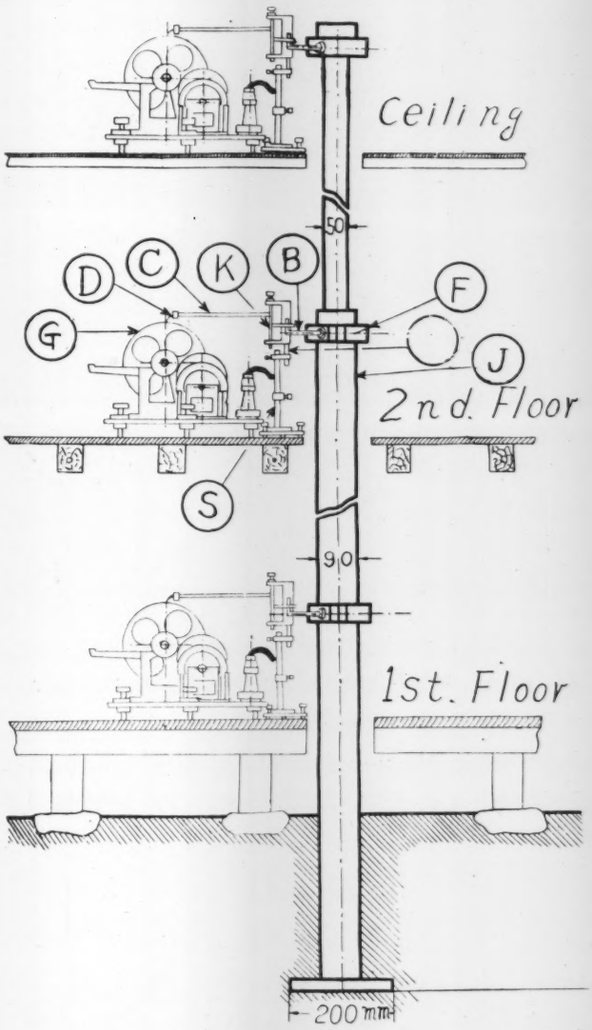

Fig. 3a. Measuring apparatus for house deformation.

Both the magnifying and recording methods for the present measurement are mechanical ones as in the case of the anemometer[4] which will be described in the next paper, and moreover they are exactly common

4) *loc. cit.*

to the three measuring points (1st floor, 2nd floor and ceiling). We will, therefore, explain them concerning the 2nd floor, and their sketch-maps are shown in Figs. 3a and 3b. Two steel rods (diameter 2 mm, length 5 mm) B are screwed normally into flange F which becomes concentric with the pipe J, and they become perpendicular with each other. The flange F is fixed by bolts and nuts to the pipe J at a desirable position in which each axial directions of the two rods become coincident with N-S and E-W directions[5] respectively. The curved end of the rod B is put into fork H of which the center rod K is pivoted by a suitable arm. Rod B makes a point contact with one of the two slightly magnetized arms of the fork H, and the arm pivoting the center rod K is put vertically on the 2nd floor by a suitable stand S as shown in Fig. 3a. The end of the recording stem C screwed into the center rod K has the recording needle D, which moves in accordance with the house-motion and records the two components of the house displacements on the smoked recording paper running with drum G. The recording drum G runs with suitable rotation speeds which are given by a phonic motor with gear mechanism.

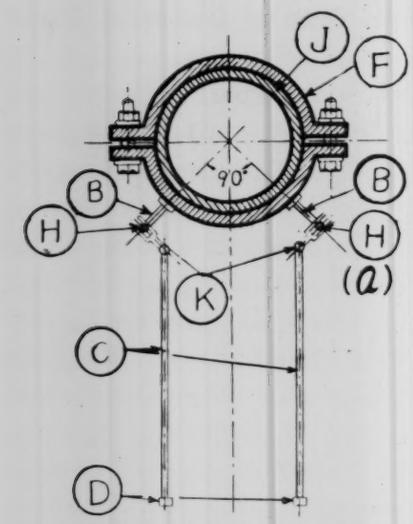

Fig. 3b. Measuring apparatus for house deformation.

For the present measuring apparatus, the mechanical magnification V of house-displacement on the 2nd floor is given by the following expression:

$$V=L/I\,,$$

where L expresses the length of recording stem C with recording needle D, and I the distance between the rotation axis of the center rod K and the point of the fork H with which the steel rod B contacts, and the value V becomes 10~13.3 for the present apparatus. The running speed of the record-paper (=peripherial speed of the recording drum) assumes three kinds values i.e. 2.09, 0.174 and 0.0145 mm/sec for the present experiment.

5) The directions of the girder and the beam of the house under measurement become respectively N-S and E-W.

3. Free Vibration of the House.

The records of horizontal free vibrations of the house due to an arbitrary shock applied to a pillar on the second floor are shown in Fig. 4. These records have been of course obtained by the apparatus

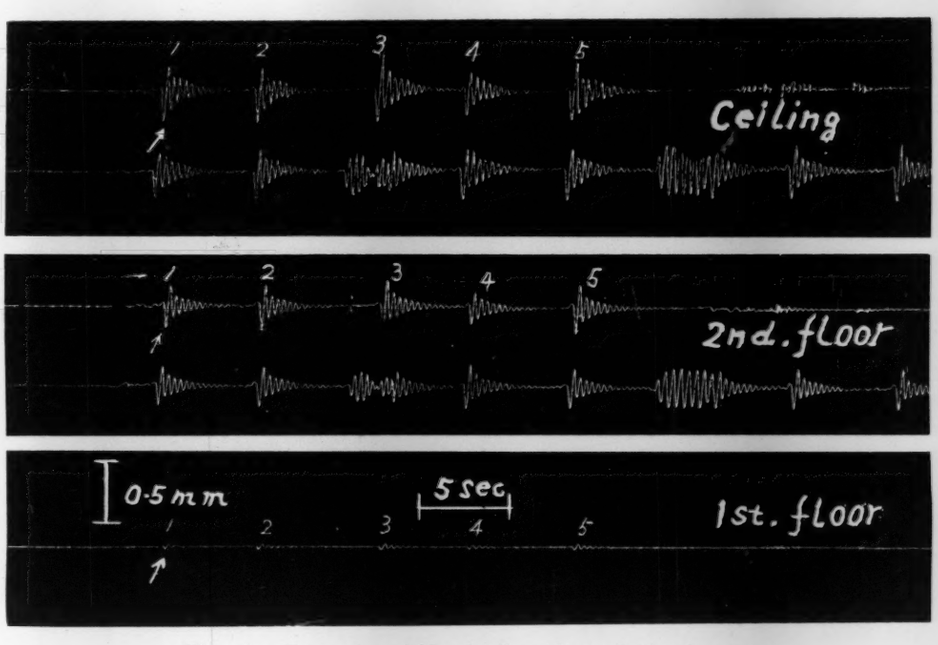

Fig. 4. Records of free vibration of the house.

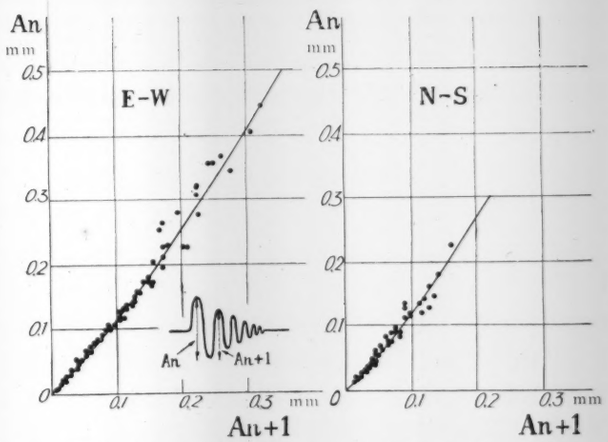

Fig. 5. Damping characters of E–W, N–S component free vibrations on the 2nd floor.

explained in the above section, and they show that the respective two components of vibration at the three places (1st floor, 2nd floor and

ceiling) are in the same phase, and that they have the same value of the free vibration period in the same time.

(1) *Damping Ratio and Amplitudes.* Taking the n-th double amplitude A_n and next $(n+1)$-th double amplitude A_{n+1} in the free vibration record of the 2nd floor, we obtain Fig. 5, which shows the damping characters of the respective E-W, N-S component vibrations on the second floor of the house. From Fig. 5, we can see that the value of A_n/A_{n+1} or the damping ratio increases with the vibration amplitude. Expressing the relation between A_n and A_{n+1} as follows:

$$A_n=a(A_{n+1})^m\,, \qquad (1)$$

we obtain the values a and m as in the following Table I.

Table I. Values of a and m for the 2nd Floor.

Components	E-W	N-S
a	1.10	1.14
m	1.13	1.20

Now, from Table II which shows the relations between the amplitude A_n and the damping ratio v for both E-W and N-S components, we find the following facts: The damping ratio increases with the

Table II. Amplitude and Damping Ratio v on the 2nd Floor.

A_n (in mm)	v (E-W component)	v (N-S component)
0.05	1.06	1.08
0.10	1.10	1.17
0.20	1.25	1.27
0.40	1.35	

amplitude; when the amplitude becomes 4 multiples of small amplitude (0.05 mm), the damping ratio increases by about 18% of the damping ratio for the case of the small amplitude (0.05 mm). When they become 8 multiples of the small amplitude (0.05 mm), the damping ratio increases by about 28% of that for the case of small amplitude.

(2) *Period and Amplitude of Free Vibration.* As regards Japanese wooden house, from the observation results of the house vibrations,

T. SAITA[6] and one of the present writers have already explained that its free vibration period becomes longer as the vibration amplitude becomes larger. For the present study, we obtained generally the same results about the relation between the periods and amplitudes of the free vibrations of the house. On the present free damped vibrations as shown in Fig. 4, for large amplitude of vibration, we will take the first five continued vibrational motions from the beginning point of vibrational motion, and also for small amplitude, we will take the last five continued vibrational motions from the end point of free vibration. Taking the mean values of the periods of the respective first and last five free vibrations on the 2nd floor, we obtained the relation between the periods and amplitudes as shown in Table III.

Table III. Free Vibration Period and Amplitude on the 2nd Floor.

No. of experiment	E-W component				N-S component				Reference
	Front part of vibration		Rear part of vibration		Front part of vibration		Rear part of vibration		
	amplitude (mm)	period (sec)	amplitude (mm)	period (sec)	amplitude (mm)	period (sec)	amplitude (mm)	period (sec)	error of calculated vibration period becomes less than 3%.
1	0.43～0.08	0.335	>0.02	0.306	0.22～0.022	0.307	>0.01	0.288	
2	0.47～0.09	0.335	>0.02	0.314	0.25～0.03	0.287	>0.01	0.286	
3	0.42～0.08	0.345	>0.02	0.306	0.23～0.03	0.307	>0.01	0.288	
mean values	0.26	0.338	>0.02	0.308	0.13	0.304	>0.01	0.287	

From Table III, we find that the free vibration period of small amplitude (rear part of free vibration) of E-W component becomes longer by just 7% than that of N-S component. We can see, moreover, that for the two cases in which the respective ranges of the vibration amplitudes for E-W and N-S components become 0.45～0.08 mm and 0.23～0.02 mm, the free vibration periods increase to be about 10% longer than that of small amplitude less than 0.02 mm for E-W component and also to be about 6% longer than that of small amplitude less than 0.02 mm for N-S component respectively.

6) T. SAITA and M. SUZUKI, *loc. cit.*

(3) *Free Vibration Modes.* The free vibration modes of the house are shown in Fig. 6, which is obtained from the observation records of free vibrations at the three points (1st floor, 2nd floor and ceiling) of the

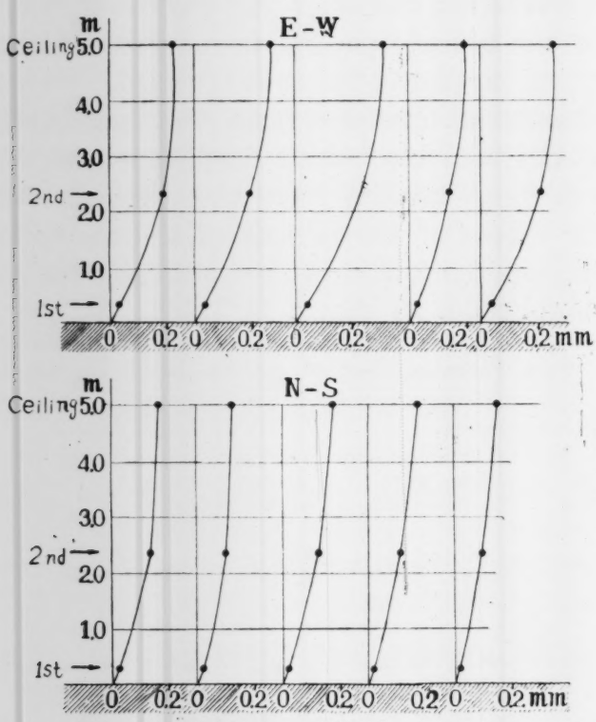

Fig. 6. Free vibration modes.

house, and Fig. 6 shows that the free vibration becomes the modes of shear vibration type. It is natural that the free vibration mode should become similar to the mode at the resonance condition of the forced vibration of the house caused by a rotary with unbalanced mass which shall be discussed in the next section.

4. Forced Vibration Caused by a Rotary with Unbalanced Mass.

To obtain the forced vibration of the house, we used SAITA's rotary[7] which is shown in Fig. 7. This rotary is mainly constructed with the rear hub and rim of a bicycle, and it is hand-driven by means of handle, chain and gear mechanism. To increase the rotation inertia of the machine, we put into the hub a lead wheel band instead of tire and tube. The unbalanced masses of 4 kinds shown in Table IV

7) T. SAITA, *loc. cit.*

are composed of lead wheel segments and they are rigidly fixed on the hub of radius 22.9 cm by bolts and nuts as shown in Fig. 7. When these four unbalanced masses are used, the hub will rotate uniformly

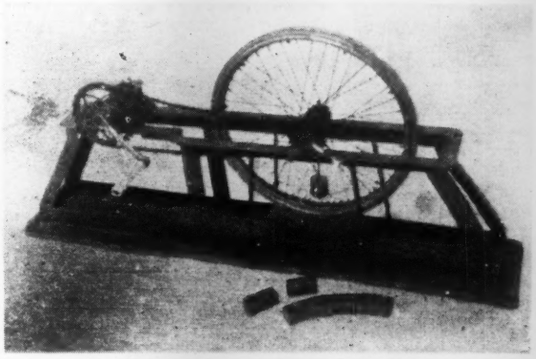

Fig. 7. Rotary with unbalanced mass.

for the range of rotation 7∼1.5 R.P.S. Of course, in the working state of the machine, it must be kept off from any displacement with rattle on the floor for the purpose of obtaining reliable records of damped forced-vibrations of the house. By hand, the hub is put into a running state with the highest possible peripherial speed, and then into a free state of damped rotation.[8]

Now we can easily obtain the following expression of the horizontal force caused by the machine which works horizontally to the house:

$$F=\frac{v^2}{r}M\cos\theta=4\pi^2\frac{r}{T^2}M\cos\theta\,, \qquad (2)$$

where F (in dyne): Horizontal force caused by the machine,
r (in cm): Distance between the center of mass of the unbalanced mass fixed to hub and the axis of the rotation of the wheel,
T (in sec.): Rotation period of the wheel,
M (in gr.): Mass of unbalanced mass,
θ (in degree): Angle between the horizontal line and the line running through the two points, one being the center of mass of the unbalanced mass and the other center of the wheel in its running condition.

Now, using the unit of kg-wt for M, we obtain the following expression of F in kg-wt:

8) In the present experiment, we put this machine on the respective positions C and C' of the 2nd floor of the house, which are shown in Fig. 1b.

$$F=0.923\,MT^{-2}. \qquad (3)$$

In Table IV, the maximum horizontal force for $T=1$ sec. is shown for respective unbalanced masses.

Table IV. Weights of Unbalanced Masses and Max. Horizontal Forces due to Them.

Kind of unbalanced mass	*Ma*	*Mb*	*Mc*	*Md*
Wt. of unbalanced mass (in Kg.)	1.00	1.70	3.40	5.10
Max. horizontal force (in Kg-wt)	0.92	1.57	3.14	4.71

For the case of free damped rotation of the rotary with unbalanced mass $M_c=3.4$ kg, we obtained the records of the forced vibrations of the respective three places (1st and 2nd floors, ceiling) as shown in Fig. 8. In this case, moreover, the record of acceleration vibrograph[9] is also shown in Fig. 8. The displacement calculated from this record becomes, of course, equal to the displacement obtained directly from the present displacement measurement apparatus.

According to the damping degree of revolution of the unbalanced mass rotary, the resonance amplitude of vibration becomes of course somewhat different, but this fact has no serious effect on the certification of the resonance period of the house. As the maximum horizontal force applied to the house by the machine becomes proportional to the square of T, we are able to calculate the maximum vibration amplitude for the constant maximum force of the respective periods. The amplitude obtained by the product of T^2 and the maximum amplitude of the respective periods becomes equal to that of the respective periods corresponding to the maximum force 0.923 M (kg-wt). From these treatment, we obtained the relations between the displacement amplitude and the period for the three respective locations (1st floor, 2nd floor, ceiling) when the maximum horizontal force becomes 3.14 kg-wt as shown in Fig. 9. From these curves in Fig. 9, we can see that for N-S component, the displacement commonly reaches its maximum when the period becomes 0.34 sec. for all three locations, and also for E-W component, it reaches its maximum when the period be-

9) The accerelation vibrograph used is ISHIMOTO's seismograph of which natural period=0.115 sec., sensibility=2.0 gal/mm, mechanical magnification=213, weight of mass=13 kg, damper=air damper, and recording method=mechanical smoked paper one. It is installed at *b* location on the 2nd floor of the house shown in Fig. 2.

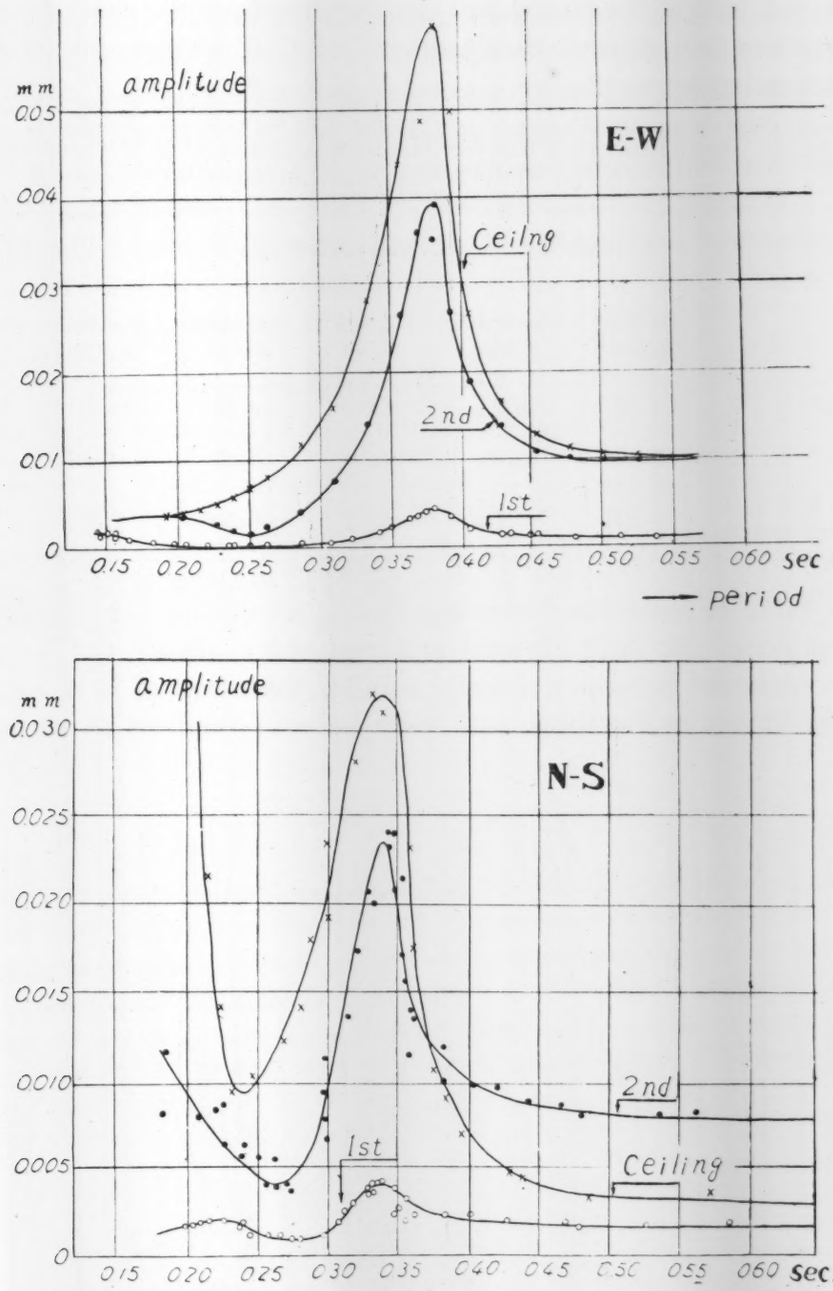

Fig. 9. Relations between displacement amplitude and period.

comes 0.38 sec. When the period of applied force becomes longer than 0.55 sec., the respective displacements for E-W and N-S components become roughly constant, and this fact shows that the problem turns into a statical one when the period surpasses 0.55 sec. Table V shows

both the N-S and E-W component displacement-amplitudes of the three locations when the statical displacement of E-W component on the 2nd floor is taken to be unit.

Table V. Displacements When Statical Displacement of E-W Component on 2nd Floor is Taken to be Unit.

Position / State / Component	Ceiling		2nd Floor		1st Floor	
	statical state	resonance state	statical state	resonance state	statical state	resonance state
E-W	1.06	6.2	1.0	4.55	0.10	0.46
N-S	0.334	3.33	0.82	2.27	0.167	0.41
ratio of N-S and E-W components	0.334	0.536	0.82	0.50	1.51	0.89

This table reveals the following facts; excepting the statical state of the 1st floor, for both statical and resonance states the amplitudes of N-S component become generally smaller than that of E-W component for all two floors and ceiling, and they become smallest at ceiling, and

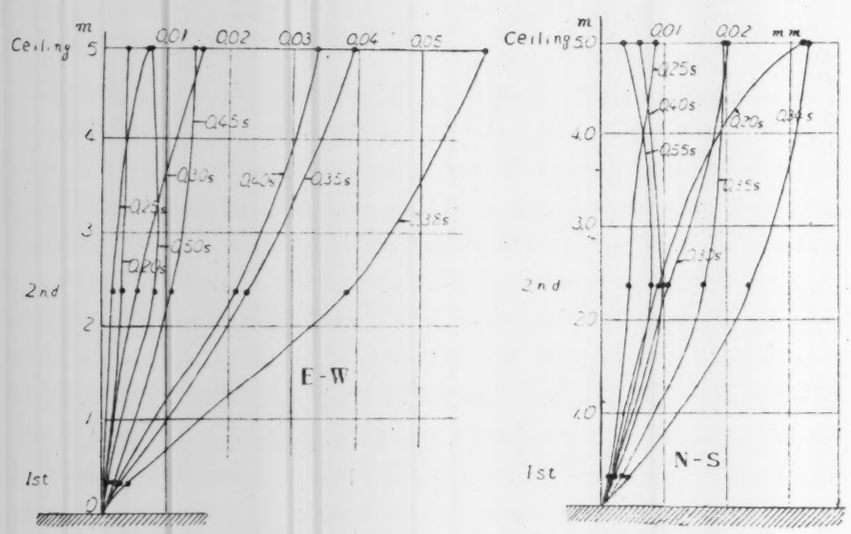

Fig. 10. Forced vibration modes.

also the ratios of N-S component and E-W component for both statical and resonance states for the upper floor have smaller values than that for the lower floor of the house. These two facts show that both the

effective statical-and dynamical-strength for N-S component of the house becomes larger than that for E-W component, and also the upper part of the house becomes effectively stronger than the lower part of it.

The vibration modes of the house for both E-W and N-S components are shown respectively in Fig. 10, in which the parameter of the curves is taken as time in sec. In Fig. 10, we can see that both the vibration modes for N-S and E-W components for resonance condition become

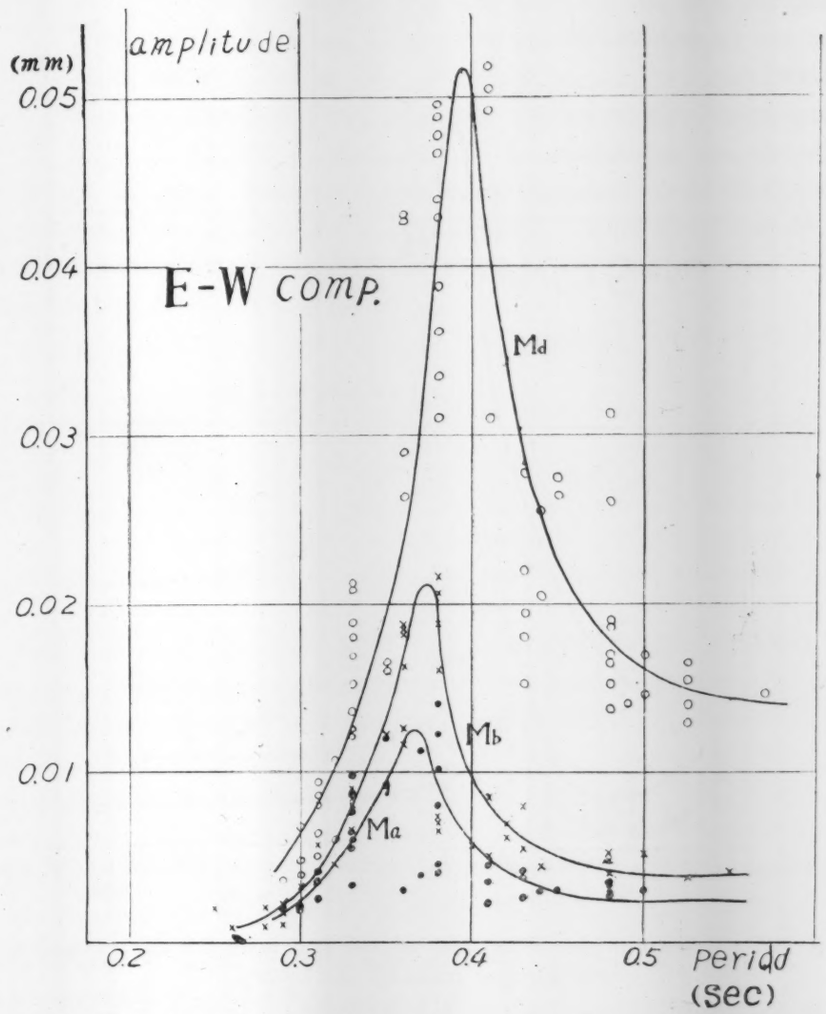

Fig. 11a. Vibration characteristics of the 2nd floor for the variation of unbalanced mass of the rotary.

naturally similar to that of the free vibration mode of the house which is already shown in Fig. 6. When the period of the applied horizontal force becomes long, the amplitude of both the 2nd floor and ceiling

become nearly equal, but in the case of more longer periods the amplitude of the 2nd floor becomes somewhat larger than that of the ceiling. This tendency appears especially more distinctly for N-S component than for E-W component. The reason why the displacement of the 2nd floor becomes distinctly large, is that the horizontal force caused by the rotary is applied on the 2nd floor and also the 2nd floor is of rather weak construction. When the period of the applied force becomes

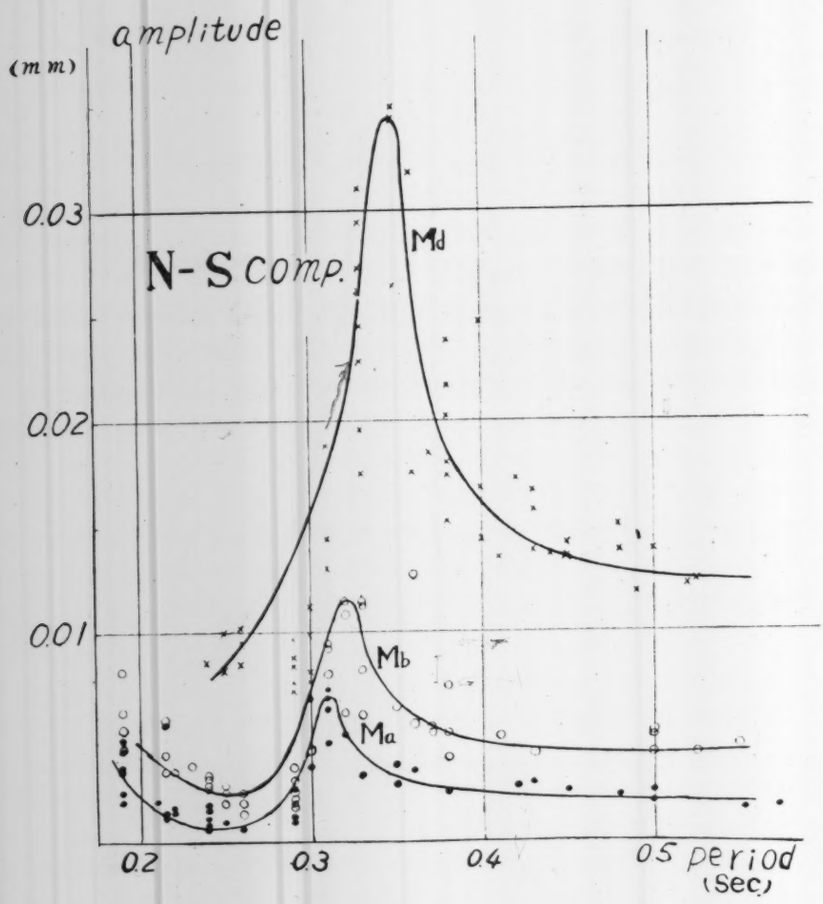

Fig. 11b. Vibration characteristics of the 2nd floor for the variation of unbalanced mass of the rotary.

shorter than the resonance period of the house, the respective three locations (1st floor, 2nd floor and ceiling) show their respective different vibrations and also seem to have their own respective resonance periods. This fact shows that the house cannot vibrate wholly as a single body, and that the three locations vibrate with their respective vibration

modes for the reason of the dynamically weak construction.

Now the vibration characteristics of the 2nd floor for the variation of unbalanced mass of the rotary on the 2nd floor are shown in Fig. 11 for E-W and N-S components respectively. In E-W component (Fig. 11a), observed points marked with ●, ×, ○ correspond to the unbalanced masses M_a, M_b and M_d respectively, and also the points marked with ●, ○, × in N-S component (Fig. 11b) shows respective cases of M_a, M_b and M_d. The vibration characteristics for the case of M_c are already shown in Fig. 9. The curves in Fig. 11 correspond of course to the maximum horizontal forces shown Table IV. From Fig. 11, we can see that the resonance period on the 2nd floor slightly varies as the unbalanced mass varys and that it shows a tendency to be elongated as the maximum force becomes larger. And this tendency appears more distinctly in the N-S component than in the E-W component. This fact shows that the dynamical construction of the N-S direction of the house may be weaker than that of the E-W component.

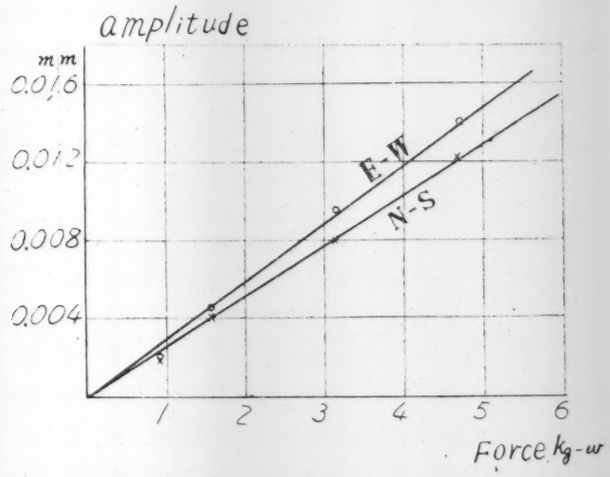

Fig. 12. Relation between the applied statical force and the maximum horizontal deflection of the 2nd floor.

From Figs. 9 and 11, we are able to obtain the relation between the force intensity applied horizontally to the house and the maximum horizontal displacements in both statical and dynamical states; Fig. 12 shows the relation between the statical force applied to the house and the maximum deflections of the house on the 2nd floor, the statical force of course being the force with the period longer than 0.55 sec. for the present house, and also Fig. 13 shows the relation between the

dynamical maximum deflection of the 2nd floor at the resonance condition and the dynamical force of period 0.32 sec. applied to the house. Of course, the two curves in both Figs. 12 and 13 are cases of N-S and E-W components respectively. From Figs. 12 and 13, we can see

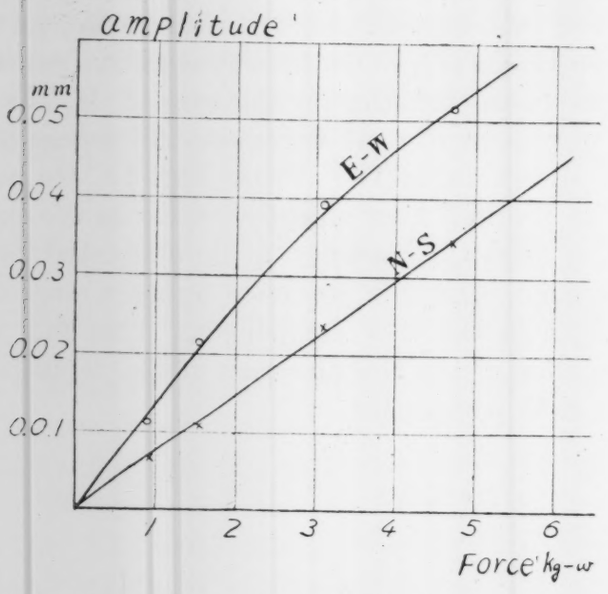

Fig. 13. Relation between applied dynamical force and maximum deflection at 2nd floor.

that the statical deflection of course becomes proportional to the applied force but the dynamical deflection does not become necessarily proportional to the intensity of applied horizontal force. As for the present house, the fact that the E-W component does not become proportional may be explained by the increase in the decaying factor worsening of the condition of the house with the increase in deflection caused by the applied force. Of course this property is mainly due to the construction of the house.

From Figs. 9 and 11, we obtain Fig. 14 which shows the variation of resonance displacement due to that of resonance period on the 2nd floor and in which the points marked with × correspond to the state of free vibration. We can understand from Fig. 14 that the resonance period of the house becomes much elongated by the finiteness of vibration amplitude, which is of course due to the intensity of the applied force. In Fig. 14, moreover, we can see that the free vibration period obtained from small vibration amplitude becomes much smaller than

that obtained from forced large vibration amplitude. The resonance period corresponding to comparatively large forced vibration amplitude, moreover, becomes comparatively longer than that of the comparatively small forced vibration amplitude. From the discussions about Fig. 14, we obtain the important fact about the resonance phenomenon of wooden

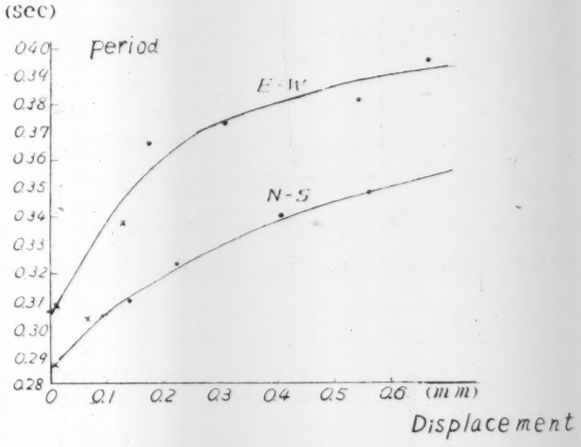

Fig. 14. Relation between displacement amplitude and resonance period.

house as follows: When the resonance period of a wooden house is discussed, it must be stated whether the vibration condition is a free or a forced one and moreover whether the vibration amplitude becomes infinitesimal or finite.

5. Vibrations due to Pressure of Natural Winds.

In the present section, we shall discuss the results of the concurrent observations of both the natural winds and the house vibrations caused by them. The apparatus used for this concurrent observations has already been introduced in the preceding section. As the method of analysis of the wind pressure will be shown in the next paper[10] in which we shall discuss the wind construction, we do not show it in this paper. In this section, we shall first discuss the relation between the wind pressure and the house displacement and next we shall study the statistical characters of the vibration periods of the house due to wind and the predominant period. The problems concerning the relation between the periods and the amplitudes of the house vibrations caused

10) *loc. cit.*

by natural wind and also the nature of the deformation vectors of the house due to natural wind will be studied in this section.

(1) *Wind Pressure and Displacement of the House.* Now we will take the following two cases of observation of winds: (1) S-E wind blowing for the space of 8 hours and 45 minutes from 22^h, Sept. 11 to 6^h45^m, Sept. 12, 1941, in which the maximum wind speed reached 23 m/s, and also (2) N-W wind lasting for the space of 23 hours and 12 minutes from 18^h48^m, Sept. 16 to 18^h, Sept. 17, 1941, in which the maximum wind speed reached 35 m/s.

Using the respective records of both wind pressures and the house vibrations, we calculated the mean values of the wind pressures of NE-SW direction and those of SE-NW direction, and also the mean values of the vibration amplitudes of E-W component and those of N-S component. By these procedures, we obtained the relations between

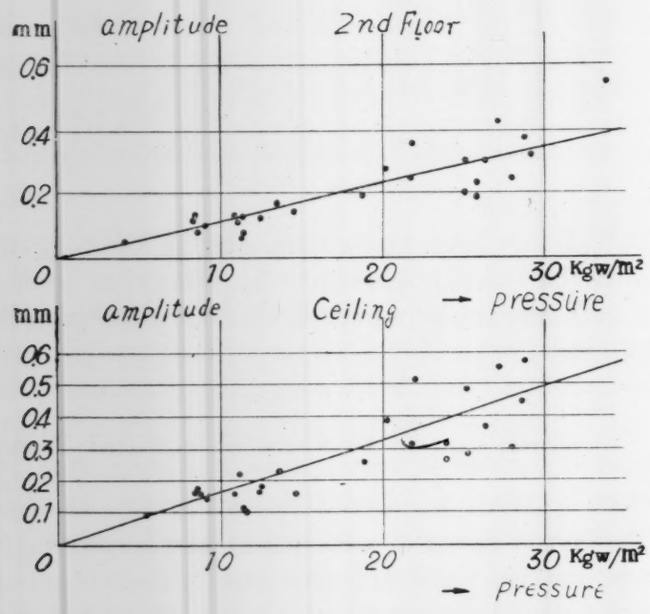

Fig. 15. Relation between wind pressure and house displacement amplitude S-W wind.

the wind pressure and the vibration amplitude of the house on the ceiling and on the 2nd floor as shown in Figs. 15 and 16. From Figs. 15 and 16, we can see that the vibration amplitudes become roughly proportional to the maximum wind pressure for both winds (S-E wind, and N-E wind). From the theoretical point of view, this character of proportionality may be of course right, but actually the respective

points marked with ● in Figs. 15 and 16 do not necessarily form a regular curve such as a straight line. This fact is of course due to the facts that both the house displacements and the wind pressures have respectively dynamical natures and also the two stations where the observation of the wind and house deformation are respectively carried out have a 40 meters' distance between them. Figs. 15 and 16

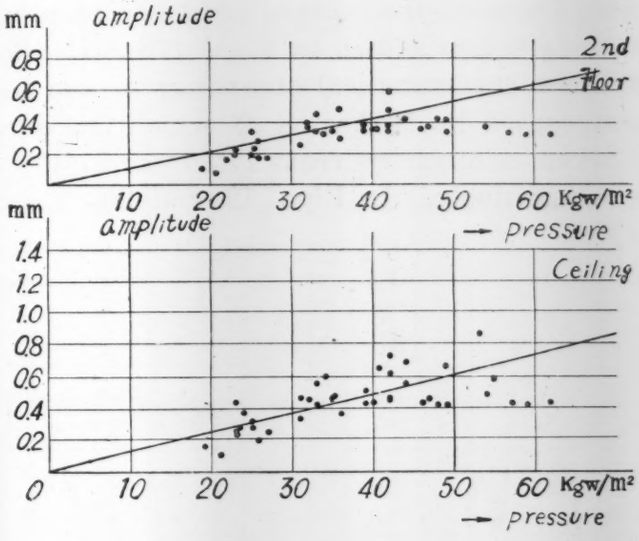

Fig. 16. Relation between wind pressure and house displacement amplitude S-W wind.

show that for the wind pressure of 30 Kg-wt/m², the two displacements on ceiling and 2nd floor become respectively 0.49 mm, 0.38 mm for S-E wind, and 0.37 mm, 0.30 mm for N-E wind. Hence we learn that the displacements on ceiling and 2nd floor due to S-E wind become larger than those due to N-W wind. We cannot, however, explain easily these facts from the theory that when the intensity of wind pressure is the same, the displacement of the house due to the wind is of the same magnitude even when the directions of the wind are diametrically opposite to each other. In the present case, as already mentioned, the two concurrent observation stations have a distance of 40 metres between them and both the environment of the houses and the topography around the house are not uniform. From these two facts, we are able to infer that the effect of N-W wind pressure on the house is more or less varied and weakened mainly by the environment of N-E side of the house.

(2) *Statistical Characters of the Vibration Periods of the House due to Wind and Their Predominant Period.* Taking two records of the house displacement which are respectively caused by N-E wind of the duration from 17^h35^m to 17^h55^m, March 2, 1941, and by S-W wind of the duration from 12^h17^m to 12^h27^m, March 4, 1941, we studied the statistical characters of the vibration period of the house. Figs. 17a and 18a show respectively the vibrations of the house for the above-mentioned two durations of time. Parts of the records of the wind pressure for these two time durations are also shown in Figs. 17b and 18b respectively. Figs. 19 and 20 show the statistical characters of the house vibrations of N-S component caused by N-E wind of which the duration of time (5 minutes) is taken arbitrarily from 17^h35^m to 17^h40^m and also from 17^h40^m to 17^h45^m respectively. In Figs. 19 and 20, the values of the

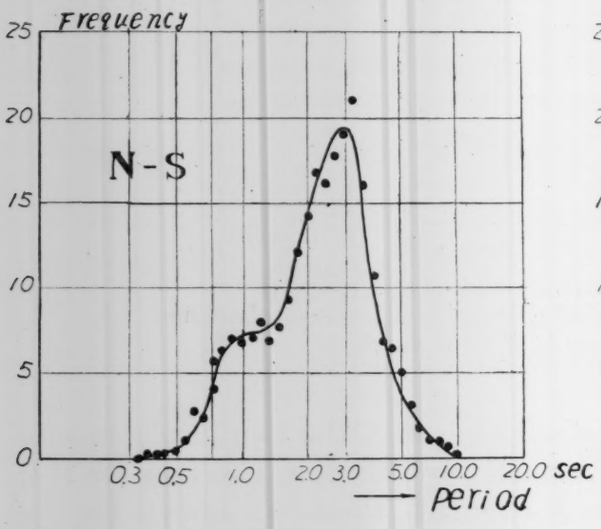

Fig. 19. Relation between vibration period of the house due to N-E wind and their predominant period. Observation time=17^h35^m~17^h40^m, March 2, 1941.

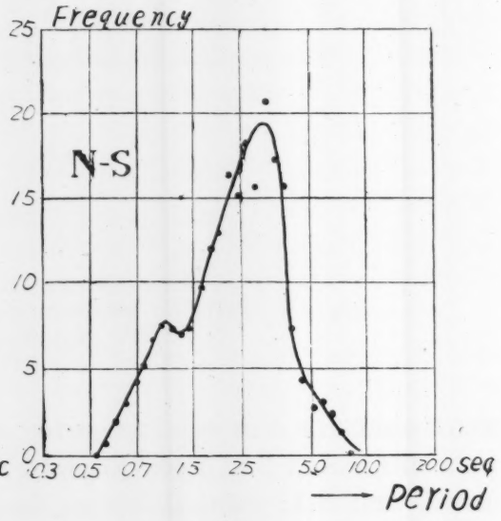

Fig. 20. Relation between vibration period of the house due to N-E wind and their predominant period. Observation time=17^h40^m~17^h45^m, March 2, 1941.

period taken on the abscissa of log. scale are obtained by the method wherein we take, as the period of the house vibrations, the time duration from a top to the next top on the recorded curve of the vibration of the house in Figs. 17a and 18a, or the time duration from a bottom to the next bottom on the same records. The ordinates in Figs. 19 and 20 show also the total numbers of which we summarized the numbers of the same values of periods for the same duration of time

(5 minutes) as in Figs. 17a and 17b. The natures shown by the curves in Figs. 19 and 20 become approximately the same, and therefore we can say that the result is same whether the observation time of

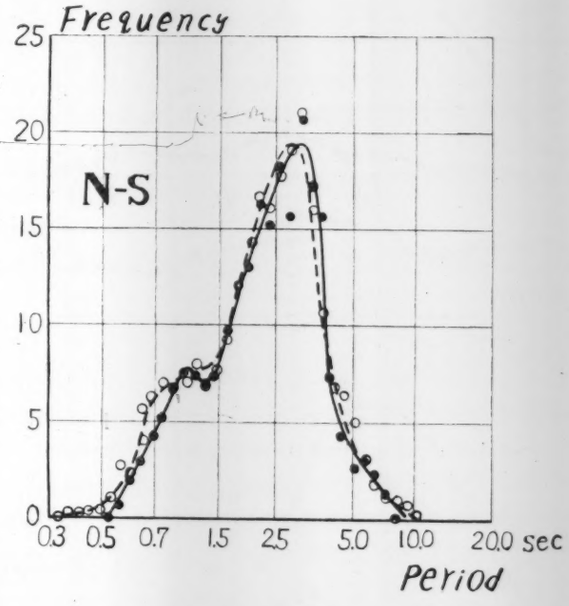

Fig. 21. Relation between vibration period of the house due to N-E wind and their predominant period.
○ 17^h35^m~17^h40^m March 2, 1941
● 17^h40^m~17^h45^m 〃 〃 〃

duration is 5 minutes or 10 minutes. From Figs. 19 and 20, or from Fig. 21 which shows the results obtained from 10 minutes observation, we learn that there are two maximum values of the vibration periods such as 1.0 sec., 3.0 sec. respectively. We shall call these values of period as the *predominant periods* of the house subject to winds. Fig. 22 shows the statistic characters of the house vibrations of the respective two components of E-W and N-S due to the same wind during the time from 17^h45^m to 17^h55^m. Fig. 22 shows that the predominant periods become 2.3 sec. for E-W component and also 2.7 sec. for N-S component respectively. In the same way, the predominant periods caused by the S-W wind become as follows: Fig. 23 shows the statistical results which are obtained from the observation time duration from 12^h17^m to 12^h27^m by the same statistical method as in the preceding case of N-E wind. From Fig. 23, we find that, for the predominant periods of the house for E-W vibration component, there are two values i.e. 0.6 sec.

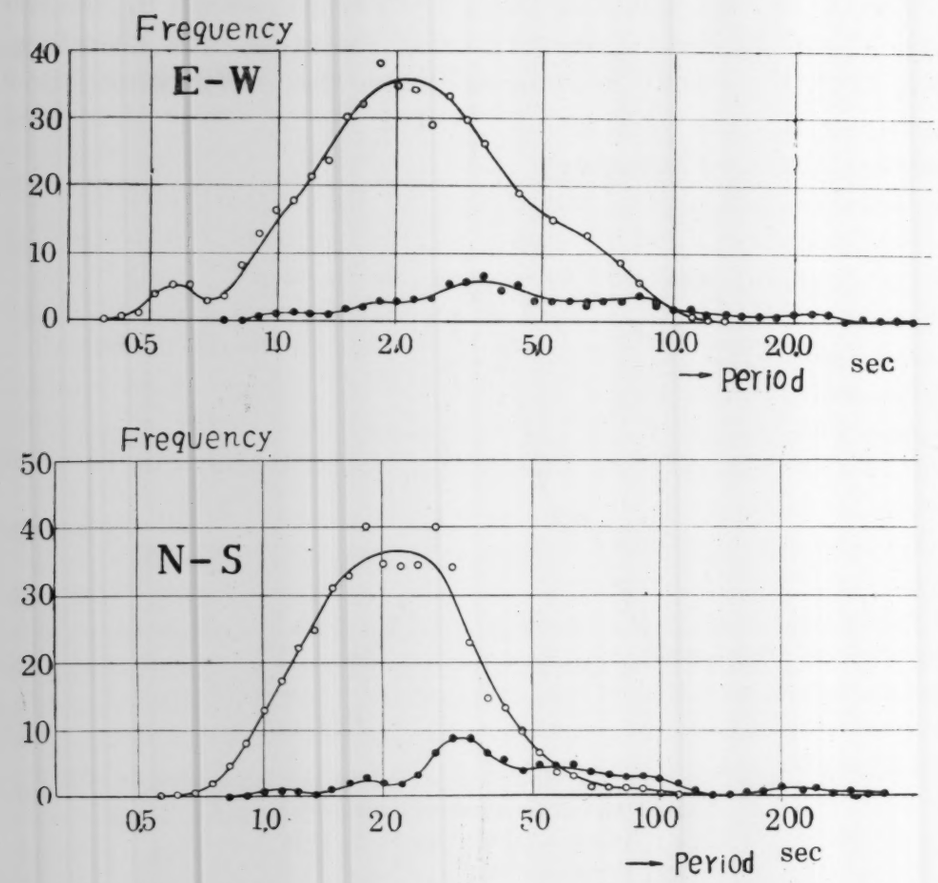

Fig. 22. Relation between vibration period of the house due to N-E wind and their predominant period. 17^h45^m to 17^h55^m March 2, 1941.

and 2.4 sec., but the predominant period for N-S direction becomes roughly 2.5 sec.

From the discussions about the predominant periods of the house vibration caused by the winds, of which the natures are shown in

Table VI. Predominant Periods of the House Vibration Caused by Natural Wind.

Wind Direction / Vibration Component	N-E Wind (sec.)		S-W Wind (sec.)	
N-S Direction	1.0	2.7, 3.0		2.5
E-W Direction		2.3	0.6	2.4

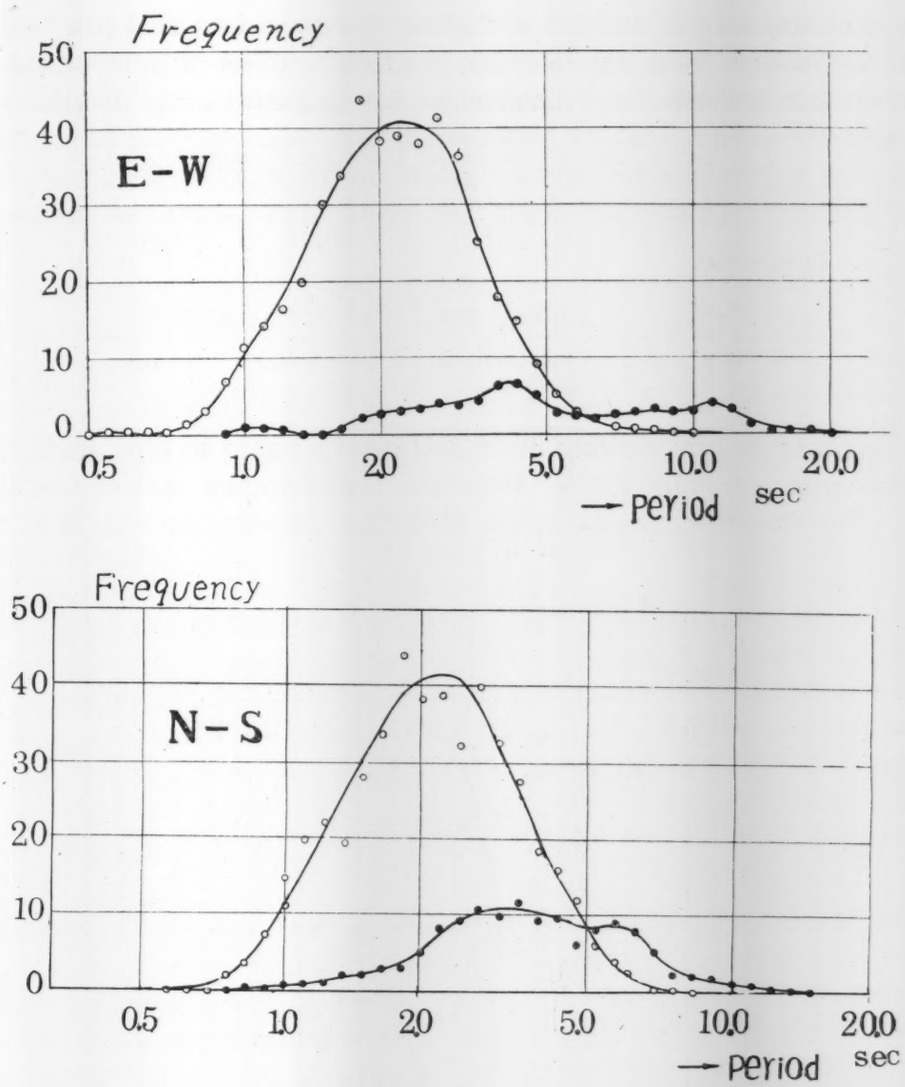

Fig. 23. Vibration period of the house due to S-W wind and their predominant period. 12^h17^m to 12^h27^m.

Figs. 26~32, we obtain Table VI in which the predominant periods are tabulated. The values of both the free vibration period and the resonance periods of this house shown in the preceding sections become of course shorter than that of the predominant periods shown in Table VI. From Table VI, we can say that the predominant periods of the house become generally longer than the proper periods of it such as free vibration periods or forced resonance periods. Now the vibrations with these predominant periods do not necessarily show the property

of the displacement of vibration during the time of these predominant periods beginning from equilibrium position or zero displacement and returning again to the zero displacement. Regarding the displacements

Table VII. Predominant Duration Times.

Kind / Component	(A)	(B)	(C)
E-W	3.8~12 sec.	3~10 sec.	20 sec.
N-S	3.0~6.0 sec.	3.5~8.0 sec.	20 sec.

which begin from zero displacement and return again to zero, its duration time becomes generally longer than the predominant periods mentioned above. For example, we take the vibration records due to N-E wind

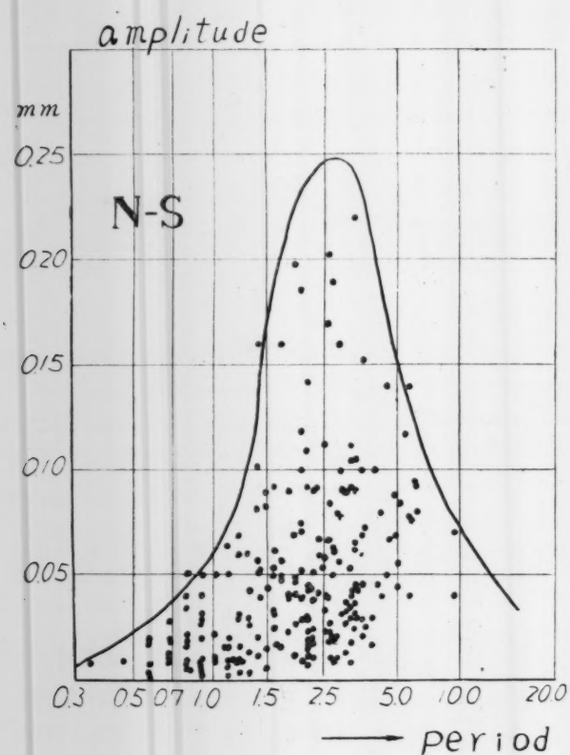

Fig. 24. Vibration period and amplitude (N-S comp.) due to E-N wind.
Obs. Time=17^{h}35^m~17^{h}40^m.

during the 5 minutes from 17^{h}45^m to 17^{h}55^m and also the 10 minutes from 12^{h}17^m to 12^{h}27^m. Using these vibration records, we analyse the

predominant duration times in which the displacement begins from zero position and again returns to zero position as shown in Table VII. In Table VII, (A) corresponds to the vibration record during the time from 17^h45^m to 17^h55^m, and also (B) corresponds to that during the time from 12^h17^m to 12^h27^m. In addition to the values corresponding to (A) and (B) shown in Table VII, from the above-mentioned vibration records

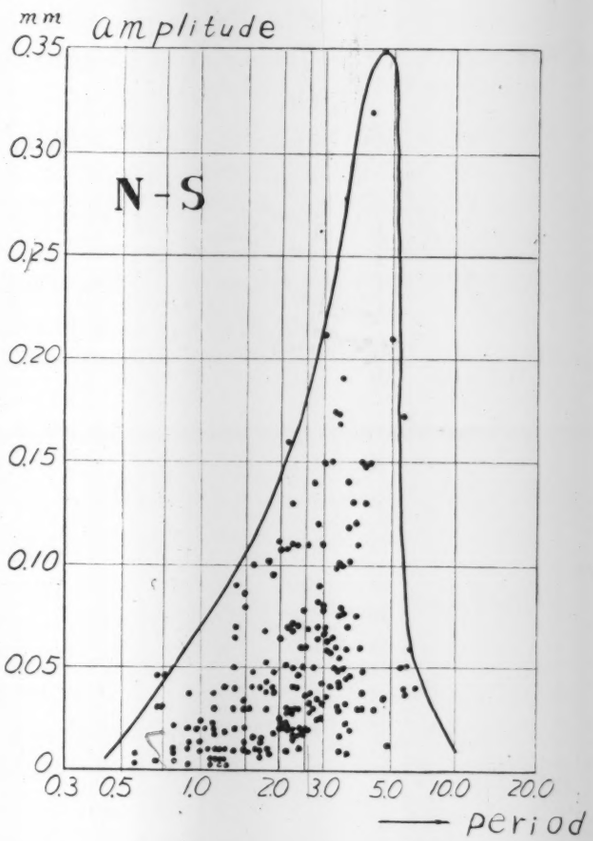

Fig. 25. Vibration period and amplitude (N-S comp.) due to E-N wind.
Obs. Time=11^h40^m~17^h45^m.

of both components N-S and E-W, we found the value 20 sec. to be the predominant period. And this value is shown in (C) kind in Table VII. Of course the free vibrations of the house must be generated by the wind, and the phases wherein the periods become 0.30~0.32 sec., are predominantly found in the records of both E-W, N-S components of vibrations, but their amplitudes become very small compared with those of the above-mentioned phases, and become moreover only about 1/20

of the amplitude of the other predominant phase which we have already explained.

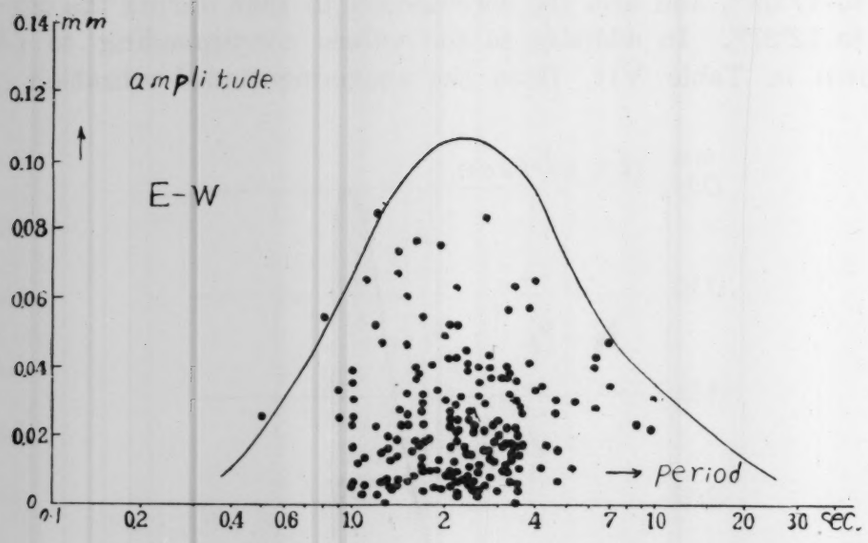

Fig. 26. Relation between vibration amplitudes and period due to S-W wind.

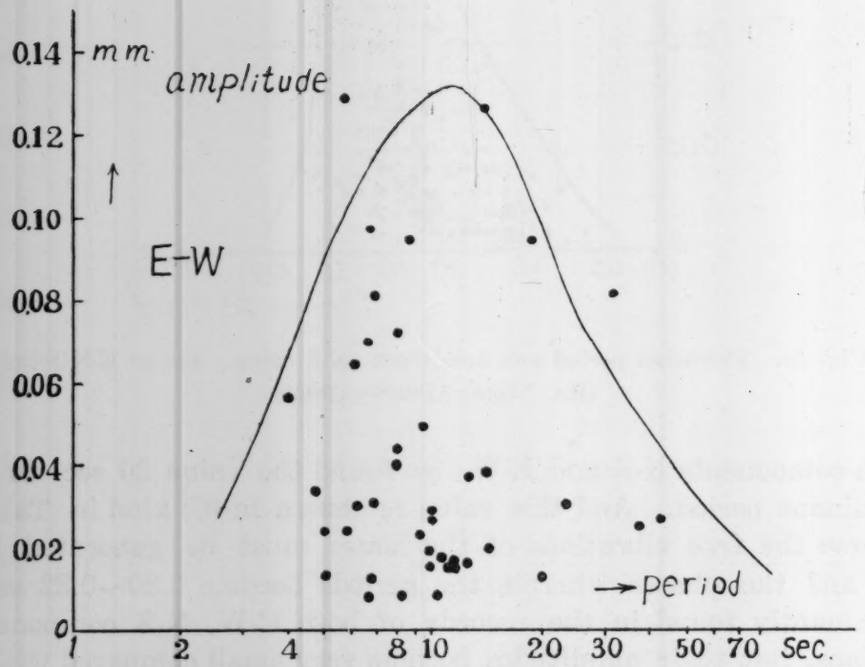

Fig. 27. Relation between vibration amplitude and period due to S-W wind.

(*3*) *Period and Amplitude.* Figs. 24 and 25 show respectively the relations between vibration amplitude and its period due to N-E wind during the 5 minutes time from 17^h35^m to 17^h40^m and also from 17^h40^m to 17^h45^m. From Figs. 24 and 25, we can see that the periods corresponding to the large amplitudes become about 3.1 sec. and 4.5 sec. respectively. Fig. 26 shows also the relation between the periods and amplitudes due to S-W wind during the 10 minutes time from 12^h17^m to 12^h27^m, from which we can see that the periods corresponding to large amplitudes become about 2.5 sec. Fig. 27 shows the relation between the time, in which the displacement begins from zero and also returns again to zero, and the maximum amplitude during this time. From Fig. 27, we can also see that the time corresponding to large amplitude becomes about 10 sec.

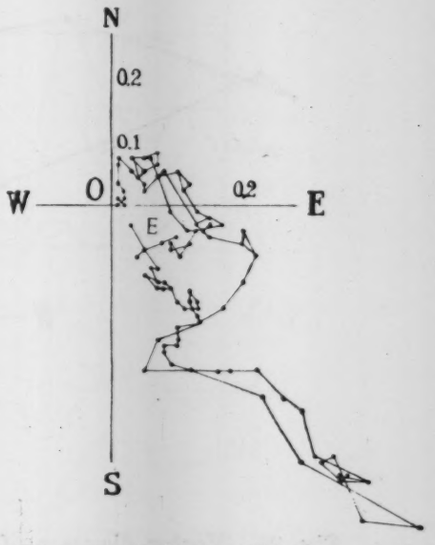

Fig. 28. Vector diagram of the house vibration due to the wind during about 60 sec. from $2^h45^m40^s$ on March 4, 1941.

(*4*) *Displacement Vectors.* Taking both E-W and N-S components of the records of the house vibrations caused by two winds, one of which is the wind (for about 60 sec.) from $2^h45^m40^s$ on March 4, 1941, and the other is the wind for about 50 sec. from 2^h45^m on March 4, 1941, we obtain the displacement vectors of the house vibration in every 0.48 sec. for both two vibrations which are shown in Figs. 28 and 29 respectively. Fig. 28 shows that the house generally moves in the direction of E-S during this time of 50 sec., and that it also returns to the same initial position passing through the same way during this wind blow of 50 sec. Fig. 29, however, shows that the house generally moves in a manner more complicated than the movement shown in Fig. 28, and that it moves through three quadrants during the wind blow of 60 sec. During two short neighbouring wind blows of S-W wind as in the present case, the motions of the house differ greatly as shown in Figs. 28 and 29. These two natures of the vibration of the house may of course be caused by the facts that the wind construction is very complicated, and that the natural wind varies greatly in its blowing directions even during tne short time of about 60 sec. These facts of the nature of the blow-

ing wind mentioned above shall be explained in the next paper[11], in which we will show the study of the wind construction by a short time observation of the blowing wind.

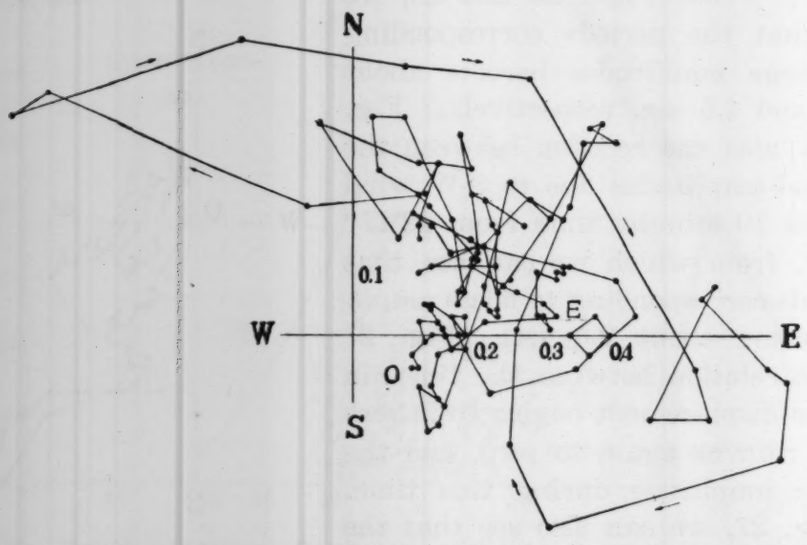

Fig. 29. Vector diagram of the house vibration due to the wind during about 50 sec. from $2^h45^m\ 0^s$ on March 4, 1941.

6. The Statical Displacement of the House due to the Sun's Radiation Heat.

It was very calm and there was no wind during the five days from 17^h, Sept. 10 to 17^h, Sept. 15, 1945. For the space of these five days, we obtained the records of the house displacement of both N-S, E-W components, and the parts of them are shown in Fig. 30, in which the upper three curves show respectively the E-W displacement components on the 1st flow, 2nd floor and ceiling, and the lower three curves correspond respectively to the N-S displacement components on the respective three places (1st floor, 2nd floor and ceiling). From Fig. 30, we can see that the two components of the respective three places have generally a common variation period of 24 h. The house begins to move in the E-S direction from 6 h morning and it returns again to the original position at about 6 h next morning, and moreover the two components of the three respective places have different residual permanent displacements respectively. The respective displacements on the 2nd floor and on the ceiling generally assume same phase with respect

11) *loc. cit.*

to both the E-W and the N-S components for the present house. The displacement magnitudes on the 1st floor become almost equal for both the E-W and the N-S components, but the displacement magnitudes of

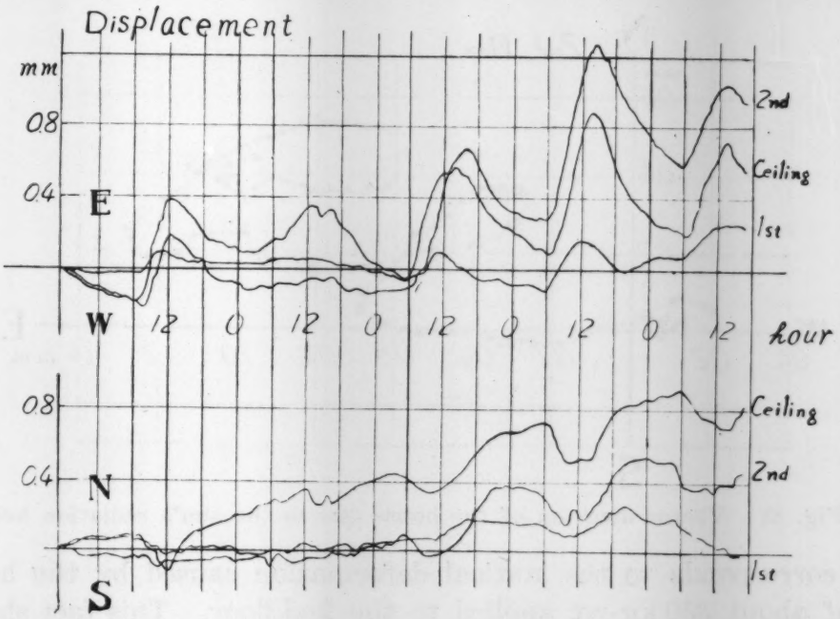

Fig. 30. Displacement of the house due to the sun's radiation heat.

the 2nd floor and ceiling on E-W component turn to be about three times of those on the S-N components shown in Fig. 39. The phase differences between the 1st and 2nd floors or between the 1st floor and ceiling become about 2 hours, and the phase of the maximum displacement on the 2nd floor has 2 hours time-lag compared with those on the 1st floor.

These phenomena concerning the deformation of the house become similar to the daily variation of the atmospheric temperature. When the daily variation of the atmospheric temperature becomes large as on a fine weather, the daily variation amplitude of the deformation of the house also becomes large, and it comes near zero when the weather is bad or rainy. These house deformations can be explained from the fact that the house is exposed to the radiation heat of the sun, and that its deformation is caused by the thermal stresses effectively induced into the house.

Using Fig. 30, we obtain Fig. 31 in which the vector diagram of the deformation of the house on the 2nd floor is shown. The numbers such as 6, 12, 18, 0 on the curve shows the time of a day in hour.

From the vector diagram in Fig. 31, we can see that the daily variation of the deformation becomes same and similar for every day, and the maximum displacement amplitude in a day becomes about 1.0 mm

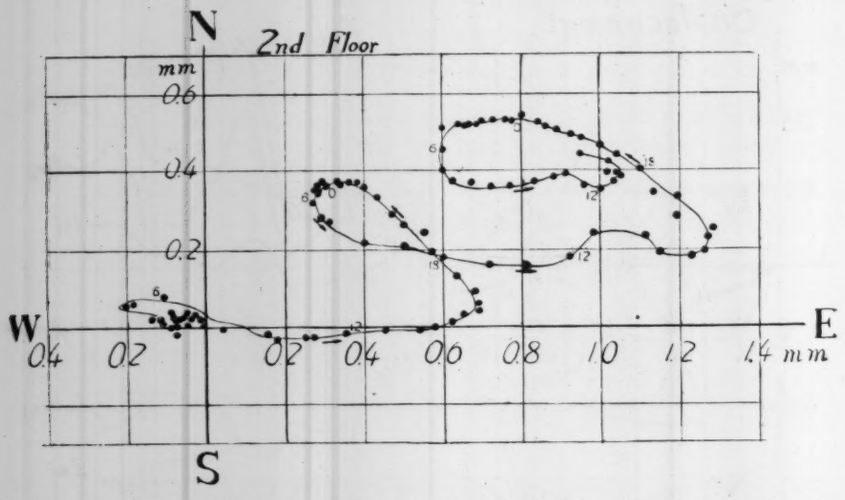

Fig. 31. Vector diagram of the house due to the sun's radiation heat.

which corresponds to the statical deformation caused by the horizontal force of about 350 kg-wt applied to the 2nd floor. This fact shows that the house deformation due to the radiation heat of the sun is large and is not negligible when we study the deformation of a Japanese wooden house.

7. Conclusion.

In the present paper, we have explained the vibration properties of a Japanese two-storied wooden house when it is subject to free vibration caused by a shock, and also to forced vibration due to unbalanced force or natural wind pressure. The house deformation due to thermal stress under the radiation heat of the sun has also been studied.

Concluding this paper, we express our thanks to the late Prof. M. Ishimoto, by whose guidance the present study has been carried out, and also to the late Yoshitaro Maeda, teacher of the Technical School, Inatori-machi, Shizuoka Prefecture, whose assistance proved valuable in the present analysis. We also wish to express our sincere thanks to Katsuzo Hosaka who constructed the present experimental apparatus designed by us. Lastly we express our thanks to the authorities of the Japan Committee for Promoting Science and Engineering for the grant in aid of the present research.

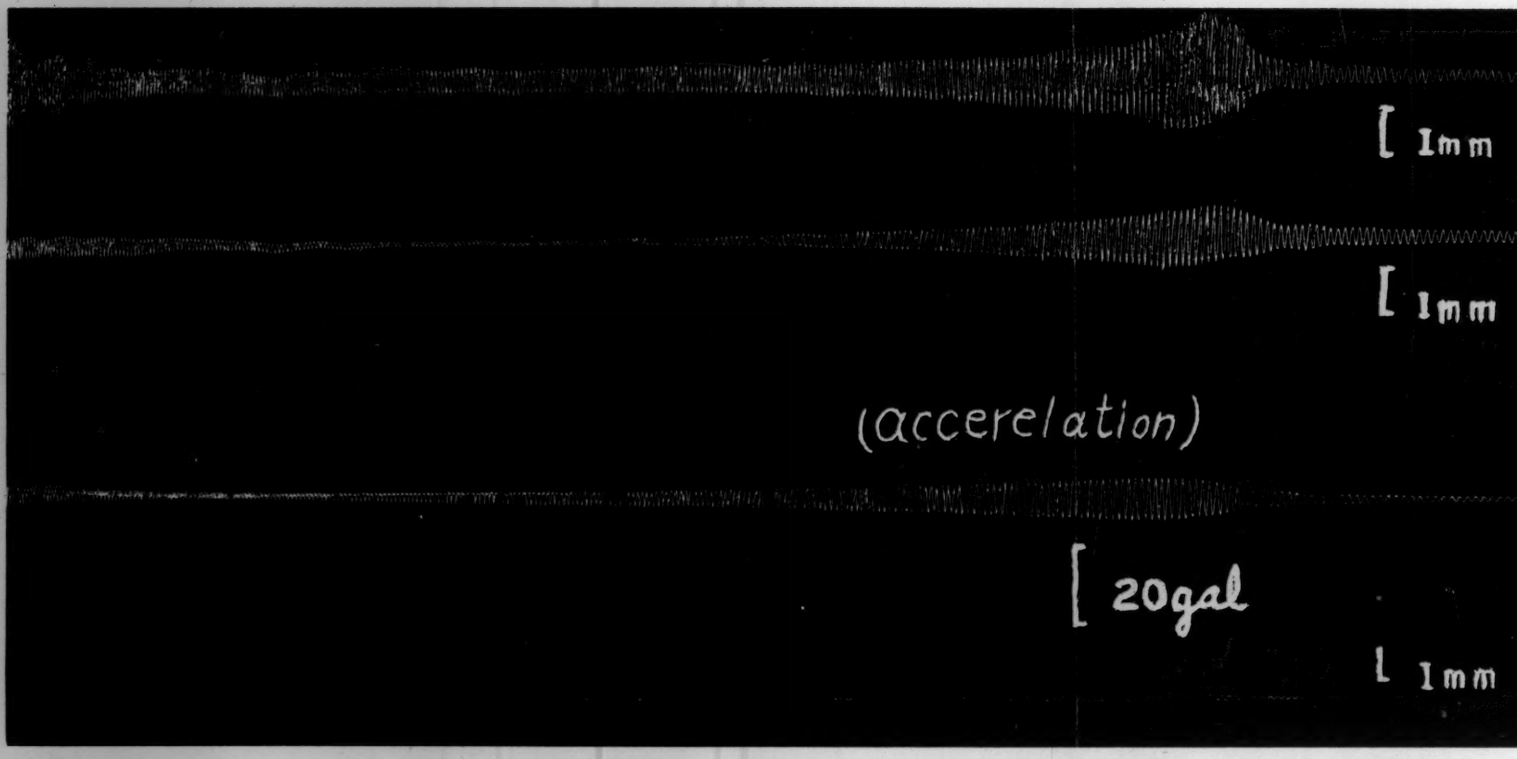

Fig. 8. E-W comp. records of the forced vibrations. Unbalanced mass M_e=3.4 kg.

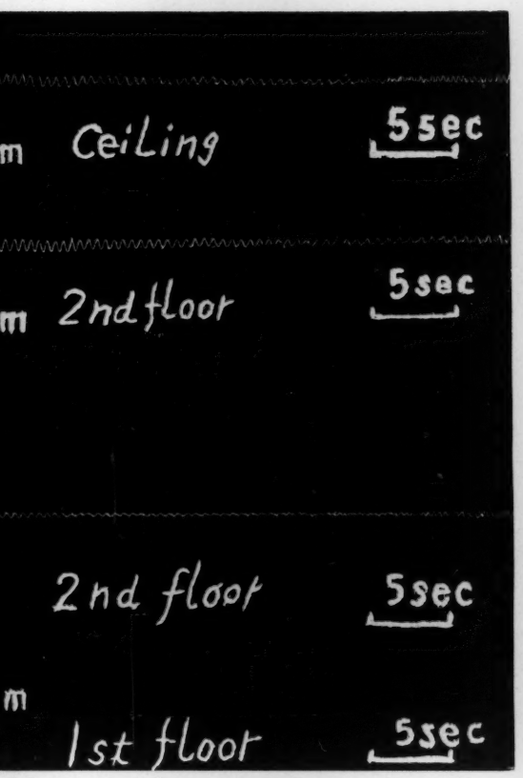
m Ceiling 5sec
m 2nd floor 5sec
2nd floor 5sec
m
1st floor 5sec

kg.

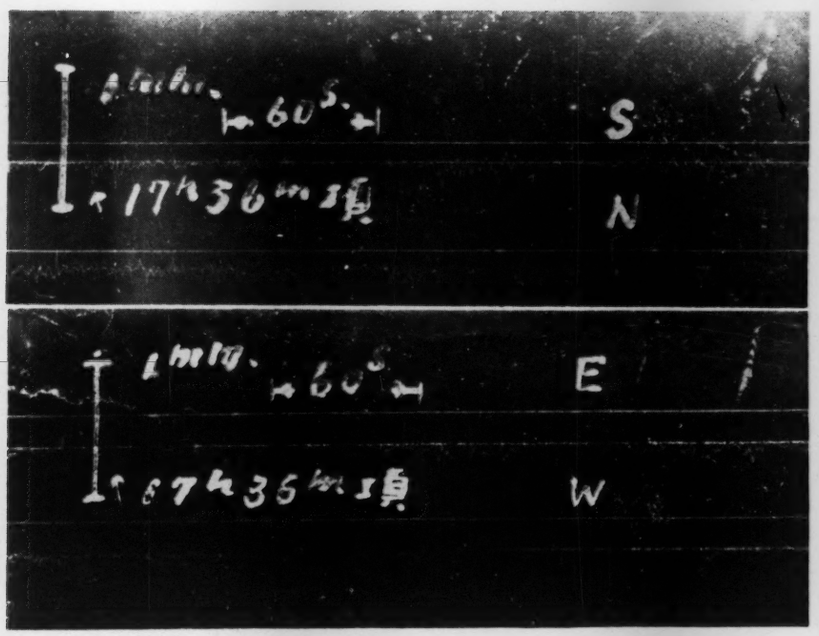

Fig. 17a. Vibration records of the house due to N-E wind.

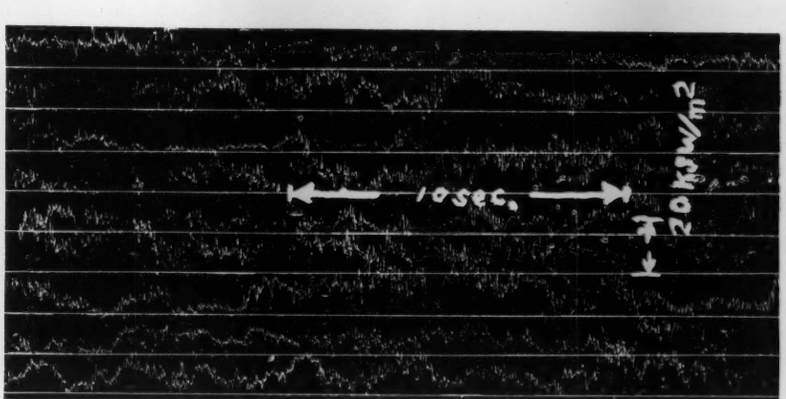

Fig. 17b. Records of N-E wind.

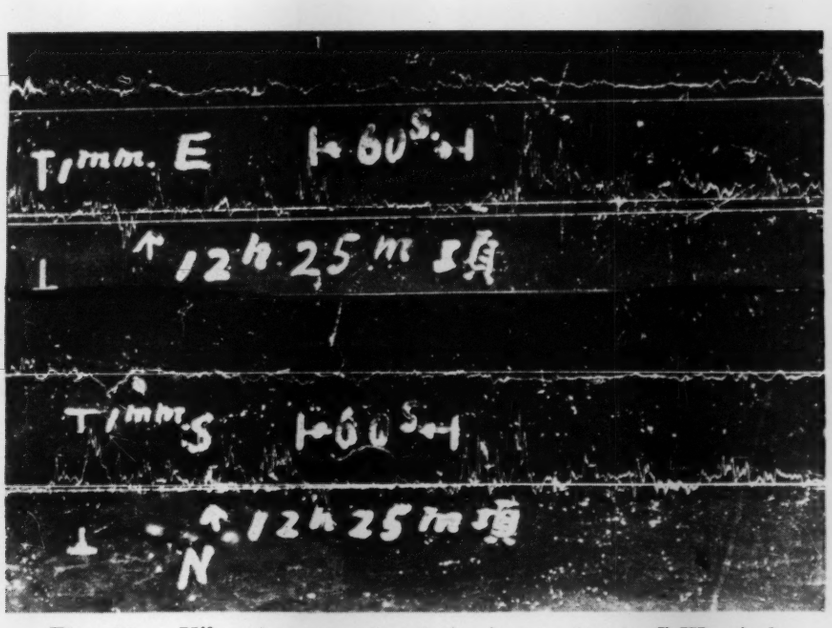

Fig. 18a. Vibration records of the house due to S-W wind.

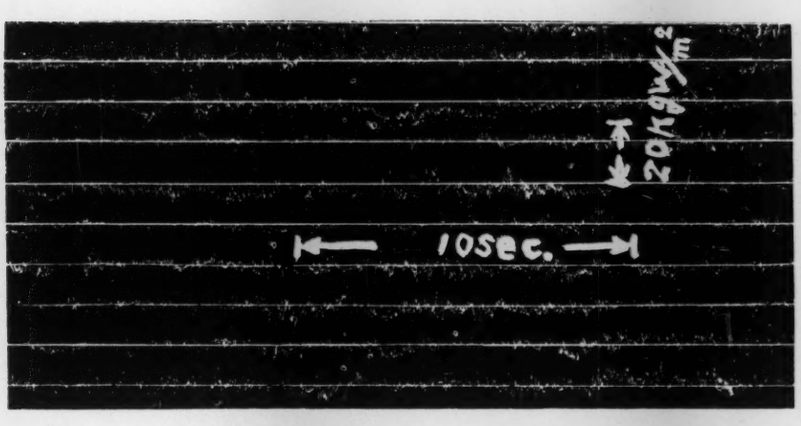

Fig. 18b. Records of S-W wind.

8. 自然風及び起振機等による木造二階建住宅の振動

地震研究所 {西村源六郎 / 鈴木正治}

筆者達は自然風の観測結果を発表したが，此の観測と共に自然風に依る木造家屋の振動観測も合せて行つた．従来木造家屋の耐風構造の問題は静的に取扱われ自然風の息に対する動的の考慮は殆んど見当らない．然しながら鉄塔及び高層建造物等の自然風に依る振動観測の結果に就いては報告されて居る．本観測は最初は風の観測点附近に実験家屋を求むる予定であつたが，適当の家屋が見当らずその地点より南方約 50 米の木造二階建の家屋を選定観測する事にした．本報告は直接風の観測と対応する部分は少なく主として直接人力に依る自由振動，起振機に依る強制振動及び日射熱に依る家屋の動きに就いてである．これを総括すれば次の如くである．

i 自由振動 自己振動週期は E–W 成分は 0.31 秒～0.34 秒，N–S 成分は 0.29 秒～0.30 秒，減衰比は E–W 成分は 1.06～1.35，N–S 成分は 1.08～1.27 で，振動振幅が増加すれば自巳振動週期及び減衰比が増加する．

ii 強制振動 自巳振動週期は自由振動の場合と同様振動振幅が増加すると，E–W，N–S 両成分共に増加する．同一加力に対して両成分を比較すると，N–S 成分は静的及び共振時に於ても加力に振幅は比例するが，E–W 成分に於ては静的には比例するが共振時には比例しない．天井 N–S 成分の静的振幅はそれの E–W 成分と比較すると 0.32 倍，二階の N–S 成分の 0.41 倍となり顕著に小さい．之は N–S 成分に壁体の効果が多いものと考えられる．

iii 自然風に対するもの

a 風圧と変位 変位は殆んど風圧に比例する．天井の変位は二階の 1.4 倍～1.2 倍である．同一風圧に対して南西風に依る場合の変位は北東風に依る場合より二階及び天井共大きい．

b 週期と頻度 家屋の卓越振動週期は，家屋の固有振動週期 0.30～035 秒附近と 2.6 秒～3.2 秒附近に卓越する，又南西風に依るものが北東風より大きな週期の波動が多い．

c 週期と変位 家屋の固有振動週期 0.30～0.35 秒附近の振動変位は小さく，最も大きい変位を与える週期は 2.0～5.0 秒である．

d 家屋の平面的運動 風力に依る家屋の変位の軌道は楕円運動で，之は風向変化と家屋の構造に依るものと考えられる．

iv 日射に依るもの

家屋は日射に依り各部の温度差に依り応力を受ける．此の結果変形するのであるが，気温変化と相似な変化をなし，その変位量は一日の温度差に比例し，曇天及雨天の日は極めて小さく，その運動の経路は楕円である．各階の各成分は大体相似で夫々異つた残留変位がある．

結　語

一般の木造住宅は其の固有週期は殆んど一秒以下である故風の息の週期に依る共振は殆んど考慮の必要なく，静的の取扱ひで充分と考えられるが，木造構造物中で其の固有振動週期の長い五重塔其の他一秒以上の固有振動週期の構造物は其の設計には一応共振を考慮した動的な取扱をなすべきであると考える，

前記装置に依つて種々の振動観測の結果について述べたが，家屋の構造及び風の性質に依つて多少は異る結果はあると思われるが，将来の研究のいとぐちともなれば著者等は満足である．

筆を擱くにあたり元稲取町実業学校教官故前田芳太郎氏に対し生前に於て観測及び御協力に依て此の研究を遂行し得たもので同氏の靈に対し感謝する次第である．尚機械の設置に関しては保坂製作所長保坂勝造氏の御協力に依るもので御礼申上げ，研究費の大部分は日本学術振興会の援助に依るもので茲に感謝の意を表す．

昭和29年6月25日印刷
昭和29年6月30日發行

東京都文京區本富士町一番地
東京大學構内
編纂兼
發行者　東京大學地震研究所

東京都千代田區富士見町一丁目十番地
印刷者　笠井康賴

東京都千代田區富士見町一丁目十番地
印刷所　株式會社國際文献印刷社

賣捌所　東京都千代田區神田一ツ橋通
岩波書店

東京都中央區日本橋通二丁目六番地
丸善株式會社

Sold by
Iwanami Shoten,
Hitotsubashi dôri, Chiyoda-ku, Tôkyô,
and
Maruzen Co., Ltd.,
Nihonbashi dôri, Chûô-ku, Tôkyô.
Price of this copy: 704 Yen. (Postage exclusive.)

BULLETIN OF

THE EARTHQUAKE RESEARCH INSTITUTE

TOKYO UNIVERSITY

Vol. XXXII, Part 1. March, 1954.

Contents.

Papers and Reports.

Page

1. T. MATUZAWA, S-Wellen an der fest-flüssigen Schichtgrenze. I. (im Deutschen) 1
2. Y. SATÔ, Study on Surface Waves X. Equivalency of SH-waves and Sound Waves in a Liquid. (in English) 7
3. I. YOKOYAMA, Geomagnetic Studies of Volcano Mihara. The 4th paper. (A Series of Geomagnetic Dip-Surveys and Continuous Observation of Changes in Geomagnetic Declination.) (in English) 17
4. H. TSUYA, R. MORIMOTO and J. OSSAKA, The 1950–1951 Eruptions of Mt. Mihara, Oshima Volcano, Seven Izu Islands, Japan. Part I. The 1950 eruption. (in English) 35
5. K. KASAHARA, Experimental Studies on the Mechanism of Generation of Elastic Waves IV. (in English) 67
6. The Research Group for Explosion Seismology, The Fourth Explosion-Seismic Observations in North-Eastern Japan. (in English) 79
7. G. NISHIMURA, M. SUZUKI and E. FURUKAWA, Theory of Eden's Twin Strips and Application of It to Magnifying Mechanism of Seismometer. (in English) 87
8. G. NISHIMURA and M. SUZUKI, Horizontal Deformations of a Japanese Two-Storied Frame-House: (1) Vibration due to an Arbitrary Shock, (2) Vibration Caused by a Rotary with Unbalanced Mass, (3) Vibration due to Natural Wind, and (4) Deformation due to the Sun's Radiation Heat. (in English) 113

(For the papers written in Japanese or in occidental languages, the abstracts are given in occidental languages or in Japanese respectively.)

BULLETIN OF THE EARTHQUAKE RESEARCH INSTITUTE,
TOKYO UNIVERSITY. Vol. XXXII, Part 2. June, 1954.

東京大學
地震研究所彙報

第 32 號　第 2 册

昭和 29 年 6 月

目　次

論文及報告

			頁
9.	Fourier 級数に関する一つの問題（英文）	高橋健人	147
10.	固体液体の境の面の S波 II（独文）	松沢武雄	155
11.	表面波の研究 XI 表面波の定義及び分類（英文）	佐藤泰夫	161
12.	三原山の地球磁気学的研究 第5報（1951年5月から1953年8月にいたる期間の地磁気三成分の変化）（英文）	横山泉	169
13.	東京横浜における加速度地震計記象の解析結果（英文）	金井清 鈴木正治	189
14.	常時微動の測定 第1報（英文）	金井清 田中貞二 長田甲斐男	199
15.	地震動の振幅と周期との関係（小引）（英文）	金井清	211
16.	大島新熔岩の粘性の熱履歴について（英文）	佐久間修三	215

所　報

(The titles in occidental languages are given on the back cover.)

本彙報ハ年4回 (但シ第1號ヨリ第6號マデハ不定期ニ, 第7號ハ3冊トシテ發行セリ), 彙報別冊ハ不定期ニ發行ス.

本彙報掲載ノ論文及ビ報告ノ内容ニ關シテハ著者ノミニ其責任アルモノトス.

本彙報ニ關スル照會通信ハ東京大學地震研究所長ヘ宛テラレタシ.

The Bulletin is published quarterly. (Vols. I–VI were published at irregular intervals and Vol. VII consisted of three parts.)
Supplementary Volume is published at irregular interval.

The authors of the papers alone are responsible for the statements and opinions contained in their respective papers.

All communications relating to this Bulletin should be addressed to the Director of the Earthquake Research Institute, Tokyo University.

9. *A Problem on Fourier Series.**

By Takehito TAKAHASHI,

Seizyo University, Setagaya, Tokyo.

(Read Jan. 26, 1954.—Received March 31, 1954.)

1.

In relation to the study of gravity Prof. C. Tsuboi has proposed the problem of finding a function whose n-th Fourier coefficient is $\varphi(n)$ (certain function of n) times that of the given function $f(x)$.

We shall give the answer when $\varphi(n)$ is either n^m (m being integer $\geqq -1$) or r^n ($|r|<1$). In the next section the fundamental case $\varphi(n)=n$ is treated under somewhat strict conditions on $f(x)$. They are mostly removed in the 3rd section from the standpoint of the theory of distributions of L. Schwarz, including the case when $\varphi(n)$ differs from n. Examples are given in the last section.

2.

Let $f(x)$ be an absolutely continuous function with period 2π. Then $f(x)$ is an integral and we can write

$$f(x)=\frac{1}{2}a_0+\sum_{n=1}^{\infty}(a_n\cos nx+b_n\sin nx)\,, \tag{1}$$

$$f'(x)\sim\sum_{n=1}^{\infty}(-a_n\sin nx+b_n\cos nx)\,. \tag{2}$$

We shall try to transform the right hand side of (2) into the series in question[1]

$$\sum_{n=1}^{\infty}n(a_n\cos nx+b_n\sin nx)\,.$$

We denote by $g(x)$ a function which, if it exists, has the above series as its Fourier series, that is

---

* Communicated by Y. Satô.

1) This series is said to be conjugate to the Fourier series (2). For the various studies on conjugate series we refer to G. H. HARDY and W. W. ROGOSINSKY, *Fourier series*. (Cambridge Tracts No. 38) 76, 99.

$$g(x)\sim\sum_{n=1}^{\infty} n(a_n\cos nx+b_n\sin nx)\ . \tag{3}$$

Now $f'(x)$ being a periodic function, we get from (2)

$$f'(x-t)\sim\sum_{n=1}^{\infty} n\{(a_n\cos nx+b_n\sin nx)\sin nt+(-a_n\sin nx+b_n\cos nx)\cos nt\}. \tag{4}$$

This formula calls for an adequate function which, being multiplied by $\sin nt$ or $\cos nt$ and integrated with t, proves to be a constant number or zero.

For this purpose we utilize the following relations:

$$\int_{-\infty}^{\infty}\frac{\sin nt}{t}dt=\pi\ , \tag{5}$$

$$P\int_{-\infty}^{\infty}\frac{\cos nt}{t}dt=\lim_{\varepsilon\to 0}\left(\int_{-\infty}^{-\varepsilon}+\int_{\varepsilon}^{\infty}\right)=0\ . \tag{6}$$

By transforming the equation (5), as

$$\int_{-\infty}^{\infty}\frac{\sin nt}{t}dt=\sum_{n=-\infty}^{\infty}\int_{(2m-1)\pi}^{(2m+1)\pi}\frac{\sin t}{t}dt$$

$$=\int_{-\pi}^{\pi}\frac{\sin nt}{t}dt+\sum_{n=1}^{\infty}\int_{-\pi}^{\pi}\left(\frac{1}{t-2n\pi}+\frac{1}{t+2n\pi}\right)\sin nt\,dt,$$

and using Euler's relation

$$\cot\frac{t}{2}=\frac{2}{t}+\sum_{n=1}^{\infty}\frac{4t}{t^2-4n^2\pi^2}\ ,$$

we obtain[2]

$$\int_{-\pi}^{\pi}\cot\frac{t}{2}\sin nt\,dt=2\pi\ , \tag{7}$$

and

$$P\int_{-\pi}^{\pi}\cot\frac{t}{2}\cos nt\,dt=0\ . \tag{8}$$

Now we are to show that

$$g(x)=\frac{1}{2\pi}P\int_{-\pi}^{\pi}f'(x-t)\cot\frac{t}{2}\,dt\ . \tag{9}$$

2) Formulas (7) and (8) may be proved directly if we notice that the left side of (7) is independent of n.

To avoid P symbol the left side is transformed into

$$\frac{1}{2\pi}\int_0^{\pi}\{f'(x-t)-f'(x+t)\}\cot\frac{t}{2}\,dt\,.$$

Then the Fourier coefficients of the above function may be given by the repeated integral of the type

$$\frac{1}{2\pi^2}\int_{-\pi}^{\pi}\sin nx\,dx\int_0^{\pi}\{f'(x-t)-f'(x+t)\}\cot\frac{t}{2}\,dt\,,$$

which proves to be the expected value na_n, if this integral exists and we can interchange the order of integration. For this, it is sufficient that the function $\{f'(x-t)-f'(x+t)\}/t$ should be continuous both in x and t.

In the case when $f'(x)$ is also absolutely continuous we get another expression for $g(x)$ by integrating (7) by parts, as

$$g(x)=\frac{1}{\pi}\int_{-\pi}^{\pi}f''(x-t)\log\left|2\sin\frac{t}{2}\right|dt\,. \tag{10}$$

This expression is sometimes useful as we need not take Cauchy's principal value because of the integrability of the logarithmic function.

Another way of integration by parts gives rise to the expression which does not contain $f'(x)$ or $f''(x)$:

$$\begin{aligned}g(x)&=\frac{1}{2\pi}\lim_{\varepsilon\to 0}\left(\int_{-\pi}^{-\varepsilon}+\int_{\varepsilon}^{\pi}\right)f(x-t)\operatorname{cosec}^2\frac{t}{2}\,dt\\&=\frac{1}{2\pi}\lim_{\varepsilon\to 0}\left\{-f(x+\varepsilon)\cot\left(\frac{-\varepsilon}{2}\right)+f(x-\varepsilon)\cot\frac{\varepsilon}{2}\right.\\&\quad\left.-\frac{1}{2}\left(\int_{-\pi}^{-\varepsilon}+\int_{\varepsilon}^{\pi}\right)f(x-t)\operatorname{cosec}^2\frac{t}{2}\,dt\right\}\\&=-\frac{1}{4\pi}\lim_{\varepsilon\to 0}\left\{\left(\int_{-\pi}^{-\varepsilon}+\int_{\varepsilon}^{\pi}\right)f(x-t)\operatorname{cosec}^2\frac{t}{2}\,dt-\frac{8f(x)}{\varepsilon}\right\}\,.\end{aligned} \tag{11}$$

After Hadamard we express this formula by the notation

$$g(x)=-\frac{1}{4\pi}P_f\int_{-\pi}^{\pi}f(x-t)\operatorname{cosec}^2\frac{x-t}{2}\,dt\,, \tag{11'}$$

which means the "finite part" of the divergent integral.

The results (9)~(11') can be easily transformed into

$$g(x)=\frac{1}{2\pi}P\int_{-\pi}^{\pi}f'(t)\cot\frac{x-t}{2}\,dt\,, \tag{9'}$$

$$g(x)=\frac{1}{\pi}\int_{-\pi}^{\pi} f''(t)\log\left|2\sin\frac{x-t}{2}\right|dt\,, \tag{10'}$$

$$=-\frac{1}{4\pi}P_f\int_{-\pi}^{\pi} f(t)\operatorname{cosec}^2\frac{x-t}{2}\,dt\,. \tag{11''}$$

3.

The theory of Fourier series becomes more natural and clear if we extend the concept of function to the framework of distributions.[3)]

For example, Dirac's delta function $\delta(x)$ which is defined for any continuous function $\varphi(x)$ by the relation

$$\delta(\varphi)\equiv\int_{-\pi}^{\pi}\delta(x)\varphi(x)dx=\varphi(0)$$

may be expanded in Fourier series

$$\delta(x)=\frac{1}{\pi}\left(\frac{1}{2}+\sum_{n=1}^{\infty}\cos nx\right).$$

In general, (periodic) distribution T is a linear and continuous functional $T(\varphi)$ defined for all indefinitely differentiable functions $\varphi(x)$ of period 2π. Any integrable periodic $f(x)$ is identified with the distribution

$$f(\varphi)=\int_{-\pi}^{\pi} f(x)\varphi(x)dx\,. \tag{12}$$

A distribution can always be expanded in its Fourier series, and every trigonometrical series with coefficients bounded by a fixed polynominal converges to some distribution having the given coefficients as its Fourier series. Term by term differentiation of Fourier series is always allowed.

Differentiation of a distribution T is defined by the relation

$$T'(\varphi)=-T(\varphi'). \tag{13}$$

When a function $f(x)$ gives a jump at $x=a$ and elsewhere has ordinary derivative $[f'(x)]$, the distribution derivative $f'(x)$ is expressed as

$$f'(x)=[f'(x)]+\{f(a+0)-f(a-0)\}\delta(x-a)\,. \tag{14}$$

Distribution-theoretically, all the procedures in the preceding section

3) L. SCHWARZ, *Théorie des distributions*, I–II (Paris, 1950–51).

are allowed only when $f(x)$ is a distribution. And we can write from (7) and (8)

$$\frac{1}{2}P\cot\frac{x}{2}=\sum_{n=1}^{\infty}\sin nx\,. \tag{15}$$

On differentiating both sides we have

$$-\frac{1}{4}P_f\operatorname{cosec}^2\frac{x}{2}=\sum_{n=1}^{\infty}n\cos nx\,. \tag{16}$$

Then the results of the preceding section (9)$\sim$(11'') are to be interpreted as the convolution products of the two distributions.

The idea of convolution product is essential in our problem: if we can find a distribution $v(x)$ whose n-th Fourier coefficient is $(\varphi(n),\ 0)$

$$v(x)=\frac{1}{2}\varphi(0)+\sum_{n=1}^{\infty}\varphi(n)\cos nx\,, \tag{17}$$

our result is expressed as the convolution product of $f(x)$ and $v(x)$

$$\int_{-\pi}^{\pi}f(t)\,v(x-t)\,dt=\frac{1}{2}a_0\varphi(0)+\sum_{n=1}^{\infty}\varphi(n)(a_n\cos nx+b_n\sin nx)\,. \tag{18}$$

Some cases are considered below.

For $\varphi(n)=r^n$ $(|r|<1)$ we may choose as $v(x)$ the real part of

$$(1-re^{ix})^{-1}-\frac{1}{2}=\frac{1}{2}+\sum_{n=1}^{\infty}r^ne^{inx}=\left(\frac{1}{2}+\sum_{n=1}^{\infty}r^n\cos nx\right)+i\sum_{n=1}^{\infty}r^n\sin nx\,, \tag{19}$$

the left side of which is equal to

$$(1-r^2)\{2(1+r^2-2r\cos x)\}^{-1}+ir\sin x\,(1+r^2-2r\cos x)^{-1}. \tag{19'}$$

Putting the real part of (19') into (18), we obtain

$$\frac{1}{2\pi}\int_{-\pi}^{\pi}f(t)(1-r^2)(1+r^2-2r\cos(x-t))^{-1}dt$$

$$=\frac{1}{2}a_0+\sum_{n=1}^{\infty}r^n(a_n\cos nx+b_n\sin nx)\,. \tag{20}$$

We find that (19') tends to $\{\pi\delta(x)+i2^{-1}P\cot(x/2)\}$ and the left side of (20) to Poisson's integral as $r\to1$.

If $\varphi(n)=1/n$ $(\varphi(0)=0)$ we integrate the imaginary part of (19) to obtain in the limit $r\to1$

$$-\log\left|2\sin\frac{x}{2}\right|=\sum_{n=1}^{\infty}\frac{\cos nx}{n}\qquad(x\neq0). \tag{21}$$

Then we get

$$-\frac{1}{\pi}\int_{-\pi}^{\pi} f(t)\log\left|2\sin\frac{x-t}{2}\right|dt=\sum_{n=1}^{\infty}\frac{1}{n}(a_n\cos nx+b_n\sin nx)\,. \tag{22}$$

In the case of $\varphi(n)=n^{2k}$ or n^{2k+1} (k positive integer) we need only differentiate the distribution $f(x)$ or $g(x)$:

$$(-1)^k f^{(2k)}(x)=\sum_{n=1}^{\infty} n^{2k}(a_n\cos nx+b_n\sin nx)\,, \tag{23}$$

$$\begin{aligned}(-1)^k g^{(2k)}(x)&=\frac{(-1)^k}{2\pi}P\int_{-\pi}^{\pi} f^{(2k+1)}(t)\cot\frac{x-t}{2}dt\\&=\sum_{n=1}^{\infty} n^{2k+1}(a_n\cos nx+b_n\sin nx)\,.\end{aligned} \tag{24}$$

4.

As an example we take up the following function:

$$f(x)=\sum_{n=1}^{\infty} n^{-2}\cos nx=\frac{1}{4}(\pi-|x|)^2-\frac{1}{12}\pi^2\,, \tag{25}$$

$$f'(x)=[f'(x)]=\begin{cases}(x-\pi)/2 & (x>0)\\(x+\pi)/2 & (x<0)\,.\end{cases} \tag{25'}$$

In this case $g(x)$ is a known function

$$g(x)=\sum_{n=1}^{\infty} n^{-1}\cos nx=-\log\left|2\sin\frac{x}{2}\right| \qquad (x\neq 0). \tag{26}$$

We first verify the formula (9′). Assuming $\pi>x>0$ we calculate as follows:

$$\begin{aligned}\frac{1}{2\pi}P\int_{-\pi}^{\pi} f'(t)\cot\frac{x-t}{2}dt&=\frac{1}{4\pi}\lim_{\varepsilon\to 0}\left\{\int_{-\pi}^{0}(t+\pi)\cot\frac{x-t}{2}\,dt\right.\\&\qquad\left.+\left(\int_0^{x-\varepsilon}+\int_{x+\varepsilon}^{\pi}\right)(t-\pi)\cot\frac{x-t}{2}dt\right\}\\&=-\frac{1}{2\pi}\lim_{\varepsilon\to 0}\left\{\left[(t+\pi)\log\left|\sin\frac{x-t}{2}\right|\right]_{-\pi}^{0}+\left[(t-\pi)\log\left|\sin\frac{x-t}{2}\right|\right]_0^{x-\varepsilon}\right.\\&\qquad\left.+\left[(t-\pi)\log\left|\sin\frac{x-t}{2}\right|\right]_{x+\varepsilon}^{\pi}-\left(\int_{-\pi}^{x-\varepsilon}+\int_{x+\varepsilon}^{\pi}\right)\log\left|\sin\frac{x-t}{2}\right|dt\right\}\\&=-\frac{1}{2\pi}\left\{2\pi\log\left|\sin\frac{x}{2}\right|+\int_{-\pi}^{\pi}\log\left|\sin\frac{x-t}{2}\right|dt\right\}\,.\end{aligned}$$

The last expression reduces itself to (26), since

$$\int_{-\pi}^{\pi} \log\left|\sin\frac{x-t}{2}\right| dt = \int_{-\pi}^{\pi} \log\left|\sin\frac{x-t}{2}\right| dt = -2\pi\log 2\,. \qquad (27)$$

If we use the formula (10′) the calculation becomes simplified. Introducing into (10′) the derivative of (25′)

$$f''(x) = \frac{1}{2} - \pi\delta(x)\,,$$

we obtain

$$\frac{1}{\pi}\int_{-\pi}^{\pi}\left(\frac{1}{2}-\pi\delta(x)\right)\log\left|2\sin\frac{x-t}{2}\right| dt$$

$$= \frac{1}{2\pi}\int_{-\pi}^{\pi} \log\left|2\sin\frac{x-t}{2}\right| dt - \log\left|2\sin\frac{x}{2}\right| = -\log\left|2\sin\frac{x}{2}\right|\,,$$

by the aid of the relation (27).

If we start from

$$f(x) = \sum_{n=1}^{\infty} n^{-1}\sin nx = \begin{cases} (\pi-x)/2 & (x>0) \\ (-\pi-x)/2 & (x<0) \end{cases}$$

$$f'(x) = -\frac{1}{2} + \pi\delta(x)\,,$$

we obtain

$$g(x) = \frac{1}{2\pi}\,P\int_{-\pi}^{\pi}\left(-\frac{1}{2}+\pi\delta(t)\right)\cot\frac{x-t}{2}\,dt = \frac{1}{2}P\cot\frac{x}{2}\,,$$

which is obviously not a function.

This example shows that we can not expect to get a function even when $f(x)$ is a function.

---

9. Fourier 級数に関する一つの問題

成城大学　高　橋　健　人

与えられた函数の n 番目の Fourier 係数を $\varphi(n)$ 倍したものを Fourier 係数とする函数を求める問題を考える．これは重力常数の研究に関聯して坪井教授によつて提出されたものである．

$\varphi(n)=r^n$ ($|r|<1$) 及び n^m (m は整数 ≥ -1) に対し解答を与えた．(公式 (9)～(11″), (20)～(24)). これらは Fourier 級数論に於て既に知られた結果を含んでいるが，函数の枠を L. Schwarz による distribution にまで拡大することによつて収斂条件等が不必要になり一般的な取扱いができる．最後に計算例をあげた．

10. *S-Wellen an der fest-flüssigen Schichtgrenze. II.*

Von Takeo MATUZAWA

Institut für Erdbebenforschung.

(Vorgelegt den 19. Feb. 1954.—Eingegangen den 23. März 1954.)

1. Verhalten der SV-Wellen an der Schichtgrenze.

In der ersten Mitteilung wurde das Verhalten der SH-Wellen an der fest-flüssigen Schichtgrenze untersucht. Natürlich kommt der Fall vom Eintritt der SV-Wellen oft vor. Als die Ergänzung wird der Fall diskutiert.

Die (x, y)-Ebene sei an der Schichtgrenze genommen und die positive z-Achse sei in die Zähflüssigkeit gerichtet.

Die Gleichung der kleine Bewegung in der Flüssigkeit lautet,

$$\left.\begin{aligned} \rho' \frac{\partial^2 u'}{\partial t^2} &= -\frac{\partial p'}{\partial x} + \nu \frac{\partial}{\partial t}\left(\frac{\partial^2 u'}{\partial x^2} + \frac{\partial^2 u'}{\partial z^2}\right), \\ \rho' \frac{\partial^2 w'}{\partial t^2} &= -\frac{\partial p'}{\partial z} + \nu \frac{\partial}{\partial t}\left(\frac{\partial^2 w'}{\partial x^2} + \frac{\partial^2 w'}{\partial z^2}\right), \\ v' &= 0 \end{aligned}\right\} \qquad (1)$$

wo, u', v' und w' Komponenten der kleinen Verschiebung des Flüssigkeitsteilchens sind,

ρ' die Dichte der Flüssigkeit ist,

ν die Viskosität der Flüssigkeit ist,

und p' der Zusatzdruck in der gestörten Flüssigkeit ist.

Nun

$$p' = -\rho' c^2 \left(\frac{\partial u'}{\partial x} + \frac{\partial w'}{\partial z}\right),$$

wo, c die Schallgeschwindigkeit in der Flüssigkeit ist.

Also aus (1)

$$\left.\begin{aligned} \rho' \frac{\partial^2 u'}{\partial t^2} &= \rho' c^2 \frac{\partial}{\partial x}\left(\frac{\partial u'}{\partial x} + \frac{\partial w'}{\partial z}\right) + \nu \frac{\partial}{\partial t}\left(\frac{\partial^2 u'}{\partial x^2} + \frac{\partial^2 u'}{\partial z^2}\right), \\ \rho' \frac{\partial^2 w'}{\partial t^2} &= \rho' c^2 \frac{\partial}{\partial z}\left(\frac{\partial u'}{\partial x} + \frac{\partial w'}{\partial z}\right) + \nu \frac{\partial}{\partial t}\left(\frac{\partial^2 w'}{\partial x^2} + \frac{\partial^2 w'}{\partial z^2}\right). \end{aligned}\right\} \qquad (2)$$

Wenn man setzt in (2)

$$u'=\frac{\partial\phi'}{\partial x}-\frac{\partial\psi'}{\partial z}\ ,$$
$$w'=\frac{\partial\phi'}{\partial z}+\frac{\partial\psi'}{\partial x}\ ,$$

dann

$$\left.\begin{aligned}&\frac{\partial u'}{\partial x}+\frac{\partial w'}{\partial z}=\frac{\partial^2\phi'}{\partial x^2}+\frac{\partial^2\phi'}{\partial z^2}\ ,\\&\rho'\frac{\partial^2}{\partial t^2}(\nabla^2\phi')=\left(\rho' c^2+\nu\frac{\partial}{\partial t}\right)\nabla^2(\nabla^2\phi')\ ,\\&\rho'\frac{\partial^2}{\partial t^2}(\nabla^2\psi')=\nu\frac{\partial}{\partial t}\nabla^2(\nabla^2\psi')\ .\end{aligned}\right\}\qquad(3)$$

Setze man

$$\phi'=A'\exp\{ih'(l_1'x+m_1'z)-ipt\}\ ,$$
$$\psi'=B'\exp\{ik'(l_2'x+m_2'z)-ipt\}\ ,$$

dann bekommt man, um den Gleichungen zu genügen,

$$\left.\begin{aligned}&\rho' p^2=(c^2\rho'-ip\nu)(\overline{h'l_1'}^2+\overline{h'm_1'}^2)\ ,\\&\rho' p^2=-ip\nu(\overline{k'l_2'}^2+\overline{k'm_2'}^2)\ .\end{aligned}\right\}\qquad(4)$$

Daher,

$$\overline{h'm_1'}^2=\sqrt{\left\{\frac{\rho' p^2\rho' c^2}{c^2\rho'^2+\overline{p\nu}^2}-\overline{h'l_1'}^2\right\}^2+\left(\frac{\rho' p^2 p\nu}{c^2\rho'^2+\overline{p\nu}^2}\right)^2}\times e^{i\varphi}\qquad(5)$$

wo

$$\tan\varphi=\frac{\rho' p^2 p\nu}{c^2\rho'^2+\overline{p\nu}^2}\Big/\left\{\frac{\rho' p^2 c^2\rho'}{c^2\rho'^2+\overline{p\nu}^2}-\overline{h'l_1'}^2\right\}.\qquad(6)$$

Dann

$$h'm_1'=+\sqrt[4]{\left\{\frac{\rho' p^2\rho' c^2}{c^2\rho'^2+\overline{p\nu}^2}-\overline{h_1'l_1'}^2\right\}^2+\left(\frac{\rho' p^2 p\nu}{c^2\rho'^2+\overline{p\nu}^2}\right)^2}\,e^{i(\varphi/2)}\ ,\qquad(7)$$

und

$$\overline{h'm_2'}^2=+\sqrt{(k'l_2')^4+\left(\frac{\rho' p^2}{p\nu}\right)^2}\,e^{-i\theta},\qquad(8)$$

wo,

$$\tan\theta=\frac{\rho' p^2}{p\nu}\Big/\overline{k'\,l_2'}^{\,2}\,. \tag{9}$$

Dann

$$k'm_2'=+i\sqrt[4]{(k'l_2')^4+\left(\frac{\rho' p^2}{p\nu}\right)^2}\,e^{-i(\theta/2)}. \tag{10}$$

Die Komponenten der Verschiebung sind also

$$\left.\begin{aligned} u_1'&=\frac{\partial\phi'}{\partial x}=ih'l_1'A'\exp\{ih'(l_1'x+m_1'z)-ipt\}\,,\\ w_1'&=\frac{\partial\phi'}{\partial z}=ih'm_1'A'\exp\{ih'(l_1'x+m_1'z)-ipt\}\,,\end{aligned}\right\} \tag{11}$$

$$\left.\begin{aligned} u_2'&=-\frac{\partial\psi'}{\partial z}=-ik'm_2'B'\exp\{ik'(l_2'x+m_2'z)-ipt\},\\ w_2'&=\frac{\partial\psi'}{\partial x}=ik'l_2'B'\exp\{ik'(l_2'x+m_2'z)-ipt\}\,.\end{aligned}\right\} \tag{12}$$

Es sei, im festen Teil, ρ die Dichte, λ und μ die Lamésche Konstanten. Die eintretende SV-Welle sei u_0, w_0, die reflektierte P-Welle u_1, w_1 und die reflektierte SV-Welle u_2, w_2.

Wie gewöhnlich setzt man,

$$\left.\begin{aligned} u_0&=-ikmB\exp\{ik(lx+mz)-ipt\}\,,\\ w_0&=iklB\exp\{ik(lx+mz)-ipt\}\,,\end{aligned}\right\} \tag{13}$$

$$\left.\begin{aligned} u_1&=ihl_1A\exp\{ih(l_1x-m_1z)-ipt\}\,,\\ w_1&=-ihm_1A\exp\{ih(l_1x-m_1z)-ipt\}\,,\end{aligned}\right\} \tag{14}$$

$$\left.\begin{aligned} u_2&=ikmB_1\exp\{ik(lx-mz)-ipt\}\,,\\ w_2&=iklB_1\exp\{ik(lx-mz)-ipt\}\,,\end{aligned}\right\} \tag{15}$$

wo

$$h^2=\frac{\rho p^2}{\lambda+2\mu}\,,\quad k^2=\frac{\rho p^2}{\mu}\,,\quad l^2+m^2=1,\quad\text{und}\quad l_1^2+m_1^2=1\,.$$

An der Schichtgrenze herrscht natürlich die Kontinuität der Verschiebung und der Spannung.

Nämlich, für $z=0$,

$$u=u'\,,\qquad w=w'\,,$$

$$-c^2\rho'\left(\frac{\partial u'}{\partial x}+\frac{\partial w'}{\partial z}\right)+2\nu\frac{\partial}{\partial t}\left(\frac{\partial w'}{\partial z}\right)=\lambda\left(\frac{\partial u}{\partial x}+\frac{\partial w}{\partial z}\right)+2\mu\frac{\partial w}{\partial z}\ ,$$

$$\nu\frac{\partial}{\partial t}\left(\frac{\partial w'}{\partial x}+\frac{\partial u'}{\partial z}\right)=\mu\left(\frac{\partial w}{\partial x}+\frac{\partial u}{\partial z}\right),$$

wo,

$$u=u_0+u_1+u_2\ , \qquad w=w_0+w_1+w_2\ ,$$
$$u'=u_1'+u_2' \quad \text{und} \quad w'=w_1'+w_2'\ .$$

Daraus bekommt man,

$$kl=h'l_1'=hl_1=k'l_2'\ , \tag{16}$$

$$\left.\begin{aligned}
&h'm_1'A'+klB'+hm_1A-klB_1=klB\ ,\\
&klA'-k'm'B'-klA-kmB_1=-kmB\ ,\\
&\left\{\frac{c^2\rho'\rho'p^2}{c^2\rho'-ip\nu}-2ip\nu\overline{h'\,m_1'}^2\right\}A'-2ip\nu k'^2l_2'm_2'B'\\
&\qquad+\{\lambda h^2+2\mu\overline{hm_1}^2\}A-2\mu k^2lmB_1=-2\mu k^2lmB\ ,\\
&-2ip\nu klh'm_1'A'+ip\nu(\overline{k'm_2'}^2-\overline{kl}^2)B'\\
&\qquad-2\mu hm_1klA-\mu k^2(m^2-l^2)B_1=\mu k^2(m^2-l^2)B\ .
\end{aligned}\right\} \tag{17}$$

2. Approximation für kleines l, nämlich für beinahe vertikalen Eintritt der SV-Wellen.

Es ist ziemlich umständlich, den allgemeinen Fall streng zu lösen. Aber im Reflexionsverfahren interessiert uns der Fall vom beinahe vertikalen Eintritt. Wenn sich die Approximation bis zur ersten Ordnung von l beschränkt, dann wird die Rechnung ziemlich vereinfacht.

Aus (6) und (7)

$$\left.\begin{aligned}
&\tan\varphi\doteqdot\frac{p\nu}{\rho'c^2}\ ,\\
&h'm_1'=\sqrt{\frac{\rho'p^2}{\sqrt{c^2\rho'^2+\overline{p\nu}^2}}}\,e^{i(\varphi/2)}\ .
\end{aligned}\right\} \tag{18}$$

Aus (9) und (10)

$$\tan\theta\doteqdot\infty, \qquad \text{also} \qquad \theta\doteqdot\pi/2\ ,$$

und

$$k'm_2'=\sqrt{\frac{\rho'p^2}{p\nu}}\,e^{(i\pi/4)}. \tag{19}$$

Nach umständlichen Rechnungen bekommt man aus (17) mit Berücksichtigung von (16), (18) und (19)

$$\frac{A'}{B}=2\left(\frac{\rho}{\rho'}\right)^2\times$$

$$\cdot\frac{\left[1+\sqrt{\frac{\rho'\mu}{\rho p_\nu}}\left\{\left(2\sqrt{\frac{\mu}{\lambda+2\mu}}-1\right)e^{i(\pi/4)}-2\frac{p_\nu}{\mu}\sqrt{\frac{\mu}{\lambda+2\mu}}e^{-i(\pi/4)}\right\}\right]l}{\left\{\sqrt{\frac{\rho}{\rho'}}\frac{\mu}{\sqrt{c^2\rho'^2+p_\nu^2}}e^{i(\varphi/2)}-\sqrt{\frac{\mu}{\lambda+2\mu}}\left(1+\frac{p_\nu}{\sqrt{c^2\rho'^2+p_\nu^2}}e^{i(\varphi-\pi)}\right)\right\}\left\{\sqrt{\frac{\rho\mu}{\rho' p_\nu}}e^{i(\pi/4)}-1\right\}}, \tag{20}$$

$$\frac{B'}{B}=2\frac{\rho}{\rho'}\frac{1}{\sqrt{\frac{\rho\mu}{\rho' p_\nu}}e^{i(\pi/4)}-1}, \tag{21}$$

$$\frac{A}{B}=2\frac{\rho}{\rho'}\times$$

$$\cdot\frac{\left\{1+\sqrt{\frac{\rho'\mu}{\rho p_\nu}}e^{i(\pi/4)}-2e^{-i(\pi/4)}-\frac{\mu}{p_\nu}e^{i(\pi/4)}\right\}l}{\left\{\sqrt{\frac{\rho}{\rho'}}\frac{\mu}{\sqrt{c^2\rho'^2+p_\nu^2}}e^{i(\varphi/2)}-\sqrt{\frac{\mu}{\lambda+2\mu}}\left(1+\frac{p_\nu}{\sqrt{c^2\rho'^2+p_\nu^2}}e^{i(\varphi-\pi)}\right)\right\}\left\{\sqrt{\frac{\rho\mu}{\rho' p_\nu}}e^{i(\pi/4)}-1\right\}}, \tag{22}$$

$$\frac{B_1}{B}=-\frac{\sqrt{\frac{\rho\mu}{\rho' p_\nu}}e^{i(\pi/4)}+1}{\sqrt{\frac{\rho\mu}{\rho' p_\nu}}e^{i(\pi/4)}-1}. \tag{23}$$

Wir sehen also, dass A' und A von der ersten Ordnung von l sind. Daher bekommt man aus (11), (12), (13), (14) und (15) in der ersten Annäherung von l,

$$\left.\begin{aligned} &u_1'\doteqdot 0,\\ &w_1'\doteqdot ih'm_1'A'\exp\{ih'(l_1'x+m_1'z)-ipt\},\end{aligned}\right\} \tag{24}$$

$$\left.\begin{aligned} &u_2'\doteqdot -ik'm_2'B'\exp\{ik'(l_2'x+m_2'z)-ipt\},\\ &w_2'\doteqdot ik'l_2'B'\exp\{ik'(l_2'x+m_2'z)-ipt\},\end{aligned}\right\} \tag{25}$$

$$\left.\begin{aligned} &u_0=-ikmB\exp\{ik(lx+mz)-ipt\},\\ &w_0=iklB\exp\{ik(lx+mz)-ipt\},\end{aligned}\right\} \tag{26}$$

$$\left.\begin{aligned} &u_1\doteqdot 0,\\ &w_1\doteqdot -ihm_1A\exp\{ih(l_1x-m_1z)-ipt\},\end{aligned}\right\} \tag{27}$$

$$\left.\begin{aligned} u_2 &\fallingdotseq ikmB_1 \exp\{ik(lx-mz)-ipt\}\,, \\ w_2 &\fallingdotseq iklB_1 \exp\{ik(lx-mz)-ipt\}\,. \end{aligned}\right\} \qquad (28)$$

3. Zusammenfassende Bemerkung.

Wenn man schreibt, B statt $-ikB$ in (26), A statt $-ik'm_2'B'$ in (25) und B_r statt $ikmB_1$ in (28), dann sieht man, dass u_2' in (25) und u_2 in (28) respektiv identisch mit v' und v_r in der ersten Mitteilung sind.

Nämlich sind die horizontale Komponente der Verschiebung in der Flüssigkeit und die der reflektierten SV-Wellen in diesem Falle bis zur zweiten Ordnung von l gleich den entsprechenden Komponenten im Falle von der SH-Wellen.

Im Falle der SV-Welle kommen noch dazu kleine vertikale Komponenten hinzu. Obendrein treten auch kleine vertikale Komponenten von P-Wellen auf.

Auf alle Fälle, was die horizontale Komponente von S-Welle betrifft, können wir die beiden Fälle von SH-Wellen und SV-Wellen in ganz gleicherweise behandeln, wenn der Eintrittswinkel klein ist.

10. Kotai-Ekitai no Sakai no Men no S-Nami. II.

Zisin-Kenkyûsyo MATUZAWA Takeo.

Kotai-Ekitai no Sakai no Men ni tyokkaku ni tikai Kakudo de SV-Nami ga hairu Baai no aramasi no Keisan wo okonatta. Hairu Kakudo no Nizyô izyô wo suteru Baai niwa S-nami no Suiheidô ni tuite wa SH-Nami no Baai to Kawari wa nai. P-Nami oyobi S-Nami no Zyôgedô ga, arawareru ga, sorewa Kakudo no Itizyô no Mono de aru.

11. *Study on Surface Waves* XI. *Definition and Classification of Surface Waves.*

By Yasuo SATÔ,

Earthquake Research Institute.

(Read May 19, 1953.—Received March 31, 1954.)

1. Introduction.

Since last century, an enormous number of investigations has appeared concerning the property of surface waves. Of these, Rayleigh-wave is most prominent, and its nature has been elucidated by many authors. Beside this wave, however, studies are made on those waves propagated upon elastic plates or in stratified media which are also called as and classified among surface waves. These waves do not always show the property first assigned by Lord Rayleigh to surface waves that the energy is concentrated near the free surface, but the amplitude often remains finite value throughout the layer or layers.[1] Then, should we exclude these waves from the category of surface waves and treat them separately from the typical kind of waves such as Rayleigh-waves?

We do not think so, for the mathematical treatment is quite analogous, and moreover, the change of the nature between these waves is so gradual that we can not make a rigorous distinction between them. Then how shall we define the term "*surface waves*"? And what is the representative nature of them?

Of course such a consideration is not always necessary. We can promote investigations without touching on such a discussion. However, the accumulated knowledge of ours is not small now, and it is not useless to dig into the problem more deeply and obtain a wide and profound view concerning our subject so that we may learn readily and systematically.

2. Definition (1).

Surface waves in a wide sense.

Here, we have no intention to assert that the surface wave is such

1) Y. SATÔ, *Bull. Earthq. Res. Inst.*, **29** (1951), 223.

and such or to propose that the definition of it should be so and so, but we want only to suggest a definition of the term "*surface wave*" for convenience and simplicity's sake.

As is stated in the above section, we cannot employ the definition that the surface wave is a wave whose energy is concentrated only near the free surface. We must notice another property which is conserved in waves such as Love-waves or those propagated in elastic plates.

Now, we will confine our problems, in this paper, to the case of parallel plane boundaries or a single boundary surface. The waves are always propagated along this plane, or the wave front of them is always perpendicular to this boundary. This is indeed the common nature of the problem, and this characterizes the waves under consideration. May it not serve as our definition of surface waves? At present we will employ the following definition.

> "When waves are propagated in a medium with a single or several parallel plane boundaries and their wave-front is perpendicular to this or these boundary surfaces, we call them surface waves".

3. Two types of surface waves.

According to the definition we have given just now, surface wave is propagated in the direction of boundary surfaces and it conserves that definite distribution of amplitude in regard to the direction perpendicular to the above one which is determined by the nature of the medium, wave length and the branch of dispersion curve to which this wave belongs. Now this amplitude distribution is classified into two groups, of which one takes a form expressed by the exponential function (as in Rayleigh-wave), and the other takes the sinusoidal form (as in the part of layer in the case of Love-wave). We will express the former by the symbol $[E]$ and the latter by $[S]$.

However, a single symbol is not always satisfactory, as is actually the case in Rayleigh-waves, which are to be expressed by two kinds of waves P (dilatational) and SV (distorsional). Therefore we put the symbol for the former in the left, and that for the latter in the right as $[EE]$. Finally we put a bar $[-]$[2] which implies a free surface,

2) $[-]$ demands the vanishing of stress and $[=]$ that of displacement. However, in the problem of elastic liquid the conditions are not identical with those in elastic solid. See foot-note 5).

e.g., $[\overline{EE}]$, and a double bar [=][3] which implies a rigid boundary.

Now, if a symbol $[\overline{EE}]$ is given, we can understand from it a sort of surface wave which is existent in a semi-infinite elastic medium and is constituted by the dilatational and the distorsional waves which have both the amplitude distribution of exponential type. This is of course the Rayleigh-wave. In this way we can express Love-waves and other kinds of surface waves symbolically; namely

$$\left.\begin{array}{ll} \Sigma\text{-wave}^{3)} \ldots\ldots\ldots & [\overline{S}]. \\ \text{Love-wave} \ldots\ldots\ldots & \left[\dfrac{S}{E}\right]. \\ \text{Stoneley-wave} \ldots\ldots & \left[\dfrac{EE}{EE}\right]. \\ \Pi_0^{-}\text{-wave}^{4)} \ldots\ldots\ldots & [\overline{EE}]. \\ \Pi_0^{+}\text{-wave}^{4)} \ldots\ldots\ldots & [\overline{EE}],\ [\overline{ES}]. \end{array}\right\} \ldots\ldots\ldots\ldots (3\cdot1)$$

4. Surface waves of *n*-phase-type.

In this section we will introduce one more new term. If a kind of surface wave is symbolically expressed by one letter E or S, we will call this wave a "one-phase-type". So, we call a surface wave which is expressed by n letters as "n-phase-type". For example, Love-wave is a surface wave of a two-phase-type, and Stoneley-wave is that of a four-phase-type.

In the previous section we have given symbolical representation of surface waves which are already known. Conversely, however, if a symbolical representation is given, we can determine what kind of surface wave it will be. And since we can easily obtain all sorts of symbolical expression as a problem of combination and permutation, we can describe the type of surface waves without exception. Even if

3) Surface waves in a elastic plate formed by SH-waves. Cf. Y. SATÔ, *Bull. Earthq. Res. Inst.*, **29** (1951), 223. Also see K. SEZAWA, *Sindôgaku*, p. 160, (in Japanese). F. PRESS and M. EWING, *Trans. Amer. Geophys. Union*, **32** (1951), 673.

4) Surface waves in a elastic plate formed by P- and SV-waves. Cf. Y. SATÔ, *Bull. Earthq. Res. Inst.*, **29** (1951), 223. Also see H. LAMB, *Proc. Roy. Soc. London*, **93** (1917), 114. K. SEZAWA, *Sindôgaku*, p. 158, (in Japanese). I. TOLSTOY and E. USDIN, *Geophys.*, **18** (1953), 844.

no surface wave can actually exist which corresponds to some symbolical description in some cases, there can never exist a surface wave which lacks its characteristic expression.

We will now show all the types of surface waves of one- and two-phase-type.[5]

$$\left.\begin{array}{ll}\text{One-phase-type;} & [\overline{E}],\ [\underline{\overline{E}}],\ [\underline{\underline{\overline{E}}}],\ [\underline{\underline{\underline{\overline{E}}}}],\ [\underline{\underline{\underline{\underline{\overline{E}}}}}]. \\ & [\overline{S}],\ [\underline{\overline{S}}],\ [\underline{\underline{\overline{S}}}],\ [\underline{\underline{\underline{\overline{S}}}}],\ [\underline{\underline{\underline{\underline{\overline{S}}}}}].\end{array}\right\} \quad \cdots\cdots\cdots\cdots\cdots(4.1)$$

$$\begin{aligned}\text{Two-phase-type;}\ & [\overline{EE}],\ [\underline{\overline{EE}}],\ [\underline{\underline{\overline{EE}}}],\ [\underline{\underline{\underline{\overline{EE}}}}],\ [\underline{\underline{\underline{\underline{\overline{EE}}}}}]. \\ & \left[\begin{matrix}E\\ \overline{E}\end{matrix}\right],\ \left[\begin{matrix}\overline{E}\\ \overline{E}\end{matrix}\right],\ \left[\begin{matrix}\underline{\overline{E}}\\ \overline{E}\end{matrix}\right],\ \left[\begin{matrix}\underline{\underline{\overline{E}}}\\ \overline{E}\end{matrix}\right],\ \left[\begin{matrix}\underline{\underline{\underline{\overline{E}}}}\\ \overline{E}\end{matrix}\right],\ \left[\begin{matrix}\underline{\underline{\underline{\underline{\overline{E}}}}}\\ \overline{E}\end{matrix}\right], \\ & [\overline{ES}],\ [\underline{\overline{ES}}],\ [\underline{\underline{\overline{ES}}}],\ [\underline{\underline{\underline{\overline{ES}}}}],\ [\underline{\underline{\underline{\underline{\overline{ES}}}}}]. \\ & \left[\begin{matrix}E\\ \overline{S}\end{matrix}\right],\ \left[\begin{matrix}\overline{E}\\ \overline{S}\end{matrix}\right],\ \left[\begin{matrix}E\\ \underline{\overline{S}}\end{matrix}\right],\ \left[\begin{matrix}\underline{\overline{E}}\\ \overline{S}\end{matrix}\right],\ \left[\begin{matrix}\underline{\underline{\overline{E}}}\\ \overline{S}\end{matrix}\right],\ \left[\begin{matrix}E\\ \underline{\underline{\overline{S}}}\end{matrix}\right],\ \left[\begin{matrix}\underline{\overline{E}}\\ \underline{\overline{S}}\end{matrix}\right],\ \left[\begin{matrix}\underline{\underline{\overline{E}}}\\ \underline{\overline{S}}\end{matrix}\right],\ \left[\begin{matrix}\underline{\underline{\underline{\overline{E}}}}\\ \underline{\overline{S}}\end{matrix}\right], \\ & \left[\begin{matrix}S\\ \overline{S}\end{matrix}\right],\ \left[\begin{matrix}\overline{S}\\ \overline{S}\end{matrix}\right],\ \left[\begin{matrix}\underline{\overline{S}}\\ \overline{S}\end{matrix}\right],\ \left[\begin{matrix}\underline{\underline{\overline{S}}}\\ \overline{S}\end{matrix}\right],\ \left[\begin{matrix}\underline{\underline{\underline{\overline{S}}}}\\ \overline{S}\end{matrix}\right],\ \left[\begin{matrix}\underline{\underline{\underline{\underline{\overline{S}}}}}\\ \overline{S}\end{matrix}\right].\end{aligned}$$

$$\cdots\cdots\cdots\cdots\cdots(4.2)$$

It is, however, another problem to find what kind of wave corresponds to one of these expressions and what its nature is. We will postpone the examination of this problem to another occassion and will discuss the definition more precisely now.

5. Definition (2).

Surface waves in a narrow sense.

Definition of the surface waves given in § 2 is a very wide one. Indeed one may think of it too loose, for the waves hitherto excluded from surface waves are involved within the category of the surface waves if we adopt above definition in a wide sense.

For example, we will take up the problem of the reflection of SH-waves at the free surface. Using ordinary notations, we have (free surface; $z=0$)

5) When the medium is liquid, some proper attention must be paid with respect to the conditions at the surface. Cf. Y. SATÔ, *Bull. Earthq. Res. Inst.*, **32** (1954), 7.

incident wave: $v=A\exp\{i\tilde{\beta}z+ifx+ipt\}$,

reflected wave: $v'=A'\exp\{-i\tilde{\beta}z+ifx+ipt\}$, ...(5.1)

where A and A' are constants and

$$\tilde{\beta}=\beta/i=\sqrt{(f^2-k^2)}/i=\sqrt{(k^2-f^2)},$$

$$k=p/V_s,$$

$V_s=\sqrt{(\mu/\rho)}$ is the velocity of S-waves.

Giving the condition of free surface, namely

$$\widehat{yz}=\mu\frac{\partial}{\partial z}(v+v')=0,$$

we have $A=A'$.

Therefore $v+v'=2A\cos\tilde{\beta}z\cdot\exp\{ifx+ipt\}$. .....(5.2)

Now this wave apparently propagates in the direction of x, and the distribution of amplitude in regard to the z-direction is given by the function $2A\cos\tilde{\beta}z$.

Shall we include this phenomenon into the group of surface waves after the former wide definition? Or shall we exclude the reflection at the free surface? In the latter case, however, the part of Love-waves in the layer cannot be regarded as the surface wave. Anyhow, giving up such considerations, we will define the "surface wave in a narrow sence", here.

When the medium extends to infinity, either $\exp(\beta z)$ or $\exp(-\beta z)$ (in case the wave is dilatational $\exp(\alpha z)$ or $\exp(-\alpha z)$[6]) diverges if β (or α) is real. That is to say, when the wave is of the $[E]$-type, only one phase is (if both of the dilatational and distorsional waves exist, only two phases are) allowed in a semi-infinite medium because of the divergency of the other one (or two) phase. On the contrary, if the wave is of the $[S]$-type two (or four) phases are allowed to exist in a semi-infinite medium.

Now we will show in the following table the number of phases which can exist in a medium and the number of boundary conditions at the free surface and at the plane of separation of two kinds of media.

Let us assume some structure of media and compare the number of the boundary conditions and that of the phases of waves existent in these media by means of the following tables, then a little figuring will show that

6) $\alpha=\sqrt{f^2-h^2}$, $h=p/V_p$.

Table I.
Number of phases.

Type	P- and SV-waves[7]		SH-waves	
	[E]	[S]	[E]	[S]
Semi-infinite elastic solid	2	4	1	2
Bounded elastic solid	4	4	2	2
Semi-infinite elastic liquid	1	2	–	–
Bounded elastic liquid	2	2	–	–

Table II.
Number of boundary conditions.

	P- and SV-waves[7]	SH-waves
Free surface of elastic solid	2	1
Free surface of elastic liquid	1	—
Plane of separation of two elastic solids	4	2
Plane of separation of elastic solid and liquid	3	1
Plane of separation of two elastic liquids	2	—

if 1) all the media are bounded (with respect to the z-direction),
or 2) the waves in the semi-infinite part assume the $[E]$-type,
two numbers are equal and the elimination of indefinite constants out of the boundary conditions gives a characteristic equation. Hence the velocity of waves is determined.

On the contrary, if one or two media extends to infinity and moreover if the waves in it or them assume the $[S]$-type, then the number of the phases of waves exceeds that of the boundary conditions. Hence there remains some indeterminateness and the period can take an arbitrary value even if the velocity is given. The problem of the reflection and refraction of the plane waves are examples of such cases, which are, for example, expressed symbolically as $[\overline{S}]$, $\left[\begin{matrix}E\\S\end{matrix}\right]$, and so on.

If we exclude such cases from the surface waves in the wide sense, we can obtain surface waves in the narrow sense, which we will write down in the following.

$$\left.\begin{array}{ll}\text{One-phase-type;} & [\overline{E}],\ [\underline{\overline{E}}],\ [\underline{\underline{\overline{E}}}],\ [\underline{\overline{\overline{E}}}],\ [\underline{\underline{\underline{\overline{E}}}}].\\ & [\overline{S}],\ [\underline{\overline{S}}],\ [\underline{\underline{\overline{S}}}].\end{array}\right\} \quad \cdots\cdots\cdots\cdots(5.3)$$

7) SV-waves (of course SH-waves, too) cannot exist in a liquid.

Two-phase-type; $[\overline{EE}]$, $[\underline{EE}]$, $[\overline{\overline{EE}}]$, $[\underline{\underline{EE}}]$, $[\overline{\underline{EE}}]$.

$$\left[\begin{matrix}E\\E\end{matrix}\right], \left[\begin{matrix}\overline{E}\\E\end{matrix}\right], \left[\begin{matrix}E\\\underline{E}\end{matrix}\right], \left[\begin{matrix}\overline{E}\\\overline{E}\end{matrix}\right], \left[\begin{matrix}\overline{E}\\\underline{E}\end{matrix}\right], \left[\begin{matrix}E\\\overline{E}\end{matrix}\right].$$

$$[\overline{ES}], [\underline{ES}], [\overline{\underline{ES}}]. \qquad \ldots(5.4)$$

$$\left[\begin{matrix}E\\S\end{matrix}\right], \left[\begin{matrix}\overline{E}\\S\end{matrix}\right], \left[\begin{matrix}E\\\underline{S}\end{matrix}\right], \left[\begin{matrix}\overline{E}\\\overline{S}\end{matrix}\right], \left[\begin{matrix}\overline{E}\\\underline{S}\end{matrix}\right], \left[\begin{matrix}E\\\overline{S}\end{matrix}\right].$$

$$\left[\begin{matrix}\overline{S}\\\underline{S}\end{matrix}\right], \left[\begin{matrix}S\\\overline{S}\end{matrix}\right], \left[\begin{matrix}\overline{S}\\\overline{S}\end{matrix}\right].$$

Here we will again remark that to examine the existence and the nature of waves corresponding to the above symbolical expression is another problem.

6. Other kind of surface waves.

We have given some consideration concerning the definition, classification and the representation of the surface waves, which, in our paper, are restricted to the plane waves propagated in one direction only, in the medium assumed to be homogeneous. On the other hand, actual waves observed on the earth are propagated in two dimensions along the curved surface of our globe, which is known to have a heterogeneous structure.

There are also waves propagated in media with cylindrical surfaces such as an elastic cylinder or a bore hole. These waves also contains some common nature with the previously treated ones and we often use the term "surface waves" without any explanation or remark. A strict definition must of course be given, which we hope to consider in a future occasion, but the similarity between these waves will be easily understood.

---

11. 表面波の研究 XI
表面波の定義及び分類

地震研究所 佐藤泰夫

1. 弾性体を伝はる表面波の研究は，前世紀以来活潑に行はれて来たが，その定義については未だに十分の論議が行はれた事を聞かず，納得のゆくものもない．"表面附近にのみエネルギーが集中し

てゐる波”といふ定義は，レーリー波については満されてゐるが，板の中を伝はる波，或は表面層を有する媒質については必ずしも適用され得ない．とは言へ，かうした種類の波もレーリー波と数学的取扱ひは極めて似かよつて居り，その間に厳密な区別をつける事は難かしい．

2. 然らば我々はいかなる定義を採用すべきであらうか，我々は従来，表面波なる言葉によつてどのやうなものを予想し，又取扱つて来たであらうか．長々しい議論は措き，ここに採らうとする定義を述べれば次の通りである．

“一つ又は幾つかの平行な境界面によつて境された弾性体（弾性流体を含む）を伝はる波の中，波面が境界面に垂直なものを表面波といふ．”

3. そして之に加へて次の如き表現法を採用したい．

“表面波のうち，境界面に垂直な方向（z- 方向）の振巾変化が exp- 函数のくみ合せであるものを [*E*]-型，sin-, cos- 函数であるものを [*S*]-型と呼ぶ”[8]

更に，[⁻] たる記号によつて自由表面を，[=] で固定表面を表現する事にすれば，

ラ　ブ　波..... $\left[\begin{matrix}S\\E\end{matrix}\right]$

レーリー波..... $[EE]$

ストーンレー波..... $\left[\begin{matrix}EE\\EE\end{matrix}\right]$

のような記号的表現が可能となる．ここに二つの文字を並べたのは，P 波に関する型を左に，S 波に関するものを右に記したものである．

4. 又，n 個の文字によつて表現される表面波を n-phase-type の表面波とよぶことにすれば

ラブ波，レーリー波；two-phase-type
ストーンレー波；　four-phase-type

となる．

我々は E, S 二つの文字と境界面を表はす記号との順列・組合せの問題として，phase の数 n が与へられれば，あらゆる表面波の型を書き下すことが可能である．この中には実在しない型をも含むかもしれないが，実在する表面波でこの中に含まれないものはない．

5. §2 に於いて述べた定義は，或はあまりにも広くゆるやかなものである，と考へられるかもしれない．何故ならば，このやうな定義による時，自由表面に於ける SH-波の反射の如き現象をも表面波の中に加へなくてはならないからである．しかしながら，このやうな場合に対しては，存在可能の phase の数は境界条件の数より多くなり，速度と振動数の間に満さるべき特性方程式もなく，従つて個有の伝播速度も存在しない．之に反して

“すべての媒質が（z-方向に）限られてゐる”

か，もしくは

“半無限体部分の波が [*E*]-型である”

ならば，phase の数は境界条件の数と等しくなり，常数を消去する事によつて振動数と速度とを含む所の特性方程式が得られる事になる．

従つて我々はこの条件を附加して，せまい意味の表面波の定義としたい．そのすべての型を one-phase 及び two-phase のものについて書き下せば (5.3), (5.4) の通りとなる．

6. 実際に観測せられる波は，一次元的に伝播するものでもなく，境界面は曲率を持ち，且媒質は不均質と考へられる．このほか円筒状の境界面をもつた弾性体を伝はる波もあり，これらには上の議論をそのままにあてはめる事はできない．従つて厳密な定義は別に行はなくてはならないが，その共通な性質は類推によつて容易に理解しうるであろう．

---

8) 佐藤泰夫「弾性体を伝わる表面波」科学 **19** (1949), 311.「弾性表面波について」地震 **[ii] 6** (1953), 13.

12. *Geomagnetic Studies of Volcano Mihara. The 5th Paper.*

(Changes in Three Geomagnetic Components during the Period from May 1951 to August 1953.)

By Izumi YOKOYAMA,

Earthquake Research Institute.

(Read Feb. 23, 1954.—Received March 31, 1954.)

1. Introduction.

In relation to the eruptions of Volcano Mihara in Ooshima Island, various studies were projected from the view-point of geomagnetism since 1950. It is of great importance and interest to accumulate data of changes in geomagnetic field related to volcanic activities as accurately as possible because very few studies of this sort have hitherto been made elsewhere. Generally speaking, observations with high accuracy are quite difficult to be conducted on volcanoes which are, as a rule, in places far from civilized area. However, Volcano Mihara is situated fairly near Tokyo and rather easily accessible. So that, it is desirable to get data as many as we can on this volcano before we start elaborate works on other volcanoes. The results got here would be helpful for general studies of this kind which should be carried out on any other volcanoes.

Some results obtained by a series of geomagnetic dip-surveys and continuous observation of changes in geomagnetic declination from July 1950 to Oct. 1953 have been reported in the previous papers.[1)2)3)4)] Although we have reported some evidences of geomagnetic changes that are related to volcanic activities, the local anomalous changes in three geomagnetic elements during the period from May 1951 to Aug. 1953 are abstracted in this paper on the basis of the data obtained by the most accurate observations. The changes are also analyzed in order to surmise their sources.

1) T. RIKITAKE, *Bull. Earthq. Res. Inst.*, **29** (1951), 161.
2) T. RIKITAKE, *Bull. Earthq. Res. Inst.*, **29** (1951), 499.
3) T. RIKITAKE, I. YOKOYAMA, A. OKADA and Y. HISHIYAMA, *Bull. Earthq. Res. Inst.*, **29** (1951), 583.
4) I. YOKOYAMA, *Bull. Earthq. Res. Inst.*, **32** (1954), 17.

2. The magnetic survey repeated in Aug. 1953.

As already reported in the 3rd paper, the magnetic survey with a first-order G.S.I. type magnetometer was carried out at ten stations suitably distributed in Ooshima Island in May 1951 when Volcano Mihara was still very active. In Aug. 1953 the volcano seemed to be rather quiescent in appearance and the survey was repeated with a newly constructed second-order G.S.I. type magnetometer,[5] the accuracies of which being 0.1 *minute* of arc in declination and inclination and 1 γ in intensities as well as the first-order one. Station No. 42, southern foot of Shiraishiyama, was added newly in this survey for future study. The results of the observations are given in Tables I~XI. At station No. 24, Oomiya park, Nomashi Village, the azimuth failed to be determined owing to the growth of pine-trees. And the observation of declination at station No. 26, Mabushi in May 1951 was found to be unreliable due to the mismanagement.

In order to eliminate the geomagnetic daily variation and disturbances that may be assumed to be almost the same within a region of a few hundred *kilometers* in distance, Kakioka Magnetic Observatory is taken as the standard point. Furthermore, differences in general secular changes between Ooshima and Kakioka are taken into consideration. Those are not negligible in two years, i.e. 0.5 *minute* of arc westward in declination and -0.4 *minute* of arc in inclination while almost zero in horizontal intensity. The local anomalous changes in three geomagnetic

Table I.

Station, No. 14 Zoo

Lat. = 34°45′.2 N Long. = 139°26′.5 E

Date	Time (J.S.T.)	D	I	H
July 31, 1953	17^h20^m	6°24′.3 W	48°18′.7	30187γ
	18 11	25.4	18.8	30188
	18 54	24.1	20.1	—
	19 26	22.4	18.4	30187
	Mean	6°24′.0	48°19′.0	30187γ

5) I. YOKOYAMA, *Bull. Earthq. Res. Inst.*, **31** (1953), 211.

Table II.

Station, No. 16 Senzu Primary School

Lat.=34°46′.6 N Long.=139°25′.3 E

Date	Time (J.S.T.)	*D*	*I*	*H*
Aug. 1, 1953	00^{h}26^m	5°25′.0 W	48°33′.0	30188γ
	00 46	25.8	33.7	30190
	02 06	25.0	33.3	—
	02 42	24.4	32.9	—
	Mean	5°25′.1	48°33′.2	30189γ

Table III.

Station, No. 19 Ooshima Meteorol. Station

Lat.=34°45′.8 N Log.=139°22′.6 E

Date	Time (J.S.T.)	*D*	*I*	*H*
Aug. 3, 1953	17^{h}36^m	6°20′.0 W	48° 7′.6	30041γ
	18 15	19.7	7.6	36
	20 16	19.1	7.1	—
	20 40	19.4	7.2	—
	Mean	6°19′.5	48° 7′.4	30038γ

Table IV.

Station, No. 24 Oomiya Park, Nomashi Village

Lat.=34°43′.8 N Long.=139°21′.5 E

Date	Time (J.S.T.)	*D*	*I*	*H*
Sept. 19, 1953	20^{h}58^m	—	47°21′.2	30683γ
	21 16	—	20.6	—
	21 40	—	21.5	30671
	Mean		47°21′.1	30677γ

Table V.

Station, No. 26 Mabushi

Lat.=34°41′.3 N Long.=139°23′.3 E

Date	Time (J.S.T.)	D	I	H
Aug. 11, 1953	09^h44^m	5°28′.5 W	46°51′.5	31558γ
	10 15	31.5	53.8	31560
	10 59	32.6	54.2	—
	11 22	33.7	53.9	31562
	Mean	5°31′.6	46°53′.4	31560γ

Table VI.

Station, No. 37 Mr. Masaka's garden, Nomashi Village

Lat.=34°43′.6 N Long.=139°21′.5 E

Date	Time (J.S.T.)	D	I	H
July 30, 1953	08^h56^m	6°10′.5 W	47°21′.2	
	10 12	09.9	21.4	
	12 42	14.2	20.6	
	14 12	14.7	25.9	
	16 10	13.2	23.4	
	17 46	11.3	23.6	
	18 30	10.4	23.3	
	21 04	06.9	21.4	
	21 34	09.7	21.7	
July 31, 1953	07 05	07.8	21.7	
	07 53	08.8	22.7	29995γ
	09 18	09.9	21.9	29996
	10 10	—	21.5	29991
	10 52	10.2	20.7	29991
	11 36	11.4	22.0	29987
	Mean	6°10′.6	47°22′.0	29992γ

Table VII.

Station, No. 38 Yuba

Lat.=34°45′.2 N Long.=139°23′.9 E

Date	Time (J.S.T.)	*D*	*I*	*H*
Aug. 3, 1953	11^h33^m	5° 5′.0 W	49° 22′.2	29004γ
	12 28	4.6	21.3	29013
	12 59	5.2	21.8	—
	13 26	5.1	21.5	29015
	Mean	5° 5′.0	49° 21′.7	29011γ

Table VIII.

Station, No. 39 Gojinka-chaya

Lat.=34°44′.2 N Long.=139°22′.9 E

Date	Time (J.S.T.)	*D*	*I*	*H*
Aug. 2, 1953	13^h40^m	3° 58′.6 W	52° 14′.2	28514γ
	14 07	57.1	13.9	28530
	14 29	57.9	14.2	28522
	Mean	3° 57′.9	52° 14′.1	28522γ

Table IX.

Station, No. 40 Suberidai

Lat.=34°42′.9 N Long.=139°22′.5 E

Date	Time (J.S.T.)	*D*	*I*	*H*
Aug. 12, 1953	18^h00^m	4° 6′.7 W	50° 40′.9	28977γ
	18 30	3.8	41.0	28967
	18 48	3.2	41.1	28968
	Mean	4° 4′.4	50° 41′.0	28971γ

Table X.

Station, No. 41 Sashikiji-Yokawa

Lat.=34°41′.5 N Long.=139°25′.6 E

Date	Time (J.S.T.)	D	I	H
Sept. 19, 1953	10^h24^m	8° 3′.3 W	48°19′.3	31666γ
	10 58	2.8	19.3	31683
	11 27	3.3	20.3	—
	12 02	3.6	19.7	31666
	Mean	8° 3′.2	48°19′.6	31672γ

Table XI.

Station, No. 42 Southern foot of Mt. Shiraishi

Lat.=34°42′.3 N Long.=139°24′.8 E

Date	Time (J.S.T.)	D	I	H
Aug. 2, 1953	17^h44^m	4°47′.3 W	47°29′.5	32480γ
	18 08	48.7	29.7	32476
	18 30	47.7	29.6	32480
	19 12	48.2	30.5	32464
	Mean	4°48′.0	47°29′.8	32475γ

Table XII.

The local anomalous changes in geomagnetic components during the period from May 1951 to Aug. 1953.

Station	ΔD W	ΔY E	ΔH	ΔZ	ΔI
No. 14 Zoo	2′.1	−19γ	22γ	7γ	−0′.9
16 Senzu Prim. School	0.1	− 1	−41	−68	−1.1
19 Ooshima Meteorol. Station	0.5	− 4	8	−22	−1.6
24 Oomiya Park, Nomashi	—	—	−42	−21	1.3
26 Mabushi	—	—	−16	−36	−1.0
37 Mr. Masaka's garden	−3.5	32	−63	−63	0.3
38 Yuba	2.9	−25	17	−56	−3.8
39 Gojinka-chaya	3.7	−32	−41	−56	−0.1
40 Suberidai	−0.1	1	0	0	0.0
41 Sashikiji-Yokawa	−2.2	21	0	−42	−2.0

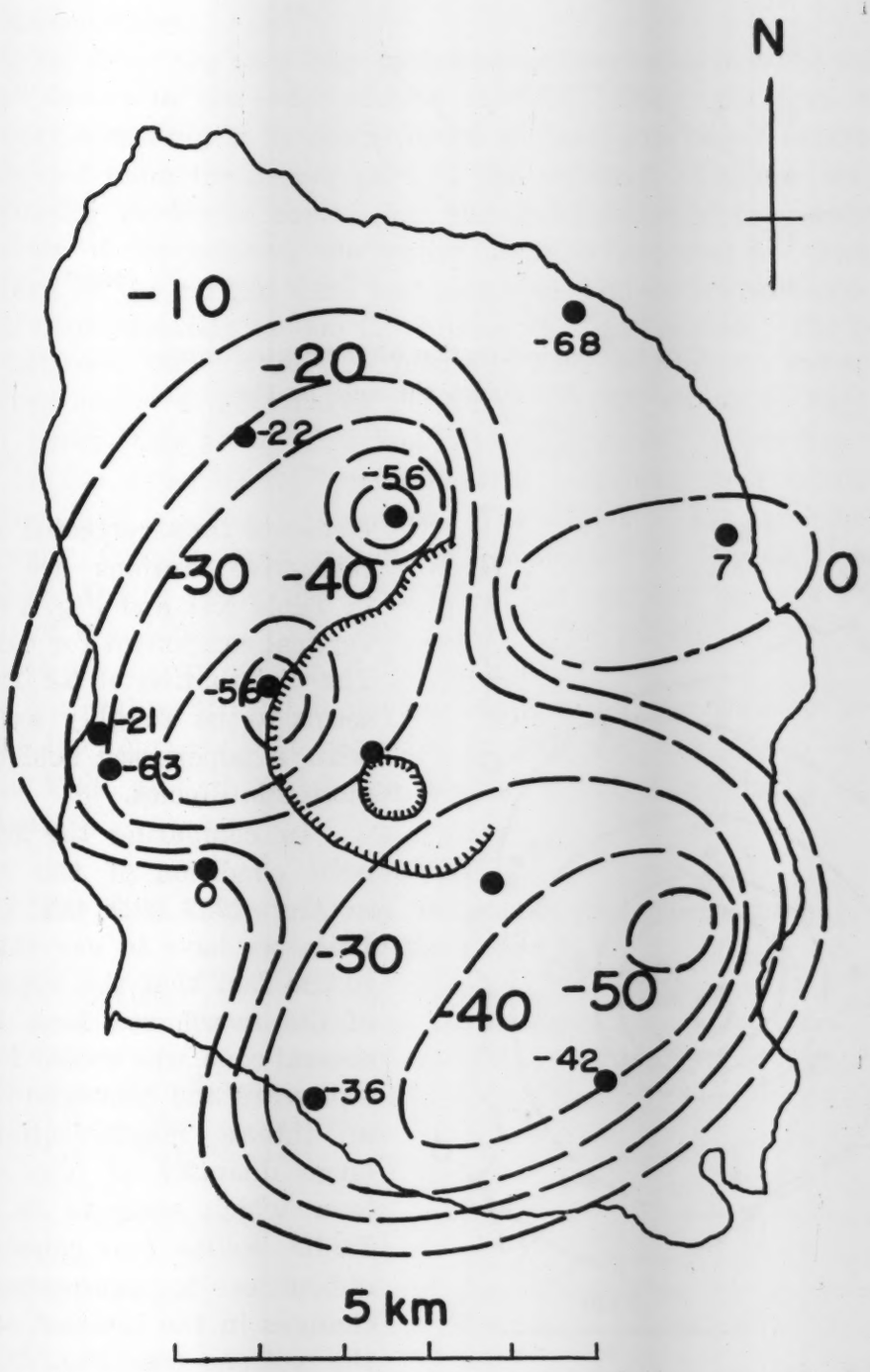

Fig. 1. The distribution of changes in vertical component during the period from May 1951 to Aug. 1953. The unit is *gamma*.

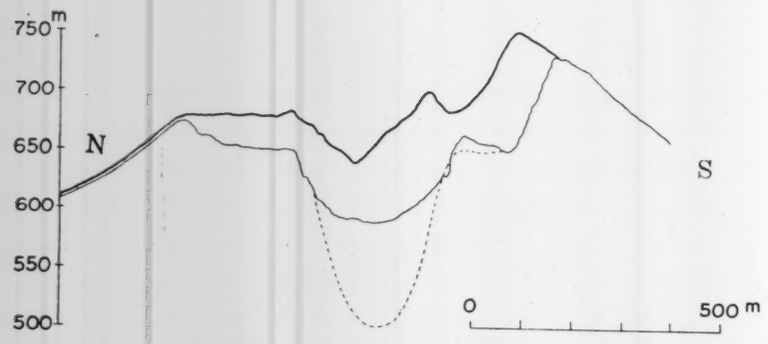

Fig. 2. Vertical section of the central cone.
—— 1951 (much the same as 1953)
—— 1950
····· 1940

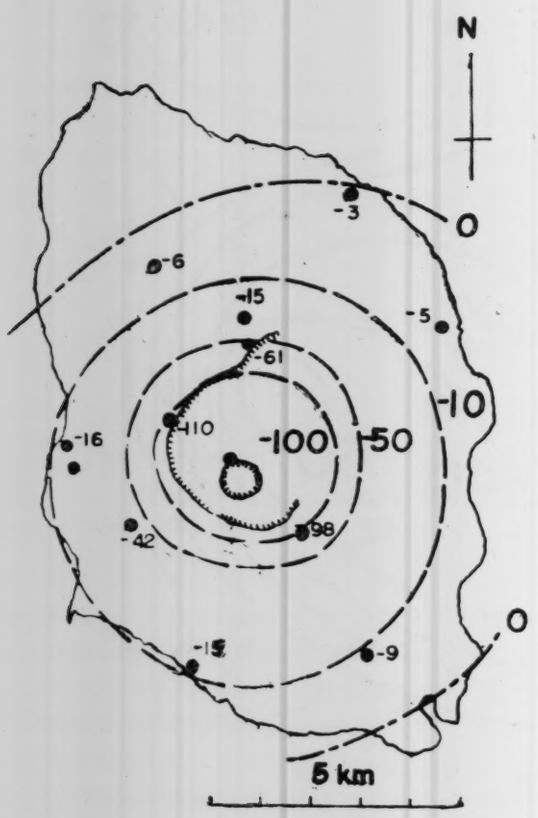

Fig. 3. The effect of ejected lava in the central cone upon the vertical component of the geomagnetic field. The unit is *gamma*.

elements thus corrected at the respective stations are shown in Table XII and Fig. 1 for the vertical component for example. The distribution of ΔZ in Fig. 1 seems to be roughly expressed with a superposed field of two magnetic dipoles.

In comparing the geomagnetic condition of the volcano in Aug. 1953 with that in May 1951, we have to pay attention to the fact that the upper part of the overflowed lava in the central cone was cooled in those two years and consequently got an intense magnetization. A large quantity of the ejected lava which amounts to about 7×10^7 *metric tons* causes some difficulties in presuming the changes in the internal state of the volcano (see Fig. 2). The effects of the lava which was magnetized during the above-

mentioned period upon the geomagnetic field are to be corrected on certain assumptions.

Judging from the fact that incandescent lava came in sight through the small fissure in the inner somma in Sept. 1952,[6] the lava in the central cone seems not to be cooled down so fast, some heat might have been supplied from the deeper part of the volcano. Though we have no convincing evidences concerning the distribution of temperature in the interior of the volcano, the writer assumes here that the upper part of the lava in the central cone had been cooled down below Curie point which is approximately at 600°C[7] during the said period. The part is shown between the contours in 1950 and 1951 in Fig. 2. Refering to the cooling curve of a fissure in the inner somma shown in Fig. 15 of the 4th paper, this assumption would be acceptable. According to the results of the experiments,[7] mean natural remanent magnetization of the ejected lava is about 0.05 *emu/cc*. The effects of the lava upon the geomagnetic field at each station are evaluated by Poisson's theorem of potential theory using the usual graphical method as was done in the case of dip-values in the 4th paper. The effects on the vertical component are shown in Fig. 3 for example.

The final values of local anomalous changes in three elements between 1951 and 1953 surveys both corrected in this way are shown in Table XIII and Figs. 4~6 in which the relation $\mathrm{rot}\,\vec{H}=0$ was taken into consideration.

Table XIII.
The final values of local anomalous changes in three geomagnetic elements.

Station	ΔY	ΔX	ΔZ
No. 14 Zoo	−20γ	21γ	12γ
16 Senzu Prim. School	− 1	−44	−65
19 Ooshima Meteorol. Station	5	0	−16
24 Oomiya Park, Nomashi	—	−34	− 5
26 Mabushi	—	−35	−21
37 Mr. Masaka's garden	33	−55	−47
38 Yuba	−25	− 2	−41
39 Gojinka-chaya	−10	−55	54
40 Suberidai	− 8	15	42
41 Sashikiji-Yokawa	18	− 5	−33

6) I. YOKOYAMA, *Bull. Earthq. Res. Inst.*, **32** (1954), 31.
7) T. NAGATA, *Journal of Geography (Tokyo)*, **60** (1951), 44.

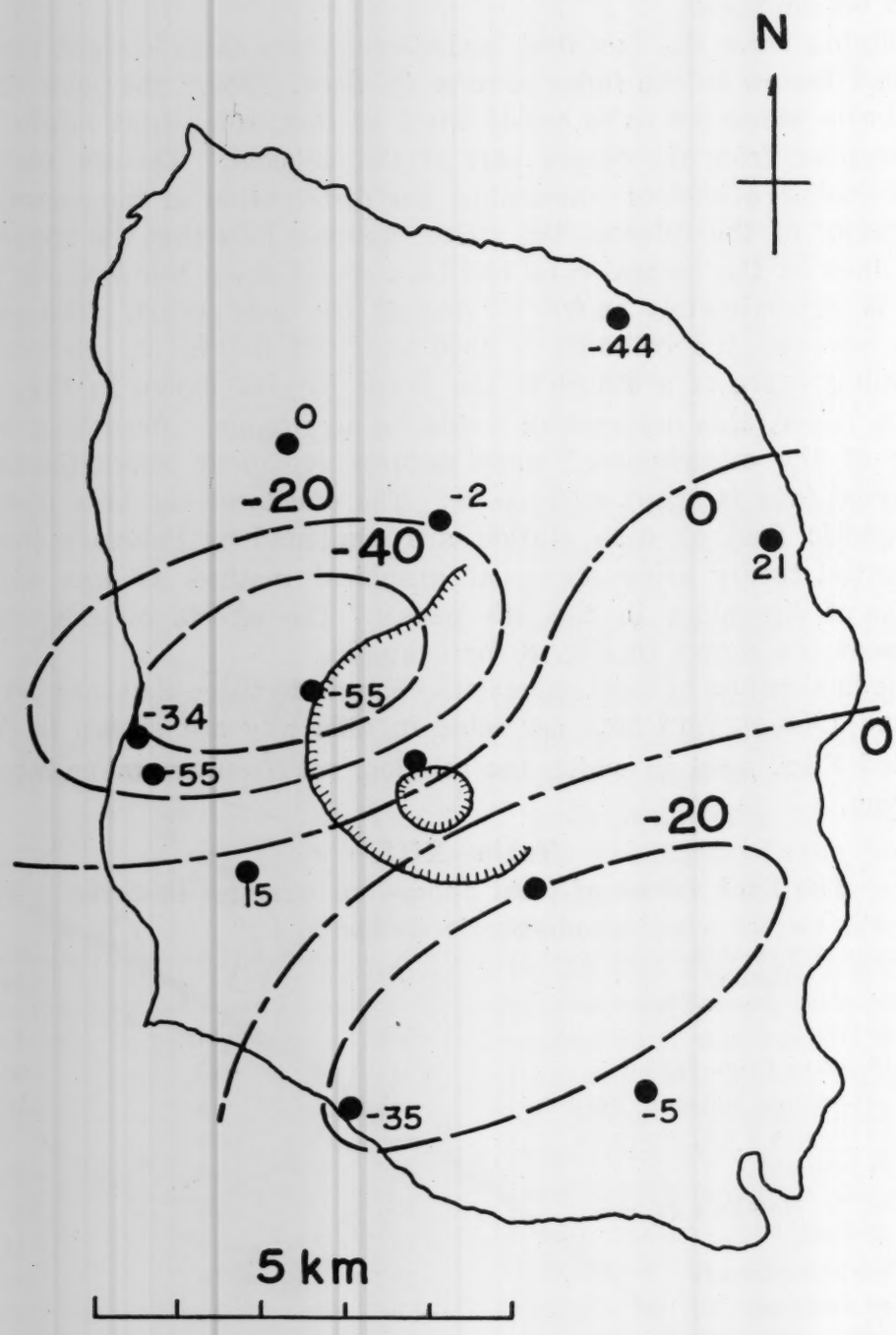

Fig. 4. The distribution of changes in geomagnetic north component. The unit is *gamma*.

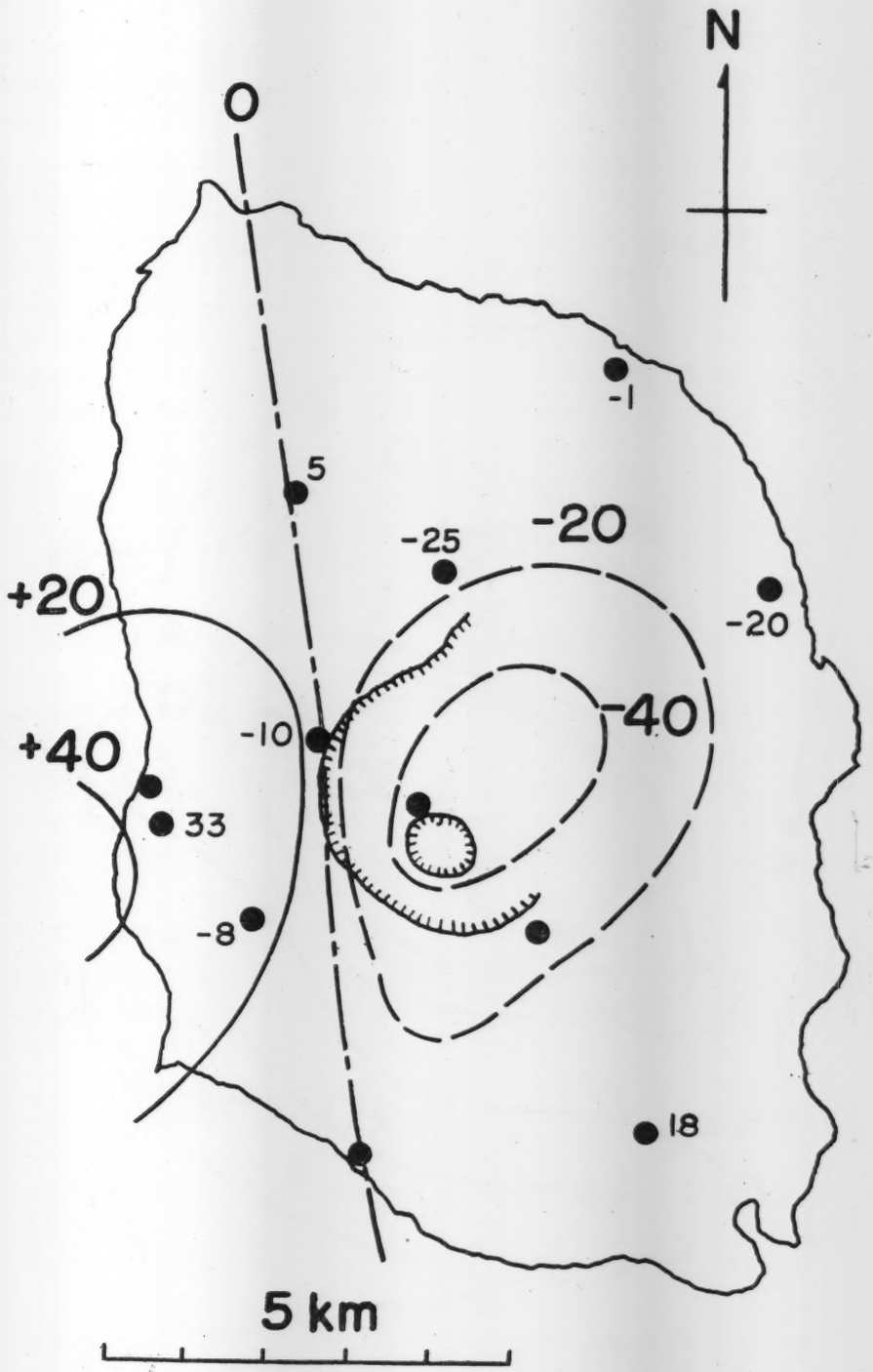

Fig. 5. The distribution of changes in geomagnetic east component. The unit is *gamma*.

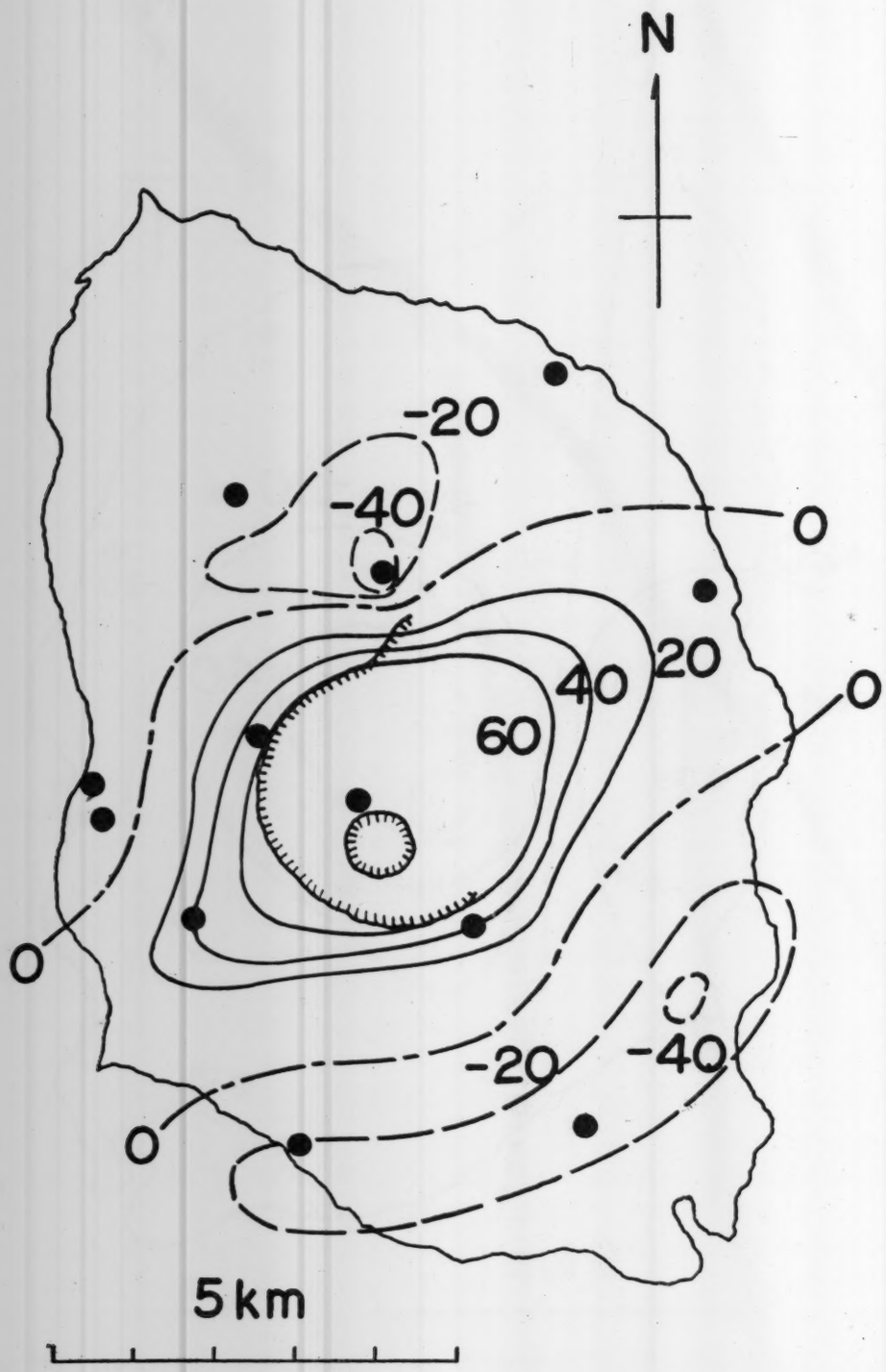

Fig. 6. The distribution of changes in vertical component. The unit is *gamma*.

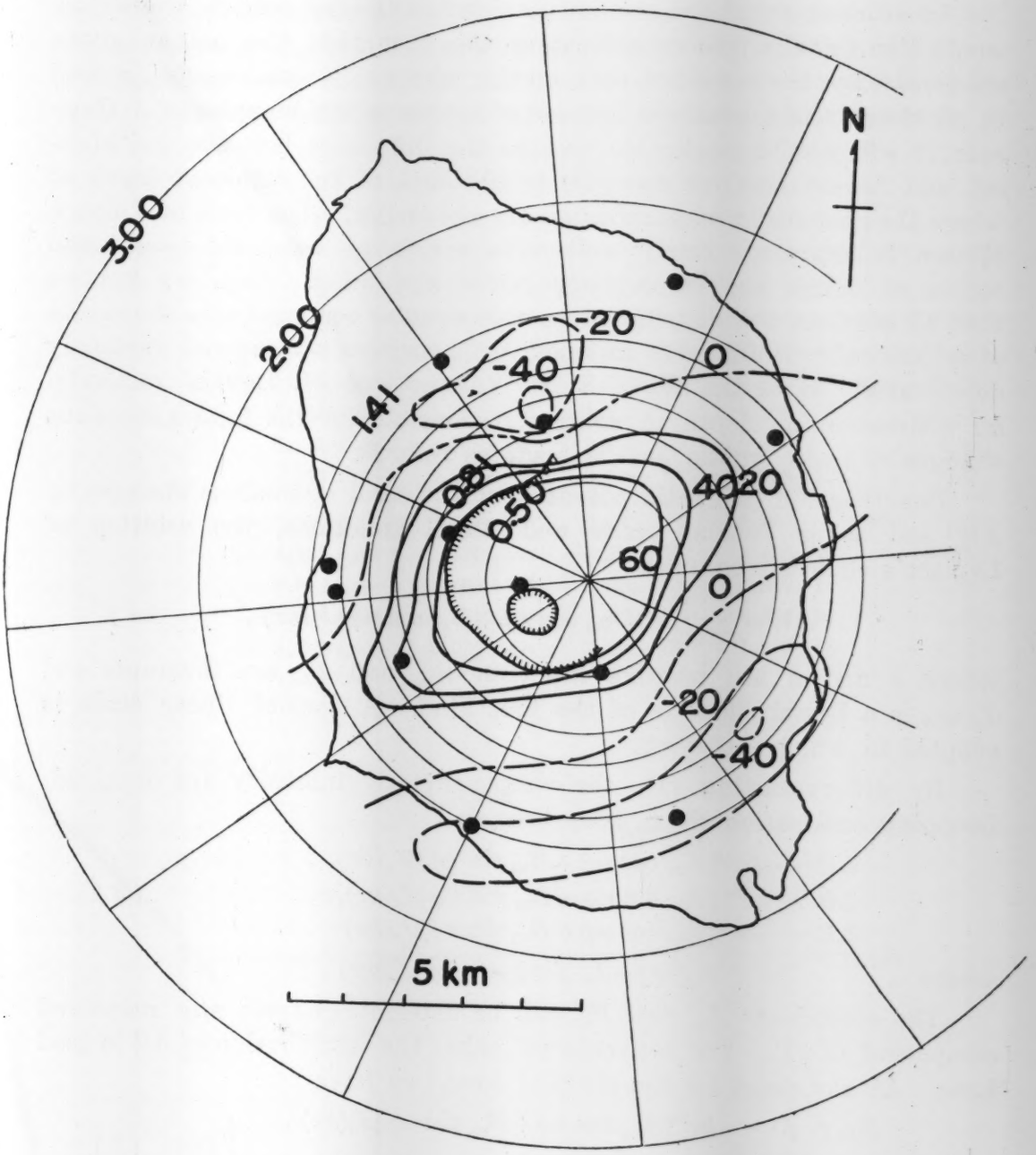

Fig. 7. Map of ΔZ distribution used in obtaining the coefficients A_{kn} and B_{kn}.

3. Determination of depth of sources.

In an analysis of the results obtained in the last section, the writer would like to take into consideration the fact that the height above sea-level is not the same for each station though it was usually ignored in all the previous analyses because of mathematical complexity. However, it will not be negligible because the difference between the highest and lowest stations amounts to 20～30% of the supposed depth at where the changes in magnetization are occurring. The form of Volcano Mihara is expressed fairly well with a circular cone, the height and radius of which are respectively 800 m and 5 km. Then we assume that all stations are distributed on this circular cone and take the origin of cylindrical coordinates on its apex with positive z measured vertically downwards. With the aid of E. H. Vestine and N. Davids' method[8], an estimation of depth of sources responsible for the local anomalous changes of geomagnetic field is made as follows.

Denoting the magnetic potential of the local anomalous changes by ΔW and using Fourier series and Bessel functions, the solution of Laplace's equation becomes

$$\Delta W=\sum_{k=0}^{K}\sum_{n=0}^{N} e^{kz}[A_{kn}\cos n\phi+B_{kn}\sin n\phi]J_n(kr)\,, \qquad (1)$$

where k and n are positive integers, A_{kn} and B_{kn} are constants and $J_n(kr)$ is a Bessel function of the first kind. A special linear scale is adopted in which 10 km=3.

By differentiating (1), the components of intensity are obtained. Dropping summation signs, they become

$$\left.\begin{aligned}\Delta R&=-ke^{kz}[A_{kn}\cos n\phi+B_{kn}\sin n\phi]\Psi_n(kr)\,,\\ \Delta\Phi&=ne^{kz}[A_{kn}\sin n\phi-B_{kn}\cos n\phi]J_n(kr)/r\,,\\ \Delta Z&=-ke^{kz}[A_{kn}\cos n\phi+B_{kn}\sin n\phi]J_n(kr)\,,\end{aligned}\right\} \qquad (2)$$

where $$\Psi_n(kr)=J_{n-1}(kr)-(n/kr)J_n(kr)\,.$$

The coefficients A_{kn} and B_{kn} can be determined from any measured component of (2). For convenience' sake, the distribution of ΔZ is used here. At any point on the circular cone, we have

$$\left.\begin{aligned}&Z(z,r,\phi)=-ke^{kz}[A_{kn}\cos n\phi+B_{kn}\sin n\phi]J_n(kr)\,,\\ &z=r\frac{800}{5000}\,.\end{aligned}\right\} \qquad (3)$$

8) E. H. VESTINE and N. DAVIDS, *Terr. Mag.*, **50** (1945), 1.

In obtaining A_{kn} and B_{kn}, a set of five circles is drawn on a map of the ΔZ distribution so as to keep away from the central region of the volcano where the correction for the lava is very rough and the Fourier analysis for each circle afford five coefficients. By means of the method of least square, A_{kn} and B_{kn} are obtained as shown in Table XIV.

Applying these coefficients, ΔZ on the circular cone and ΔW on the various horizons both in the NS direction are calculated as shown in

Table XIV.

The values of A_{kn} and B_{kn}.

	n \ k	1	2	3	4	5
A_{kn}	0	5.32	-4.050×10^{3}	6.16	-8.75	-0.49
	1	1.723×10^{3}	-9.078×10^{2}	3.268×10^{2}	-7.853×10^{1}	6.78
	2	-2.964×10^{4}	7.370×10^{3}	-1.652×10^{3}	2.726×10^{2}	-18.75
	3	1.045×10^{4}	-1.108×10^{4}	1.123×10^{3}	-2.279×10^{3}	-15.17
	4	1.031×10^{4}	-2.508×10^{2}	-3.045×10^{1}	6.02	0.79
	5	7.911×10^{4}	2.327×10^{3}	-5.836×10^{2}	5.528×10^{1}	0.29
B_{kn}	1	-1.473×10^{2}	6.688×10^{1}	0.43	-5.29	5.92
	2	-4.106×10^{4}	1.010×10^{4}	-2.225×10^{3}	3.458×10^{2}	-20.37
	3	-1.882×10^{5}	1.999×10^{4}	-2.036×10^{3}	4.867×10^{1}	25.86
	4	2.890×10^{2}	-4.049×10^{2}	1.235×10^{2}	-2.452×10^{1}	2.49
	5	-1.742×10^{5}	-5.989×10^{3}	1.394×10^{3}	-1.215×10^{2}	-3.17

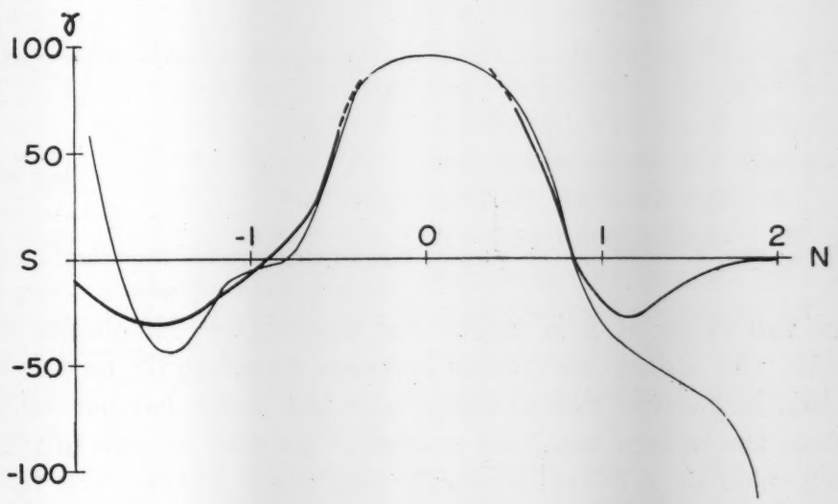

Fig. 8. ΔZ on the circular cone in the NS direction.
—— observed values —— calculated values

Figs. 8 and 9. In these figures, there are some discrepancies in distant parts from the origin. These may be ascribed to the extrapolation of the expression whose coefficients are determined with the values of inner region.

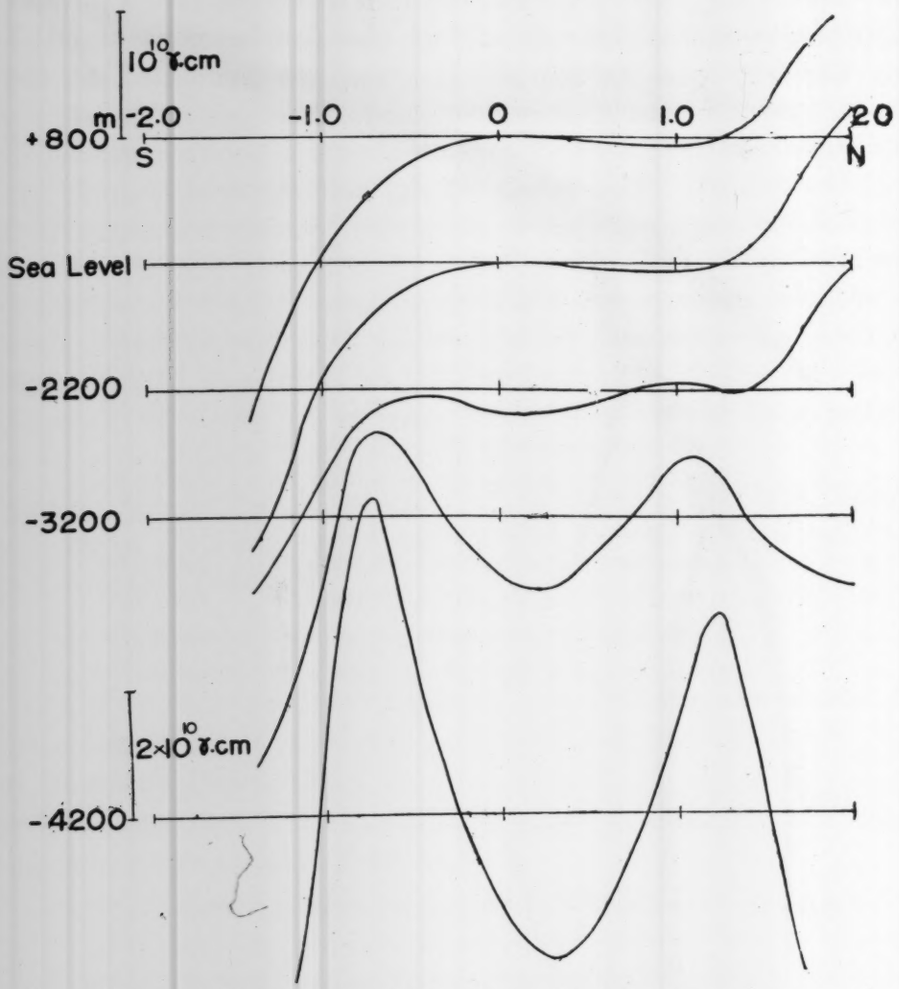

Fig. 9. ΔW on the various horizons in the NS direction.

Since the value of k is larger for the higher harmonics than the lower ones, the higher harmonics increase prominently as the source is approached, but never exceed materially the lower harmonics in amplitude unless the source has been reached. As may be seen in the figures, the distribution of ΔW at a depth less than 2200 m are fairly convergent, while it seems more divergent according as the depth becomes great. Hence, we may assume that the sources are to be found at

2~3 *km* depth from the sea-level.

4. Determination of a magnetic dipole.

In order to compare with the analyses of the 1950 survey in which T. Rikitake took a conventional dipole model, the position, intensity and direction of an underground magnetic dipole corresponding the magnetic changes on the earth's surface are determined with the aid of the method devised by Rikitake.[9]

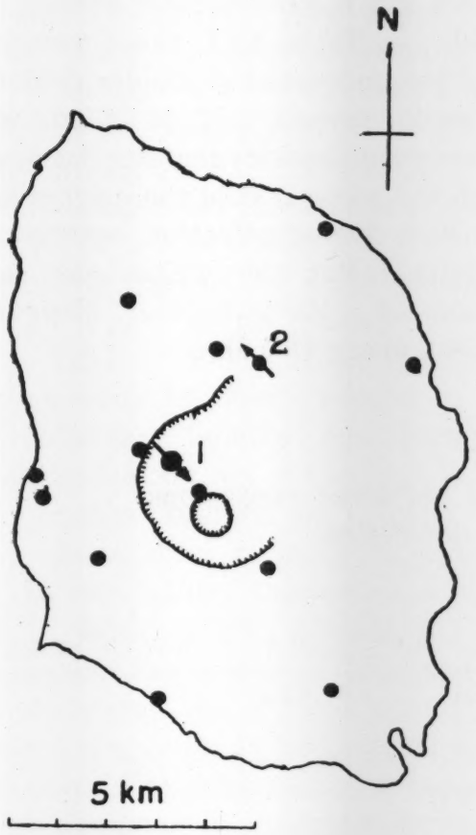

Fig. 10. The directions and positions of the magnetic dipoles corresponding to the changes in geomagnetic field.
1: July—Sept. 1950.
2: May 1951—Aug. 1953.

The distributions of geomagnetic components are expressed in the next form

$$\left.\begin{aligned}
\Delta X &= A_1 + B_1 x + C_1 y + D_1 x^2 \\
&\quad + E_1 xy + F_1 y^2 + G_1 x^3 \\
&\quad + H_1 x^2 y + I_1 xy^2 + J_1 y^3 , \\
\Delta Y &= A_2 + B_2 x + C_2 y + \cdots \\
&\quad \cdots\cdots\cdots , \\
\Delta Z &= A_3 + B_3 x + C_3 y + \cdots \\
&\quad \cdots\cdots\cdots ,
\end{aligned}\right\} \quad (4)$$

where the origin is taken at that of the cylindrical coordinates in the last section. Using the values of three components at ten points, the constants $A_1, B_1, C_1, \cdots\cdots, A_2, B_2, C_2, \cdots\cdots, A_3, B_3, C_3, \cdots\cdots$ are determined by means of the method of least squares.

The coefficients of spherical harmonic expansion of magnetic potential on a sphere of radius a are obtained by solving certain simultaneous equations which contain the constants $A_1, B_1, C_1, \cdots\cdots, A_2, B_2, C_2, \cdots\cdots, A_3, B_3, C_3, \cdots\cdots$. Then adjusting a so as to minimize the square sum of the second degree coefficients, the depth of the magnetic centre is determined to be 4.7 *km*,

9) T. RIKITAKE, *Journ. Geomagn. Geoelectr.*, **2** (1950), 20 and 25.

while the position is also obtained as shown in Fig. 10. The obtained quantities are tabulated in Table XV. Table XVI shows all the results obtained by Rikitake and the writer concerning the magnetic centre corresponding the local anomalous changes in Ooshima by now. The remarkable changes observed in Sept. 1950 seem to have recovered about one tenth by Aug. 1953 though the changes between the period from Sept. 1950 to May 1951 are not clear. This result may harmonize with the fact that the minor activities took place in Oct. 1953 and afterwards. The volcano seems still active though we got a geomagnetic change in an opposite sense to that occured in 1950. In Table XVI, the directions of magnetization and demagnetization of the underground dipoles deviate from the geomagnetic north as much as 45 *degrees*. If it is so, we might expect some other causes for the geomagnetic changes because the direction should agree with that of the general field there provided we only consider simple magnetization and demagnetization associated with rises and falls of volcanic activity. But the writer can say nothing about another causes at the moment. Many further observations would be needed for any discussions along this line.

Table XV.

The coefficients of spherical harmonic expansions and determined quantities.

Coef.	a_1^0	a_1^1	b_1^1	a_2^0	a_2^1	b_2^1	a_2^2	b_2^2
Value	0.8	−54.9	−61.5	0.3	16.7	20.9	0.8	2.1 γ

$x=2.7\,km$, $y=-0.1\,km$, $z=4.7\,km$

Table XVI.

The determined magnetic dipoles corresponding to the changes during various periods in Ooshima.

Period	Depth of centre	Azimuth of north seeking end	Dip of dipole	Magnetic moment
1936—1951	6.1 *km*	N 18°W	−17°	2.8×10^{15} *emu*
July—Sept. 1950	5.5 *km*	S 42°E	−63°	6.3×10^{14} *emu*
May 1951—Aug. 1953	4.7 *km*	N 48°W	88°	8.6×10^{13} *emu*

5. Summary and conclusion.

Analyzing the geomagnetic data obtained in May 1951 and Aug. 1953, the writer abstracted the local anomalous changes in geomagnetic components during this period. The effects of the lava cooled down on the surface was eliminated under certain assumptions. Using the distribution of ΔZ, an estimation of depth of sources was made by seeking the point where the solution of the magnetic potential becomes divergent. Thus upper limit of the sources was found to be about 2~3 *km* beneath the volcano.

With the aid of Rikitake's method, the depth of the magnetic centre is also determined to be 4.7 *km* using the partial derivatives of distributions of ΔX, ΔY and ΔZ.

Judging from the results and associated analyses of the geomagnetic studies, it is likely that the activity of the volcano which gave rise to a great change in the earth's magnetic field in 1950 is still continuing though a part of the change has been recovering during the period from 1951 to 1953. Although the main part of volcanic geomagnetic change would be closely related to the thermal condition in the interior of volcanoes, simple considerations concerning magnetization and demagnetization are not enough to explain rather complicated features of the changes observed on Volcano Mihara. Further observations should be made in order to study in detail.

In concluding, the writer wishes to express his sincerest thanks to Dr. T. Rikitake who advised and encouraged the writer from England throughout the course of this study. To Prof. T. Nagata for his helpful criticisms, the writer's cordial thanks are also due. Mr. A. Okada assisted the writer in field works, to whom the writer's hearty thanks are also due. The writer also acknowledges the facilities given by Tokai Kisen Company in magnetic surveys.

12. 三原山の地球磁気学的研究
第 5 報
(1951年5月から1953年8月にいたる期間の地磁気三成分の変化)

地震研究所 横山 泉

第 3 報において報告したように，1951 年 5 月地理調査所型磁気儀を用いて，大島全島 10 点について地磁気三成分の最高度の精密測定を行つた．以来 2 年余，三原山は外見的には一応静穏に返つたようであつた．この間における一連の伏角測量と，地磁気偏角の連続観測との結果は第 4 報で報告した．これらの観測結果を更に確めるために，1953 年 8 月再測を行い，この 2 年間における局地的異常変化を求めた．この際地磁気日変化及び擾乱ならびに永年変化の影響を除去し，又，地下の状態変化を推論するために，この二回の観測の間に冷却したであろうと考えられる噴出熔岩の一部が地球磁場に及ぼす効果を計算して，これを補正した．この際，火口内の熔岩の幾何の深さまでが Curie 点以下に冷却したかが問題である．この評価はなるべく慎重に行つたつもりであるが，今後も注目すべき現象の一つと思われる．

この地磁気の異常変化の源を推算するために，E. H. Vestine–N. Davids の方法を用い，測点が必ずしも同一平面上にないことを考慮すると，大体，源の上限は海面下 2～3 km となる．

力武の方法を用いて磁気異常中心の深さを求めると，約 4.7 km となり，前記結果とも矛盾しない．又，新たに生じた帯磁の方向及び磁気能率等は第 1 報から第 4 報にいたる総ての結果と調和する．

13. *Analytical Results of the Acceleration Seismograms obtained at Tokyo and Yokohama.*

By Kiyoshi KANAI and Masazi SUZUKI,

Earthquake Research Institute.

(Read Dec. 18, 1951 and March 23, 1954.—Received March 31, 1954.)

1. Introduction.

It is very clear from the records of earthquakes in the past that the degree of damage to houses by earthquake changes considerably with place. Particularly the damage to the houses of old Japanese style differ remarkably according to place, concerning which there are numerous records. This phenomenon may be in close relation to the problem of damage prevention, and many studies have been made to bring the cause of it to light in such fields of science as seismology, architecture and civil engineering, since seismology was established systematically as a science. But a satisfactory solution to this has not yet been given.

The conception that the property of earthquake motion depends on the nature of ground was deduced from many observational studies together with a number of mathematical ones. But the relation existing between earthquake motion which is variable according to ground property and the earthquake damage to houses cannot be represented quantitatively. It is a subject involving many unsolved problems.

As to the relation of earthquake damage to ground property, the first key for its solution was the fact that houses are damaged by acceleration of earthquake motion and that the acceleration depends on the ground property.

Then an acceleration seismograph having been invented, the acceleration of earthquake motion was directly measured, and it was found that the maximum acceleration of earthquake motion is hardly varies even if extremely different cases are compared, e.g. the case when old Japanese-style houses suffered seriously and the case when the earthquake damage was almost negligible. It was also found from the observation that every place has the predominant period of earthquake motion.[1)]

1) M. ISHIMOTO, *Bull. Earthq. Res. Inst.*, **10** (1932), 171; **12** (1934), 234; **13** (1935) 592; **14** (1936), 240; **15** (1937), 536.

When this predominant period of the ground is approximate to the natural period of building, a resonance-like phenomenon is apt to occur to the building. Consequently it was concluded that earthquake damage to buildings has a close relation to the predominant period of the ground.[2)]

In this paper, referring to the acceleration seismograms and the results mentioned above, the accelerations of earthquake motion observed at several places in Tokyo and Yokohama are compared and it is aimed to clear up the relation of acceleration amplitude to predominant period as well as the relation of the number in succession of a definite period to the period of earthquake motion.

2. The maximum acceleration of earthquake motion observed at several places in Tokyo and Yokohama.

From the observations made at several places in Tokyo and Yokohama by means of acceleration seismographs, Ishimoto found that, in the earthquake of which the distance from the earthquake origin is short, the acceleration on firm ground, as in the up-town of Tokyo, is greater than on soft ground, while earthquake of long distance from the origin becomes slightly greater on softer ground as in the down-town of Tokyo.[3)]

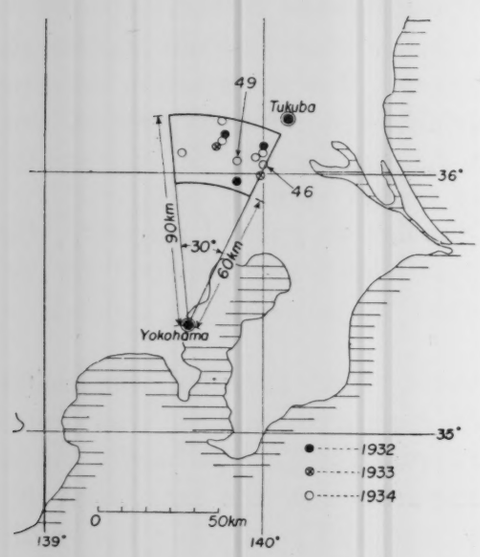

Fig. 1. The positions of the earthquake origins accepted as data in Yokohama.

The characteristics of earthquake motion is determined from the mechanism of seismic-wave generation and the materials of the pass of wave propagation besides the distance from the origin. In the case of analytical investigation of the seismograms obtained at Yokohama, the influence from these factors was eliminated with all caution possible. It was decided that earthquakes in a limited region should be accepted as data for study in order to investigate the relation between the property of earthquake motion at a certain place and the crust structure and the material

2) T. SAITA, *Shinsai* (Iwanami-Shoten, Tokyo, 1935), pp 283–324, (in Japanese).
3) M. ISHIMOTO, *loc. cit.*, 1), **10**, **13**.

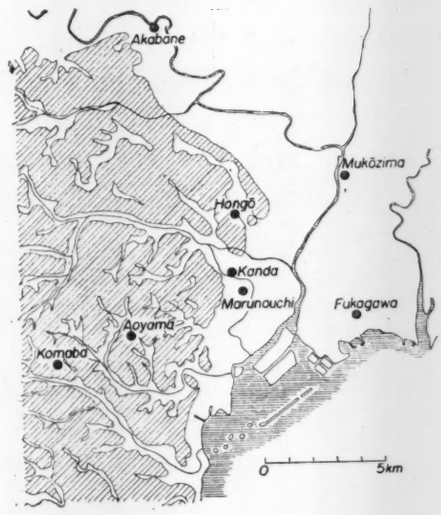

Fig. 2a. The positions of the temporary observing stations in Tokyo. Blank region and hatched one represent alluvium and other geological formations respectively.

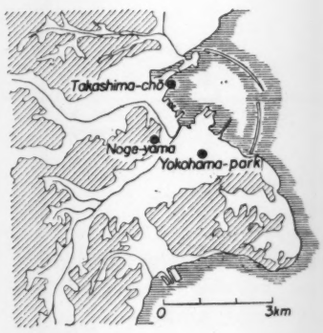

Fig. 2b. The positions of the temporary observing stations in Yokohama. Blank region and hatched one represent alluvium and other geological formations respectively.

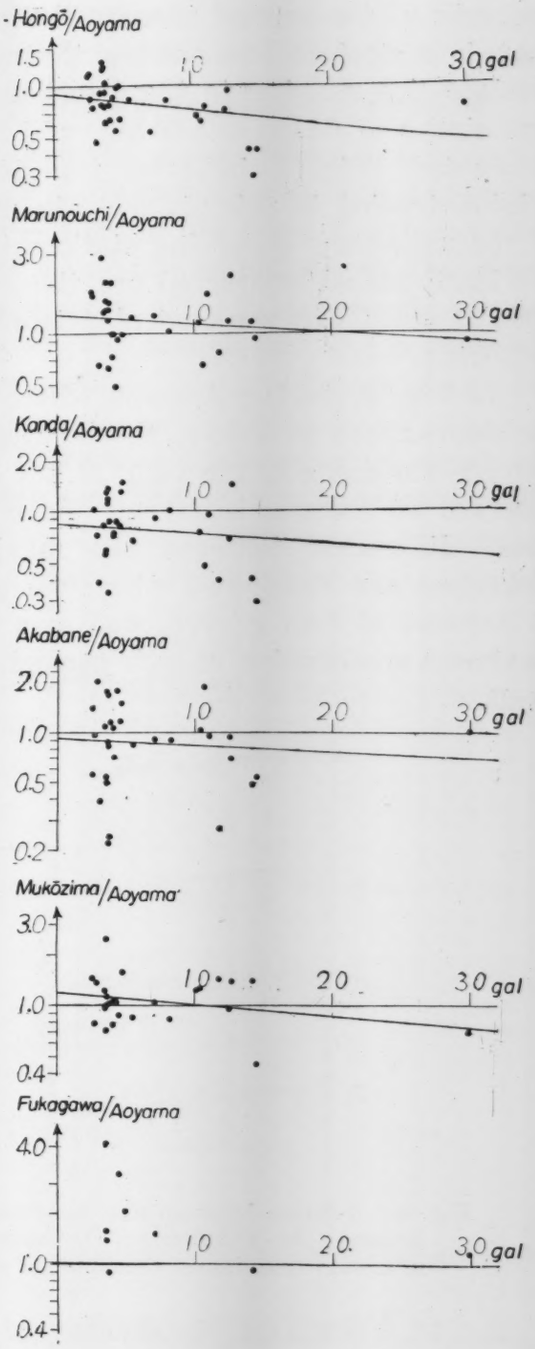

Fig. 3. Relation between the maximum acceleration and the ground property in Tokyo. Ordinate: maximum acceleration ratio; abscissa: maximum acceleration amplitude at Aoyama.

property of the ground there. The region enclosed within four lines, that is a straight line passing through Yokohama and Mt. Tsukuba, a straight line running to the direction of 30° west from Yokohama and two circles of 60 km and 90 km radii of which the centers are Yokohama, is adopted. Fig. 1 indicates the limited region and the earthquake origins treated in this paper. Fig. 2 shows the geographical positions of the temporary observing stations in Tokyo and Yokohama.

Earthquakes concerned are the ones which are recorded as seismic scale II and III by the Central Meteorological Observatory, Tokyo, during 1932–1934.

In Fig. 3, taking Aoyama where the ground is firm as the standard for observations at Tokyo, the relation between the maximum acceleration at Aoyama and the ratio of the maximum in several places to that observed at Aoyama is shown. As is seen from Fig. 3, there are only small differences between the maximum accelerations at Akabane, Mukōzima and Fukagawa where the ground is soft and the maximum at Aoyama of firm ground, and as a whole the former ones, that is the maximum acceleration at soft ground, show a tendency of being rather small.

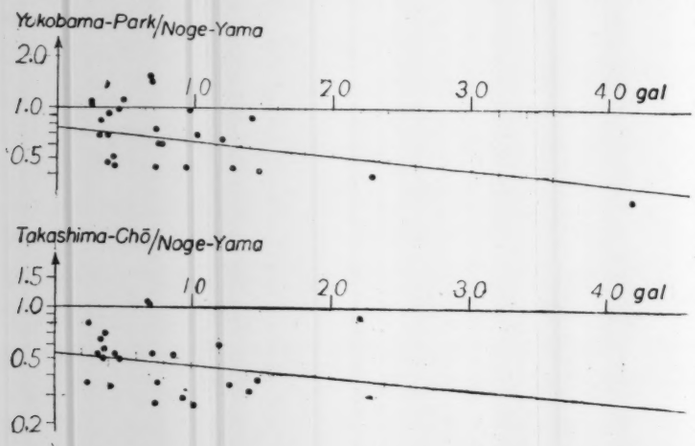

Fig. 4. Relation between the maximum acceleration and the ground property in Yokohama. Ordinate: maximum acceleration ratio; abscissa: maximum acceleration amplitude at Nogeyama.

As to Yokohama, Nogeyama of firm ground was taken as the standard, Fig. 4 illustrates the comparison of the acceleration at Nogeyama with those obtained at the Yokohama Park and Takashima-chō where the ground is soft. Fig. 4 indicates that the maximum accelerations at the Yokohama Park and Takashima-chō are almost one half

of the maximum at Nogeyama of firm ground.

3. The relations of frequency to period and acceleration to period.

Concerning several earthquakes observed at such places in Yokohama as Nogeyama, the Yokohama Park and Takashima-chō, the following facts were studied. As to all waves coming out from the time when the acceleration becomes half of the maximum amplitude to the time when it reduces itself to the same amount after it rises to the maximum, the relation of the frequency to the period and the relation of the acceleration to the period were studied. The results are shown in Figs. 5 and 6.

Figs. 5 and 6 indicate that at Nogeyama the number of waves of 0.3—0.4 sec period are predominant and the maximum acceleration

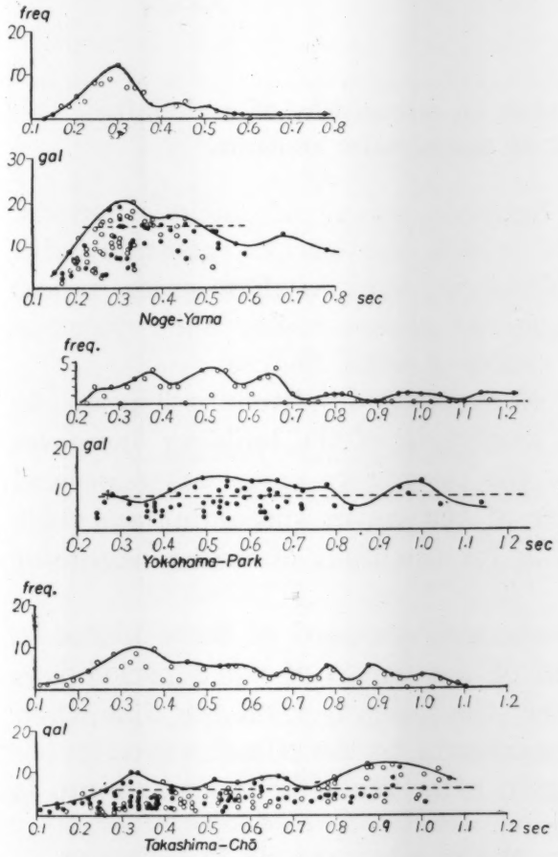

Fig. 5. Relations of frequency-period and of acceleration-period concerning the earthquake of 1934 VIII 3 at three places in Yokohama.

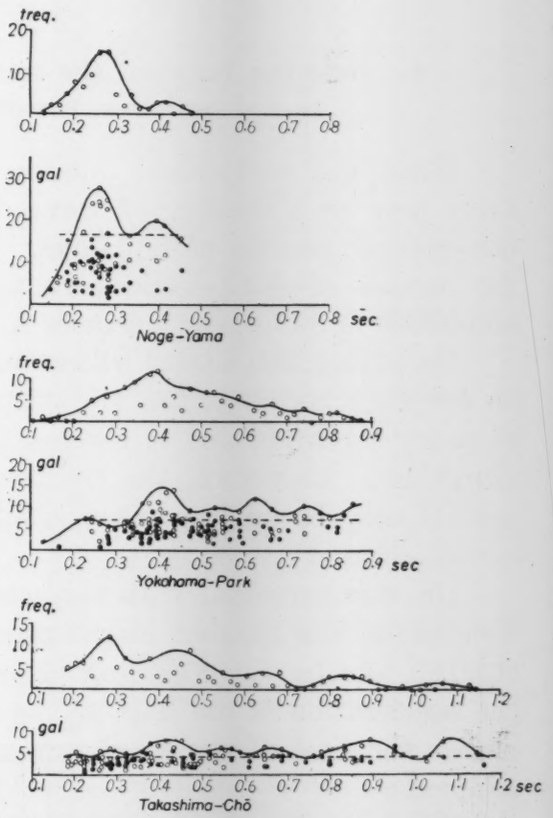

Fig. 6. Relations of frequency-period and of acceleration-period concerning the earthquake of 1934 IX 1 at three places in Yokohama.

are also at such periods. Although the frequency of the period at the Yokohama Park is different in respective earthquakes, it may be true that in many cases the maximum frequency appears around the period of 0.3–1.0 sec. Also it may be certain that the acceleration becomes larger around the period when the frequency is large. In the relationship of the wave number and the acceleration amplitude to the period of earthquake motion at Takashima-chō, there are no clear peaks, while in the relation of frequency-period and that of acceleration-period there is a considerable likeness.

Generally speaking, in firm ground the curve of frequency-period has a sharp peak, while in the ground of thick alluvium it is flat. Then it may be concluded that in firm ground the acceleration becomes specially large at a certain period, but it becomes smaller at other periods. In softer ground large acceleration covers a considerably wide range of period.

4. Relation between the number in succession of a definite period and that period of earthquake motion.

Since the earthquake motion involves waves of various periods, there may be a number of waves of which the periods coincide with the natural periods of buildings. However, even in those cases, unless the waves of such periods continue for some while, the vibration amplitude of buildings increases in rather a small degree.

By giving the forced vibration of constant amplitude and period to an ordinary building, the vibration amplitude of the building increases at every vibration and it reaches to the asymptote value after several vibrations. Therefore, the frequency of the waves succeeding and their periods may be an important problem for the study of earthquake-proof construction.

On this occasion, with the seismograms obtained at three places in Yokohama, the number in succession of the waves of equal period was studied. As in the preceding chapter, the interval from the time when the acceleration is the half of the maximum to the time when it becomes the half of the maximum again after reaching the maximum is adopted.

As to the period, it is considered to be equal in three ways; that is in the first case $\pm 5\%$ is accepted to be the allowable limit, the second $\pm 10\%$ and the last $\pm 20\%$. Concerning the two earthquakes of 1934

VIII 3 and 1934 IX 1, the seismograms obtained at Nogeyama, the Yokohama Park and Takashima-chō in Yokohama were analysed, with the results given is in Figs. 7 and 8.

These figures show that in the case where the error of period is within $\pm 5\%$, the maximum number in succession is four at all places.

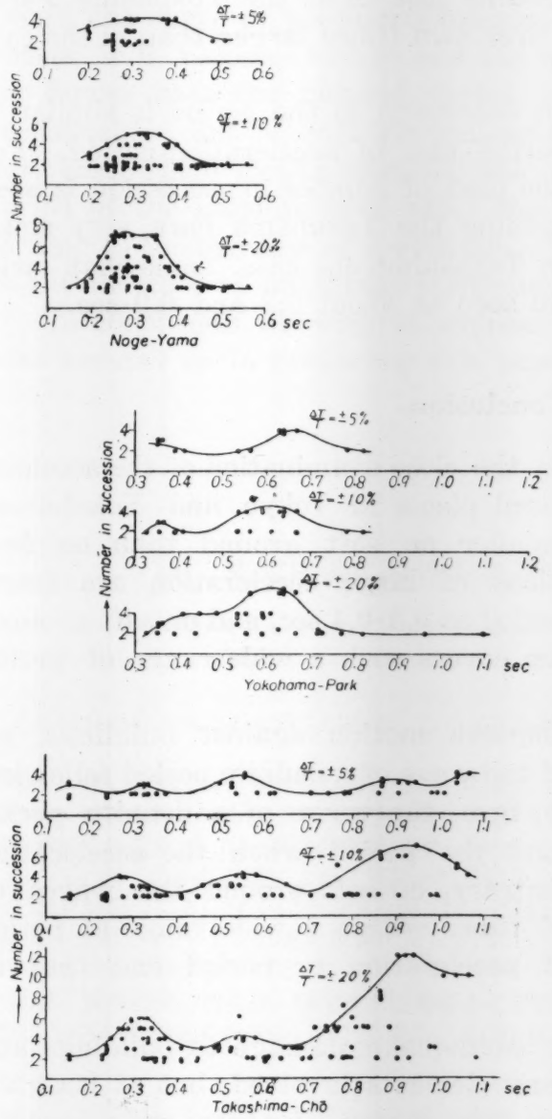

Fig. 7. Distribution of the number in succession of the waves of a definite period concerning the earthquake of 1934 VIII 3 at three places in Yokohama.

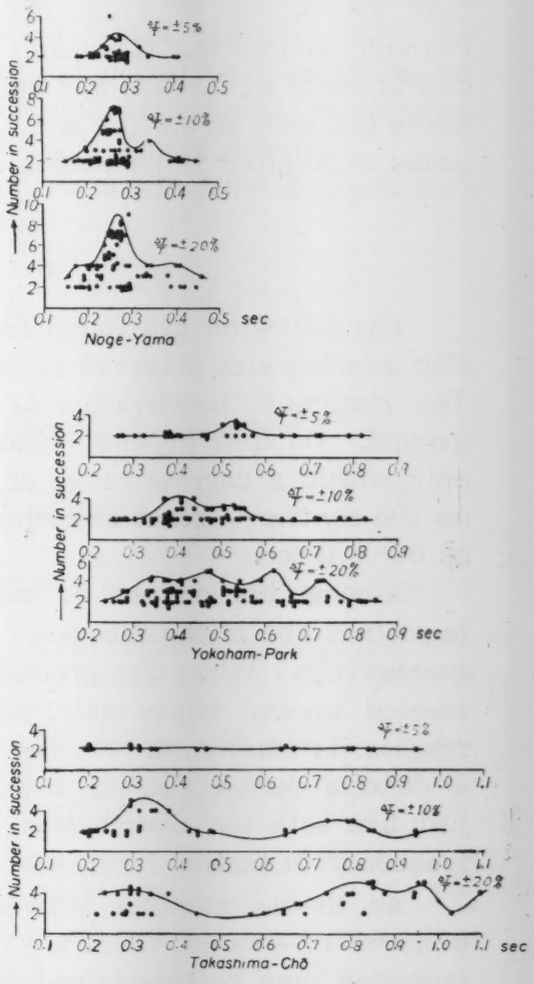

Fig. 8. Distribution of the number in succession of the waves of a definite period concerning the earthquake of 1934 IX 1 at three places in Yokohama.

In case of ±20%, it is only five at the Yokohama Park, while at Nogeyama it is about eight, two times larger than in case of ±5% error. At Takashima-chō the number in succession is different in each earthquake and when the error allowable is ±20%, there will be two different results. One is that the number in succession is unchanged from the case of ±5% error allowable just as at the Yokohama Park, and the other is that it becomes over two times larger than in the case of ±5% error.

The distribution of number in succession to the period is similar to both the curves of frequency-period and of acceleration-period. For example, concerning Nogeyama the peak of number in succession is seen clearly about at 0.30 sec and concerning the Yokohama Park very small peaks are seen at 0.3–0.7 sec. In Takashima-chō case, somewhat large peaks of number in succession are seen at about 0.3 and 0.9 sec.

6. Conclusion.

The following are found from the close examination of the acceleration seismograms observed at several places in Tokyo and Yokohama: The maximum acceleration is smaller on soft ground than on firm ground. On firm ground, vibrations of large acceleration are found only within a narrow range of period as 0.3–0.4 sec, and on soft ground, on the contrary, great acceleration covers such a wide range of period as 0.2–1.0 sec.

Among the actions of earthquake motion against buildings, an important one is the frequency of the wave of a definite period following successively. When the ground is firm, the waves of a definite period succeed several times only around the period when the acceleration reaches its maximum. On the contrary, on soft ground the waves of a definite period succeed several times within a wide range of period just like both the distribution of acceleration to period and that of frequency to period.

As to the relation between earthquake damage to buildings and property of ground, there are many elements involved, but at least the following may be ascertained from this study: Japanese-style wooden houses and other buildings do not always show an equal tendency as to the relation between earthquake damage and ground property. Japanese-style wooden houses on soft ground are damaged seriously, while the damage to the buildings of other types are not so clearly influenced by

the ground property and in some cases it is influenced reversely to the case of Japanese-style wooden houses.[4)]

Such a phenomenon can be explained from the peculiarity of Japanese-style wooden houses. The natural period of such houses becomes as much as two times longer before they collapse. On the firm ground where the curve of acceleration-period has a sharp peak, the period of houses will become longer and the amplitude stops increasing even if the houses have the natural period which coincides with that of an earthquake. But on soft ground, as the curve of acceleration-period is flat, earthquake motion involves the period which coincides with the period of the building even after the natural period becomes larger according to the increase of amplitude. Then on soft ground, consequently the increase of amplitude continues till the houses collapse.

In conclusion we wish to express our thanks to Miss S. Yoshizawa who assisted us in preparing this paper.

---

13. 東京横浜における加速度地震計記象の解析結果

地震研究所 {金井 清 / 鈴木正治}

東京横浜の数ケ所で石本博士が観測した加速度地震計記象を，詳しくしらべた結果，次の事柄がわかつた．

即ち，堅い地盤では，加速度が大きく，一定周期の波が数回続く地震動は，狭い範囲の周期，0.3～0.4 sec，に限られている．それにひきかえて，軟い地盤では，加速度が或程度大きく，一定周期の波が数回続く地震動が，広い範囲の周期，0.2～1.2 sec，にわたつている．

従つて，極く微小な破壊によつて周期が急速に長くなるような構造物は，堅い地盤では，たとえ共振的現象が起つても，すぐにその域を脱け出る可能性が大きい．これに反して，このような構造物は，軟い地盤では，一たび共振的現象に入ると，たとえ破壊によつてその構造物の周期がのびても，どこまでも共振現象が続くことになる．

地盤と震害程度の関係は，日本式木造家屋とその他の構造物とでは，傾向がかなりちがう．その原因は，いろいろ考えられるが，以上の事は，その大きなものの 1 つであろう．

---

4) K. KANAI, *Bull. Earthq. Res. Inst.*, **27** (1949), 97.
K. KANAI and S. YOSHIZAWA, *Bull. Earthq. Res. Inst.*, **29** (1951), 209.

14. *Measurement of the Micro-tremor. I.*

By Kiyoshi KANAI, Teiji TANAKA
and Kaio OSADA,

Earthquake Research Institute.

(Read Jan. 26, 1954 and March 23, 1954.—Received March 31, 1954.)

1. Introduction.

It is certain that the ground is always vibrating at a minute amplitude about 1 micron. Such vibrations are called micro-tremor.

The studies concerning the micro-tremor were started soon after seismology had been established systematically as a branch of science. First it was noted that the mean period of micro-tremor of a definite place has a particular value.[1] Since then, only several studies about the amplitude besides those concerning period have been made intermittently.[2]

The present paper describes the systematical measurement of micro-tremor observed at various places in Tokyo, and the properties of ground deduced from the characteristics of micro-tremor are utilized for the determination of the coefficient of ground relating to earthquake-proof construction. At the same time it is intended that by researching the micro-tremor in full as a wave problem, contribution to the study of earthquake motion will be made.

2. Measuring instrument.

As the measurement in the present study needs much time, for financial reasons paper smoked by oil-lamp and needle for recording are adopted.

For measurement of horizontal motion inverted-pendulum-type transducer is used, and the vertical motion Ewing-type is used. Both have the natural period of 1.0 sec. The motion of the pendulum is transduced into the change of electrical quality by means of the moving coil. The sensitivity is 7.0 volt/kine. The amplifier is of resistance coupled 3 stages, the maximum amplification amount to 90 db and the

1) F. OMORI, *Bull. Earthq. Inv. Comm.*, **2** (1908), 1.
2) W. INOUYE, *Bull. Earthq. Res. Inst.*, **10** (1932), 83.
M. ISHIMOTO, *Bull. Earthq. Res. Inst.*, **15** (1937), 697.

conductance between input and output is 28 mho.

In order to make the behavior of the amplifier stable and to improve its characteristic, push-pull connection and the stabilized power supply are adopted.

This measuring apparatus may distinguished by the recorder.[3] Its constructional features are shown in Fig. 1. The mechanism is as follows. A moving coil supported by a bakelite plate of suitable stiffness moves back and forth in the radial magnetic field caused by a permanent magnet. The back-and-forth motion of the coil is changed into the rotary motion due to an Eden's spring.[4] The Eden's spring has a straw arm at the end, and a recording needle is at the end of the straw arm. Thus the motion of the moving coil is magnified 30 times. There are hardly any solid friction and play in the magnification system in which an Eden's spring is applied. The vibration system is activated by the electro-magnetic damping due to the coil bobbin made of duralumin.

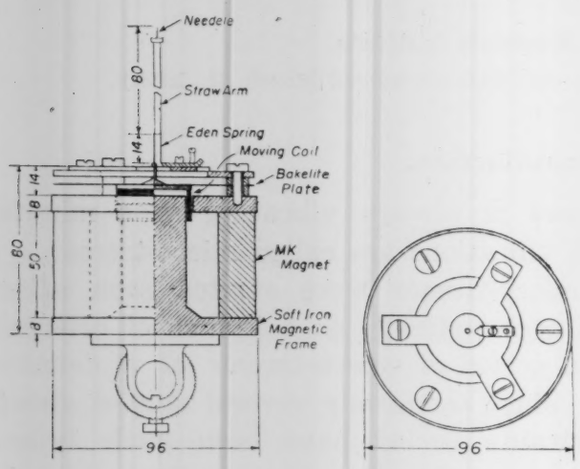

Fig. 1. Construction features of the recorder.

Two natural frequencies of the recorder are available, viz. 20 c/s and 40 c/s, by exchanging Eden's spring. D. C. sensitivities are 0.5 mA/mm and 2.0 mA/mm respectively.

The sensitivity of the vibrograph as a whole, that is the combination of transducer, amplifier and recorder,

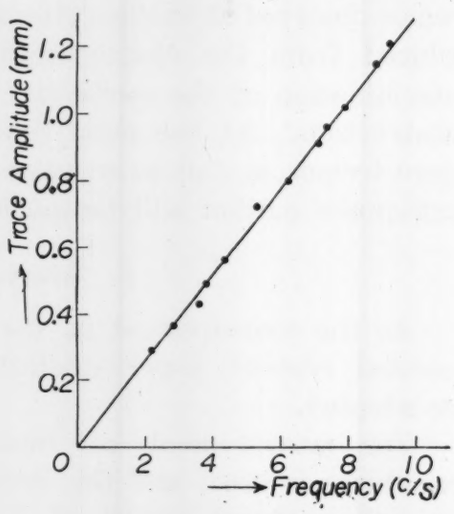

Fig. 2. Characteristic of the vibrograph. Trace amplitude means the record-amplitude corresponding to the 1 μ vibration-table amplitude, as the case of 1/500 of full gain.

3) T. TANAKA and K. KANAI, *Journ. Seism. Soc. Japan.*, [ii], **5** (1952), 43.

4) G. NISHIMURA, M. SUZUKI and E. FURUKAWA, *Bull. Earthq. Res. Inst.*, **32** (1954), 87.

amounts to the maximum of 1.0×10^4 cm/kine. This means the magnification is about 65,000 in case of sinusoidal wave of 1 c/s. The characteristic of the vibrograph as a whole is shown in Fig. 2. Fig. 3 is the photograph of the measuring equipment.

This time the micro-tremor observations were continued for 30 minutes in day-time and at midnight respectively. Midnight observation was performed automatically by using time-switch.

The sensitivity of amplifier was regulated according to place and time so that the maximum of the recorded amplitude may become 10 mm. The driving speed of records is 10 mm/sec. Time was marked by interrupting the output of amplifier at every 15 sec by using a specially made watch.

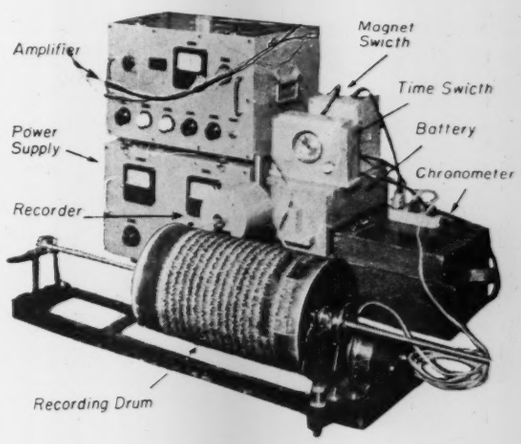

Fig. 3. Measuring equipment.

3. Relation of frequency to period of micro-tremor.

By taking any part of two minutes from the records of micro-tremor, the interval from the time the wave crosses 0-line till it comes to 0-line again is measured. The time thus read is doubled and it is considered to be the period. Then taking the period on the abscissa and the number of waves of each period on the ordinate, the curve of frequency-period is drawn as in Figs. 4–6. (Since this seismograph is an instrument which measures the velocity of waves, the time during which waves cross 0-line twice corresponds to the time needed for the maximum displacement of micro-tremor to come to the next maximum.)

Any place has a definite frequency-period curve of micro-tremor and it is very similar to that of the earthquake motion at the said place.

From Figs. 4–6 it is found that the frequency-period curves of micro-tremor observed in various place in Tokyo can be roughly classified into three groups. The curves which have one sharp peak belong to the first group, those having several peaks to the second, and to the last very flat curves belong.

Among the records of the micro-tremor in various places, the representative records belong to the first, the second and the third

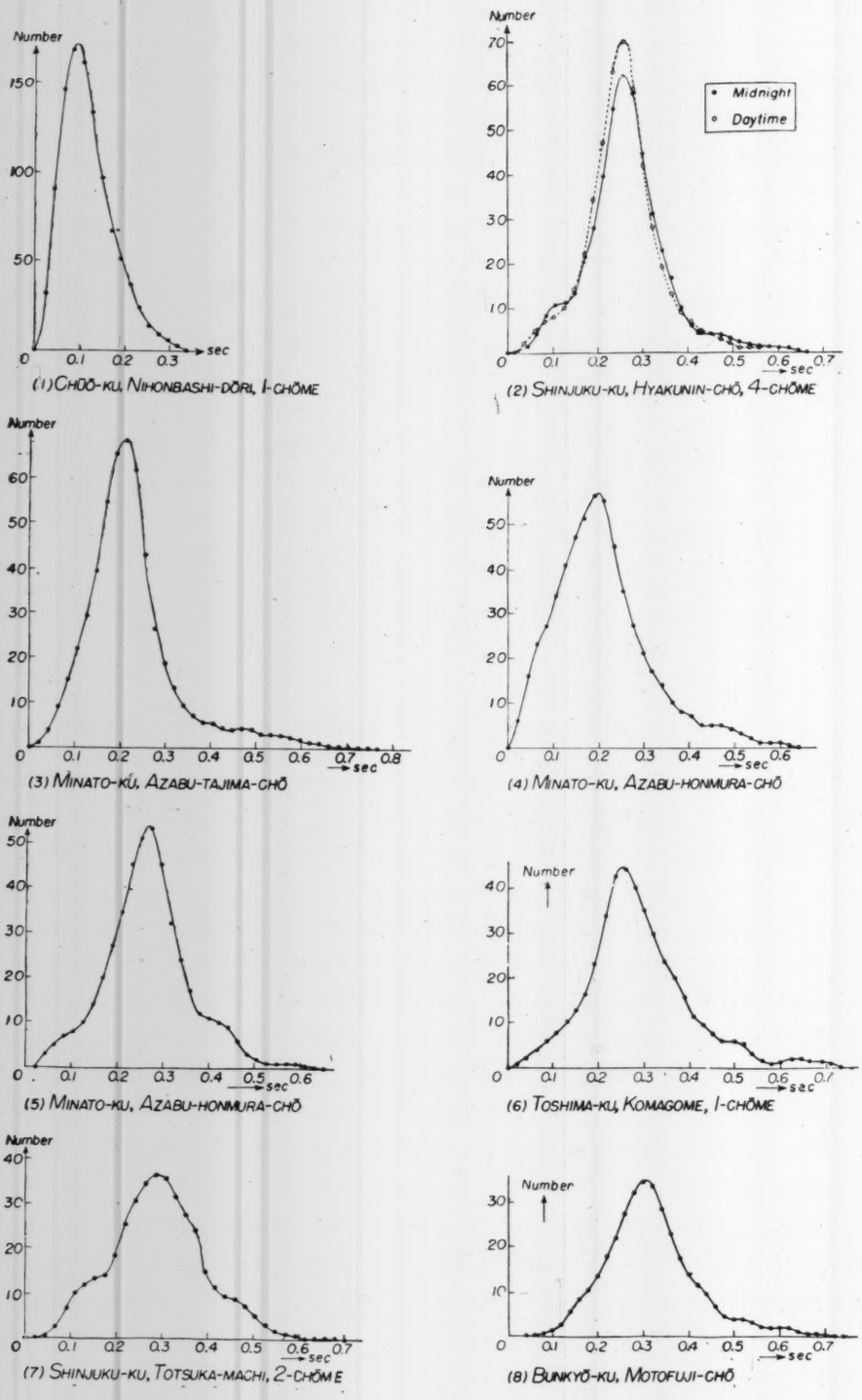

Fig. 4. Frequency-period curves belong to the first group.

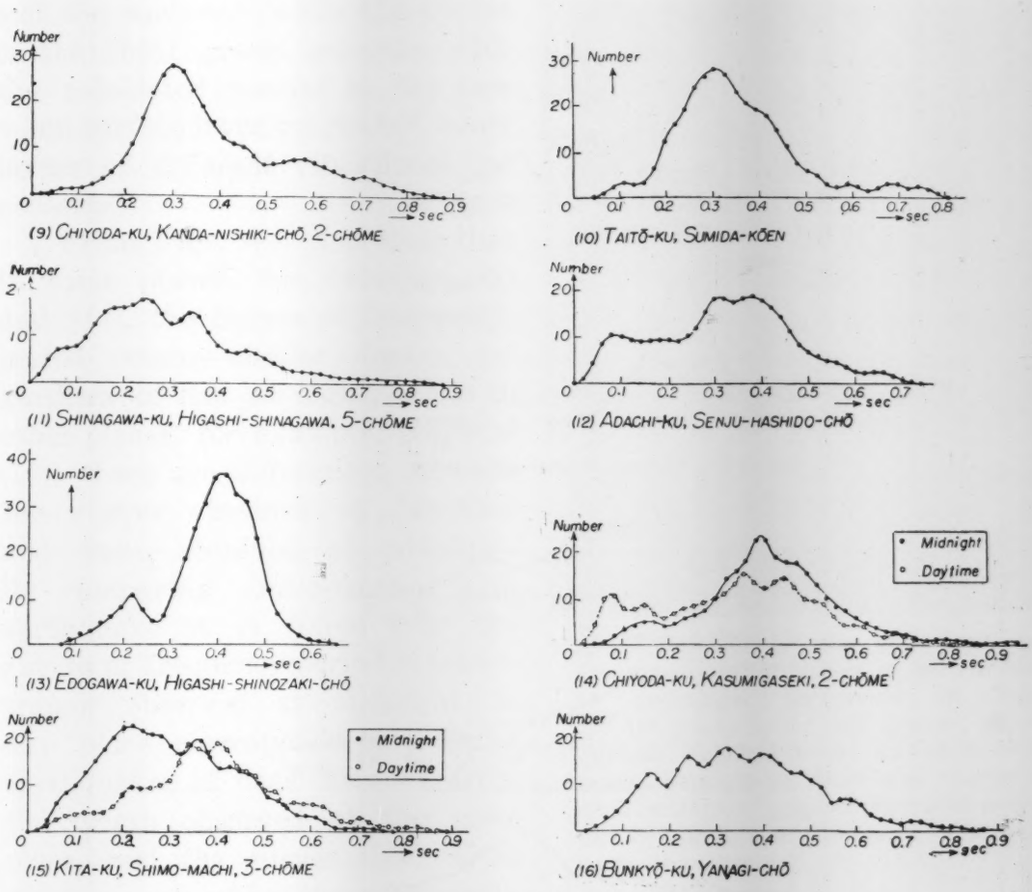

Fig. 5. Frequency-period curves belong to the second group.

groups concerning day-time and midnight are shown in Fig. 7.

Such a classification is illustrated in Fig. 8 as a geological map from which we can deduce the following: The curves of the first group belong to such geological formation as very thin alluvium, diluvium and tertiary. The curves of the second group belong to alluvium of over several meters' thickness. The curves of the third group appear at the special ground among the geological formation of alluvium with thickness of over 25 m.

On the other hand the curves of the first group correspond to the mathematical results concerning the relationship of amplitude-period in case of a surface layer.[5] The curves of the second group are very similar to the calculated results concerning the case when there are two or three layers of different vibrational impedance between the bed rock

5) K. KANAI, *Bull. Earthq. Res. Inst.*, **28** (1950), 31.

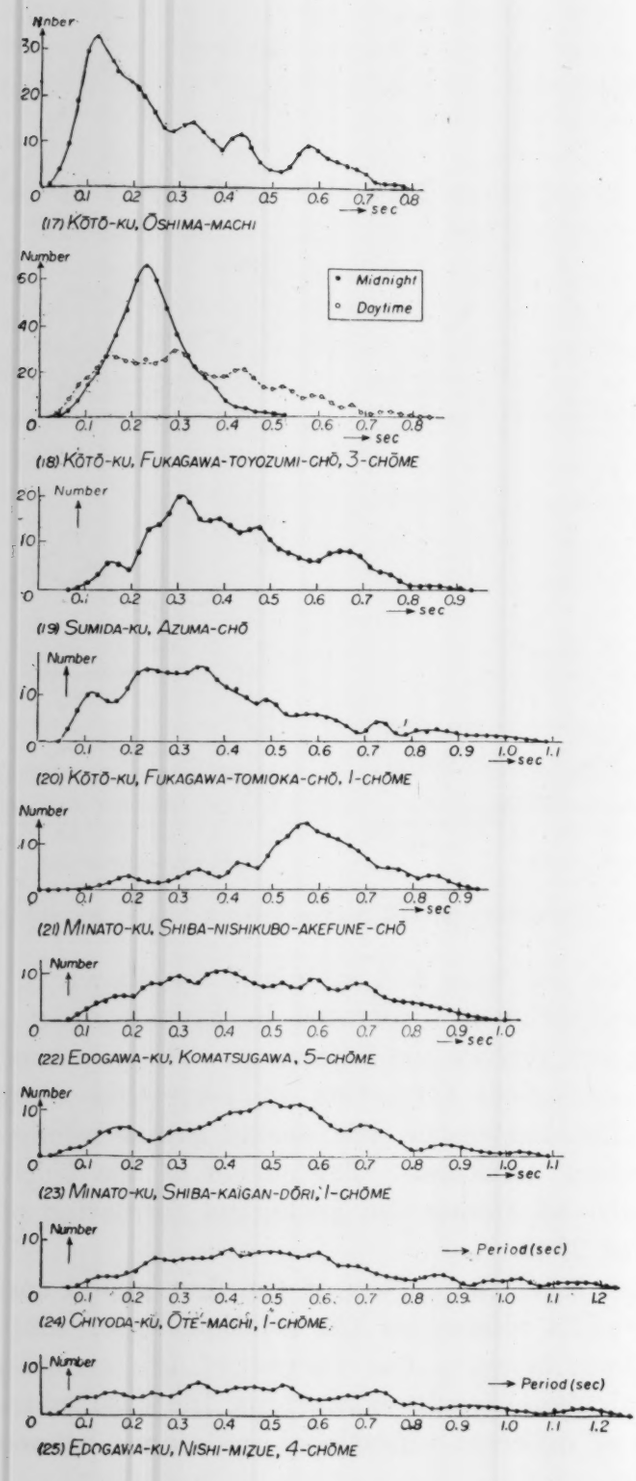

Fig. 6. Frequency-period curves belong to the third group.

and the surface,[6] while the curves of the third group coincide with the calculated results in the case when surface layer consists of many layers of different vibrational impedance.[7]

From Figs. 4–6 it is clear that in some places, for example, (2) and (14), the curves of frequency-period retain similar figure regardless of day or night, while in other places, for example, (15) and (18), there are differences between the curves obtained at day-time and those obtained at midnight. By comparing micro-tremor with earthquake it is found that the curves of frequency-period of micro-tremor observed at midnight in any place corresponds to those of earthquakes of near distance from the origin observed at the same place, and the curves observed at day-time resembles those of earthquake of remote distance from the origin.[8]

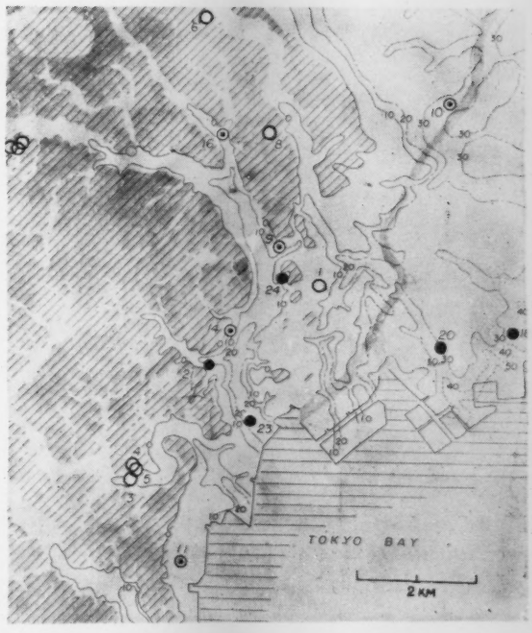

Fig. 8. Relation of the classification of frequency-period curves of micro-tremor to geological formation in Tokyo. ○: 1st group; ◉: 2nd group; ●: 3rd group. Hatched zone: diluvium or tertiary; blank zone: alluvium. Large and small letters of number represent position number and the thickness of alluvium in m respectively.

4. Relation of amplitude to period of micro-tremor.

If the period and amplitude of the waves of micro-tremor are read one by one from the records, they can be plotted as shown in Figs. 9–12.

From these figures it is known that the amplitude is at its maximum at the period when the waves reach the maximum in number. Also it is found that the relation of the lower limit of amplitude to the period which traces a going-up slope appears to follow a certain law. Picking up the minimum amplitudes of respective periods and their ratio to the minimum amplitude of a definite period they are plotted in Fig. 13

6) K. KANAI, *Bull. Earthq. Res. Inst.*, **31** (1953), 219,
K. KANAI and S. YOSHIZAWA, *Bull. Earthq. Res. Inst.*, **31** (1953), 275.
7) K. SEZAWA and K. KANAI, *Bull. Earthq. Res. Inst.*, **13** (1935), 484.
8) M. ISHIMOTO, *Bull. Earthq. Res. Inst.*, **12** (1934), 234 and **13** (1935), 592.

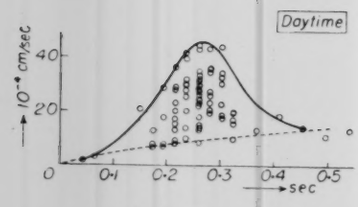

Fig. 9. Amplitude-period curves of micro-tremor at, (2), 4-chōme, Hyakunin-chō, Shinjuku-ku.

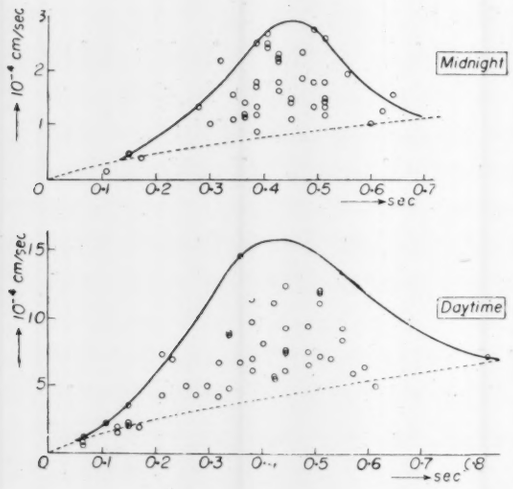

Fig. 10. Amplitude-period curves of micro-tremor at, (14), 2-chōme, Kasumigaseki, Chiyoda-ku.

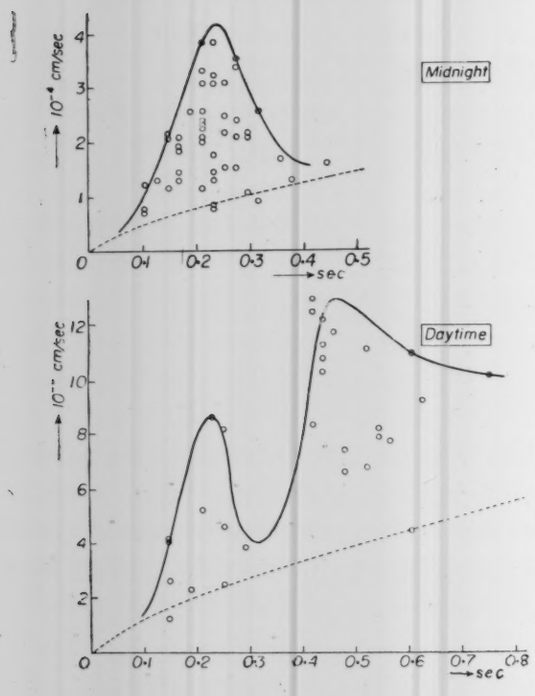

Fig. 11. Amplitude-period curves of micro-tremor at, (18), 3-chōme, Fukagawa-toyozumi-chō, Kōtō-ku.

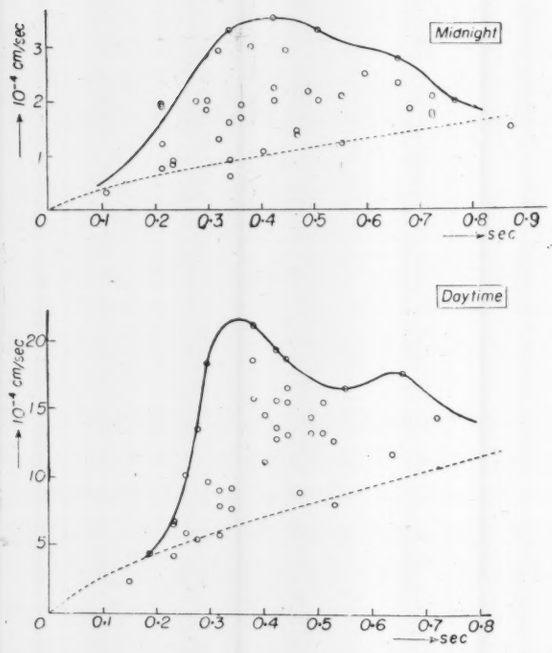

Fig. 12. Amplitude-period curves of micro-tremor at, (20), 1-chōme, Fukagawa-tomioka-chō, Kōtō-ku.

which, roughly speaking, proves the relation of $V \propto T^{0.7}$, at least, at the period ranging 0.1～1 sec. Such a relation is represented by the lower

curves written in Figs. 9–12.

Now let the lower limit of amplitude be the amplitude of the original waves of micro-tremor. Then it may be considered that the upper boundary indicates the amplification concerning every period. The maximum amplitudes shown in Figs. 9–12 being divided by the amplitudes of lower limit at the corresponding periods, the numerical values of the maximum amplification of grounds are given as shown in Table I.

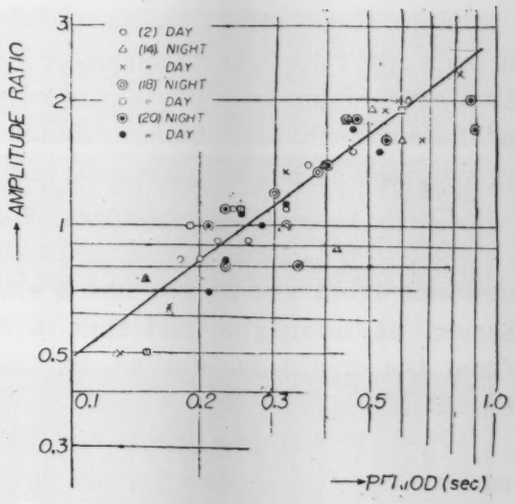

Fig. 13. Relation of lower limit amplitude to period.

The maximum amplification which shows slight difference between day and night at every place and is independent of the property of ground becomes 3–4 in general. (As the amplitude of lower limit is considered to be twice as large as the original amplitude, which is due to the reflection of waves at free surface, the doubled values of the calculated results mentioned above are regarded as the amplification of ground. Those values coincide with the amplification of earthquake motion at ground surface[9].)

Table I.
The values of the maximum amplification of grounds.

Position	Time	Value
(2)	Day	4.4
(14)	Night	3.5
	Day	3.6
(18)	Night	4.4
	Day	4.1, 3.8
(20)	Night	3.2
	Day	3.2

$V \propto T^{0.7}$ means that displacement D is in the relationship of $D \propto T^{1.7}$ and this coincides with the displacement-period relation of earthquake motion which was described in the preceding paper.[10]

5. Conclusion.

As the results of the measurement of micro-tremor made at many places in Tokyo, the following become clear :

9) K. KANAI, K. OSADA and S. YOSHIZAWA, *Bull. Earthq. Res. Inst.*, **31** (1953), 227.
10) K. KANAI and M. SUZUKI, *Bull. Earthq. Res. Inst.*, **32** (1954), 187.

(i) The relation curve of frequency-period of micro-tremor shows a definite form for respective districts. This form coincides with that of earthquake motion and has a close relation with the geology of a district. On the firm ground a sharp peak appears at 0.1–0.3 sec period, and on the soft ground at 0.4–0.6 sec. On especially soft ground the curve is flat at the period ranging 0.3–1 sec.

(ii) The frequency-period curve of earthquake motion of near distance from the origin has a similarity to that of micro-tremor observed at midnight, and that of earthquake motion of remote distance from the origin is similar to that of the micro-tremor observed at day-time.

(iii) Presuming the cause of micro-tremor, the relation of displacement to period at every place is considered to be $D \propto T^{1.7}$, at least, at the period ranging 0.1～1 sec. This is coincident with that of the earthquake motion at bed rock.

(iv) In the case when the presumption in (iii) is taken into consideration, the maximum amplification of micro-tremor is considered almost independent of the property of ground and becomes 6–8 in general. Such values correspond to those of earthquakes.

From the results of the measurement of micro-tremor described in this paper it is shown that there seem to be some similarities between the generation mechanism of micro-tremor and seismic waves which arrive at bed rock.

In conclusion we wish to express our thanks to the Science Section of Educational Ministry and the Bureau of Architecture, Tokyo-Metropolis, for the financial aid granted us for the present investigations. Thanks are also due to the residents of the observation districts for their cooperation, and to Miss S. Yoshizawa who assisted us in preparing this paper.

---

14. 常時微動の測定 第1報

地震研究所 金井 清
田中貞二
長田甲斐男

東京都内の多くの場所で常時微動を観測した結果，次の事柄がわかつた．

(i) 常時微動の頻度—周期関係は各場所について，きまつた型である．この型は，同じ場所における地震動の頻度—周期関係の型によく似ており，その場所の地質と関係が深い．

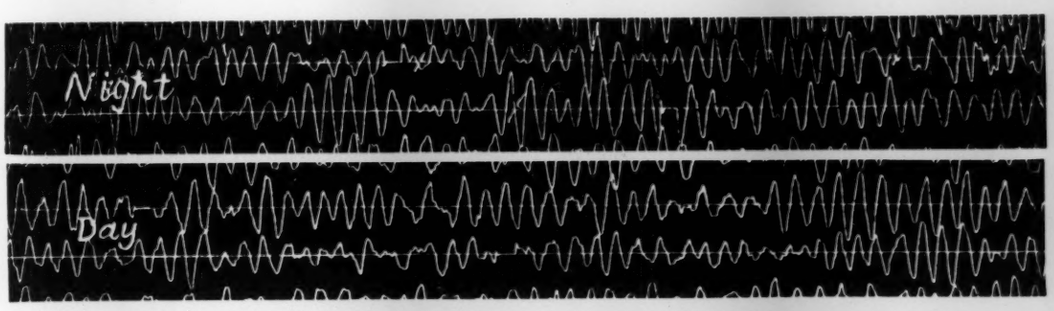

(2). 4-chōme, Hyakunin-chō, Shinjuku-ku.

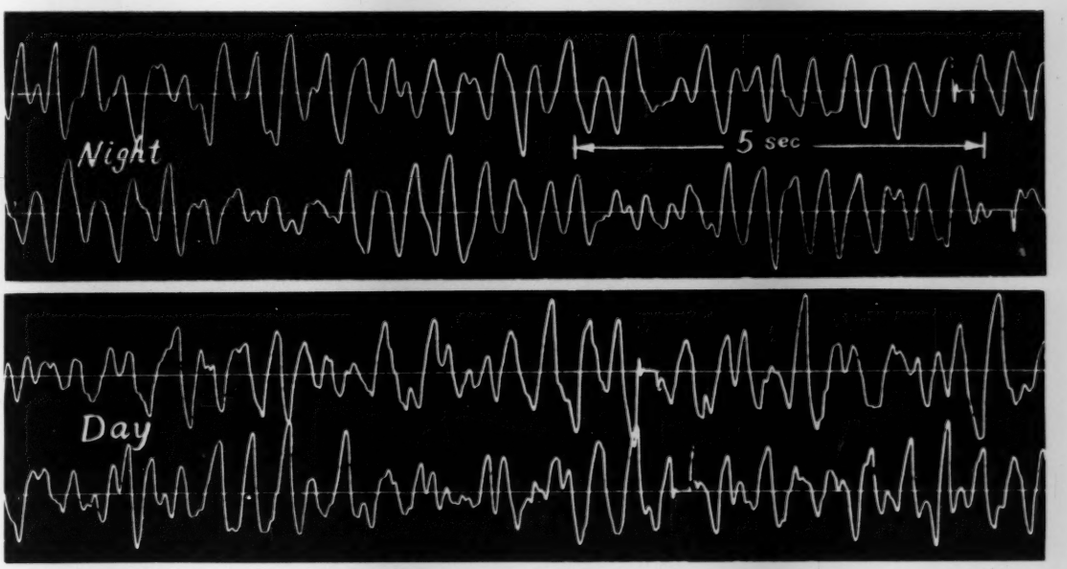

(15). 3-chōme, Shimo-machi, Kita-ku.

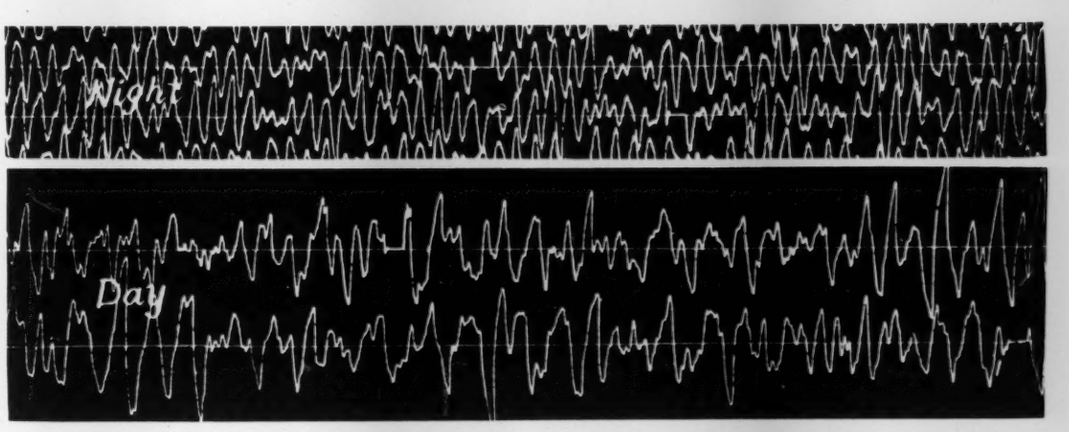

(18). 3-chōme, Fukagawa-toyozumi-chō, Kōtō-ku.

Fig. 7. Representative records of micro-tremor belong to the 1st, 2nd and 3rd groups. Upper: midnight; lower: day-time. Original size.

即ち，堅い地盤では 0.1～0.3 sec に鋭い山ができる．軟い地盤では 0.4～0.6 sec に山ができる．非常に軟い地盤では 0.3 sec から 1 sec 以上にわたつて平である．

(ii) 常時微動の深夜の頻度—周期曲線は近地地震のものに似ており，昼のものは遠地地震のものに似ている．

(iii) 常時微動を起すもとになるものを，或解析のやりかたの結果から仮想すると，少くとも 0.1～1 sec のものについては，変位と周期の関係は $D \propto T^{1.7}$ と考えられる．

この関係は基盤における地震動のものに合う．

(iv) (iii) のように考えると，常時微動の地盤による最大増巾度は 6～8 となる．この値は地震動の場合に合う．

(v) 常時微動の頻度—周期曲線は，耐震構造上からの地盤係数を求める手段として利用することができそうである．

15. *A Short Note on the Relation of Amplitude-Period of Earthquake Motion.*

By Kiyoshi KANAI,

Earthquake Research Institute.

(Read March 23, 1954.—Received March 31, 1954.)

From Figs. 5, 6 in the preceding paper[1] and the observational results in Tokyo[2] and Fukui[3], the relation between the maximum acceleration of earthquake motion A_{max} and the predominant period T_0 is obtained as shown in Fig. 1. From Fig. 1 the relation as the average becomes

$$A_{max} \propto T_0^{-0.6\pm0.1}. \quad (1)$$

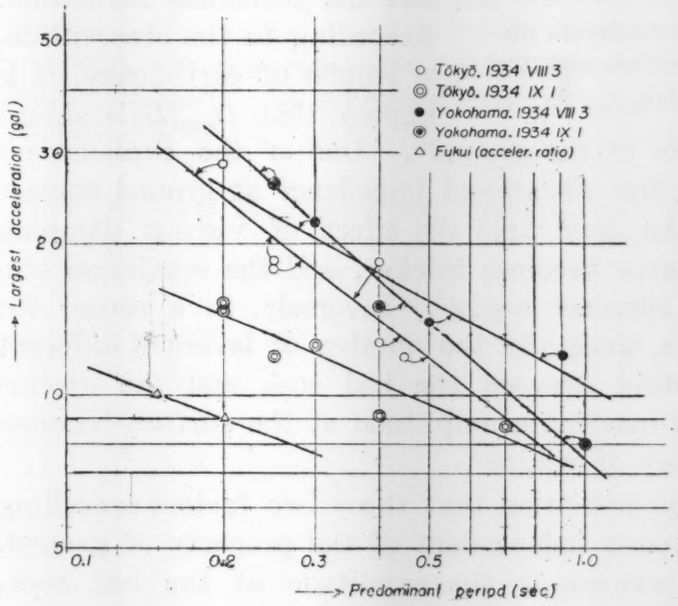

Fig. 1. Relation between the maximum acceleration of earthquake motion and the predominant period of ground.

Then, as will be seen from the observation results of after-shocks in Nankai[4] and Fukui[5] earthquakes and compared results of observations made at two places in Tokyo and Hyōgo prefecture[6], the relation between the maximum displacement of earthquake motion D_{max} and the predominant period T_0 becomes as shown in Fig. 2. Fig. 2 leads to the relation as the average which is

1) K. KANAI and M. SUZUKI, *Bull. Earthq. Res. Inst.*, **32** (1954), 187.
2) M. ISHIMOTO, *Bull. Earthq. Res. Inst.*, **13** (1935), 594, Table II.
3) T. MINAKAMI, *Report of the Fukui Earthquake Committee* (1950), 84, Table 18.
4) T. MINAKAMI and S. SAKUMA, *Bull. Earthq. Res. Inst.*, **26** (1948), 63, Figs. 3, 4 and 64, Fig. 6.
5) T. MINAKAMI, *loc. cit.*, 3).
6) K. KANAI and T. SUZUKI, *Bull. Earthq. Res. Inst.*, **31** (1953), 312, Table IV, V.

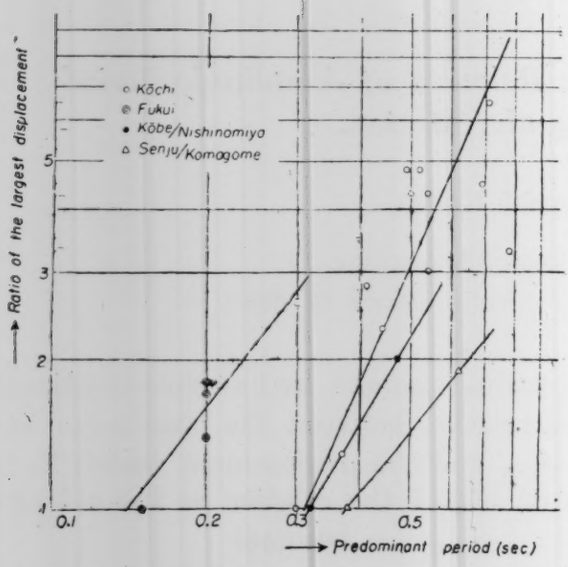

Fig. 2. Relation between the maximum displacement of earthquake motion and the predominant period of ground.

$$D_{max}=T_0^{1.7\pm0.2}. \qquad (2)$$

Now, let the wave amplitude at the bed rock be D and the maximum amplitude at the ground surface be D_{max}. Then their relation is represented as follows;

$$\frac{D_{max}}{D}=f(L), \qquad (3)$$

where $f(L)$ is the coefficient depending on both the material existing between the bed rock and the ground surface and the geological formation. According to the observational results of earthquake, it is known that D_{max}/D is almost independent of the property of the ground[7]. One of the explanations to this is that generally the vibrational impedance at ground surface tends to decrease and at the same time the effect of viscous damping decreases as the surface layer becomes thicker, and the maximum amplitude at ground surface becomes larger[8]. Inversely, in a sense, the thicker the surface layer is, generally the number of layers of different vibrational impedance existing between the bed rock and the ground surface increases, and the maximum amplitude at the surface becomes smaller due to the coherency of waves[9].

These facts lead to a presumption that these two factors cancelling each other, $f(L)$ becomes almost independent of the property of ground. Consequently the relation between D, the amplitude at the bed rock, and T, the period of waves, may be represented as follows

$$D\propto T^{1.7\pm0.2}. \qquad (4)$$

Concerning seismic waves, if the law of equipartition of energy holds good and seismic wave is affected by viscous damping in the course of

7) K. KANAI, K. OSADA and S. YOSHIZAWA, *Bull. Earthq. Res. Inst.*, **31** (1953), 229, Fig. 6 and 230, Fig. 7.
8) K. KANAI, *Bull. Earthq. Res. Inst.*, **30** (1952), 35.
9) K. KANAI and S. YOSHIZAWA, *Bull. Earthq. Res. Inst.*, **31** (1953), 275.

transmission, the relation represented by equation (4) is acceptable so far as it goes.

In conclusion the author wishes to express his thanks to Miss S. Yoshizawa who assisted him in preparing this paper.

---

15. 地震動の振幅と周期との関係 (小引)

地震研究所　金　井　　清

東京，横浜，福井の各種の地盤で，周期 0.1 sec の地震計を使つて，地震の比較観測を行つて得られた結果から，ある基準地の最大加速度に対する各地の最大加速度の割合と夫々の土地の卓越周期との関係を求めると，

$$A_{max} \propto T_0^{-0.6 \pm 0.1} \qquad (1)$$

となつた．

又，高知，福井，東京，兵庫の各種の地盤で，周期 1 sec の地震計を使つて地震の比較観測を行つて得られた結果から，ある基準地の最大変位に対する各地の最大変位の割合と夫々の土地の卓越周期の間には次の関係があることになつた．

$$D_{max} \propto T_0^{1.7 \pm 0.2} \qquad (2)$$

(1), (2) 式を使つて，地震波の性質，地盤係数についての議論を行つた．

---

16. *Effect of Thermal History on Viscosity of Oosima-lavas.*

(Elastic and Viscous Properties of Volcanic Rocks. Part 4.)

By Shūzō SAKUMA,

Earthquake Research Institute.

(Read Jan. 26 and March 23, 1954.—Received March 31, 1954.)

Introduction.

One of the factors which characterize volcanic activities is the viscosity of the intruding, extruding and flowing lavas during the course of the respective activities. The scale of upheaval and subsidence around the volcanoes, the frequency and magnitude of volcanic earthquakes as well as the intensity of explosions are affected without exception by the viscosity of lavas. Lava is the product of magma at its last stage of evolution. The viscosity of magma varies with the development of crystallization in it, and crystallization is a certain complicated function of temperature and the rate of cooling. Accordingly, viscosity will be influenced seriously by the thermal state in which the magma has been placed to the present. Especially, when the lava is ejected to the earth's surface and has to cool in the air, the rate of nucleation and growth of crystals cannot keep up with the rapid rate of cooling, and the lava remains as a heterogeneous mixture of crystals and glass.

The viscosity of flowing lavas of various volcanoes has been estimated by many investigators. However, we do not know how the character of extruding lava is affected by various complicated parameters in such transient circumstances. The question, which arose as to the mode of development of dynamical properties in the interior of lava, leads the writer to conduct the present experimental study concerning the effect of thermal history on the viscosity of Oosima-lavas.

It was already pointed out in the previous papers[1] that heat treatment of Oosima-lava in the laboratory causes irreversible changes both in Young's modulus and in the viscosity. It was found that the viscosity always increases with the repetition of heating experiment, but the previous procedures of experiments need some alterations.

1) S. SAKUMA, *Bull. Earthq. Res. Inst.*, **30** (1952), 269 ; **31** (1953), 63 and 291.

Method.

The fundamental principle of experiment remains the same. Specimens are cut from lava blocks, ground and polished into thin plates of ca. 0.3 cm × 1 cm × 8 cm. The lava-plate is supported on two knife-edges at its ends and is loaded at the centre through another knife-edge, and the specimen continues to sag by the constant load. The whole contrivance is inserted in the electric furnace. In the previous experiments, elasticity and viscosity were measured at constant temperatures by the deformation of specimen due to application and removal of load. The load was not applied while the temperature was being raised and lowered to the next constant temperature. But such step-by-step procedure is not suitable for the present purpose to find the effect of thermal history, for the reason that the step-by-step heating complicates the history of the specimen. In the present studies, the temperature is raised not step by step but at a constant and definite rate and the load is applied from long before the commencement to the end of heating, to avoid the above-mentioned defect.

However, this method of experiment has still some other defects, which shall be discussed here.

1) Possible lag of temperature in the specimen.

Because the temperature in the furnace increases with time and is not kept constant, the distribution of temperature in the specimen as well as in the furnace is not perfectly uniform and constant. Accordingly, the temperature in the specimen will lag more or less behind the temperature which the thermocouple indicates. If we regard the specimen as an infinite plate with thickness l for mathematical simplicity, and assume the temperature at the surface as

$$T=\beta t \qquad (\text{at} \quad x=0 \quad \text{and} \quad x=l),$$

the temperature in the specimen is given from the theory of conduction of heat by

$$T=\frac{4\beta}{\pi}\sum_{n=1}^{\infty}\frac{1}{n}\sin\frac{n\pi}{l}x\left\{t-\frac{l^2}{\kappa n^2\pi^2}\left(1-\exp\left(-\frac{\kappa n^2\pi^2}{l^2}t\right)\right)\right\}, \qquad (1)$$

in which κ is the thermal diffusivity and n the odd integer. Put $x=\frac{l}{2}$, and

$$T=\beta t-\frac{\beta l^2}{8\kappa}+\frac{4\beta l^2}{\kappa\pi^3}\left\{\exp\left(-\frac{\kappa\pi^2}{l^2}t\right)-\frac{1}{3^3}\exp\left(-\frac{9\kappa\pi^2}{l^2}t\right)+\cdots\right\}. \qquad (2)$$

Put $\kappa=3\times10^{-3}$ cm^2/sec and $\beta=600°$/h, and we find that the lag is only 0.7°C even at the centre. Subsequently, this kind of lag can be neglected.

2) Lag of deformation due to elastic after-effect.

If the specimen is the Newtonian viscous liquid, the velocity of deformation will represent its viscosity for the temperature at the very instant. But the actual lava has been proved to be a visco-elastic material except at high temperatures. Put

$$\tau'\ddot{e}+\dot{e}=\frac{P}{3\eta} \qquad (3)$$

for the present specimen, where P and e are stress and strain, E is Young's modulus, η is viscosity and τ' is the relaxation time for strain under constant stress. τ' is the cause of the lag in question. The approximate value of τ' was given in the previous report. If the temperature increases as $T=\beta t$, and $\eta=\eta_0$ at $t=0$, the equation (3) becomes

$$\dot{e}=\exp\left(-\int\frac{dt}{\tau'}\right)\left\{C+\int\frac{P}{3\eta\tau'}\exp\left(\int\frac{dt}{\tau'}\right)dt\right\}. \qquad (4)$$

If we assume that $1/\eta=M\exp(mT-kt')$, on the basis of the result of experiment which will be seen on Figs. 2(a)-(b), and that, for simplicity's sake, $\tau'=\bar{\tau}'=$ constant, we obtain

$$\dot{e}=\frac{PM}{3}\left\{\frac{m\beta\bar{\tau}'}{1+m\beta\bar{\tau}'}\exp\left(-\frac{T}{\beta\bar{\tau}'}\right)+\frac{1}{\bar{\tau}'\beta}\cdot\frac{\exp(kT_0/\beta)}{m-k/\beta+1/\beta\bar{\tau}'}\cdot\exp\left(mT-\frac{kT}{\beta}\right)\right\}. \qquad (5)$$

$$(t'=t-T_0/\beta)$$

After some approximate numerical calculations ($T_0=150$°C, $k=10^{-4}$, $\beta=600°$/h, $m=2\times10^{-2}$), we find that the first term, which includes the delayed elasticity principally, is of the same order of magnitude of the second term at 600°C and is not negligible, and that it vanishes at above 800°C owing to the decrease of $\bar{\tau}'$ at higher temperatures. If $\beta=100°$/h, the first term vanishes even at 600°C. In short, the present method of experiment is trustworthy at least at temperatures higher than 800°C.

Tested Specimens.

Three kinds of new lavas[2] from Oosima were compared with one another. The three were already described with photo-micrographs in

2) H. Tsuya, R. Morimoto & J. Ossaka, *Bull. Earthq. Res. Inst.*, **29** (1951), 563; **30** (1952), 231.

the preceding paper[3] on the elasticity at high temperatures.

One was found at the side of a fluidal lava-flow and remains glassy, one was in a deep crevice in the slowly solidified lava-pool and is highly crystalline, and the other is of an intermediate character of the above two.

Comparison of grain-size among the specimens were done by a modified method of volumetry. Petrographical constituents on photomicrographs were classified into three groups: (1) light-colored minerals (2) gray (on black and white photo)-colored minerals (3) dark-colored minerals and glass. Preliminary inspection by microscope showed that group (1) consists largely of plagioclases, (2) of pyroxynes and (3) of glass and few magnetites. Straight lines are drawn on the photomicrographs in cross-stripes. Length of every segment (x) of line which crosses a mineral or glass is regarded as the size of the part. The distribution of grain-size of minerals and the relative area occupied by the respective groups could be estimated roughly by this procedure.

More exactly, however, the average length which is occupied by one mineral differs from every one of its sides. An example will be shown in the followings. Assume the cross-section of a mineral to be a rectangle the sides of which are A and qA. The average length of the segments for all possible orientation of the rectangle to straight lines is given by

$$\bar{x}=\frac{2qA}{\pi\sqrt{1+q^2}}\log\frac{\tan\left(\frac{\pi}{4}+\frac{\lambda}{2}\right)}{\tan\frac{\lambda}{2}}, \qquad (\tan\lambda=1/q) \qquad (6)$$

$$\therefore \quad \bar{x}=\begin{cases}0.80a & \text{for} \quad q=1\\ 0.78a & ,, \quad q=2\\ 0.63a & ,, \quad q=10\,.\end{cases}$$

where a is the geometrical mean of the sides. Subsequently, it is not accurate to regard the length of the segment as the grain-size and the abscissae of Figs. 1 (a) and 1 (b) should be corrected.

In spite of that, the difference between the glassy and the crystalline lavas shown by this method deserves notice. The area of glass is about 50% for the glassy one and about 20% for the crystalline one. The difference was found to have been caused by the abundant presence of fine grains of minerals in the groundmass of crystalline lava. Phenocrysts occupy about 10% of total area in common. They are omitted from the figures.

3) S. SAKUMA, *loc. cit.*, 1).

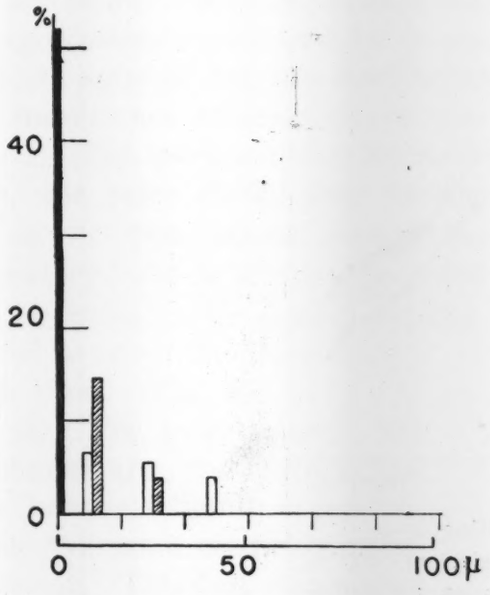

Fig. 1(a). Glassy lava. (phenocrysts (14%) are omitted from the figure.)

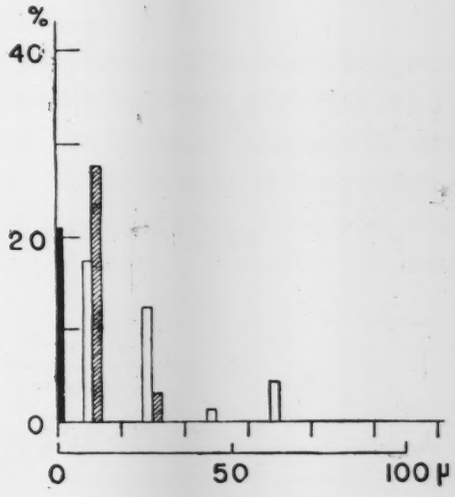

Fig. 1(b). Crystalline lava. (phenocrysts (13%) are omitted from the figure.)

Fig. 1. Area (in %) occupied by the minerals of various grain-size.
White columns: plagioclases,
Hatched columns: pyroxynes,
Black column: glass and magnetites.

Results of Experiments.

Viscous flow of specimens was studied by measuring its deformation every few minutes or every thirty seconds. The specimens were dealt

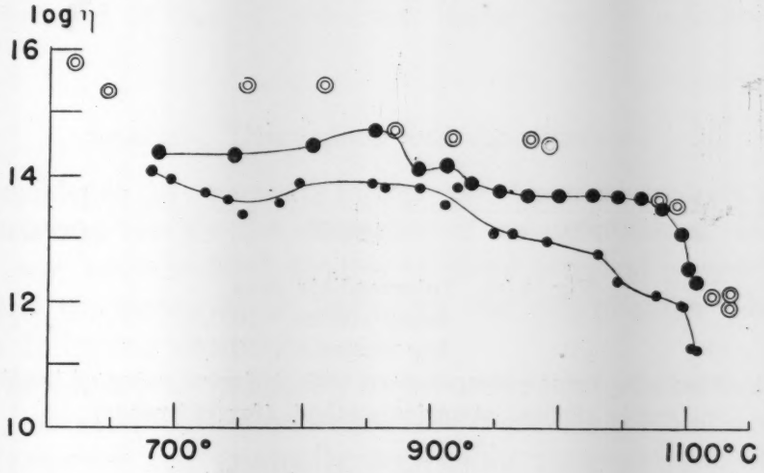

Fig. 2(a). Glassy lava.
Small circles: 600°/h,
Big circles: 100°/h.

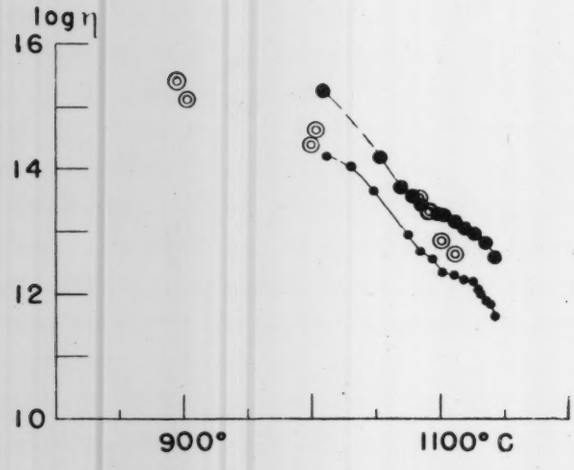

Fig. 2(b). Crystalline lava.
Small circles: 600°/h,
Big circles: 100°/h.

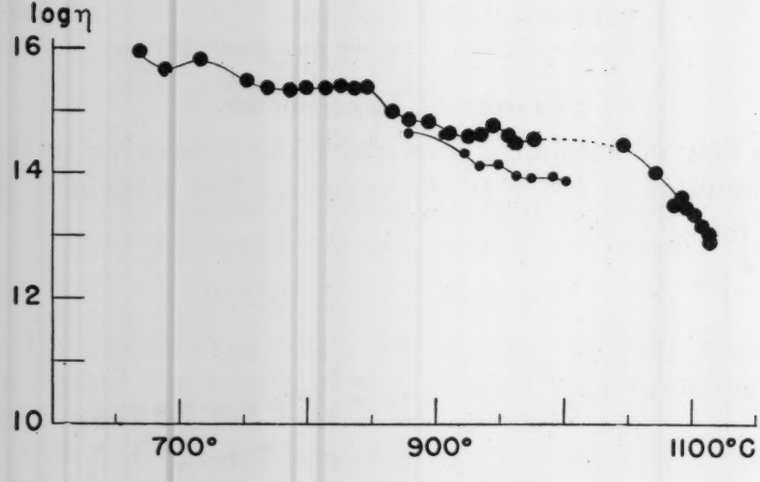

Fig. 2(c). Intermediate lava.
Small circles: 100°/h,
Big circles: 30°/h.

Fig. 2. Viscosity versus temperature with different rates of heating.
Double circles: stepwise method. (for reference)

with under various rates of increase of temperature, i.e. 600°/h, 100°/h and 30°/h. The applied stress is kept same for all experiments so that

the structural viscosity, if any, may not affect the results. The results of experiments were found to be reproducible within the error of about 20%, in spite of the non-equilibrium character of the experiments.

Results are summarized as follows.

(1) The more rapidly the specimens are brought to high temperature, the more fluidal they become. Viscosity depends not only on T, but on $\dot{T}$. This shows merely the effect of thermal history in the laboratory, and it will be discussed later. Experiments under constant temperatures, after heated rapidly to the temperatures, were also conducted to prove the dependence of viscosity on time. Viscosity increases with time. (Fig. 3)

(2) The more glassy the specimens are, the more fluidal they behave without exception, under the same condition of experiment. This fact means that the lavas of Oosima are always affected by their respective thermal histories, which they have experienced under natural conditions.

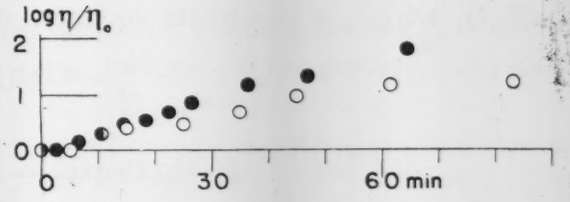

Fig. 3. Change of viscosity whit time at constant high temperatures.
Closed circles:
1130°C±4°C, crystalline lava,
Open circles:
1000°C±3°C, intermediate lava.

The previous experiments by increasing the temperature step by step failed to show the transient character in viscosity of lavas. The remarkable discontinuity in viscosity which was observed in the previous experiments at about 1130°C will perhaps correspond to one of eutectics under nearly equilibrium conditions.

Analysis, Discussions and Application.

The dependence of viscosity upon the thermal history of lava is one of the keys to clarify the character of volcanic rocks, although it complicates our experimental studies of their physical properties. The writer wishes to throw some light on the complicated phenomenon through the following discussions.

The lavas cannot be imagined to be under perfect thermodynamical equilibrium. Crystallization under perfect thermodynamical equilibrium, under high pressure and gradually decreasing temperature, would have rendered the magma a different igneous rock.

At first, let us consider the lava cooling under natural conditions.

Because it is not in equilibrium and the reactions lag behind cooling, the quantity of crystalline phase is inevitably less than that which may be expected under equilibrium conditions. The existence of the supercooled glass will be the main cause of the phenomenon to be examined here. The quantity as well as quality of the phase which is not in thermodynamical equilibrium is a function not only of temperature but of time. Let us assume secondly that the fluidity, or the reciprocal of viscosity, can be divided into two parts, which correspond to the stable and unstable phases respectively.

$$\frac{1}{\eta}=c(T)+b'(T,t)\,. \tag{7}$$

$b'(T,t)$, which is the unstable part, will vary in the following manner.

$$\frac{\partial b'}{\partial t}=-k'(T)b'. \tag{8}$$

$$\therefore \quad b'=b_0(T)\exp\left\{-\int k'(T)dt\right\}. \tag{9}$$

And $T=T(t)$ in general,

$$\therefore \quad \frac{1}{\eta}=c(T)+b_0(T)\exp\left\{-\int_{T_0}^{T}\frac{k'(T)}{\dot{T}}dT\right\}. \quad (T_0>T) \tag{10}$$

$c(T)$ and $b_0(T)$ may depend partly on the quality of the liquid phase at the temperature and partly on the quantity of it, as well as the mode of aggregation of the crystals. More precisely, $b'(T,t)$ may consist of more than one component. But only one main term is to be discussed here, because of the limited accuracy of the present experiment and because the reactions can be supposed to be eutectic, in which various minerals crystallize together.

When we heat the specimens in the laboratory, the change of viscosity with time will be similar to (7) and

$$\frac{\partial b}{\partial t}=-k(T)b\,. \tag{11}$$

In the last place, viscosity at heating in the laboratory is given approximately by

$$\frac{1}{\eta}=c(T)+b'_0(T)\exp\left\{-\int_0^t k(T)\,dt\right\} \tag{12}$$

where the origin of time is taken at the beginning of the experiment. The initial state of (12) is the final state of (10).

$$\therefore \quad \begin{cases} \frac{1}{\eta} = c(T) + I(T) \exp\left\{-\int_0^T \frac{k(T)}{\dot{T}} dT\right\}, & (13) \\ I(T) \equiv b_0(T) \exp\left\{-\int_{T_0}^0 \frac{k'(T)}{\dot{T}} dT\right\}. & (14) \end{cases}$$

Then we enter into analysis of the results of experiments on the basis of the above-mentioned assumptions.

(A) Evaluation of k.

A-1) Experiments under linearly increasing temperatures, in which $T=\alpha_n t$, $\alpha_n=600°/\text{h}$, $100°/\text{h}$ and $30°/\text{h}$.

$$\therefore \quad \frac{1}{\eta_n} = c(T) + I(T) \exp\left\{-\frac{1}{\alpha_n}\int_0^T k dT\right\}. \qquad (15)$$

At first we compare the viscosity with one another among the same kind of specimens, which has the same history in the nature, i.e. $I(T)$ is common.

$$\frac{1}{\eta_1} - \frac{1}{\eta_3} = I(T)\left\{\exp\left(-\frac{1}{\alpha_1}\int_0^T k dT\right) - \exp\left(-\frac{1}{\alpha_3}\int_0^T k dT\right)\right\}$$

$$\frac{1}{\eta_2} - \frac{1}{\eta_3} = I(T)\left\{\exp\left(-\frac{1}{\alpha_2}\int_0^T k dT\right) - \exp\left(-\frac{1}{\alpha_3}\int_0^T k dT\right)\right\}.$$

If we take $\alpha_3 \ll \alpha_1$ and α_2, we can put as follows approximately, because $c(T)$ is far less than $b(T)$ below 1100°C.

$$ln\frac{\eta_2}{\eta_1} = \left(\frac{1}{\alpha_2} - \frac{1}{\alpha_1}\right)\int_0^T k dT. \qquad (16)$$

Then we get $\int_0^T k dT$ as a function of T, as far as the assumptions

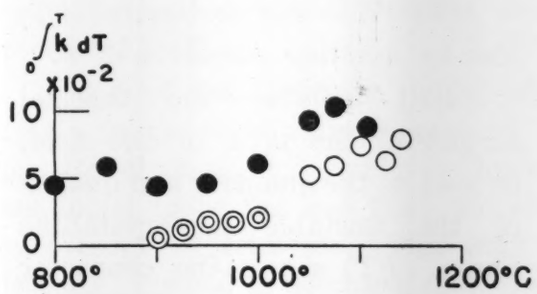

Fig. 4. $\int_0^T k(T)dT$ as a function of T.
Closed circles: glassy lava,
Open circles: crystalline lava,
Double circles: intermediate lava.

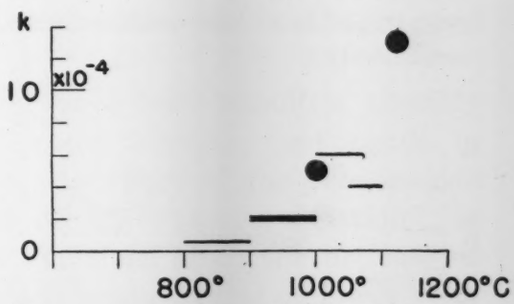

Fig. 5. k versus temperature.
Circles: obtained from Fig. 3.
Segments: obtained from Fig. 4.

stand right. The probable error of k is estimated at about 60% for the observed fluctuation in viscosity (20%).

A-2) Experiments under constant temperatures.

Specimens are heated in the same way as in 1), i.e. $T=\alpha t$, and then the temperature is kept constant at a definite temperature. In this case,

$$\frac{1}{\eta}=c(T)+I(T)\exp\left\{-\frac{1}{\alpha}\int_0^T k dT\right\}\exp\left(-k(T)t\right), \qquad (17)$$

in which t is the time elapsed at the constant temperature T. We can obtain k by this method too. If we could observe η for a long enough time, we would obtain $c(T)$ also.

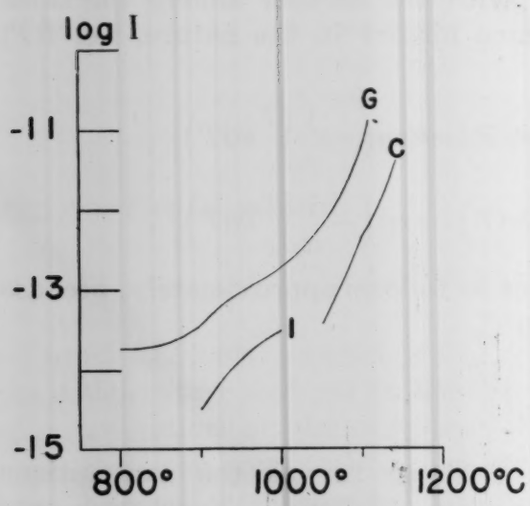

Fig. 6. I versus temperature.
(suffixes G, C and I are for glassy, crystalline and intermediate lavas respectively.)

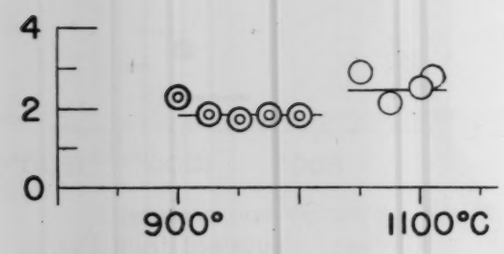

Fig. 7. ΔlnI.
Open circles: lnI_G-lnI_C,
Double circles: lnI_G-lnI_I.

As will be seen in Fig. 5, k is not remarkable at lower than 800°C, and it appears to increase at higher temperatures. The general tendency is common among the crystalline, intermediate and glassy lavas, even though there are some differences in details. Viscosity increases as much as ca. 2.7 times in $1/k$ seconds under constant temperature, so far as $c(T)$ is small. This is quite a remarkable fact.

(B) We can estimate $I(T)$ also by availing ourselves of k.

$I(T)$ includes the thermal history of the lava in the field, as well as the quantity and quality of the unstable non-crystalline phase. $I(T)$ shows the character of the relative change of viscosity with temperature. When we compare the $I(T)$s of the crystalline and the glassy one, we find that

$$ln\frac{I_G}{I_C}=ln\frac{b_{0G}}{b_{0C}}+\left\{-\int_{T_0}^{0}\frac{k'_G}{\dot{T}}dT+\int_{T_0}^{0}\frac{k'_C}{\dot{T}}dT\right\}. \qquad (18)$$

Fig. 7 shows that the logarithms of the ratio of I_G to other lavas are positive and nearly constant respectively. This fact is consistent with the prevailing idea that the glassy lava has cooled faster than the others. The rates of cooling cannot be estimated from the present data, because of the integrated form of the equation (18), even if we assume $k=k'_G=(k'_C)$ and $b_{0G}=b_{0C}$. But the obtained ratios are not unreasonable quantitatively.

(C) Let us consider the meaning of k and suppose the mode of change of viscosity with temperature and time, on the basis of the experiments. In the writer's opinion, the increase of k at high temperatures may imply mainly the increase of velocity of crystallization from the supercooled glass in the groundmass. The $k-T$ curve on Fig. 5 can be expressed approximately by the equation:

$$k=C\exp(-W/RT_K) \qquad (19)$$

where T_K is the absolute temperature, and the activation energy W is estimated at about 30 kcal/mol.

When we heat the specimens in the laboratory, velocity of crystallization of the supercooled part will get larger with rise of temperature, and a part of the supercooled glass is transformed into the crystalline phase. This increase of solid phase will surpass the decrease due to remelting of crystals, when the unstable part is predominant. This may be the main cause of the observed irreversibility in viscosity and elasticity. This progress of crystallization should be accompanied with separation and escape of volatile constituents too, as in the natural process of cooling.

Some of the crystals, which should have been remolten, possibly remain in the solid state in case of too rapid heating, and result in opposite change in viscosity. However, the effect of the phenomenon was found to be far less than the effect of the "recrystallization" in the present experiments. This may be explained from the increase of viscosity, instead of decrease, under constant temperatures at lower than 1130°C.

The state of matters in the interior of the specimens is, of course, not perfectly the same as that which occurred in its natural process of cooling. Crystallization in its natural state should have taken place in

the hydrothermal conditions. However, it was found that bubbles and fine vesicles grew up in the specimens during the present experiments too. This fact suggests that the lava still includes some volatile constituents. Consequently, it is not so unreasonable to infer that the changes in the properties of lavas in the laboratory are similar, at least qualitatively, to those in the natural cooling. We should be careful, of course, in extrapolating the present results to the phenomena in the nature.

(D) We have discussed hitherto the effects of crystallization upon viscosity. We must now try to infer the viscosity of lavas under natural conditions. If we assume that the equation (10) can be applied to nature and that $k=k'$, the necessary quantity to be determined further is the rate of cooling in the field.

T. Minakami[4] measured the flowing velocity, temperature and the dimension of one of the 1951 lava-flows of Oosima, and estimated its viscosity. He did not measure the cooling rate of lava, but it can be calculated from his published data. Because the quantity of the flowing mass (Q) through every cross-section of the flow is nearly constant, the flow can be duly regarded as steady. And we can put (cooling rate)=(space-gradient of T)$\times$(velocity of flow). Thus the rate of cooling was estimated as a function of temperature, within the range of 1125°–950°C. Then we can calculate $\exp\left(-\int_{950°}^{1125°}\frac{k}{\dot{T}}dT\right)$, but $\exp\left(-\int_{0}^{950°}\frac{k}{\dot{T}}dT\right)$ remains unknown and this should be treated as a constant term in the calculation. η is calculated by availing ourselves of the observed I_a and k. A glance at Fig. 8 will be sufficient to convince us that the gradients of

Table I.
Cooling rate of the lava in the field.

T (°C)	Distance (m)	Q (cc/sec)	$\dot{T}$ (°C/sec)
1125	140	3.5×10^{5}	-8.3×10^{-2}
1108	110	2.8	−5.7
1083	200	2.4	−2.6
1038	500	2.6	−1.4
(950)			

4) T. MINAKAMI, *Bull. Earthq. Res. Inst.*, **29** (1951), 427.
T. MINAKAMI and S. SAKUMA, *Bull. Volcanol.*, **14** (1953), 79.

the increase in viscosity with the decrease in temperature resemble each other satisfactorily, i.e. between the calculated and the observed ones.

Accordingly, we will be able to tell the viscosity of lavas in its natural molten state by k and I obtained in the laboratory, if we can assume their rates of cooling in the field, although it is not permitted without limit.

(E) There remains two essential problems to be solved. One is: what petrographical changes correspond to the changes in viscosity? The other is: in what manner does the viscous flow take place in the specimens?

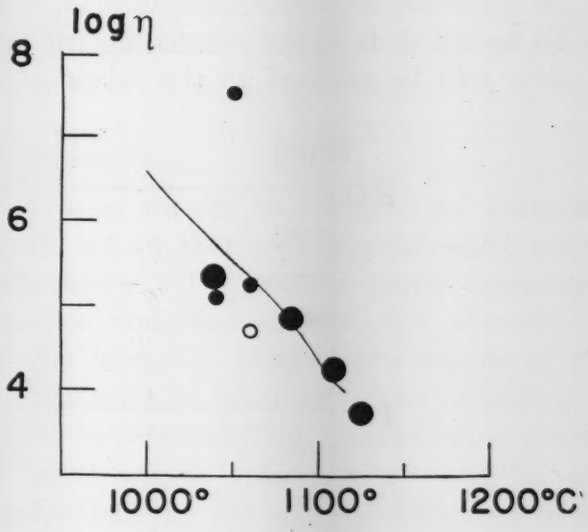

Fig. 8. Viscosity of Oosima-lava cooling in the field.

Line: calculated from $\dot{T}$ in Table I,
Circles: observed in the field,
(big closed ones: T. Minakami, small closed ones: S. Murauchi and A. Sugimura, open one: R. Takahasi and T. Nagata[5].)

The changes in viscosity, reversible or irreversible, must be accompanied by changes in the quantity of minerals and in the mode of aggregation of them. The difference between the crystalline and the glassy specimens are fairly distinct, as mentioned in the preceding paragraph. But petrographical change in the specimens by heating in the laboratory was found to be less distinct at least below 1130°C. Significant increase or decrease in the quantity of mineral grains could not be ascertained by microscopic studies, except increase of fine grains of magnetite in the glassy part. There is little ground at present to decide whether the physico-chemical process which produces magnetite as a result is the main cause of the observed change in viscosity, or not. More detailed and precise studies on the crystallinity and the mode of aggregation of constituent minerals under various conditions will be useful in this connection.

The origin of viscous flow in the mixture of crystals of various size and intercrystalline materials is also still vague at present. The recent progress in the physics of liquid state revealed that liquids can

5) R. TAKAHASI and T. NAGATA, *Bull. Earthq. Res. Inst.*, **15** (1937), 1047.

be regarded as aggregates of fine, unstable crystallites. This idea may be accepted as quite reasonable for lavas too. Accordingly, the viscous flow will be realized as the result of slips at boundaries of grains of

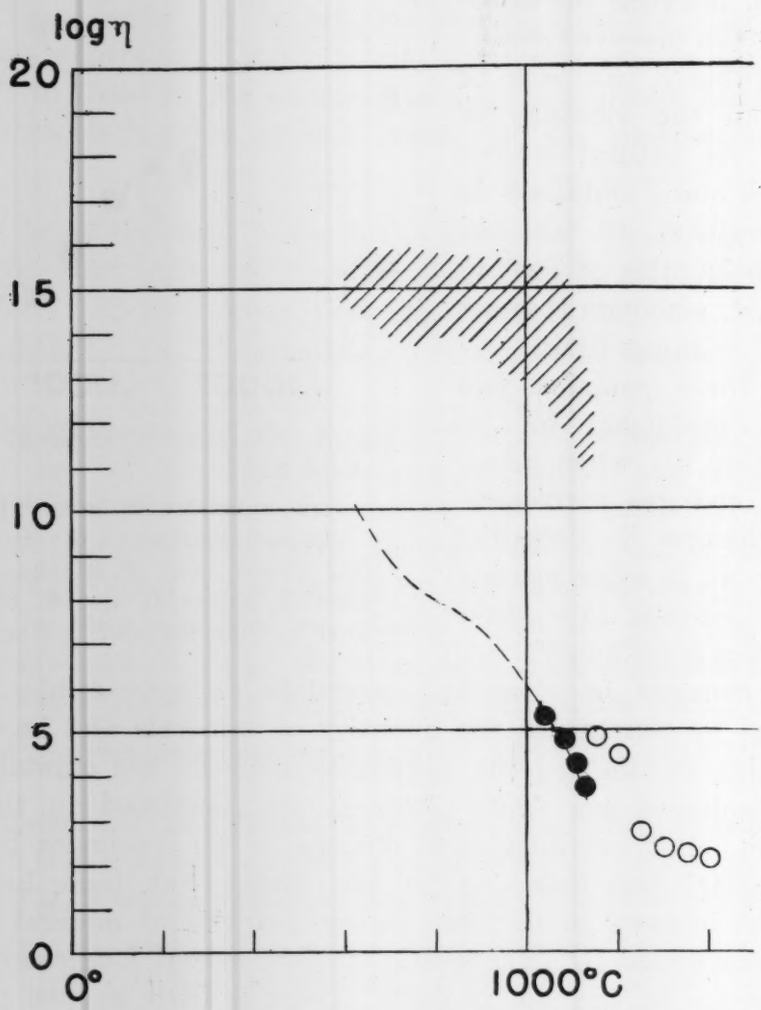

Fig. 9. Comparison of viscosity-coefficients obtained in the field and in the laboratory.
Hatched area: range of viscosity by the present experiment,
Open circles: K. Kani's experiment[6],
Closed circles: observed viscosity in the field (T. Minakami),
Broken line: calculated viscosity for an assumed cooling rate.

various sizes and forms macroscopically as well as microscopically. Those experimental studies will be of great use which deal with the

6) K. KANI, *Proc. Imp. Acad. Japan*, **10** (1934), 79.

apparent viscosity of the mixture of solid grains and viscous liquid, in order to clarify the functional relation of viscosity to the mode of aggregation of grains.

Conclusion.

The character of viscosity of lava should be realized as transient essentially. The lavas are always not in thermodynamical equilibrium, both in the field and in the laboratory. The present paper dealt with the specimens from Volcano Oosima, and showed that the viscosity is a function of the history of the lava, i.e. that of the degree of the development of crystallization. Viscosity of lavas of other volcanoes at the time of their ejection may also be inferred from similar experiments.

The variety in viscosity of lavas among volcanoes, or even in one volcano, might have been caused chiefly by the original difference in the chemical compositions among their magmas concerned.[7] But partly it must have been caused by the difference in their stage of development of crystallization at the time when the magmas obtained sufficient energy for them to struggle ahead to the earth's surface.

In concluding, the writer wishes to express his cordial thanks to Dr. T. Minakami, Dr. T. Nagata and Mr. J. Ossaka for the facilities and advices given to him.

16. 大島新熔岩の粘性の熱履歴について

地震研究所　佐久間修三

前報では熔岩試料の温度を徐々に階段的に変えて実験していた．しかしその実験により，熔岩の粘性には加熱により増加する傾向があることが判つたので，試料の加熱速度を系統的に変えて実験した．これによつ判明した粘性の熱履歴の性質は次の通りである．(第 2–3 図).

(1) 速かに高温に至らせれば粘性はより小となる．

(2) 試料が玻璃を多く含む程粘性は小さい．

(3) 一定温度下では粘性は時間と共に増す．

熔岩中にある過冷却非晶質部分が加熱により更に晶出することがこの熱履歴の主因であると考えると実験事実をよく説明出来る．この考えで実験結果を整理して，この再晶出の速度は温度が高いほ

7) T. MINAKAMI, *Bull. Volcanol.*, **10** (1950), 59.
T. MINAKAMI and S. SAKUMA, *loc. cit.*, 4).
M. P. VOLAROVIC and others, *Comp. Rend. Acad. Sci.*, No. 9 (1934), 561; **1** (1936), 321.

ど大きいことを示した.(第 5 図)

実験によつてこのような晶出に伴う粘性の変化の性質を知れば，その熔岩が自然で冷えて来た途中での粘性をも或程度推定出来る．但し冷却速度をも知らなければならない．大島熔岩流について計算した 1 例（第 8–9 図）を示す.

一言にしていえば，熔岩の粘性は温度のみの函数ではなく，本質的に過渡現象として考察されねばならない.

——所　　報——

◎談話会記事

第 307 回談話会（昭和 29 年 1 月 26 日）

1. Fourier 級数論における坪井の問題について　高橋健人
（佐藤所員紹介）
2. 弾性波の発生機構に関する実験（第 5 報補遺）　笠原慶一
3. 常時微動の測定（第 1 報）　金井清・田中貞二
4. 建物の固有周期を測定する計器の試作　田中貞二
5. 岩石物性研究用超音波装置の試作　下鶴大輔
6. 樽前山熔岩円頂丘の帯磁　佐久間修三
7. 大島新熔岩の粘性の熱履歴　佐久間修三

第 308 回談話会（昭和 29 年 2 月 23 日）

1. 建物の固有周期を測定する計器の試作　田中貞二
2. 三原山の地球磁気学的研究
第 5 報　地磁気三成分の再測結果　横山泉
3. 檜俣拱堰堤岩盤傾斜測定　岡本舜三・北川英夫
4. 液体固体の境の面の SV 波　松沢武雄

第 309 回談話会（昭和 29 年 3 月 23 日）

1. 東京，横浜における加速度地震計記象の解析結果（第 1 報補遺）　金井清・鈴木正治
2. 常時微動の測定（第 2 報）　金井清二・田中貞・長田甲斐男
3. 和歌山附近頻発地震群の観測（第 2 報）　宮村摂三・堀実・辻浦賢・松本英照
4. 大島新熔岩の粘性の熱履歴（続報）　佐久間修三
5. 融解点附近の弾性の研究
其の 1　弾性波の速度と振巾に就いて　下鶴大輔
6. 土地の脈動の観測方法について　岸上冬彦

第 310 回談話会（昭和 29 年 4 月 27 日）

1. 坪井・永田の方法について　佐藤泰夫
2. 道路における振動測定　岸上冬彦
3. ベヨネイヅ列岩の岩石　森本良平
4. 地殻の変動解析について　荒川秀俊
（河角所員紹介）
5. 藤原咲平博士遺稿，諏訪湖結氷期日及び御神渡期日表について　荒川秀俊
（河角所員紹介）

第 311 回談話会 (昭和 29 年 5 月 25 日)

1. 長周期地震波による地球内部構造の解析　　松　夫・三　松　三　悖
2. 震源決定の精度について (第 1 報)　　佐藤泰利
3. 和歌山市湯浅町間の水準再測量結果　　松本周一
4. 地震動による建物振動の観測結果 (第 3 報)　　浅野　清
5. 建物の振動減衰性について (第 2 報)　　岡田　清郎
　　金井富三
　　鈴木清

第 312 回談話会 (昭和 29 年 6 月 22 日)

1. 弾性波の発生機構に関する実験　第 6 報　　笠原慶一郎
2. マグネチツクテープを用いた地震動の常時観測　第 1 報　　表俊一郎・宮村摂三・山崎雄博・浅田敏
3. 地震の場の論—楕円形の場　　松沢武雄・長谷川忠望
4. 九州地方に於ける重力異常の分布　　坪井忠二・実川広幸・田島顕一・井上和子・関井忠
5. 日本に於ける重力異常の分布とその解釈　第 1 報　　坪井忠二

昭和29年7月30日印刷
昭和29年8月5日發行

東京都文京區本富士町一番地
東京大學構内
編纂兼發行者　東京大學地震研究所

東京都千代田區富士見町一丁目十番地
印刷者　笠井康賴

東京都千代田區富士見町一丁目十番地
印刷所　株式會社國際文献印刷社

賣捌所　東京都千代田區神田一ツ橋通
岩波書店

東京都中央區日本橋通二丁目六番地
丸善株式會社

Sold by
Iwanami Shoten,
Hitotsubashi dôri, Chiyoda-ku, Tôkyô,
and
Maruzen Co., Ltd.,
Nihonbashi dôri, Chûô-ku, Tôkyô.
Price of this copy: 283 Yen. (Postage exclusive.)

BULLETIN OF

THE EARTHQUAKE RESEARCH INSTITUTE

TOKYO UNIVERSITY

Vol. XXXII, Part 2. July, 1954.

Contents.

Papers and Reports.

Page

9. T. TAKAHASHI, A Problem on Fourier Series. (in English) 147
10. T. MATUZAWA, S-Wellen an der fest-flüssigen Schichtgrenze. II. (im Deutschen) 155
11. Y. SATÔ, Study on Surface Waves XI. Definition and Classification of Surface Waves. (in English) 161
12. I. YOKOYAMA, Geomagnetic Studies of Volcano Mihara. The 5th paper. (Changes in Three Geomagnetic Components during the Period from May 1951 to August 1953.) (in English) 169
13. K. KANAI and M. SUZUKI, Analytical Results of the Acceleration Seismograms obtained at Tokyo and Yokohama. (in English) 189
14. K. KANAI, T. TANAKA and K. OSADA, Measurement of the Micro-tremor. I. (in English) 199
15. K. KANAI, A Short Note on the Relation of Amplitude-Period of Earthquake Motion. (in English) 211
16. S. SAKUMA, Effect of Thermal History on Viscosity of Ooshima-lavas. (Elastic and Viscous Properties of Volcanic Rocks. Part 4.). (in English). 215

Institute Notes.

(For the papers written in Japanese or in occidental languages, the abstracts are given in occidental languages or in Japanese respectively.)

BULLETIN OF THE EARTHQUAKE RESEARCH INSTITUTE,
TOKYO UNIVERSITY. Vol. XXXII, Part 3. September, 1954.

東京大學
地震研究所彙報

第 32 號　第 3 册

昭和 29 年 9 月

目　次

論文及報告

			頁
17.	地震の場の論: 楕円形の場 (独文)	松沢武雄 長谷川博	231
18.	層のある地球の弾性振動 (第1種の振動の周期) (英文)	松本利松 佐藤泰夫	247
19.	坪井・永田の方法について (英文)	佐藤泰夫	259
20.	融解点附近の弾性の研究　其の一　縦波の性質 (英文)	下鶴大輔	271
21.	玄武洞周辺の磁気異常とその玄武岩の帯磁 (英文)	横山泉	281
22.	伊豆大島三原山昭和25年及26年の噴火　その2　昭和26年の噴火 (A) 第2期の活動 (英文)	津屋弘逵 森本良平 小坂丈予	289
23.	逆立振子型風力計による自然風の観測と解析 (英文)	西村源六郎 鈴木正治	313

(The titles in occidental languages are given on the back cover.)

本彙報ハ年4回 (但シ第1號ヨリ第6號マデハ不定期ニ，第7號ハ3冊トシテ發行セリ)，彙報別冊ハ不定期ニ發行ス．

本彙報掲載ノ論文及ビ報告ノ内容ニ關シテハ著者ノミニ其責任アルモノトス．

本彙報ニ關スル照會通信ハ東京大學地震研究所長ヘ宛テラレタシ．

The Bulletin is published quarterly. (Vols. I–VI were published at irregular intervals and Vol. VII consisted of three parts.)
Supplementary Volume is published at irregular interval.

The authors of the papers alone are responsible for the statements and opinions contained in their respective papers.

All communications relating to this Bulletin should be addressed to the Director of the Earthquake Research Institute, Tokyo University.

17. *Feldtheorie der Erdbeben: Elliptisches Quellengebiet.*

Von Takeo MATUZAWA und Hirosi HASEGAWA,

Geophysikalisches Institut.

(Vorgelegt den 22. Juni 1954.—Eingegangen den 28. Juni 1954.)

1. Spannung in einer elliptischen Platte, die am Rande befestigt ist und an einer Seite konstantem Druck unterliegt.

In der vorigen Mitteilung[1] untersuchten wir den Spannungszustand in einer Kreisplatte, die der oben gegebenen Bedingung genügt. Dort[2] wurde auch bemerkt, dass das Kreisplattenmodell grosse horizontale Verschiebung der Verwerfung nicht geben kann, aber elliptische oder rechteckige Quellengebiete beträchtliche horizontale Verschiebung geben können.

Hier wollen wir die Sache zahlenmässig beweisen. Die x and y Achsen werden in der Mittelfläche der Platte gelegt und die grosse Achse der Ellipse wird in der x Richtung genommen.

Die Dicke der Platte sei $2h$ und die Ellipse sei

$$\frac{x^2}{a^2}+\frac{y^2}{b^2}=1\,.$$

Die Randbedingungen sind

$$\left.\begin{aligned} &Z_z=X_z=Y_z=0\,, && \text{für} \quad z=-h\,,\\ &Z_z=-p\,,\ X_z=Y_z=0\,, && \text{für} \quad z=h\,, \end{aligned}\right\} \qquad (1)$$

$$u=v=w=0\,,\quad \frac{\partial w}{\partial \nu}=0\,,\quad \text{für}\quad z=0\quad \text{und}\quad \frac{x^2}{a^2}+\frac{y^2}{b^2}=1\,, \qquad (2)$$

wo ν nach aussen gerichteter Normalvektor ist.

Wir folgen hier auch der Love'schen Methode wie folgt.

Die Gleichungen des elastischen Gleichgewichtes sind wie gewöhnlich

$$\left.\begin{aligned} &\frac{\partial X_x}{\partial x}+\frac{\partial X_y}{\partial y}+\frac{\partial X_z}{\partial z}=0\,,\\ &\frac{\partial Y_x}{\partial x}+\frac{\partial Y_y}{\partial y}+\frac{\partial Y_z}{\partial z}=0\,,\\ &\frac{\partial Z_x}{\partial x}+\frac{\partial Z_y}{\partial y}+\frac{\partial Z_z}{\partial z}=0\,. \end{aligned}\right\} \qquad (3)$$

1) T. MATUZAWA, *Bull. Earthq. Res. Inst.*, **31** (1953), 189.
2) *ibid.*, 200.

Mit der Hilfe von den Gleichungen

$$\left.\begin{aligned} &X_x=\lambda\Delta+2\mu\frac{\partial u}{\partial x}\,, \qquad Y_y=\lambda\Delta+2\mu\frac{\partial v}{\partial y}\,, \qquad Z_z=\lambda\Delta+2\mu\frac{\partial w}{\partial z}\,,\\ &Y_z=\mu\Big(\frac{\partial w}{\partial y}+\frac{\partial v}{\partial z}\Big)\,, \qquad Z_x=\mu\Big(\frac{\partial u}{\partial z}+\frac{\partial w}{\partial x}\Big)\,, \qquad X_y=\mu\Big(\frac{\partial v}{\partial x}+\frac{\partial u}{\partial y}\Big)\,, \end{aligned}\right\} \tag{4}$$

wo

$$\Delta=\frac{\partial u}{\partial x}+\frac{\partial v}{\partial y}+\frac{\partial w}{\partial z}\,,$$

bekommen wir

$$\Theta=X_x+Y_y+Z_z=(3\lambda+2\mu)\Delta\,, \tag{5}$$

$$\nabla^2X_x=2\mu\nabla^2\frac{\partial u}{\partial x}=-2(\lambda+\mu)\frac{\partial^2\Delta}{\partial x^2}\,, \quad \text{u.s.w.} \tag{6}$$

Nämlich

$$\left.\begin{aligned} &\nabla^2X_x=-\frac{1}{1+\sigma}\frac{\partial^2\Theta}{\partial x^2}\,, \quad \nabla^2Y_y=-\frac{1}{1+\sigma}\frac{\partial^2\Theta}{\partial y^2}\,, \quad \nabla^2Z_z=-\frac{1}{1+\sigma}\frac{\partial^2\Theta}{\partial z^2}\,,\\ &\nabla^2Y_z=-\frac{1}{1+\sigma}\frac{\partial^2\Theta}{\partial y\partial z}\,, \quad \nabla^2X_z=-\frac{1}{1+\sigma}\frac{\partial^2\Theta}{\partial z\partial x}\,, \quad \nabla^2X_y=-\frac{1}{1+\sigma}\frac{\partial^2\Theta}{\partial x\partial y}\,, \end{aligned}\right\} \tag{7}$$

zusammen mit

$$\nabla^2\Delta=\nabla^2\Theta=0\,, \quad \text{und} \quad \frac{2(\lambda+\mu)}{3\lambda+2\mu}=\frac{1}{1+\sigma}\,,$$

wo σ die Poissonsche Konstante ist.

Also sehen wir ohne weiteres

$$\nabla^4Z_z=0\,. \tag{8}$$

Aus (1) und (3) haben wir

$$\left.\begin{aligned} &\frac{\partial Z_z}{\partial z}=0\,, \qquad Z_z=-p\,, \qquad \text{für} \quad z=h\,,\\ &\frac{\partial Z_z}{\partial z}=0\,, \qquad Z_z=0\,, \qquad \text{für} \quad z=-h\,. \end{aligned}\right\} \tag{9}$$

Eine Lösung von Z_z, die den Bedingungen (8) und (9) genügt, lautet,

$$Z_z=\frac{1}{4}h^{-3}p(z^3-3h^2z-2h^3)\,.$$

Daher aus (7) bekommt man,

$$\frac{\partial^2\Theta}{\partial z^2}=-\frac{3}{2}(1+\sigma)h^{-3}pz\,.$$

Mit $\nabla^2\Theta=0$, können wir setzen

$$\Theta=-\frac{1}{4}(1+\sigma)h^{-3}pz^3+\frac{3}{4}(1+\sigma)h^{-3}pz\left(\frac{\alpha^2\beta^2}{\alpha^2+\beta^2}\right)\left(\frac{x^2}{\alpha^2}+\frac{y^2}{\beta^2}\right), \quad (10)$$

wo α und β Parameter sind, die nachher bestimmt werden.

Um X_z und Y_z zu bestimmen, aus (3) und (7) mit (10), haben wir

$$\frac{\partial X_z}{\partial x}+\frac{\partial Y_z}{\partial y}+\frac{3p}{4h}(z^2-h^2)=0\,,$$

$$\nabla^2X_z=-\frac{3}{2}h^{-3}p\frac{\beta^2}{\alpha^2+\beta^2}x\,,$$

$$\nabla^2Y_z=-\frac{3}{2}h^{-3}p\frac{\alpha^2}{\alpha^2+\beta^2}y\,.$$

Die den Randbedingungen $X_z=Y_z=0$ für $z=\pm h$ genügenden Lösungen sind

$$\left.\begin{aligned}X_z&=\frac{3}{4}h^{-3}p\frac{\beta^2}{\alpha^2+\beta^2}(h^2-z^2)x\,,\\ Y_z&=\frac{3}{4}h^{-3}p\frac{\alpha^2}{\alpha^2+\beta^2}(h^2-z^2)y\,.\end{aligned}\right\} \quad (11)$$

Daher aus (3)

$$\left.\begin{aligned}\frac{\partial X_x}{\partial x}+\frac{\partial X_y}{\partial y}&=\frac{3}{2}h^{-3}p\frac{\beta^2}{\alpha^2+\beta^2}xz\,,\\ \frac{\partial X_y}{\partial x}+\frac{\partial Y_y}{\partial y}&=\frac{3}{2}h^{-3}p\frac{\alpha^2}{\alpha^2+\beta^2}yz\,.\end{aligned}\right\} \quad (12)$$

Aus (7)

$$\left.\begin{aligned}\nabla^2X_x&=-\frac{3}{2}h^{-3}pz\frac{\beta^2}{\alpha^2+\beta^2}\,,\\ \nabla^2Y_y&=-\frac{3}{2}h^{-3}pz\frac{\alpha^2}{\alpha^2+\beta^2}\,,\\ \nabla^2X_y&=0\,.\end{aligned}\right\} \quad (13)$$

Aus (5) und (10)

$$X_x+Y_y=\Theta-Z_z$$
$$=-\frac{1}{4}(2+\sigma)h^{-3}pz^3+\frac{3}{4}h^{-1}pz+\frac{2}{4}p+\frac{3}{4}(1+\sigma)h^{-3}pz\left(\frac{\alpha^2\beta^2}{\alpha^2+\beta^2}\right)\left(\frac{x^2}{\alpha^2}+\frac{y^2}{\beta^2}\right). \quad (14)$$

Man führe eine Funktion χ ein, so dass

$$\left.\begin{aligned} X_x &= \frac{3}{2}h^{-3}pz\left(\frac{\alpha\beta^2}{\alpha^2+\beta^2}\right)^2\left(\frac{x^2}{\alpha^2}+\frac{y^2}{\beta^2}\right)+\frac{\partial^2\chi}{\partial y^2}, \\ Y_y &= \frac{3}{2}h^{-3}pz\left(\frac{\alpha^2\beta}{\alpha^2+\beta^2}\right)^2\left(\frac{x^2}{\alpha^2}+\frac{y^2}{\beta^2}\right)+\frac{\partial^2\chi}{\partial x^2}, \\ X_y &= -\frac{\partial^2\chi}{\partial x\partial y}, \end{aligned}\right\} \tag{15}$$

wo

$$\frac{\partial^2\chi}{\partial x^2}+\frac{\partial^2\chi}{\partial y^2} = -\frac{1}{4}(2+\sigma)h^{-3}pz^3+\frac{3}{4}h^{-1}pz + \frac{1}{2}p+\frac{3}{4}(-1+\sigma)h^{-3}pz\left(\frac{\alpha^2\beta^2}{\alpha^2+\beta^2}\right)\left(\frac{x^2}{\alpha^2}+\frac{y^2}{\beta^2}\right).$$

(13) und (15) geben uns

$$\left.\begin{aligned} \frac{\partial^2}{\partial x^2}(\nabla^2\chi) &= -\frac{9}{2}h^{-3}pz\frac{\alpha^2}{\alpha^2+\beta^2}, \\ \frac{\partial^2}{\partial y^2}(\nabla^2\chi) &= -\frac{9}{2}h^{-3}pz\frac{\beta^2}{\alpha^2+\beta^2}, \\ \frac{\partial^2}{\partial x\partial y}(\nabla^2\chi) &= 0. \end{aligned}\right\} \tag{16}$$

Daher sehen wir, dass die folgende Gleichung

$$\nabla^2\chi+\frac{9}{4}h^{-3}pz\left(\frac{\alpha^2\beta^2}{\alpha^2+\beta^2}\right)\left(\frac{x^2}{\alpha^2}+\frac{y^2}{\beta^2}\right)$$

lineär von x und y sein muss.

Als die Lösung bekommt man

$$\chi = \frac{2+\sigma}{8}\frac{pz^3}{h^3}\left\{\frac{z^2}{10}-\frac{\alpha^2\beta^2}{\alpha^2+\beta^2}\left(\frac{x^2}{\alpha^2}+\frac{y^2}{\beta^2}\right)\right\}-\frac{1}{8}\frac{pz^3}{h}-\frac{1}{4}pz^2+z\chi_1''+\chi_0'',$$

mit

$$\chi_1'' = -\frac{3}{4}(1-\sigma)\frac{p}{h^3}\frac{\alpha^2\beta^2}{\alpha^2+\beta^2}\left(\frac{x^2}{a^2}+\frac{y^2}{b^2}\right)^2+\frac{3p}{8h}\frac{\alpha^2\beta^2}{\alpha^2+\beta^2}\left(\frac{x^2}{\alpha^2}+\frac{y^2}{\beta^2}\right),$$

und

$$\chi_0'' = \frac{1}{4}p\frac{\alpha^2\beta^2}{\alpha^2+\beta^2}\left(\frac{x^2}{\alpha^2}+\frac{y^2}{\beta^2}\right),$$

mit den Bedingungen

$$\left.\begin{aligned} \frac{3}{a^4}+\frac{1}{a^2b^2}&=\frac{1}{4\alpha^2}\,,\\ \frac{3}{b^4}+\frac{1}{a^2b^2}&=\frac{1}{4\beta^2}\,. \end{aligned}\right\} \tag{17}$$

Man bekommt also,

$$\left.\begin{aligned} X_x&=\frac{3}{2}\,h^{-3}pz\Big(\frac{\alpha\beta^2}{\alpha^2+\beta^2}\Big)^2\Big(\frac{x^2}{\alpha^2}+\frac{y^2}{\beta^2}\Big)-\frac{2+\sigma}{4}\,\frac{pz^3}{h^3}\,\frac{\alpha^2}{\alpha^2+\beta^2}\\ &\quad -3(1-\sigma)\frac{pz}{h^3b^2}\,\frac{\alpha^2\beta^2}{\alpha^2+\beta^2}\Big(\frac{x^2}{a^2}+3\frac{y^2}{b^2}\Big)+\frac{\alpha^2}{\alpha^2+\beta^2}\,p\Big(\frac{3}{4}\,\frac{z}{h}+\frac{1}{2}\Big)\,,\\ Y_y&=\frac{3}{2}\,h^{-3}pz\Big(\frac{\alpha^2\beta}{\alpha^2+\beta^2}\Big)^2\Big(\frac{x^2}{\alpha^2}+\frac{y^2}{\beta^2}\Big)-\frac{2+\sigma}{4}\,\frac{pz^3}{h^3}\,\frac{\beta^2}{\alpha^2+\beta^2}\\ &\quad -3(1-\sigma)\frac{pz}{h^3a^2}\,\frac{\alpha^2\beta^2}{\alpha^2+\beta^2}\Big(3\frac{x^2}{a^2}+\frac{y^2}{b^2}\Big)+\frac{\beta^2}{\alpha^2+\beta^2}\,p\Big(\frac{3}{4}\,\frac{z}{h}+\frac{1}{2}\Big)\,,\\ X_y&=6(1-\sigma)\frac{pz}{h^3}\,\frac{\alpha^2\beta^2}{\alpha^2+\beta^2}\,\frac{xy}{a^2b^2}\,. \end{aligned}\right\} \tag{18}$$

Die entsprechenden Komponenten u, v, und w der Verschiebung werden wie folgt gegeben.

Aus

$$\frac{\partial u}{\partial x}=\frac{1}{E}\{X_x-\sigma(Y_y+Z_z)\}\,,\qquad \text{u.s.w.,}$$

$$\frac{\partial w}{\partial y}+\frac{\partial v}{\partial z}=2\frac{(1+\sigma)}{E}\,Y_z\,,\qquad \text{u.s.w.,}$$

bekommt man

$$\left.\begin{aligned} u&=-\frac{1+\sigma}{E}\,\frac{px}{4h^3}\,\frac{1}{\alpha^2+\beta^2}\{(2\alpha^2-\sigma\beta^2)z^3-3\alpha^2h^2z-2\alpha^2h^3\}\\ &\quad+\frac{3}{2}\,\frac{pzx}{Eh^3}\,\frac{\alpha^2\beta^2}{\alpha^2+\beta^2}\Big[\frac{1}{\alpha^2+\beta^2}\Big(\frac{x^2}{3\alpha^2}+\frac{y^2}{\beta^2}\Big)(\beta^2-\sigma\alpha^2)-2(1-\sigma)\\ &\quad\times\Big\{\frac{1}{b^2}\Big(\frac{x^2}{3a^2}+3\frac{y^2}{b^2}\Big)-\frac{\sigma}{a^2}\Big(\frac{x^2}{a^2}+\frac{y^2}{b^2}\Big)\Big\}\Big]\,,\\ v&=-\frac{1+\sigma}{E}\,\frac{py}{4h^3}\,\frac{1}{\alpha^2+\beta^2}\{(2\beta^2-\sigma\alpha^2)z^3-3\beta^2h^2z-2\beta^2h^3\}\\ &\quad+\frac{3}{2}\,\frac{pzy}{Eh^3}\,\frac{\alpha^2\beta^2}{\alpha^2+\beta^2}\Big[\frac{1}{\alpha^2+\beta^2}\Big(\frac{x^2}{\alpha^2}+\frac{y^2}{3\beta^2}\Big)(\alpha^2-\sigma\beta^2)-2(1-\sigma) \end{aligned}\right\}$$

$$\times\left\{\frac{1}{a^2}\left(\frac{y^2}{3b^2}+3\frac{x^2}{a^2}\right)-\frac{\sigma}{b^2}\left(\frac{x^2}{a^2}+\frac{y^2}{b^2}\right)\right\}\Big],$$

$$w=\frac{1+\sigma}{E}\frac{p}{16h^3}\Big[(1+\sigma)z^4-6h^2z^2-8h^3z+6\frac{\alpha^2\beta^2}{\alpha^2+\beta^2}(h^2-\sigma z^2)\left(\frac{x^2}{\alpha^2}+\frac{y^2}{\beta^2}\right)$$

$$-12(1-\sigma)\frac{\alpha^2\beta^2}{\alpha^2+\beta^2}\left(\frac{x^2}{a^2}+\frac{y^2}{b^2}\right)^2\Big]. \qquad (19)$$

An der Zentralebene, nämlich für $z=0$, haben wir

$$W=-\frac{1}{4}\frac{p}{D}\frac{\alpha^2\beta^2}{\alpha^2+\beta^2}\left\{2\left(\frac{x^2}{a^2}+\frac{y^2}{b^2}\right)^2-\frac{h^2}{1-\sigma}\left(\frac{x^2}{\alpha^2}+\frac{y^2}{\beta^2}\right)\right\},$$

$$\left(\frac{\partial^4}{\partial x^4}+2\frac{\partial^4}{\partial x^2\partial y^2}+\frac{\partial^4}{\partial y^4}\right)W=-\frac{p}{D},$$

wo

$$D=\frac{2}{3}\frac{Eh^3}{1-\sigma^2}.$$

Die bisherigen Lösungen genügen den Bedingungen an beiden Seiten der Platte aber nicht am Rande der Platte. Dafür müssen wir geeigneten Druck und Drehmoment an den Rand hizufügen.

Erstens wollen wir die Zusatzlösung für $u=0$, $v=0$ an $z=0$ finden. Dafür muss man geeigneten Druck an den Rand ausüben. Dann ist der Spannungszustand in der Platte zweidimensional.

Nämlich

$$X'_z=Y'_z=Z'_z=0.$$

Aus (7)

$$\frac{\partial\Theta'}{\partial z}=\kappa \quad \text{(konst.)}$$

Also

$$\Theta'=\Theta'_0+\kappa z, \qquad (20)$$

wo Θ'_0 eine Funktion von x und y allein ist.

Daher

$$\frac{\partial^2\Theta'_0}{\partial x^2}+\frac{\partial^2\Theta'_0}{\partial y^2}=0. \qquad (21)$$

X'_x, Y'_y und X'_y werden von Spannungsfunktion $\chi(x,y,z)$ abgeleitet.

Weil $\left(\frac{\partial^4}{\partial x^4}+2\frac{\partial^4}{\partial x^2\partial y^2}+\frac{\partial^4}{\partial y^4}\right)\chi=0$ ist, ist $\left(\frac{\partial^2}{\partial x^2}+\frac{\partial^2}{\partial y^2}\right)\chi=\Theta_0'+\kappa z$.

Aus (7), (20) und (21) haben wir

$$\left.\begin{aligned}
&\frac{\partial^2}{\partial y^2}\left(\frac{\partial^2\chi}{\partial z^2}+\frac{\sigma}{1+\sigma}\Theta_0'\right)=0\,,\\
&\frac{\partial^2}{\partial x^2}\left(\frac{\partial^2\chi}{\partial z^2}+\frac{\sigma}{1+\sigma}\Theta_0'\right)=0\,,\\
&\frac{\partial^2}{\partial x\partial y}\left(\frac{\partial^2\chi}{\partial z^2}+\frac{\sigma}{1+\sigma}\Theta_0'\right)=0\,.
\end{aligned}\right\} \tag{22}$$

Daher ist der Klammerausdruck in (22) eine lineäre Funktion von x und y. Wir können sie null setzen, ohne Einfluss auf Ableitung von X_x', Y_y' und X_y' auszuüben.

Darum

$$\chi=\chi_0+\chi_1 z-\frac{1}{2}\frac{\sigma}{1+\sigma}\Theta_0' z^2\,, \tag{23}$$

wo

$$\left(\frac{\partial^2}{\partial x^2}+\frac{\partial^2}{\partial y^2}\right)\chi=\Theta_0'\,,\qquad \left(\frac{\partial^2}{\partial x^2}+\frac{\partial^2}{\partial y^2}\right)\chi_1=\kappa\,.$$

Wenn man Θ_0', χ_0 und χ_1 so wählen, dass

$$\Theta_0'=-\frac{1}{2}\frac{1+\sigma}{1-\sigma}p\,,$$

$$\chi_0=-\frac{1}{4}\frac{p}{1-\sigma}\frac{1}{\alpha^2+\beta^2}\{(\sigma\alpha^2+\beta^2)x^2+(\alpha^2+\sigma\beta^2)y^2\}\,,$$

und

$$\chi_1=0\,,$$

dann

$$\left.\begin{aligned}
&X_x'=\frac{\partial^2\chi}{\partial y^2}=-\frac{1}{2}\frac{p}{1-\sigma}\frac{\alpha^2+\sigma\beta^2}{\alpha^2+\beta^2}\,,\\
&Y_y'=\frac{\partial^2\chi}{\partial x^2}=-\frac{1}{2}\frac{p}{1-\sigma}\frac{\sigma\alpha^2+\beta^2}{\alpha^2+\beta^2}\,,\\
&X_y'=-\frac{\partial^2\chi}{\partial x\partial y}=0\,.
\end{aligned}\right\} \tag{24}$$

$$\left.\begin{aligned}
&u'=\frac{1}{E}\left\{\Theta_0'x-(1+\sigma)\frac{\partial\chi_0}{\partial x}+\frac{1}{2}(1+\sigma)p\frac{\alpha^2}{\alpha^2+\beta^2}x\right\}=-\frac{1}{2}\frac{1+\sigma}{E}p\frac{\alpha^2}{\alpha^2+\beta^2}x\,,\\
&v'=\frac{1}{E}\left\{\Theta_0'y-(1+\sigma)\frac{\partial\chi_0}{\partial y}+\frac{1}{2}(1+\sigma)p\frac{\beta^2}{\alpha^2+\beta^2}y\right\}=-\frac{1}{2}\frac{1+\sigma}{E}p\frac{\beta^2}{\alpha^2+\beta^2}y\,,\\
&w'=\frac{p\sigma}{2E}\frac{1+\sigma}{1-\sigma}pz\,.
\end{aligned}\right\} \tag{25}$$

Wenn man diese Lösung hinzufügt, dann bekommt man

$$u=0\,, \qquad v=0\,, \qquad \text{für} \qquad z=0\,.$$

Zweitens wollen wir die Zusatzlösung finden, so dass

$$w=0\,, \qquad \frac{\partial w}{\partial \nu}=0\,, \qquad \text{für} \qquad z=0 \qquad \text{und} \qquad \frac{x^2}{a^2}+\frac{y^2}{b^2}=1\,.$$

Um diese Bedingung zu erfüllen, muss man geeigneten Drehmoment an den Rand ausüben, so dass die Mittelfläche die folgende Form nimmt, nämlich

$$W=C\left(\frac{x^2}{a^2}+\frac{y^2}{b^2}-1\right)^2\,.$$

In diesem Falle können X_z'' und Y_z'' nicht null sein, aber $X_z''=Y_z''=Z_z''=0$ für $z=\pm h$. Z_z'' muss überall gleich null sein, weil

$$\nabla^1 Z_z''=0 \qquad \text{und} \qquad \frac{\partial Z_z''}{\partial z}=0 \qquad \text{an} \qquad z=\pm h\,,$$

was aus (9) ganz klar ist.

Aus

$$\nabla^2\Theta=0 \qquad \text{und} \qquad \nabla^2 Z_z''=-(1+\sigma)^{-1}\frac{\partial^2\Theta}{\partial z^2}\,,$$

hat Θ eine Form wie $\Theta_0''+z\Theta_1''$, wo Θ_0'' und Θ_1'' harmonische Funktion von x und y sind.

Was Θ_0'' betrifft, wird es in Θ_0' eingeschlossen.

Aus (7) und

$$X_z''=Y_z''=0 \text{ an } z=\pm h\,,$$

bekommen wir

$$X_z''=\frac{1}{2}\frac{1}{1+\sigma}(h^2-z^2)\frac{\partial\Theta_1''}{\partial x}\,,$$

$$Y_z''=\frac{1}{2}\frac{1}{1+\sigma}(h^2-z^2)\frac{\partial\Theta_1''}{\partial y}\,.$$

(3) und (7) geben uns

$$\frac{\partial X_x''}{\partial x}+\frac{\partial X_y''}{\partial y}-\frac{z}{1+\sigma}\frac{\partial\Theta_1''}{\partial x}=0\,, \qquad \frac{\partial X_y''}{\partial x}+\frac{\partial Y_y''}{\partial y}-\frac{z}{1+\sigma}\frac{\partial\Theta_1''}{\partial y}=0\,,$$

$$\nabla^2 X_x''+\frac{z}{1+\sigma}\frac{\partial^2\Theta_1''}{\partial x^2}=0\,, \qquad \nabla^2 Y_y''+\frac{z}{1+\sigma}\frac{\partial^2\Theta_1''}{\partial y^2}=0\,,$$

$$\nabla^2 X''_y + \frac{z}{1+\sigma}\frac{\partial^2 \Theta''_1}{\partial x \partial y} = 0 , \qquad X''_x + Y''_y = z\Theta''_1 .$$

Daraus bekommt man

$$\left.\begin{aligned} X''_x &= \frac{z}{1+\sigma}\Theta''_1 + \frac{\partial^2 \chi''}{\partial y^2} , \qquad Y''_y = \frac{z}{1+\sigma}\Theta''_1 + \frac{\partial^2 \chi''}{\partial x^2} , \\ X''_y &= -\frac{\partial^2 \chi''}{\partial x \partial y} , \end{aligned}\right\} \tag{26}$$

wo

$$\nabla^2 \chi'' = -\frac{1-\sigma}{1+\sigma} z\Theta''_1 .$$

Auch aus

$$\frac{\partial^2}{\partial y^2}\left(\frac{\partial^2 \chi''}{\partial z^2} - \frac{2-\sigma}{1+\sigma} z\Theta''_1\right) = 0 , \qquad \frac{\partial^2}{\partial x^2}\left(\frac{\partial^2 \chi''}{\partial z^2} - \frac{2-\sigma}{1+\sigma} z\Theta''_1\right) = 0 ,$$

$$\frac{\partial^2}{\partial x \partial y}\left(\frac{\partial^2 \chi''}{\partial z^2} - \frac{2-\sigma}{1+\sigma} z\Theta''_1\right) = 0 ,$$

ergibt sich, dass der Klammerausdruck lineär von x und y sein muss, was man gleich null setzen kann, weil das keinen Einfluss auf Spannungskomponente hat.

Daher

$$\chi'' = z\chi''_1 + \frac{2-\sigma}{6(1+\sigma)} z^3 \Theta''_1 ,$$

wo

$$\left(\frac{\partial^2}{\partial x^2} + \frac{\partial^2}{\partial y^2}\right)\chi''_1 = -\frac{1-\sigma}{1+\sigma}\Theta''_1 .$$

Also

$$\left.\begin{aligned} u'' &= -\frac{1}{E}\left[(1+\sigma) 2\frac{\partial \chi''_1}{\partial x} + \frac{1}{6}(2-\sigma) z^3 \frac{\partial \Theta''_1}{\partial x}\right] , \\ v'' &= -\frac{1}{E}\left[(1+\sigma) 2\frac{\partial \chi''_1}{\partial y} + \frac{1}{6}(2-\sigma) z^3 \frac{\partial \Theta''_1}{\partial y}\right] , \\ w'' &= \frac{1}{E}\left[(1+\sigma)\chi''_1 + \left(h^2 - \frac{1}{2}\sigma z^2\right)\Theta''_1\right] . \end{aligned}\right\} \tag{27}$$

Zusammenfassend bekommen wir die vertikale Verschiebung der Mittelfläche $W = (w + w' + w'')_{z=0}$ wie folgt.

$$W=\frac{1}{E}\{(1+\sigma)\chi_1''+h^2\Theta_1''\}-\frac{1}{4}\frac{p}{D}\frac{\alpha^2\beta^2}{\alpha^2+\beta^2}\left\{2\left(\frac{x^2}{a^2}+\frac{y^2}{b^2}\right)^2-\frac{h^2}{1-\sigma}\left(\frac{x^2}{\alpha^2}+\frac{y^2}{\beta^2}\right)\right\}. \tag{28}$$

Am Rande der Ellipse, nämlich, an $\frac{x^2}{a^2}+\frac{y^2}{b^2}=1$ müssen $W=0$ und $\frac{\partial W}{\partial \nu}=0$ sein.

Nämlich

$$(1+\sigma)\chi_1''+h^2\Theta_1''-\frac{1}{4}\frac{pE}{D}\frac{\alpha^2\beta^2}{\alpha^2+\beta^2}\left\{2-\frac{h^2}{1-\sigma}\left(\frac{x^2}{\alpha^2}+\frac{y^2}{\beta^2}\right)\right\}=0,$$

und

$$\left(\frac{x}{a^2}\frac{\partial}{\partial x}+\frac{y}{b^2}\frac{\partial}{\partial y}\right)\{(1+\sigma)\chi_1''+h^2\Theta_1''\}-8\frac{pE}{D}\frac{\alpha^2\beta^2}{\alpha^2+\beta^2}\left\{\frac{1}{a^4}\left(1-\frac{3h^2}{1-\sigma}\frac{1}{a^2}\right)x^2+\frac{1}{b^4}\left(1-\frac{3h^2}{1-\sigma}\frac{1}{b^2}\right)y^2-\frac{h^2}{4(1-\sigma)}\frac{1}{a^2b^2}\right\}=0.$$

Daraus bekommt man

$$\chi_1''=\frac{E}{1+\sigma}\frac{p}{D}\frac{\alpha^2\beta^2}{\alpha^2+\beta^2}\left[\frac{x^2}{a^2}+\frac{y^2}{b^2}-\frac{h^2}{4(1-\sigma)}\left(\frac{x^2}{\alpha^2}+\frac{y^2}{\beta^2}\right)+\frac{2h^2}{1-\sigma}\left\{\frac{1}{a^2}+\frac{1}{b^2}-\frac{h^2}{4(1-\sigma)}\left(\frac{1}{\alpha^2}+\frac{1}{\beta^2}\right)\right\}-\frac{1}{2}\right],$$

$$\Theta_1''=-\frac{2E}{1-\sigma}\frac{p}{D}\frac{\alpha^2\beta^2}{\alpha^2+\beta^2}\left\{\frac{1}{a^2}+\frac{1}{b^2}-\frac{h^2}{4(1-\sigma)}\left(\frac{1}{\alpha^2}+\frac{1}{\beta^2}\right)\right\}.$$

Wenn man diese Ausdrücke in (26), (27) und (28) einsetzt, dann

$$W=-\frac{1}{2}\frac{p}{D}\frac{\alpha^2\beta^2}{\alpha^2+\beta^2}\left(\frac{x^2}{a^2}+\frac{y^2}{b^2}-1\right)^2, \tag{29}$$

$$\left.\begin{aligned}
u''&=-\frac{2p}{D}\frac{\alpha^2\beta^2}{\alpha^2+\beta^2}\left(\frac{1}{a^2}-\frac{h^2}{4(1-\sigma)}\frac{1}{\alpha^2}\right)zx,\\
v''&=-\frac{2p}{D}\frac{\alpha^2\beta^2}{\alpha^2+\beta^2}\left(\frac{1}{b^2}-\frac{h^2}{4(1-\sigma)}\frac{1}{\beta^2}\right)zy,\\
w''&=\frac{p}{D}\frac{\alpha^2\beta^2}{\alpha^2+\beta^2}\left[\frac{x^2}{a^2}+\frac{y^2}{b^2}-\frac{h^2}{4(1-\sigma)}\left(\frac{x^2}{\alpha^2}+\frac{y^2}{\beta^2}\right)-\frac{1}{2}\right]\\
&\quad+\frac{\sigma}{1-\sigma}\frac{p}{D}\frac{\alpha^2\beta^2}{\alpha^2+\beta^2}z^2\left\{\frac{1}{a^2}+\frac{1}{b^2}-\frac{h^2}{4(1-\sigma)}\left(\frac{1}{\alpha^2}+\frac{1}{\beta^2}\right)\right\}.
\end{aligned}\right\} \tag{30}$$

$$\left.\begin{aligned} X''_x &= -\frac{2E}{1-\sigma^2}\frac{p}{D}\frac{\alpha^2\beta^2}{\alpha^2+\beta^2}z\left[\frac{1}{a^2}+\frac{\sigma}{b^2}-\frac{h^2}{4(1-\sigma)}\left(\frac{1}{\alpha^2}+\frac{\sigma}{\beta^2}\right)\right], \\ Y''_y &= -\frac{2E}{1-\sigma^2}\frac{p}{D}\frac{\alpha^2\beta^2}{\alpha^2+\beta^2}z\left[\frac{\sigma}{a^2}+\frac{1}{b^2}-\frac{h^2}{4(1-\sigma)}\left(\frac{\sigma}{\alpha^2}+\frac{1}{\beta^2}\right)\right], \\ X''_y &= 0\,, \qquad X''_z = Y''_z = Z''_z = 0\,. \end{aligned}\right\} \tag{31}$$

Alles zusammenfassend bekommen wir die endliche Lösung des Problems, nämlich, $u+u'+u''$, $v+v'+v''$, $w+w'+w''$, $X_x+X'_x+X''_x$, $Y_y+Y'_y+Y''_y$, Z_z, X_y, Y_z und Z_x.

Wir enthalten uns des Niederschreibens im Ganzen.

2. Horizontale Schubspannung an der Oberfläche.

Die Spannung $X'_{y'}$ in der vertikalen Ebene mit Richtungskosinussen $l=\cos\theta$, $m=\sin\theta$ und $n=0$ ergibt sich

$$X'_{y'}=\tfrac{1}{2}(Y_y-X_x)\sin 2\theta+X_y\cos 2\theta\,.$$

Die Richtung der maximalen Schubspannung wird gegeben durch

$$\tan 2\theta=\frac{Y_y-X_x}{2X_y}\,,$$

und die entsprechende maximale Schubspannung τ_m ist

$$\tau_m=\tfrac{1}{2}\sqrt{(Y_y-X_x)^2+4X_y^2}\,,$$

Nun

$$\begin{aligned} Y_y-X_x &= \frac{3}{h^3}\frac{\alpha^2\beta^2}{\alpha^2+\beta^2}pz\Big[(1-\sigma)\left\{\left(\frac{1}{b^2}-\frac{3}{a^2}\right)\frac{x^2}{a^2}+\left(\frac{3}{b^2}-\frac{1}{a^2}\right)\frac{y^2}{b^2}\right\} \\ &\quad +\frac{1}{2}\frac{\alpha^2-\beta^2}{\alpha^2+\beta^2}\left(\frac{x^2}{\alpha^2}+\frac{y^2}{\beta^2}\right)+(1-\sigma)\left(\frac{1}{a^2}-\frac{1}{b^2}\right)+\frac{2+\sigma}{12}\frac{\alpha^2-\beta^2}{\alpha^2\beta^2}z^2\Big], \\ X_y &= 6(1-\sigma)\frac{pz}{h^3}\frac{\alpha^2\beta^2}{\alpha^2+\beta^2}\frac{xy}{a^2b^2}\,. \end{aligned}$$

Beim Kreisplattenmodell ist $\alpha=\beta$ und $a=b$.

Mit der Hilfe von (17) können wir diese Ausdrücke wie folgt umschreiben.

$$Y_y-Y_x=\frac{3}{h^3}\frac{pzab}{4\left\{3\left(\frac{b^2}{a^2}+\frac{a^2}{b^2}\right)+2\right\}}\left[(1-\sigma)\left\{\left(\frac{a}{b}-\frac{3b}{a}\right)\frac{x^2}{a^2}+\left(\frac{3a}{b}-\frac{b}{a}\right)\frac{y^2}{b^2}\right\}\right.$$

$$+\frac{1}{2}\frac{3\left(\frac{a^2}{b^2}-\frac{b^2}{a^2}\right)}{3\left(\frac{b^2}{a^2}+\frac{a^2}{b^2}\right)+2}\left\{4\left(\frac{3b}{a}+\frac{a}{b}\right)\frac{x^2}{a^2}+4\left(\frac{3a}{b}+\frac{b}{a}\right)\frac{y^2}{b^2}\right\}$$

$$+(1-\sigma)\left(\frac{b}{a}-\frac{a}{b}\right)+(2+\sigma)\left(\frac{a}{b^3}-\frac{b}{a^3}\right)z^2\Big],$$

$$X_y=6(1-\sigma)\frac{pzxy}{h^3}\frac{1}{4\left\{3\left(\frac{b^2}{a^2}+\frac{a^2}{b^2}\right)+2\right\}}. \qquad (32)$$

3. Zahlenmässige Rechnung eines besonderen Falles.

Im Allgemeinen ist der Spannungszustand ziemlich kompliziert. Also wollen wir einen besonderen Fall zeigen.

Es sei $b=2h$, $a=4h$, $\sigma=1/4$ und $z=-h$.

Dann

$$Y_y-X_x=-\frac{9}{59}p\left\{\frac{1}{4}\left(\frac{x^2}{4h^2}+11\frac{y^2}{h^2}\right)+\frac{30}{59}\left(\frac{7}{4}\frac{x^2}{h^2}+13\frac{y^2}{h^2}\right)-3\times\frac{1}{16}\right\},$$

$$=-p\left(0.1453\frac{x^2}{h^2}+1.427\frac{y^2}{h^2}-0.02860\right). \qquad (33)$$

$$X_y=-\frac{9}{118}p\frac{xy}{h^2}=-0.07630p\frac{xy}{h^2}. \qquad (34)$$

$$\tan 2\theta=0.952\frac{x^2}{h^2}+9.350\frac{y^2}{h^2}-0.1875. \qquad (35)$$

$$\frac{\tau_m}{p}=\frac{1}{2}\sqrt{\left(0.1453\frac{x^2}{h^2}+1.427\frac{y^2}{h^2}-0.02860\right)^2+4\times0.0763^2\frac{x^2y^2}{h^4}}, \qquad (36)$$

Durch die Transformation $\xi=\frac{x}{h}$, $\eta=\frac{y}{h}$,

$$\frac{\tau_m}{p}=\sqrt{0.00528\xi^4+0.5100\eta^4+0.1096\xi^2\eta^2-0.00208\xi^2-0.02040\eta^2+0.0002045}. \qquad (36')$$

4. Annäherungsform der Iso-$\left(\frac{\tau_m}{p}\right)$ Kurve.

Aus (36)

$$f=\left(\frac{\tau_m}{p}\right)^2=A'\xi^4+B'\eta^4+C'\xi^2\eta^2-D'\xi^2-E'\eta^2+F' ,$$

$$\frac{\partial f}{\partial \xi}=2\xi(2A'\xi^2+C'\eta^2-D') ,$$

$$\frac{\partial f}{\partial \eta}=2\eta(2B'\eta^2+C'\xi^2-E') ,$$

$$\frac{\partial^2 f}{\partial \xi^2}=12A'\xi^2+2C'\eta^2-2D' ,$$

$$\frac{\partial^2 f}{\partial \eta^2}=12B'\eta^2+2C'\xi^2-2E' ,$$

$$\frac{\partial^2 f}{\partial \xi\partial \eta}=4C'\xi\eta ,$$

wo

$$A'=.00528 , \quad B'=.5100 , \quad C'=.1096 , \quad D'=.00208 , \quad E'=.02040$$

und

$$F'=.0002045 .$$

Am Maximum- oder Minimum-Punkt muss es notwendig sein, dass

$$\frac{\partial f}{\partial \xi}=\frac{\partial f}{\partial \eta}=0 ,$$

nämlich

$$(\xi=0 , \quad \eta=0) , \qquad \left(\xi=0 , \quad \eta=\sqrt{\frac{E'}{2B'}}=.1414\right) ,$$

$$\left(\xi=\sqrt{\frac{D'}{2A'}}=.444 , \quad \eta=0\right) ,$$

oder

$$\left(\xi=\sqrt{\frac{2B'D'-C'E'}{4A'B'-C'^2}}=.302 , \quad \eta=\sqrt{\frac{2A'E'-C'D'}{4A'B'-C'^2}}=.098\right) .$$

Die Indikatrix am $(\xi=0 , \eta=0)$ ist

$$\delta f=\frac{1}{2}\frac{\partial^2 f}{\partial \xi^2}\delta\xi^2+\frac{\partial^2 f}{\partial \xi\partial \eta}\delta\xi\delta\eta+\frac{1}{2}\frac{\partial^2 f}{\partial \eta^2}\delta\eta^2=-.00208\delta\xi^2-.02040\delta\eta^2 .$$

Daher ist $(\xi=0 , \eta=0)$ ein Maximum-Punkt und

$$f_{\max}=.0002045\ .$$

Nämlich $\tau_m/p=.0143\ .$

Die Indikatrix am $(\xi=0\ ,\ \eta=.1414)$ ist

$$\delta f=.00011\delta\xi^2+.0408\delta\eta^2\ .$$

Daher ist dieser Punkt ein Minimum-Punkt und $f_{\min.}=0$, was aus (36) direkt klar zu sehen ist.

In gleicher Weise am $(\xi=.444\ ,\ \eta=0)$ auch $f_{\min.}=0$.

Am $(\xi_0=.302\ ,\ \eta_0=.098)$ sind

$$\frac{\partial^2 f}{\partial\xi^2}=2\times 4A'\xi_0^2=2\times.001924\ ,$$

$$\frac{\partial^2 f}{\partial\xi^2}=2\times 4B'\eta_0^2=2\times.01973\ ,$$

$$\frac{\partial^2 f}{\partial\xi\partial\eta}=.01296\ .$$

Daher ist die Indikatrix

$$\delta f=.00192\delta\xi^2+.01296\delta\xi\delta\eta+.01973\delta\eta^2=.01973(\delta\eta+.430\delta\xi)(\delta\eta+.226\delta\xi)\ .$$

Also ist dieser Punkt ein Sattelpunkt, und in dem schmalen Gebiet zwischen den Linien $\delta\eta+.430\delta\xi=0$ und $\delta\eta+.226\delta\xi=0$ nimmt δf ab, vice versa.

$$f_{\min.\text{-}\max}=.000005\ .$$

In diesem Bereich aber ist (τ_m/p) ganz klein und es interessiert uns nicht viel. Ausserhalb dieses Gebietes nimmt (τ_m/p) nach aussen immer zu.

Nun, in der Nähe von $(\xi=0\ ,\ \eta=2)$, wenn man setzt $\xi=\delta\xi$, $\eta=2-\delta\eta$, dann, $f=8.09-16.15\delta\eta$.

Nämlich $$(\tau_m/p)\fallingdotseq 2.85(1-\delta\eta)\ . \qquad (37)$$

Wir sehen also, dass Iso-(τ_m/p) Linie parallel zu dem Rande läuft, und τ_m ungefähr gleich 3 mal p ist.

Ähnlicherweise in der Nähe von $(\xi=4\ ,\ \eta=0)$,

$$f\fallingdotseq 1.320(1-\delta\xi)\ .$$

Also

$$\tau_m/p\fallingdotseq 1.15(1-0.5\delta\xi)\ .$$

Daher ist die Schubspannung am Rande in der langen Achse erheblich kleiner als die in der kurzen Achse.

Am Rande der Ellipse, nämlich an der Linie $(\xi^2/4^2)+(\eta^2/2^2)=1$, haben wir

$$f=.0098\xi^4-.579\xi^2+8.90\,.$$

Funktion f hat weder Maximum noch Minimum im Bereich $0\leqq\xi\leqq 4$. Nämlich, nimmt die Maximum-Schubspannung am Rande von der kleinen Achse nach der langen allmählich ab.

5. Hauptspannungen am unteren Rande.

An der beiden Seiten der Platte sind die Hauptspannungen natürlich Z_z und der horizontale Zug (oder Druck). Besonders in der x-Achse oder y-Achse sind sie einfach $\sum X_x$, $\sum Y_y$ und Z_z.

Nun, am Punkte $x=0$, $y=2h$, $z=h$,

$$\begin{aligned}\sum X_x&=X_x+X_x'+X_x''=-1.455p\,,\\ \sum Y_y&=Y_y+Y_y'+Y_y''=4.35p\,,\\ Z_z&=-p\,.\end{aligned}$$

Also ergibt sich die Maximum-Schubspannung in der horizontalen Richtung zu

$$\tau_m/p=2.90\,,$$

und die Maximum-Schubspannung, derer Richtung in der (y,z) Ebene liegt, ergibt sich zu

$$\tau_m/p=2.68\,.$$

Am Punkte $x=4h$, $y=0$, $z=h$ haben wir

$$\begin{aligned}\sum X_x&=-.541p\,,\\ \sum Y_y&=19.1p\,,\\ Z_z&=-p\,.\end{aligned}$$

Also ist die Maximum-Schubspannung erheblich kleiner hier als am Punkte $x=0$, $y=2h$, $z=h$.

An der freien Oberfläche, am Punkte $x=0$, $y=2h$, $z=-h$, haben wir

$$\begin{aligned}\sum X_x&=1.14p\,,\\ \sum Y_y&=-4.69p\,,\\ Z_z&=0\,.\end{aligned}$$

Die Maximum-Schubspannung in der horizontalen Richtung ist,

$$\frac{\sum Y_y-\sum X_x}{2}=-2.90p\,,$$

was natürlich mit (37) übereinstimmt.

Die Maximum-Schubspannung in der (y,z) Ebene ist

$$\frac{\sum Y_y-Z_z}{2}=-2.35p\,.$$

Wir sehen also, dass die Maximum-Horizontalschubspannung grösser als die überschiebende Spannung ist. Aber die beiden Werte sind nicht viel verschieden. Daher können wir ruhig vermuten, dass die beiden Verwerfungen gleichzeitig auftreten können, was manchmal der Fall ist.

Am Punkte $x=4h$, $y=0$, $z=-h$ haben wir

$$\sum X_x = 0.233p\,,$$
$$\sum Y_y = -.055p\,,$$
$$Z_z = 0\,.$$

Also sehen wir wieder, dass die Spannungen in der nähe von diesem Punkt erheblich kleiner als die in der Nähe von $x=0$, $y=2h$, $z=-h$.

Alles zusammenfassend können wir natürlicherweise erklären, dass beim elliptischen Quellengebiet oder im allgemeinen beim etwas verlängerten Quellengebiet nicht nur Überschiebungen sondern auch horizontale Verwerfungen vorkommen können.

Wir sind der Meinung, dass das Nachbebengebiet ungefähr mit dem Quellengebiet des Hauptbebens übereinstimmt. Mehrere Nachbebengebiete sind wirklich elliptisch in Form, wie man in vielen Beispielen von Grossbeben deutlich sehen kann, die S. Homma[3] u.a. gegeben hatten.

Die Richtung der maximalen Schubspannung stimmt im allgemeinen nicht mit der der Iso-τ_m/p Linie überein. Andererseits kommt das System der horizontalen Verwerfungen beim Grossbeben im allgemeinen in Echelon Form vor[4]. Unser Rechenresultat erklärt wenigstens qualitativ diese Tatsache.

---

17. Zisin no Ba no Ron: Daenkei no Ba.

Tikyû Buturigaku Kyôsitu Matuzawa-Takeo to Hasegawa-Hirosi.

Matuzawa ga mae ni Zisin no Ba wo ronzita toki niwa Aturyoku no okoru Kuiki wo Enkei to site Kangae wo susumeta. Kono Toki niwa yokosuberi no Dansô wo setumeisuru Koto wa Muri de atta.

Kono Ronbun dewa Daenkei no Aturyoku no Ba ni yotte zyûbun ôkii yoko no Zuri-Hariai no okoru koto wo simesita.

Zisin no Ba no Ron dewa Yosin no okoru Kuiki wa Tikara no Hassei no Ba to daitai itti suru Mono to Kangaeru ga, zissai no Yosin-Kuiki mo Daenkei no Baai ga ôi.

Yoko no Zuri-Hariai no Kyokudai no Hôkô to sono Kyokudai no Atae no hitosii Sen towa ippan niwa itti sinai. Kono Koto wa Yokosuberi-Danso no iwayuru 'Gankô' wo setumei suru to omowareru.

3) S. Homma und A. Seki, *Zisin* [ii], **2** (1949), 37–40; **3** (1951), 44–48.

4) S. Fujiwhara und T. Takayama, *Bull. Earthq. Rest. Inst.*, **9** (1931), 50–79.

18. *On the Vibration of an Elastic Globe with One Layer. The Vibration of the First Class.*

By Tosimatu MATUMOTO and Yasuo SATÔ,

Earthquake Research Institute.

(Read May 25, 1954.—Received June 30, 1954.)

1. Introduction.

It is one of the most important problems in the field of geophysics to make researches on the internal constitution of the earth, and since the 19th century many authorities have attacked this problem by means of statical, dynamical[1)-11)] as well as a thermo-dynamical and other methods.

Recently M. Ewing and F. Press[12)] suggested that it may be possible to make use of a long surface wave with a period of several hundred seconds for investigating the interior of the earth, especially with respect to the part of the mantle. This is a hopeful idea and it is reasonable

1) H. LAMB, "The Vibration of an Elastic Sphere," *Proc. Math. Soc. London*, **13** (1882), 189–212.

2) H. LAMB, "On the Vibration of a Spherical Shell," *Proc. Math. Soc. London*, **14** (1883), 50–56.

3) T. J. BROMWICH, "On the Influence of Gravity on Elastic Waves, and in Particular, on the Vibrations of an Elastic Globe," *ibid.*, **30** (1899), 98–120.

4) J. H. JEANS, "On the Vibrations and Stability of a Gravitational Planet," *Phil. Trans. Roy. Soc. London*, **201** (1903), 157–184.

5) J. H. JEANS, "The Propagation of Earthquake Waves," *Proc. Roy. Soc. London*, **102** (1923), 554–574.

6) K. SEZAWA, "On the Propagation of Rayleigh-waves on Plane and Spherical Surfaces," *Bull. Earthq. Res. Inst.*, **2** (1927), 21–28.

7) K. SEZAWA, "Dispersion of Elastic Waves Propagated on the Surface of Stratified Bodies on Rayleigh-wave having some Azimuthal Distribution," *ibid.*, **3** (1927), 1–18.

8) K. SEZAWA, "Further Studies on Rayleigh-wave having some Azimuthal Distribution," *ibid.*, **6** (1929), 1–18.

9) K. SEZAWA, "Propagation of Love-waves on a Spherical Surface and allied Problems," *ibid.*, **7** (1929), 473–455.

10) K. SEZAWA, Sindôgaku, (Iwanami, 1931), 147–152.

11) R. YOSHIYAMA, "Love-wave Propagation in Heterogeneous Elastic Sphere," *Zisin*, [i], **10** (1938), 272–276, (in Japanese).

12) M. EWING and F. PRESS, "An Investigation of Mantle Rayleigh Wave," *Bull. Seism. Soc. Amer.*, **44** (1954), 127–148.

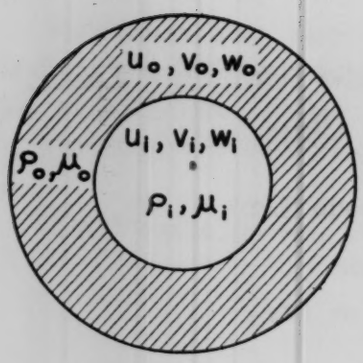

Fig. 1.

to expect that if the wave length of the surface wave becomes as long as the earth's radius, the dispersive property of the wave may be affected by the density and rigidity of the deeper part of the earth; therefore it may be possible to infer the state of the earth's interior by the dispersive property of the long surface wave.

In order to make clear whether such an analysis is possible or not, we calculated the vibration of the first class[13] of the earth model, which we assumed to be composed of two parts, namely the core and the mantle. In each part, the density and rigidity of the medium are assumed to be uniform, and are denoted by ρ_0, μ_0 in the mantle, and ρ_i, μ_i in the core respectively.

2. Vibration of the elastic sphere.

Fundamental equation of motion in a homogeneous, isotropic and perfectly elastic medium is given by the following expression

$$\rho\frac{\partial^2 \boldsymbol{u}}{\partial t^2}=(\lambda+\mu)\ \text{grad div}\ \boldsymbol{u}+\mu\nabla^2\boldsymbol{u}\,, \tag{2.1}$$

where $\boldsymbol{u}$ expresses the displacement vector.

If we take the divergence and the rotation of the above vectorial equation, and express them referring to the spherical coordinates, we get the equations of motion which give the dilatation Δ and the rotation components $\tilde{\omega}_r$, $\tilde{\omega}_\theta$ and $\tilde{\omega}_\phi$ as follows:

$$\left.\begin{aligned}
\rho\frac{\partial^2\Delta}{\partial t^2}&=(\lambda+2\mu)\left[\frac{1}{r^2}\frac{\partial}{\partial r}\left(r^2\frac{\partial\Delta}{\partial r}\right)+\frac{1}{r^2\sin\theta}\frac{\partial}{\partial\theta}\left(\sin\theta\frac{\partial\Delta}{\partial\theta}\right)+\frac{1}{r^2\sin^2\theta}\frac{\partial^2\Delta}{\partial\phi^2}\right],\\
\rho\frac{\partial^2\tilde{\omega}_r}{\partial t^2}&=\mu\left[\frac{\partial^2\tilde{\omega}_r}{\partial r^2}+\frac{4}{r}\frac{\partial\tilde{\omega}_r}{\partial r}+\frac{2}{r^2}\tilde{\omega}_r+\frac{1}{r^2\sin\theta}\frac{\partial}{\partial\theta}\left(\sin\theta\frac{\partial\tilde{\omega}_r}{\partial\theta}\right)+\frac{1}{r^2\sin^2\theta}\frac{\partial^2\tilde{\omega}_r}{\partial\phi^2}\right],\\
\rho\frac{\partial^2\tilde{\omega}_\theta}{\partial t^2}&=\mu\left[\frac{1}{r}\frac{\partial^2(\tilde{\omega}_\theta r)}{\partial r^2}+\frac{1}{r^2\sin^2\theta}\frac{\partial^2\tilde{\omega}_\theta}{\partial\phi^2}-\frac{1}{r^2\sin^2\theta}\frac{\partial^2(\tilde{\omega}_\phi\sin\theta)}{\partial\phi\partial\theta}-\frac{1}{r}\frac{\partial^2\tilde{\omega}_r}{\partial r\partial\theta}\right],\\
\rho\frac{\partial^2\tilde{\omega}_\phi}{\partial t^2}&=\mu\left[\frac{1}{r}\frac{\partial^2(\tilde{\omega}_\phi r)}{\partial r^2}+\frac{1}{r^2}\frac{\partial}{\partial\theta}\left(\frac{1}{\sin\theta}\frac{\partial(\tilde{\omega}_\phi\sin\theta)}{\partial\theta}\right)\right.
\end{aligned}\right\}$$

13) "First (and second) class" of vibration is the term adopted by H. LAMB. The vibration of the first class corresponds to the transversal vibration.

$$-\frac{1}{r^2}\frac{\partial}{\partial\theta}\left(\frac{1}{\sin\theta}\frac{\partial\tilde{\omega}_\theta}{\partial\phi}\right)-\frac{1}{r\sin\theta}\frac{\partial^2\tilde{\omega}_r}{\partial r\partial\phi}\Bigg]. \Bigg\} \tag{2.2}$$

The typical solutions of these equations were obtained by K. Sezawa in the following forms[10]:

$$\left.\begin{aligned}
\Delta &= A_{m\cdot n}\frac{J_{n+1/2}(hr)}{\sqrt{r}}P_n^m(\cos\theta)\begin{Bmatrix}\cos\\ \sin\end{Bmatrix}m\phi\, e^{ipt}\ ,\\
2\tilde{\omega}_r &= B_{m\cdot n}\frac{J_{n+1/2}(kr)}{r^{3/2}}P_n^m(\cos\theta)\begin{Bmatrix}\sin\\ -\cos\end{Bmatrix}m\phi\, e^{ipt}\ ,\\
2\tilde{\omega}_\vartheta &= \Bigg[C_{m\cdot n}\frac{J_{n+1/2}(kr)}{\sqrt{r}}\frac{P_n^m(\cos\theta)}{\sin\theta}\\
&\quad + B_{m\cdot n}\frac{1}{n(n+1)}\frac{1}{r}\frac{d}{dr}(\sqrt{r}\,J_{n+1/2}(kr))\frac{dP_n^m(\cos\theta)}{d\theta}\Bigg]\begin{Bmatrix}\sin\\ -\cos\end{Bmatrix}m\phi\, e^{ipt}\ ,\\
2\tilde{\omega}_\phi &= \Bigg[C_{m\cdot n}\frac{1}{m}\frac{J_{n+1/2}(kr)}{\sqrt{r}}\frac{dP_n^m(\cos\theta)}{d\theta}\\
&\quad + B_{m\cdot n}\frac{m}{n(n+1)}\frac{1}{r}\frac{d}{dr}(\sqrt{r}\,J_{n+1/2}(kr))\frac{P_n^m(\cos\theta)}{\sin\theta}\Bigg]\begin{Bmatrix}\cos\\ \sin\end{Bmatrix}m\phi\, e^{ipt}\ ,
\end{aligned}\right\}$$

$$h^2=\rho p^2/(\lambda+\mu)\ ,\quad k^2=\rho p^2/\mu\ , \tag{2.3}$$

where $J_{n+1/2}$ means the Bessel function of the first kind and $P_n^m(\cos\theta)(=\sin^m\theta\,(d/d\cos\theta)^m P_n(\cos\theta))$ the associated Legendre function.

Modifying the equation (2.3), we can obtain the expressions giving the displacement components, which we denote as u(r-component), v(θ-component) and w(φ-component) respectively[14].

The displacement components cited above are resolved into three parts[15], as for example, $u=u_1+u_2+u_3$.

We offer the set of displacement (u_2, v_2, w_2) as the solution of the first class, in which the dilatation Δ and the radial displacement u both vanish, and with which alone we can satisfy the boundary conditions at the spherical surface. The other set of displacement (u_1+u_3, v_1+v_3, w_1+w_3) is given as the solution of the second class, in which the rotation component $\tilde{\omega}_r$ vanishes.

As a first step, we will consider only the solution of the first class in this paper, leaving that of the second class to the future.

It is easily proved that this solution of the first class is not affected

14) K. Sezawa, "Amplitude of P- and S waves at Different Focal Distances," *Bull. Earthq. Res. Inst.*, **10** (1932), 299–334.

15) *loc. cit.*, 10). See p. 556–562.

by gravity owing to the property $u=0$ and $\Delta=0$[16]. This nature, which does not hold in the case of second class vibration, is convenient for our study which aims at making clear the change of the period caused by the variation of elastic constants and the density of the earth's interior.

3. Vibration of the first class generated in the layered earth's model.

In later sections, we will adopt the simplified model of the layered earth whose radius of the outer mantle is a and that of the internal surface of separation between the mantle and the core is b.

It is easily shown that the displacement components of the first class, which are denoted by suffix "o" in the mantle and "i" in the core, are as follows:

$$\left.\begin{aligned} u_0 &= 0\ , \\ v_0 &= \frac{m}{n(n+1)}\frac{1}{\sqrt{r}}\begin{Bmatrix} B_n J_{n+1/2}(k_0 r) \\ B'_n Y_{n+1/2}(k_0 r) \end{Bmatrix}\begin{Bmatrix} D_m P_n^m(\cos\theta) \\ D'_m Q_n^m(\cos\theta) \end{Bmatrix}\frac{1}{\sin\theta}\begin{Bmatrix} \cos \\ \sin \end{Bmatrix} m\phi\, e^{ipt}\ , \\ w_0 &= -\frac{1}{n(n+1)}\frac{1}{\sqrt{r}}\begin{Bmatrix} B_n J_{n+1/2}(k_0 r) \\ B'_n Y_{n+1/2}(k_0 r) \end{Bmatrix}\begin{Bmatrix} D_m dP_n^m(\cos\theta)/d\theta \\ D'_m dQ_n^m(\cos\theta)/d\theta \end{Bmatrix}\begin{Bmatrix} \sin \\ -\cos \end{Bmatrix} m\phi\, e^{ipt}\ , \\ &\qquad \text{for} \qquad b \leqq r \leqq a\ . \end{aligned}\right\} \tag{3.1}$$

and

$$\left.\begin{aligned} u_i &= 0\ , \\ v_i &= \frac{m}{n(n+1)}\frac{1}{\sqrt{r}} E_n J_{n+1/2}(k_i r)\begin{Bmatrix} D_m P_n^m(\cos\theta) \\ D'_m Q_n^m(\cos\theta) \end{Bmatrix}\frac{1}{\sin\theta}\begin{Bmatrix} \cos \\ \sin \end{Bmatrix} m\phi\, e^{ipt}\ , \\ w_i &= -\frac{1}{n(n+1)}\frac{1}{\sqrt{r}} E_n J_{n+1/2}(k_i r)\begin{Bmatrix} D_m (dP_n^m(\cos\theta)/d\theta) \\ D'_m (dQ_n^m(\cos\theta)/d\theta) \end{Bmatrix}\begin{Bmatrix} \sin \\ -\cos \end{Bmatrix} m\phi\, e^{ipt}\ , \\ &\qquad \text{for} \qquad 0 \leqq r \leqq b\ , \end{aligned}\right\} \tag{3.2}$$

where $k_0^2=p^2\rho_0/\mu_0$ and $k_i^2=p^2\rho_i/\mu_i$.

The boundary conditions are given as follows:
For the outer free surface (where $r=a$):

$$\frac{\partial}{\partial r}\frac{v_0}{r}=0\ , \qquad \left(\frac{\partial}{\partial r}\frac{w_0}{r}=0\right)\ , \tag{3.3a}$$

16) H. TAKEUCHI, "On the Earth Tide," *Jour. Fac. Sci., Univ. Tokyo*, **7** (1951), 23–29.

and for the boundary surface between the mantle and the core (where $r=b$) :

$$\mu_0\frac{\partial}{\partial r}\frac{v_0}{r}=\mu_i\frac{\partial}{\partial r}\frac{v_i}{r}\ , \quad \left(\mu_0\frac{\partial}{\partial r}\frac{w_0}{r}=\mu_i\frac{\partial}{\partial r}\frac{w_i}{r}\right), \tag{3.3b}$$

$$v_0=v_i\ , \qquad (w_0=w_i)\ . \tag{3.3c}$$

Introducing the equations (3.1) and (3.2) into the above conditions, we get three homogeneous, linear equations, from which by eliminating the coefficients B_n, B'_n and E_n, we can obtain the determinantal equation of the following form

$$\mathfrak{D}_n=\begin{vmatrix} \frac{\partial}{\partial a}\left\{\frac{J_{n+1/2}(k_0a)}{a^{3/2}}\right\} & \frac{\partial}{\partial a}\left\{\frac{Y_{n+1/2}(k_0a)}{a^{3/2}}\right\} & 0 \\ \frac{\partial}{\partial b}\left\{\frac{J_{n+1/2}(k_0b)}{b^{3/2}}\right\} & \frac{\partial}{\partial b}\left\{\frac{Y_{n+1/2}(k_0b)}{b^{3/2}}\right\} & -\frac{\mu_i}{\mu_0}\frac{\partial}{\partial b}\left\{\frac{J_{n+1/2}(k_ib)}{b^{3/2}}\right\} \\ J_{n+1/2}(k_0b) & Y_{n+1/2}(k_0b) & -J_{n+1/2}(k_ib) \end{vmatrix}=0\ . \tag{3.4}$$

This equation involves the variables n and $k_0a(\equiv\xi)$, and parameters k_i/k_0, μ_i/μ_0 and b/a.

3.1. Meaning of n and m.

To make clear the physical meaning of the equation (3.4), we will consider what sort of quantity n and m mean.

When the conditions $n\gg m$ and $n\gg 1$ are both satisfied, it is well known that the associated Legendre function has the approximation formulae

$$\left.\begin{aligned} P_n^m(\cos\theta)&\sim\left(\frac{1}{n\sin\theta}\right)^{1/2}\sin\{(n+1/2)\theta+\delta\}+0\left(\frac{1}{n^{3/2}}\right), \\ Q_n^m(\cos\theta)&\sim\left(\frac{1}{n\sin\theta}\right)^{1/2}\cos\{(n+1/2)\theta+\delta\}+0\left(\frac{1}{n^{3/2}}\right). \end{aligned}\right\} \tag{3.5}$$

Substituting the above equation into (3.1) and (3.2), and assuming the value of D'_m/D_m to be $-i$, we get, as R. Yoshiyama[17] has proved before,

$$\tilde{\omega}_r\sim R_{(r)}\left\{\begin{matrix}\sin\\-\cos\end{matrix}\right\}m\phi\, e^{i\{pt-(n+1/2)\theta\}}. \tag{3.6}$$

(3.6) indicates that $p/(n+1/2)$ represents the angular velocity in the θ-direction in rough approximation, and therefore, $(n+1/2)$ represents the number of waves involved in a spherical surface in the direction of θ.

17) *loc. cit.*, 11).

However, if the condition $n \gg 1$ is not satisfied, $1/n^{3/2}$ cannot be neglected compared with $1/n^{1/2}$. Since we are now considering the case in which n takes small value, the approximation mentioned above is not admissible in our problem.

When n is not so large compared with unity, $p/(n+1/2)$ loses the meaning of angular velocity in the θ-direction, therefore we must consider what meaning the variable of n has. From the nature of Legendre's associated function P_n^m and Q_n^m, we know that $(n-m)$ represents the number of nodal lines in θ-direction, and m the number of nodal lines in ϕ-direction. Therefore we will regard n and m as the parameter by which we can define the mode of vibration.

Here it should be added that m must be an integer, while n can take any arbitrary positive real value. When n is an integer, (3.1) and (3.2) represent a stationary vibration, while if n does not take an integral value, (3.1) and (3.2) represent a vibration in which the nodal lines moves with the lapse of time, or a wave.

3.2. Modification of the equation of vibration.

Now, we will try a modification of fundamental equation of vibration (3.4) in order to get a more simplified form of equation.

First, we will introduce a new quantity

$$\xi = k_0 a = \frac{2\pi a}{V_{s0}} \Big/ T \,, \tag{3.7}$$

where V_{s0} means the velocity of S-waves in the mantle, and $\frac{1}{\xi} = T \Big/ \frac{2\pi a}{V_{s0}}$ the period of vibration, the time unit of which is the time necessary for the S-wave to travel around the earth's surface.

Introducing (3.7) into (3.4), we have

$$\mathfrak{D}_n\left(\xi, \frac{k_i}{k_0}, \frac{\mu_i}{\mu_0}, \frac{b}{a}\right) = -J_{n+1/2}(k_i b)\mathrm{L}_n\left(\xi, \frac{b}{a}\right) + \frac{\mu_i}{\mu_0}\frac{\partial}{\partial b}\left\{\frac{J_{n+1/2}(k_i b)}{b^{3/2}}\right\} R_n\left(\xi, \frac{b}{a}\right), \tag{3.8}$$

where

$$L_n = \begin{vmatrix} \dfrac{\partial}{\partial a}\left\{\dfrac{J_{n+1/2}(k_0 a)}{a^{3/2}}\right\} & \dfrac{\partial}{\partial a}\left\{\dfrac{Y_{n+1/2}(k_0 a)}{a^{3/2}}\right\} \\ \dfrac{\partial}{\partial b}\left\{\dfrac{J_{n+1/2}(k_0 b)}{b^{3/2}}\right\} & \dfrac{\partial}{\partial b}\left\{\dfrac{Y_{n+1/2}(k_0 b)}{b^{3/2}}\right\} \end{vmatrix} ,$$

$$R_n=\begin{vmatrix} \dfrac{\partial}{\partial a}\left\{\dfrac{J_{n+1/2}(k_0a)}{a^{3/2}}\right\} & \dfrac{\partial}{\partial a}\left\{\dfrac{Y_{n+1/2}(k_0a)}{a^{3/2}}\right\} \\ J_{n+1/2}(k_0b) & Y_{n+1/2}(k_0b) \end{vmatrix} . \qquad (3.9)$$

4. Determination of the Period of Vibration.

Calculations were performed for two special models of the earth. In the first model, we assumed the core to be in rigid state, and in the second, the core to be in liquid state. In both models, we put the ratio of b (radius of the core) and a (radius of the free surface) as 0.5469 (=2900/6370). The numerical calculations were performed by means of series expansion.

Case I. When the core is perfectly rigid, the ratio k_0/k_t becomes infinite and μ_0/μ_t vanishes. Then in the right hand member of equation (3.8) the first term is neglected compared with the second term, and the period equation takes the following form

$$R_n(\xi, b/a)=s_n(\xi)\cos(1-b/a)\xi+t_n(\xi)\sin(1-b/a)\xi=0 , \qquad (4.1)$$

or in a different expression

$$\tan\left(1-\frac{b}{a}\right)\xi=-\frac{s_n(\xi)}{t_n(\xi)} , \qquad (4.2)$$

in which $s_n(\xi)$ and $t_n(\xi)$ are obtained expanding the Bessel functions;

$$\left.\begin{aligned} s_n(\xi)=\xi^{-(n+3)}\eta^{-(n+1/2)}\Bigg\{&\sum_{r=0}^{<n>}\sum_{p=0}^{<n>}(-1)^{r+p}c_{2r,n}c_{2p,n}\xi^{2r+1}\eta^{2p} \\ &+\sum_{r}^{<n-1>}\sum_{p}^{<n-1>}(-1)^{r+p}c_{2r+1,n}c_{2p+1,n}\xi^{2r+2}\eta^{2p+1} \\ &+\sum_{r}^{<n>}\sum_{p}^{<n-1>}(-1)^{r+p+1}(n-2r+2)c_{2r,n}c_{2p+1,n}\xi^{2r}\eta^{2p+1} \\ &+\sum_{r}^{<n-1>}\sum_{p}^{<n>}(-1)^{r}(n-2r+1)c_{2r+1,n}c_{2p,n}\xi^{2r+1}\eta^{2p}\Bigg\} , \\ t_n(\xi)=\xi^{-(n+3)}\eta^{-(n+1/2)}\Bigg\{&\sum_{r=0}^{<n>}\sum_{p=0}^{<n>}(-1)^{r+p+1}(n-2r+2)c_{2r,n}c_{2p,n}\xi^{2r}\eta^{2p} \\ &+\sum_{r}^{<n-1>}\sum_{p}^{<n-1>}(-1)^{r+p+1}(n-2r+1)c_{2r+1,n}c_{2p+1,n}\xi^{2r+1}\eta^{2p+1} \\ &+\sum_{r}^{<n>}\sum_{p}^{<n-1>}(-1)^{r+p+1}c_{2r,}c_{2p+1,n}\xi^{2r+1}\eta^{2p+1} \\ &+\sum_{r}^{<n-1>}\sum_{p}^{<n>}(-1)^{r+p}c_{2r+1,n}c_{2p,n}\xi^{2r+2}\eta^{2p}\Bigg\} , \end{aligned}\right\} \qquad (4.3)$$

where

$$\eta=\frac{b}{a}\xi\,,$$

and

$$<n>=\begin{cases} n/2 & \text{when } n \text{ is even,} \\ (n-1)/2 & \text{when } n \text{ is odd .} \end{cases}$$

In this equation, the coefficients c_{pq} which are obtained from the coefficients of the expansion of Bessel Function are calculated as follows:

$c_{00}=1$

$c_{01}=1$ $c_{11}=1$

$c_{02}=3$ $c_{12}=3$ $c_{22}=1$

$c_{03}=15$ $c_{13}=15$ $c_{23}=6$ $c_{33}=1$

$c_{04}=105$ $c_{14}=105$ $c_{24}=45$ $c_{34}=10$ $c_{44}=1$

$c_{05}=945$ $c_{15}=945$ $c_{25}=420$ $c_{35}=105$ $c_{45}=15$ $c_{55}=1$

The roots of equation (4.2) are given by the ordinates of cross point of the curves of $\tan(1-b/a)\xi$ and $-s_n(\xi)/t_n(\xi)$. For any arbitrarily given n (of which the physical meaning is discussed in section 3), we can get a series of roots ξ_n, which are tabulated in Table I. The letter

Table I. The Roots of Characteristic Equation $R_n(\xi, b/a)=0$.

$\left(\text{Rigid Core,}\quad 1/\xi=T\Big/\frac{2\pi a}{V_{s0}}\,,\quad k_0/k_i=\infty\,,\quad \mu_0/\mu_i=0\,,\quad b/a=0.5469\right)$

n \ N	0		I		II		III	
	ξ	$1/\xi$	ξ	$1/\xi$	ξ	$1/\xi$	ξ	$1/\xi$
0	1.160	0.8261	9.963	0.1014	17.05	0.0587	24.08	0.0415
1	2.000	0.5000	10.14	0.0986	17.15	0.0583	24.2	0.0413
2	3.045	0.328	10.49	0.0953	17.4	0.0575	24.4	0.0410
3	4.30	0.233	10.8	0.0936	17.5	0.0570		
4	5.40	0.185	11.5	0.0870				

N stands for the number of nodal plane in r-direction, which should be explained in a latter section.

Case II. After the same method as the foregoing calculation, we can obtain the roots for the case of liquid core. In this case the ratio

k_0/k_i vanishes and μ_0/μ_i becomes infinite. Then the period equation (3.8) takes the following form

$$L_n(\xi, b/a)=g_n(\xi)\cos(1-b/a)\xi+h_n(\xi)\sin(1-b/a)\xi=0\ , \qquad (4.4)$$

in which $g_n(\xi)$ and $h_n(\xi)$ are obtained as before, namely

$$\left.\begin{aligned}
g_n(\xi)=(\xi\eta)^{-n-3}\Bigg\{&\sum_{r=0}^{<n>}\sum_{p=0}^{<n>}(-1)^{r+p+1}(n-2p+2)c_{2r,n}c_{2p,n}\xi^{2r+1}\eta^{2p}\\
&+\sum_{r}^{<n-1>}\sum_{p}^{<n-1>}(-1)^{r+p+1}(n-2p+1)c_{2r+1,n}c_{2p+1,n}\xi^{2r+2}\eta^{2p+1}\\
&+\sum_{r}^{<n>}\sum_{p}^{<n>}(-1)^{r+p}(n-2r+2)c_{2r,n}c_{2p,n}\xi^{2r}\eta^{2p+1}\\
&+\sum_{r}^{<n-1>}\sum_{p}^{<n-1>}(-1)^{r+p}(n-2r+1)c_{2r+1,n}c_{2p+1,n}\xi^{2r+1}\eta^{2p+2}\\
&+\sum_{r}^{<n>}\sum_{p}^{<n-1>}(-1)^{r+p}(n-2r+2)(n-2p+1)c_{2r,n}c_{2p+1,n}\xi^{2r}\eta^{2p+1}\\
&+\sum_{r}^{<n-1>}\sum_{p}^{<n>}(-1)^{r+p+1}(n-2r+1)(n-2p+2)c_{2r+1,n}c_{2p,n}\xi^{2r+1}\eta^{2p}\\
&+\sum_{r}^{<n>}\sum_{p}^{<n-1>}(-1)^{r+p}c_{2r,n}c_{2p+1,n}\xi^{2r+1}\eta^{2r+2}\\
&+\sum_{r}^{<n-1>}\sum_{p}^{<n>}(-1)^{r+p+1}c_{2r+1,n}c_{2p,n}\xi^{2r+2}\eta^{2p+1}\Bigg\}\ ,\\
h_n(\xi)=(\xi\eta)^{-n-3}\Bigg\{&\sum_{r=0}^{<n>}\sum_{p=0}^{<n>}(-1)^{r+p}c_{2r,n}c_{2p,n}\xi^{2r+1}\eta^{2p+1}\\
&+\sum_{r}^{<n-1>}\sum_{p}^{<n-1>}(-1)^{r+p}c_{2r+1,n}c_{2p+1,n}\xi^{2r+2}\eta^{2p+2}\\
&+\sum_{r}^{<n>}\sum_{p}^{<n>}(-1)^{r+p}(n-2r+2)(n-2p+2)c_{2r,n}c_{2p,n}\xi^{2r}\eta^{2p}\\
&+\sum_{r}^{<n-1>}\sum_{p}^{<n-1>}(-1)^{r+p}(n-2r+1)(n-2p+1)c_{2r+1,n}c_{2p+1,n}\xi^{2r+1}\eta^{2p+1}\\
&+\sum_{r}^{<n>}\sum_{p}^{<n-1>}(-1)^{r+p+1}(n-2r+2)c_{2r,n}c_{2p+1,n}\xi^{2r}\eta^{2p+2}\\
&+\sum_{r}^{<n-1>}\sum_{p}^{<n>}(-1)^{r+p}(n-2r+1)c_{2r+1,n}c_{2p,n}\xi^{2r+1}\eta^{2p+1}\\
&+\sum_{r}^{<n>}\sum_{p}^{<n-1>}(-1)^{r+p}(n-2p+1)c_{2r,n}c_{2p+1,n}\xi^{2r+1}\eta^{2p+1}\\
&+\sum_{r}^{<n-1>}\sum_{p}^{<n>}(-1)^{r+p+1}(n-2p+2)c_{2r+1,n}c_{2p,n}\xi^{2r+2}\eta^{2p}\Bigg\}\ .
\end{aligned}\right\} \qquad (4.5)$$

The roots of this equation are shown in Table II.

In the Tables I and II there exist many roots ξ_n for a given value of n (which are denoted by the letter $N=0$, I, II, III, $\cdots$). These roots give the same distribution of displacement on the spherical surface, but

Table II. The Roots of Characteristic Equation $L_n(\xi, b/a)=0$.

(Liquid Core. $1/\xi = T\Big/\frac{2\pi a}{V_{s0}}$, $k_0/k_l=0$, $\mu_0/\mu_l=\infty$, $b/a=0.5469$.)

n \ N	0		I		II	
	ξ	$1/\xi$	ξ	$1/\xi$	ξ	$1/\xi$
0	—	—	7.362	0.1358	14.1	0.0709
1	—	—	7.62	0.131	14.2	0.0704
2	2.415	0.414	8.18	0.122	14.5	0.0690
3	3.79	0.264	8.9	0.112	14.9	0.0671
4	4.9	0.20	9.9	0.101		

differ in its distribution of amplitude in r-direction. For example, calculated distribution of amplitude in r-direction for the branch N=0, I, and II ($n=2$, rigid core) are shown in Fig. 2. Here we can observe that the branch number 0, I and II indicate the number of nodal planes in r-direction. The branch 0 gives the lowest value of ξ_n, that is, the longest period of vibration.

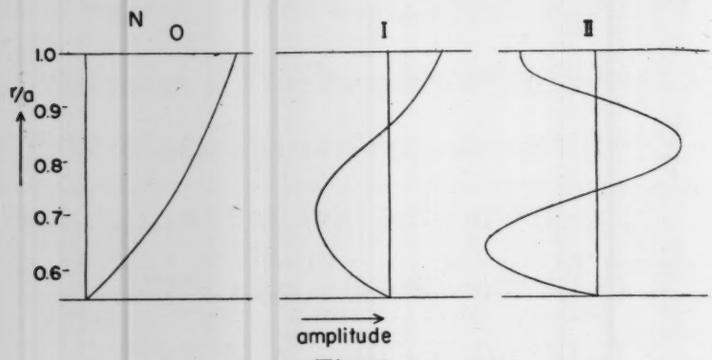

Fig. 2.

5. Conclusion.

The results of calculation are shown in Fig. 3. As stated above, the longest period of vibration is given by the reciprocal of the root on branch $N=0$. In the case of $n=2$, for instance, the longest period measured by the unit $2\pi a/V_{s0}$ $\left(\text{see (3.7)}, \frac{1}{\xi}=T\Big/\frac{2\pi a}{V_{s0}}\right)$ are 0.328 for rigid core and 0.414 for liquid core respectively. If we adopt 6.5

km./sec. as the S-wave velocity in the mantle, the actual periods will be expressed by the relation

$$T=1/\xi\times 6.16\times 10^3 \quad \text{sec.}$$

and are about 33.7 min. for rigid core and 42.5 min. for liquid core.

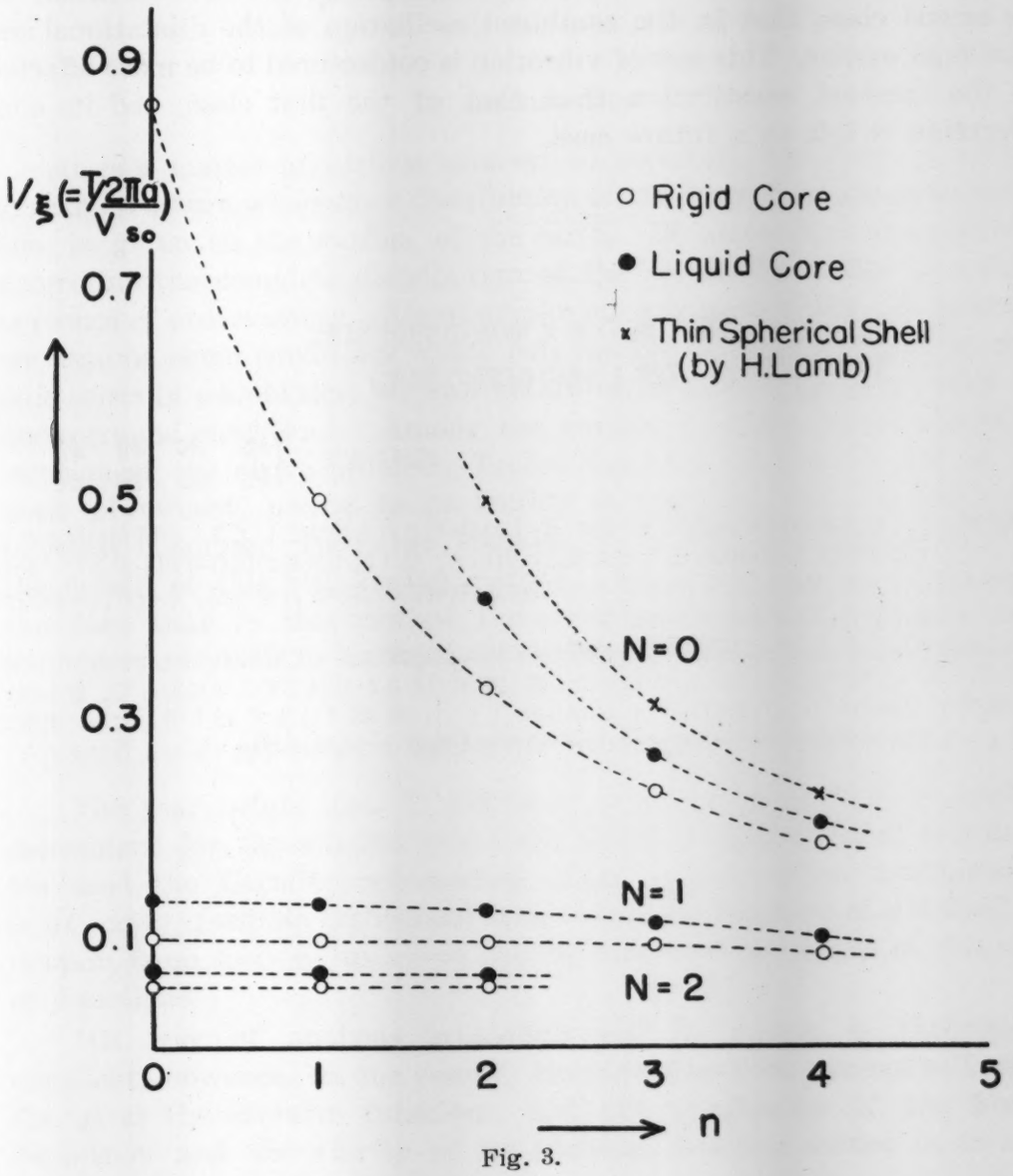

Fig. 3.

When the ratios k_0/k_i and μ_0/μ_i are finite and give the intermediate state of rigid and liquid core, the periods will also give the intermediate values of them.

Thus it may be possible to infer the ratios k_0/k_i and μ_0/μ_i if we have enough observations distributed over the earth's surface to make clear the period and the mode of vibration. But in actual observations such long period as cited above must be left to future consideration.

It is also necessary to calculate the period of the vibration of the second class, that is, the combined oscillation of the dilatational and rotational motion. This sort of vibration is conjectured to be more affected by the internal constitution than that of the first class, and its consideration is left to a future case.

---

18. 層のある地球の弾性振動
(第1種の振動の周期)

地震研究所 松本利松
佐藤泰夫

弾性球としての地球の固有振動については H. Lamb のそれを始めとして多くの研究がなされている．ここでは Core と Mantle より成る地球に対して，第1種の振動の固有周期を求めた．振動の球面上における各 Mode についてそれぞれ一連の固有周期の群が存在するが，それらは半径方向に異なった振巾分布を示す振動に対応する．

この振動周期は核の内外における弾性常数及び密度の比の値によって変化するが，$n=2$ (θ- 又は φ- 方向に2つの節平面が存在する)の場合には核が剛体であるか流体であるかに従って，最も長い固有周期は，Mantle の S- 波速度を 6.5km/sec として，約 33.7分及び 42.5分となる．実際にこのような振動が観測されれば，地球の Core の状態を推定する有力な手懸りを与えるであろう．

---

19. *A Note on Tsuboi-Nagata's Method.*

By Yasuo SATÔ,

Earthquake Research Institute.

(Read April 27, 1954.—Received June 30, 1954.)

1. Introduction

It is a matter of serious interest to ascertain the state of subterranean structure when some distribution of the gravity or the geomagnetism is given on the surface of the earth. Of course it is impossible to determine the complete distribution of the matter by means of a single sequence of observations without employing any assumption. If, however, we assume some conditions which can readily be acknowledged by common sense in geophysics, we can obtain some knowledge concerning the underground conditions. Among the various methods, which aim at the solution of the above problem, Tsuboi-Nagata's method[1] is one of the most prominent, owing to its facility of treatment and its lucidity of physical meaning. Here, we suppose, it is not necessary to describe the details of this well-known method. We will only call attention to the fact that in this method the observed distribution on some finite domain is assumed to be repeated cyclically outside the said domain.

2. Rikitake's method using Hermite functions

The year before last, T. Rikitake[2] proposed a method of analysis convenient for the solution when the distribution of anomaly is isolated. He used the Hermite polynomials $H_n(x)$, which, when multiplied by $\exp(-x^2/2)$, form an orthogonal system and any function of x defined in a domain from $x=-\infty$ to $x=\infty$ can be expanded by means of this series of functions.

His way of analysis is superb and its course is theoretically excellent, however, to our regret, Hermite functions are not so familiar for us as the circular functions, and the familiarity of the Fourier expansion and the clarity of its physical meaning induce us to apply

1) C. TSUBOI and T. FUCHIDA, *Bull. Earthq. Res. Inst.*, **15** (1937), 636. T. NAGATA, *ibid.*, **16** (1938), 550.

2) T. RIKITAKE, *Bull. Earthq. Res. Inst.*, **30** (1952), 293.

Tsuboi-Nagata's method even to the problem of isolated distribution of anomalies[3].

3. Tsuboi-Nagata's method

The principle of Tsuboi-Nagata's method resides in the following property, i.e., corresponding to the subterranean distribution of anomaly

$$A \exp\{ix\} \quad \cdots\cdots\cdots\cdots\cdots\cdots (3.1a)$$

there exists on the surface a distribution

$$K \cdot A \exp\{ix\} \quad \cdots\cdots\cdots\cdots\cdots\cdots (3.1b)$$

where K is independent of x, but depends on the depth of the plane of anomaly. Since the linearity of the fundamental equation of potential theory secures the law of superposition, corresponding to the underground distribution

$$\sum_{\alpha} A_{\alpha} \exp\{i\alpha x\} \quad \cdots\cdots\cdots\cdots\cdots\cdots (3.2a)$$

we have

$$\sum_{\alpha} K_{\alpha} \cdot A_{\alpha} \exp\{i\alpha x\} \quad \cdots\cdots\cdots\cdots\cdots\cdots (3.2b)$$

on the surface. Or, if the distribution of anomaly

$$\tilde{\phi}(x) = \sum \phi_{\alpha} \exp\{i\alpha x\} \quad \cdots\cdots\cdots\cdots\cdots\cdots (3.3a)$$

is at first given on the surface, we should assume subterranean distribution

$$\tilde{\Phi}(x) = \sum L_{\alpha} \cdot \phi_{\alpha} \exp\{i\alpha x\} \quad \cdots\cdots\cdots\cdots\cdots\cdots (3.3b)$$

where Fourier coefficients ϕ_{α} is expressed as

$$\phi_{\alpha} = \frac{1}{2\pi} \int_{-\pi}^{\pi} \tilde{\phi}(t) \exp(-i\alpha t) dt \quad \cdots\cdots\cdots\cdots\cdots\cdots (3.4)$$

Now, suppose an isolated distribution of anomaly $\phi(x)$ on the surface, shown, for example, in Fig. 1.

If we apply Fourier's double integral theorem to the function $\phi(x)$, we have at once

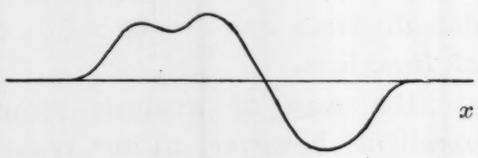

Fig. 1.

3) Moreover, the expansion due to the Hermite functions is not uniquely determined, for we can take any point as the origin of the coordinates, and any length as the unit, and every different combination of the origin and unit length gives different expression of expansion.

$$\phi(x)=\int_{-\infty}^{\infty}\phi^*(\xi)\exp(i\xi x)d\xi\,, \qquad \cdots\cdots\cdots\cdots(3.5)$$

where

$$\phi^*(\xi)=\frac{1}{2\pi}\int_{-\infty}^{\infty}\phi(t)\exp(-i\xi t)dt\,. \qquad \cdots\cdots\cdots(3.6)$$

The corresponding underground distribution is expressed by the function

$$\Phi(x)=\int_{-\infty}^{\infty}L(\xi)\phi^*(\xi)\exp(i\xi x)dx\,, \qquad \cdots\cdots\cdots(3.7)$$

where $\phi^*(\xi)$ has the same meaning with that in the expression (3.6).

As we have just said before, $\phi(x)$ shows an isolated distribution and may be assumed to vanish outside the finite domain, say $(-\pi, \pi)$, and $\phi^*(\xi)$ can be modified as

$$\phi^*(\xi)=\frac{1}{2\pi}\int_{-\pi}^{\pi}\phi(t)\exp(-i\xi t)dt\,. \qquad \cdots\cdots\cdots(3.8)$$

This expression has an identically equal form with (3.4), therefore we have

$$\phi_\alpha=\phi^*(\alpha)\,, \qquad \cdots\cdots\cdots\cdots\cdots(3.9)$$

from which we can deduce the property that in such a case Fourier coefficient is equal to the value of Fourier's conjugate function at the same point.

3.1. Tsuboi-Nagata's method from the point of view of spectrum

If we discuss the problem borrowing the terms of optics, in Tsuboi-Nagata's method we are using a line spectrum ϕ_α as a substitute for a continuous spectrum $\phi^*(\xi)$ (cf. Fig. 2). In this case, if the breadth b is not sufficiently narrow, a series of line spectrum may fail to be a good substitute for a continuous one[4].

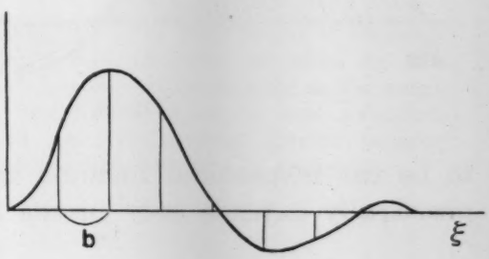

Fig. 2.

4) Information theory will give some clue with respect to the density we are to give to the line spectrum.

3.2. Tsuboi-Nagata's method as the approximation of an integral

Rigorous solution of the underground distribution is expressed by the formula

$$\Phi(x)=\int_{-\infty}^{\infty} L(\xi)\phi^*(\xi)\exp(i\xi x)d\xi\ , \qquad \cdots\cdots (3.7\text{ bis})$$

while the same distribution is given by Tsuboi-Nagata's method

$$\tilde{\Phi}(x)=\sum_{\alpha} L_\alpha\cdot\phi_\alpha \exp(i\alpha x). \qquad \cdots\cdots\cdots\cdots (3.3\text{b bis})$$

Since ϕ_α is equal to $\phi^*(\alpha)$, the latter expression proves to be an approximation of the former integral by the rectangular formula, which fact will be understood by the Fig. 3. The curve C in the figure represents the integrand of the expression (3.7) and the area of the hatched part represents $\tilde{\Phi}(x)$ in (3.3 b), or the value given by Tsuboi-Nagata's method. If curve C vanishes outside a finite domain (R_1,R_2), (practically our problems satisfy such a condition, for the amplitude of extremely rapid oscillation is generally very small), the rectangular formula proves to be the trapezoidal formula as shown in Fig. 4 and our integration practically extends only in the finite region (R_1, R_2).

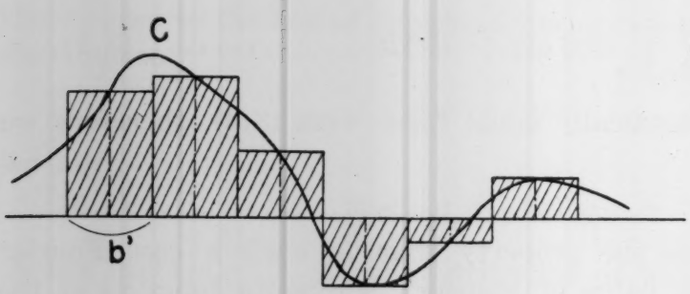

Fig. 3.

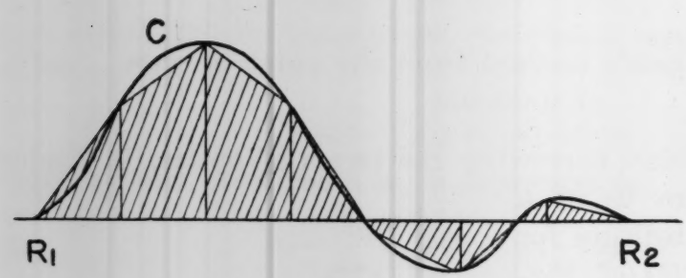

Fig. 4.

4. Modification of Tsuboi-Nagata's method

Now, in order to obtain a good approximation of an integral, we must, it is evident, make the breadth b' of the division narrower. Since this quantity b' is nothing but the breadth b in Fig. 2, we have at once

$$b'=b=2\pi/[\text{fundamental period of } \tilde{\phi}(x) \text{ in (3.3a)}]\,, \quad \ldots.(3.10)$$

and to take b' small means to take the fundamental period of $\phi(x)$ large, namely to insert a zone where the anomaly is null between the regions of anomaly which appears cyclically. (cf. Figs. 5b, c, d). This is our proposal in this paper.

5. Explanation by means of an example

We will explain the details of this circumstance in this section employing the example already used in Rikitake's paper.

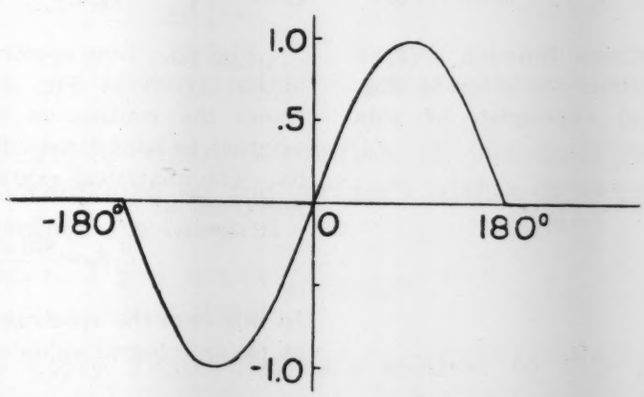

Fig. 5a. Original distribution of an anomaly in the vertical geomagnetic component used in the calculation in § 5.

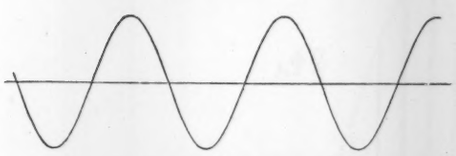

Fig. 5b. Distribution of the anomaly used for the analysis after Tsuboi-Nagata's method. The original anomaly is the one shown in Fig. 5a.

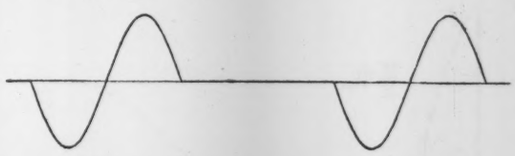

Fig. 5c. The distribution of anomaly used in the analysis proposed in this paper. Null region as wide as the original breadth of anomaly was assumed, hence the fundamental period became twice the breadth of the anomaly.

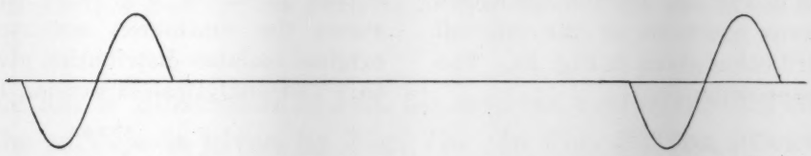

Fig. 5d. The second trial of the analysis based on the method proposed. A distribution with a fundamental period four times with the breadth of the original one was assumed, inserting a null region three times as wide as the part of anomaly.

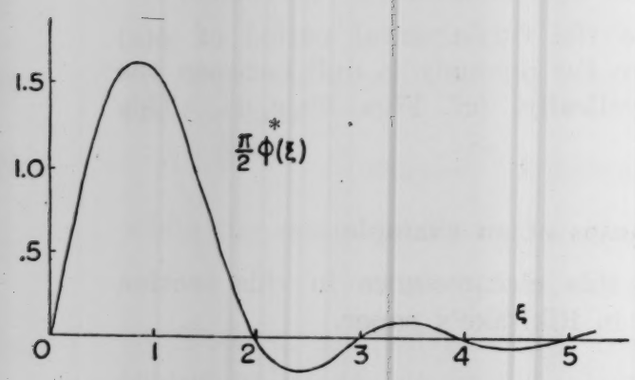

Fig. 6a. Spectrum function $\phi^*(\xi)$ of the isolated distribution $\phi(x)$ given in Fig. 5a. The analytical expression of this spectrum is:

$$\frac{\pi}{2}\phi^*(\xi)=\frac{\sin \xi\pi}{1-\xi^2}.$$

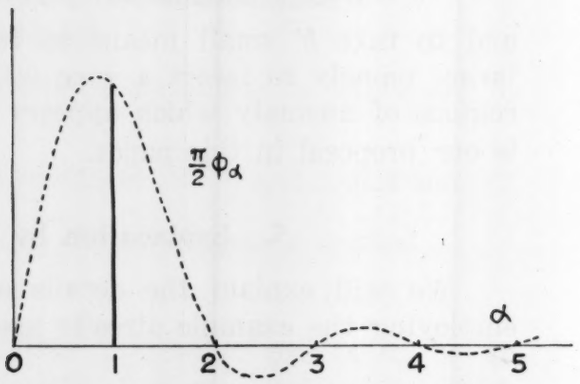

Fig. 6b. Line spectrum of the distribution given in Fig. 5b. Broken line shows the continuous spectrum of the original isolated distribution given in Fig. 5a. The analytical expression of the line spectrum is:

$$\frac{\pi}{2}\phi_\alpha=\frac{\sin \alpha\pi}{1-\alpha^2}.$$

In this case the spectrum lines are taken at every integral value of α.

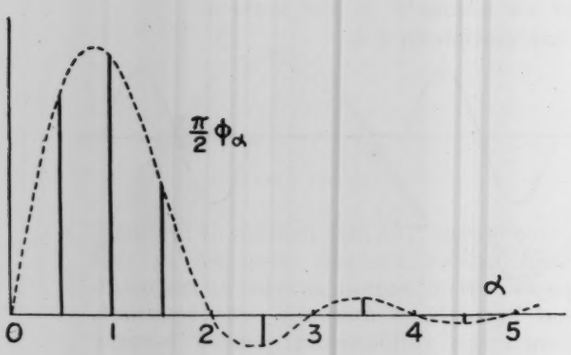

Fig. 6c. Line spectrum of the distribution given in Fig. 5c. Broken line shows the continuous spectrum of the original isolated distribution given in Fig. 5a. The analytical expression is:

$$\frac{\pi}{2}\phi_\alpha=\frac{\sin \alpha\pi}{1-\alpha^2}.$$

In this case the interval of spectrum lines is 1/2.

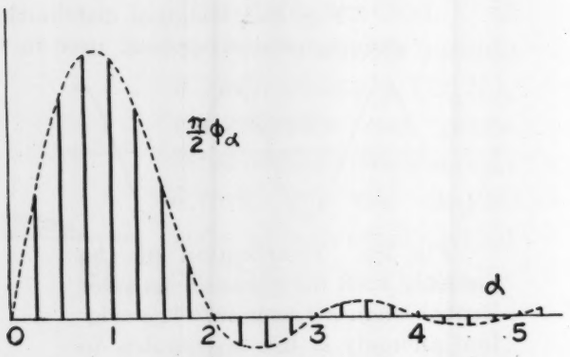

Fig. 6d. Line spectrum of the distribution given in Fig. 5d. Broken line shows the continuous spectrum of the original isolated distribution given in Fig. 5a. The analytical expression is:

$$\frac{\pi}{2}\phi_\alpha=\frac{\sin \alpha\pi}{1-\alpha^2}.$$

In this case the spectrum lines are taken at every 1/4.

Fig. 5a is the original distribution of anomaly in the vertical geomagnetic component given on the surface.

The analytic expression of this function is

$$\phi(x)=\begin{cases}0 & \cdots\cdots\ x<-\pi\ , \\ \sin x & \cdots\cdots\ -\pi<x<\pi\ , \\ 0 & \cdots\cdots\ \pi<x\ .\end{cases} \qquad \cdots\cdots\cdots(5.1)$$

Of course, this function has a continuous spectrum, which is shown in Fig. 6a, and its functional form is

$$\begin{aligned}\phi^*(\xi)&=\frac{1}{2\pi}\int_{-\pi}^{\pi}\sin t\cdot(-i\sin\xi t)dt \\ &=\frac{-i}{\pi}\cdot\frac{\sin\xi\pi}{1-\xi^2}\ . \qquad \cdots\cdots\cdots\cdots\cdots\cdots(5.2)\end{aligned}$$

In order to get a rigorous solution of the distribution of the magnetization concentrated on the surface[5] with a downward direction, we ought to calculate the integral

$$\frac{1}{\pi^2}\int_0^{\infty}\frac{1}{\xi}\frac{\sin\xi\pi}{1-\xi^2}\sin\xi x dx^{6}\ . \qquad \cdots\cdots\cdots\cdots(5.3)$$

Now, if we apply Tsuboi-Nagata's method to this problem, the function treated in this case is not the original isolated one shown in Fig. 5a, but the cyclic distribution shown in Fig. 5b. The spectrum

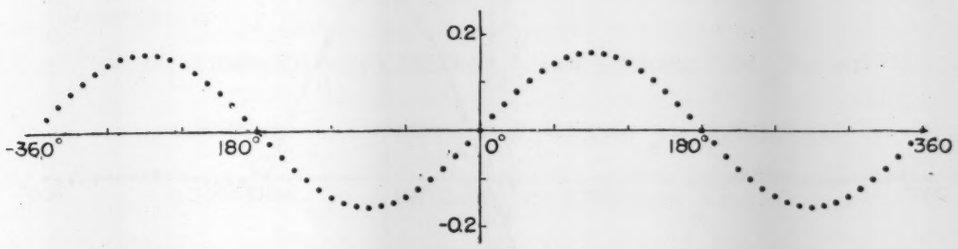

Fig. 7b. Obtained geomagnetization by means of the ordinary Tsuboi-Nagata's method. The original anomaly is shown in Fig. 5a, but the distribution used for the analysis in this case is the one given in Fig. 5b.

of this function is illustrated in Fig. 6b, and the corresponding magnetization on the surface is given by Fig. 7b. In Fig. 9b the integrand of

5) In this problem we cannot obtain the concentrated underground magnetization rigorously satisfying the given surface anomaly of the vertical geomagnetic component.

6) T. NAGATA, *loc. cit.*, 1).

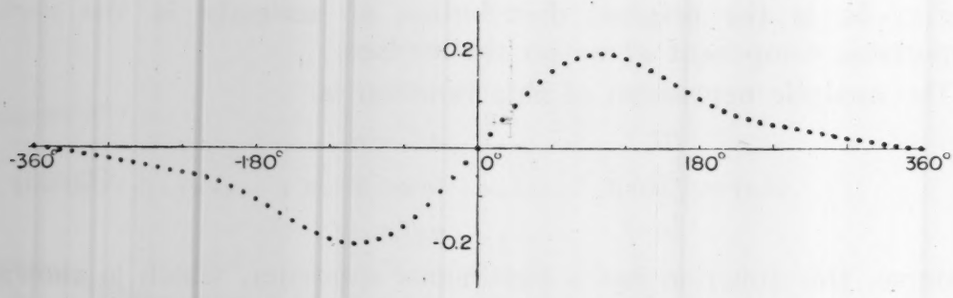

Fig. 7c. Distribution of magnetization corresponding to the anomaly in the vertical geomagnetic component shown in Fig. 5c.

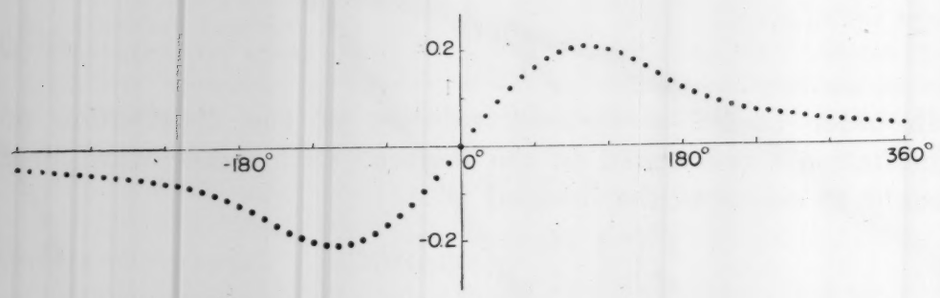

Fig. 7d. Distribution of magnetization corresponding to the anomaly in the vertical geomagnetic component shown in Fig. 5d.

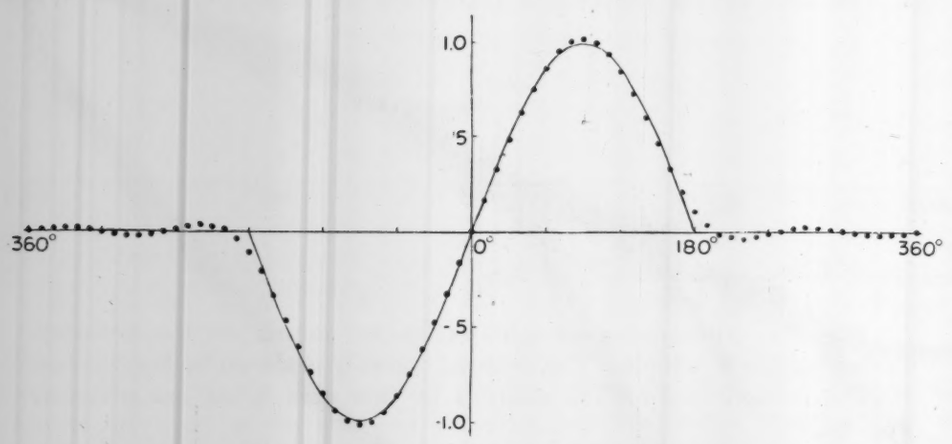

Fig. 8c. Bold line is the original distribution of the vertical geomagnetic component, while the black circles show the approximation due to Fourier series with a fundamental period two times as wide as the original breadth of the distribution as shown in Fig. 5c. The analytical expression is:

$$\frac{\pi}{2}\cdot\tilde{\phi}(x)=\left[1.33333\sin\frac{1}{2}x+\frac{\pi}{2}\sin x+0.8\sin\frac{3}{2}x-0.19048\sin\frac{5}{2}x\right]\Big/2\ .$$

(5.3) and the approximation due to the rectangular (or trapezoidal) formula is illustrated taking some moderate value of x.

As mentioned above, we are not, of course, satisfied by this solution, hence we tried two other solutions adopting the idea described in the previous section. First, we inserted a null region as wide as the original breadth of anomaly as shown in Fig. 5c. The spectrum of this distribution is given in Fig. 6c. Fig. 7c is the obtained distribution of

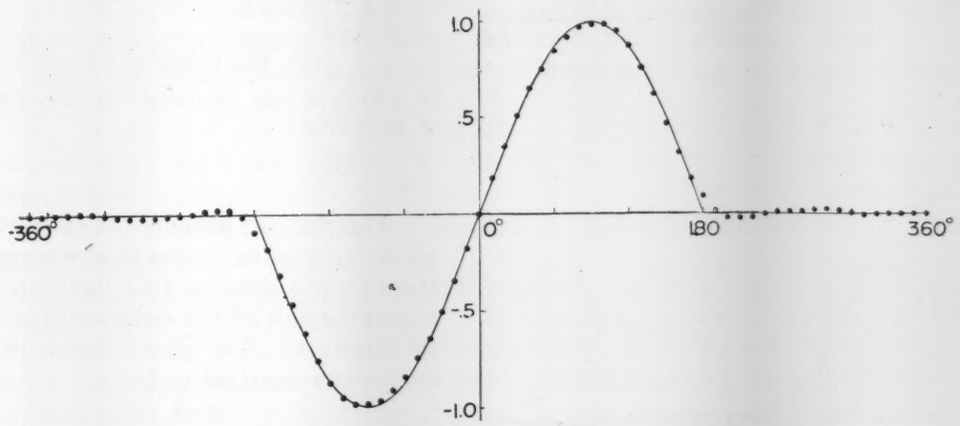

Fig. 8d. Bold line is the original distribution of the vertical geomagnetic component, while the black circles show the approximation due to Fourier series with a fundamental period four times as wide as the original breadth of the distribution as shown in Fig. 5d. The analytical expression is:

$$\frac{\pi}{2}\tilde{\phi}(x)=\Big[0.75425\sin\frac{1}{4}x+1.33333\sin\frac{1}{2}x+1.61624\sin\frac{3}{4}x+\frac{\pi}{2}\sin x$$
$$+1.25708\sin\frac{5}{4}x+0.8\sin\frac{3}{2}x+0.34284\sin\frac{7}{4}x-0.17406\sin\frac{9}{4}x$$
$$-0.19048\sin\frac{5}{2}x-0.10775\sin\frac{11}{4}x+0.07395\sin\frac{13}{4}x$$
$$+0.08889\sin\frac{7}{2}x-0.05413\sin\frac{15}{4}x\Big]\Big/4\,.$$

magnetization. Approximate distribution of geomagnetic component represented by a few terms of Fourier series which were used in this analysis is shown in Fig. 8c. Fig. 9c is an illustration of the approximate integration of the integral in (3.7).

Secondly we have assumed a distribution with a fundamental period four times as wide as the breadth of the original one, or in other words, inserting a null region three times as wide as the part of anomaly, we adopted a distribution as shown in Fig. 5d. Figs. 6d, 7d, 8d and 9d

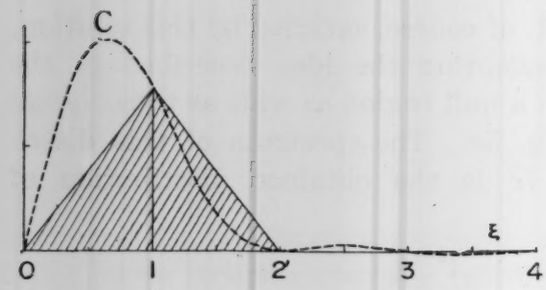

Fig. 9b. Illustration of the Tsuboi-Nagata's method from the viewpoint of the approximate integration. The curve C is the integrand and the area between C and the ξ-axis gives the result. The hatched area shows the value given by the ordinary Tsuboi-Nagata's method. In the case of an isolated anomaly the error becomes fairly large. The analytical expression of the curve C is

$$\frac{1}{\xi}\frac{\sin \xi\pi}{1-\xi^2}\sin \xi x$$

(viz. the integrand in (5.3)),

in which x was assumed, in this figure, to be unity.

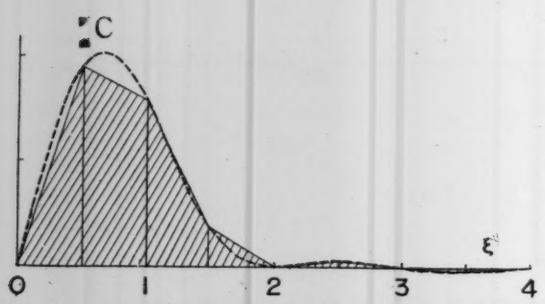

Fig. 9c. To assume the distribution given by Fig. 5c proves that we employ the hatched area in this figure as the approximation of the definite integral of the curve C. The parameter x of the curve was assumed to be

$$x=1.$$

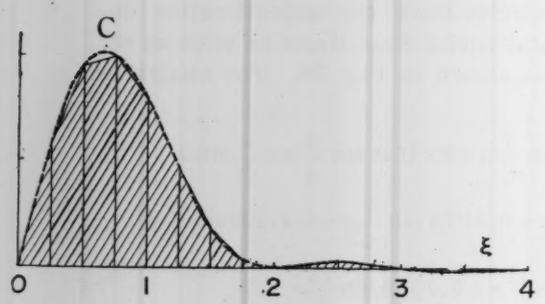

Fig. 9d. If we assume the distribution of anomaly given by Fig. 5d instead of the one given by Fig. 5b or 5c, the approximation becomes as is shown by the hatched part of this figure. x was assumed to be unity.

show similar process with which the analysis was performed in this case. From these illustrations one may understand what the modified method in this paper means and also may briefly estimate the error involved in this calculation. Needless to say, the result coincides fairly well with that obtained by T. Rikitake[7].

7) *loc. cit.*, 2).

19. 坪井·永田の方法について

地震研究所　佐藤泰夫

重力·地磁気等の地表における異常の分布から，内部の構造を推論することは，地球物理学に於いてもっとも重要な問題の一つであり，幾つもの方法が提案されてゐるが，坪井·永田の方法[1]はその中でも最もすぐれたものの一つであらう．(§1).

しかし既に力武も指摘してゐる様に[2]，此の方法では，測定された分布は，その範囲外においても，全く同様な変化を周期的にくり返す事を必然的に仮定しなくてはならない．かうした制約は弧立した異常分布に対しては無理なものであり，これを改善する爲に，力武は Hermite 函数を用ゐる極めて巧妙な方法を提案したのである[2]．しかしこれにも一二困難な点がないわけではなく，坪井·永田の方法の持つ長所——方法の容易な点，物理的意義の明らかな点等——は捨て去りがたい．(§2).

弧立した函数 $\phi(x)$ のスペクトル——共軛函数——は連続スペクトルであり，坪井·永田の方法で Fourier 係数を用ゐる事は，連続スペクトルの代用として線スペクトルを使用する事を意味する．(Fig. 2 参照)，(§3.1).

又，この方法を積分の近似計算として見るならば，矩形公式による近似となってゐる．(Fig. 2 参照)，(§3.2).

従って良好な近似を得ようとすれば，分割の幅をせまくすべきであるし，この事は又線スペクトルの間隔を密にとる事と同意義である．ところが基本周期はスペクトルの間隔に逆比例するから，この間隔をせまくとる事は基本周期を長くする事となり，従って又，坪井·永田の方法では不可避の事である異常分布の周期的なくりかえしに於て，中間に異常のない部分を挿入する事になる．(Fig. 5b, c, d 参照)，(§4).

最後に，この間の事情を，実例により，グラフを用ゐて説明した．基本周期をどの程度にのばすべきか，換言すればどのくらい異常のない部分をさしはさむかは，§4 の見方よりすればポテンシアル論に関する物理的常識によって，§3.2 の観点に立てば，矩形公式による積分の近似の誤差に関する見積りから，§3.1 のやうに，線スペクトルによって連続スペクトルを代表すると考へるならば Information theory における解析論の考へから，定める事ができるであらう．

このやうにして求めた結果は，当然のことであるが，力武によって得られたものとよく一致する．(§5).

20. *Study on the Elasticity near the Melting Point. Part I. Nature of Dilatational Wave.*

By Daisuke SHIMOZURU,

Earthquake Research Institute.

(Read Feb. 23, 1954.—Received June 30, 1954.)

Introduction.

Recent discussions on the constitution of the earth's interior, especially those on the state of the earth's core, have brought out the scantiness of relevant experiments. Particularly, the elastic behavior of rocks in the neighborhood of the melting point is one of the most urgent questions. But, our knowledge concerning this is very poor because of the lack of definite theory of fusion and experimental facts.

Theory of fusion has been advocated by many authorities such as Brillouin[1], Born[2], Fürth[3], Lindemann[4], Lennard-Jones and Devonshire[5], Kirkwood[6]. But there exists no exact theory based upon the concept of the statistical mechanics.

On the other hand, there are a few experimental data in the literature on the behavior of the elastic moduli of solids in the neighborhood of their melting point.

Birch and Bancroft[7] reported the temperature variations of the rigidity modulus of polycrystalline Al up to 650°C i.e. 13° below the melting point.

Siegel and Cummerov[8] compared the above data with other data[9], [10], [11] such as Young's modulus of a single crystal of Pb at temperatures up to 325°C, 2° below the melting point. He stated that these data do

1) L. BRILLOUIN, *Phys. Rev.*, **54** (1938).
2) M. BORN, *Jour. Chem. Phys.*, **7** (1939).
3) R. FÜRTH, *Proc. Cambr. Phil. Soc.*, **37** (1941).
4) F. A. LINDEMANN, *Phys. Zeits.*, **11** (1910).
5) LENNARD-JONES and DEVONSHIRE, *Proc. Roy. Soc. A*, **169**, **170** (1939).
6) J. G. KIRKWOOD, *Jour. Chem. Phys.*, **9** (1941).
7) BIRCH and BANCROFT, *Jour. Chem. Phys.*, **8** (1940).
8) SIEGEL and CUMMEROV, *Jour. Chem. Phys.*, **8** (1940).
9) QUIMBY and SIEGEL, *Phys. Rev.*, **54** (1938).
10) F. C. ROSE, *Phys. Rev.*, **49** (1936).
11) M. DURAND, *Phys. Rev.*, **50** (1936).

not agree with Sutherland's curve[12] quoted by Brillouin, in which the melting temperature was assumed to be that at which the rigidity vanishes.

Hunter and Siegel[13] measured the principal elastic moduli of single crystal rods of NaCl over the temperature range from 20°C to 804°C, that is, the melting point. According to them, the shear constants C_{44} and $C_{11}-C_{12}$ decrease almost linearly with temperature, but they do not become zero at the melting point.

Kornfeld[14] has investigated the propagation of transverse vibrations in rosin for different temperatures between 20°C and 70°C. Using Maxwell's theory, Kornfeld obtained for rigidity modulus a value of the order of 10^{10} dynes/cm^2 at 20°C, which decreased by a factor of 10 as the temperature was raised to 70°C. In the case of stearin the approach to the melting point is accompanied by a catastrophic drop in rigidity modulus.

Bordoni and Nuovo[15] measured the frequency of fundamental resonance of a small cylinder by an electro-acoustic method for five metals at elevated temperatures up to the vicinity of the fusion point, and the logarithmic variation with temperature of the velocity of propagation was compared with the behavior of cubic dilatation.

Pochapsky[16),17] measured the variation of the velocity of propagation of a short train of ultra high frequency compressional acoustic waves in liquid sodium with temperature between 371°K and 545°K. He calculated the temperature coefficient of velocity and adiabatic compressibility between the aforementioned temperatures. He stated that no change in the temperature coefficient of velocity was detected in the neighborhood of the freezing point.

These experimental investigations give, however, no definite figure of the variation of elasticity in the neighborhood of the melting point and its relation to the variation of density, specific heat or other physical quantities. As for the field of seismology or the research on the constitution of the earth's interior, it is very interesting to know how the elasticity or the velocity and amplitude of elastic waves change when

12) SUTHERLAND, *Phil. Mag.*, **32** (1891).
13) HUNTER and SIEGEL, *Phys. Rev.*, **61** (1942).
14) M. O. KORNFELD, *C. R. Ac. Sci. U.R.S.S.*, **36** (1942).
15) BORDONI and NUOVO, *Ric. Sci.*, **23**, **4** (1953).
16) POCHAPSKY and QUIMBY, *Phys. Rev.*, **79** (1950).
17) T. E. POCHAPSKY, *Phys. Rev.*, **84** (1951).

the first phase transition from solid to liquid occurs.

The ultimate object of the present study is the measurement of the variation of the elastic moduli of rocks at elevated temperatures. As is well known, rocks are in general composed of glass and minerals, which in turn are solid solutions. Accordingly, phenomena of fusion of rocks is exceedingly complex. Therefore, it will be the proper course to take at first the chemical elements or binary or ternary eutectic alloy as the test materials.

As a preliminarly experiment, the present paper describes a series of experiments on the temperature variation of the velocity of ultrasonic compressional wave in Wood's metal for the range between 10°C and 90°C.

Apparatus.

The ultrasonic apparatus has been constructed for the measurement of the velocity of elastic wave in rocks. The apparatus is similar to that which has been described by Hughes *et al.*[18] The basic instrument is composed of an electronic apparatus for generating pulses and that for measuring the transmission time (Fig. 1).

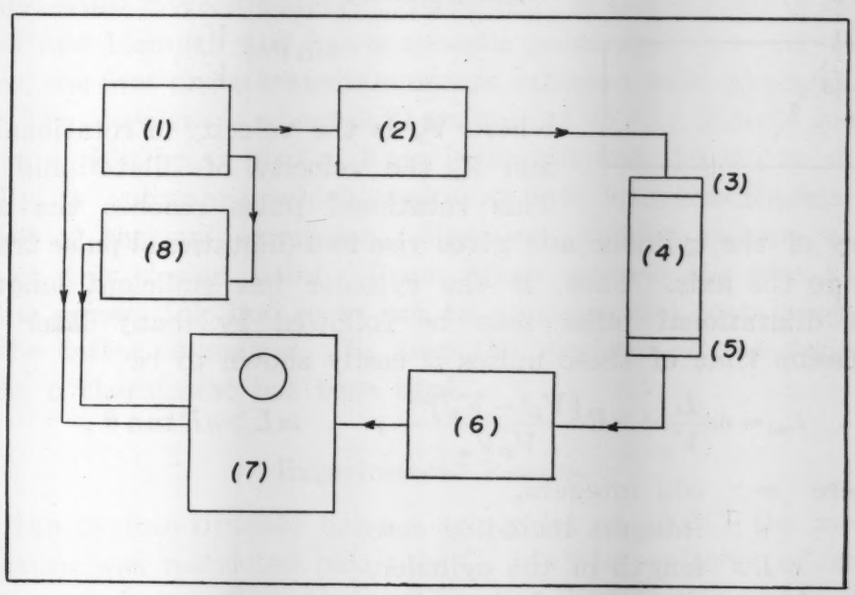

Fig. 1. Functional Diagram of the Apparatus. (1) Main trigger generator. (2) Pulse generator. (3) Driving crystal. (4) Sample. (5) Receiving crystal. (6) Video amplifier. (7) Cathode ray oscilloscope. (8) Time mark circuit.

18) HUGHES *et al.*, *Phys. Rev.*, **75** (1949), 1552–1556.

This pulse generator provides pulses with a rise time of about 0.2 microsecond. These sharp pulses are impressed on a 1 MC crystal which generates very sharp elastic pulse waves in the specimen. These waves are received at the opposite end of the specimen by a similar crystal. Although, X-cut quartz crystals are common as a driver and a receiver, 1 MC barium-titanate of 25 mm diameter was used in the present experiment. The output of the receiving crystal goes through a video-amplifier to a cathode ray oscilloscope. It is equipped with sweeps of two durations 100 and 10 microseconds. Time marks are indicated on each sweep at the interval of 1/10 sweep. Two kinds of sweeps are ultilized as follows. When the transmitted pulse appears on the screen of the oscilloscope, say, between 20 and 30 microseconds, units and fractions of the transmission time in microsecond are measured by switching the interval on the 10 microsecond sweep which has the time mark of each 1 microsecond.

Recently, Hughes and others found in their study of the velocity measurements of elastic waves that a plane dilatational pulse travelling parallel to the axis of a circular cylinder gives rise at the cylindrical boundary to rotational pulses which leave the boundary at the critical angle given by

$$\sin\theta=\frac{V_R}{V_D},$$

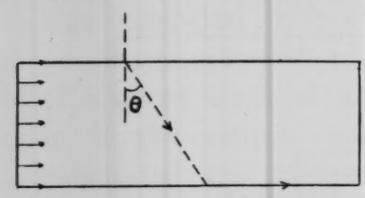

Fig. 2.

where V_R is the velocity of rotational waves and V_D the velocity of dilatational waves. This rotational pulse reaches the opposite boundary of the cylinder and gives rise to a dilatational pulse travelling parallel to the axis. Thus, if the cylinder has sufficient length, the original dilatational pulse may be followed by many later phases. Transmission time of these pulses is easily shown to be

$$t_{mn}=m\frac{L}{V_D}+nR\frac{[V_D^2-V_R^2]^{1/2}}{V_DV_R}, \qquad mL\geqslant nR\tan\theta,$$

where m : odd integers,
n : integers including zero,
L : length of the cylinder,
R : diameter of the cylinder.

For a metallic cylinder, many later phases have been observed. With rocks, however, number of later phases is rather few. In this case, the first and the second phases must be used to measure the velocity

of dilatational and rotational waves. Fig. 3 shows the example of the screen pattern of the pulse transmitted respectively through an aluminum rod and a sandstone rod.

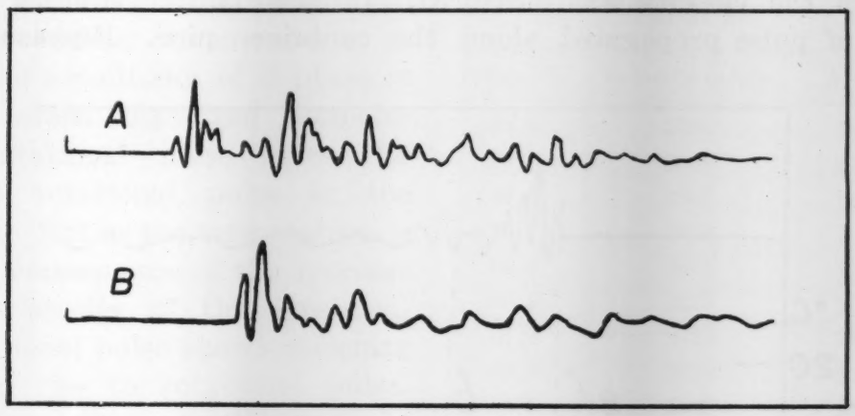

Fig. 3. Examples of the screen pattern of received pulse.
(A) Aluminum. (B) Sandstone.

Specimen Material.

As a preliminary experiment, a kind of low melting point alloy, generally called "Wood's Metal", was used. It is composed of cadmium, tin, lead and bismuth and has a eutectic point at 73°C. At this temperature, the first phase transition occurs between solid phase and liquid phase. The density is about 9.81 gr./cm^3 at 15°C. Wood's metal was casted in a thin brass pipe of 5 cm in length and 2.5 cm in diameter. Generally, a substance which melts at low temperature has a large coefficient of thermal expansion. Moreover, sudden volume expansion occurs at this fusion point. From these reasons the pipe has a cut along the generating line so as not to compress the containing sample when the latter is melted. To keep the specimen at the desired temperature, a thermostat has been used.

Experimental Results.

As the barium-titanate has a Curie point at 120°C, the measuring temperature was restricted below 90°C. As the velocity of sound in brass is much larger than that in Wood's alloy, the first arriving pulse ought to have the direct path along the environing brass pipe.

However, the amplitude of such pulse is very small compared with that of pulse propagated through the specimen material in question.

Therefore, below 60°C when the gain of amplifier is not high, the phase through brass is not distinguishable. Fig. 4 shows one of wave patterns obtained in the present experiment. Ordinate indicates the temperature at which the velocity was measured. In this figure, A-phase is the arrival of pulse propagated along the container pipe. B-phase is the

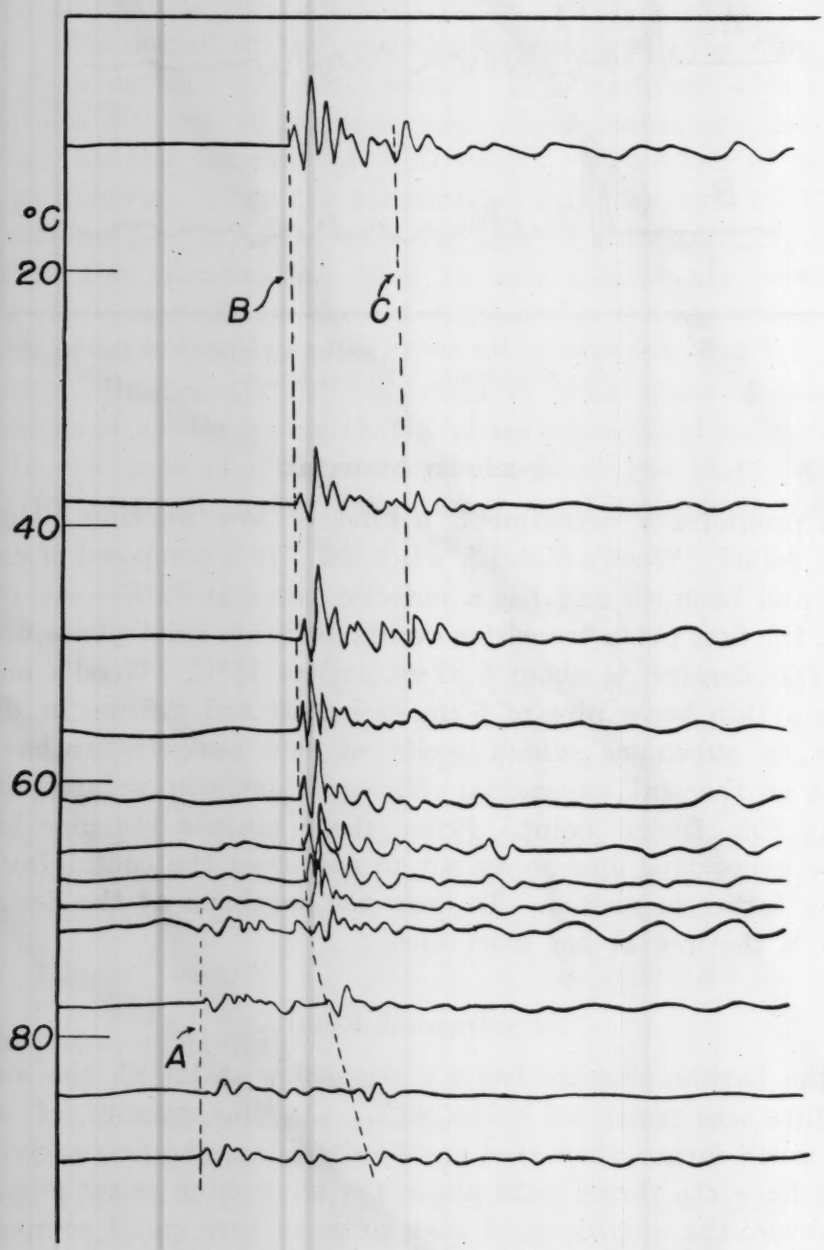

Fig. 4. Wave patterns as the function of temperature.

arrival of dilatational wave transmitted directly through the specimen material. C-phase is the second arrival of dilatational wave which was partly transmitted as rotational wave. Table I shows the tabulated values of the velocity of dilatational wave for various temperatures as well as the amplitudes of B-phase in arbitrary scale. At room temperature, dilatational pulse gives rise easily to rotational pulse at the boundary. But as the temperature is raised, in consequence of the increase of solid viscosity of the specimen, the dilatational pulse shows difficulty in giving rise to rotational pulse. Therefore, C-phase could not be detected distinctly in this experiment. This is the reason why we confine our study only to the nature of dilatational wave. Velocity of dilatational wave or amplitude versus temperature are plotted in Fig. 5 and Fig. 6 respectively.

Table I.

Temp. °C	Velocity m/sec.	Ampl.
10.0	2785	21.0
38.0	2665	21.0
48.5	2650	20.8
55.7	2620	19.0
61.5	2585	17.8
65.9	2556	16.2
67.9	2520	15.5
69.8	2510	14.8
73.5	2345	13.7
77.7	2320	9.8
84.9	2190	7.0
90.1	1953	3.5

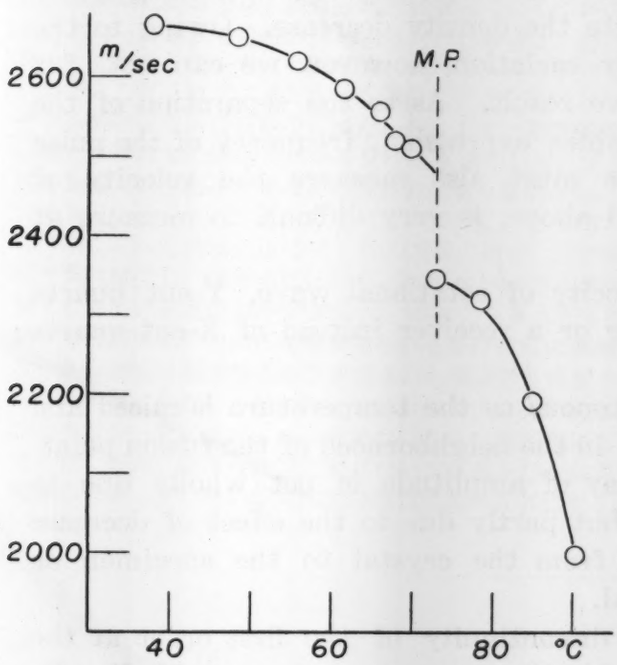

Fig. 5. Velocity of dilatational wave vs. temperature. M.P. stands for melting point.

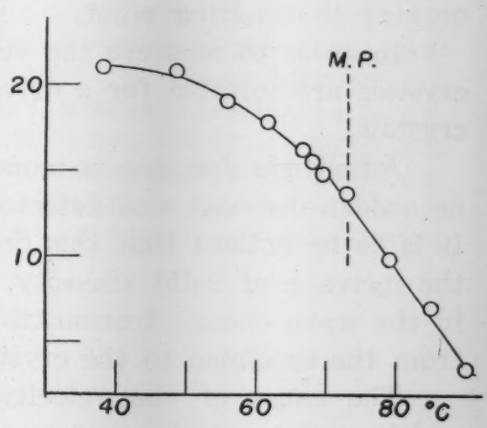

Fig. 6. Amplitude of dilatational wave vs. temperature.

Discussions.

The velocity of dilatational wave decreases continuously as the temperature is raised up to the melting point, where the velocity shows a discontinuous decrease. From the melting point up to 90°C, the velocity decreases more rapidly than at the solid state. The discontinuous jump in the velocity from 2510 m/sec. to 2345 m/sec. at the fusion point is the most conspicuous feature. As we must treat the test material as a visco-elastic medium, the velocity of dilatational wave propagated through it is given by the complex velocity. In order to calculate the complex moduli from this velocity, the density must be known at different temperatures. We could unfortunately find no data about the thermal expansion of Wood's metal nor the expansion coefficient of it. It is a fact however that Wood's metal shows a sudden remarkable volumic expansion by melting, so the density must undergo a sudden decrease. This decrease in the density must result in the increase of the propagation velocity, if the elastic modulus is unchanged. In reality, we have a very remarkable decrease in the propagation velocity of elastic waves. We can therefore conclude that the complex modulus must make a very sudden, remarkable decrease at the melting point more than enough to compensate the density decrease. Owing to the lack of numerical data of density variation, however, we can not, for the present, give any quantitative result. As to the separation of the real elastic moduli from the complex expression, frequency of the pulse wave must be changed, and we must also measure the velocity of rotational wave which, as cited above, is very difficult to measure at or near the melting point.

In order to measure the velocity of rotational wave, Y-cut quartz crystals are suitable for a driver or a receiver instead of X-cut quartz crystals.

Amplitude decrease is monotonous as the temperature is raised and no sudden decrease was detected in the neighborhood of the fusion point. It is to be noticed that this decay of amplitude is not wholly due to the increase of solid viscosity, but partly due to the effect of decrease in the wave energy transmitted from the crystal to the specimen or from the specimen to the crystal.

The cause of the velocity discontinuity of the first order at the melting point, which was detected in the present experiment with Wood's metal, will be studied in near future using more simple material such

as alkali metal, of which the density variation or other physical quantities are well known as the function of temperatures.

Acknowledgments.

The writer gratefully acknowledges his indebtedness to Prof. R. Takahasi of the Institute for his encouragement throughout this study. His thanks are also due to the members of the Radar Section of Japan Radio Company who kindly designed the electronic equipments and assisted the writer in construction of it.

---

20. 融解点附近の弾性の研究
其の一 縦波の性質

地震研究所 下 鶴 大 輔

最近の地球内部構造論に関しては，実験事実の貧困さが，その理論的発展を阻害している．特に，物質が融けた時に，その弾性的性質が，どうなるかという問題は，未だ殆んど手をつけられていない．融解点近傍までは，固有振動法に依っていくつかの研究があるが，この方法では，更に融けて液体になった後までの事が実験出来ない．著者は，岩石物性研究の超音波装置を試作し，先づその第一の実験として，岩石の融解点における弾性の研究をとり上げた．此の論文では，その研究の第一段階として，ウツド金と称する低融点合金を試料とした．実験装置の概略は，電気的なパルスをチタン酸バリウムの振動子に加え，それより，弾性縦波として試料中を通し，他端で同じく，チタン酸バリウムで，通過パルスを受けとり増巾して，ブラウン管オツシロスコープにて，その伝播時間を測定し，試料中を通る弾性縦波の速度を算出した．試料部分を恒温槽に入れ，測定温度を次第に変えてその速度の変化をしらべた．測定温度は 10°C より 90°C までであって，ウツド金の場合，73°C に共晶点(融解点)がある．此の実験の結果，次の事がわかった．即ち温度が上ると縦波の速度は次第に減少し，融解点において，2510 m/sec から 2345 m/sec へ不連続的に減少し，更に温度が高くなると，速度の減少の割合は，固体のときよりも更に著しくなる．此の様に融解点に於いて，縦波の速度に第一次の不連続が見られる事は非常に興味深い．粘弾性体として取扱わなくてはならないから速度は複素数の形で表現され，複素弾性常数を計算する為めには温度による密度変化が判らなくてはならない．然るにウツド金の場合，密度変化が不明なので，複素弾性常数を計算する事が出来なかった．故に，此の実験で得られた融解点における縦波速度の不連続の機巧を説明する為めには，是非，簡単な化学元素について実験を行う必要がある．或る種のアルカリ金属に就いては実験中であって，その結果は次の機会に述べる事にする．

---

21. *Geomagnetic Anomalies related to the Magnetization of the Basalt in the Vicinity of Gembudō.*

By Izumi YOKOYAMA,

Earthquake Research Institute.

(Read December 22, 1953.—Received June 30, 1954.)

1. Introduction.

Gembudō is a famous rocky cave for its singular sight of columnar joints, and is situated at a distance of about 110 *kilometers* north-west from Kyoto. It is one of the outcrops of the basaltic rocks which are scattered along the catchment basin of the river Maruyama. The epoch of its ejection has not been confirmed by geologists. Topographical map and geological sketch map are shown in Figs. 1 and 2 respectively.

As for the magnetization of the basalt from Gembudō, M. Matuyama has made some studies as early as in 1929[1]. He found out a magnetization almost reverse to the present geomagnetic field which attracted attention of many geophysicists. Following his pioneer works, more detailed studies are now under way at the Geophysical Institute of Tokyo University from the view-point of rockmagnetism which has remarkably developed in these several years.

In November 1953, the writer carried out a dip-survey with a miniature earth-inductor[2] in the vicinity of Gembudō to study the relation between the geomagnetic anomalies and the reverse natural remanent magnetization of the rocks.

2. Results of dip-survey and the magnetization of the basaltic rocks.

The error of each measurement in the dip-survey was about 1 *minute* of arc. The observed values are shown in Table I and Fig. 3, in which daily variation is corrected. The normal value of dip-angle for this district is about 49°30′. As seen in Fig. 3, the differences of dip-angles for various places are not large. However we can see a

1) M. MATUYAMA, *Proc. Imp. Acad. Japan*, **5** (1929), 203.
2) T. RIKITAKE, *Bull. Earthq. Res. Inst.*, **29** (1951), 147.

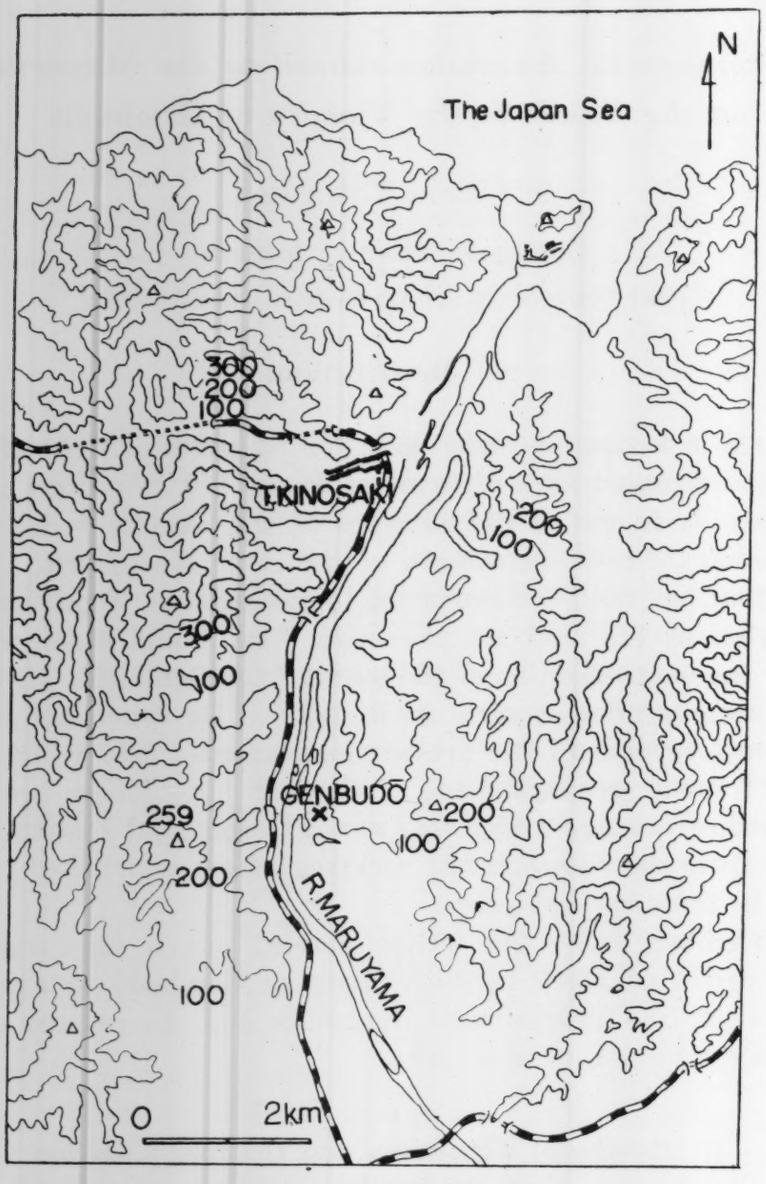

Fig. 1. Topographical map in the vicinity of Gembudō.

negative anomaly in the southern part of this region whose centre is the triangular point of which altitude is 259 *meters*.

Oriented rock samples were taken from 12 sites which are shown in Fig. 2. The columnar joints are found at the olivine basalt region in the figure. All samples were cut from these jointed basaltic rocks except samples No. 01 and No. 12 which are both augite-hypersthene

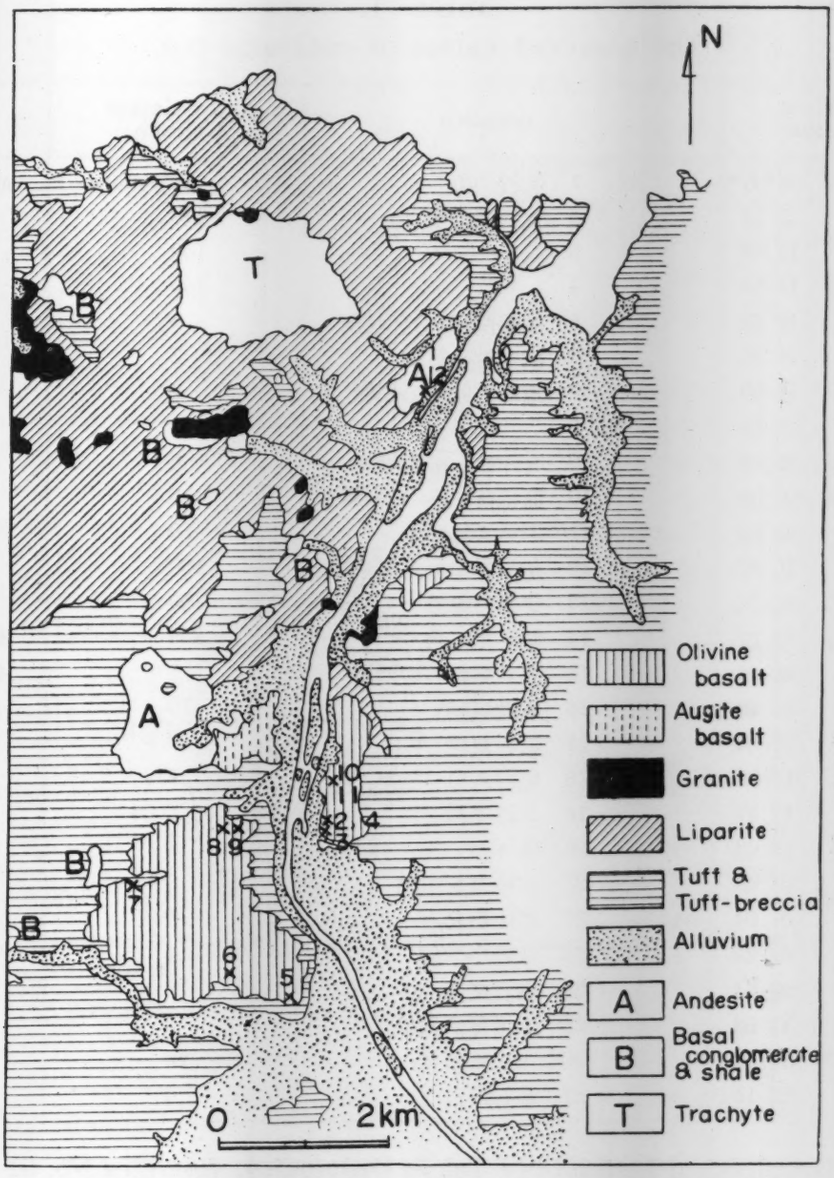

Fig. 2. Geological sketch map in the vicinity of Gembudō.
(After the Geological Institute of Kyoto University)

andesite. These rocks do not seem to be suffered from any displacements since their consolidation. The natural remanent magnetization (N.R.M.) of the samples were measured by an astatic magnetometer. The results are shown in Table II and the directions of magnetization are represented as the points in the lower hemisphere of the Schmidt's equal-area projection in Fig. 8 together with those obtained by M. Matuyama

Table I.
The observed values of magnetic dip.

Time (1953)		Locality		Approximate Altitude	Dip
Nov. 2	12^h47^m	No. 1	結村の奥	15 *meters*	49°20′
	13 15	2	玄武洞の上	140	36
	13 39	3	〃	160	21
	14 14	4	〃	150	41
	17 23	5	吊橋西口	3	19
	19 33	6	城崎町小島橋	2	27
	19 55	7	城崎町北方の川岸	2	31
	20 15	8	〃	2	38
	20 48	9	今津渡しの西岸	2	22
Nov. 3	09 08	10	滝部落	10	15
	09 59	11	不動の滝の上	90	13
	10 37	12	伊賀谷道の高原中央	160	23
	12 14	13	伊賀谷部落	90	15
	13 27	14	259 米三角点	259	48 52
	15 06	15	玄武洞渡しの西岸	5	49 13
	15 49	16	玄武洞前	10	25
	17 04	17	結村東岸	5	29
	17 25	18	結村入口	5	27
	17 47	19	戸島部落	5	23
	18 03	20	楽々浦	5	20
Nov. 4	06 45	21	城崎町新田橋	3	00
	07 04	22	城崎町北方	3	17
	09 28	23	城崎小学校	4	32
	09 54	24	来日部落	5	07
	11 03	25	上山部落入口	5	32
	11 21	26	上山部落奥	20	12
	12 15	27	赤石附近	5	18

and the Geophysical Institute of Tokyo University. Samples No. 01 and No. 12 from the northern district of Kinosaki Town are rather normal as can be seen in Fig. 8, while the other samples from the outcrops of the basaltic rocks are almost reverse to the present geomagnetic field except sample No. 06.

Taking into consideration the fact that the basalt in this district has reverse N.R.M. in general, the said negative anomaly of dip-angle seems to be caused by this anomalous magnetization. If this view-point is taken, it is likely that the basaltic rocks welled up near the 259

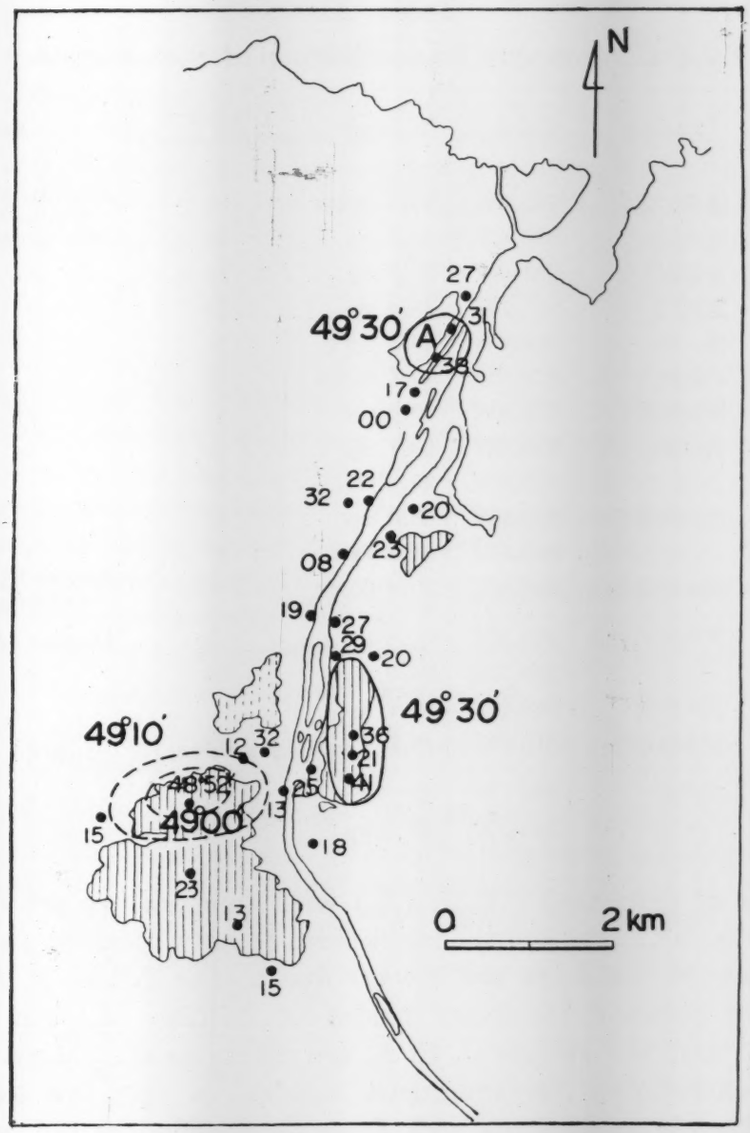

Fig. 3. Distribution of magnetic dip-angle.

meter-triangular point and flowed down to the lower regions.

The results of the experiments on the magnetic properties of the rock samples made by the Geophysical Institute of Tokyo University are shown in Figs. 9 and 10[3]. It is made clear that the reverse N.R.M. is not due to the self-reversal of thermo-remanent magnetization because

3) T. Nagata, S. Akimoto, S. Uyeda, K. Momose and E. Asami, *Tech. Comm. Palaeomagnetism*, Xth Assembly, ATME, Rome (1954), 29.

Table II.

Natural remanent magnetization of rock-samples.

Sample No.	Locality	Decli.	Dip	Intensity in 10^{-4} *emu/g*	Rock
IY 53110201	城崎町北方	N63.5W	27.3 down	7	Augite-hypersthene andesite
02	玄武洞	S36.4E	36.4 up	10	Olivine basalt
03	青竜洞	S33.0W	11.3 up	10	〃
04	玄武洞	S11.1W	24.4 up	19	〃
05	森　津	S09.6W	45.9 up	24	〃
06	不動滝	N76.9W	40.1 down	8	〃
07	伊賀谷道	S29.4W	40.8 up	4	〃
08	上山道	S09.2W	50.1 up	6	〃
09	〃	S20.6W	36.8 up	14	〃
10	玄武洞北方	S36.0W	55.0 up	17	〃
11	〃	S50.4W	37.2 up	10	〃
12	城崎町北方	S70.9W	60.6 down	1	Augite-hypersthene andesite
SA 5207282a	玄武洞入口	S19.9W	75.0 up	7	Olivine basalt
2b	〃	S20.0W	34.9 up	14	〃
03	玄武洞奥	S14.7E	34.1 up	9	〃
05	青竜洞中央	S12.7W	42.0 up	12	〃
M1	玄武洞	S30 W	49 up	16	〃
M7	〃	S44 W	57 up	57	〃

the changes of saturated T.R.M. (J_{Tc}) with temperature are normal as shown in Fig. 9[4]. Though the rocks seem to have received no geological changes, their N.R.M.s are not always due to the T.R.M. since there is no similarity between the decay modes of N.R.M. (J_n) and saturated T.R.M. (J_{Tc}) and the ratioes J_n to J_{Tc} are rather small. Moreover, Curie point of rock-forming ferromagnetic mineral is very low as shown in Fig. 10. That is to say, the rock from Gembudō does not seem to be a very reliable tool for palaeomagnetism at the present stage.

3. Conclusion.

The relation between reverse natural remanent magnetization of the rocks from Gembudō and geomagnetic anomaly in the vicinity of the place was studied. The writer could roughly determine the negative anomaly area which is closely related to the reverse N.R.M. though the

4) T. NAGATA, S. UYEDA and S. AKIMOTO, *Journ. Geomag. Geoel.*, **4** (1952), 22.

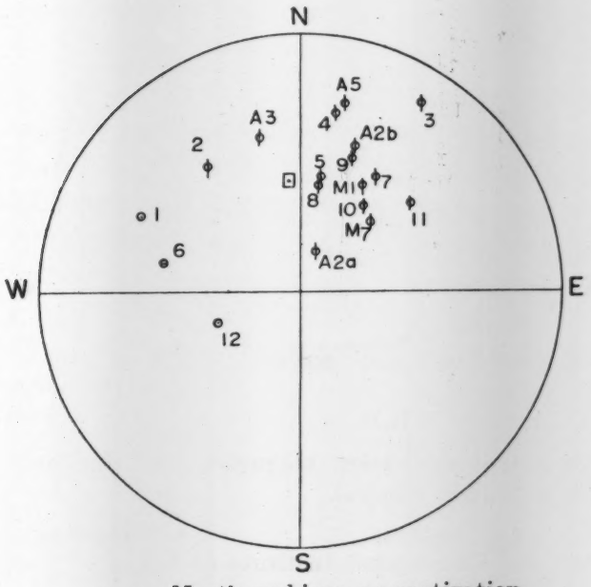

● : North-seeking magnetization

ϕ : South-seeking magnetization

⊡ : Earth's present field

Fig. 8. Equal-area plot of magnetization of rock samples.

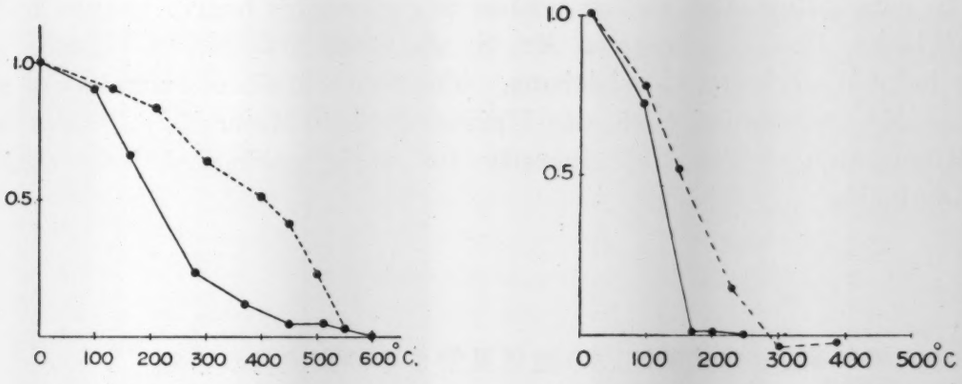

(a) Reverse N.R.M. (b) Normal N.R.M. (IY53110206)

Fig. 9. Changes of N.R.M. (J_n) and saturated T.R.M. (J_{Tc}) with temperature.
——— N.R.M. decay mode ····· T.R.M. decay mode

	J_n emu/g	J_{Tc} emu/g	J_n/J_{Tc}
a)	1.41×10^{-3}	2.76×10^{-3}	0.51
b)	1.74×10^{-3}	8.58×10^{-3}	0.20

(After the Geophysical Institute of Tokyo University)

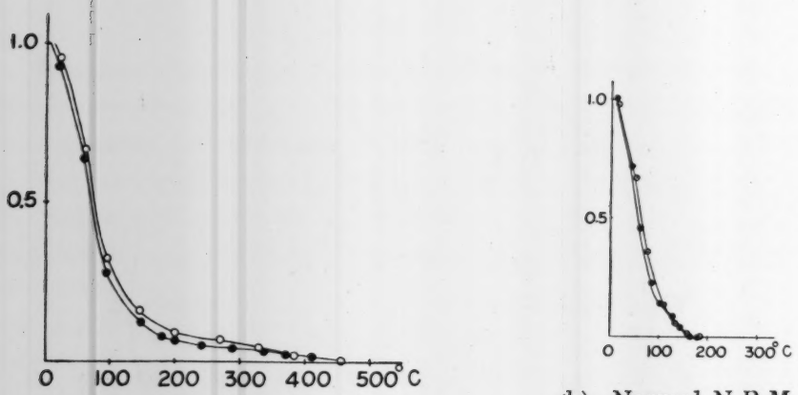

(a) Reverse N.R.M. (b) Normal N.R.M. (IY53110206)

Fig. 10. Changes of saturation magnetization (J_s) with temperature of rock-forming ferromagnetic mineral.

o : Cooling • : Heating

(After the Geophysical Institute of Tokyo University)

origin of the reverse magnetization is still not clear. From the viewpoint of palaeomagnetism, the rocks from Gembudō do not seem to be useful because their N.R.M.s are not always due to the normal thermoremanent magnetization.

In concluding, the writer wishes to express his hearty thanks to Dr. T. Rikitake, Prof. T. Nagata, Mr. S. Akimoto and Mr. S. Uyeda for their helpful advices and criticisms. The writer's sincere thanks are also due to Mr. N. Kawai of Kyoto University and Messrs. J. Ossaka and H. Mukaiyama of Tokyo University for their geological informations on Gembudō.

21. 玄武洞周辺の磁気異常とその玄武岩の帯磁

地震研究所 横山 泉

玄武洞はその柱状節理で有名であると同時に，その玄武岩の逆帯磁において顕著である．この逆帯磁に関連する磁気異常を求めるため，1953年11月，小型地磁気感応儀を用いて，玄武洞周辺の伏角測量を行った．同時に岩石試料12ケを採り，その自然残留磁気を測定した．

理学部地球物理学教室永田研究室における岩石磁気学的研究の成果を参考にすると，玄武洞の玄武岩は古地磁気学的には，必ずしも信頼し得る資料とはいえない．現在の段階においては，その逆帯磁は未解明に属するようである．

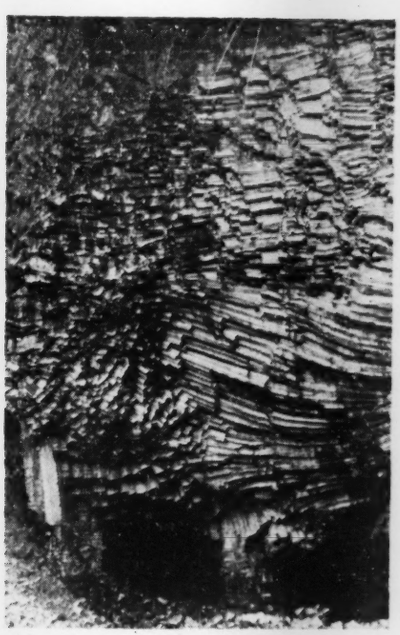

Fig. 4. The scene of Gembudō.

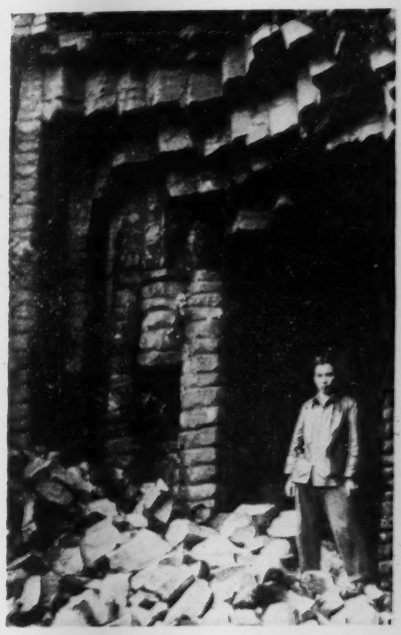

Fig. 5. The place where the rock samples No. 02 and No. 04 were taken. (Gembudō)

Fig. 6. The place where the rock sample No. 07 was taken. (Igaya)

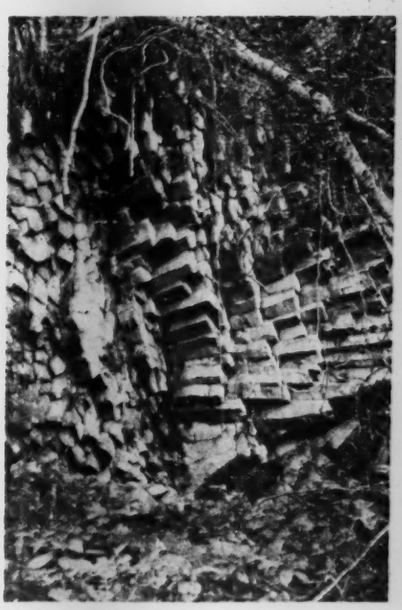

Fig. 7. The place where the rock sample No. 09 was taken. (Kamiyama)

22. *The 1950-1951 Eruptions of Mt. Mihara, Oshima Volcano, Seven Izu Islands, Japan. Part II. The 1951 eruption.*

A. Activity of the second period.

By Hiromichi TSUYA, Ryōhei MORIMOTO and Joyo OSSAKA,

Earthquake Research Institute.

(Read March 18, 1952.—Received June 30, 1954.)

VI. Temporary suspension of eruption of Mihara crater during Sept. 24, 1950—Feb. 3, 1951.

Mihara crater on the central cone (Miharayama) of Oshima volcano was active for 70 days from July to Sept. 23, 1950, without any day-long or longer break of eruption[28]. By the eruption, the crater and its central pit were filled with new lava; part of the lava ran over the crater-rim both to the north and to the northwest, flowing down to the foot of the central cone; and a cinder cone, about 50 m in height above the crater-floor, was formed outside of the former central pit and near the southern wall of the crater.

The sudden stoppage of eruption on Sept. 23, 1950, marked the end of the 1950 eruption—the first period of the present activity of the volcano. From that day on, the crater had been virtually dormant for 130 days until Feb. 4, 1951, when it began to show again signs of reopening eruption. Thus during that dormant period, there occurred neither eruptive activity nor any remarkable topographical changes in and about the crater, although both the cinder cone and the lava in the crater seemed to have subsided but slightly, though having collapsed here and there, probably due to the withdrawal of some underlying molten lava and/or shrinkage of the solidifying mass of new ejecta (Figs. 62, 63). Some fume or misty vapour was occasionally visible rising through several fissures in the cinder cone, and about the middle of October there remained still visible glow from cracks in the lava at

28) H. TSUYA, R. MORIMOTO and J. OSSAKA, "The 1950-1951 Eruptions of Mt. Mihara, Oshima Volcano, Seven Izu Islands, Japan. Part I. The 1950 eruption," *Bull. Earthq. Res. Inst.*, **32** (1954), 35–66.

a few spots near Kakôjaya (tea-house on the crater-rim). On Jan. 10, 1951, according to S. Watanabe, a photographer of Motomura village, the cinder cone was found to have been cut by several large fissures at the summit and on measuring was found to have depressed more than 1 m. White vapours were issuing, continually and vigorously, through some of the fissures and from the summit bowl-shaped depression (1950 explosive vent) of the cone. However, the general feature of Mihara crater at that time remained nearly the same as that observed immediately after the 1950 eruption stopped.

During the remainder of January and in the first three days of February, the crater maintained again its quiescence as before, displaying nothing worth special mentioning, although steaming of the cinder cone was rather continuous with the rise and fall of its intensity. Neither volcanic earthquakes nor tremors were recorded on the seismographs at the Oshima Meteorological Observatory[29]. Thus there had been no forewarning of the coming danger, even within a few hours just before the 1951 eruption began on Feb. 4.

From Feb. 4 on, the volcano had been in a state of eruptive activity for 148 days, until June 28, 1951, when it finished once again its apparent surface activity. The first half (Feb. 4–April 1) of this activity was an almost continuous eruption attaining its height towards the end of March, while the next half (April 2–June 28) was characterized by recurrence of rather short-lived eruptions with intervening quiet phases. Preceded by the 1950 eruption as the first period and rising phase of the 1950–1951 activity, the former represented the second period and the peak of the activity, and the latter, the third period and declining phase.

VII. Course of the eruption in the second period.

(1) *Opening of the 1951 eruption, Feb. 4, 1951:*

On Feb. 4, 1951, the cinder cone in Mihara crater was steaming all day as usual, not only from its summit crater but from fissures in its outer slopes. Thus white vapour was rising most actively from three radial fissures that ran through the western slope of the cinder cone all the way up to the point where they joined some concentric steaming fissures on its summit crater-rim. Two of the radial fissures, lying about 20 m apart, were trending northwest toward the base of the

29) Y. KIZAWA, "Volcanic tremor," *Jour. Geogr.*, **60** (1951), 28.

cinder cone (Fig. 67).

At about 12 h 40 m, Feb. 4, 1951, following small explosions with a little black ash-cloud, red-hot lava began to be ejected from a vent (a), about 1 m in diameter, newly opened on one of fissures in the 1950 lava adjoining the northwest base of the cinder cone (Figs. 64, 65). Ejection of fragmentary red-hot lava, up to a height of about 100 m in the air, was repeated every two to three minutes, continuing at each time for several minutes, accompanied with loud detonation. The solidified 1950 lava, adjacent to the new vent, was moving up and down, probably owing to pressure of the gases rising from below to be discharged explosively through the vent. At the same time, continuous rocking of the ground was felt distinctly at a distance of about 100 m from the vent, on the crest of western rim of Mihara crater. The vent (a) had stopped its activity within 24 hours without forming any large heap of cinder and/or spattery ejecta around it, although the activity opened the way for more spectacular ones at several adjoining vents, which followed in succession soon afterwards.

(2) *Activity of spatter cones at the western foot of the cinder cone, Feb. 5–19:*

Early in the morning of Feb. 5, adjoining to the south of vent (a), a new vent (b in Fig. 67) was opened to eject red-hot lava in the same way as displayed at the preceding vent. The same day, at about 16 h, a similar ejection of red-hot lava started at another new vent (c in Fig. 67) situated several meters away to the southeast of the vent (b). From that time on, these two vents (b and c) were almost continually active side by side, but without any sympathetic rise and fall of their activities. On Feb. 6, at 15 h, the vent (b) was found to have grown into a spatter cone, about 5 m in relative height, while the vent (c) still remained as it was in the preceding day, without being surrounded by conical heap of spattery ejecta. With an intermission of less than one minute, a detonation lasting for 4 to 5 minutes was being repeated, and at the same time fragments of red-hot lava were being thrown up to a height of about 30 m in the air.

On Feb. 7, at 10 h 30 m, two active vents (b and c) were displaying ejection of red-hot lava as before, and sending forth white vapours in addition. A hissing noise like that caused by a flying cannon-ball was heard almost continuously, but with a short intermission at intervals of 4 to 5 minutes. Besides, about that time, considerable white

vapours were visible rising along several cracks in the 1950 lava about the active vents, and also at a few sunken areas south and southeast, on the western foot of the main cinder cone (Figs. 66, 68).

On Feb. 9, at 10 h 50 m, one of the active vents (c) was found to have grown into a spatter cone, about 5 m in relative height, and was ejecting lava spatter side by side with the other vent (b). Emission of a bluish fume was being accompanied with an almost continuous hissing noise. But they became feeble or stopped while the lava spattering was going on. Two days later, explosions were heard, together with puffs, almost continuously from early morning to evening hours and with increasing intensity, even at Goshinka-jaya (tea-house) on the somma. The spatter heaps at b and c had extended largely so that their skirts joined with each other. One vent (c), a few meters in diameter, was ejecting lava fragments from two spots in it, to a height of more than 100 m in the air, while the other (b) was at a standstill, but glowing inside. The neighbouring sunken areas that had been steaming vigorously for the preceding few days were visible without sending forth vapour clouds so thick as to veil themselves. One of them, situated about 100 m south of the vent (c), was circular in its outline with a diameter of about 50 m, standing out clear with white and yellowish patches of incrustation due to some solfataric action, and having a glowing spot in its central part. Between the said area and the vent (c), and adjacent to the west foot of the main cinder cone, there was another sunken area wherein a little red-hot lava was exposed.

On Feb. 13, about 13 h, red-hot lava began to gush from a new vent (d in Fig. 69) in one of the above-mentioned sunken areas, and about an hour later, the lava was flowing northwards along the western wall of the Mihara crater, after having spread over the area about the new vent. In the vent was a red-hot lava pool, about 20 m in diameter, surging incessantly and displaying explosive fountainings at intervals of several minutes, by which spattery lava fragments were thrown up to a height of about 100 m in the air. About that time, the vents (b) and (c) continued to be active in building their respective cones with spattery ejecta, and the sunken area southeast of the vent (c) seemed to have a red-hot lava pool, about 30 m in diameter.

Lava outflowing from the vent (d) had already stopped early in the next morning, whereas explosive lava fountainings at the same vent lasted for several days. Thus on Feb. 15, at 11 h, the fountaining

activity was in progress at the vent (d), which had been surrounded with its own-building spatter cone, about 10 m in height and 40 m in diameter at the base. The neighbouring vents (b) and (c) also continued to spatter red-hot lava, although their activities were far less in intensity than that at the vent (d). The spatter cones at (b) and (c) were measured respectively 8 m and 11 m high, and 35 m across at their combined basal part. In the sunken area southeast of the vent (c), there were two glowing spots, and faint bluish fume was rising from the ground thereabout. Soon after these two glowing spots became active in succession, forming separate vents (e and f in Figs. 70, 71) that displayed lava spatterings side by side. Thus on Feb. 17, at 12 h 30 m, these two vents continued to spatter red-hot lava, each being surrounded with its own spatter cone, about 5 m in height. At that time the neighbouring three vents (b, c and d) were also actively piling their spattery ejecta higher and higher around them.

For the next two days, Feb. 18–19, the five vents (b, c, d, e and f) were active, every one of them, vying with one another in making flings of spattery red-hot lava, together with detonations accompanied by puffs of blue gas. The lava spatterings and detonations were going on almost continuously at b and e, while they occurred about every two minutes at d and f. On Feb. 19, at 10 h 30 m, the spatter cones b—f measured 20 m, 20 m, 30 m, 10 m and 8 m in height respectively, and the lava spatterings that were still going on, were some 50 m, 30 m, 150 m, 100 m and 20 m in height above their respective vents. With the simultaneous lava spatterings on that day as a climax, these vents declined in activity rapidly afterwards. Thus on Feb. 21, at 11 h, three (c, d and f) of the five vents were found to have already stopped their lava spattering activity, although the rest (b and e) still remained active with some lava spatterings continuing until the beginning of the next month.

(3) Revival of eruption of the 1950 cinder cone, Feb. 20, 1951:

While the lava spattering activity was spreading among the six vents (a—f) as mentioned above, both fissuring accompanied by local collapse and emission of whitish vapour-clouds on the 1950 cinder cone were being increased remarkably. In the afternoon of Feb. 6, S. Watanabe went to the summit of the cone on the southern rim of its crater-bowl; no further sign of activity of the crater could be detected, except voluminous liberation of whitish vapours, although the cone was still very hot only a few centimeters beneath its surface, even on its

outer slope, and there were several fissures glowing inside. There was steam on the outer slopes of the cone and inner walls of its crater-bowl, and lines of vapour vents could be followed all way up the western slope, which might represent upright fissures in the cone. There were also several steam lines parallel with the rim of the crater, which marked concentric fissures in the cone (Figs. 65, 67).

The steaming activity of the cone increased in intensity day by day, but there was sometimes apparent lull in the activity as on Feb. 9, when only a faint blue fume could be seen rising on the cone.

On Feb. 9, the cone was found to have settled remarkably in its western sector between two steaming fissures extending from near the crater-rim half way down the outer slope. Within sunken area and half way down the western slope of the cone, there had developed a bowl-shaped opening, about 30 m in diameter, whence steam could be seen rising in quantity on Feb. 13. This new opening on the cone had gradually been enlarged and deepened by slumping of its walls and possibly by steam blasts. On Feb. 17, it had grown into a crateriform depression vomiting whitish vapour-clouds (Fig. 70).

A new feature on the cinder cone, as observed on Feb. 20, was a black ash-cloud rising from an explosive vent, a few meters in diameter, that newly opened on that day close to the down-slope side of the above-mentioned depression on the western slope of the cone (vent 1, Fig. 73). The next day, bombs of red-hot lava was being ejected in succession from the new vent, together with black ash-clouds. This was the first time after the early days in the second period of activity that the ejection of red-hot lava had come into play from a vent on the 1950 cone.

On Feb. 23, at 15 h 30 m, heavy volumes of black ash-clouds were rising from the Feb. 20 vent, while red-hot bombs were being ejected from another new vent (vent 2, Fig. 73), several meters in diameter, that had been opened close to the downhill side of the preceding one. At the same time the first depression on the northwest side of the top of the cone had grown into a new crater. Thus having been enlarged and deepened markedly since the beginning of collapse about Feb. 11, it took the form of a circular crater several scores of meters across, with its southeast rim close to the northwest rim of the 1950 crater of the cone (vent 3, Fig. 73). Vapour clouds were rising from both old and new craters. It was evident that the new crater was being extended by fissuring and slumping of loose ejecta on the surrounding walls.

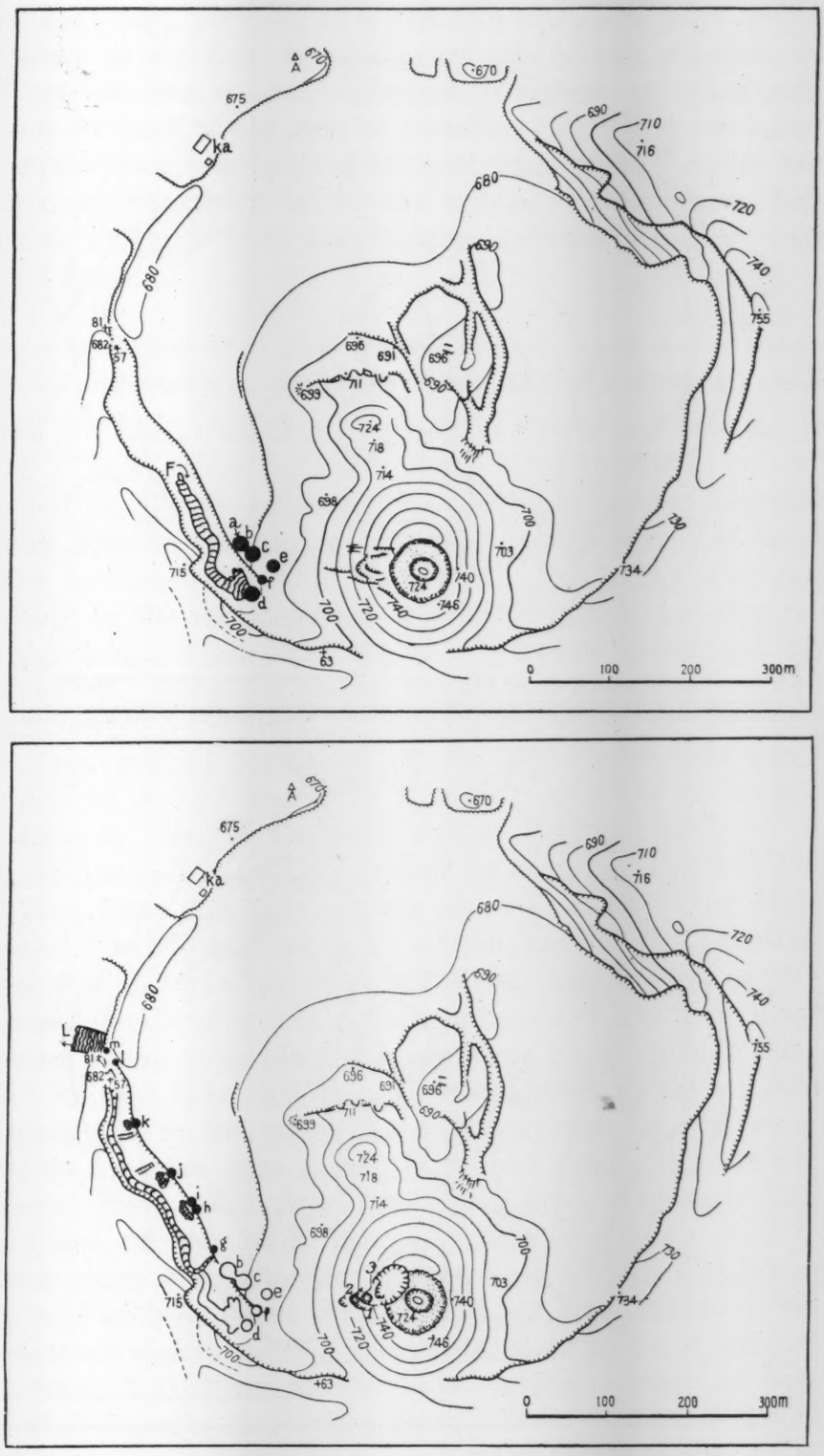

Fig. 72. Map of Mihara crater.

a) Showing new spatter cones (b—f).

b) Showing new spatter cones (g—l) and new vents (1—3) on the main cinder cone.

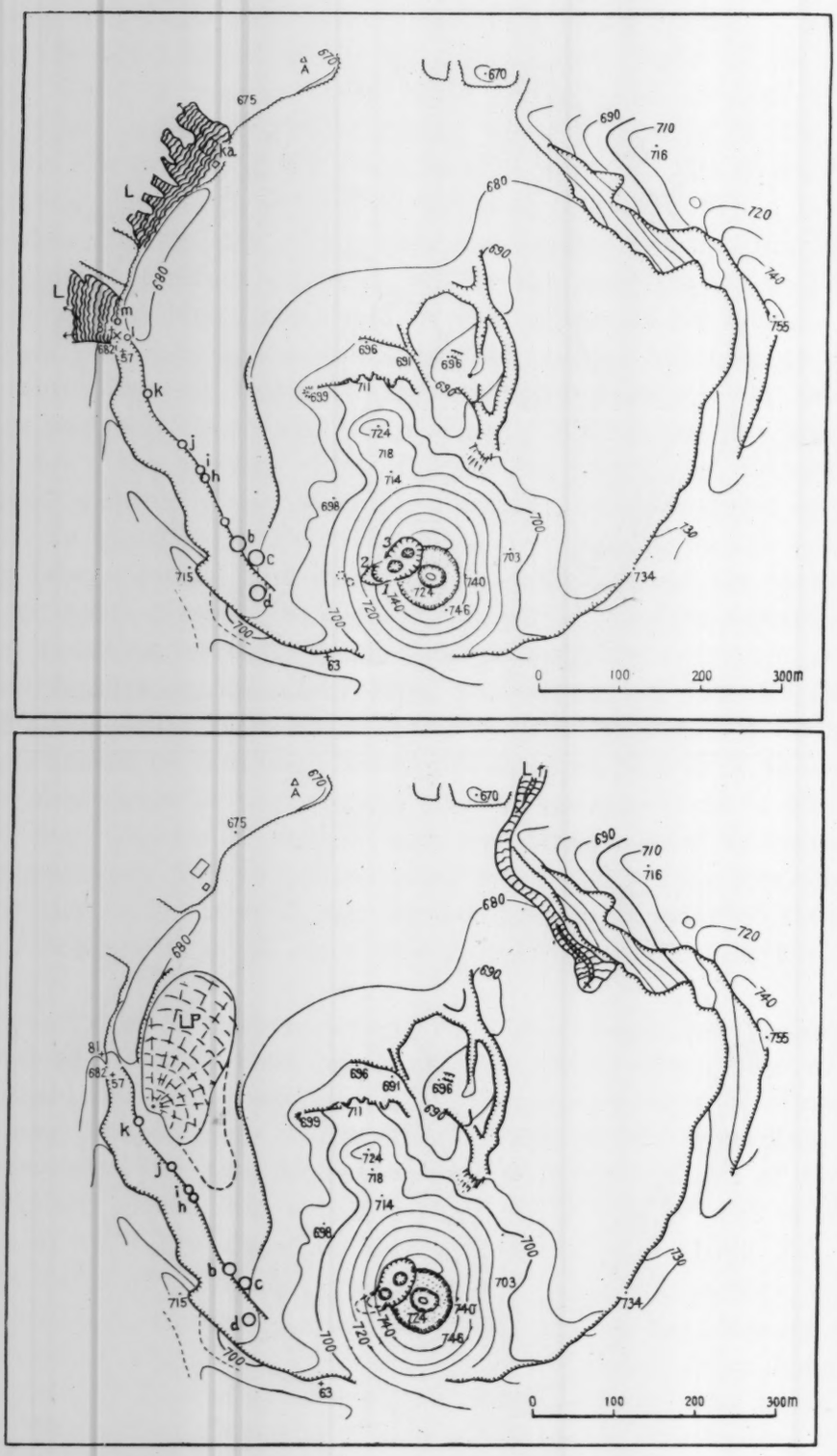

Fig. 73. Map of Mihara crater.
Showing development of new vents on the main cinder cone.

The next day, between 13 h and 16 h 40 m, explosive eruption was taking place at the Feb. 23 vent every one or two minutes, with ejection of red-hot bombs and occasional spoutings of black ash clouds. For the most part of the rest of February, an almost incessant activity of the cinder cone was notified by explosions so loud as to be audible every several minutes even at the village of Motomura, but it was visible only at times from Goshinkajaya because of cloudy weather with occasional rains.

(4) *Appearance of a line of new spatter cones, and upheaval of the inside of Mihara crater, late in February, 1951:*

Since the beginning of the present activity on Feb. 4, 1951, the inside of Mihara crater had been rising little by little, but with some intervening small halt and subsidence, as confirmed by observing several landmarks both on the top of the 1950 cinder cone and on the 1950 lava-flows accumulated within the crater. The rising was remarkable particularly in the northwestern half of the crater including the central mound that had been thrusted out of the former central pit during the 1950 eruptions. Thus the central mound and the vicinity were observed to have upheaved 5–6 meters by the end of February. Besides, on Feb. 23, the lava ground northwest of the 1950 cinder cone was found to have upheaved several meters in a night, covering an area of about 150 m × 50 m in front of the west wall of Mihara crater.

On the just-mentioned lava ground, prior to its remarkable upheaval, a faint blue fume was seen already about Feb. 17, rising from a small area, about 1 m in diameter, with whitish and yellowish coatings. Since then, the fuming area had been spreading day by day until Feb. 23 when, immediately after the sudden upheaval of the lava ground, blue fumes were rising with hissing noises from many spots on the upheaved ground. By that time this ground was traversed by several large cracks opened deep due to its upheaval, and moreover its surface part was broken into countless lava pieces, large and small, to form an impassable chaotic mass. Blue fume was rising most vigorously from several spots on one of the large cracks, which run from near the aforementioned group of spatter cones northwestward for a distance of about 500 m. And at last, about Feb. 25, red-hot lava began to be thrown out as spattery ejecta from a fuming spot near the southeastern end of that crack, and a new spatter cone, several meters in height, was formed at the spot a short time later. From then onward lava ejection

spread rapidly all along the same crack, and on March 2 there developed six new spatter cones forming a line along the crack (g, h, i, j, k and l in Fig. 72 b).

(5) *Lava overflowing onto the western flank of Mt. Mihara, Feb. 28, 1951:*

The proceeding of the activity of Mihara crater in February suggests that, after travelling a long way upward through the permanent lava-conduit underneath the volcano, a molten lava again came up to the crater bottom, intruding in sequence into different parts of the crater filling. Thus the molten lava approached the ground in succession: first in a small area including the spatter cones (b)—(f); second on the western flank of the cinder cone; and third in the northwestern part of the crater, particularly along a fissure by the SE.-NW. line of spatter cones (g)—(l). As the activity continued, the inside of the crater was subject to a differential upheaval, suggesting that intrusions were going on within the heap of ejecta filling the crater, forcibly but with different rates of progress in different parts of the crater. The molten lava which intruded must have had an unconquerable gas potential actuating it, and consequently, upon approaching the surface of the ground, it caused an explosive liberation of gases, resulting in eruptions of red-hot lava breaking through different parts of the ground as already described. But, for three weeks after the present activity began on Feb. 4, 1951, the eruptions were no more than almost incessant spatterings of red-hot lava accompanied by occasional puffings of black ash-clouds, with the exception of a small lava-flow brought by the fountaining activity at the vent (d) on Feb. 13.

It was on Feb. 28 that the 1951 lava overflowed for the first time the northwestern rim of Mihara crater and descended the western flank of Mt. Mihara onto the sandy flat called Sabaku (desert)—part of the atrio between the somma and the central cone (Mt. Mihara). Thus, according to I. Takagi, a member of the family who manages the Goshinkajaya rest house, this day about 1 h, a red-hot lava was observed from his house, descending the western steep slope of Mt. Mihara in a cascade of fire along the margin of the southernmost of the 1950 lava-flows. The same day, at 11 h, the new lava was found to have reached the flat of Sabaku, a distance of more than 1 km from its source, forming a narrow stream, a few meters in width, on the steep slope of Mt. Mihara, and spreading out as a broader fan over the flat of Sabaku.

The lava front, which showed the form of a levee about 1.3 m high, was still creeping ahead sluggishly with a rattling noise made by *aa* blocks tumbling down from the front as it advanced.

The lava did not come directly as a surface flow neither from the 1950 cinder cone nor from any one of the spatter cones on the floor of Mihara crater, but it issued from a new vent opened in the pile of 1950 lava on the northwestern rim of the crater, just at the northwestern end of the fissure on which several spatter cones (g—l) were being formed. It must have been fed by a molten lava that moved sideways from the inside of the crater through the said fissure beneath the surface. Possibly about that time, lava stood molten in the fissure at levels high enough to permit spatter ejection on the one hand, and outflowing in a red-hot fluidal state on the other.

For more than a month after its start on Feb. 28, the lava outflowing went on with increasing intensity, and in the latter half of March it showed itself as the climax of the present activity, together with the concurrent Strombolian eruptions on the 1950 cinder cone.

(6) *Climax of the present activity, March, 1951:*

i) Activity of spatter cones: Early in March, lava spatterings were in progress to build up several spatter cones in the line of activity (g—l, Fig. 74) that had developed late in the preceding month along the crack about 500 m long, trending southeast-northwest across the upheaved lava floor in the northwestern part of Mihara crater. Besides the active vents with growing spatter cones, there had developed a number of fuming (or steaming) spots in the same line of activity, where the rock was covered with whitish and yellowish coatings. The spatter cones were very changeable in activity without any sympathetic or antipathetic relation between them. Thus on March 4, of the three spatter cones (i), (j) and (k), all of which towered far above the rest, with a height of 5 m or so, the last one was throwing out spatters of red-hot lava every three minutes to a height of several meters in the air, while the other two were sending out white vapours only without regard to their vents glowing inside; on March 6, the spatter cone (k) displayed neither lava spattering nor steaming, whereas (i) and (j) were in the midst of their lava spatterings side by side, and (j) was spilling small lava-flows from its side openings (Fig. 75). But the line of activity appeared to be most active as a whole on March 7, when lava spatterings were going on side by side on the four spatter cones (i, j,

k and l), besides lava squirtings in the form of a small river of fire from a vent adjacent to (g). The same day, at 20 h, incandescent lava from this vent was seen flowing with a velocity of about 0.5 m/sec, at first to the west for a distance of about 50 m, then to the north for a distance of about 300 m along the western wall of Mihara crater (Fig. 76).

The lava floor on both sides of the just-mentioned line of activity had been upheaved several meters in the few days before March 10, together with the adjoining central upthrusted mound[30]. But after March 11, these parts showed a tendency to depress, and at the same time, lava spatterings and other activities in that line of activity also dwindled rapidly. Thus on March 16, when one of the writers (Tsuya) visited the volcano, lava spatterings were found to have stopped at all the vents in the line of activity but two (h and i), which were ejecting a few blocks of red-hot lava every several minutes; blue fumes were rising from (j) and (k) with loud hissing noises; and only heat was noticeable at (l) and (m). At that time these last two were forming chimney-shaped spiracles a few meters high, surrounded with agglutinated spattery ejecta, while each of the other four vents (h, i, j and k) was atop a beehive cone about 10 m high, built up with agglutinated spattery ejecta and partly covered by small aprons of lava-flows (Figs. 77, 78). The southeasternmost vent (g) seemed to have disappeared in the heap of later ejecta from neighbouring vents. On the other hand, in the older group of vents adjacent to the west of the 1950 cinder cone, the twin spatter cones (b and c) were ejecting only one or two blocks of red-hot lava at a time but spasmodically, and the spatter cone (d), the largest of all, had a crateriform vent at its top, whence a bluish flame of burning gases was rising like a torchlight, with intervening spasmodical ejections of a few red-hot lava blocks. Covered with cinders ejected from the 1950 cone, these older spatter cones were about 30 m in height, whereas the rest in the same group (e and f) had vanished from sight.

ii) Activity of the main cinder cone: The explosive eruption of the 1950 cone, which was resumed in February at two vents on its northwestern side, became more spectacular in the next month. Thus, on March 2, after having been shrouded by thick rainy cloud throughout Feb. 28 and March 1, the cone was seen displaying explosive ejections

30) Cf. Figs. 31 and 61 of our previous paper (H. TSUYA, R. MORIMOTO & J. OSSAKA, *ibid.* p. 44.).

of red-hot lava from the two side vents (Feb. 20 and Feb. 23 vents), at intervals of about thirty seconds and occasionally accompanied with puffings of black ash-cloud. Close to the downslope side of the Feb. 23 vent there had developed two other vents, one inactive and the other issuing steam, whose exact date of birth was quite unknown.

The vents on the northwest side of the cone subsided virtually within the first ten days of March and all activity became centred in the summit depression afterwards, which had become enlarged by the slumping and fissuring of the surrounding walls. Thus, on March 16, the summit depression was found to have become a new crater consisting of two active vents linked with each other. The crater formed a circular funnel, about 80 m in diameter at the upper rim and more than 30 m in depth, encircled with steeply sloping walls on all sides but the west where it opened to the much shallower hollow of one of the formerly active side vents. With a low-pitched detonation, the crater bursted into a spectacular eruption repeatedly : one (west vent) of the two active vents in the crater belched a jet of fire carrying cinders and bombs of red-hot lava, at intervals of four to five seconds; and the other (east vent) sent up puffs of black ash-cloud only at a little longer but irregular intervals (Figs. 79, 80). During a spasm of the eruption red-hot bombs were being thrown into the air up to a height of about 200 m above the top of the cone. Observations from the west rim of Mihara crater, at a point about 300 m west of the centre of activity, showed that most of the flings were getting back into the crater from where they came, and only a few were falling outside the crater and rolling down the slopes of the cone. During the flight through the air, bombs generally followed towering parabolic trajectories, high and low, except those which shot straight upward above the crater (Figs. 81–84). But there were occasionally observed some lava clots taking irregular, wavy paths, and seemingly floating to flutter like burning paper. Larger bombs made a whirring noise by friction with the air while flying through it, and also made a pounding noise as they flopped down on the ground. None of the flings, however, reached to the observation point, because at that time explosions were not forcible enough and the wind was from the southwest, carrying smaller flings (cinders and ashes) to the leeward (northwest) side of the cone. Therefore, nothing dangerous was met during the half-day's stay as that point for observing the eruption, although harmonic tremors of the ground, which were felt just like the roll and pitch of a boat,

were strong enough to cause a little uneasiness to the observers on the scene, together with the larger shocks felt at times but usually in company with the explosions.

The explosive activity of the cinder cone, pulsating in character, continued until about March 25, with little change except the particularly heavy explosions in the afternoon of March 20, which were accompanied with spatterings of lava clots, more than 1 m in diameter, up to the height of about 100 m in the air and at the rate of ten times a minute.

From March 25 on throughout the rest of the month, the cinder cone became less active, the major portion of its activity being explosive puffings of black ash-cloud and continual emission of white vapor-cloud. On March 31, only white vapours were seen rising from the cone, in company with light explosions, at intervals of several seconds. Thus the most thriving activity of the cinder cone seemed to have come to an end by March 25, after continuing for about two weeks from March 10. At the village of Motomura, during this period, explosions were not only heard but also frequently notified by rattlings of doors, casements, etc; spectacular glowing cloud effects over the mountain could be seen occasionally at night, with the glow waxing and waning; and observation from sea in a starlit night showed red-hot bombs being shot up like hundreds of shooting stars.

iii) West lava-flows: The lava outflows on the outside of Mihara crater, which started on Feb. 28, went on rather steadily throughout the next month, but with occasional changes of its source (Fig. 85). On March 2, at 17 h, red-hot, fluidal lava was spurting out of a vent in the solidified lava, situated just inside the northwestern rim of Mihara crater, and it was pouring away in torrents down the mountain slope (Fig. 85). Thus, advancing downwards as well as sidewise, the new flood of lava was being enlarged on the western steep slope of Mt. Mihara (central cone) and the adjoining flat of Sabaku, besides flowing over the older still-moving flows (Fig. 87, 88). On March 6 and 7, lava was issuing not only from a vent in the edge of the already-solidified lava on the northwestern rim of Mihara crater, but also from two or three holes in the fresh flows halfway down the steep outer slope (Figs. 89, 90).

The Mihara Shrine, a stone building a few meters high situated at the western base of Mt. Mihara, was buried underneath the flood of advancing lava on March 9 (Fig. 87, 120). The same day, at 16 h 10 m,

Kakôjaya (tea-house) on the north-northwestern rim of Mihara crater was also destroyed by a new lava-flow whose front by that time was about to run over the crater-rim at the south of the house. On March 10, at 5 h 30 m, this new flow was found to have advanced downhill just north of the 1950 west flow (Nomashi lavas shown in Fig. 30) and partly overlapping it. Thus, by that time, the flow had spread out as a broad fan over the flat sandy terrain (Sabaku) adjacent to the northwest base of Mt. Mihara and only a few hundreds of metre distant from Goshinkajaya (tea-house) on the northwestern caldera-rim; its farthest front had reached a distance of about 1200 m from the rim of Mihara crater, and the front was still moving forward at the rate of 0.5 m per minute. On March 12 the new lava flow on the north side of the 1950 west flow was found to have coalesced with the flow on the south side at their fronts, with several islands of the 1950 flow left uncovered between them.

From then on, during the two weeks to March 25, lava flows continued to pour out of temporary, changeable vents in the older already-solidified lava either on the crater-rim or on the steep outer slope of the mountain, and run downhill either in two or three separate torrents or as braided, branching streams, and spread over the flat ground of Sabaku. One of more thriving and long-lived flows in that period was that which on March 17–18 was seen running down along the south margin of the already-solidified flows on the western slope of the mountain. The main source of the flow was on the northwestern rim of Mihara crater, near the northwestern end of the previously-mentioned line of spatter cones, where brilliant golden-yellow molten lava was welling out continuously and silently from an opening, about 0.5 m in diameter, in the solid crust of an older flow (Fig. 92). After crawling once under the solid crust and passing through a tunnel about 20 m long, the molten lava again welled out of another opening at the lower end of the tunnel to flow downhill in a single stream (Figs. 93, 94). Moreover, in the evening hours of March 17, molten lava was seen gushing out of the side opening (grotto) on a small lava-cone, about 2 m in height and situated on the steep slope at a short distance north of the last-mentioned lava source, and flowing in torrents into the main lava stream in question (Figs. 91, 100). The lava-cone seemed to be a lump of lava which, upon reaching this point as a surface flow or through a tunnel, had been prevented temporarily from further flowing downhill by some obstacles.

Table XII. Temperatures of the 1951 flows.*

Date	Lava temp. (°C)	Locality
March 16	800	Loc. a, on the NW. slope, outside of Mihara crater.
March 21	850	Loc. b, south of the source vent of the west flows, on the NW. crater rim.
〃 〃	1120	Loc. c, in a crack on the lava flow, 130 m SE. of loc. b.
〃 〃	850	Loc. d, south side of one of the west flows on the NW. slope.
〃 〃	850	Loc. e, lateral front of one of the west flows, below the NW. caldera wall, 150 m north of the passage to Nomashi village.
March 22	1000	Loc. f, the farthest front of the west flows, 300 m NE. of Goshinka-jaya.
〃 〃	980	Loc. g, ditto.
〃 〃	1050	Loc. h_1, ditto.
〃 〃	1050	Loc. h_2, ditto.

* Observed by J. Ossaka and others[31], by means of an optical pyrometer. Localities are shown in Fig. 120.

Table XIII. Hourly rates of advance of the lava fronts.*

Date	Rate of advance, m/hr	Locality
March 16	3	Loc. x, the farthest front of the west flows, 95 m E. of the passage to Nomashi village.
March 19	6	Loc. y, immediately below the caldera wall at Goshinka-jaya.
March 22	3	Loc. z, the farthest front of the west flows, 300 m NE. of Goshinka-jaya.
〃 〃	2 (m/day)	Loc. w, lateral front of one of the west flows, 150 m N. of the passage to Nomashi village.

* Observed by J. Ossaka and others[31]. Localities are shown in Fig. 120.

31) In this matter, the writers owe much to Messrs. S. ÔYA, S. HADA, K. ISA, N. OGUSHI, S. SAKURAI, H. OBA, K. ONO, F. KINOSHITA and K. GOTÔ of the Geological Institute of our University.

The just-mentioned flow of glowing lava was running in rather straight stream like a moving belt-conveyor or escalator, with a velocity of about 0.5 m per second on the steep slope (25° or so) near its source. It was about one metre wide, becoming wider farther down the slope and exhibiting a widening into delta shape at the front on the flat ground several hundreds of metre down the slope (Figs. 95–97). At the source the glowing liquid was bright orange in colour, its heat radiation was strong enough to prevent us from approaching within two meters, and its viscosity was such as to allow us to push the tip of a long stick narrowly into it with both hands. The flow became dotted with black patches of solidified crust shortly after its departure from the source vent, and as the flow advanced downhill, these patches increased until at last they covered the whole surface of the flow. The crust thus formed tended to wrinkle into festoons of ropes with convexity downstream, making the flow less rapid and more restrained, with the greatest drag at the stream margins (Figs. 97, 98). Besides, the flow was building up natural levees of dark clinkers at each side, about 1 m high, making the flow more and more high than its surroundings. Upon arriving at the flat ground, the flow changed into a bank of *aa*, 2–3 m high and several meters wide, and as it was pushed from behind, its front was creeping forward at the rate of a few meters per hour, with the behaviour like a moving caterpillar tractor. Thus as the front advanced, its wall was impelled forward to be broken into pieces; as blocks fell off from the frontal wall and lumps of red-hot lava inside fell out on the ground below, with rustling noises; sometimes the front pushed its way through the soft sands on the flat ground, folding the latter into a low, wave-like ridge; and in some places the hardened crust of the flow broke open and gave vents to new lava-tongues which, after emerging as rounded bulbs of newly formed crust, projected ahead and sideways like arms and toes (Figs. 99, 101).

Between Feb. 28 and March 25, the almost continuous outflowing of lava resulted in an enormous volume covering practically the whole of the northwestern slope of Mt. Mihara and the adjoining flat ground of Sabaku (caldera floor), covering not only the greater part of the 1950 west flow but also the much larger surrounding area and several islands left uncovered in it (Figs. 102–104). Thus all the new flows that ran down the northwestern slope united below into one, and spread together westward against the northwestern caldera wall and then northeastward along the base of the wall. On March 17, part of the lateral front of

the flow had reached a point about 50 m distant from the deepest gap in the northwestern caldera wall, the passage to the village of Nomashi, and was advancing very slowly farther towards the gap. Lest they should suffer damage from the flood pouring out through the gap, the villagers tried to prevent by a ditch the further advance in that direction of the flow (Figs. 105–108). Seeing that the artificial ditch thus formed, about 1 m deep and 1.5 m wide, proved to be ineffective, they constructed a stone-wall about 2 m high to block the gap in the caldera wall. But this stone-wall was in reality of no use, because the lava was flowing down the gently-sloping ground northeastwards and along the base of the caldera wall, instead of attaining the level of the stone-wall whose base was several meters higher in level than the surface of the lava flow below. On March 18, the farthest front of the flow reached a point near the caldera wall just below Goshinka-jaya (tea-house), a distance of about 2 km from the rim of Mihara crater, and thereafter it advanced farther northward for about 700 m until it virtually stopped still on March 28 (Figs. 109, 110). During the last few days the lava front was advancing over a bushy land with a danger of setting fire to the surrounding bushes, but the fire was prevented by the villagers who cutdown these bushes.

The new lava flows that covered wholly the northwestern caldera floor thus formed a great lava field, about 2.7 km in length, 700 m in width at the middle, and narrowing into a 20–30 m flow at the northern end (Fig. 111). The thickness of the lava is probably about 8 to 10 m in the central part of the field and less than 1 m in its marginal part. The surface of the lava flows is largely covered with clinker-like blocks of *aa* type, but each flow is massive inside, forming a continuous ledge beneath its own crust of *aa* blocks, as may be seen in many contraction cracks formed during its cooling. Besides, in some places of the lava field, a very rough surface of "shark-skin" type is exposed patchwise without any blanket of clinkers, showing parallel grooves in the direction of flow. Along the margin of the field, particularly at its lower part, there developed a number of short tongues and toes of lava having a relatively smooth surface. But a typical *pahoehoe* is found within a short distance from the source vents on the rim of Mihara crater, where the lava is covered with a thin crust easy to break and contorted into a complex ropy structure.

The general feature of the lava field just outlined shows that the change from *pahoehoe* to *aa* took place shortly after the lava came out

of the vent of outflow, *aa* being characteristic of all the long flows far down the mountain slope. The flows that came out secondarily from cracks or tunnels in their predecessors were not typical *aa* even at their outlets, possibly owing to the fact that they maintained a relatively low temperature at the time of outflow. One of the writers (Ossaka) and students of the Geological Institute observed the lava temperatures with an optical pyrometer at several points of the flows, with the results as shown in Table XII. Hourly rates of advance of the lava fronts, observed by them, are shown in Table XIII.

iv) Lava pool: On the morning of March 25, shortly before the cessation of lava outpourings on the northwestern slope, a temporary lava pool was developed in the source area of the lava flows, just on the east side of the line of spatter cones (g–1 in Fig. 73) in the Mihara crater. The sudden stoppage of continuous drainage of lava-flows down the mountain slope must have caused the pool on their source vents in that part of the crater floor where molten lava was still continuing to issue from some underlying feeders. The lava pool thus formed became a shallow, oval basin, about 250 m in N.-S. diameter and 150 m in E.-W., bordered on its northwestern side with a slump scarp a few meters high, so that the molten lava in the pool could not overflow the northwestern mountain slope (Fig. 112).

The lava pool was glowing brilliantly with a darker scum forming on the surface and was so fluid that it was continually agitated with waves breaking against the shore[32] (Figs. 113, 114). In the pool, near its western shore, a group of lava fountains was in rapid succession welling up a dome (big bubble) of molten lava a few meters high above the pool, then bursting into pieces to be scattered about (Fig. 115 a-h). An ever-changing, glowing cobweb pattern, radial and concentric to the fountain group, was seen with zigzag bright lines between the skins of molten lava, fanning out to the east. Thus the lava streams in the pool flowed outward from the fountain group, and upon reaching the surrounding shore, they flowed under the solid lava on the shore, as if engulfed from within, instead of flowing outside over the slump scarp and other beach ramparts. It seemed likely that a convectional circulation of molten lava was taking place within the pool, although at the same time there was also a possibility of leaking out of the lava down

32) The activity of this lava pool may be clearly seen on the 16 mm telephoto motion pictures (The Eruption of the Volcano Oshima in 1950–51.) taken by the Ministry of Education, Japan.

to the northwestern slope through some passages under the slump scarp on the shore of the pool. The fountain group seemed to be the main source supplying molten lava to the pool, and as far as could be ascertained, it was situated close to the line of the spatter cones (g–l) whose gas activity still asserted itself in continual hissing noises from the glowing vents on the spatter cones (h), (i) and (j). These features seemed rather to favour the supposition that the lava pool was fed through the fountain group from that rift which had given birth to the line of the spatter cones.

Toward the end of March, the lava pool was found to have become smaller and less active. On March 30, it was about 50 m×100 m in area and much crusted, and by the beginning of the next month, it was crusted all over its surface.

v) Northeast lava flows. The eastern half of Mihara crater had displayed nothing particular to be mentioned until the end of March. Thus, for about 55 days from the beginning of the 1951 eruption on Feb. 4, neither lava flow nor spattering occurred on the northeastern floor of Mihara crater, and no eruptive vent was formed on the east side of the 1950 cinder cone. Being filled with the 1950 lava flows and partly covered with new ejecta (ashes and cinders) from the 1950 cone, the crater floor showed pressure ridges and mounds and irregular hardened flow patterns, with chasms and cracks particularly conspicuous near the east side of the central upthrusted mound now occupying the site of the former central pit. There were the usual steaming cracks about the crater floor, white vapours being seen rising vigorously during damp and cool weather. Several lines of vapour vents could be followed up the eastern slope of the 1950 cone, but hardly any spot of red-hot heat was visible thereabouts (Fig. 116).

On March 28, at 16 h 30 h, a river of red-hot lava was seen flowing for the first time in 1951 over the northeastern rim of Mihara crater (Fig. 73 b), running down the northern slope of the central cone, along the east margin of the 1950 northern flow (Senzu lavas shown in Fig. 30), and partly over-lapping it. Upon reaching the gentler slope at the base of the cone, the new lava flow deflected its course northeastward, and advanced about 3 km within a day into the desert land in the northeastern gap of the somma mountain. The flow was of the *aa* type, advancing in the same manner as observed on the already-mentioned west flows. It was about 10 m in width in the upper course, about 400 m in the middle with a long island left uncovered, and became

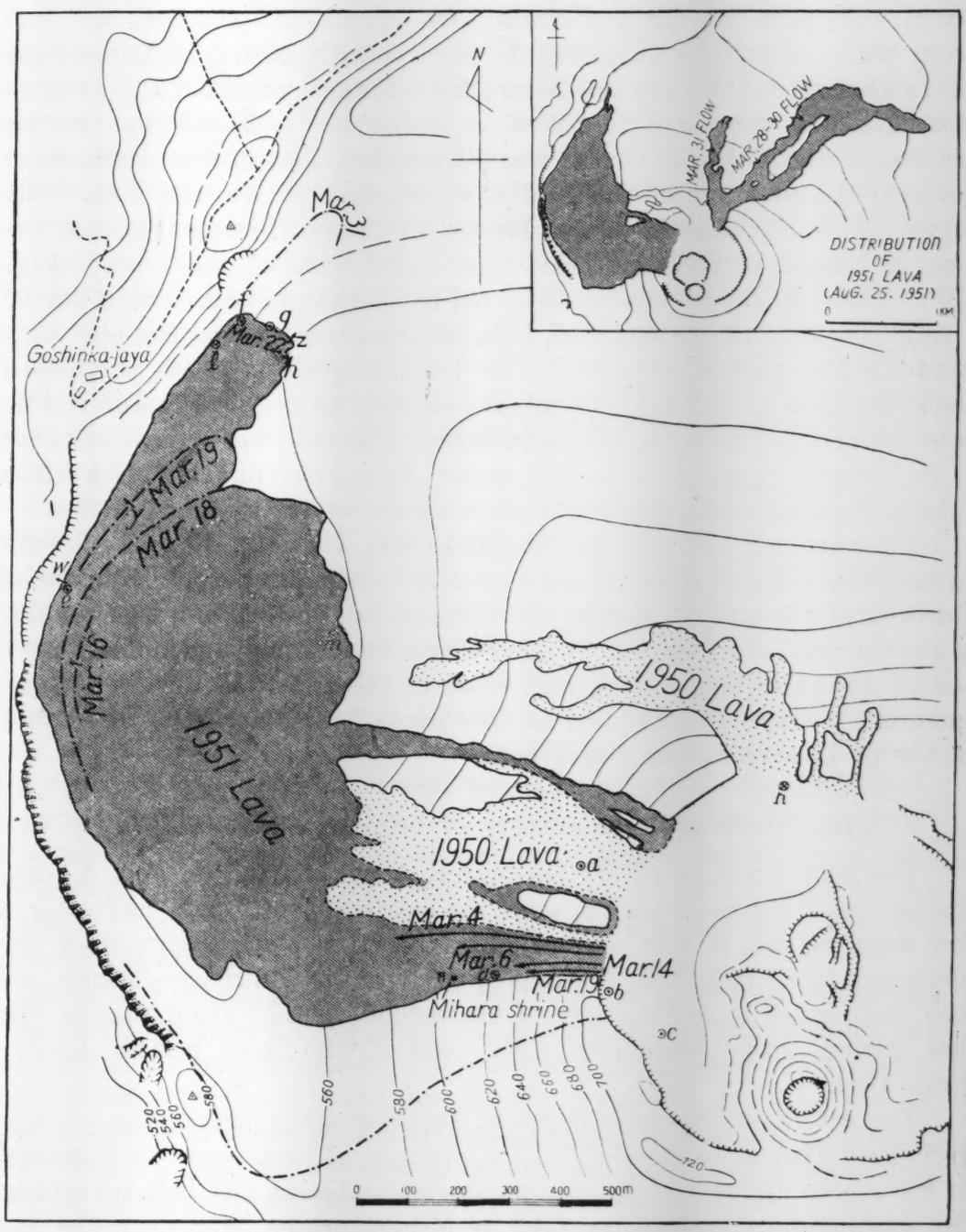

Fig. 120. Distribution of the lavas from Mihara crater during March, 1951. Arrows show the direction of lava-flowing. Chained lines show the fronts or margins of the lavas. Double circles and crossed circles indicate the points where the temperatures of the lavas were measured and the localities of some collected specimens respectively.

100 m wide near its farthest front. On March 31, another flow ran down the northern slope along the west margin of the just-mentioned one, and advanced straight northward for a distance of about 1 km within two days. It was 50 m to 150 m in width in its lower and middle courses, while its upper course was joined with that of the northeastern flow and also with one of the 1950 flows (Figs. 117, 118, and 120). The source vent of these flows was located in the northeastern part of the floor of Mihara crater, just below the inner wall of the crater (Fig. 119). Thus on March 30, at 15 h, red-hot lava was seen oozing out of a small opening in the solidified lava on the crater floor, flowing in a stream a few meters wide, and after travelling about 150 m northward along the base of the crater wall, it was flowing over the crater rim to pour in torrents down the mountain slope. The flow was typical *pahoehoe* in its extreme upper part on the crater floor, but on the steep slope outside the crater it quickly changed to *aa*.

The northern and northeastern flows had virtually stopped already on April 5, without making any remarkable advance beyond their fronts observed at the end of March. The course of these flows was similar to that of 1777–78 (An'ei lava flows), and they would undoubtedly have poured into the sea on the east coast of the island as the An'ei flows had done, if they had continued to flow for a longer period with further supply of lava from the source vent.

VIII. Review of the activity of February—March, 1951.

The 1951 eruption of Mihara crater, which started on Feb. 4, continued for about two months until the beginning of April, and after a few days' repose, it was resumed, but this time with intermittent explosions. Reviewing the continuous activity of February—March, we may distinguish it as "activity of the second period" from that of the first period, July—September, 1950, and of the third period, April—June, 1951.

The activity of the second period represented the peak of the volcanic cycle 1950–1951 as inferred from the changes of eruptions. It appeared to have been influenced by the northwest-southeast rift belt traversing the southwestern part of the floor of Mihara crater from near the top of the 1950 cinder cone to the northwestern rim of the crater. A line of activity had developed along the rift belt with explosions and lava outpourings, the explosive activity progressing along the rift from the crater floor toward the top of the 1950 cinder cone, and the effluent

activity in the opposite direction as far as the northwestern crater rim. Thus, the explosive activity started with a number of spatter cones on the crater floor, settled down to steady eruption at the top of the main cinder cone, while the effluent activity started with a few small lava flows at some of the new spatter cones, settled down to long-dated outflows from vents around the northwestern crater rim, with the result of forming an extensive lava field in the northwestern part of the caldera floor. At the final stage of the activity of the second period, a short-lived effluent activity occurred at the northeastern corner of Mihara crater, with lava-flows pouring over the northern crater-rim towards the northern and northeastern skirts of the central cone. This may be regarded as a prelude to the forthcoming activity of the third period, seeing that the latter took place exclusively in the eastern half of the crater floor.

During the entire course of the activity of the second period, the western half of the crater floor kept rising day by day, together with the 1950 cinder cone and the central upthrusted mound, although there occurred some intervening sinking locally as well as temporarily. Toward the end of March, immediately after the activity came to a halt, the crater floor tended to make rapid sinking. Certain changes in height of the crater floor, excepting those due to new filling and settling of the ground, seem to favour the supposition that there was a steady upward pressure of magma released partially by an occasional outbreaking, causing the rise and fall of the crater floor during the activity. The magma that took part in the activity of the second period may have been the same as that of 1950, still liquid in the conduit below, recharging itself with gases until it could extrude through the northwest-southeastern rift referred to.

During the activity characteristic harmonic tremors were registered at the Meteorological Observatory at Motomura almost continuously, although there were fluctuations in number and amplitude of the tremors, in accordance with the ebb and flow of the eruption. In the cases of larger eruptions as those of March 14–24, explosions were heard as thudding detonations, and in other cases they were felt at as far as Motomura, accompanied with the rattling of houses caused by air shocks.

(To be continued)

22. 伊豆大島三原山昭和25年及26年の噴火
その2 昭和26年の噴火 (*A*) 第2期の活動

地震研究所 津屋弘達・森本良平・小坂丈予

伊豆大島三原山の昭和26年の噴火は，2月4日開始，4月1日頃まで約2ケ月間，連続噴火し，小休止ののち，更に間歇的噴火を繰返して6月28日に終った．2月及び3月の噴火は，昭和25年，26年の噴火期間を通じての最高潮であった．われわれは，この連続噴火を，第2期の活動として，前回詳述した昭和25年7月16日—9月23日の第1期の活動[地震研究所彙報32号，第1冊，35–66頁]及び，4月2日以降6月28日に至る第3期の活動と区別して，ここにその噴火経過を詳しく記述した．

第2期の噴火は，三原火口の西半で行われた．とくに，前年の噴火によって生じた噴石丘頂上附近から，火口北西縁に至る，南東一北西方向の裂線に沿って演ぜられた（第72–73図参照），すなわち，爆発的活動は，噴石丘西側火口底に形成された熔岩々滴丘の活動に始まって，噴石丘頂上火孔の定常的爆発活動へと，南東に移行し，一方，熔岩の溢流は，熔岩々滴丘よりの流出に出発して，火口北西線に沿う火孔群から長期にわたって溢流するようになる．この結果，火口原（カルデラ底）北西に拡がる熔岩原が形成された（第120図）．この期の終りに，噴火は，火口の東半に移り，次期活動の前駆と見なされる，火口北東隅からの熔岩溢流がはじまる（第73図b）．

この期間を通じて，火口中央の噴石丘をも含めて，火口底の西半は，局部的及び一時的沈下はあったが，全般的に，上昇を続け，3月下旬活動休止後急激に沈下した．この火口底の上昇，沈下は，それぞれ，岩漿の上昇と，熔岩溢出によるガス圧の低下によるものである．火山微動の盛衰も，この火口における噴火の消長と，きわめてよく調和していた（未完）．

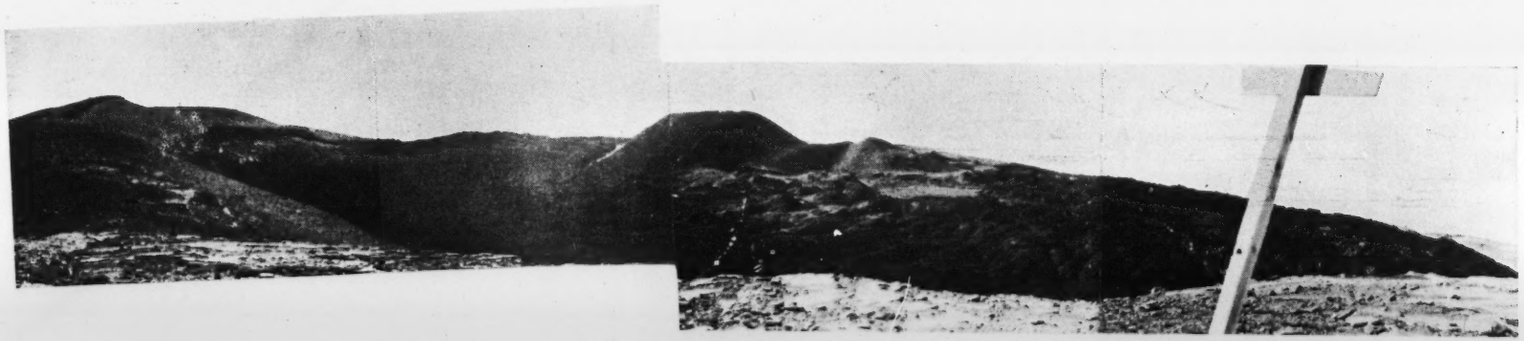

Fig. 62. Mihara crater at the time of quiescence following the 1950 eruption, with the 1950 cinder cone in the centre, Dec. 11, 1950. Looking south from the north rim of the crater.

Fig. 63. The northern inner wall of summit crater of the 1950 cinder cone, with the highest rim (Kenga-miné) of Mihara crater in the back ground, Dec. 11, 1950.

→

Fig. 64. Vapour rising from vent (a) on the western floor of Mihara crater, showing the opening of the 1951 eruption, Feb. 4, 1951.
Photo. Miyajima.

Fig. 65. Explosive emission of incandescent lava from vent (a), with the 1950 cinder cone in the background, Feb. 4, 1951.
Photo. S. Watanabe. ↓

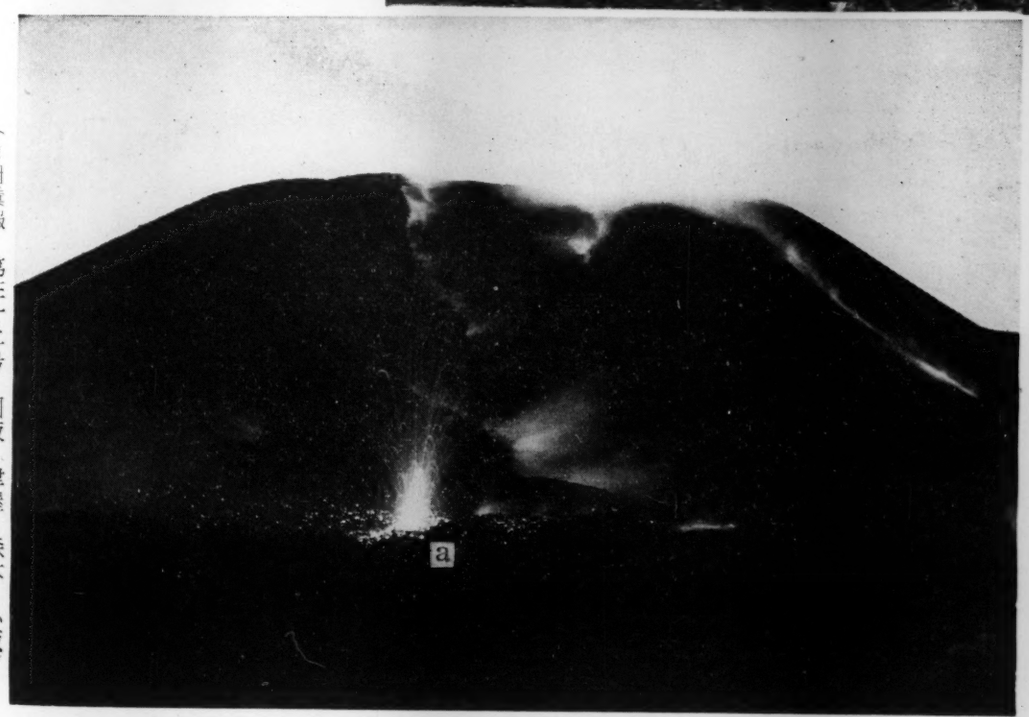

（震研彙報 第三十二号 図版 津屋・森本・小坂）

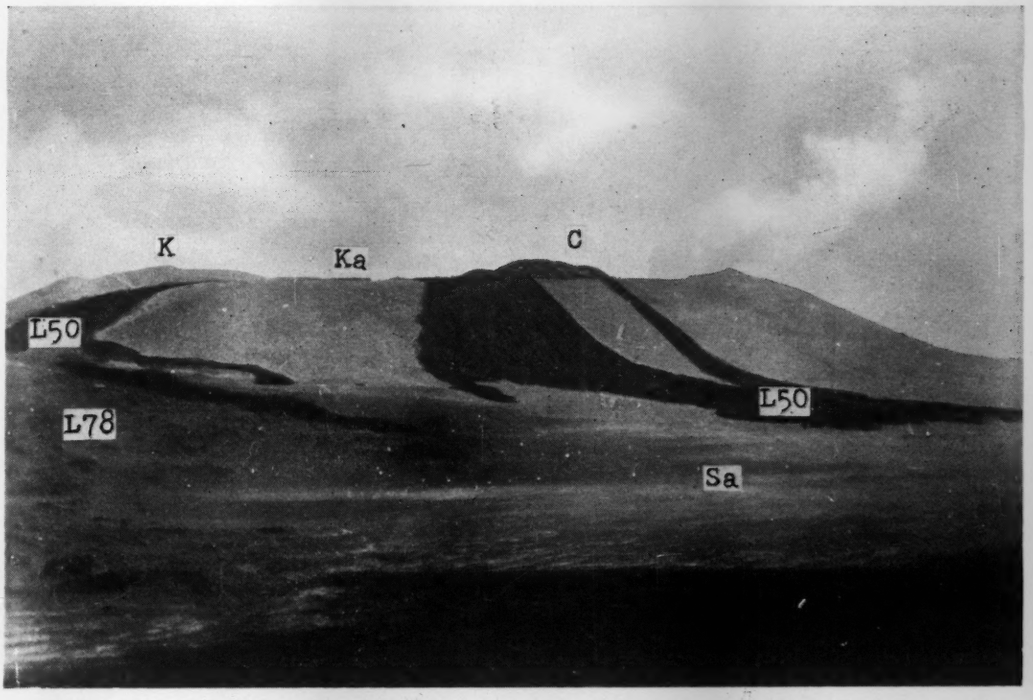

Fig. 66. Mt. Mihara as viewed southeastward from Goshinka-jaya showing vapour-cloud rising from the western floor of Mihara crater (on the right of C), Feb. 6, 1951. C:1950 cinder cone. L50:1950 lava flows. L78:1778 lava. K:Kenga-miné. Ka: Kakô-jaya. Sa: Sabaku (caldera floor). Photo. S. Watanabe.

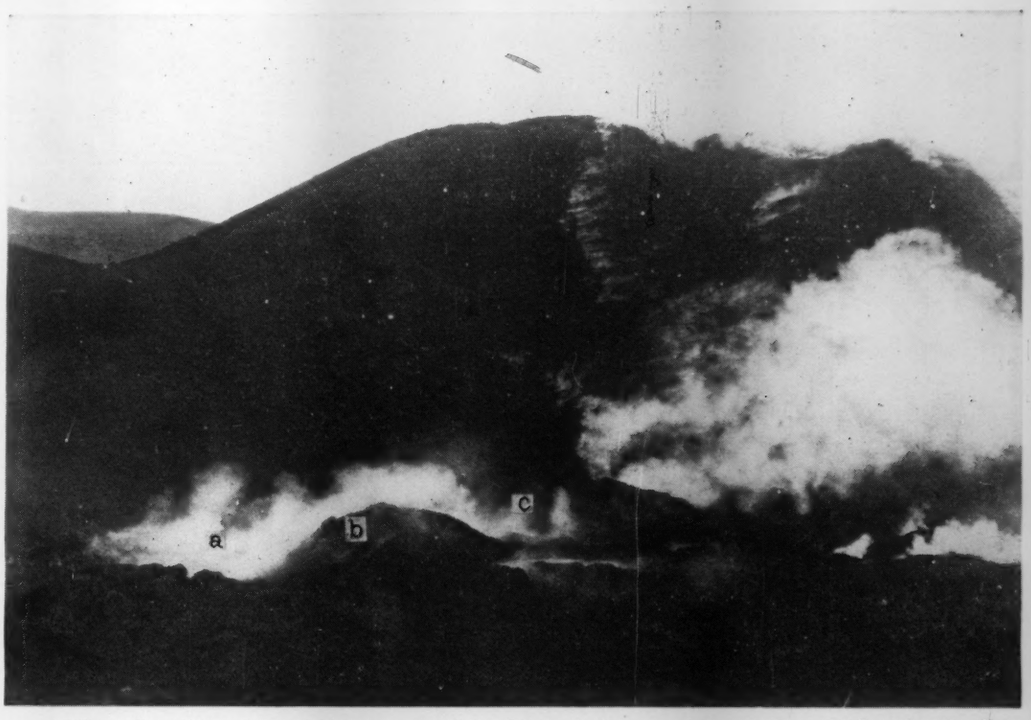

Fig. 67. Showing active vents (a), (b) and (c) on the northwest base of the 1950 cinder cone, Feb. 6, 1951. Photo. S. Watanabe.

Fig. 68. Showing active vents (b) and (c), Feb. 9, 1951. Vent (d) was formed within the steaming area on the right. Photo. S. Watanabe.

Fig. 69. Vent (d), showing lava spattering with flow, Feb. 13, 1951.
Photo. S. Watanabe.

Fig. 70. Spatter cones covered with cinders and bombs (b~f), Feb. 17, 1951. The 1950 cinder cone in the back shows new steam vents formed by fissuring and slumping on its northwest side. Photo. S. Watanabe.

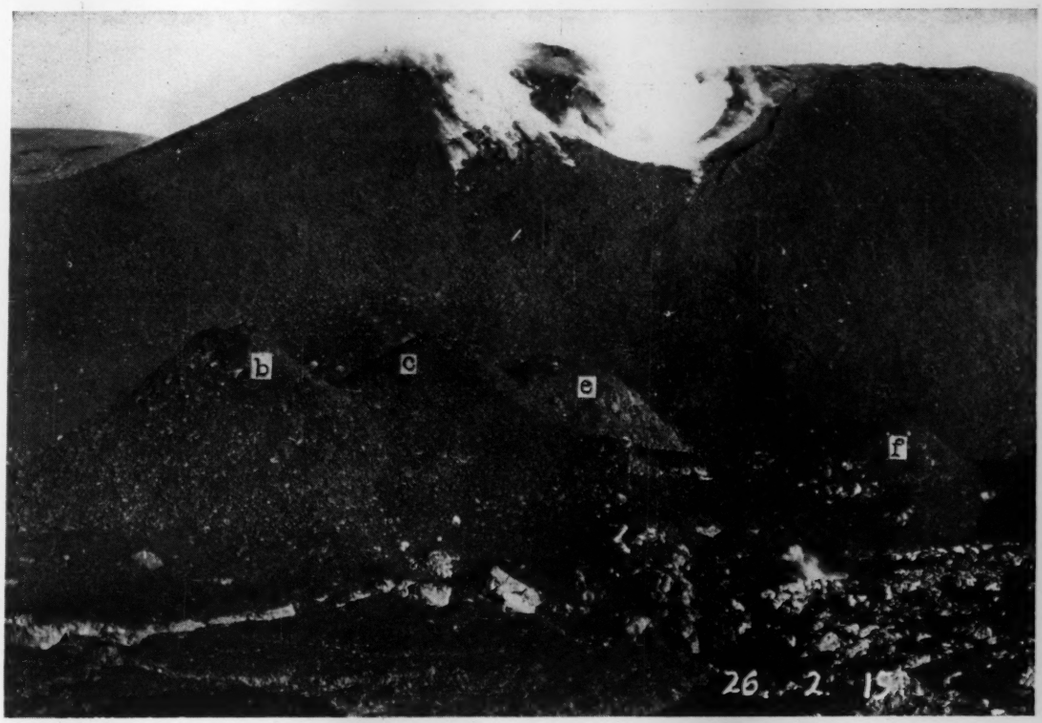

Fig. 71. Ditto. Feb. 19, 1951. Photo. M. Miyajima.

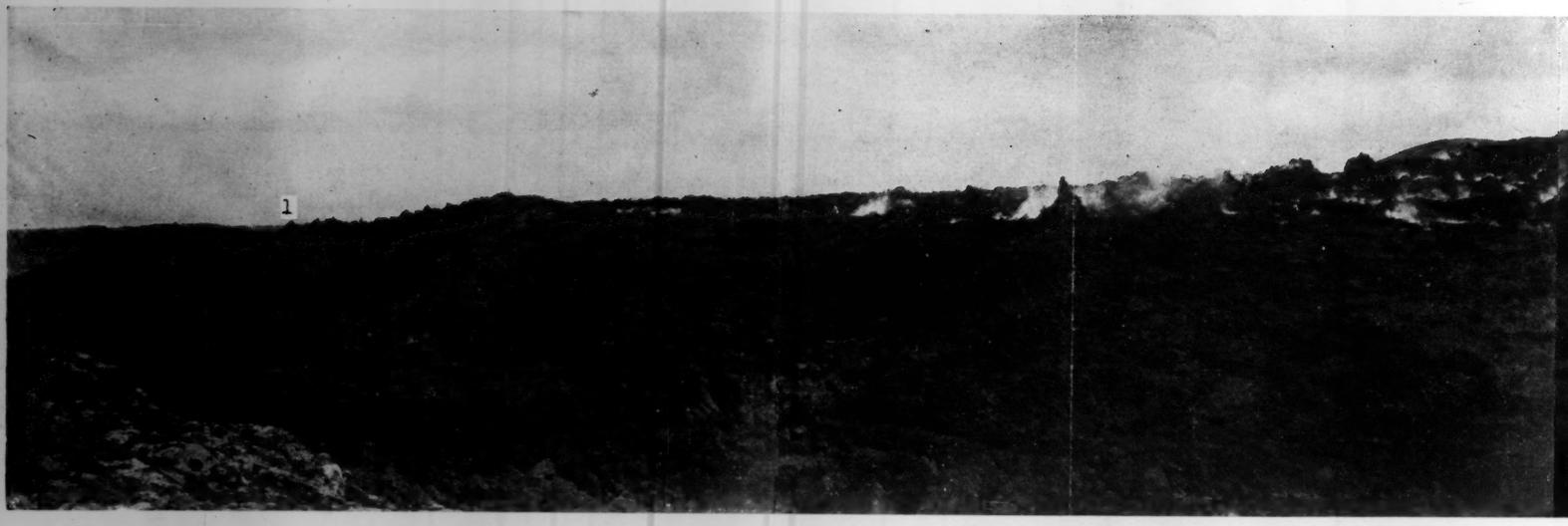

Fig. 74. The western half of Mihara crater,
right background, March 2, 1951. The lower hil

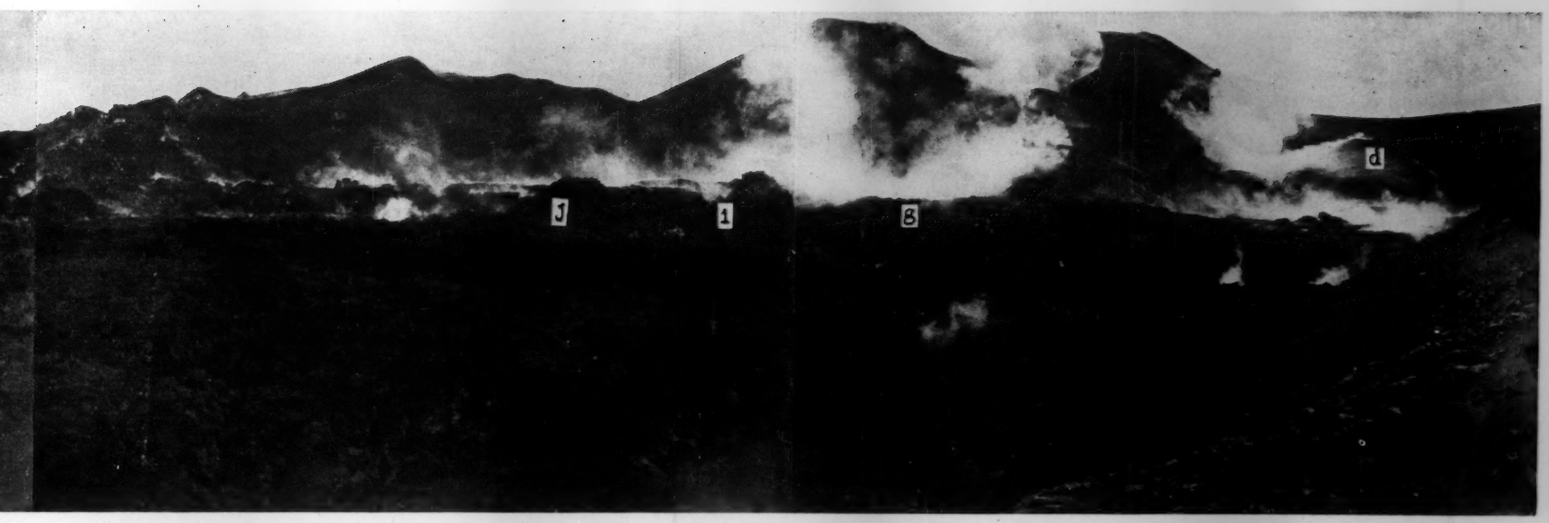

ater, showing line of active vents (b—l) on the crater floor, with the new active craters on the 1950 cinder cone in the
hill on the left of the cinder cone is the central mound upthrusted from below at the site of the former central pit.
Photo. S. Watanabe.

Fig. 75. Small lava flows on the sides of the spatter cone (j), March 6, 1951.
Photo. S. Watanabe.

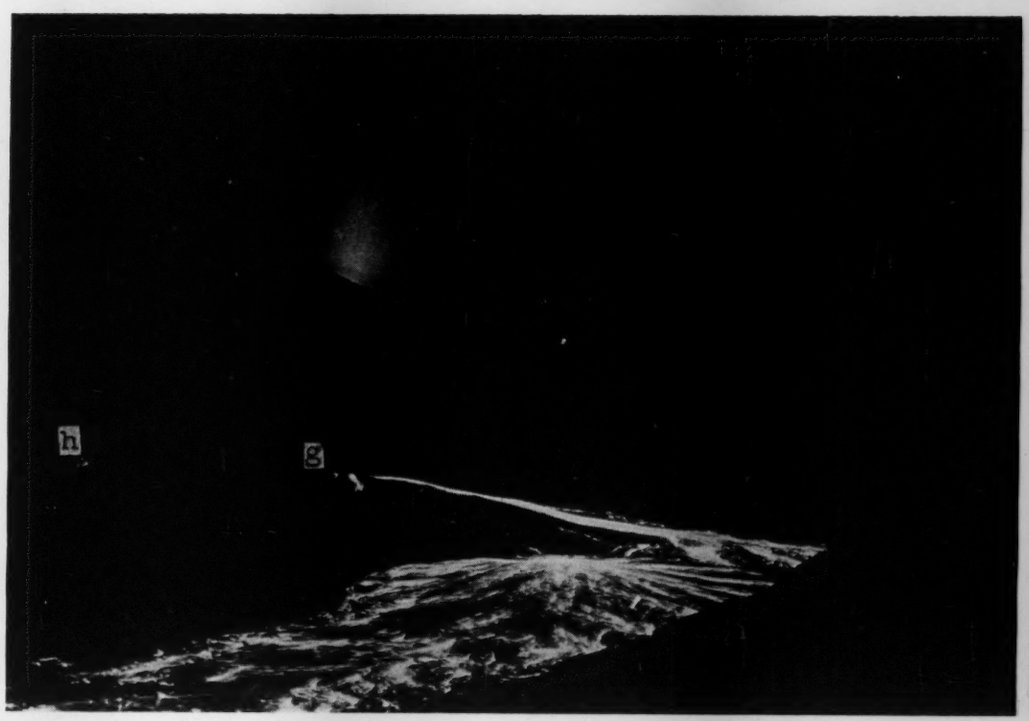

Fig. 76. Night view of lava flow from a temporary vent near the vent (g), with explosive emission of lava on the 1950 cone in the background, March 7, 1951. Photo. S. Watanabe.

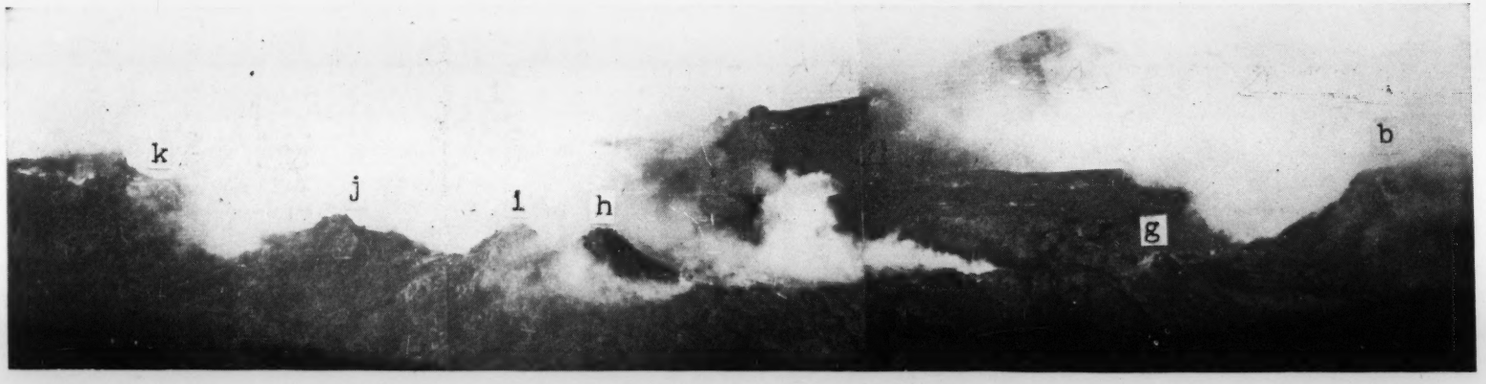

Fig. 77. The western part of Mihara crater, showing line of the fully-developed spatter cones (b—k), March 16, 1951.

Fig. 78. Spatter cones (l) and (m) on the northwestern extension of the line g—k (Fig. 77) and close to the northwestern rim of Mihara crater. One of the source vents of lava flows on the northwest slope was located at V, March 16, 1951.

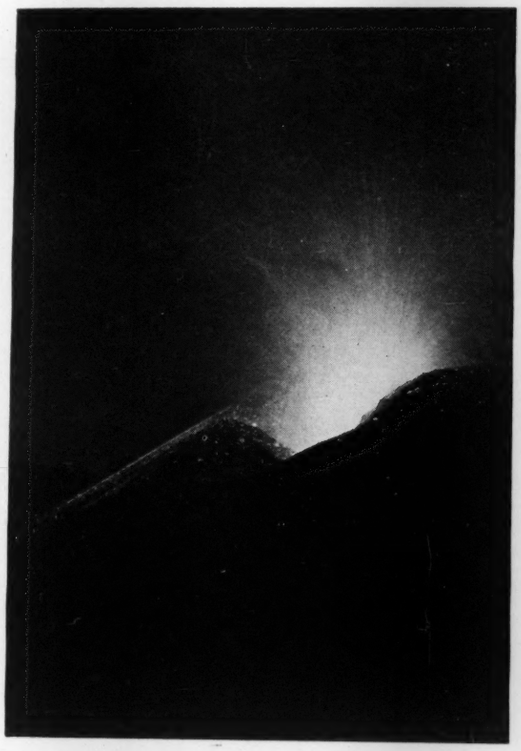

Fig. 79. Explosive emission of incandescent lava at the new main vent on the 1950 cinder cone, March 16, 1951.
Photo. S. Watanabe.

Fig. 80. Black ash cloud vomiting from the new main vent on the 1950 cinder cone, March 16, 1951. Spatter cone (d) lower right.
Photo. S. Watanabe.

Fig. 81. Explosive emission of lava at the new main vent on the 1950 cinder cone, March 20, 1951.
Photo. S. Watanabe.

Fig. 82. Ditto. (night view), March 16, 1951.

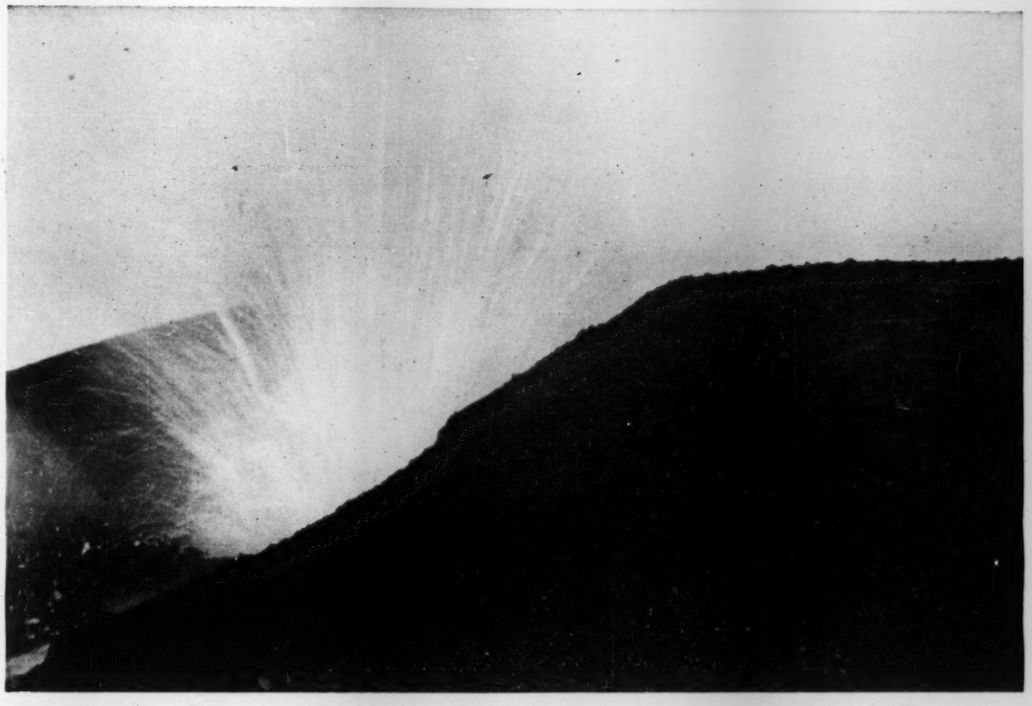

Fig. 83. Close-up of trajectories of incandescent masses thrown from the main vent on the 1950 cinder cone, March 18, 1951. (Telephoto.)

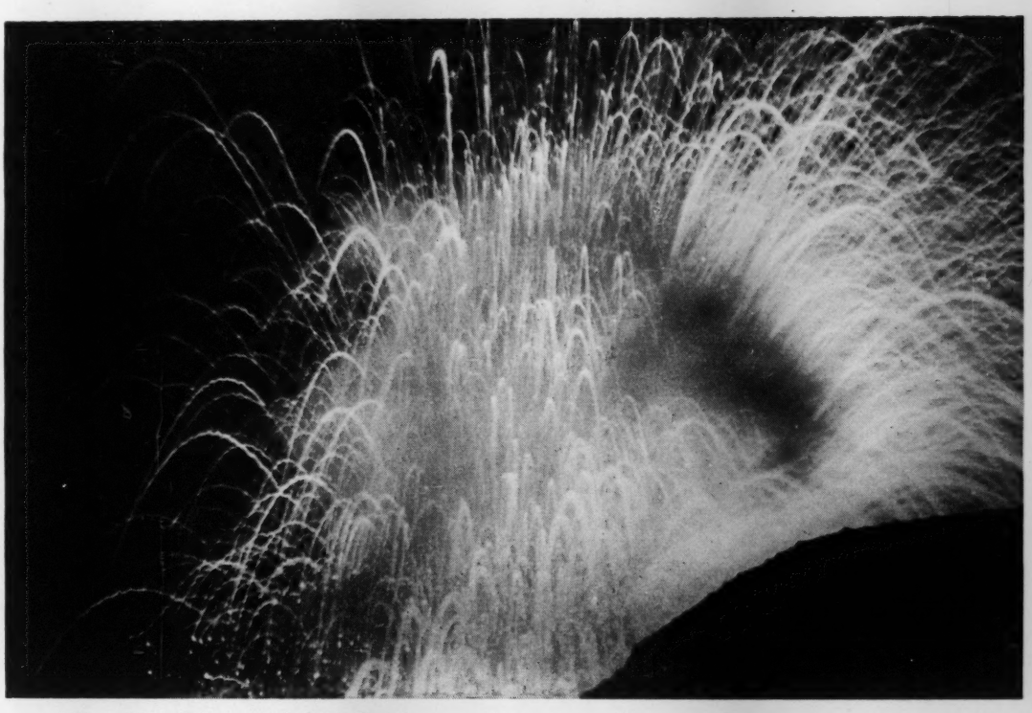

Fig. 84. Ditto. (night view)

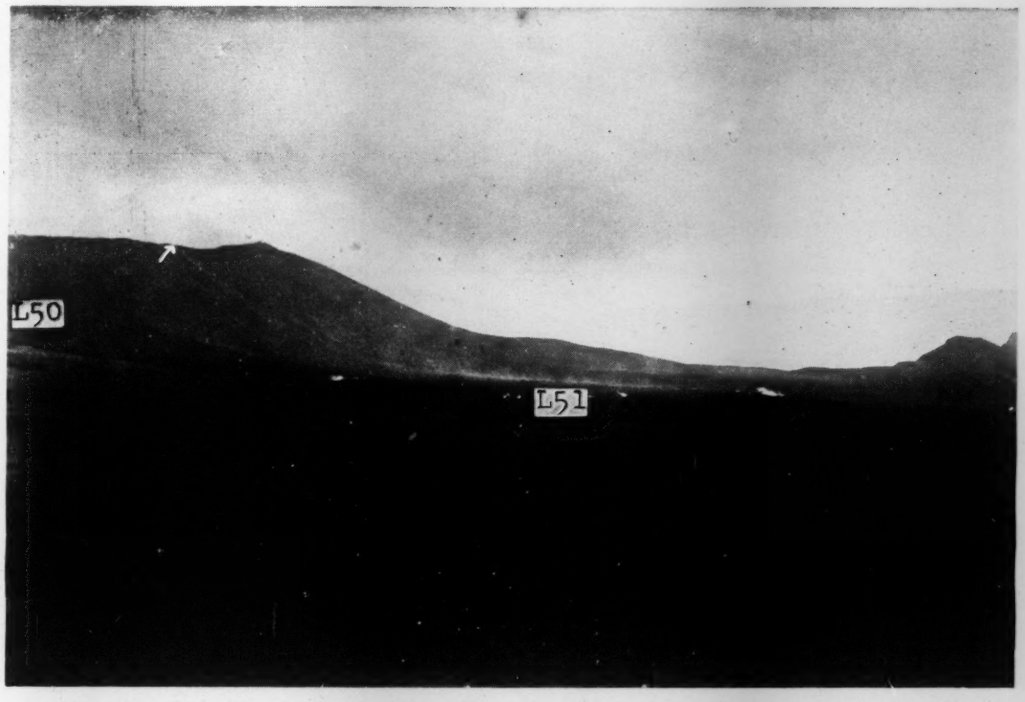

Fig. 85. New lava flowing down the northwestern slope (arrow's head) of Mt. Mihara and spreading over the flat ground of Sabaku (caldera floor), March 1, 1951. L50:1950 lava. L51:1951 lava. Photo. S. Watanabe.

Fig. 36. Incandescent lava spurting from a vent on the northwest rim of Mihara crater and flowing away downslope, March 2, 1951.
Photo. S. Watanabe.

Fig. 87. Incandescent lava flowing down the western slope of Mt. Mihara, March 7, 1951. The small shrine (Mihara-jinja) at the right was about to be destroyed by the advancing lava. Photo. S. Watanabe.

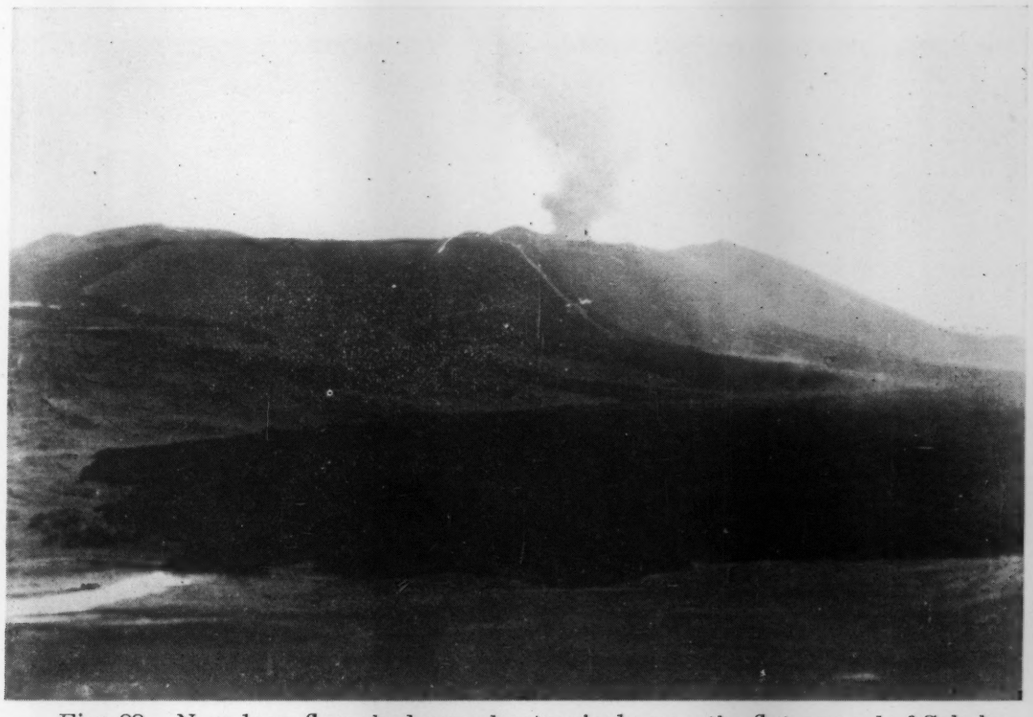

Fig. 88. New lava flows had spread extensively over the flat ground of Sabaku (caldera floor), the farthest front coming close to the caldera wall near Goshinka-jaya, March 12, 1951. Photo. S. Watanabe.

Fig. 89. Telephoto view of three source vents of lava flows on the northwest slope of Mt. Mihara, March 17, 1951. See Fig. 90.

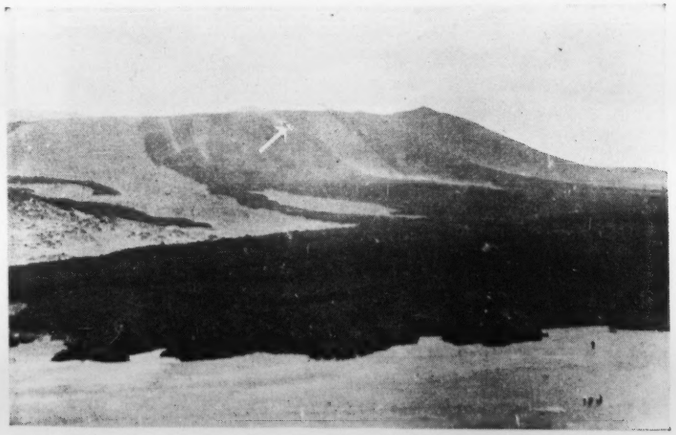

Fig. 90. Steaming lava flows and their source vents (shown by arrow's head) on the northwest slope of Mt. Mihara, March 17, 1951.

Fig. 91. Lava grotto (shown by arrow's head) from which an incandescent lava was cascading the day before to join into the main flow, March 18, 1951. See Fig. 100.

Fig. 92. Source vent (V) of an incandescent lava flow, March 18, 1951.

Fig. 93. Incandescent lava flow near its outlet in the edge of a lava tunnel, March 18, 1951.

Fig. 94. Close-up detail of the same flow as shown in Fig. 93, March 18, 1951.

Fig. 95. Lava flow, March 18, 1951.

Fig. 96. Ditto. Looking upstream, March 18, 1951.

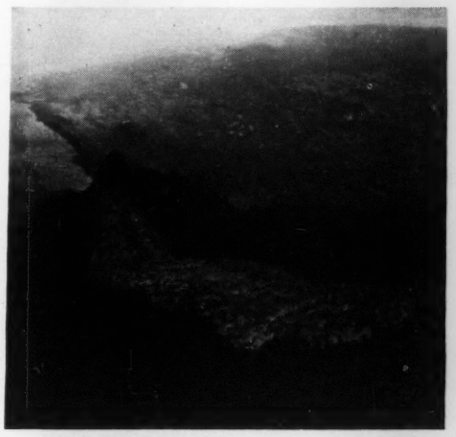

Fig. 97. Ditto. Looking downsteam, March 18, 1951.

Fig. 98. Ditto. Showing ropy crust, March 18, 1951.

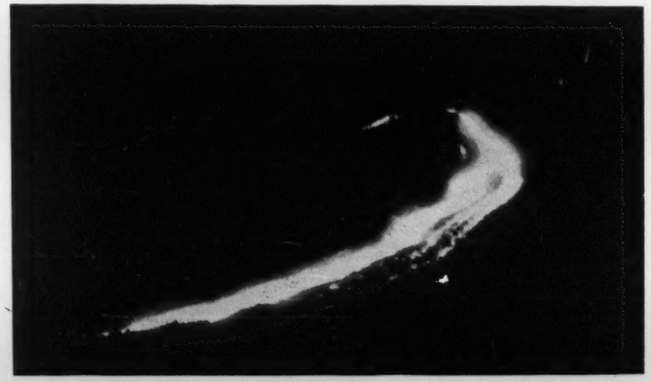

Fig. 99. Night view of lava flowing down the west slope of Mt. Mihara, March 18, 1951.

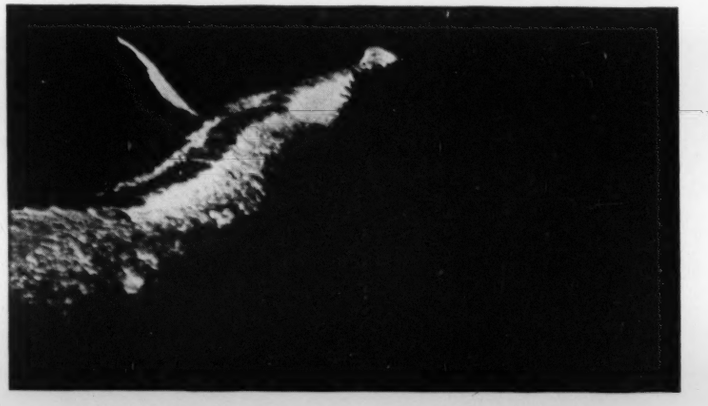

Fig. 100. Night view of lava flowing down the west slope, March 17, 1951. Lava cascade (upper left) joining into the main flow (right). See Fig. 91.

Fig. 101. Night view of Mt. Mihara from Goshinka-jaya, March 18, 1951.

Fig. 102. The same by day, March 16, 1951.

(震研彙報 第三十二号 図版 津屋・森本・小坂)

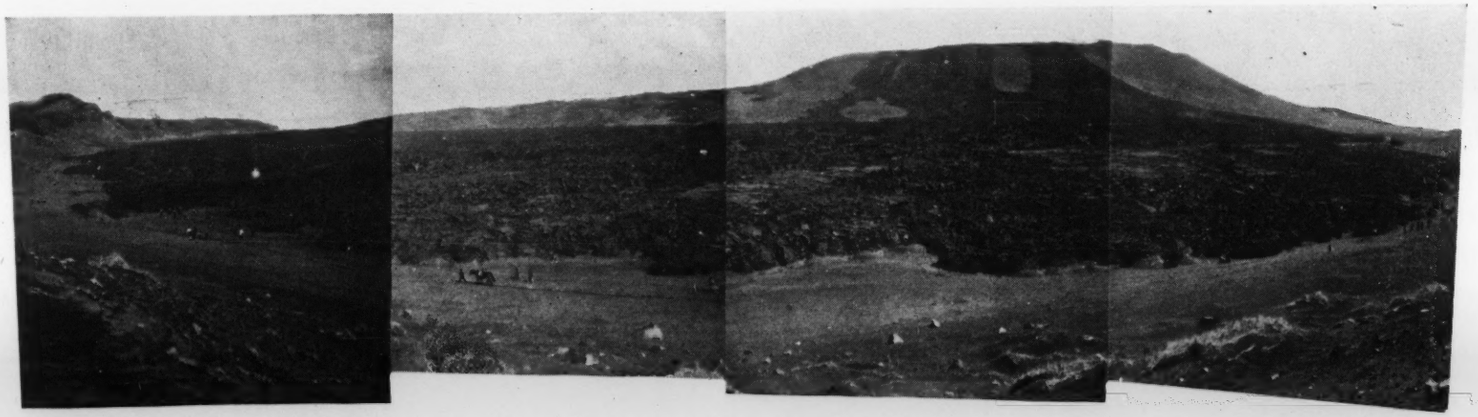

Fig. 103. New lava flows, as viewed east from the talus slope on the western caldera wall, March 18, 1951.

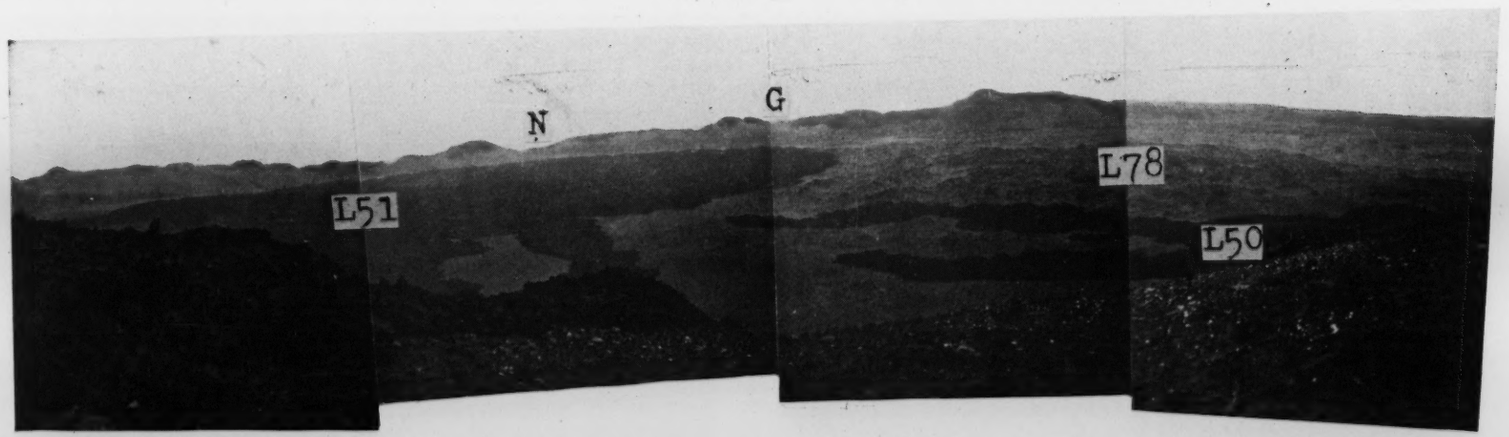

Fig. 104. New lava flows, looking down west from the northern rim of Mihara crater, March 17, 1951. L51: 1951 lava. L50: 1950 lava. L78: 1778 (An'ei) lava. G: Goshinka-jaya. N: Passage to Nomashi village.

Fig. 105. Lava front near Goshinka-jaya, March 18, 1951.

Fig. 106. Lava front creeping into an artifical ditch, March 18, 1951. G: Goshinka-jaya.

Fig. 107. *Aa* front approaching the western caldera wall, March 18, 1951.

Fig. 108. The southern margin of lava flows, March 18, 1951. The Mihara Shrine had already been buried under the flows.

Fig. 109. The farthest front (arrow's head) advancing into bushy land northeast of Goshinka-jaya, March 22, 1951. Photo. S. Watanabe.

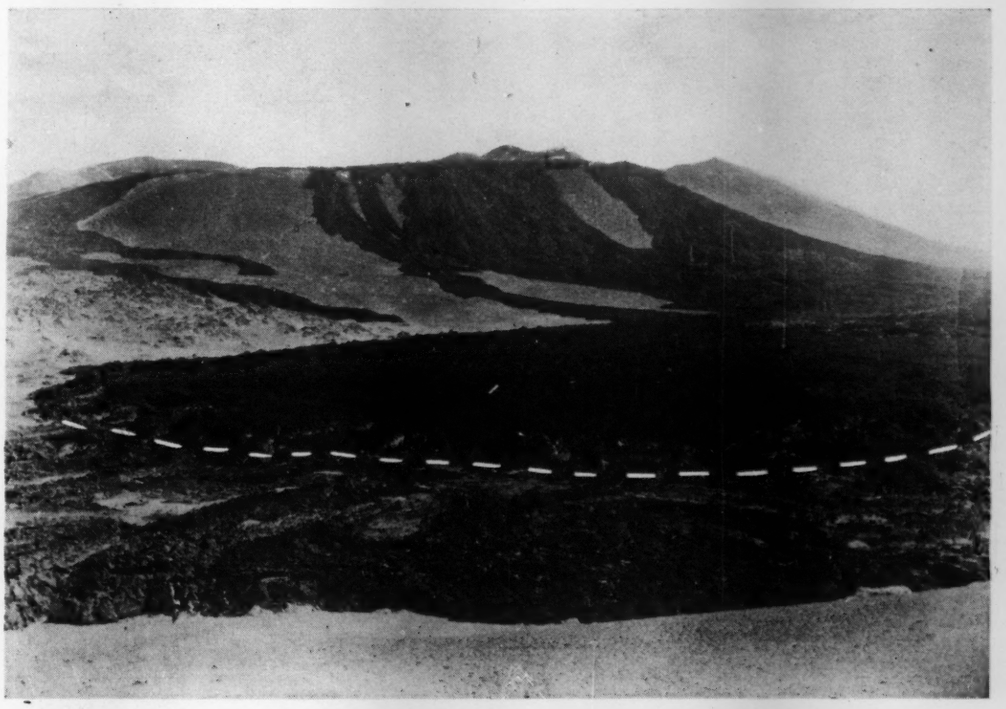

Fig. 110. New lava flows, showing flow advance by outflow from secondary vents (tunnels and cracks) on the front, March 23, 1951. Chain line shows the front on March 12. Cf. Figs. 78, 100. Photo. S. Watanabe.

Fig. 111. Aerial view of Oshima volcano, showing Mihara crater (K—M) with new lava flows and the steaming cinder cone, March 23, 1951. G: Goshinka-jaya. N: Passage to Nomashi village. S: Shiroishi-yama. G—N—S: Somma. (The Yomiuri Press.)

（震研彙報 第三十二号 図版 津屋・森本・小坂）

Fig. 112. Lava pool looking northeast from the west rim of Mihara crater, March 25, 1951. The spatter cone (j) near centre right. Photo. S. Watanabe.

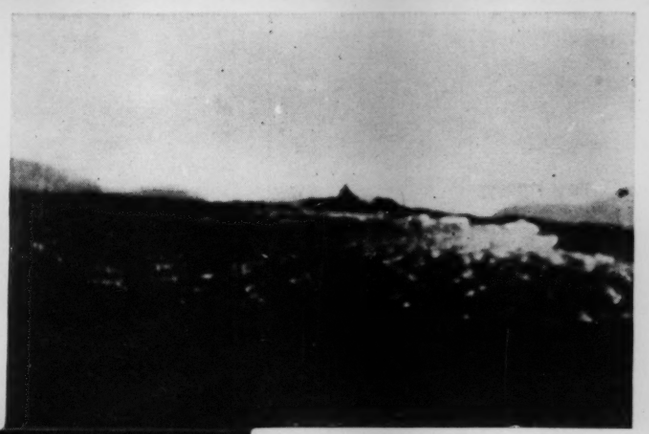

Fig. 113. vLaa pool looking southwest, with bright zigzag lines in the lava crust, March 25, 1951. (One cut from the 16 mm moving pictures taken by the Ministry of Education.)

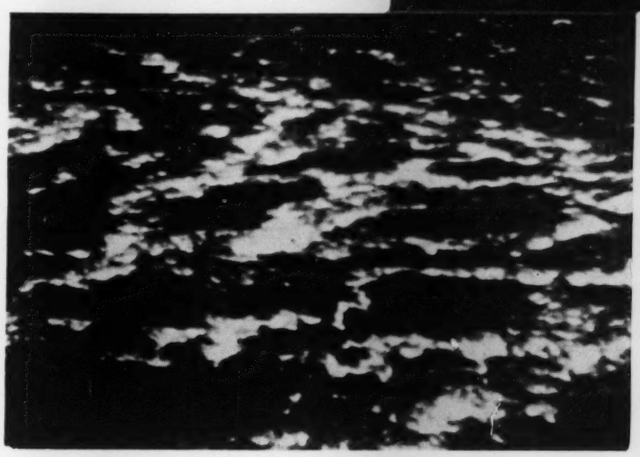

← Fig. 114. Detail of the bright lines in the lava pool, March 25, 1951. (Ditto.)

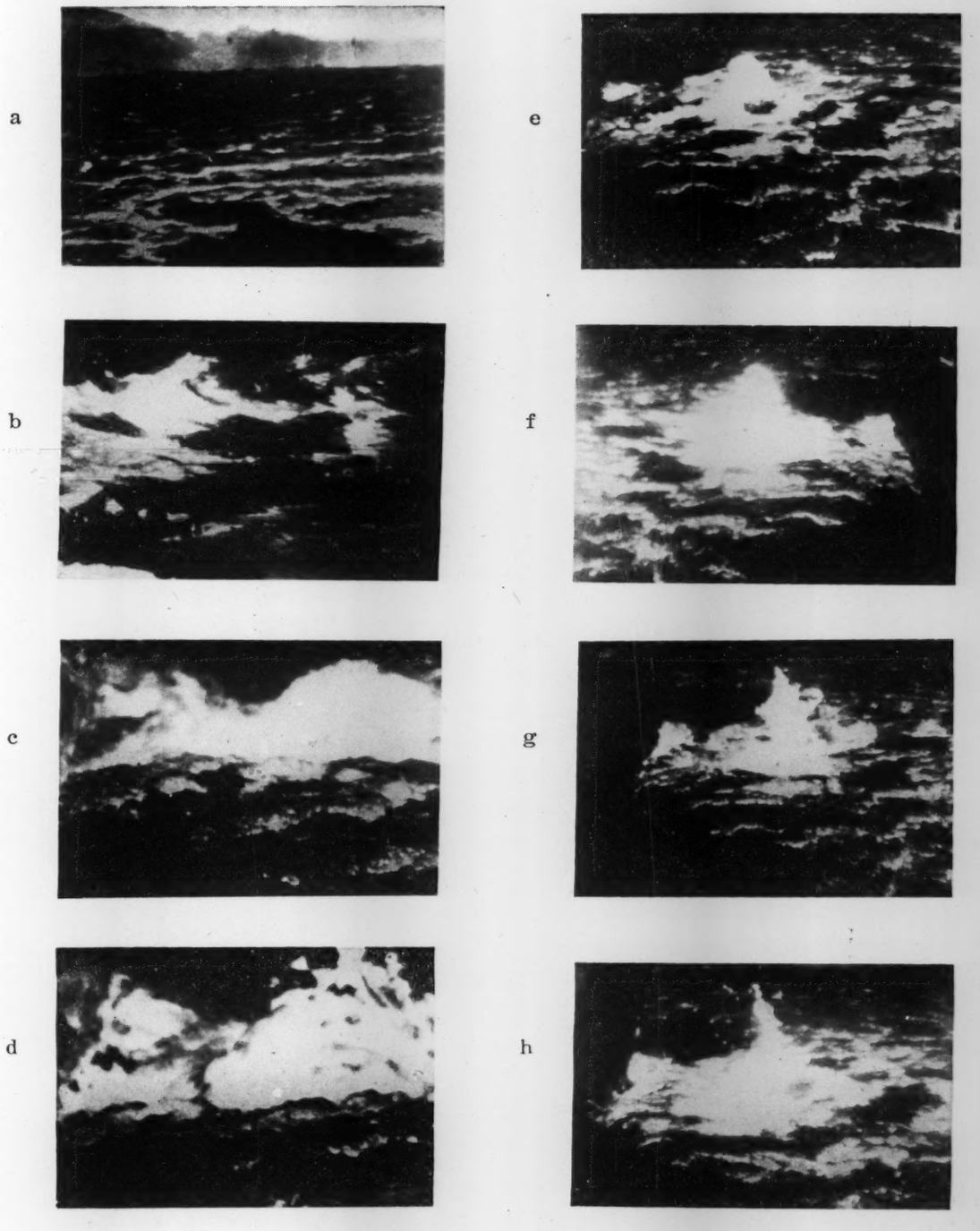

Fig. 115. Lava pool with its source fountain.
a, b. Pool lava flowing toward and into grotto on the shore near the fountain.
c, d. Pool lava doming up and spattering at the fountain.
e~h. Successive views of the lava fountain.
(Cuts from the 16 mm moving pictures taken by the Ministry of Education.)

Fig. 116. Eastern half of Mihara crater, looking southeast from near the highest point (Kengaminé) on the east rim of the crater, March 17, 1951.

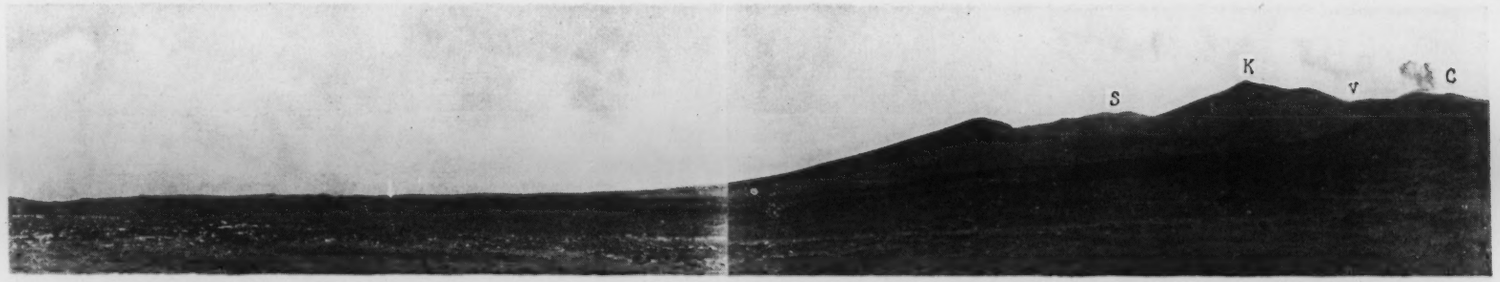

Fig. 117. New lava flows on the northeast slope of Mt. Mihara, March 29, 1951. Arrow's head shows farthest front. K: Kengaminé, S: Shiroishiyama (somma), C: 1951 cinder cone, v: Outlet of the flows on the northeast rim of Mihara crater. Photo. S. Watanabe.

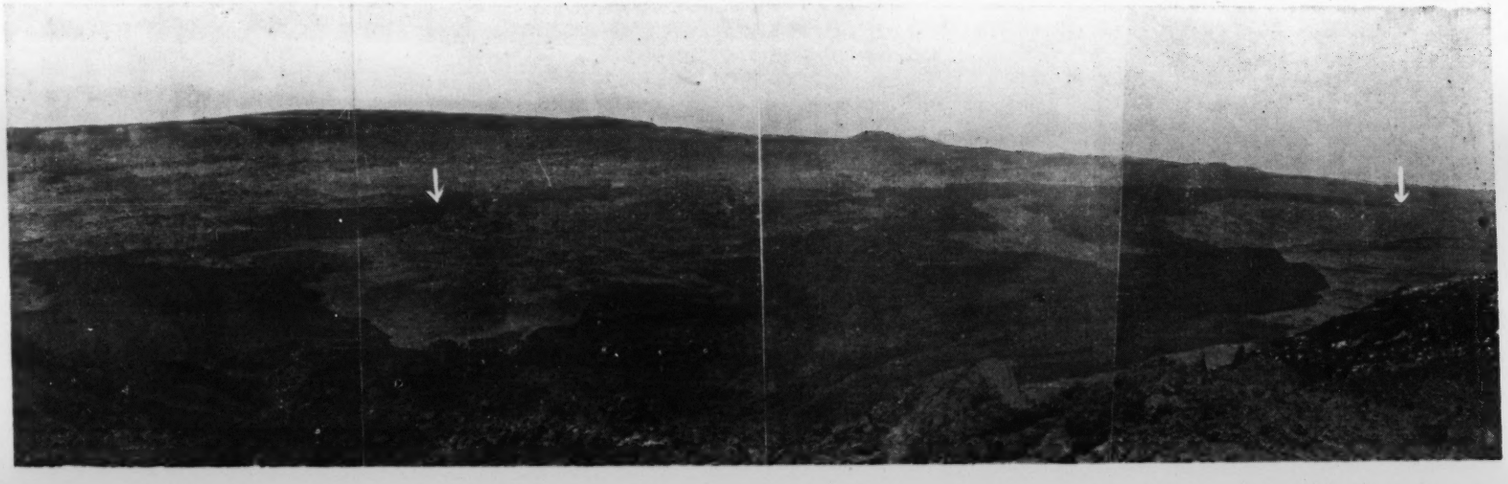

Fig. 118. New lava flows, looking down north from near the outlet of the flows on the northeast rim of Mihara crater, April 30, 1951.

Fig. 119. Lava oozing out of *pahoehoe* crust on floor of the northeastern corner of Mihara crater, March 30; 1951. The 1950 cinder cone on the left back ground. Photo. S. Watanabe.

（震研彙報 第三十二号 図版 津屋・森本・小坂）

23. *Anemometer of Inverted Pendulum Type and Wind Construction Studied with It.*

By Genrokuro NISHIMURA and Masazi SUZUKI,

Earthquake Research Institute.

(Read Dec. 19, 1940 and July 3, 1941.—Received June 30, 1954.)

1. Introduction.

At the occasion when we investigated the kaze-tsunami[1] caused by the Muroto Typhoon in 1934, we observed actually the damage done to Japanese wooden houses at Kansai District by this typhoon. At that time, the late Prof. M. Ishimoto, the director of the Earthq. Res. Inst., suggested to us that in order to clarify the relations between the damage[2] to houses and the blowing wind, it is necessary to study the wind constructions, and that in short time intervals such as one or two minutes. He also encouraged us, by making every effort to furnish the necessary funds, to take up the study of wind construction. Writing the present paper, we worship heartily the spirit of the late Prof. M. Ishimoto, and also pray for his happiness.

Now, we know that there are various types of anemometers such as Robinson's or Dynes', which are, however, not suitable for our purpose of studying the construction of natural wind. Therefore, we designed new a suitable anemometer which shall be shown in this paper. The present new-designed anemometer is of an inverted pendulum type, and it can actually catch the natural winds with variation periods equal to or longer than 0.1 sec. Moreover, by the present anemometer, we are able to obtain accurately the records of two components of the natural wind velocity which becomes equal to or smaller than 60 m/s.

The anemometer was installed on the roof of a Japanese ware-house which was situated in the neighbourhood of the sea coast of Inatori-machi, Izu Peninsula, Shizuoka Prefecture. The respective records of winds in the seasons of both spring and winter were obtained at the prescribed locality. The records of the winds of typhoon could not,

1) G. NISHIMURA and T. TAKAYAMA, *Bull. Earthq, Res. Inst., Suppl. Vol.*, **2** (1935).

2) The vibrations of a Japanese two-storied frame-house due to natural wind were also studied by us, and the mesurement of the wind pressure related to this study was done by the same anemometer described in the present paper.

G. NISHIMURA and M. SUZUKI, "Horizontal Deformations of a Japanese Two-Storied Frame-House," *Bull. Earthq. Res. Inst.*, **32** (1954).

however, be obtained in the course of observation by the present apparatus. Therefore, in this paper, we analysed the records obtained by the anemometer at the above-mentioned time, and obtained some interesting results concerning the wind constructions.

The present paper contains the following studies: (1) New-designed anemometer, (2) Time variation of wind pressure (Breath of wind pressure) and predominant periods of breath, (3) Breath and pressure of natural wind, and (4) Blowing direction and pressure of natural wind.

Of course, the present study of the natural winds is that of the winds at special locality and special observation times, and therefore the results obtained by the present analysis are not necessarily appropriate for the general study of the general characters of the natural winds. The present writers, however, hope that the present analysis will make a contribution to the study of the natural winds.

2. Theory and design of anemometer of inverted pendulum type.

We assume that the horizontal intensity of the pressure of the natural wind becomes W kg-wt/cm^2, and the total horizontal pressure exerted on a sphere of which the outer diameter becomes d, is W kg-wt. When the said sphere constructs an inverted pendulum as shown in Fig. 1, we can easily obtain the following equation of motion of the pendulum:

$$\frac{d^2\theta}{dt^2}+2\varepsilon\frac{d\theta}{dt}+\omega^2\theta=hW/I_0\,, \quad \cdots\cdots\cdots\cdots(1)$$

where $2\varepsilon=\lambda_0/I_0$, $\omega^2=K_0/I_0$, and I_0=the moment of inertia of the inverted pendulum about the rotation axis of the pendulum weight, λ_0=the constant related to the damping of the free vibration of the pendulum when the damping force becomes proportional to the rotation velocity $d\theta/dt$ of the pendulum, K_0=the restitutive moment of the pendulum, h=the distance between the rotation axis of the pendulum and the action point of the total pressure W on the top sphere of the pendulum, and θ, t, of course, show respectively the angle of rotation of the pendulum and the time of motion of the pendulum. Of course, in the present theory, the wind pressure W is the force acting on the pendulum perpendicular to the axis of the pendulum and also works in the plane in which the pendulum's motion is constrained.

Now, assuming that the functional form $f(t)$ of the wind force W becomes as follows:

(a) $W=f(t)=W_m(1-\cos \mu t)/2$,

(b) $W=f(t)=W_m \gamma t \cdot \exp(1-\gamma t)$,

(c) $W=f(t)=W_m \gamma^2 t^2/2 \cdot \exp(2-\gamma t)$,

(d) $W=f(t)=W_m \exp(-\gamma t)\cdot \sin \mu' t$,

(e) $W=f(t)=W_m\{1-\exp(-\gamma'' t)\}$,

we studied the characters of the pendulum motion. These expressions show respectively the different characters of the wind force with respect to time t, and we can easily obtain the solutions of the equation (1) for the respective five cases of W shown in the expressions (a)~(e). In these expressions (a)~(e), the quantities such as μ, μ', γ, γ', γ'' having $[1/T]$ dimension are respectively the factors controlling both the sharpness and the acting time of the wind force. The analytical solutions of (1) corresponding to the respective cases of W shown in the expressions (a)~(e) show that when the proper period of the inverted pendulum is made short and the damping force is not so large, the angle of the deflection of the pendulum θ coincides nearly with the amplitude $-f(t)/\omega^2$. The sensibility of the inverted pendulum, however, becomes inverse-proportional to the square of the natural period of it. And, therefore, when we make the period as short as possible, it is difficult to obtain a suitable mechanical magnification from the technical point of view. Of course, it is desirable to make the damping small to a certain degree, because when it becomes large, the phase-lag becomes large. But it is not desirable to make the damping too small, because the free vibration of

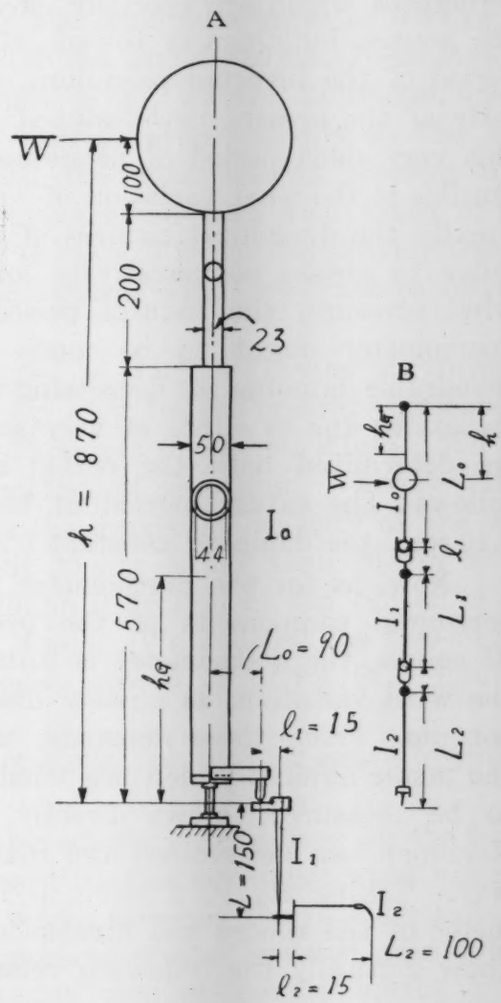

Fig. 1.

the inverted pendulum may be excited by the pressure of shock type of the natural wind.

Now, our object to obtain the wind variation with the anemometer is to catch the wind variation which becomes much effective on structures such as wooden houses or other tall towers. As a matter of fact, the free vibration periods of these structures are not very short as shown in the foot note[3]. Therefore, as we want to study the wind structures which are specially effective on the dynamical properties of the houses, buildings or towers, it is not desirable to make the natural period of the inverted pendulum, which is used for the main function body of the present new-designed anemometer, very short. Because, by this very short period of pendulum, the anemometer becomes of course sensible to the wind variation of very short periods which do not affect greatly the dynamical natures of vibration of the building. Thus, in order to obtain comparatively long variation of the period of natural wind pressure, the natural period of the inverted pendulum of the anemometer ought to be made comparatively long and to have a favourable damping for decreasing the sensitiveness to very short periodic variations due to winds of very short period. From these discussions, we determined both the period and the damping of the pendulum as follows: The natural period of the inverted pendulum $T_n=0.05$ sec.$\sim$ 0.10 sec., the damping constant $\varepsilon/\omega=0.5\sim0.6$.

Now, as for the anemometer, it is necessary to obtain the two horizontal components of the pressure intensity of the natural wind. Of course, the anemometer is installed at a certain position to observe the wind variation, as already discussed, of the two horizontal components. From these demands, we must use a sphere as the part of the meter against which the wind, of which the pressure intensity is to be measured, blows directly, as schematically shown in Fig. 1. Hereupon, we determined the diameter of the sphere in the following way. Taking R_e, V, d and ν as Reynolds number, wind velocity, diameter of the sphere and kinematic viscosity of the air respectively, we know generally the following relation:

$$R_e=V\cdot d/\nu\,. \qquad \cdots\cdots\cdots\cdots\cdots\cdots(2)$$

Putting $R_e=3\times10^5$, $\nu=0.1456$ cm^2/sec, and $V=60$ m/sec, we obtain

3) The free vibration periods of wooden houses are 0.1$\sim$1.0 sec. for one-storied and three-storied house, those of Gojyu-no-Tô tower are 1.0$\sim$2.0 sec., and those of steel towers for electric transmission lines are nearly 1.0 sec.

the following value of d: $d=7.28$ cm. Therefore, when we take the value of d as 10 cm, the total resistance of the sphere increases proportionally to the wind velocity, or the wind pressure, and for the values of the wind velocity 0~44 m/s (wind pressure 0~119 kg-wt/m^2), and for the case of $V=44$ m/sec, the total resistance of the sphere becomes 0.39 kg. The relation (2) shows us, moreover, that for the respective spheres of $d=15$ cm and 20 cm, the total resistances of them become proportional to the wind velocity $V=0\sim29.1$ m/sec. and $V=0\sim21.9$ m/sec. respectively, and they show equally the maximum value of 0.39 kg for the two cases, i.e. $d=15$ cm, $V=29.1$ m/sec. and $d=20$ cm, $V=21.9$ m/sec. When the diameter of the sphere is 7.28 cm, we are, of course, able to make the resistance of the sphere increase proportionally to the wind pressure or the wind velocity until the wind velocity becomes about 60 m/sec, but for the present anemometer we take two kinds of the sphere of which the diameters are 15 cm and 20 cm respectively because in the case of small velocity of the natural wind, we want to increase the sensibility of the anemometer.

As already mentioned, we adopted a machine having an inverted pendulum with the sphere on the top of it for the present anemometer, the sphere being composed of two diameters $d=15$ cm, 20 cm. We also adopted a mechanical magnifying method of recording. Therefore from technical reasons it is desirable that the maximum velocity of the wind be recorded at the length of about 20 mm or less than 20 mm on the recording paper and also the maximum deflection of the center of the sphere be about 1 mm less than 4 mm. We adopted the two-stepped magnifying mechanism with the lever system of about 66.5 multiple lever magnification.

We will use the following notations for the respective quantities shown in Fig. 1:

y_A=Max. deflection of the center of the sphere fixed on the top of the inverted pendulum caused by the maximum wind velocity,
l=Length of the flat spring which becomes the rotation axis and also gives the restitutive moment of the inverted pendulum,
L=Distance between the rotation axis of the flat spring of the inverted pendulum and the center of the top sphere,
I_s=Sectional moment of inertia of the flat spring of the pendulum,
E=Longitudinal modulus of elasticity of the flat spring of the pendulum,
W_m=Maximum wind pressure,

C_x=Resistance coefficient of the sphere of the pendulum,
S=Max. sectional area of the sphere of the pendulum.
Then, the following formula is easily obtained:

$$y_A=\frac{Ll(L-l)}{EI_s}C_xW_mS. \quad \cdots\cdots\cdots\cdots\cdots\cdots(3)$$

Using this formula, we determined the dimensions of the flat spring of the pendulum as follows. Assuming that $E=2.1\times10^{12}$ dyne/cm^2, $y_a=0.14$ cm, $l=3$ cm, $W_m=52.7$ kg/m^2, $C_x=0.42$, $S=\pi d^2/4$, $d=15$ cm, and $L=84.3$ cm, we obtained the following value of I_s: $I_s=6.43\times10^2$ cm^4. Therefore, when the two flat springs of breadth of 2.5 cm are used, the respective values of thickness of the two springs become 2.04 mm. Of course, in order to obtain the expression y_A, it was assumed that the upper part of the pendulum stem above the flat spring does not show any deformation due to the wind pressure applied on the sphere fixed to the top of the pendulum stem. To satisfy this assumption, as shown in Fig. 1, the structure of the stem becomes as follows: The lower part of the stem is an aluminium pipe having the length of 570 mm and the outer and inner diameters of 50 mm & 44 mm, and the upper part of it becomes also an aluminium rod of the length of 200 mm and the diameter of 23 mm. The lower part of the rod and upper part of the pipe are fixed to each other by screwing, and therefore the transversal vibration period of these combined stem becomes very short as about 0.007 sec., which is the calculated value.

Now, as the magnifying method for the present anemometer, we adopted the mechanical one which is quite of the same mechanism as the acceleration-seismometer[4] designed by the late Prof. Ishimoto. As shown in Fig. 1, the present magnifying mechanism is of the two-stepped lever system and the levers have the characters shown in Table 1.

Table I.

Lever \ Arms	Length of short arm	Length of long arm	Moment of inertia
The first-step magnifying lever	$l_1=15$ mm	$L_1=150$ mm	$I_1=250$ gr cm^2
The second-step magnifying lever	$l_2=15$ mm	$L_2=100$ mm	$I_2=10$ gr cm^2

The distance L_0 between the rotation axis of the inverted pendulum

4) M. ISHIMOTO, *Bull. Earthq. Res. Inst.*, **9** (1931).

and the first-step magnifying lever is taken as 9.0 cm for the present case. The equation of motion of the present anemometer due to wind pressure W is expressed by

$$\left(I_0+I_1\frac{L_0^2}{l_1^2}+I_2\frac{L_0^2L_1^2}{l_1^2l_2^2}\right)\frac{d^2\theta}{dt}+\lambda\frac{d\theta}{dt}+K_0\theta=Wh\,. \quad \cdots\cdots(4)$$

From this equation, we can see that the moments of inertia I_0, I_1, I_2, especially those of the first-step and the second-step magnifying levers I_1 and I_2 should be as small as possible, because they have the tendency to prolong the natural period[5] of the anemometer. The moment of inertia of the spherical head on the top of the pendulum stem has of course the large effect to increase the moment of inertia I_0, and therefore for minimizing it the spherical head used for the present machine is of copper-made thin shell. The details of the construction of it is explained in page 325 of this paper. Therefore, the moment of inertia of the pendulum body I_0 is taken as 13,000 gr cm^2, and the respective values of I_1 and I_2 are shown in Table I. The sectional form of the first-step lever of aluminium is of the cross type and the long arm of the second-step lever is a straw pipe of about 2 or 3 mm diameters. Therefore, the increase of the moment of inertia of the anemometer due to both the mechanical magnifying mechanism and the mechanical recording system becomes only about 2% for both two spheres which are fitted to the top of the stem of the inverted pendulum.

We adopted for the anemometer an air damper with an aluminium piston of 10 cm in outer diameter and an aluminium cylinder of 10.02 cm inner diameter. The clearance[6] between the piston and the cylinder

---

5) Natural period $T=2\pi\sqrt{\dfrac{I}{K_0}}$, where $I=I_0+I_1\dfrac{L_0^2}{l_1^2}+I_2\dfrac{L_0^2L_1^2}{l_1l_2}$.

6) The clearance e becomes as follows:

$$e=\left(\frac{6\pi\eta l}{\lambda}\right)^{1/3}\cdot rL\,, \quad \text{where}$$

r=Outer radius of the piston of the air damper,
l=Height of the same piston,
L=Distance between the rotation axis of the inverted pendulum of the anemometer and the piston axis of the air damper,
$\lambda=2\varepsilon I=2\omega I=\dfrac{4\pi I_0}{T_0}$ where $\varepsilon/\omega=1$,
T_0=Natural period of the inverted pendulum of the anemometer,
I_0=Moment of inertia of the inverted pendulum of the anemometer,
η=Coefficient of viscosity of air.

For the present anemometer, taking $r=5$ cm, $L=18$ cm, $l=5$ cm, $T_0=0.1$ sec, $I_0=4\times10^6$ gr-cm^2. and $\eta=1.81\times10^{-4}$ in C. G. S. Unit, we obtained $e=0.01$ cm.

inner wall becomes, therefore, 0.01 cm. The precision adjustment of the damping degree of the air damper is made by handling the cock attached to the damper to secure suitable entrance and exit of air through the cock.

By using the design of the anemometer discussed in the preceding section, we obtained the two new-designed anemometers which are shown in Figs. 2a, 2b & 2c. As shown in Figs. 2a, 2b and 2c, the actual anemometer is constructed so as to obtain the two components of the horizontal wind pressure, and therefore the springs used for the rotation axes of the inverted pendulum are composed of two sets and one of them is connected to the base plate of the anemometer and the other to the lower end of the pendulum stem, and each set has two flat springs. Of course, these two sets of spring are fixed to form a right angle with each other. Each set of spring is composed of two flat spring plates which give the restitutive force to the inverted pendulum of the anemometer. Therefore these two sets of spring give respectively the restitutive forces whose direction of action is perpendicular to each other. Two air-dampers are used, as shown in Figs. 2b and 2c, of which the one cylinder is fixed to the base of the anemometer, and the other cylinder is fixed to the stem of the inverted pendulum and can move freely in two horizontal components of direction.

The recording system of the present anemometer is a kind of mechanical one, and is composed of smoked paper system which is commonly used in the field of seismometer in Japan. The driving motor of the recording drum for the present recording apparatus is a synchronous motor of 6 watt and 1 r.p.m.

By the gear mechanism, the peripheral speeds of the recording smoked paper on the drum are made to have three kinds such as 0.4 cm/sec, 0.1 cm/sec and 0.04 cm/sec. The drum is made of aluminium, as in the case of the Ishimoto acceleration-seismometer[7].

As may be seen in Fig. 2a, all the parts except the spherical part blown directly by wind of the present anemometer are set in a suitable cover for the purpose of avoiding the attack of the wind pressure. The lower part of the cover is a cylinder, which forms the foundation of the anemometer. Both the top and bottom thick plates of it is made of casting, and the top thick plate becomes the base plate for the inverted pendulum of the anemometer. Of course, to this base plate is fixed one of the two sets of the flat springs giving the restitutive

7) M. ISHIMOTO, *loc. cit.*

forces to the pendulum. The recording drum is set on the bottom plate of this cylinder foundation, and the diameter and the height of this cylinder become 80 cm and 50 cm respectively, and the top and bottom plates are made of cast iron and the cylinder wall is composed of common steel plate. The total height of the anemometer becomes 200 cm, and it is made heavy, the weight being 100 kg-wt, so as to avoid the rattling and shaking motions of the base and the cover of the anemometer when attacked by a strong wind.

3. The character test of the anemometer.

The records of the wind pressure are taken by the smoked paper method as already explained. Therefore solid friction between the recording needle and the smoked paper affects badly the sensitivity of the anemometer. This needle is pivoted to the end of the straw pipe which becomes the long arm of the second-step magnification. We first studied this solid friction by a common method as follows:

The solid friction term ρ and the damping ratio V are connected by $V=\{W_k-2\rho(1+V)\}/W_{k+1}$, where W_k, W_{k+1} are respectively the Kth and $(K+1)$th double amplitudes recorded on the smoked paper in the state of free damped vibration of the anemometer. Therefore, plotting W_k and W_{k+1} on the section papers as shown in Fig. 3, we obtained, using the above expression and Fig. 3, the following values of V and ρ:

$V=1.05$, $\rho=0.025$ mm.

Therefore the solid friction ρ' becomes as follows:

$\rho'=1.86\ \text{kg/m}^2\times 0.025\ \text{mm}$

$=0.46\ \text{kg/cm}^2$.

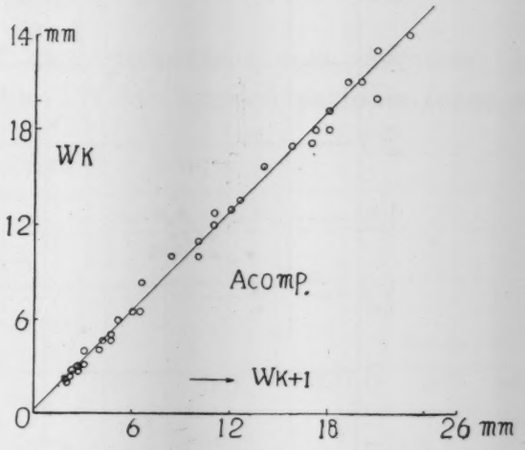

Fig. 3.

From this experiment, we can see that the present anemometer with smoked paper recording mechanical method cannot record wind pressure less than 0.46 kg/cm², or in other words, it can record wind velocity greater than 0.9 m/sec.

Now, due to its construction, the present anemometer has some effective inertia. Therefore, when its foundation is vibrated through

some source, it comes to have the tendency of doing the action of a vibrograph. Of course, the effective masses of the inverted pendulum are made as small as possible, but the unavoidable fact is that the moment inertia of the apparatus does its action as a vibrograph which is caused by a vibration source applied to the base of the foundation of the machine. Hereupon, using a rotary with an unbalanced mass of small scale, we applied a horizontal force to the anemometer to obtain the sensibility as a vibrograph, and in addition to this experiment we installed a acceleration seismograph[8] on the top face-plate of the base cylinder, for comparing both of these experimental results. The experimental results are shown in Figs. 4a and 4b, in which the abscissae show the varied period of the applied unbalanced forces and the ordinates the deflection a_1 of the anemometer in Fig. 2a and the deflection a_2 of the acceleration seismograph. Moreover, Figs. 4a and 4b show the respective results referring to the two components A and B. These figures show that the present anemometer has somewhat the properties

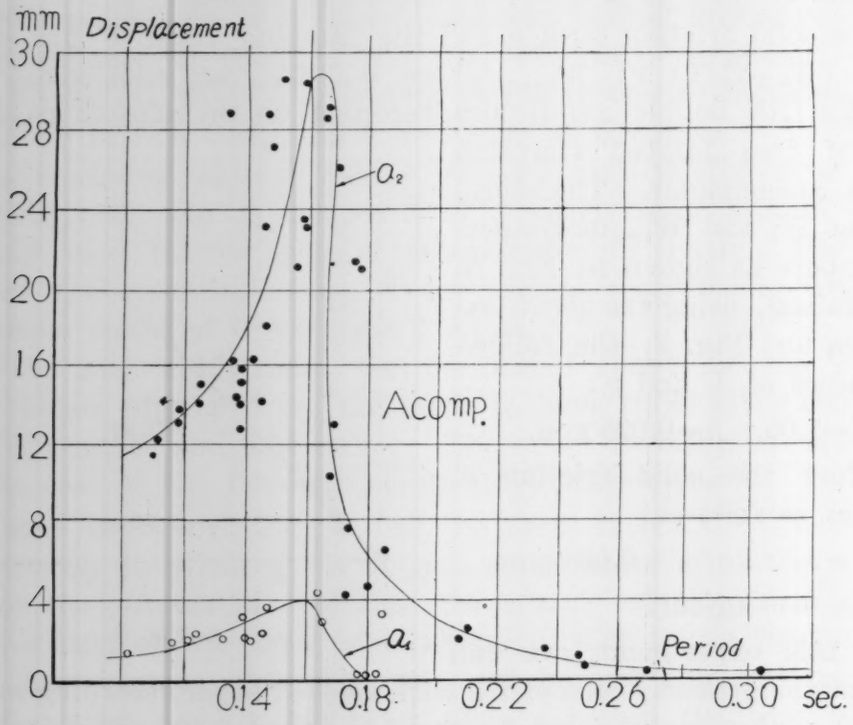

Fig. 4a. A comp.

8) Portable acceleration seismograph of period 0.1 sec, sensibility = 2.0 gal per mm on the record and critical damping.

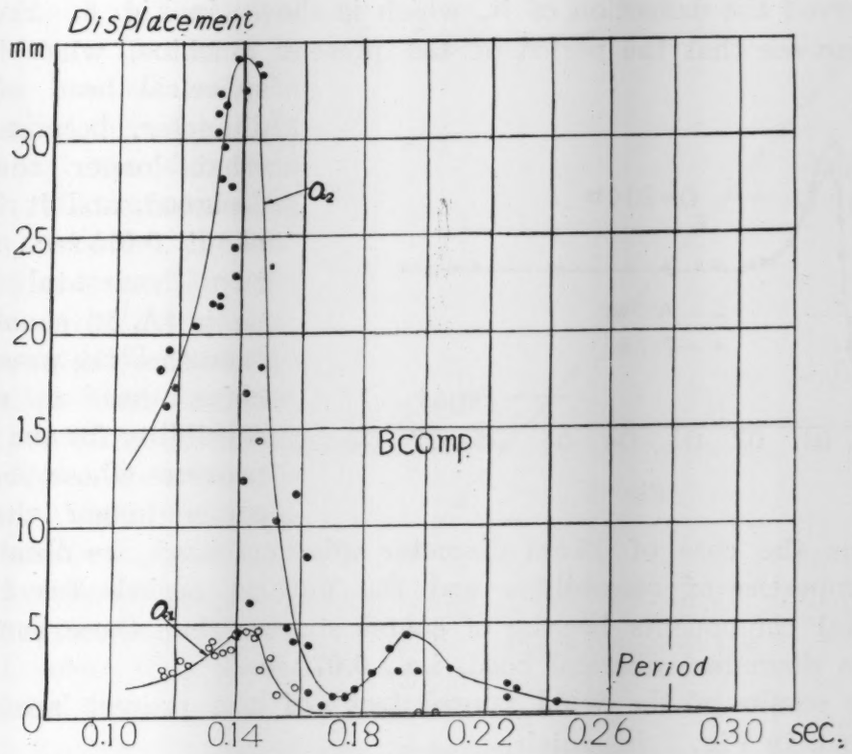

Fig. 4b. B comp.

of a vibrograph, but the ratio of two deflections a_1/a_2 assumes, as shown in Fig. 5, the constant value 1/8 for applied periodic force of which the period becomes greater than 0.12 sec. Therefore, we can correct the recorded deflections of the anemometer by installing an acceleration seismograph in the base cylinder of the anemometer.

Next, as a sensibility test of the present anemometer the following experiment was carried out. Applying the periodic force horizontally on the center of the spherical head of the present machine,

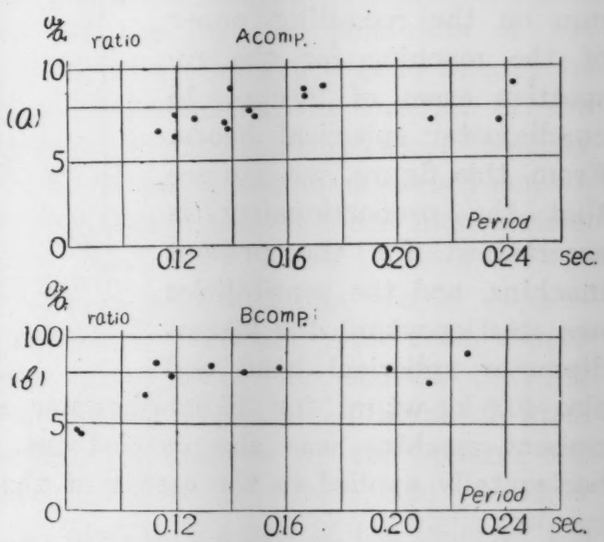

Fig. 5. A comp. B comp.

we observed the deflection of it, which is shown in Fig. 6. From Fig. 6, we can see that the period of the present machine, when it has a spherical head of 20 cm diameter, becomes somewhat longer than that designed, and it becomes about 0.075 sec. for the two horizontal components (A, B) equally, and therefore the present machine has a constant sensibility for the periodic pressure whose period becomes longer than 0.20 sec. For the case of 15 cm diameter spherical head, we obtained the same properties of sensibility, and the natural periods for the two horizontal components become of course shorter than those in the case of 20 cm diameter spherical head, i.e., 0.070 sec.

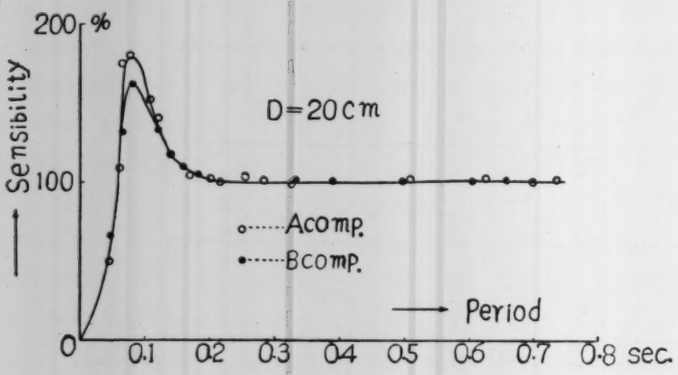

Fig. 6.

The results of the wind tunnel test[9] of the present anemometer are shown in Fig. 7 in which the abscissa corresponds to wind pressure in kg-wt/m² and the ordinate to the reading of the displacement in mm on the recording paper of the machine for the respective cases of 20 cm-, 15 cm-diameter spherical heads. From this figure, we can see that the proportionality is ascertained for the present machine, and the sensibilities are 28.0 kg-wt/m² for 20 cm-diameter spherical head and also 45.5 kg-wt/m² for 15 cm-diameter one. The statical test of the present machine was also carried out, in which the statical loads are horizontally applied to the center of the spherical head.

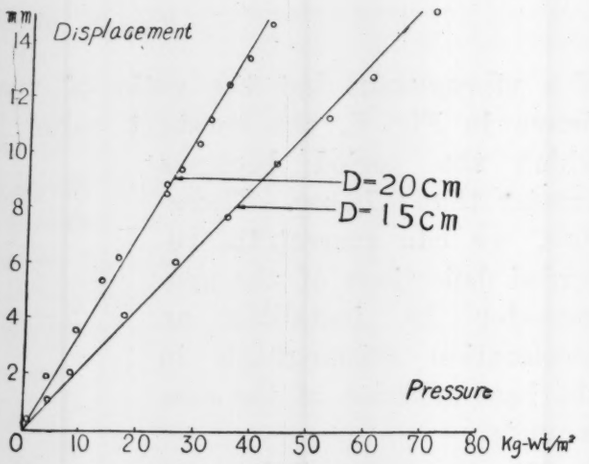

Fig. 7. Wind tunnel test.

9) The test was carried out with 1.5 m–3.0 m section wind tunnel belonging to the former Aeronautical Research Inst., University of Tokyo.

The results of the statical test are shown in Fig. 8 in which the statical loads in gram applied are taken in abscissa, and the deflection δ in mm of the recording needle in ordinate. In this figure, we can see that the deflection $\delta=1.0$ cm corresponds to the total resistance 435 gr for the 20 cm diameter spherical head and 443 gr for the 15 cm diameter one respectively. Therefore, using the relation $R=C_xq\cdot S$, where R=total resistance, q=pressure in unit area, and S=diametral area of section, we calculated the value of the resistance coef. C_x as follows;

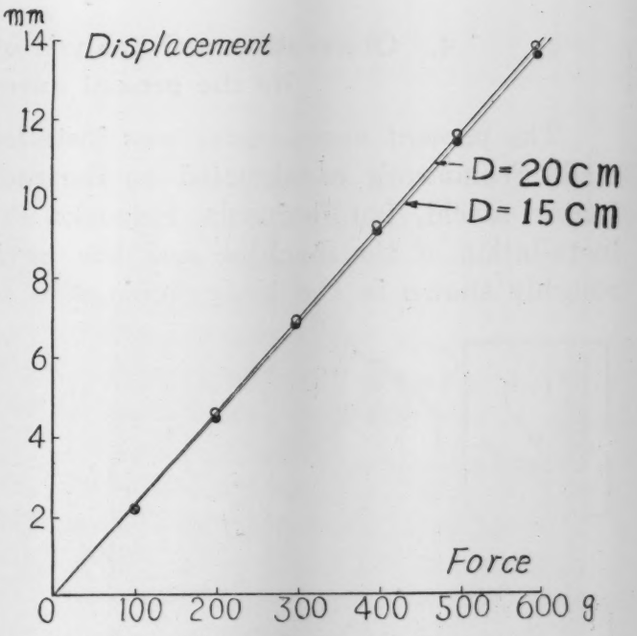

Fig. 8. Statical test.

$C_x=0.48$ for 20 cm dia. spherical head,
and $C_x=0.53$ for 15 cm dia. spherical head.

The value of this resistance coefficient for 15 cm diameter spherical head becomes larger than that for 20 cm dia. spherical head about 5%. This fact, we think, may be explained as follows: The aluminium bowl fixed to the top of the stem of the inverted pendulum of the machine, the position of which is under the spherical head as may be seen in Fig. 2a, 2b, for the purpose of protecting the interior of the machine against rain, affects unfavourably the wind resistance. Namely the effect of this bowl, of which the effective section area is 7 cm, on the resistance for the case of 15 cm diameter head becomes more serious than for the case of 20 cm diameter head.

The spherical heads used for the present machine are of copper-made thin shell, and the two spherical bowls are made from copper plate of 0.5 mm thickness by the operation of the spatula drawing method, and are soldered at the diametral circle. A stem of steel rod of 10 mm diameter is set through the interior of the sphere, one end of it is soldered to the interior top of the sphere, and the other end, which is outside the sphere, is fixed to the top of the stem of the inverted pendulum by screw.

4. Observation and analysis of the natural wind by the present anemometer.

The present anemometer was installed on the floor of a wooden-made framework constructed on the roof of a Japanese ware-house at Inatori-machi, Izu Peninsula, Shizuoka Prefecture. The location of the installation of the machine and the environment of the location are roughly shown in the topographic map of Fig. 9. The east side of the location faces Pacific Ocean, and both the north and west sides face the Izu mountain range. Fig. 10 is the photograph of the anemometer installed on the roof of the ware-house at the location explained above.

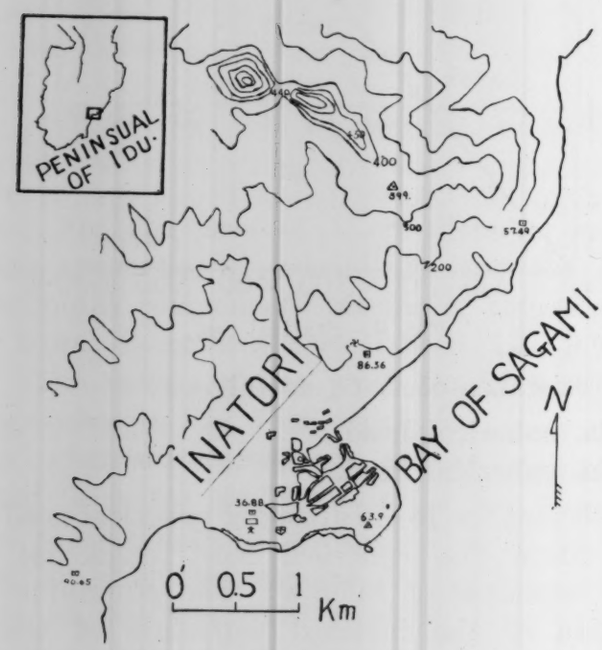

Fig. 9.

Now, some of the records of natural winds obtained by the present anemometer are shown in Figs. 11a, 11b. They are so complicated that it is very difficult to study the structure or the breath of the natural winds. Thus, it is also difficult to obtain the so-called breaths of natural wind or the periods of variation of the wind pressure or wind velocity.

By the following method, we analysed the records in order to obtain the period of the natural wind. The records used for the present analysis are those of the monsoons of the South-West wind of December 2, 1940, as well as those of the North-East wind of March 2, 1941, both having their own peculiar characters.

By investigating these records minutely, we found that during the period between two zero wind pressures there are complicated undulations of wind pressure, and also many maximum and minimum pressure intensities, and that the wind having the greatest intensity may be expected during this period. Therefore, it may be reasonable to assume that the variation of the wind pressure are generally expressed by the

diagrammatic schema shown in Fig. 12.

Considering the upper schema shown in Fig. 12, we shall assume T_0 to be the period of zero wind pressure. T_0 in this case is the duration time from the 1st zero wind pressure to the next zero wind pressure. We will also assume the largest wind pressure in this period T_0 to be Q_0.

As may be seen in the lower schema shown in Fig. 12, the wind pressures have a complicated undulation character with many maximum and minimum values of pressures for the duration time T_0. Putting the duration time between the two continued minimum points as t_1, we will assume t_1 to be the period of the 1st order. (see t_1 of Fig. 12.)

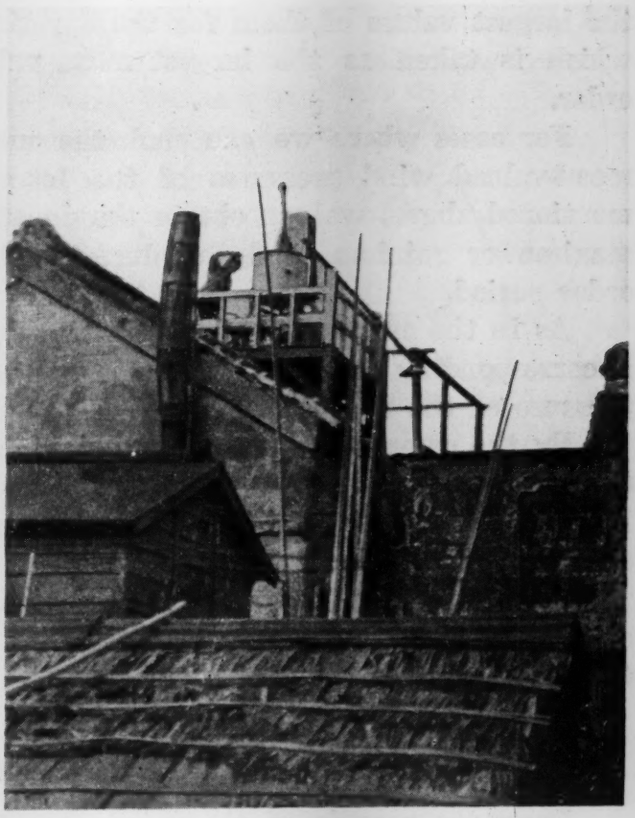

Fig. 10. Anemometer installed on the roof of a ware-house.

We assume that the respective two differences between both two extreme ends of the time t_1, or two continued minima and the maxima in time t_1 are shown by q_i and q_{i+1}.

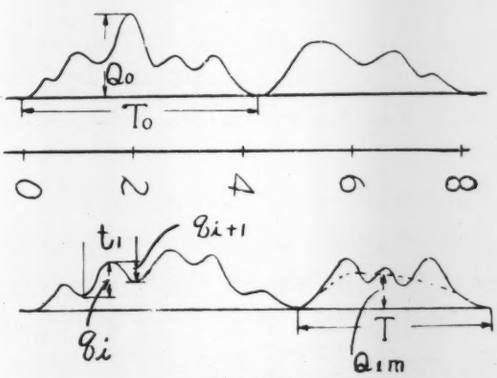

Fig. 12.

Then putting the arithmetic mean of q_i and q_{i+1} as q_1 or $q_1=(q_i+q_{i+1})/2$, we will assume q_1 to be the maximum wind pressure with period t_1.

The mean valued curves connecting the mean values of the maxima and minima which occur between the time T_0, shall be taken as the mean wind pressures of the 1st order. We will also express

the largest values of them for the duration time T_0 by the letter Q_1 which is taken as the largest mean valued wind pressure of the 1st order.

For cases where we can find the maxima and minima in these mean-valued wind pressures of the 1st order, by the same method as mentioned above, we can obtain the duration time t_2 of continued two maxima or minima, and this duration time t_2 shall be called the 2nd order period.

As in the cases of obtaining q_1 and Q_1, the largest wind pressure q_2 corresponding to the period t_2, and the largest mean-valued wind pressure of the 2nd order Q_2 are also generally obtainable.

By the same treatment as explained above, the 3rd order quantities t_3, q_3, Q_3, and the 4th order quantities t_4, q_4, Q_4, etc. are also obtainable. In brief, by using these obtained quantities such as T_0, Q_0 and t_1, q_1, Q_1, t_2, q_2, Q_2, ..., t_n, q_n, Q_n, we intend to conduct analysis of the natural wind structures for the following three cases; (1) breath of natural wind, (2) wind pressure and breath, and (3) wind pressure and the blowing direction.

5. Analysis results I. Breath or period of natural wind.

From the records of the wind pressure obtained by the present anemometer on Dec. 2 in 1940 and March 2 in 1941, we read first the values of T_0 and t_1 which are already respectively defined in the preceding section.

Then, grouping the values of T_0 and t_1 by the following method, we will study the statistical natures of them respectively.

For example, express the two values of T_0 by T_{0i} and T_{0i}' respectively. Then, all the values of T_0 between T_{0i} and T_{0i}' are represented by the mean value of T_{0i} and T_{0i}' or T_{0m} in case $T_{0m}=(T_{0i}+T_{0i}')/2$, when they are satisfied by the following expression:

$$2(T_{0i}-T_{0i}')/(T_{0i}'+T_{0i})=1/10 \quad \text{.....(10)}$$

Now we assume that the total sum n of all the values of T_0 between T_{0i} and T_{0i}' under the condition expressed by (10) shows the fluctuation degree of T_0. By this conception, we obtained the frequency curve of T_0 or $T_0 \sim n$ curve which is necessary for studying the statistical natures of the variation of the breath of the natural wind.

Figs. 13 and 14 show $T_0 \sim n$ curves for the 10 minutes observation for the two cases, i.e., the SW wind from 14 h 5 m to 14 h 15 m on Dec.

2, 1940 and NE wind from 16 h 21 m to 16 h 31 m on March 2, 1941. From these figures, we can see that for the SW wind, T_0 whose values are 1.7 sec., 3.2 sec., 6.1 sec. and 15 sec., become predominant and for the NE wind T_0 whose values are 0.5 sec. and 1.6 sec. become predominant.

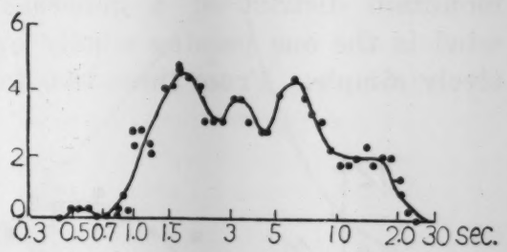

Fig. 13. Statistics of T_0 period of SW wind from 14 h 5 m to 14 h 15 m, Dec. 2, 1940.

Next, taking the record of SW wind from 14 h 14 m to 14 h 15 m 20 s on Dec. 2, 1940 and that of NE wind from 16 h 21 m to 16 h 23 m on March 2, 1941 by the same procedures as in the preceding cases of T_0, we obtained $t_1 \sim n$ curves as shown in Figs. 15 and 16 in which t_1 becomes the period of the 1st order explained in the preceding section. From these figures, we can see that for SW wind, t_1 with value of 0.6 sec. and 0.95 sec. become predominant and for NE wind, t_1 with value of 0.5 sec. becomes predominant.

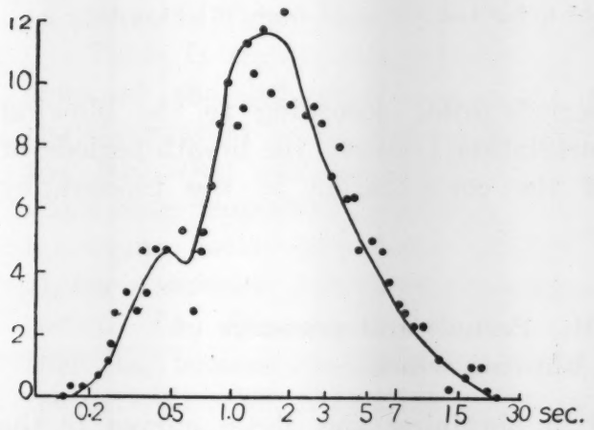

Fig. 14. Statistics of T_0 period of NE wind from 16 h 21 m to 16 h 31 m, March 2, 1941.

From these four figures (Figs. 13, 14, 15 and 16), we can see generally that for two cases of breath such as T_0 and t_1, those corresponding to the SW wind become somewhat longer than those corre-

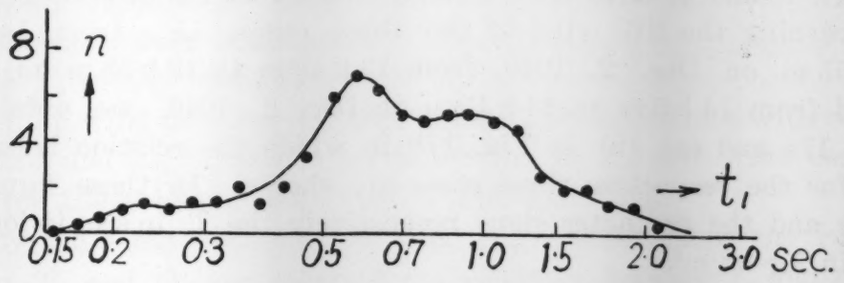

Fig. 15. Frequency curve of t_1 for the SW wind from 14 h 14 m to 14 h 15 m 20 s, Dec. 2, 1940.

sponding to the NE wind.

Now we can see that the SW wind is the one passing over the mountain district of a generally complicated topography and the NE wind is the one passing wholly over the sea surface which is comparatively simple. From these two facts, we can say, about the properties

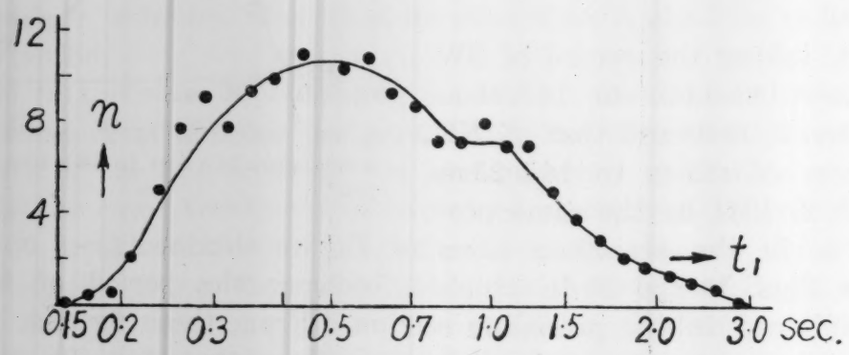

Fig. 16. Frequency curve of t_1 for the NE wind from 16 h 21 m to 16 h 23 m, March 2, 1941.

of natural wind breath whose periods differ according to the blowing directions, that there is some correlation between the breath periods of natural winds and the degree of the complication of the topography over which the wind blows.

6. Analysis results II. Periods and pressures of natural blowing winds.

With the same records used in obtaining the $T_0 \sim n$ curves in the preceding section, we will study the properties of $T_0 \sim Q_0$, $T_1 \sim Q_1$, $t_1 \sim q_1$ curves in this section. Of course, the respective measurings of Q_0, T_1, Q_1, t_1 and q_1 have been already defined in the preceding section.

Concerning the SW wind of the three cases, i.e., from 14 h 14 m to 14 h 15 m on Dec. 2, 1940, from 13 h 49 m to 13 h 59 m on Dec. 2, 1940 and from 14 h 5 m to 14 h 15 m on Dec. 2, 1940, we obtained (a) in Figs. 17a and (a), (b) in Fig. 17b in which the relation between T_0 and Q_0 for the respective three cases are shown. In these figures the abscissae and the ordinates show respectively the T_0 in sec. in log. scale and Q_0 in kg-wt/m^2.

Next, concerning the NE winds of the three cases, i.e., from 16 h 21 m to 16 h 22 m on March 2, 1941, from 16 h 21 m to 16 h 31 m on

March 2, 1941, from 17 h 45 m to 17 h 55 m on March 2, 1941, and from 16 h 22 m to 16 h 23 m on March 2, 1941, we obtained (a) in Fig. 18a, (a), (b) in Fig. 18b and (a) in Fig. 18a, in which the relations of T_0 and Q_0 of these four cases are shown respectively. The units of both abscissae and ordinates in these figures, are the same as in the figures for SW winds. From these figures for both the SW and the NE winds, we can see that the breaths of period T_0 having the effective maximum pressure become as shown in Table II.

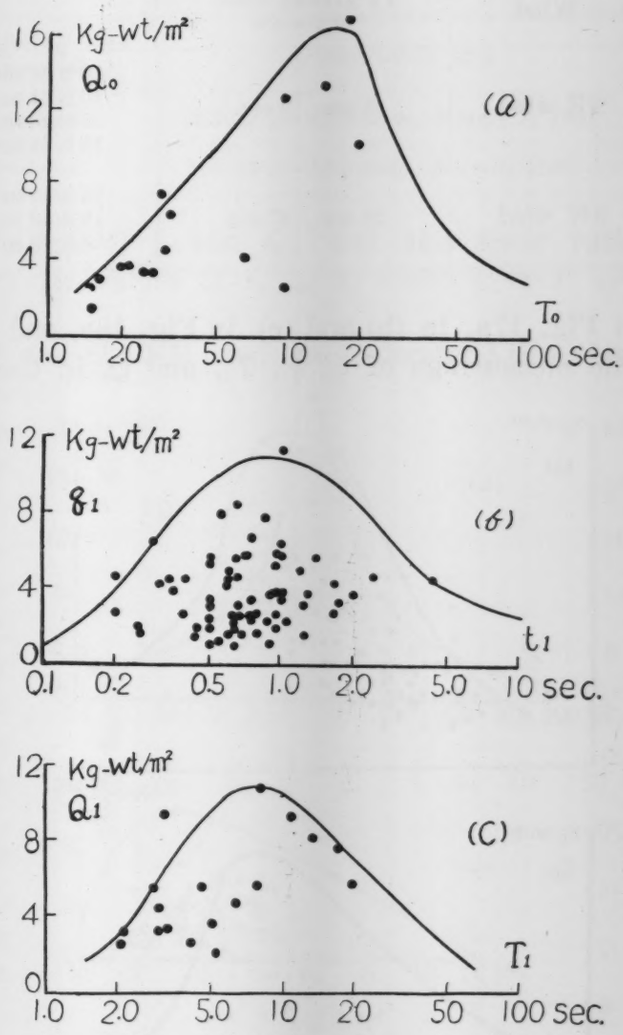

Fig. 17a. The SW wind of 14 h 14 m~14 h 15 m, Dec. 2, 1940.
(a): $T_0 \sim Q_0$, (b): $t_1 \sim q_1$, and (c): $T_1 \sim Q_1$.

Table II shows that in spite of the difference of the observation time, both the NE wind and the SW wind have respectively the maximum wind pressures Q_0 for a suitable breath of period T_0. For example, they (Q_0) become maximum respectively when breath T_0 becomes 5 or 9 sec. for the NE wind, and when T_0 becomes 15 or 17 sec. for the SW wind. Moreover, it is a remarkable fact, that the breath T_0 giving effectively maximum wind pressure becomes different in accordance with the blowing direction and the breath T_0 corresponding to the SW wind becomes two or three times longer than that of the NE wind.

By the same treatment as that which made clear the relation between T_0 and Q_0, we obtained the relations between t_1 and q_1 and also those between T_1 and Q_1, which are respectively shown in (b) and (c)

Table II. Breath period T_0 of maximum pressure Q_0.

Wind	T_0 giving max. pressure	Observation date
NE wind	5 sec., 9 sec.	16 h 21 m~16 h 22 m, 16 h 21 m~16 h 31 m, 17 h 45 m~17 h 55 m, 16 h 22 m~16 h 23 m } March 2, 1941.
SW wind	15 sec., 17 sec.	14 h 14 m~14 h 15 m, 13 h 49 m~13 h 59 m, 14 h 5 m~14 h 15 m } Dec. 2, 1940.

in Fig. 17a, in (b) and (c), in Fig. 18a, and also in (b) and (c) in Fig. 18c. The measurings of t_1, q_1, T_1, and Q_1 in these Figs. have already been defined in the preceding section. These figures show that the wind pressures defined by q_1 and Q_1 have also the maximum values corresponding to suitable breaths of period t_1 and T_1 respectively in spite of the difference of the blowing direction of the wind, and the values of t_1 and T_1 giving maximum values as shown in Table III.

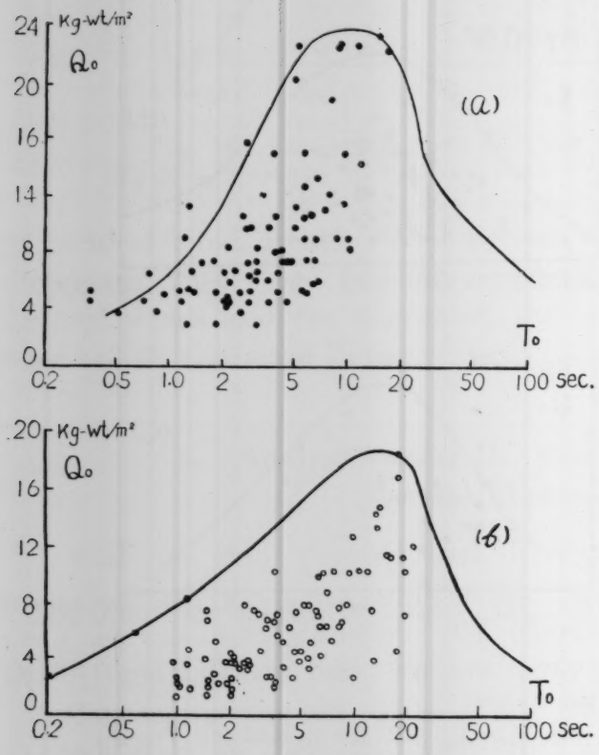

Fig. 17b. (a): T_0~Q_0 for the SW wind of 13 h 49 m~13 h 59 m, Dec. 2, 1940.
(b): T_0~Q_0 for the SW wind of 14 h 5 m~14 h 15 m, Dec. 2, 1940.

From Table III, we can see that, as in the case of T_0 and Q_0 shown in Table II, in spite of the blowing direction of natural wind, there are wind breath periods T_1 and t_1 which give respectively maximum wind pressure defined by Q_1 and q_1 respectively. It is also remarkable that the breath periods t_1, T_1 of the SW wind becomes two times longer than those of the NE wind. Now, for the respective winds of NE and SW under discussion in the above paragraph, we obtained Table IV, in which the

Table III. The breath periods t_1, T_1 giving the maximum values of q_1 and Q_1 wind pressure distribution.

Wind direction	t_1 giving max. values of q_1	T_1 giving max. values of Q_1	Observation date
NE wind	0.4–1.0 sec.	4 sec.	16 h 21 m~16 h 22 m, March 2, 1941
SW wind	0.9 sec.	8 sec.	14 h 14 m~14 h 15 m, Dec. 2, 1940

maximum values of wind pressure of q_1 and Q_1, and also their ratio q_1/Q_1 are given in addition to the values of t_1/T_1, in which t_1 & T_1 are given in Table III.

Comparing the SW wind and the NE wind, we understand that they have respectively some interesting characters, as may be seen in Table IV. For SW wind, in the breath period T_1 such as 8 sec. of pressure intensity Q_1=11 kg-wt/m², there is a breath period t_1 of about 1/10 times of T_1, but their pressure intensity q_1 becomes 11 kg-wt/m² which is equal to Q_1. For the NE wind, in the breath period T_1 such as 4 sec., there is a breath period t_1 of about 1/10~1/4 times of T_1 of which the max. pressure intensity q_1 becomes about 60% of Q_1.

This analysis shows that the structure of the SW natural wind becomes more complicated than that of the NE natural wind, which fact is clear when we compare the two records of both winds. (See Figs. 11a, b.) And this property, we think, may perhaps be explained from the

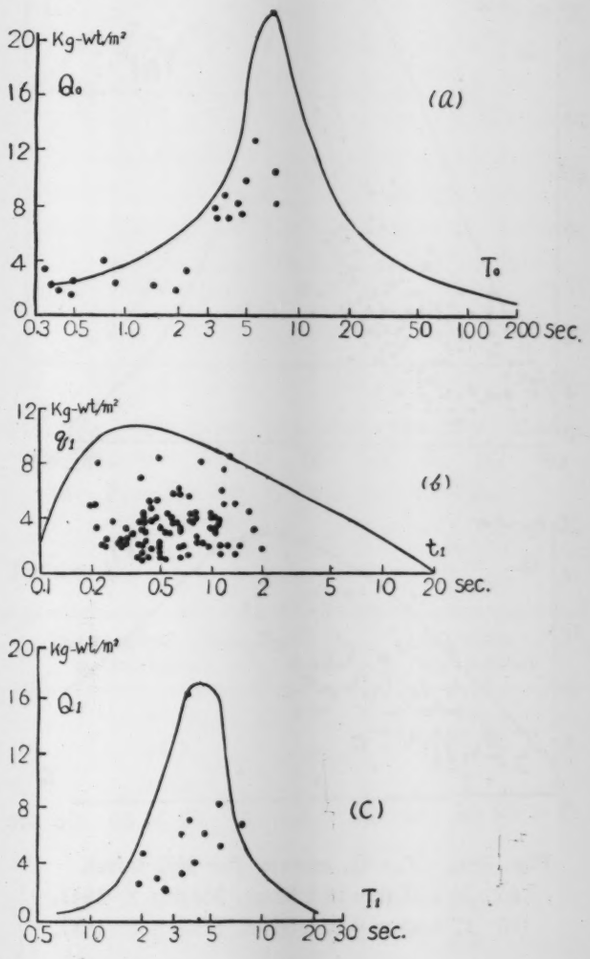

Fig. 18a. NE wind, 16 h 21 m~16 h 22 m, March 2, 1941.
(a) T_0~Q_0, (b) t_1~q_1, (c) T_1~Q_1.

Table IV. Max. values of q_1 and Q_1.

Kind	Max. wind pressure			Ratio of Periods of breath t_1/T_1
	q_1 in kg-wt/m²	Q_1 in kg-wt/m²	Ratio q_1/Q_1	
NE wind	10.5	17.0	0.62	0.10
SW wind	11.0	11.0	1.0	0.11

(Remark: t_1 and T_1 are given in Table III.)

effect of the topography of the districts over which the natural wind blows, as already discussed in the preceding section.

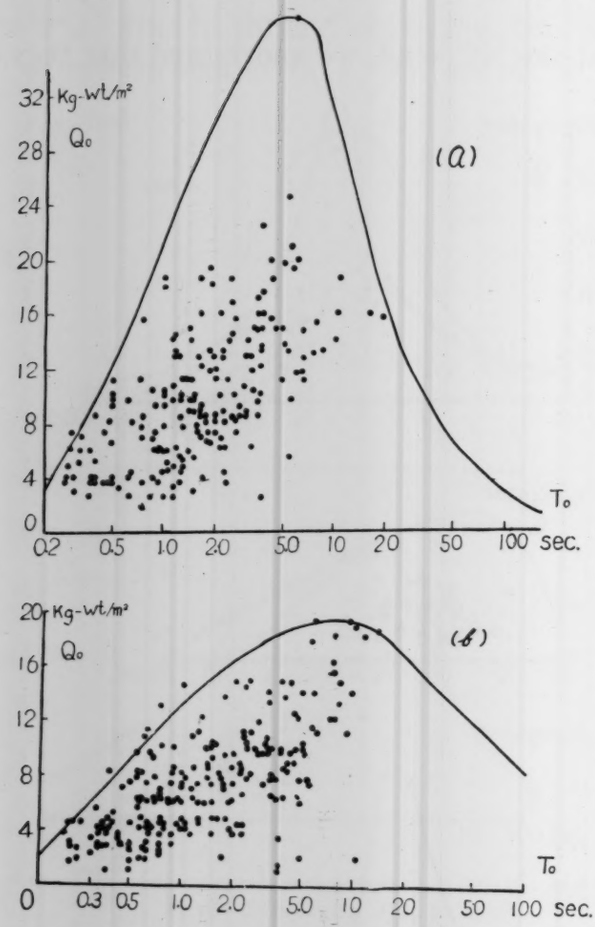

Fig. 18b. $T_0 \sim Q_0$ curves for NE wind.
(a) 16 h 21 m~16 h 31 m, March 2, 1941.
(b) 17 h 45 m~17 h 55 m, March 2, 1941.

7. Analysis results III. Wind pressures and wind directions.

For the purpose of studying the relation between the wind pressure and the wind direction, using the rectangular coordinates (x-, y-axis), we obtained (a), (b), (c) and (d) in Fig. 19, for the SW wind on Dec. 2, 1940, in which the plotted points correspond to every two components of wind pressures for each 5 sec. Of course these two components were obtained by the present anemometer, and the x-axis becomes the NE-O-SW component of the present position of the anemometer and the y-axis the NW-O-SW component. The four graphs (a), (b), (c) and (d) in Fig. 19 correspond to the duration time of 1 minute from 13 h 52 m to 13 h 53 m, from 13 h 57 m to 13 h 58 m, from 14 h 0 m to 14 h 1 m and from 14 h 14 m to 14 h 15 m on Dec.

2, 1940 respectively. By the same way as in Fig. 19, concerning the NE wind on March 2, 1941, we obtained five graphs as shown in Figs. 20 (a), (b), (c), (d) and (e). In these graphs, the plotted points correspond to every two components of wind pressure for every 0.25 sec.

By using the wind pressure records of the two components p_x and p_y of the natural wind, we could obtain the resultant pressure p, while its blowing direction φ may be obtained by using the following relations:

$$\left.\begin{aligned} p^2&=(p_x)^2+(p_y)^2\,,\\ \varphi&=\tan^{-1}(p_y/p_x)\,. \end{aligned}\right\} \quad \cdots (11)$$

By this method, we are able to study the variations of p and φ with time variation.

From Figs. 19 and 20, we can see that both the SW- and the NE-winds have the same nature, i.e., all the points showing the wind

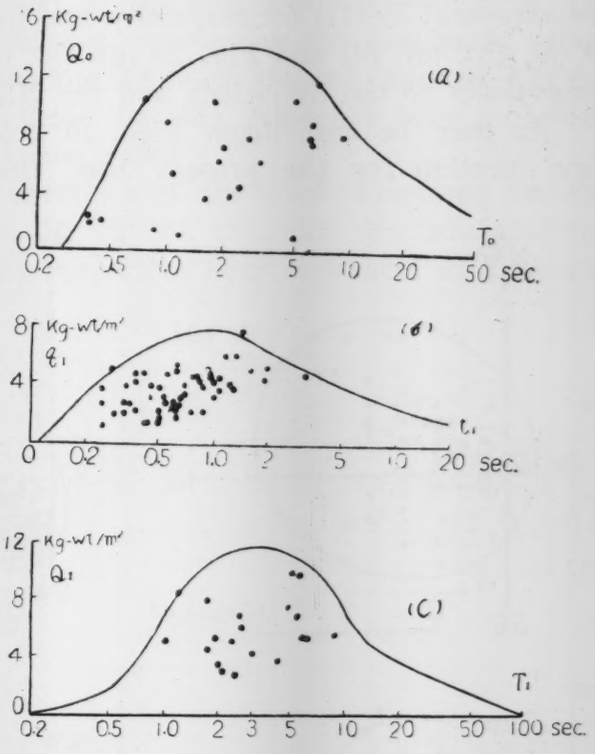

Fig. 18c. SW wind, 16 h 22 m~16 h 23 m, March 2, 1941.
(a) T_0~Q_0, (b) t_1~q_1, (c) T_1~Q_1.

Table V.

Wind	Observation date	Max. wind pressure p (in kg-wt/m²)	Direction φ (in degree)
SW-wind	13^h52^m~13^h53^m	12.8	36
	13 57 ~13 58	13.8	−61
	14 0 ~14 1	16.9	57
	14 14 ~14 15 20^s	16.5	16
NE-wind	15^h18^m~15^h19^m	19.0	191
	16 21 ~16 22	39.7	174
	16 22 ~16 23	18.9	169
	16 31 ~16 32	26.1	188
	17 41 ~17 42	18.5	180

pressure for a certain time interval are included in an ellipse of which the long axis becomes the maximum wind pressure for that time interval.

Table V shows the maximum pressure p and its direction φ which are expressed by (11) for respective one minute durations shown in Fig. 19 (a), (b), (c), (d) and Fig. 20 (a), (b), (c), (e) and (d) which correspond respectively to the SW-winds and the NE-winds.

As may be seen from Figs. 19 & 20 and also Table V, for these time duration for the present case, the blowing directions of these

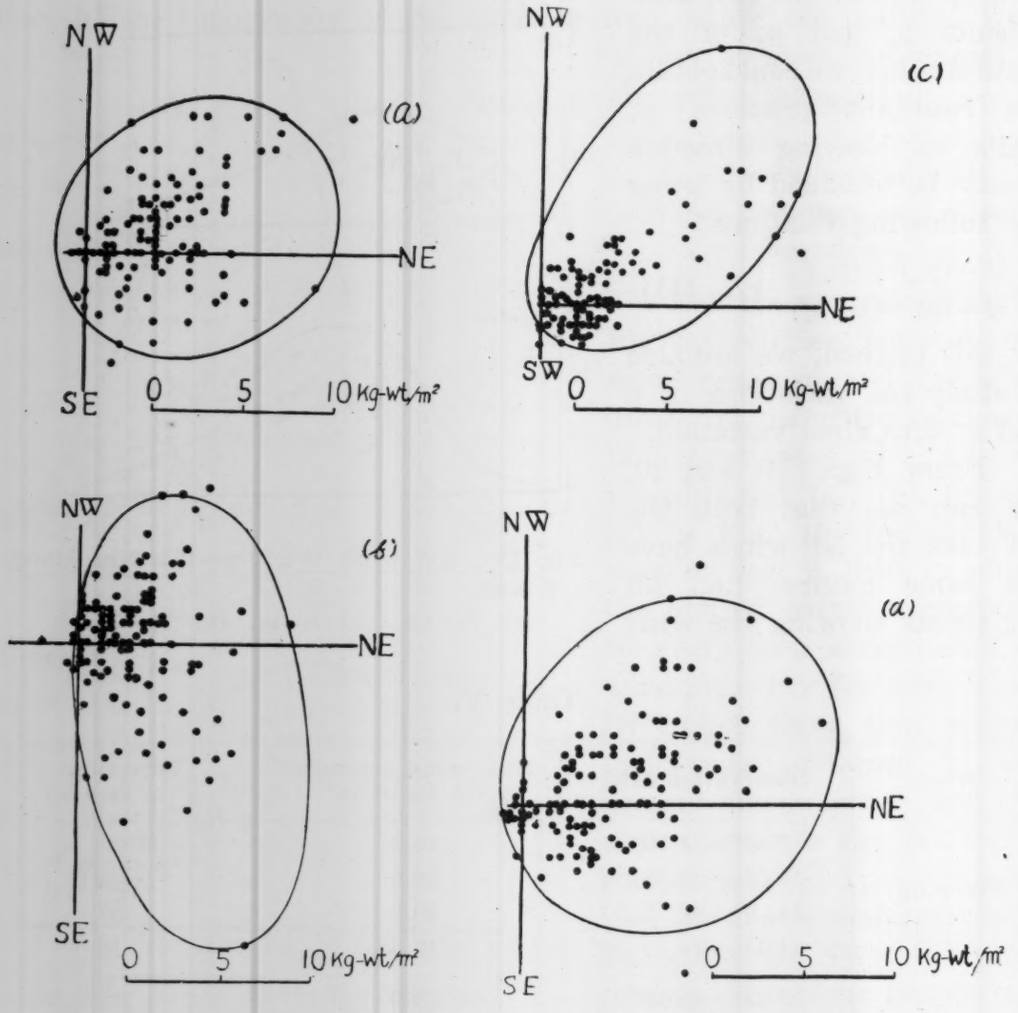

Fig. 19. Relation between wind pressure and wind direction for the SW wind.
(a) 13 h 52 m~13 h 53 m, Dec. 2, 1940,
(b) 13 h 57 m~13 h 58 m, Dec. 2, 1940,
(c) 14 h 0 m~14 h 1 m, Dec. 2, 1940,
(d) 14 h 14 m~14 h 15 m 20 s, Dec. 2, 1940.

maximum pressure for the SW wind vary distinctly for wide range such as 118° from 57° to −61°, but those for the NE wind do not have a distinct wide variation range, and it becomes the value such as 22° from 169° to 191°. On the contrary, concerning the maximum values of their wind pressure, those for the SW-wind do not have a distinct variation of wide range, but those for the NE-wind have a distinct variation of range of about 2 times wider.

Table VI shows the time variations of the wind directions for the time durations shown in Figs. 19 and 20, in which are tabulated the following four quantities : (1) the respective long and short axes 2a and

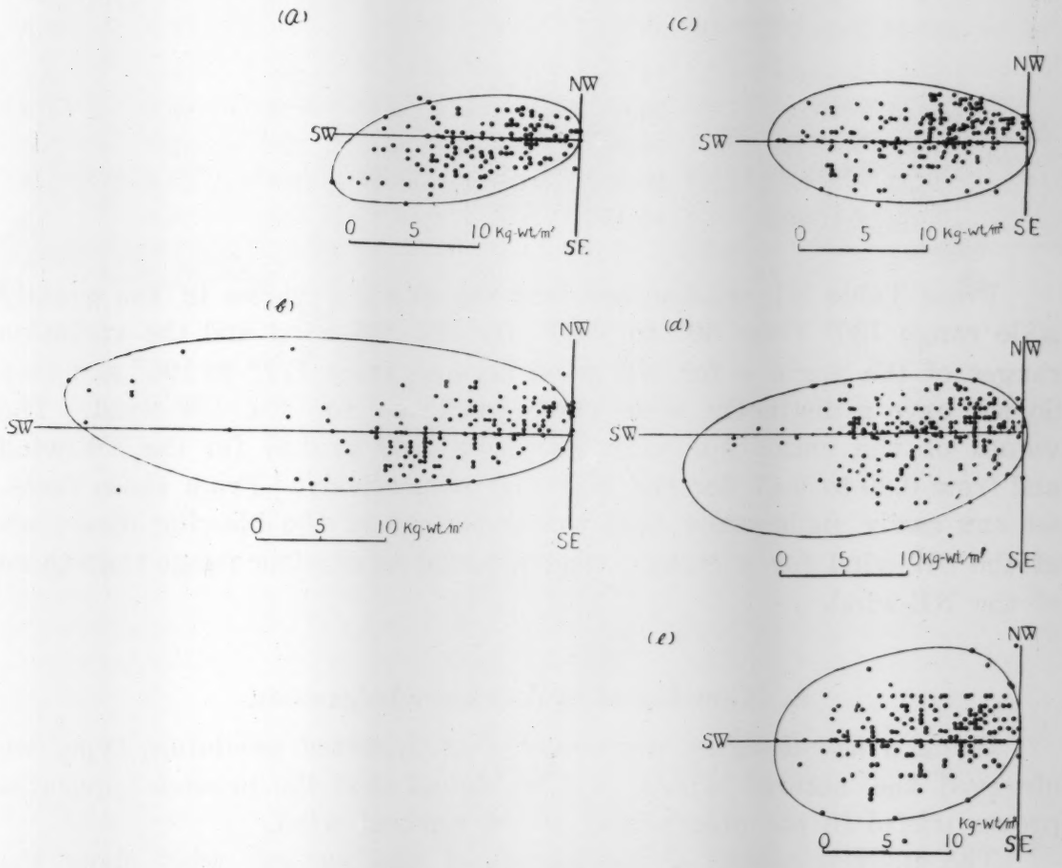

Fig. 20. Relation between wind pressure and wind direction for the NE wind.
(a) 15 h 18 m~15 h 19 m, March 2, 1941,
(b) 16 h 21 m~16 h 22 m, March 2, 1941,
(c) 16 h 22 m~16 h 23 m, March 2, 1941,
(d) 16 h 31 m~16 h 32 m, March 2, 1941,
(e) 17 h 41 m~17 h 42 m, March 2, 1941.

2b of the ellipses shown in Figs. 19 and 20, (2) the angle φ between the long axis of the ellipse and the axis of NE-O-SW, (3) the coordinates of (x, y) of the center of the ellipse and also (4) the ratio b/a between the long and short axes 2a and 2b respectively.

Table VI.

Wind	Date	$2a$ (in kg-wt/m^2)	$2b$ (in kg-wt/m^2)	b/a	φ (in degree)	x (in kg-wt/m^2)	y (in kg-wt/m^2)
SW-wind	$13^h52^m\sim13^h53^m$	15.0	13.5	0.87	34	6.0	1.1
	13 57 ~13 58	25.2	12.2	0.49	−80	6.0	4.2
	14 0 ~14 1	19.5	11.1	0.57	50	6.7	5.8
	14 14 ~14 15 20^s	19.1	16.3	0.85	44	8.0	2.2
NE-wind	$15^h18^m\sim15^h19^m$	19.3	8.0	0.41	190	4.5	1.1
	16 21 ~16 22	39.0	11.7	0.30	177	27.8	1.9
	16 22 ~16 23	19.3	8.9	0.46	180	9.7	0
	16 31 ~16 32	26.6	12.3	0.46	188	12.9	1.9
	17 41 ~17 42	19.1	12.8	0.67	195	8.9	0.5

From Table VI, we can see that the angle φ varies in the greatly wide range 130° from 50° to −80° for the SW-wind and the variation ranges of the angle φ for NE wind become from 177° to 195° and they do not have a distinctly wide range such as for the SW-wind. The values of the ratios b/a vary also from 0.49 to 0.87 for the SW-wind and from 0.30 to 0.67 for the NE-wind respectively. From those facts, we can easily understand that the variations of the blowing directions of the SW-wind for a certain time interval have wider range than those of the NE-wind.

8. Conclusion and acknowledgement.

Using a new-designed anemometer of inverted pendulum type, we observed the natural winds, and we found that the present apparatus proves useful in the observation of the natural wind.

The analysis results of the records of the natural wind show the complication of the structure of the natural wind, and they confirm the existence of the predominant period of the breath of the wind and the difference of those breath due to the blowing directions of the wind. There are interesting natures for the relations between the breath and the maximum wind pressure and also between the blowing

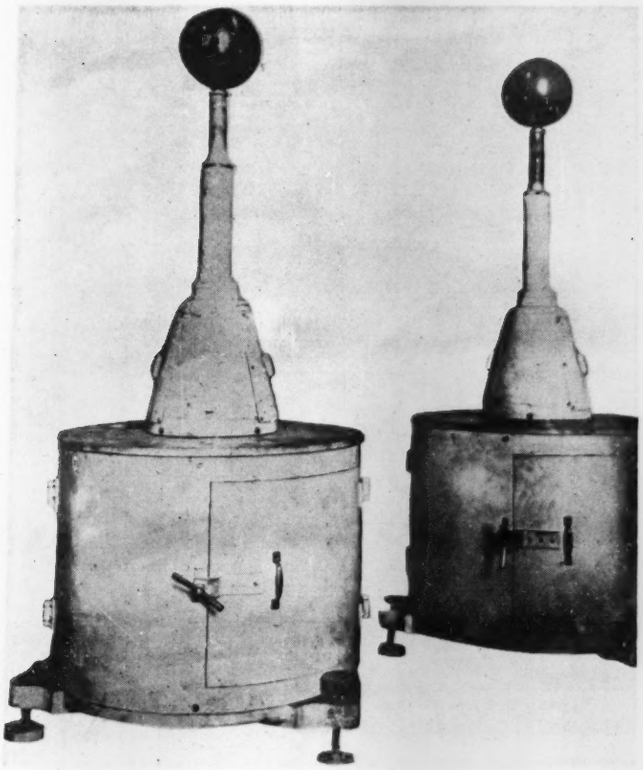

Fig. 2a.

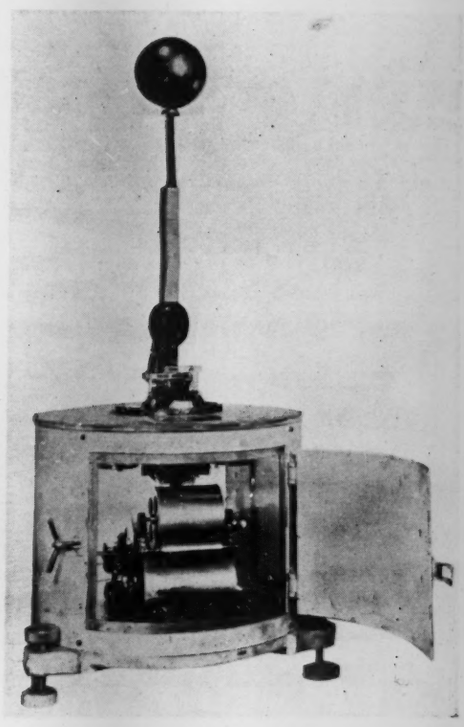

Fig. 2b.

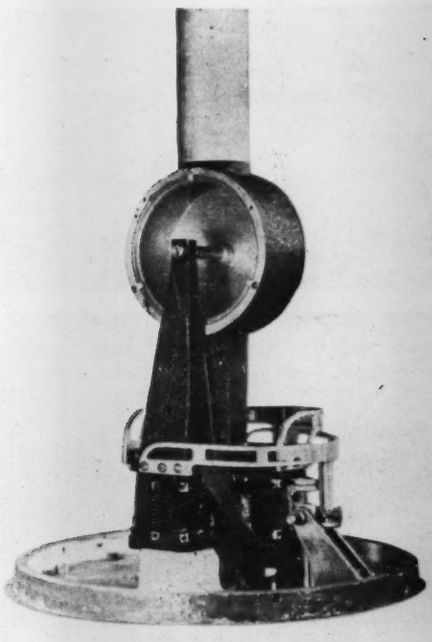

Fig. 2c.

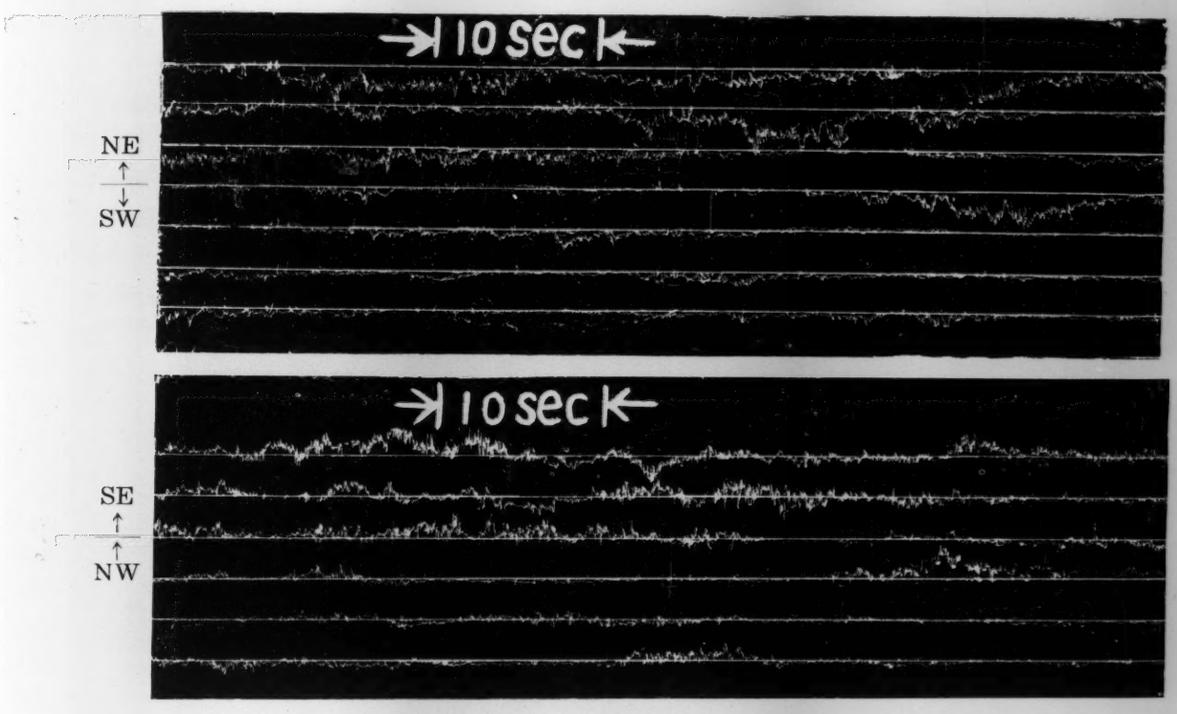

Fig. 11a. Records of natural wind. (14 h, Dec. 2, 1940.)

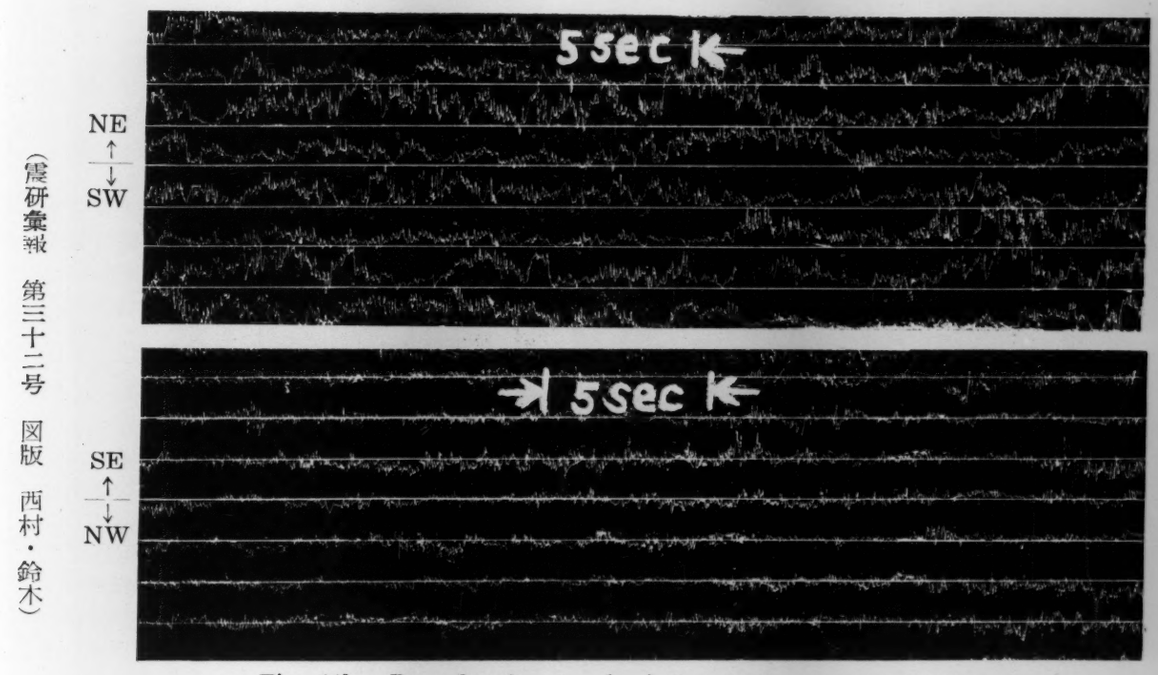

Fig. 11b. Records of natural winds. (13 h, March 2, 1941.)

（震研彙報 第三十二号 図版 西村・鈴木）

direction and the wind pressure.

In conclusion, the authors express sincere thanks to the late Mr. Yoshitaro Maeda, by whose enthusiastic assistance in the field observation the present study was carried out. The authors also express hearty thanks to Professor I. Tani who afforded readily facility for using the wind tunnel which belonged to the former Aeronautical Research Institute, Univ. of Tokyo. Lastly the authors express thanks to the authorities of the Institute of the Promotion of Science and Technology of Japan, for appropriating to one of the present writers funds which helped in carrying out the present investigation.

---

23. 逆立振子型風力計による自然風の観測と解析

地震研究所 {西村源六郎 / 鈴木正治}

新型自記風力計と本計器を用いて自然風の観測結果の解析を行い，自然風の構造の研究を行った．本計器は逆立振子型自記風力計であって，週期，感度，抵抗係数，槓杆倍率，測定範囲等については次表に示す．

第1表　風力計常数

球の直径	感度	週期 (sec.)	抵抗係数 (Cx)	槓杆倍率	測定範囲
20 cm	28.0 kg-wt/m²	0.075	0.48	66.5	0～20 m/sec
15 cm	45.5 kg-wt/m²	0.070	0.53	66.5	0～40 m/sec

尙制振器は空気制振器であり，記録法は煤煙紙式で，記録用ドラムの駆動は 6 W, 1 r p m の同期電動機により，記録紙速度は 0.4 cm/sec, 0.1 cm/sec, 0.04 cm/sec の三種に変える事が出来，又総重量は約 100 kg-wt, 容積は 80 cm×80 cm×200 cm である．

尙本器の特徴は構造が比較的簡単で丈夫，風圧の瞬時値を精密に記録する事が出来，互に直角な水平二成分を一つの記録用ドラムに記録する事が出来るのでこれを合成する事によって刻々の風向も算出する事が出来る．伊豆稲取町で行った自然風の観測結果の解析によれば，自然風にはその週期即ち息には大体卓越した値が存在すること，また風の方向によってその値が異っており，その最大風圧と息の関係，風圧と風向との関係なども特殊の性質がみられることがわかった．

本計器を用いて自然風についての重要な研究事項，例えば自然風に対する地形の影響，最大風圧と，平均風圧との関係，あるいは週期の持続性の問題，また構造物に対する影響，あるいは脈動に対する影響など，その他種々の研究調査し得べき事項が残されていることは著者等のよくしるところであるが，本報告が自然風の研究者，構造物の設計者，その他この方面に興味をもたられる方に多少でも参考になるところがあれば著者等の幸とするところである．

筆をおくにあたり，著者等の畏敬せる元実業学校教官故前田芳太郎氏の生前における研究に対する御理解によって同氏の家屋を長期間にわたって観測用に用いることができ，同時に同氏の熱心なる観測に対する御援助と御協力とによって全く本研究は遂行し得たものであることを述べ，ことに同氏の霊に感謝する次第である．

なお本研究は日本学術振興会の多大なる援助において遂行し得たものであって，ここに同会に対し感謝の意を表すとともに同会第二特別委員会員である西村に対し各委員が甚大なる御注意及び御指導を下されしことに対し厚く御礼申し上げる次第である．

昭和29年10月25日印刷
昭和29年10月30日發行

東京都文京區本富士町一番地
東京大學構内
編纂兼發行者 東京大學地震研究所

東京都千代田區富士見町一丁目十番地
印刷者 笠井康賴

東京都千代田區富士見町一丁目十番地
印刷所 株式會社 國際文献印刷社

賣捌所 東京都千代田區神田一ツ橋通
岩波書店

東京都中央區日本橋通二丁目六番地
丸善株式會社

Sold by
Iwanami Shoten,
Hitotsubashi dôri, Chiyoda-ku, Tôkyô,
and
Maruzen Co., Ltd.,
Nihonbashi dôri, Chûô-ku, Tôkyô.
Price of this copy: 536 Yen. (Postage exclusive.)

BULLETIN OF

THE EARTHQUAKE RESEARCH INSTITUTE

TOKYO UNIVERSITY

Vol. XXXII, Part 3. September, 1954.

Contents.

Papers and Reports.

Page

17. T. MATUZAWA und H. HASEGAWA, Feldtheorie der Erdbeben: Elliptisches Quellengebiet. (im Deutschen) 231
18. T. MATUMOTO and Y. SATÔ, On the Vibration of an Elastic Globe with One Layer. The Vibration of the First Class. (in English) 247
19. Y. SATÔ, A Note on Tsuboi-Nagata's Method. (in English) 259
20. D. SHIMOZURU, Study on the Elasticity near the Melting Point. Part I. Nature of Dilatational Wave. (in English) 271
21. I. YOKOYAMA, Geomagnetic Anomalies related to the Magnetization of the Basalt in the Vicinity of Gembudō. (in English) 281
22. H. TSUYA, R. MORIMOTO and J. OSSAKA, The 1950–1951 Eruptions of Mt. Mihara, Oshima Volcano, Seven Izu Islands, Japan. Part II. The 1951 eruption. A. Activity of the second period. (in English) 289
23. G. NISHIMURA and M. SUZUKI, Anemometer of Inverted Pendulum Type and Wind Construction Studied with It. (in English) 313

(For the papers written in Japanese or in occidental languages, the abstracts are given in occidental languages or in Japanese respectively.)

BULLETIN OF THE EARTHQUAKE RESEARCH INSTITUTE,
TOKYO UNIVERSITY. Vol. XXXII, Part 4. December, 1954.

東京大學
地震研究所彙報

第 32 號　第 4 冊

昭和 29 年 12 月

目　次

論文及報告

頁

24. 地震の場の論　更に精しく力の起る区域に就て（独文） ..... 松沢武雄 341
25. 表面波の研究　XII. 分散性のない表面波（英文） ..... 佐藤泰夫 349
26. 地下深所における地震動の観測結果 第5報（地震動の連の問題）（英文） ..... 金井清・長田甲斐男・吉沢静代 361
27. 震源決定の精度について（第一報）（英文） ..... 浅野周三 371

所報

索引

(The titles in occidental languages are given on the back cover.)

本彙報ハ年4回 (但シ第1號ヨリ第6號マデハ不定期ニ，第7號ハ3冊トシテ發行セリ)，彙報別冊ハ不定期ニ發行ス．

本彙報掲載ノ論文及ビ報告ノ内容ニ關シテハ著者ノミニ其責任アルモノトス．

本彙報ニ關スル照會通信ハ東京大學地震研究所長ヘ宛テラレタシ．

The Bulletin is published quarterly. (Vols. I–VI were published at irregular intervals and Vol. VII consisted of three parts.)
Supplementary Volume is published at irregular interval.

The authors of the papers alone are responsible for the statements and opinions contained in their respective papers.

All communications relating to this Bulletin should be addressed to the Director of the Earthquake Research Institute, Tokyo University.

24. *Feldtheorie der Erdbeben: Näheres über das Quellengebiet.*

Von Takeo MATUZAWA,

Geophysikalisches Institut.

(Vorgelegt den 28. Sept. 1954.—Eingegangen den 29. Sept. 1954.)

1. Weiteres über die Energetik der Grossbeben.

In der ersten Mitteilung[1] wurde eine Erdbebenmaschine vorgelegt und zwar ganz schematisch erörtert. Dabei wurde die Idee des Quellengebietes eingeführt, wo der Phasenübergang zwischen den festen und flüssigen Zuständen stattfinden müsste. Dort wurde angenommen, dass das Quellengebiet sich unter dem durch dessen Druckzunahme gespannten Krustenteile ebenenartig befindet. Bei dieser Annahme war die Erklärung der Wärmebilanz ohne Einführung irgendeiner Konvektion der Wärme unter der Kruste ziemlich schwer. Nach der Schätzung von K. Aki[2] unter der Voraussetzung von Konvektion in Zähflüssigkeit ist ziemlich starke Strömung der Materie, z.B. 50 m/Jahre nötig, um die nötigen Zuführung der Wärme zu bewirken, wenn die lineäre Dimension der Zirkulation etwa 100 km ist.

Anderseits wurde auch bemerkt, dass die meisten Nachbeben in dem Krustenteile gleich oberhalb des Quellengebietes entstehen werden. Nämlich, nach meiner Meinung muss das Nachbebengebiet mit dem vor dem Hauptbeben wesentlich gespannten Krustenteile übereinstimmen.

In dieser Beziehung muss die Arbeit von S. Honma und A. Seki[3] eingeführt werden. Sie forschten die Beziehung zwischen der horizontalen Flächengröße des Nachbebengebietes und der grössten Entfernung des Ortes, wo das Hauptbeben menschlich gefühlt wurde.

Anderseits zeigte K. Sagisaka[4] die Beziehung zwischen der Wellenenergie eines Grossbebens und dessen grössten Entfernung von menschlich fühlbaren Orten.

Diese beiden Resultate sind in Fig. 1 zusammenfassend eingetragen. Daraus bekommt man Fig. 2, wo die Beziehung zwischen der

1) T. MATUZAWA, *Bull. Earthq. Res. Inst.*, **31** (1953), 179–201.
2) K. AKI, *Zisin*, [ii], **7** (1954), no. 2, 65–76.
3) S. HONMA and A. SEKI, *Zisin*, [ii], **2** (1949), 37–40: **3** (1951), 45–48.
4) K. SAGISAKA, *Kensin-zihô*, **10** (1940), 385–448.

Wellenenergie des Grossbebens und der Nachbebengebietes gezeigt wird.

Abgesehen von den Verschiedenheiten zwischen den Landbeben und Ozeanbeben, können wir ganz klar sehen, dass die Energie ganz schnell im Vergleich mit dem Nachbebengebiet wächst und zwar wenigstens schneller als die zweiten Potenz von Nachbebengebiet.

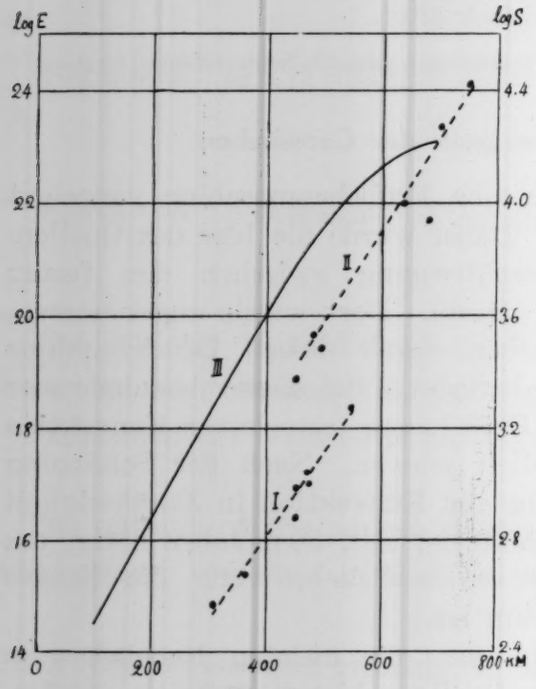

Fig. 1.
I: log S, Landbeben.
II: log S, Ozeanbeben.
III: log E
E Erg:S Km².

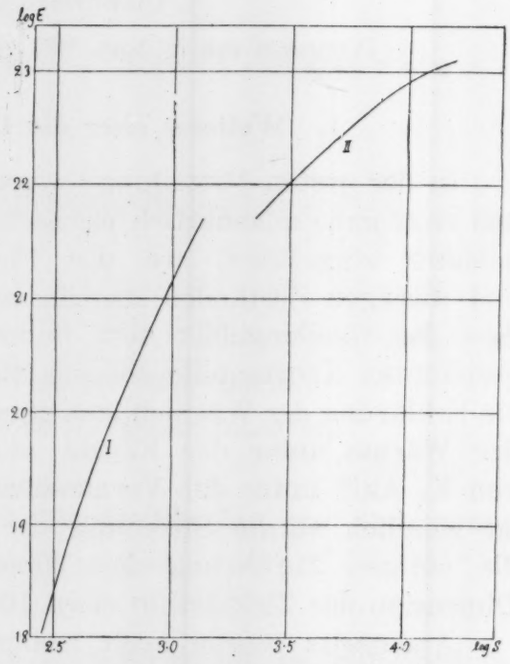

Fig. 2. E Erg:S Km².

In anderen Worten, je kleiner das Hauptbeben ist, desto grösser ist das Nachbebengebiet im Vergleich mit der Wellenenergie des Hauptbebens.

Nun müssen die obengenannten Tatsachen erklärt werden und die Energetik der Grossbeben muss verbessert werden.

Gelegentlich möchte ich hier eine Erwiderung zur Kritik von H. Kawasumi[5] gegen die potentielle Energie der Hebungen und Senkungen der Kruste in meiner Arbeit hinzufügen. Der Kernpunkt seiner Kritik

5) H. KAWASUMI, *International Association of Seismology and Physics of the Interior of the Earth. Rome Assembly, Sept. 1954. Seismology and Physics of the Interior of the Earth in Japan, 1951–1953. National report presented by the Section of Seismology, National Committee for Geodesy and Geophysics, Science Council of Japan.*

ist mir etwas unklar, aber es scheint mir, dass er weitere Beschreibung gewissen kausalen Zusammenhanges zwischen der Wellen-Energie und der potentielle Energie erfordert hätte. Aber nach meiner Überlegung kann man sie beide in diesem Falle vereinzelt betrachten. Nämlich stammen beide Formen Energie gleichfalls von der Druckänderung im Quellengebiet. Also auch wenn die Änderung der potentielle Energie nicht mit der Wellenenergie übereinstimmte, sollte man sich um nichts kümmern.

Beim Gross-Kantôbeben vom 1. Sept. 1923 z.B. fanden grosse Hebungen ausnahmslos in Gegenden mit grossen positiven Anomalien der Schwere, d. h. in entgegengesetzter Richtung zur Isostasieförderung, statt[6)7)]. Daher müsste diese Arbeit gegen die Schwere durch gewisse andere Kraft als die Schwere geleistet werden. In diesem Falle, nämlich, kann man sehr wahrscheinlich vermuten, dass die Wellenenergie dieses Bebens nicht durch die Schwere erzeugt wurde.

Selbstverständlich will ich nicht alle Möglichkeiten der Erzeugung der Erdbeben durch die Schwere ausschliessen. Ein gutes Beispiel davon ist der Fall der Johannesburger Beben, die von P. G. Gane, A. L. Hales, H. A. Oliver, und P. L. Willmore[8)] untersucht worden sind. In diesem Falle bildet der Minengang sozusagen das Quellengebiet mit negativem Zusatzdruck (in Wirklichkeit Nulldruck) und die umgebende Kruste wird durch die Schwere verzerrt. Dieses Quellengebiet wird natürlich durch menschliche Arbeit erzeugt.

Hier möchte ich wieder bemerken, dass die Tiefe der hiesigen kleinen Beben ungefähr 1.6 km ist, wo Druck von etwa 300～500 Atm. herrschen muss. Meiner Meinung nach ist nicht nötig, dass die Energie der Hebung der Gesteine, nämlich 10^{22} erg/Jahre nach der Schätzung von den Autoren, ganz in Wellenenergie verwandert wird. Das Leistungsvermögen der hiesigen Erdbebenmaschine ist nicht nötig, 100 Prozent zu sein.

Schwärme von ganz kleinen Beben neben den grossen Deichen für Wasserbecken, welche von P. Caloi[9)] untersucht wurden, sind auch Beispiele im gleichen Sinne.

---

6) Land Survey Department, *Bull. Earthq. Res. Inst.*, **1** (1926), 65.

7) C. Tsuboi, A. Jitsukawa und H. Tajima. *Proc. Jap. Acad.*, **29** (1953), No. 10. 556–560.

8) P. G. Gane, A. L. Hales and H. A. Oliver, *Bull. Seism. Soc. Am.*, **36** (1946), No. 2. 49–80: P. L. Willmore, A. L. Hales, and P. G. Gane, *Bull. Seism. Soc. Am.*, **42** (1952), No. 1. 53–80.

9) P. Caloi, *Ann. d. Geofisica*, **6** (1953), n. 3, 321–366.

2. Form des Quellengebietes und Zweiphasen-Konvektion.

Wenn die Wellenenergie eines Grossbebens mit oberflächennahen Herd von der Ordnung von 10^{25} erg ist, dann ist die Schmelzwärme unter meiner Hypothese von der Ordnung von 10^{27} erg unbedingt nötig. Um die Schwierigkeiten der zu starken Wärmeleitung oder Konvektion bei der Wärmezufuhr von unten zu vermeiden, müsste man den Flächeninhalt des Quellengebietes vermehren, z.B. es sich verzweigen lassen, etwa wie in Fig. 3 schematisch gezeigt.

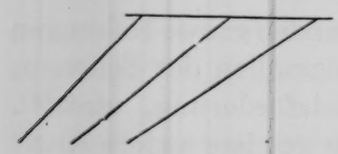

Fig. 3.

Bei der Abspannung der oberen Kruste, beziehungsweise der Druckverminderung im oberen Teil des Quellengebietes, wird das Arbeitsmittel im flüssigen Zustand in unteren Zweigen nach oben geschoben, und folglich muss die umgebende Materie im festen Zustand sicher sich senken. In dieser Weise auch kann die Zweiphasen-Konvektion stattfinden, wie schon in meiner früheren Arbeit[10] anderweitig bemerkt wurde.

In dieser Beziehung interessieren uns die Arbeiten von N. Nasu, T. Hagiwara, und S. Omote[11] oder von K. Wadati und Y. Iwai[12]. Nach Nasu u.a. war die Raumverteilung der Bebenherde in Kantô Distrikt nach dem Gross-Kantôbeben vom 1923 ungefähr trichterförmig und zwar der Mund des Trichters dehnt sich gangweise seitwärts und neigt sich schief nach unten. Die Arbeit von K. Wadati und Y. Iwai zeigt im grossen und ganzen auch ähnliche Verteilung. Auch interessiert uns sehr die Tatsache, dass das Gebiet der stärksten Senkung beim Grossbeben ungefähr mit dem Bereich oberhalb des gangartigen Gebietes mit Mitteltiefherdbeben übereinstimmt[13].

Durch die Einführung der Verzweigung ist die Form des Quellengebietes immer ähnlicher der bienenstockartigen Konstruktion des Kessels der Dampfmaschine geworden.

Nun liegt die Vermutung nahe, dass je weniger die Verzweigung des Quellengebietes ist, desto kleiner das Hauptbeben ist. In dieser Weise kann man die Beziehung zwischen der Energie des Hauptbebens und der Nachbebengebiete von S. Honma und A. Seki gut erklären.

10) T. MATUZAWA, *Bull. Earthq. Res. Inst.*, **31** (1953), 194.

11) N. NASU, T. HAGIWARA und S. OMOTE, *Bull. Earthq. Res. Inst.*, **14** (1936), 427–437.

12) K. WADATI und Y. IWAI, *Geophys. Mag.*, **25** (1954), no. 3–4. 167–173.

13) *loc. cit.* (6).

3. Tiefherdbeben und Mangel an Nachbeben davon.

Bei Tiefherdbeben kann die isostatische Störung ausser acht gelassen werden. Dagegen kann der Vorgang wie unsere Erdbebenmaschine auch im Tiefherdbebengebiet unter günstigen Umständen vorkommen. Bei sehr tiefen Quellengebieten, etwa über 200Km., kann die wesentliche Wirkung der Erdoberfläche fast vernachlässigt werden. Nämlich, kann ein Quellengebiet als vereinzelt angesehen werden. Darauf können wir z.B. den von T. Hirono und T. Usami[14] gerechneten Spannungszustand in der Umgebung von einem sphäroidischen Raum, in dem hydrostatischer Druck wirkt, anwenden.

Nun wenn der Druck im Quellengebiet genug erhöht wird, die angespannten Umgebung zu brechen, dann wird die feste Umgebung sich brechen und ein Erdbeben kann entstehen. Dabei wird der Volumeninhalt des Quellengebietes plötzlich zunehmen und das Arbeitsmittel im Quellengebiet wird adiabatisch ausgedehnt. Folglich wird dessen Druck vermindert. Bei oberflächennahen Grossbeben erreichen die Verwerfungen die Erdoberfläche und der Krustenteil oberhalb des Quellengebietes muss ziemlich schwach gemacht werden, und Brechungen können hintereinander folgen, nämlich können viele Nachbeben folgen.

Dagegen in der grossen Tiefe kann die Bruchstärke der Umgebung nach einem Beben fast ungeändert wie vor der Abspannung bleiben. Die Erzeugung der Gleitung bei der Abspannung mag nichts zu tun mit dem Fortschritt der Brechung haben, weil dort sehr hoher Druck herrscht, und die Reibungskraft keinen Unterschied von der Schubkraft haben kann[15].

Daher können wir leicht den Mangel an Nachbeben bei Tiefherdbeben vermuten. In Wirklichkeit haben wir bisher fast kein Beispiel von Nachbeben bei Tiefherdbeben gehabt, obgleich die letzten von der bedeutenden Grösse waren. Diese Tatsache wurde schon von K. Wadati und K. Masuda[16] einmal betont. Nach ihnen schien das Tiefherdbeben vom 26. Mai 1932 im Süden von Fiji Inseln nur einzige Ausnahme zu sein. Der Erdbebenbericht vom Dominion Observatory, Wellington, New Zealand, sagte, sechs kleine Nachbeben würden registriert in 12 Stunden nach dem Hauptbeben. Wenn alle diese kleinen Beben von derselben

14) T. Hirono and T. Usami, *Papers in Meteorology and Geophysics:* **5** (1954), no. 1, 64–88.

15) Dies kann auch die Erwiderung zur Kritik von H. Kawasumi gegen meine Arbeit sein, loc. cit. (5), obschon dieser Umstand auch schon dort kurz bemerkt wurde.

16) K. Wadati und K. Masuda, *Kensin-Ziho,* **8** (1934), no. 1, 11–20.

Herkunft sein wären, dann hätte es eine echte Ausnahme sein können.

Nach K. Wadati und K. Masuda war dieses Beben ein Doppelbeben. Daher liegt eine Vermutung nahe, dass zwei naheliegende Quellengebiete fast gleichzeitig tätig geworden wären. In solchem Falle können sie leicht miteinander gekoppelt werden und im dazwischen liegenden Bereiche können möglicherweise mehrere Nachbeben folgen.

In diesem Sinne können wir sagen, dass das oberflächennahe Quellengebiet mit der Erdoberfläche gekoppelt ist.

Weil die Tiefherdbeben selbstverständlich einigen Hunderten von kilometern von Beobachtungsorten entfernt sind, können sehr kleine Beben der Beobachtung entgehen. Aber bei oberflächennahen Grossbeben mit ähnlichen Grössen und Herdentfernungen können wir meistens viele Nachbeben beobachten. Das kommt bei Tiefherdbeben gar nicht vor. Also ist der Mangel an Nachbeben wenigstens mit gewöhnlicher Energie beim Tiefherdbeben ziemlich sicher.

4. Miszellaneen.

Meine Theorie steht nicht in Widerspruch mit der Benioff'schen Theorie[17] der Bruchbewegungen bei Erdbeben. Die konstante äussere Kraft F in seiner Theorie entspricht dem Druck im Quellengebiet in meiner Theorie, obgleich dieser Druck säkulären Änderung unterliegt.

B. Gutenberg und C. F. Richter[18] haben Existenz der Schichten mit Wellengeschwindigkeiten, die kleiner als in obenliegender Schicht sind, gezeigt. In Japan haben W. Inouye und G. Murai[19] auch gezeigt, dass es eine Schicht mit niedrigen S-Wellengeschwindigkeit in der Tiefe etwa 300 km. gibt.

Gutenberg'sche Vermutung[20], dass diese Verminderung der Wellengeschwindigkeiten teilweise durch Vermengungen der verflüssigten Teile verursacht würde, steht im Einklang mit meiner Idee. Aus meiner Theorie, aber, könnte von selbst folgen, dass diese Charakteristik der Erdinnere besonders in seismisch regsamen Gegenden bestehen wollte.

Gelegentlich möchte ich noch eine Bemerkung zur Temperaturerhöhung im Quellengebiet hinzufügen. Beim kreisförmigen Quellengebiet war Temperaturerhöhung von etwa 5°C im Quellengebiet nötig, um

17) H. BENIOFF, *Bull. Seism. Soc. Am.*, **41** (1951), No. 1. 31–62.

18) B. GUTENBERG and C. F. RICHTER, *Bull. Seis. Soc. Am.*, **29** (1939), 531–537.

19) Vorgelegt bei der Tagung der Seismologischen Gesellschaft, Japan, den 31. Okt. 1953. den 23. April 1954.

20) B. GUTENBERG, *Bull. Geolog. Soc. Am.*, **65** (1954), 337–348.

genügende Schubkraft für Erdbeben zu erzeugen. Aber beim elliptischen Quellengebiet[21] kann nur eindrittel der Temperaturerhöhung im vorigen Fall, nämlich etwa 1.7°C, genug sein, weil die Maximum-Schubspannung 3 mal Druck im Quellengebiet erreicht.

---

24. Zisin no Ba no Ron: Sara ni kuwasiku Tikara no okoru Kuiki ni tuite.

Zisin Kenkyû-syo Matuzawa Takeo

Oozisin no Energie no Deiri no Mondai, Oozisin no Energie to Yosin-Kuiki tono Mondai nado wo sara ni yoku setumei suru tame ni Tikara no okoru Kuiki no Katati ni tuite Kangae wo susumeta. Tumari sono Kuiki ga Edawakare site iru to suru node aru. Kono yô ni suru to Zyôki-kikan no Kama no Kôzô ni masumasu yoku nite kuru.

Sono hoka hukai Zisin ni Yosin no hotondo nai koto no Setumei wo kokoromiru. Mata Gutenberg, Inouye nado no Zisin-nami no Sokudo no osoi Sô ni tuite no Kangae wo noberu.

Ziban no Agari-sagari to Zyûryoku-Potential tono Mondai, Zyûryoku no Sigoto ni yotte okoru Zisin ni tuiteno Tyûi wo noberu. Kono Baai no Quellengebiet wa Mawari ni kurabete Aturyoku no tiisai Kuiki to naru.

---

21) T. Matuzawa und H. Hasegawa, *Bull. Earthq. Res. Inst.*, **32** (1954), 231–246.

25. *Study on Surface Waves* XII. *Non-Dispersive Surface Waves.*

By Yasuo SATÔ,

Earthquake Research Institute.

(Read May 19, 1953.—Received Sept. 30, 1954.)

1. Introduction.

Among the various properties of Love-waves, the dispersion seems to be the most remarkable and well-known one, and makes the matter greatly complicated as well as interesting. Although Rayleigh-wave when propagated in a semi-infinite elastic medium does not show such a property, the actually observed waves of Rayleigh type are known to be dispersive. This paradox, after remaining unsolved for a pretty long time, was made clear by A. E. H. Love[1] some forty years ago. In his celebrated memoir he calculated the velocity of Rayleigh waves propagated upon the layered medium and proved that the velocity is the function of frequency. Now, the next question which naturally occurs is why Love- and Rayleigh-waves propagated in the layered structure show dispersive nature. Are there any surface waves, besides Rayleigh- and Stoneley-waves, which are non-dispersive? We will answer this question in the following sections.

2. Dimensional analysis.

We will employ the following notations;

V; Velocity of surface waves.
L; Wave-length.
λ, μ; Lamé's constants.
ρ; Density.

If the surface waves are propagated upon a semi-infinite body, its velocity must be expressed in the following form;

$$V=F_1(\lambda, \mu, \rho, L)\,. \qquad \cdots\cdots\cdots\cdots\cdots\cdots (2\cdot1)$$

Now, from the consideration with respect to dimensions, V must have the form;

1) A. E. H. LOVE, *Some Problems on Geodynamics* (1911).

$$V=\left(\frac{\mu}{\rho}\right)^{\frac{1}{2}}F_2\left(\frac{\lambda}{\mu}\right). \qquad \text{.....(2.2)}$$

Thus the wave-length L cannot have any relation with the velocity, or in other words, the waves are non-dispersive in this case.

If, however, the medium has a layered structure, which has some definite thickness, say H, we have the following relation

$$V=G_1(\lambda, \lambda', \mu, \mu', \rho, \rho', L, H), \qquad \text{.....(2.3)}$$

where the new notations have the following meaning:

λ', μ'; Lamé's constants in the part of layer.
ρ'; Density in the part of layer.

By a similar consideration as with the former case, we have

$$V=\left(\frac{\mu}{\rho}\right)^{\frac{1}{2}}G_2\left(\frac{\lambda}{\mu}, \frac{\lambda'}{\mu'}, \frac{\mu'}{\mu}, \frac{\rho'}{\rho}, \frac{L}{H}\right). \qquad \text{.....(2.4)}$$

In this expression the function G_2 involves a variable L/H, which fact implies the dependency of V on L/H, namely the dispersive property of this case. Thus it was made clear that the existence of a layer makes the surface waves, which are propagated in this medium, dispersive.

3. Non-dispersive surface waves.

In the previous paper[2] we have described the examples of the types of surface waves with one- and two-phase. We will now pick out all the types of waves which are non-dispersive, i.e. the surface waves existent in the medium without layer structure. The symbolical expressions of the type of waves in a non-stratified medium are the following seven, the existence of which will be examined in the following section.

1) $[\overline{E}]$, 2) $[\overline{\overline{E}}]$,
3) $[\overline{EE}]$, 4) $[\overline{\overline{EE}}]$,
5) $\left[\frac{E}{E}\right]$, 6) $\left[\frac{EE}{E}\right]$, ...(3.1)
7) $\left[\frac{EE}{EE}\right]$.

2) Y. SATÔ, "Study on Surface Waves XI. Definition and Classification of Surface Waves," *Bull. Earthq. Res. Inst.*, **32** (1954), 161.

3.1 Examination of the seven types of waves.

We will now examine the above seven types of waves one by one.

3.11 $[\overline{E}]$

We have proved in our former paper that the waves of this type may be the SH-waves or the sound waves in an elastic liquid, but neither of them can satisfy the boundary condition of free surface.

3.12 $[\overline{\overline{E}}]$

In this case also no wave satisfying the fundamental wave equation and the boundary condition can exist.

3.13 $[\overline{EE}]$

This is the well-known Rayleigh-waves.

3.14 $[\overline{\overline{EE}}]$

Taking the displacement potential

$$\begin{cases} \phi = A\exp(\alpha z + ifx + ipt), & \alpha = \sqrt{f^2 - h^2}, \\ \psi = B\exp(\beta z + ifx + ipt), & \beta = \sqrt{f^2 - k^2}, \end{cases} \qquad \ldots\ldots(3.2)$$

(z-axis is taken upward and the medium is in the negative part of z.)

$$\begin{cases} h = p/V_P, & V_P = \sqrt{\{(\lambda+2\mu)/\rho\}}, \\ k = p/V_S, & V_S = \sqrt{(\mu/\rho)}, \end{cases}$$

we have

$$\begin{cases} u = \dfrac{\partial\phi}{\partial x} + \dfrac{\partial\psi}{\partial z} = Aif\cdot\exp(\alpha z + ifx + ipt) \\ \qquad\qquad + B\beta\cdot\exp(\beta z + ifx + ipt), \\ w = \dfrac{\partial\phi}{\partial z} - \dfrac{\partial\psi}{\partial x} = A\alpha\cdot\exp(\alpha z + ifx + ipt) \\ \qquad\qquad - Bif\cdot\exp(\beta z + ifx + ipt). \end{cases} \qquad \ldots\ldots(3.3)$$

If the boundary surface is expressed by $z=0$, the condition at this plane is

$$u=0, \quad w=0. \qquad \ldots\ldots(3.4)$$

Therefore

$$\begin{cases} Aif + B\beta = 0, \\ A\alpha - Bif = 0. \end{cases} \qquad \ldots\ldots(3.5)$$

Eliminating A and B we have

$$\begin{aligned} f^2&=\alpha\beta \\ &=\sqrt{f^2-h^2}\sqrt{f^2-k^2}\,. \end{aligned} \qquad \cdots\cdots\cdots\cdots\cdots\cdots(3.6)$$

By a glance it will become recognized that this equation cannot be satisfied by the real values of α and β. Consequently we must conclude that the waves of the type $[\overline{\overline{EE}}]$ also cannot exist actually.

3.15 $\left[\frac{E}{E}\right]$

If we take

$$\begin{cases} v=A\exp(-\beta z+ifx+ipt)\,, \\ v'=A'\exp(\beta' z+ifx+ipt)\,, \end{cases} \qquad \cdots\cdots\cdots\cdots\cdots(3.7)$$

where

$$\begin{aligned} \beta'&=\sqrt{(f^2-k'^2)}\,, \\ k'&=p/V_s'\,, \\ V_s'&=\sqrt{(\mu'/\rho')}\,, \end{aligned}$$

the next conditions must hold at the boundary surface $z=0$.

Continuity of displacement; $A=A'$,

Continuity of stress; $A\mu(-\beta)=A'\mu'\beta'$. $\qquad \cdots\cdots\cdots(3.8)$

These conditions cannot be satisfied simultaneously, so we must conclude, in this case also, that the surface waves of the type $\left[\frac{E}{E}\right]$ do not exist.

3.16 $\left[\frac{EE}{E}\right]$

Next we will examine the type $\left[\frac{EE}{E}\right]$.

In the part of solid, we take

$$\begin{cases} \Delta=A\exp(-\alpha z+ifx+ipt)\,, \\ \tilde{\omega}=C\exp(-\beta z+ifx+ipt)\,, \end{cases} \qquad \cdots\cdots\cdots\cdots\cdots(3.9)$$

where Δ is the dilatation and $\tilde{\omega}$ the component of rotation vector. Since

$$\begin{cases} \rho\dfrac{\partial^2 u}{\partial t^2}=(\lambda+2\mu)\dfrac{\partial\Delta}{\partial x}+\mu\dfrac{\partial\tilde{\omega}}{\partial z}\,, \\ \rho\dfrac{\partial^2 w}{\partial t^2}=(\lambda+2\mu)\dfrac{\partial\Delta}{\partial z}-\mu\dfrac{\partial\tilde{\omega}}{\partial x}\,, \end{cases} \qquad \cdots\cdots\cdots\cdots\cdots(3.10)$$

we have

$$\begin{cases} u=-\dfrac{1}{\rho p^2}\{(\lambda+2\mu)Aif\cdot\exp(-\alpha z+ifx+ipt) \\ \qquad\qquad +\mu C(-\beta)\cdot\exp(-\beta z+ifx+ipt)\}\,, \\ w=-\dfrac{1}{\rho p^2}\{(\lambda+2\mu)A(-\alpha)\cdot\exp(-\alpha z+ifx+ipt) \\ \qquad\qquad -\mu C(if)\cdot\exp(-\beta z+ifx+ipt)\}\,, \end{cases} \quad \ldots.(3.11)$$

and

$$\begin{aligned} \widehat{zz}&=\lambda\Delta+2\mu\frac{\partial w}{\partial z} \\ &=\mu\left[\left\{\frac{\lambda}{\mu}-\frac{2\alpha^2}{h^2}\right\}A\cdot\exp(-\alpha z)+2\frac{-if\beta}{k^2}C\cdot\exp(-\beta z)\right] \\ &\qquad\qquad\cdot\exp(ifx+ipt)\,. \end{aligned} \quad \ldots(3.12)$$

In the part of liquid we have

$$\begin{cases} \rho^*\dfrac{\partial^2 u^*}{\partial t^2}=\lambda^*\dfrac{\partial\Delta^*}{\partial x}\,, \\ \rho^*\dfrac{\partial^2 w^*}{\partial t^2}=\lambda^*\dfrac{\partial\Delta^*}{\partial z}\,, \\ \widehat{zz}^*=\lambda^*\Delta^*\,, \end{cases} \quad \ldots\ldots\ldots\ldots\ldots\ldots(3.13)$$

where the asterisk implies the quantity in the liquid.

Putting $\Delta^*=B\exp(\alpha^* z+ifx+ipt)$

we have

$$\begin{cases} u^*=-\dfrac{if}{h^{*2}}B\exp(\alpha^* z+ifx-ipt)\,, \\ w^*=-\dfrac{\alpha^*}{h^{*2}}B\exp(\alpha^* z+ifx-ipt)\,, \\ \widehat{zz}^*=\lambda^* B\exp(\alpha^* z+ifx-ipt)\,, \quad \widehat{xz}^*=0. \end{cases} \quad \ldots\ldots\ldots\ldots(3.14)$$

The boundary conditions are the continuity of the vertical component of displacement and that of the stress. Hence we have

$$\begin{cases} \dfrac{\alpha}{h^2}A+\qquad\dfrac{if}{k^2}C=-\dfrac{\alpha^*}{h^{*2}}B\,, \\ \mu\left\{\dfrac{\lambda}{\mu}-\dfrac{2\alpha^2}{h^2}\right\}A+\mu 2\dfrac{-if\beta}{k^2}C=\lambda^* B\,, \\ \dfrac{i2f\alpha}{h^2}A+\quad\dfrac{k^2-2f^2}{k^2}C=0\,. \end{cases} \quad \ldots\ldots\ldots(3.15)$$

We will introduce the following new notations :

$$\begin{aligned} &\gamma^2 \equiv V_p^2/V_s^2 = (\lambda+2\mu)/\mu, \\ &\gamma^{*2} \equiv V^{*2}/V_s^2 = k^2/h^{*2}, \\ &\Gamma \equiv \rho^*/\rho, \\ &v \equiv V/V_s = k/f, \ (V \text{ is the velocity of the surface waves.}) \end{aligned} \qquad \cdots\cdots\cdots\cdots\cdots\cdots\cdots\cdots (3.16)$$

Introducing these relations we have

$$\begin{aligned} &\lambda^*/\mu = \Gamma\gamma^{*2}, \\ &\beta/f = \sqrt{(1-v^2)}, \\ &\alpha/f = \sqrt{(1-v^2/\gamma^2)}, \\ &\alpha^*/f = \sqrt{(1-v^2/\gamma^{*2})}. \end{aligned} \qquad \cdots\cdots\cdots\cdots\cdots\cdots\cdots\cdots (3.17)$$

Then eliminating A, C and B from the expression (3.15), we have

$$\begin{vmatrix} \sqrt{(1-v^2/\gamma^2)} & 1 & \sqrt{(1-v^2/\gamma^{*2})} \\ v^2-2 & -2\sqrt{(1-v^2)} & -\Gamma v^2 \\ -2\sqrt{(1-v^2/\gamma^2)} & v^2-2 & 0 \end{vmatrix} = 0, \quad \cdots (3.18)$$

or

$$\begin{aligned} &\frac{1}{4}\Gamma v^4 \sqrt{(1-v^2/\gamma^2)} + \sqrt{(1-v^2/\gamma^{*2})} \cdot \left(1-\frac{1}{2}v^2\right)^2 \\ &\qquad = \sqrt{(1-v^2)} \cdot \sqrt{(1-v^2/\gamma^2)} \cdot \sqrt{(1-v^2/\gamma^{*2})}. \end{aligned} \qquad \cdots\cdots (3.18)'$$

3.161 We will examine the equation (3.18)′ and investigate the range of existence and other properties of this wave.

First we will assume that the solid is perfectly rigid, and glance at the nature of the matter briefly. In this case

$$\gamma^2 = \infty, \qquad \cdots\cdots\cdots\cdots\cdots\cdots (3.19)$$

and the equation (3.18)′ takes the following simple form

$$\frac{1}{4}\Gamma v^4 + \sqrt{(1-v^2/\gamma^{*2})} \cdot \left(1-\frac{1}{2}v^2\right)^2 = \sqrt{(1-v^2)}\sqrt{(1-v^2/\gamma^{*2})}. \qquad (3.20)$$

Now, this is an expression connecting Γ, γ^* and v, and since it does not contain any quantity such as period or wave length, the waves in question are, as have been expected, non-dispersive.

Solving the equation numerically we can obtain the relation velocity $v(=V/V_s)$ versus $\Gamma(=\rho^*/\rho)$ with a parameter $\gamma^*(=V^*/V_s)$. The following table and figure show this relation explicitly. As is clear from the figure, we can find a positive solution of v corresponding to any set of

values of γ^* and Γ. This is a very conspicuous property when compared with the Stoneley waves which can exist only under a very restricted conditions.

By a similar method we can get the solution when the solid is not rigid and γ has a finite value. The results of the numerical calculations when $\gamma^2=4$, or $\lambda=2\mu$ (cf. Table II and Fig. 2) and $\gamma^2=3$, or $\lambda=\mu$ (cf. Table III and Fig. 3) are shown here. Even if the parameter γ^2 takes other arbitrary values, we can easily infer, from

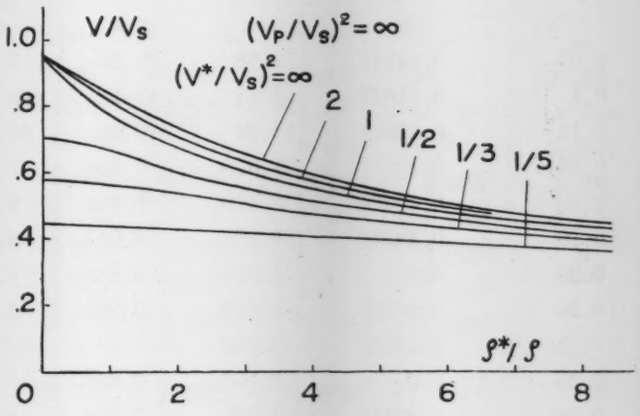

Fig. 1.

Table I. Values of Γ $(=\rho^*/\rho)$ when $\gamma^2=\infty$, (incompressible).

υ^2 \ γ^{*2}	υ	∞	10	2	1	1/2	1/3	1/5
0	0	∞	∞	∞	∞	∞	∞	∞
0.02	0.14142	108.5	108.4	108.0	107.4	106.3	105.2	102.9
0.10	0.31623	18.47	18.38	17.96	17.52	16.52	15.46	13.06
0.12	0.34641	15.13	15.04	14.67	14.20	13.19	12.11	9.572
0.16	0.4	10.866	10.779	10.403	9.959	8.961	7.836	4.860
0.18	0.42426	9.560	9.474	9.120	8.657	7.648	6.485	3.023
0.20	0.44721	8.443	8.358	8.010	7.552	6.540	5.334	0
0.25	0.5	6.426	6.345	6.011	5.565	4.544	3.213	
0.30	0.54772	5.074	4.998	4.678	4.245	3.209	1.605	
1/3	0.57735	4.394					0	
0.36	0.6	3.938	3.867	3.566	3.151	2.084		
0.40	0.63246	3.365	3.297	3.010	2.607	1.505		
0.46	0.67823	2.683	2.621	2.365	1.972	0.7590		
0.48	0.69282	2.492	2.431	2.171	1.797	0.4983		
0.50	0.70711	2.314	2.255	2.004	1.636	0		
0.6	0.77460	1.583	1.535	1.324	1.001			
0.7	0.83666	1.022	0.9858	0.8242	0.5599			
0.8	0.89443	0.5451	0.5228	0.4222	0.2438			
0.9	0.94868	0.06779	0.06467	0.0504	0.02144			
0.91	0.95394	0.01291	0.01231	0.0106	0.003873			
0.912618	0.95531	0	0	0	0			

Table II. Values of Γ $(=\rho^*/\rho)$ when $\gamma^2=4$, $(\lambda=2\mu)$.

v^2 \ γ^{*2}	v	∞	2	1	1/2	1/3	1/5
0	0	∞	∞	∞	∞	∞	∞
0.02	0.14142	73.89	73.52	73.14	72.40	71.64	70.10
0.1	0.31623	13.88	13.52	13.16	12.41	11.61	9.811
0.12	0.34641	11.37	10.98	10.66	9.909	9.093	7.189
0.16	0.4	7.878	7.556	7.220	6.496	5.681	3.523
0.18	0.42426	7.179	6.849	6.501	5.744	4.869	2.270
0.20	0.44721	6.338	6.013	5.669	4.910	4.009	0
0.25	0.5	4.820	4.509	4.175	3.408	2.401	
0.30	0.54772	3.798	3.501	3.177	2.402	1.201	
1/3	0.57735	3.282				0	
0.36	0.6	2.936	2.659	2.349	1.554		
0.40	0.63246	2.500	2.236	1.936	1.118		
0.46	0.67823	1.978	1.735	1.453	0.5593		
0.48	0.69282	1.830	1.595	1.319	0.3659		
0.50	0.70711	1.692	1.466	1.197	0		
0.6	0.77460	1.122	0.9387	0.7096			
0.7	0.83666	0.6740	0.5434	0.3691			
0.8	0.89443	0.2781	0.2165	0.1250			
0.869599	0.93252	0	0	0			

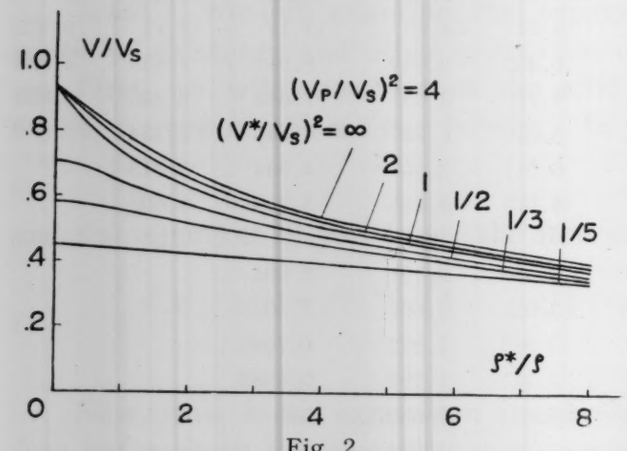

Fig. 2.

the form of the expression, that the equation has a solution, hence some special surface waves can propagate along the plane of separation of the solid and liquid medium for any given set of values of Γ and γ^*.

The curves in the three figures all show the general feature of monotonously decreasing. If, however, we glance at the portion $\Gamma\equiv\rho^*/\rho=0$, we shall find some peculiar aspect, for some of the curves start from a single point, while the others do not. (Cf. Fig. 4.) Now, we will explain this matter briefly.

Putting $\Gamma\equiv\rho^*/\rho=0$ .....(3.21)

Table III. Values of Γ $(=\rho^*/\rho)$ when $\gamma^2=3$, $(\lambda=\mu)$.

υ^2 \ γ^{*2}	υ	∞	2	1	1/2	1/3	1/5
0	0	∞	∞	∞	∞	∞	∞
0.02	0.141421	65.76	65.43	65.10	64.43	63.76	62.39
0.1	0.31623	12.30	11.99	11.67	11.00	10.29	8.700
0.12	0.34641	10.064	9.721	9.441	8.774	8.051	6.365
0.16	0.4	6.928	6.646	6.350	5.713	4.996	3.098
0.18	0.42426	6.323	6.032	5.726	5.059	4.289	2.000
0.20	0.44721	5.600	5.313	5.009	4.338	3.542	0
0.25	0.5	4.247	3.973	3.678	3.003	2.124	
0.30	0.54772	3.337	3.076	2.792	2.110	1.055	
1/3	0.57735	2.878				0	
0.36	0.6	2.568	2.326	2.055	1.359		
0.40	0.63246	2.178	1.948	1.687	0.9742		
0.46	0.67823	1.711	1.501	1.257	0.4839		
0.48	0.69281	1.578	1.376	1.138	0.3156		
0.50	0.70711	1.455	1.260	1.029	0		
0.6	0.77460	0.9403	0.7867	0.5947			
0.7	0.83666	0.5322	0.4291	0.2915			
0.8	0.89443	0.1676	0.1298	0.07497			
0.845306	0.919405	0	0	0			

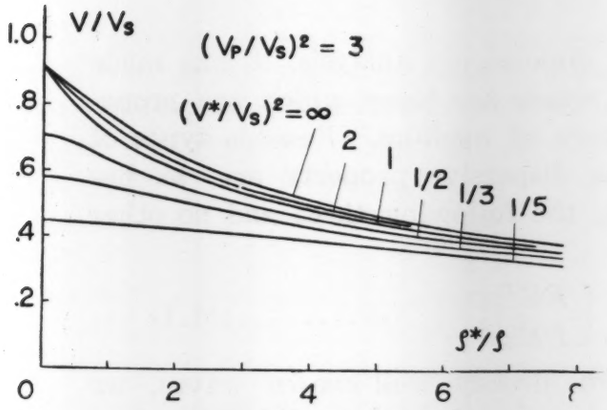

Fig. 3. $V/V_S=\upsilon$, $\rho^*/\rho=\Gamma$.

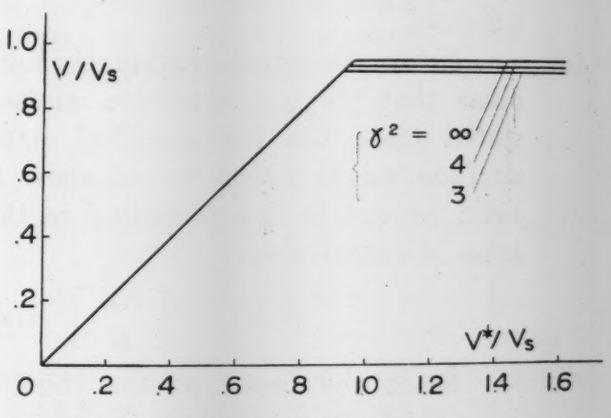

Fig. 4. $V/V_S=\upsilon$, $V^*/V_S=\gamma^*$.

into the equation (3.18)′,we have

$$\sqrt{(1-\upsilon^2/\gamma^{*2})}\cdot\{(1-\upsilon^2/2)^2-\sqrt{(1-\upsilon^2)}\cdot\sqrt{(1-\upsilon^2/\gamma^2)}\}=0\,. \quad \ldots\ldots(3.22)$$

If the factor $\sqrt{(1-\upsilon^2/\gamma^{*2})}$ does not vanish, the expression in the parenthesis must be equal to zero, namely

$$(1-v^2/2)^2=\sqrt{(1-v^2)}\cdot\sqrt{(1-v^2/\gamma^2)}\,, \qquad \text{.....(3.23)}$$

which gives the velocity of ordinary Rayleigh-waves. This is a very natural consequence, for the condition $\Gamma\equiv\rho^*/\rho=0$ implies that the liquid is infinitely rarefied. However, contrary to our common sense, if the sound velocity in the liquid is smaller than that of the Rayleigh-waves in the solid medium (viz. $V^*<V_{\text{Rayleigh}}$), the case is different.

Under such a condition we must abandon the equation (3.23) and adopt

$$v=\gamma^*. \qquad \text{.....(3.24)}$$

for the velocity of surface waves of $[E]$-type must be smaller than any other velocity of bodily waves. The result of calculations is shown in the Fig. 4, which will readily show the above circumstances.

3.17 $\left[\dfrac{EE}{EE}\right]$

This is the well-known Stoneley waves, whose range of existence was examined precisely by K. Sezawa[3] and K. Kanai some fifteen years ago.

4. Conclusion.

Thus our examination of the non-dispersive surface waves was finished.

From the consideration through dimensional analysis, it was made clear that the non-dispersive surface waves are those which are propagated upon the non-stratified structure of medium. Possible types of surface waves which do not show the dispersive property are, as has been proved in the preceding section, the following three and no other type is conceivable.

$$[\overline{EE}]\,, \quad \left[\frac{EE}{E}\right] \text{ and } \left[\frac{EE}{EE}\right]. \qquad \text{.....(4.1)}$$

Since the first and the third are already well-known waves, we examined the second type which always exists unconditionally, and obtained the velocity as the function of $\Gamma(\equiv\rho^*/\rho)$ and $\gamma^*(\equiv V^*/V_s)$.

---

3) K. SEZAWA and K. KANAI, "The Range of Possible Existence of Stoneley-Waves, and Some Related Problems," *Bull. Earth. Res. Inst.*, **17** (1939), 1.

25. 表面波の研究 XII.
分散性のない表面波

地震研究所 佐藤泰夫

1. 半無限体を伝はるレーリー波は分散性を持たない事が知られてゐるにもかかはらず，実際に観測されるものは明らかに分散性を示す．これは地球が表面層を持つ為と考へられてゐるが，同様に層のある媒質を伝はるラブ波も亦分散を行ふ．然らば表面層と分散とは不可分の関係にあるのであろうか．又，レーリー波，ストンレー波の他には分散性のない表面波は存在しないのであらうか，これらの問題を以下に取り上げる．

2. 半無限体を伝はる表面波の速度 V は

$$V=F_1(\lambda, \mu, \rho; L) \qquad \cdots\cdots\cdots\cdots\cdots\cdots\cdots\cdots\cdots\cdots(2.1)$$

と書ける筈であるが（λ, μ は Lamé の常数，ρ は密度，L は波長），次元解析によれば，これは

$$V=\left(\frac{\mu}{\rho}\right)^{\frac{1}{2}}\cdot F_2\left(\frac{\lambda}{\mu}\right) \qquad \cdots\cdots\cdots\cdots\cdots\cdots\cdots\cdots\cdots\cdots(2.2)$$

の形に変形される事がわかる．この式には波長 L を含まない，従つて速度 V は波長に関係しない．この事は，とりもなほさず分散性のない事を示す．

これに反して，もし表面層（その厚さを H; Lamé 常数 λ', μ'; 密度 ρ' とする）がある場合には，速度はこれらの函数，即ち

$$V=G_1(\lambda, \lambda', \mu, \mu', \rho, \rho', L, H) \qquad \cdots\cdots\cdots\cdots\cdots\cdots\cdots\cdots\cdots\cdots(2.3)$$

の形をとる事になるが，上と同様の考へから，これは又

$$V=\left(\frac{\mu}{\rho}\right)^{\frac{1}{2}}\cdot G_2\left(\frac{\lambda}{\mu}, \frac{\lambda'}{\mu'}, \frac{\mu'}{\mu}, \frac{\rho'}{\rho}, \frac{L}{H}\right) \qquad \cdots\cdots\cdots\cdots\cdots\cdots\cdots\cdots(2.4)$$

と書かれなくてはならない，この式は L/H を変数として持つ．つまり V は波長の函数となり，分散性を示す．以上によつて，層の存在が表面波を分散性ならしめる所以である事が明らかとなつた．

3. 従つて，分散性のない表面波は，層を有しない媒質内を伝はるものの中に求められるべきであるが，その凡ての型を列挙すれば次の通りである．

$$\begin{aligned}
&1)\ [\overline{E}], && 2)\ [\overline{\overline{E}}],\\
&3)\ [\overline{EE}], && 4)\ [\overline{\overline{EE}}],\\
&5)\ \left[\frac{E}{E}\right], && 6)\ \left[\frac{EE}{E}\right], \qquad \cdots\cdots\cdots\cdots\cdots\cdots(3.1)\\
&7)\ \left[\frac{EE}{EE}\right].
\end{aligned}$$

この中で，1), 2), 4), 5) に対応するものは存在しない事が証明せられる．3) はレーリー波，7) はストンレー波としてよく知られているから，こゝでは従来調べられていない 6) の型のものについて立入つた議論を行つた．これは半無限の弾性固体と流体との接触面に沿つて伝はる波である．速度をきめる方程式は

$$\frac{1}{4}\Gamma\mathfrak{v}^4 V(1-\mathfrak{v}^2/\gamma^2)+V(1-\mathfrak{v}^2/\gamma^{*2})\cdot\left(1-\frac{1}{2}\mathfrak{v}^2\right)^2 = V(1-\mathfrak{v}^2)\cdot V(1-\mathfrak{v}^2/\gamma^2)\cdot V(1-\mathfrak{v}^2/\gamma^{*2}) \qquad \cdots\cdots\cdots\cdots(3.18)'$$

但し

$$\mathfrak{v}\equiv V/V_s,$$
$$\gamma\equiv V_p/V_s,\ \gamma^*\equiv V^*/V_s,\ \Gamma\equiv\rho^*/\rho$$

V_s, V_p, V^* は夫々固体中の P 波，固体中の S 波，流体中の音波の速度．

ストンレー波の存在が狭い範囲に限られているのに引きかへ，上述の表面波は殆ど無条件に存在し，その速度 V は Γ, γ^*, γ の函数として与へられる．(Table I, II, III; Fig. 1, 2, 3, 参照) 但しこゝで面白いことに，$\Gamma(=\rho^*/\rho)\to 0$ の極限では上の方程式は

$$V(1-v^2/\gamma^{*2})\cdot\{(1-v^2/2)^2-V(1-v^2)\cdot V(1-v^2/\gamma^2)\}=0 \quad \cdots\cdots\cdots\cdots(3.22)$$

となり，この方程式の根によつて与へられる速度は，流体中の音波の速度が固体内のレーリー波のそれ (V_{Rayleigh}) より大きければ V_{Rayleigh} にひとしく，小さければ流体中の音波の速度にひとしくなる．(Fig. 4 参照)．

以上によって分散性のない表面波は盡されたことになる．

26. *Observational Study of Earthquake Motion in the Depth of the Ground. V. (The Problem of the Ripple of Earthquake Motion)*

By Kiyoshi KANAI, Kaio OSADA and Shizuyo YOSHIZAWA,

Earthquake Research Institute.

(Read Sept. 28, 1954.—Received Sept. 30, 1954.)

1. Introduction.

It was found from the records of displacement seismograph shortly after the invention of seismograph towards the end of 19th century that in most cases the waves of short period and small amplitude, the so-called ripples, overlap those of large amplitude and long period[1].

It also became clear from the records of acceleration seismograph that there is a period peculiar to each ground property of which the frequency is predominant[2]. In using an acceleration seismograph waves of comparatively short period such as ripples tend to appear prominently, therefore the predominant period peculiar to each ground property may be due to the property of ripples. Then it is easily assumed that the ripples are the waves generated near the ground surface.

Thus it becomes fundamentally necessary to investigate the property of ripples thoroughly not only for the purpose of clarifying the nature of seismic waves but also for the promotion of engineering seismology.

In this paper, using the results of observation made at the ground surface and 300 m under the ground at Hitachi Mine in Ibaraki Prefecture, the property of the ripples of earthquake motion is investigated.

2. Frequency of the period of earthquake motion.

In Table I the constants of the seismograph used in the observation made at the above-mentioned places are shown.

Although the period frequency of earthquake motion is observed from a number of earthquakes, those which were examined with special

1) F. OMORI, *Pub. Earthq. Inv. Com.*, **10** and **11** (1902).
2) M. ISHIMOTO, *Bull. Earthq. Res. Inst.*, **12** (1934), 234.

Table I.

Position	Horizontal			Vertical		
	Period (sec)	Damp. ratio	Magnif.	Period (sec)	Damp. ratio	Magnif.
0m	EW 0.97 NS 0.87	13:1	EW 220 NS 290	0.10	13:1	2.2 gal/mm
300m	EW 0.91 NS 1.02	13:1	EW 200 NS 240	0.26	13:1	0.3 gal/mm

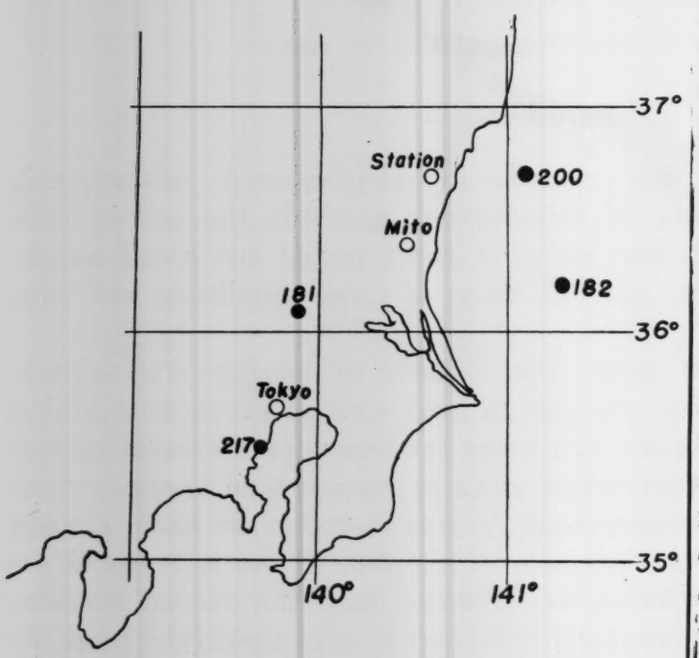

Fig. 1.

preciseness are written in Table II, and the representative seismograms of them are illustrated in Figs. 2 and 3.

From the horizontal seismograms of these earthquakes, the number of waves and their periods i.e. the frequency of period, concerning both the preliminary tremor and the main shock, are found. The period is accepted in two ways. In one way, the interval between neighbouring points at which the wave cross the 0-line is accepted as the period, and in the other way, the interval between neighbouring peaks of the seismogram is accepted. The results are shown in Figs. 4～7.

Table II.

Earthquake Number	Date	Origin		
		φ	λ	Depth (km)
181	1952 II 20	36.1	139.9	55
182	1952 II 26	36.2	141.3	40
200	1952 III 10	36.7	141.1	40
217	1952 IV 8	35.5	139.7	110

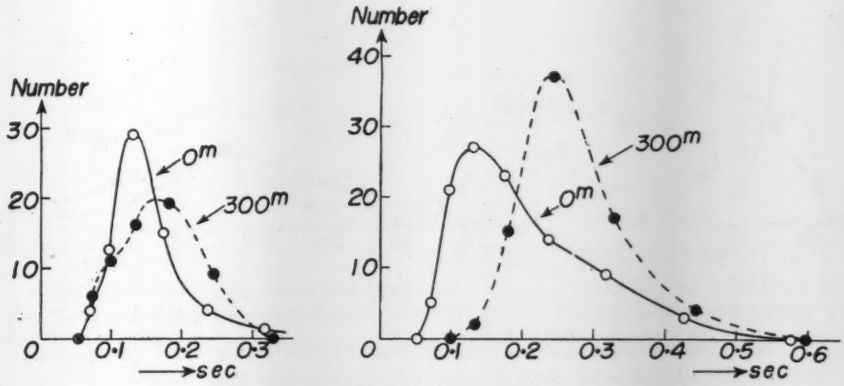

Interval between neighbouring peaks is period.

Interval between neighbouring zero amplitudes is period.

Fig. 4a. The frequency-period relation of the horizontal component of the preliminary tremor of No. 181.

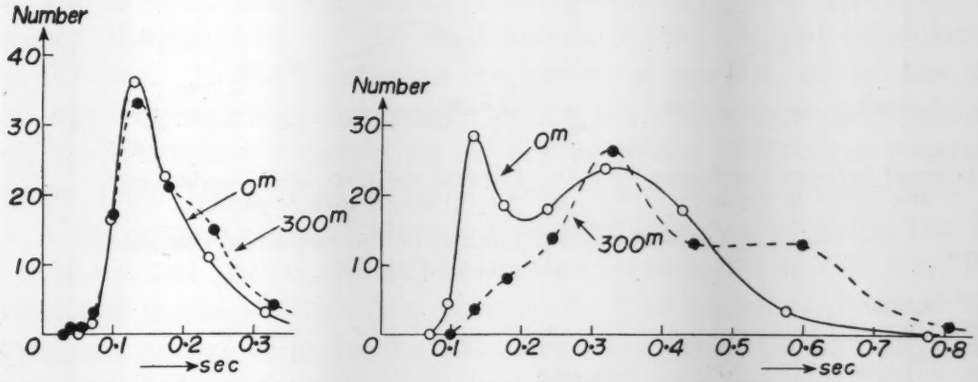

Interval between neighbouring peaks is period.

Interval between neighbouring zero amplitudes is period.

Fig. 4b. The frequency-period relation of the horizontal component of the main shock of No. 181.

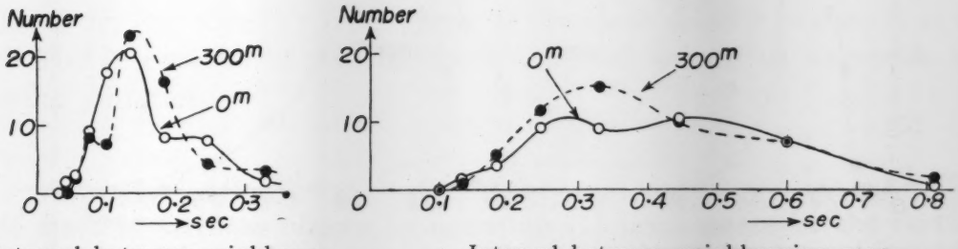

Interval between neighbouring peaks is period.

Interval between neighbouring zero amplitudes is period.

Fig. 5. The frequency-period relation of the horizontal component of the preliminary tremor of No. 182.

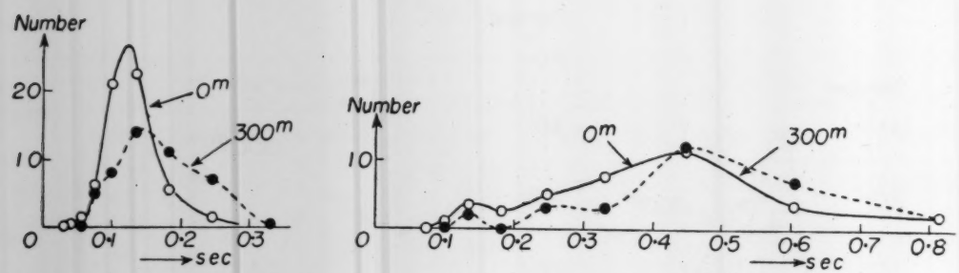

Interval between neighbouring peaks is period.

Interval between neighbouring zero amplitudes is period.

Fig. 6a. The frequency-period relation of the horizontal component of the preliminary tremor of No. 200.

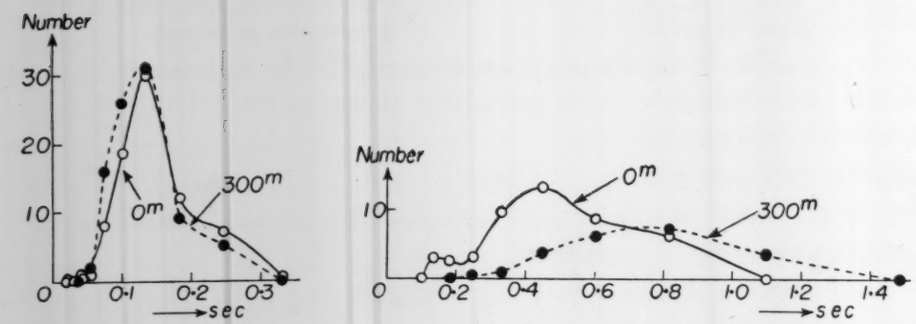

Interval between neighbouring peaks is period.

Interval between neighbouring zero amplitudes is period.

Fig. 6b. The frequency-period relation of the horizontal component of the main shock of No. 200.

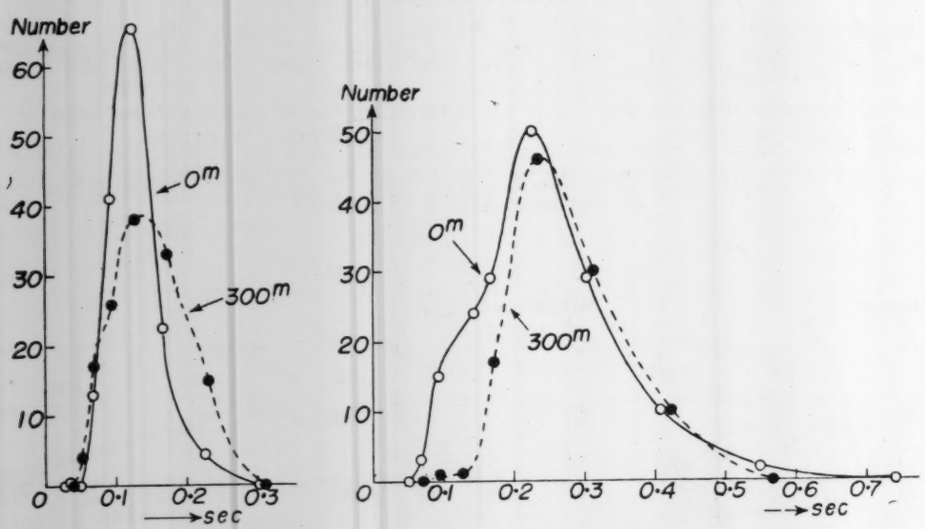

Interval between neighbouring peaks is period.

Interval between neighbouring zero amplitudes is period.

Fig. 7a. The frequency-period relation of the horizontal component of the preliminary tremor of No. 217.

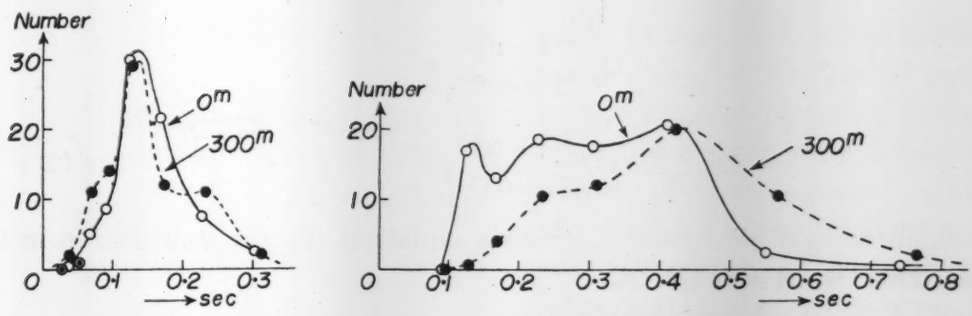

Interval between neighbouring peaks is period.

Interval between neighbouring zero amplitudes is period.

Fig. 7b. The frequency-period relation of the horizontal component of the main shock of No. 217.

From these figures it is easily seen that if the period is considered to be the interval between the neighbouring peaks of seismogram, the frequency distribution at 0 m coincides well with that obtained at 300 m under the ground, and the period corresponding to the maximum of frequency distributions of all earthquakes is definite, its value being about 0.13 sec. In the case when the period is accepted to be the interval between neighbouring points where the 0-line meets the seismogram, the frequency distribution at 0m coincides with that obtained at 300m under the ground in some cases, while in other cases there is quite a difference between them. Moreover each earthquake has its own predominant period. When the period is accepted in this way, the predominant period at 0m often becomes 0.13 sec which is equal to the predominant period value in the case when the period is assumed to be the interval between neighbouring peaks of seismogram. This holds true in the case of P-wave of No. 181.

3. The consideration on the generation of ripples of earthquake motions.

In order to simplify the form of incident seismic wave, it is assumed that it consists of two different kinds of waves, as shown in the following equation.

$$u_0 = A_1 e^{-\frac{(vt-x)^2}{c_1^2}} + A_2 e^{-\frac{(\overline{vt-\tau}-x)^2}{c_2^2}} \quad . \qquad (1)$$

If such a wave as shown in equation (1) propagates in the vertical direction, the vibrations of ground surface will be as expressed in equation (2) due to the multiple reflection of wave in the surface layer.[3)]

3) K. SEZAWA, *Bull. Earthq. Res. Inst.*, **8** (1930), 1.

$$u'_H = 4A_1 \sum_{m=0}^{\infty} (-1)^m \frac{(1-\alpha)^m}{(1+\alpha)^{m+1}} e^{-\frac{\beta^2(v't-\overline{2m+1}H)^2}{c_1^2}}$$

$$+4A_2 \sum_{m=0}^{\infty} (-1)^m \frac{(1-\alpha)^m}{(1+\alpha)^{m+1}} e^{-\frac{\beta^2(v'\overline{t-\tau}-\overline{2m+1}H)^2}{c_2^2}} \qquad (2)$$

in which $\alpha=\rho'v'/\rho v$, $\beta=v/v'$. Using equation (2) the calculation in two cases, that is, $A_1=-1/2$, $A_2=1$ and $A_1=-2$, $A_2=1$, beside the conditions $\rho=\rho'$, $v=6v'$, $\tau=4H/v'$, $c_1=3H$ and $c_2=30H$, is carried out, and it becomes as shown in Figs. 9 and 10.

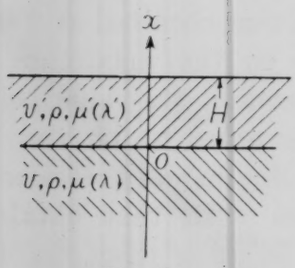

Fig. 8.

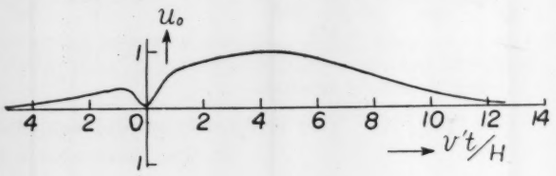

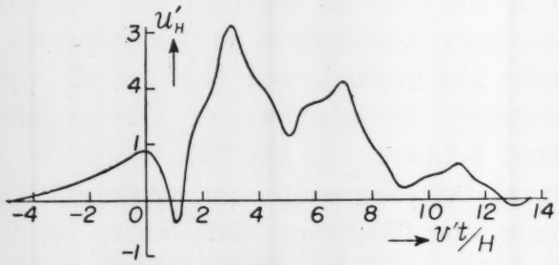

Fig. 9. $A_1=-1/2$, $A_2=1$.

When there are waves of the period equal to or shorter than the natural period of surface layer in incident seismic wave, the natural period of surface layer is apt to appear in the vibration at ground surface. This is clear from Figs. 9 and 10.

It is also seen from Fig. 9 that the wave-form of so-called ripple appears in the vibration at ground surface when the waves of shorter period are of smaller amplitude. P-wave of No. 200 is just an example of this case. In the case when the amplitude of the waves of shorter period is comparatively large, the wave-form of ripple cannot be seen at the ground surface. This will be seen in Fig. 10. P-wave of No. 181 belongs to this case.

From Figs. 9 and 10 it is found that if the interval between neighbouring peaks of seismogram is assumed to be the period, there will be many waves of the period equal to the natural period of surface layer. In other words, the predominant period of the ripples of earthquake motion may be assumed, as the first approximation, to be the natural period of the surface layer. On the other hand, if the interval between neighbouring points where the 0-line meets the seismo-

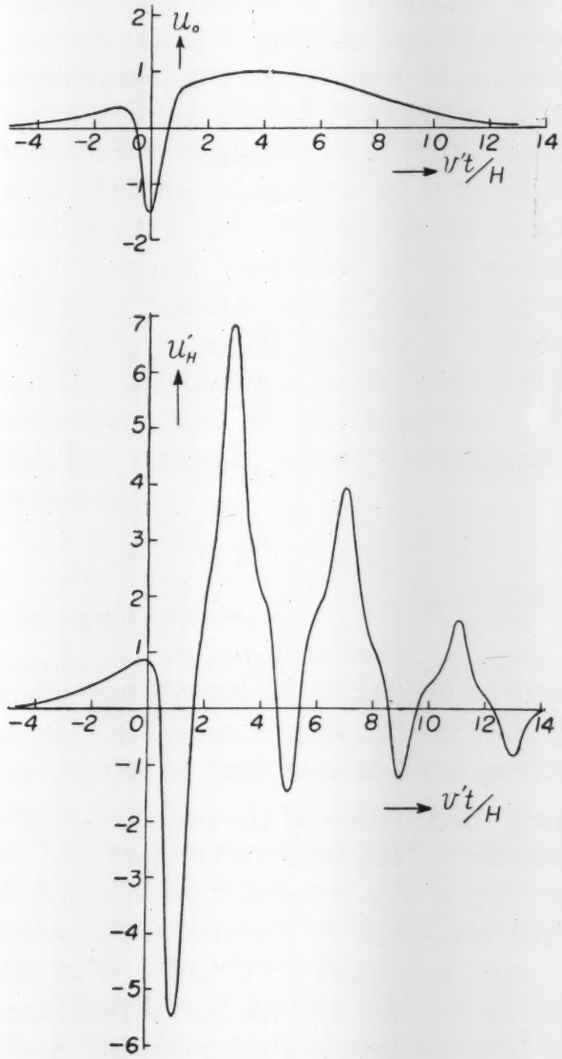

Fig. 10. $A_1 = -2$, $A_2 = 1$.

gram is regarded as the period, many waves of the period equal to the natural period of surface layer can be seen only when the waves of short period which are found among incident seismic waves are of considerably large amplitude. Consequently, in order to find the natural period of the surface layer from seismograms, it may be better to adopt the interval between neighbouring peaks of displacement seismogram as the period.

4. Study of the property of surface layer through the ripples.

Fig. 11 shows the frequency of the period obtained from the vertical seismogram of earthquake motion at the ground surface. The period to which the maximum of the frequency corresponds becomes about 0.07 sec.

The ratio of the predominant period of the horizontal component of earthquake motion to that of the vertical one is 0.13/0.07 $\fallingdotseq$1.7 which corresponds to the velocity ratio of S-wave to P-wave on the assumption that Poisson's ratio of the material of surface layer is 1/4. Since the propagation direction of the seismic waves near the surface is considered to be nearly vertical[4], in P-waves vertical motion is predominant and in S-waves horizontal motion is so, and the predominant periods of both the horizontal and vertical motions correspond to

4) T. Matuzawa, K. Hasegawa and S. Haeno, *Bull. Earthq. Res. Inst.*, **4** (1928), 85.

T. Suzuki, *Bull. Earthq. Res. Inst.*, **10** (1932), 517.

the natural periods of surface layer concerning P-waves and S-waves respectively. From this it is clear that there are ripples due to S-waves in the preliminary tremor and ripples due to P-waves in the main shock.

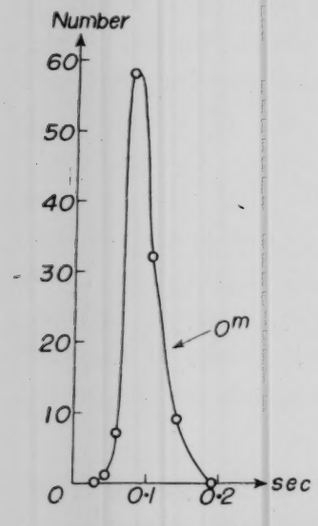

Fig. 11a. The frequency-period relation of the vertical component of the preliminary tremor of No. 182.

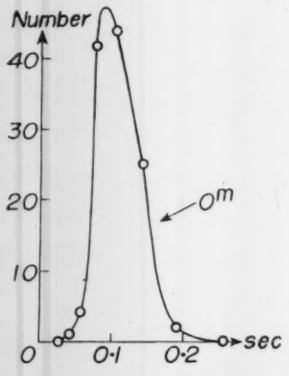

Fig. 11b. The frequency-period relation of the vertical component of the main shock of No. 182.

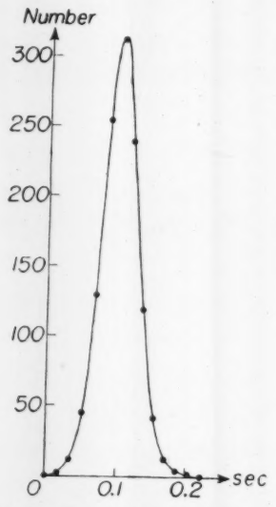

Fig. 12. The frequency-period relation of micro-tremor.

Fig. 12 illustrates the frequency distribution of the period of micro-tremor measured at the ground surface of the observation spot and its maximum value comes to 0.13 sec. From Fig. 12 and Figs. 4～7, it is found that the period to which the maximum of the period frequency of the micro-tremor at a certain place corresponds coincides with the period at the same place to which the maximum of the period frequency corresponds in the case where the interval between neighbouring peaks of seismogram is the period.

This means that the ripples of earthquake motion represent the characteristics of the ground just as the property of micro-tremor does.

In the previous research the relation between the amplitudes at the ground surface and at 300 m under the ground was studied and the result was that the maximum value of the ratio of the amplitude at the ground surface to that of the vibration at 300 m under the ground becomes about 6[5], which is acceptable by assuming that the ratio of the vibration impedance of under ground layer material to that of the

5) K. KANAI, K. OSADA and S. YOSHIZAWA, *Bull. Earthq. Res. Inst.*, **31** (1953), 226, Fig. 6.

surface layer material is 3.

From recent observations it became clear that at the observation spot here concerned there is a soil layer near the ground surface in which the velocity of P-waves is about 500 m/sec. And the previous observation made it clear that there are rocks under the said layer where the mean velocity of P-waves is 1500 m/sec.[6] Consequently, assuming that the ratio of density is approximately 1, the ratio between the vibration impedance of the material of lower medium and that of soil layer becomes 3 and it coincides with the above-mentioned value.

Next, from the velocity of P-waves at the surface layer, 500 m/sec, and the predominant period obtained from the seismogram of vertical component, 0.07 sec, the thickness of the soil layer is found to be 10 m. This is a plausible value in consideration of the conditions of the observation spot.

5. Conclusion.

From the seismograms obtained at the ground surface and 300 m under the ground at Hitachi Mine in Ibaraki Prefecture, the property of the so-called ripples of earthquake motion is studied. Considering the results of both this and the previous study, the following fact is found.

When waves with period equal to or shorter than the natural period of the surface layer are found among the incident seismic waves, the wave form of ripple will originate due the multiple reflection of seismic waves in the surface layer.

Therefore it can be said that the predominant period of the ripple of earthquake motion corresponds to the natural period of surface layer.

Then, in studying the property of surface layer by finding the predominant period from seismogram, it may be appropriate to regard the interval between neighbouring peaks of displacement seismogram as the period.

Finally, it is found that P-waves have a natural period different from that of S-waves, and the period to which the maximum of the period frequency of micro-tremor corresponds is coincident with the natural period of surface layer in case of S-waves, which is of important meaning from the engineering point of view.

In conclusion, we wish to express our hearty thanks to the members

6) K. KANAI, *Bull. Earthq. Res. Inst.*, **29** (1951), 506, Fig. 4.

of Motoyama Office, Hitachi Mine. We also wish to express our thanks to Messrs. T. Tanaka and T. Suzuki who took part in the observation.

26. 地下深所における地震動の観測結果　第5報
(地震動の漣の問題)

地震研究所　金井　清
長田甲斐男
吉沢静代

茨城県日立鉱山の地表面及び地下 300 m における地震記録から，いわゆる地震動の漣の性質をしらべたところ，次の事柄がはつきりした．

地震波の中に地表層の固有周期と同程度の周期の波又はそれよりも短い周期の波が混つていると，地震波が地表層の中で重複反射することによつて，いわゆる漣と称される波形が発生する．そして，漣を発生するもとになる波の振幅が小さいときは，漣は振幅が大きく周期の長い波の上に重なつてあらわれることになる．

従つて，地震動の漣の卓越周期を求めると，これは地表層の固有周期に近い値をとることになる．

それで，地震記象から卓越周期を求めて，表面層の性質をしらべようとする場合には，地震勤の変位の山から山の間を周期とすることが適当ということになる．

なお，表面層の固有周期は P-波の場合と S-波の場合とで値がちがうわけであるが，常時微勤の周期の頻度の最大になる周期は，工学方面で大切な，S 波による表面層の固有周期にあたることが確められた．

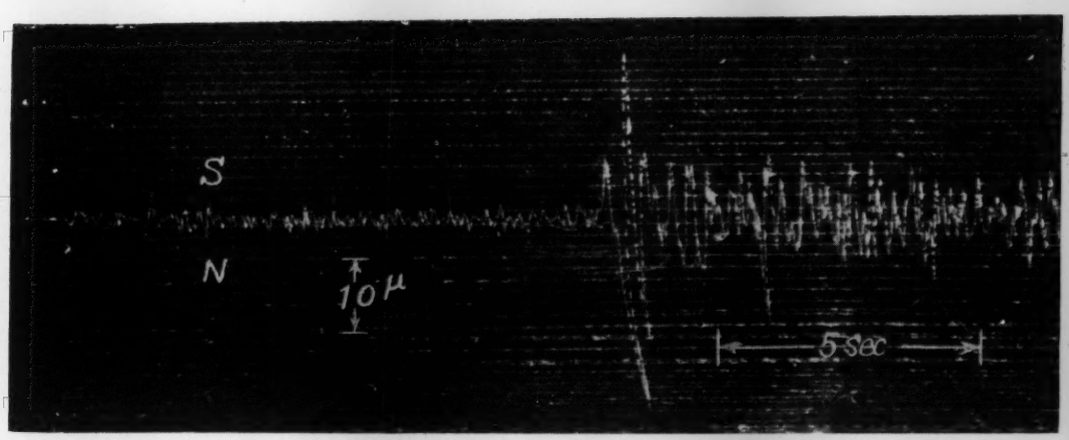

Fig. 2a. Seismogram of No. 181 at the ground surface.

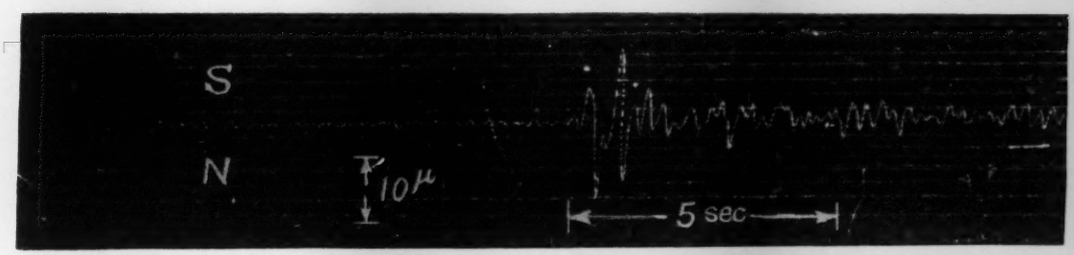

Fig. 2b. Seismogram of No. 181 at 300 m under the ground.

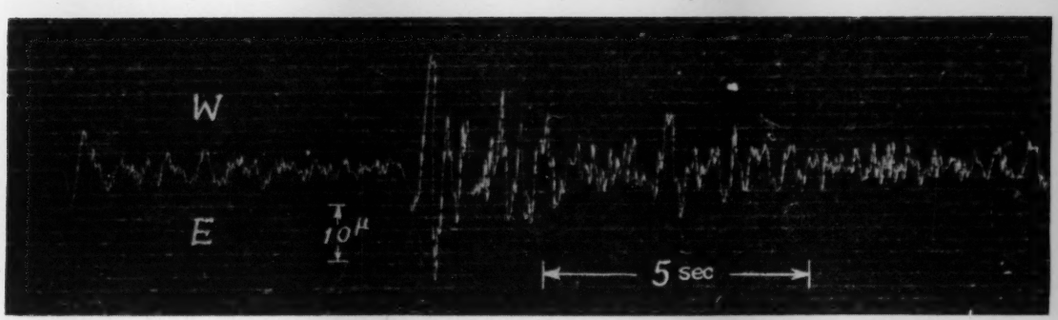

Fig. 3a. Seismogram of No. 200 at the ground surface.

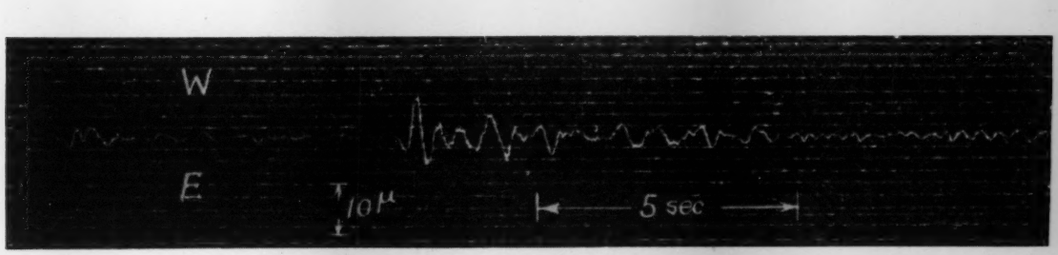

Fig. 3b. Seismogram of No. 200 at 300 m under the ground.

27. *On the Accuracy of Hypocentre Determination I.*

By Shūzō ASANO,

Earthquake Research Institute.

(Read May 25, 1954.—Received Sept. 30, 1954.)

1. Introduction.

Recently the structure of the earth's interior which is the field of earthquake occurrence has been discussed widely and vigorously on the theoretical basis of the property of material. Owing to the light thrown by the elucidation of the mechanism of earthquake occurrence and the propagation of seismic waves and so forth much importance is being attached to these studies by the seismologists at large. It is well known that most of the fundamental physical quantities used in these studies, such as density, pressure, elastic constants, etc., are basically dependent on the velocity distribution of seismic waves within the earth as derived from the travel-time curve. It is also known that incessant efforts have hitherto been made to derive a standard travel-time curve by senior investigators, among which the names of H. Jeffreys, K. E. Bullen, B. Gutenberg and C. F. Richter are to be specially mentioned. However, the discrepancies between the velocity distributions as worked out by these authorities are not small enough to be discarded from the above point of view. It is therefore necessary to examine the main causes of the inaccuracies of the travel-time curve, among which those of hypocentre determination are deemed to be of the prime importance. Among the difficulties in the accurate determination of hypocentre, such inevitable factors as the finite and irregular shape of hypocentral region may perhaps be counted, but there must be other factors which can be eliminated by modifying our method concerned. To contribute to this problem, the writer intended to carry out some critical examinations of the current procedure in these studies, and here in this paper the writer wishes to report a part of his study.

Now, in natural earthquakes, difficulties arise from the fact that we cannot control the time and position of earthquake occurrence, while in seismic prospecting, these factors are within our control so that we can arrange to carry out our observation as accurately as possible. The writer therefore made an experimental study to infer the accuracy of

hypocentre determination, taking the advantages of the field experiments of prospecting by the teams of "Jisin-Tankō Jikken Group" (Seismic Exploration Group). For providing this opportunity the writer is thankful to the members of this group. In this trial the position of shot point and shot time are assumed to be unknown and, using the time of arrival of P waves, they are determined by the usual method of least-squares as in natural earthquakes. Thus if we compare such items as the position of hypocentre and origin time as determined in this way with the actual values, we can gain some clue as to the accuracy of hypocentre determination.

2. Materials used.

The records used in this study were obtained by the experiments carried out in Feb., 1954 at the Tanasi experimental farm of the Tokyo University by courtesy of "Jisin-Tankō Jikken Group". Both vertical electro-magnetic seismographs of about 20 c/s in natural frequency and

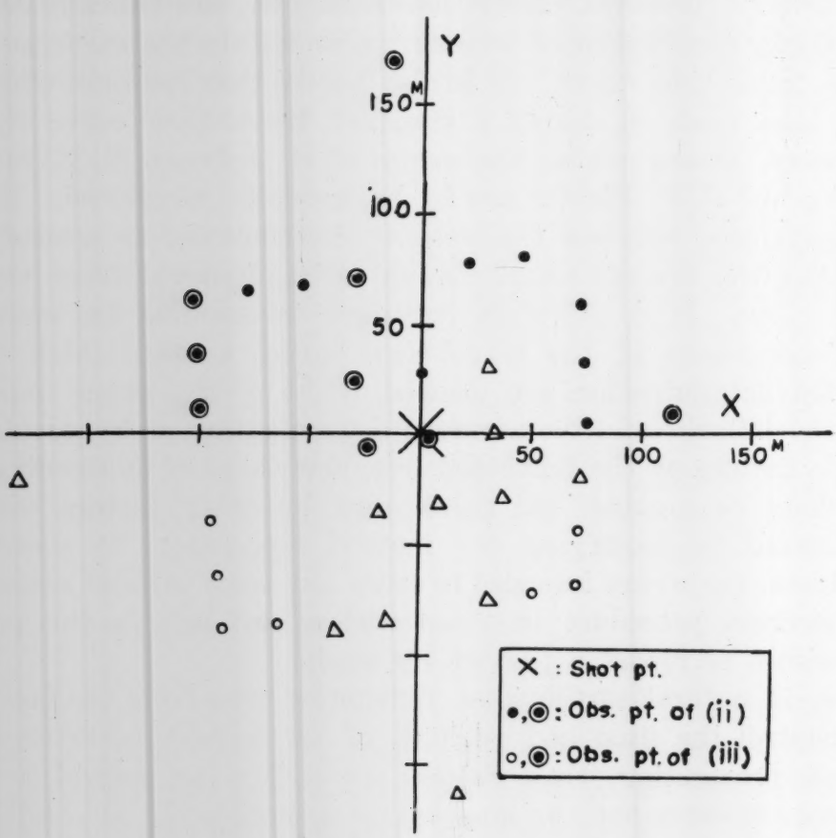

Fig. 1. Shot and observation points.

oscillographs used in this experiment were of the E. T. L.- and Tōsiba-type. Fig. 1 shows the positions of shot and seismographs. The spread was extended to about 180 m. from the origin. The exact positions of shot and seismographs were determined by plane table survey and the uncertainty of coordinates of a point is less than 20 to 30 cm. The oscillograph-paper speed was about 0.4 mm. per 1 millisec. and time signal is marked every 10 milliseconds on the records by means of a tuning fork. Fig. 8 is an example of the records.

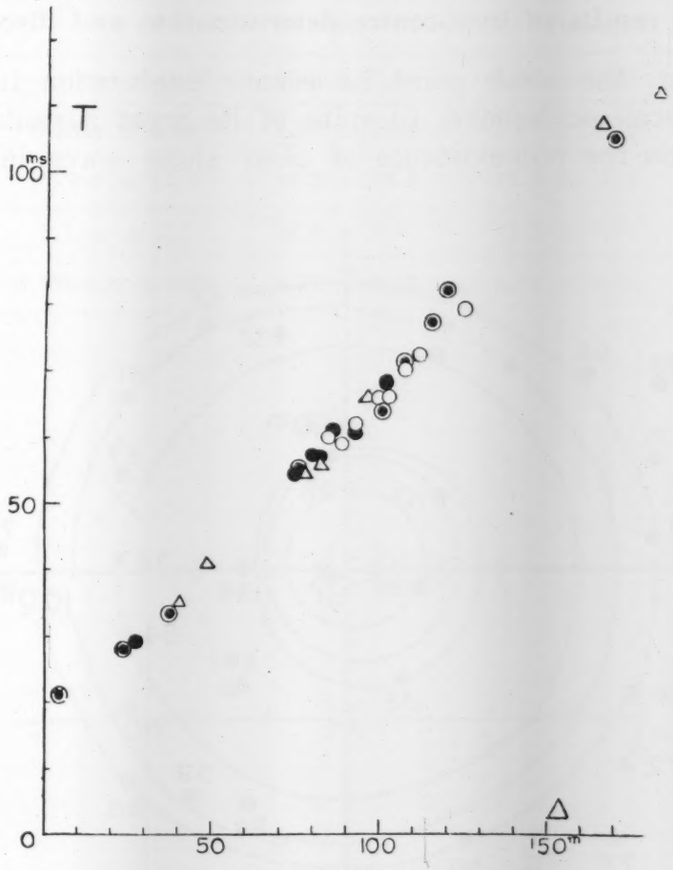

Fig. 2. The actual travel-time curve (The same marks as in Fig. 1 are used).

Using 281 g. or 70 g. of dynamite with a piece of blasting cap, the explosion was carried out at the bottom of a hole with a diameter of about 10 cm. and depth of 14 m. The oscillograms obtained gave very clear onsets and we can easily read off the phase from almost all the traces, although some of the traces were disturbed by

some inductions and ground noises. Three pairs of available data under almost same conditions were obtained, and the mean travel-time curve obtained from them is given in Fig. 2. Fluctuations of each observed travel-time are less than 3 millisec. and the allowable breadth of travel-time curve may thus be considered to be less than 5 millisec. as seen from Fig. 2. So the uncertainty of shot time, that is, the irregularity in delay time of blasting cap which seems to be a few millisec. is negligible in this study.

3. The results of hypocentre determination and discussions.

At present, the weak point in seismic exploration in comparison with the natural earthquake, in spite of its great advantages as mentioned above, is the non-existence of clear shear wave in the ground

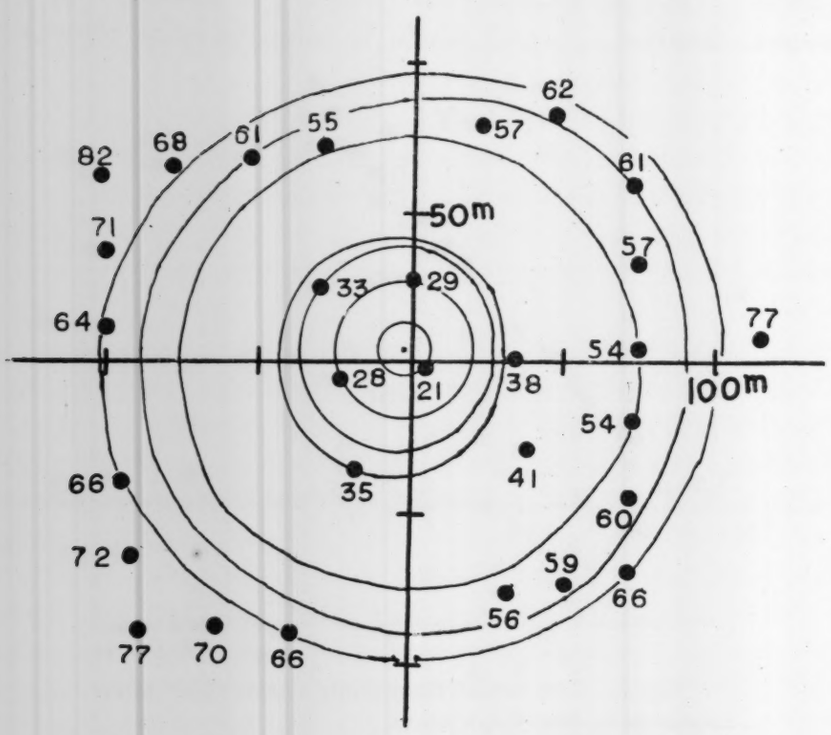

Fig. 3. Isochronals with arrival time in millisecond.

motion caused by explosion, and therefore we can not make use of P~S interval to estimate the epicentre approximately. So the epicentre of first approximation was estimated as $x_0=-3.00$ m. and $y_0=3.00$ m. by using isochronals (Fig. 3) and the travel-time curve was drawn. From this

travel-time curve the velocity, origin time and focal depth were determined to be 1.8 km/sec., 11 millisec., and 16 m. respectively, on the assumption of a uniform structure. The least-squares solution was obtained by using the formula

$$(x_0-x_i)\delta x_0+(y_0-y_i)\delta y_0+z_0\delta z_0+v_0^2(t_i-t_0)\delta t_0-v_0(t_i-t_0)^2\delta v_0=v_0^2(t_i-t_0)\delta t_i$$

where suffix 0 and i gives the quantities concerning the hypocentre and i-th observation point respectively.

Table I. The comparison of each case.

	(i)	(ii)	(iii)	Actual value
x_0	−1.50m ± 0.66	0.43 ± 0.90	−0.83 ± 0.89	0
y_0	0.38m ± 0.64	2.05 ± 2.06	−1.77 ± 1.10	0
z_0	27.9m ± 12.7	16.2 ± 14.6	13.8 ± 17.3	14
t_0	7.1ms ± 2.3	10.9 ± 3.0	11.2 ± 3.8	0
v_0	1.79km/s ± 0.04	1.77 ± 0.06	1.81 ± 0.07	

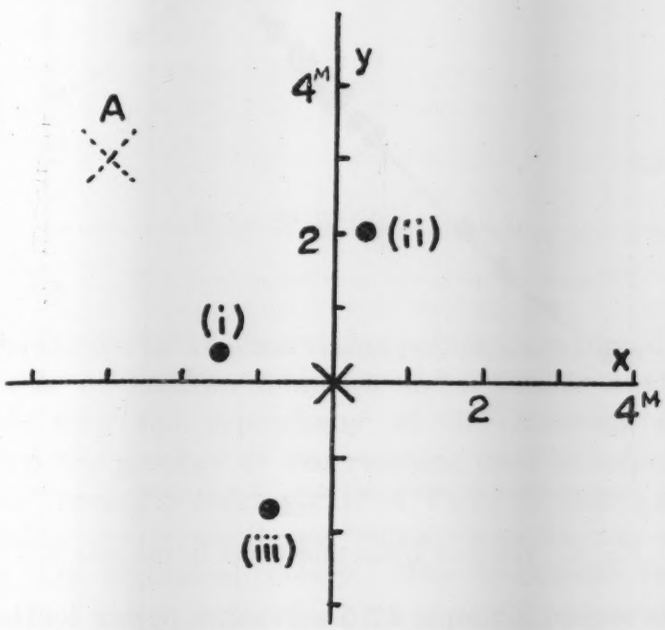

Fig. 4. The relative position of determined epicentre to the actual one. (A: epicentre of first approximation)

Three interesting cases were treated and the observation points used in each case were shown in Fig. 1 and Fig. 2:—

(i) In the first trial all observation points except four at which large

deviations from the mean travel-time curve are observed, that is, 31 seismographs were used. The results obtained are given in the column (i) of Table I and the relative place of determined epicentre to the actual one is shown in Fig. 4.

From the results we see that (1) the epicentre is relatively well-determined, while (2) the determination of focal depth and origin time is not so accurate as might have been expected. For example the focal depth is twice as deep as the actual one and this is probably due to the assumption of uniform structure. Fig. 5 gives the final travel-time curve based on this hypocentre.

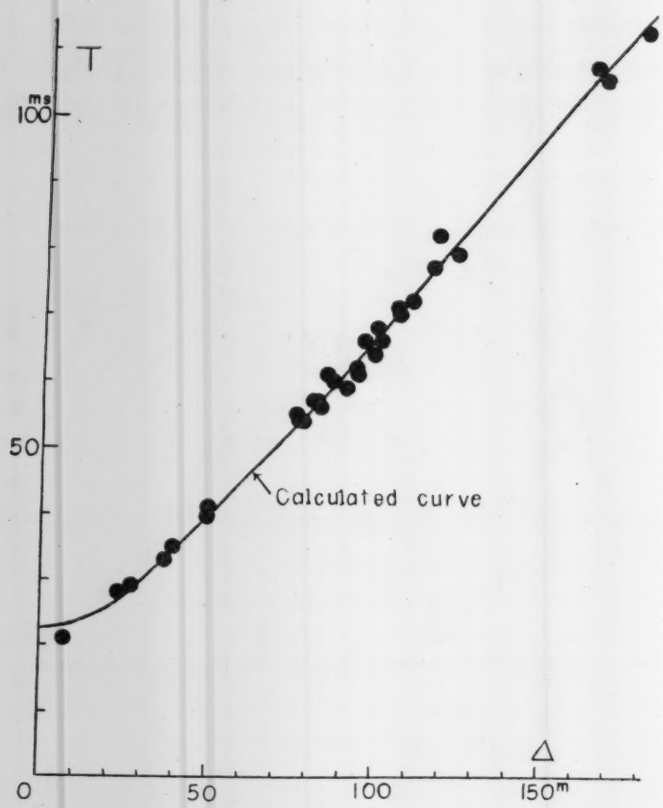

Fig. 5. The final travel-time curve in the case (i).

(ii) In the second example 17 observation points located in the first and second quadrants were used. This trial provides an example of asymmetric distribution of observatory relative to epicentre. The results in this case are entered in the column (ii) of Table I, from which we can see that in comparison with (i) the shot time is determined later and the focal depth is shallow and apparently close to the actual value,

but its probable error is larger. Furthermore the place of epicentre deviates more from the actual one than in (i) (Fig. 4). Fig. 6 gives the final travel-time curve.

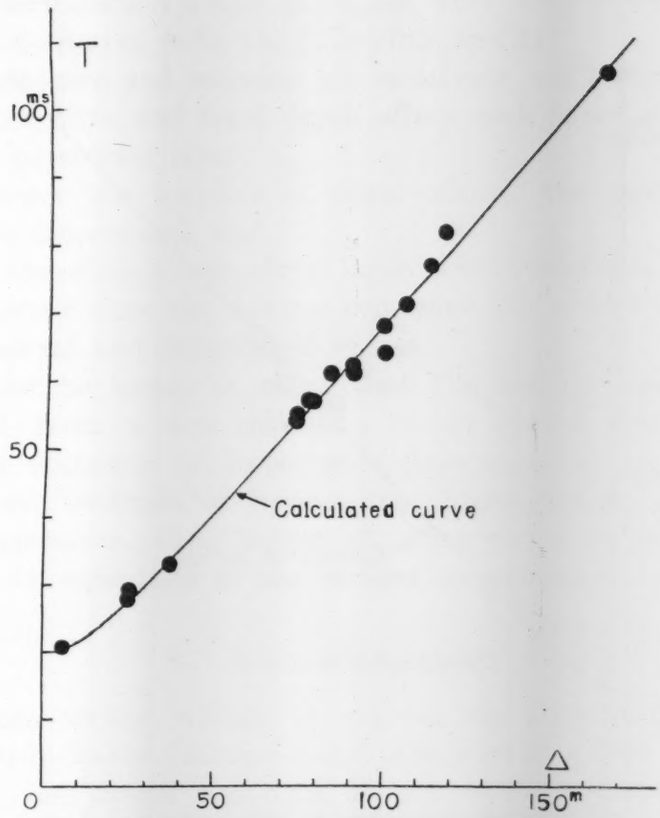

Fig. 6. The final travel-time curve in the case (ii).

(iii) In the third trial 17 observation points were picked up at random by using a table of random numbers and a similar analysis was then made. In this way the dependency of the accuracy of hypocentre determination on the number of observations used is inferred. And the result (as seen from the column (iii) of Table I) shows a marked fact that the probable errors are larger than those in the case (i) as is expected from the statistical theory. The tendencies relative to the first case resembles those obtained in the case (ii), especially in respects of shot time, focal depth and their probable errors. On the other hand, if we compare the results of (iii) with those of (ii), the place of epicenter in the case (iii) is closer to the actual one than in the case (ii) (Fig. 4) and its probable error in (iii) is a little smaller than that in (ii) although equal numbers of observations were used in both cases. This is what we

have expected from the distribution of observing points. Fig. 7 gives the final travel-time curve.

It is to be noticed from Table I that in all cases the velocity is well-determined.

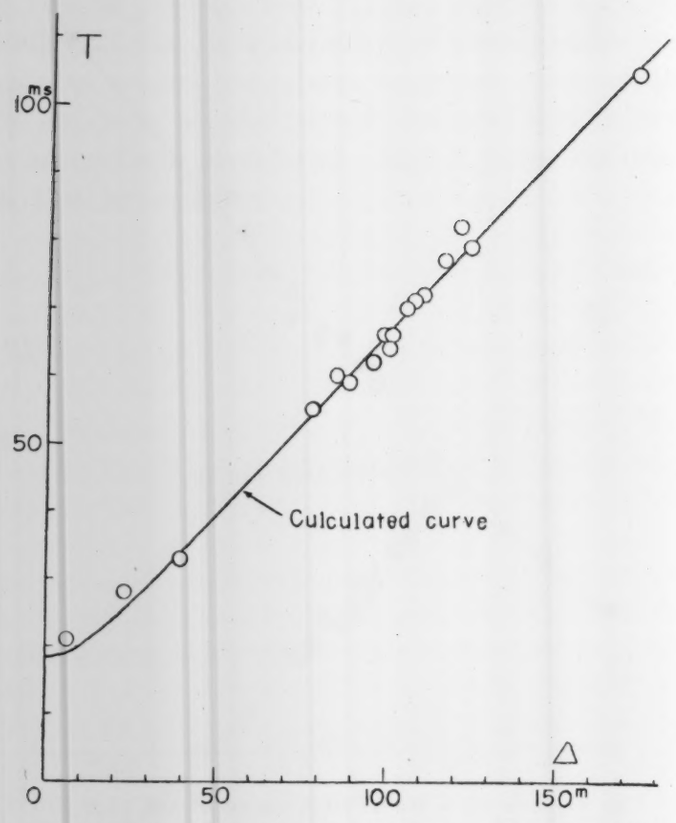

Fig. 7. The final travel-time curve in the case (iii).

These three cases give only a few examples under special conditions depending on the crustal structure of the experimental field, the shot depth, the amount of explosives, and the distribution of errors, etc., and also on the method of hypocentre determination. Throughout the above trials, the assumption of uniform structure was adopted, but if the effect of superficial layer is taken into account, the results will be expected to approach to the actual one. The writer hopes to examine the effects of superficial layer, methods of hypocentre determination, dimension of hypocentre and inclined structure, etc., on the accuracy of hypocentre determination, and reports will be given in near future.

4. Summary.

In view of the importance of the examination of accuracy of hypocentre determination a few examples were worked out by the usual method of least-squares with the following results:

1) the epicentre and velocity are relatively well-determined,

2) the shot time and focal depth affect each other and seem to be sensitive to a superficial layer,

3) the larger the number of observations, the more accurate is the hypocentre determined, and

4) when the effect of superficial layer is not taken into consideration, the probable error does not always represent the extent of discrepancy between the actual and determined values.

But it must be borne in mind that the results mentioned above were obtained from a few examples under special conditions. Such effects on the accuracy of hypocentre determination as those of the superficial layer, methods of hypocentre determination, dimension, the amount of explosives, distribution of observation points and inclined structure will be examined at the earliest opportunity.

5. Acknowledgement.

The present writer wishes to express his sincere thanks to the members of "Jisin-Tankō Jikken Group" who showed a deep understanding of this study and placed the data at the writer's disposal. He also cordially expresses thanks to Asst. Prof. S. Omote who gave him the chance and encouragements to carry out this study. To Prof. H. Kawasumi for his helpful suggestions and encouragements, the writer's hearty thanks are also due.

27. 震源決定の精度について（第一報）

地震研究所　浅野周三

爆発物を利用する地震探鉱では予め爆破点，爆破時刻，地震計の配置等を適当にし得るが，此の利点を生かし爆破点の位置，爆破時刻を未知と仮定し自然地震に於けると同様に最小自乗法により其等を定め実際と比較し自然地震で行われている震源決定の精度に関する目安を得る事を試みた．地殻構造，震源決定の方法，爆破点の深さ，薬量，地震計の配置等の点で単なる一例にすぎないが次の如き結果が得られた．

(1) 震央と速度は比較的よく定まる．
(2) 深さと発震時はお互に影響し合い表面層に敏感である様である．
(3) 同じような配置なら地震計の数の多い方がよく定まる．
(4) 蓋然誤差は定められた値と実際との相違に対する目安を必ずしも与へない様である．

以上の結果は一様の構造を仮定して得られたものであるが，表面層，震源決定の方法，爆破点の深さ，薬量，震源の大きさ，地震計の配置等の影響の考察は近い将来行つてみたいと考へている．

尚用いられた材料は「地震探鉱実験グループ」によつて得られたもので記して感謝の意を表する．

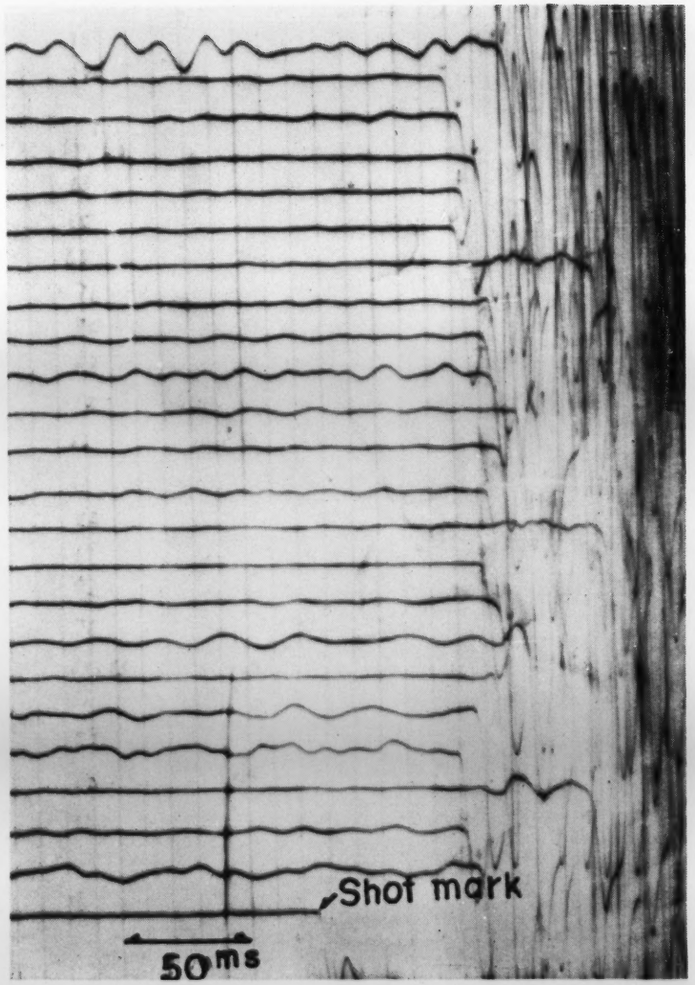

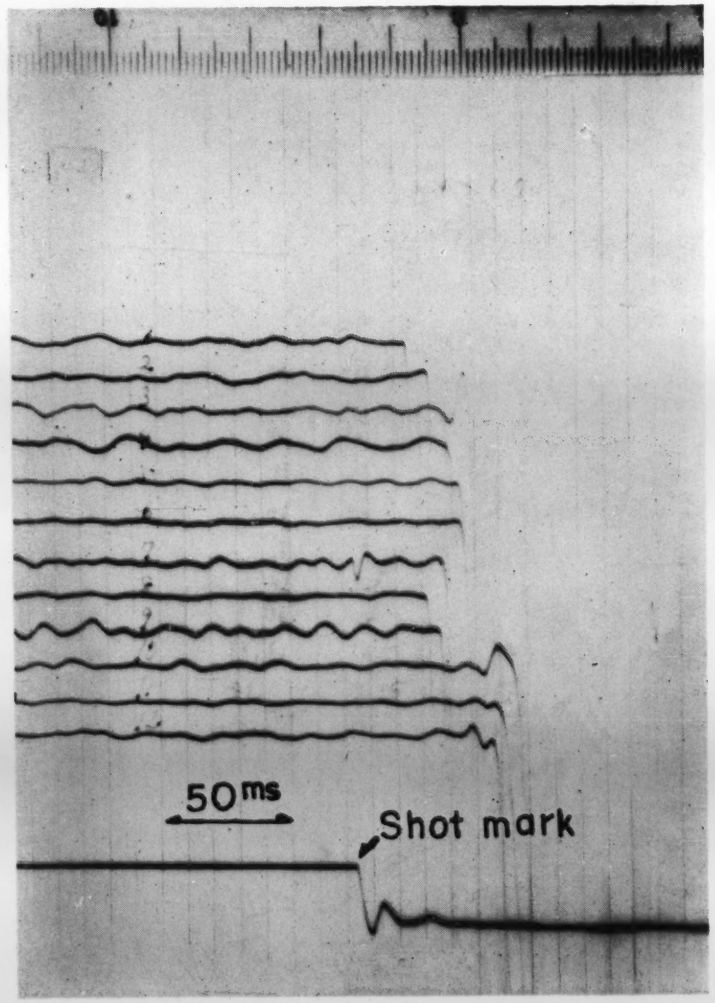

Fig. 8. An example of a pair of oscillograms.
A: an oscillogram obtained by the oscillograph of E. T. L.-type.
B: 〃 〃 〃 〃 of Tōsiba-type.

——所　　報——

◎談話会記事

第 313 回談話会 (昭和 29 年 7 月 20 日)

1.	ラブ及びレーリー両波の分散と地殻構造	三東哲夫
2.	三鷹市新川における振動実験 (建物内外に据えた起振機による建物補強前後の振動測定)	三鷹測定班 (金井清)

第 314 回談話会 (昭和 29 年 9 月 28 日)

1.	初動の押し引きに関する実験	嶋悦三
2.	分散した地震波の解析 (2)	佐藤泰夫
3.	常時観測用電磁型高倍率地震計	表俊一郎 山崎良雄
4.	芦の平における浅間火山地震の臨時観測	表俊一郎 山崎良雄 小林直吉
5.	地下深所における地震動の観測結果 (第 5 報) (地震動の漣の問題)	金井清 長田甲斐男 吉沢静代
6.	地震動による建物振動の観測結果 (第 3 報) 補遺	金井清 鈴木富三郎
7.	地震の場の論 —— 更にくわしく力の起る区域について	松沢武雄

第 315 回談話会 (昭和 29 年 10 月 26 日)

1.	岩石弾性の異方性に関する実験	下鶴大輔 村井勇
2.	表面波の分散と地殻構造	三東哲夫
3.	移動平均を用いた地震波形の解析	松本利松
4.	起振機による建物の振動試験について	高橋竜太郎

第 316 回談話会 (昭和 29 年 11 月 16 日)

1.	震源決定の精度について (第 2 報)	浅野周三
2.	分散した地震波の解析 (3)	佐藤泰夫 山口林造
3.	三鷹の運輸技術研究所にある起振機による土地の振動軌跡	岸上冬彦
4.	取壊中の高層ビルディング振動実験 (附話, 大型起振機の製作)	震研測定班
5.	建物ロッキングの測定 (其の 1)	金井清 那須信治

Index to Vol. XXXII.

Page

ASANO, S., (27) On the Accuracy of Hypocentre Determination I. (in English) 371

FURUKAWA, E., NISHIMURA, G. and SUZUKI, M., (7) Theory of Eden's Twin Strips and Application of It to Magnifying Mechanism of Seismometer. (in English) 87

HASEGAWA, H. and MATUZAWA, T., (17) Feldtheorie der Erdbeben: Elliptisches Quellengebiet. (im Deutschen) 231

KANAI, K., (15) A Short Note on the Relation of Amplitude-Period of Earthquake Motion. (in English) 211

KANAI, K. and SUZUKI, M., (13) Analytical Results of the Acceleration Seismograms obtained at Tokyo and Yokohama. (in English) 189

KANAI, K., OSADA, K. and YOSHIZAWA, S., (26) Observational Study of Earthquake Motion in the Depth of the Ground. V. (The Problem of the Ripple of Earthquake Motion) (in English) 361

KANAI, K., TANAKA, T. and OSADA, K., (14) Measurement of the Micro-tremor. I. (in English) 199

KASAHARA, K., (5) Experimental Studies on the Mechanism of Generation of Elastic Waves IV. (in English) 67

MATUMOTO, T. and SATÔ, Y., (18) On the Vibration of an Elastic Globe with One Layer. The Vibration of the First Class. (in English) 247

MATUZAWA, T., (1) S-Wellen an der fest-flüssigen Schichtgrenze. I. (im Deutschen) 1

MATUZAWA, T., (10) S-Wellen an der fest-flüssigen Schichtgrenze. II. (im Deutschen) 155

MATUZAWA, T., (24) Feldtheorie der Erdbeben: Näheres über das Quellengebiet. (im Deutschen) 341

MATUZAWA, T. und HASEGAWA, H., (17) Feldtheorie der Erdbeben: Elliptisches Quellengebiet. (im Deutschen) 231

MORIMOTO, R., TSUYA, H. and OSSAKA, J., (4) The 1950–1951 Eruptions of Mt. Mihara, Oshima Volcano, Seven Izu Islands, Japan. Part I. The 1950 eruption. (in English) 35

MORIMOTO, R., TSUYA, H. and OSSAKA, J., (22) The 1950–1951 Eruptions of Mt. Mihara, Oshima Volcano, Seven Izu Islands, Japan. Part II. The 1951 eruption. A. Activity of the second Period. (in English) 289

NISHIMURA, G. and SUZUKI, M., (8) Horizontal Deformations of a

Japanese Two-Storied Frame-House: (1) Vibration due to an Arbitrary Shock, (2) Vibration Caused by a Rotary with Unbalanced Mass, (3) Vibration due to Natural Wind, and (4) Deformation due to the Sun's Radiation Heat. (in English) 113
NISHIMURA, G. and SUZUKI, M., (23) Anemometer of Inverted Pendulum Type and Wind Construction Studied with It. (in English) 313
NISHIMURA, G., SUZUKI, M. and FURUKAWA, E., (7) Theory of Eden's Twin Strips and Application of It to Magnifying Mechanism of Seismometer. (in English) 87
OSADA, K., KANAI, K. and TANAKA, T., (14) Measurement of the Micro-tremor. I. (in English) 199
OSADA, K., KANAI, K. and YOSHIZAWA, S., (26) Observational Study of Earthquake Motion in the Depth of the Ground. V. (The Problem of the Ripple of Earthquake Motion) (in English) 361
OSSAKA, J., TSUYA, H. and MORIMOTO, R., (4) The 1950–1951 Eruptions of Mt. Mihara, Oshima Volcano, Seven Izu Islands, Japan. Part I. The 1950 eruption. (in English) 35
OSSAKA, J., TSUYA, H. and MORIMOTO, R., (22) The 1950–1951 Eruptions of Mt. Mihara, Oshima Volcano, Seven Izu Islands, Japan. Part II. The 1951 eruption. A. Activity of the second period. (in English) 289
SAKUMA, S., (16) Effect of Thermal History on Viscosity of Ooshima-lavas. (Elastic and Viscous Properties of Volcanic Rocks. Part 4.). (in English) 215
SATÔ, Y., (2) Study on Surface Waves X. Equivalency of SH-waves and Sound Waves in a Liquid. (in English) 7
SATÔ, Y., (11) Study on Surface Waves XI. Definition and Classification of Surface Waves. (in English) 161
SATÔ, Y., (19) A Note on Tsuboi-Nagata's Method. (in English) ... 259
SATÔ, Y., (25) Study on Surface Waves XII. Non-Dispersive Surface Waves. (in English) 349
SATÔ, Y. and MATUMOTO, T., (18) On the Vibration of an Elastic Globe with One Layer. The Vibration of the First Class. (in English) 247
SHIMOZURU, D., (20) Study on the Elasticity near the Melting Point. Part I. Nature of Dilatational Wave. (in English) 271
SUZUKI, M. and KANAI, K., (13) Analytical Results of the Acceleration Seismograms obtained at Tokyo and Yokohama. (in English) 189
SUZUKI, M. and NISHIMURA, G., (8) Horizontal Deformations of a

Japanese Two-Storied Frame-House: (1) Vibration due to an Arbitrary Shock, (2) Vibration Caused by a Rotary with Unbalanced Mass, (3) Vibration due to Natural Wind, and (4) Deformation due to the Sun's Radiation Heat. (in English) 113
SUZUKI, M. and NISHIMURA, G., (23) Anemometer of Inverted Pendulum Type and Wind Construction Studied with It. (in English) 313
SUZUKI, M., NISHIMURA, G. and FURUKAWA, E., (7) Theory of Eden's Twin Strips and Application of It to Magnifying Mechanism of Seismometer. (in English) 87
TAKAHASHI, T., (9) A Problem on Fourier Series. (in English) 147
TANAKA, T., KANAI, K. and OSADA, K., (14) Measurement of the Micro-tremor. I. (in English) 199
TSUYA, H., MORIMOTO, R. and OSSAKA, J., (4) The 1950–1951 Eruptions of Mt. Mihara, Oshima Volcano, Seven Izu Islands, Japan. Part I. The 1950 eruption. (in English) 35
TSUYA, H., MORIMOTO, R. and OSSAKA, J., (22) The 1950–1951 Eruptions of Mt. Mihara, Oshima Volcano, Seven Izu Islands, Japan. Part II. The 1951 eruption. A. Activity of the second period. (in English) 289
YOKOYAMA, I., (3) Geomagnetic Studies of Volcano Mihara. The 4th paper. (A Series of Geomagnetic Dip-Surveys and Continuous Observation of Changes in Geomagnetic Declination.) (in English) 17
YOKOYAMA, I., (12) Geomagnetic Studies of Volcano Mihara. The 5th paper. (Changes in Three Geomagnetic Components during the Period from May 1951 to August 1953.) (in English) 169
YOKOYAMA, I., (21) Geomagnetic Anomalies related to the Magnetization of the Basalt in the Vicinity of Gembudō. (in English). 281
YOSHIZAWA, S., KANAI, K. and OSADA, K., (26) Observational Study of Earthquake Motion in the Depth of the Ground. V. (The Problem of the Ripple of Earthquake Motion) (in English) 361
The Research Group for Explosion Seismology, (6) The Fourth Explosion-Seismic Observations in North-Eastern Japan. (in English) 371

索 引 第 32 号

頁

浅野周三 (27) 震源決定の精度について (第一報) (英文) 371
古川英一·西村源六郎·鈴木正治 (7) エデン平行薄片の理論と地震計への応用 (英文) 87
長谷川博·松沢武雄 (17) 地震の場の論 楕円形の場 (独文) 231
金井 清 (15) 地震動の振幅と周期との関係 (小引) (英文) 211
金井 清·鈴木正治 (13) 東京横浜における加速度地震計記象の解析結果 (英文) 189
金井 清·長田甲斐男·吉沢静代 (26) 地下深所における地震動の観測結果 第5報 (地震動の漣の問題) (英文) 361
金井 清·田中貞二·長田甲斐男 (14) 常時微動の測定 第1報 (英文) 199
笠原慶一 (5) 弾性波の発生機構に関する実験 (第4報) (英文) 67
松本利松·佐藤泰夫 (18) 層のある地球の弾性振動 (第1種の振動の周期) (英文) 247
松沢武雄 (1) 固体液体の境の面の S-波 (独文) 1
松沢武雄 (10) 固体液体の境の面の S-波 II (独文) 155
松沢武雄 (24) 地震の場の論 更に精しく力の起る区域に就て (独文) 341
松沢武雄·長谷川博 (17) 地震の場の論 楕円形の場 (独文) 231
森本良平·津屋弘逵·小坂丈予 (4) 伊豆大島三原山昭和25年及び26年の噴火 その1 昭和25年の噴火 (英文) 35
森本良平·津屋弘逵·小坂丈予 (22) 伊豆大島三原山昭和25年及26年の噴火 その2 昭和26年の噴火 (A) 第2期の活動 (英文) 289
西村源六郎·鈴木正治 (8) 自然風及び起振機等による木造二階建住宅の振動 (英文) 113
西村源六郎·鈴木正治 (23) 逆立振子型風力計による自然風の観測と解析 (英文) 313
西村源六郎·鈴木正治·古川英一 (7) エデン平行薄片の理論と地震計への応用 (英文) 87
長田甲斐男·金井 清·田中貞二 (14) 常時微動の測定 第1報 (英文) 199
長田甲斐男·金井 清·吉沢静代 (26) 地下深所における地震動の観測結果 第5報 (地震動の漣の問題) (英文) 361
小坂丈予·津屋弘逵·森本良平 (4) 伊豆大島三原山昭和25年及び26年の噴火 その1 昭和25年の噴火 (英文) 35
小坂丈予·津屋弘逵·森本良平 (22) 伊豆大島三原山昭和25年及び26年の噴火 その2 昭和26年の噴火 (A) 第2期の活動 (英文) 289
佐久間修三 (16) 大島新熔岩の粘性の熱履歴について (英文) 215
佐藤泰夫 (2) 表面波の研究 X 流体中の音波と SH-波のつくる表面波の対応性 (英文) 7

佐藤泰夫 (11) 表面波の研究 XI 表面波の定義及び分類（英文） 161
佐藤泰夫 (19) 坪井·永田の方法について（英文） 259
佐藤泰夫 (25) 表面波の研究 XII 分散性のない表面波（英文） 349
松本利松·佐藤泰夫 (18) 層のある地球の弾性振動（第1種の振動の周期）（英文） 247
下鶴大輔 (20) 融解点附近の弾性の研究 其の一 縦波の性質（英文） 271
鈴木正治·金井 清 (13) 東京横浜における加速度地震計記象の解析結果（英文） 189
鈴木正治·西村源六郎 (8) 自然風及び起振機等による木造二階建住宅の振動（英文） 113
鈴木正治·西村源六郎 (23) 逆立振子型風力計による自然風の観測と解析（英文） 313
鈴木正治·西村源六郎·古川英一 (7) エデン平行薄片の理論と地震計への応用（英文） 87
高橋健人 (9) Fourier 級数に関する一つの問題（英文） 147
田中貞二·金井 清·長田甲斐男 (14) 常時微動の測定 第1報（英文） 199
津屋弘逵·森本良平·小坂丈予 (4) 伊豆大島三原山 昭和25年及び26年の噴火 その1 昭和25年の噴火（英文） 35
津屋弘逵·森本良平·小坂丈予 (22) 伊豆大島三原山 昭和25年及び26年の噴火 その2 昭和26年の噴火 (*A*) 第2期の活動（英文） 289
横山 泉 (3) 三原山の地球磁気学的研究 第4報 (一連の伏角測量と偏角変化の連続観測)（英文） 17
横山 泉 (12) 三原山の地球磁気学的研究 第5報 (1951年5月から1953年8月にいたる期間の地磁気三成分の変化)（英文） 169
横山 泉 (21) 玄武洞周辺の磁気異常とその玄武岩の帯磁（英文） 281
吉沢静代·金井 清·長田甲斐男 (26) 地下深所における地震動の観測結果 第5報 (地震動の連の問題)（英文） 361
爆破地震動研究グループ (6) 東北日本における第4回爆破地震動観測（英文） .. 79

BULLETIN

OF THE

EARTHQUAKE RESEARCH INSTITUTE

TOKYO UNIVERSITY

VOL. XXXII

1954

東京大学

地震研究所彙報

第 32 號

昭和 29 年

CONTENTS.

Vol. XXXII.

Part 1. March, 1954.

Papers and Reports.

Page

1. T. MATUZAWA, S-Wellen an der fest-flüssigen Schichtgrenze. I. (im Deutschen) 1
2. Y. SATÔ, Study on Surface Waves X. Equivalency of SH-waves and Sound Waves in a Liquid. (in English) 7
3. I. YOKOYAMA, Geomagnetic Studies of Volcano Mihara. The 4th paper. (A Series of Geomagnetic Dip-Surveys and Continuous Observation of Changes in Geomagnetic Declination.) (in English) 17
4. H. TSUYA, R. MORIMOTO and J. OSSAKA, The 1950–1951 Eruptions of Mt. Mihara, Oshima Volcano, Seven Izu Islands, Japan. Part I. The 1950 eruption. (in English) 35
5. K. KASAHARA, Experimental Studies on the Mechanism of Generation of Elastic Waves IV. (in English)..... 67
6. The Research Group for Explosion Seismology, The Fourth Explosion-Seismic Observations in North-Eastern Japan. (in English)..... 79
7. G. NISHIMURA, M. SUZUKI and E. FURUKAWA, Theory of Eden's Twin Strips and Application of It to Magnifying Mechanism of Seismometer. (in English) 87
8. G. NISHIMURA and M. SUZUKI, Horizontal Deformations of a Japanese Two-Storied Frame-House: (1) Vibration due to an Arbitrary Shock, (2) Vibration Caused by a Rotary with Unbalanced Mass, (3) Vibration due to Natural Wind, and (4) Deformation due to the Sun's Radiation Heat. (in English) 113

Part 2. July, 1954.

9. T. TAKAHASHI, A Problem on Fourier Series. (in English) 147
10. T. MATUZAWA, S-Wellen an der fest-flüssigen Schichtgrenze. II. (im Deutschen)..... 155

11. Y. SATÔ, Study on Surface Waves XI. Definition and Classification of Surface Waves. (in English)..... 161
12. I. YOKOYAMA, Geomagnetic Studies of Volcano Mihara. The 5th paper. (Changes in Three Geomagnetic Components during the Period from May 1951 to August 1953.) (in English) 169
13. K. KANAI and M. SUZUKI, Analytical Results of the Acceleration Seismograms obtained at Tokyo and Yokohama. (in English) 189
14. K. KANAI, T. TANAKA and K. OSADA, Measurement of the Micro-tremor. I. (in English)..... 199
15. K. KANAI, A Short Note on the Relation of Amplitude-Period of Earthquake Motion. (in English)..... 211
16. S. SAKUMA, Effect of Thermal History on Viscosity of Ooshima-lavas. (Elastic and Viscous Properties of Volcanic Rocks. Part 4.). (in English) 215

Part 3. September, 1954.

17. T. MATUZAWA und H. HASEGAWA, Feldtheorie der Erdbeben: Elliptisches Quellengebiet. (im Deutschen)..... 231
18. T. MATUMOTO and Y. SATÔ, On the Vibration of an Elastic Globe with One Layer. The Vibration of the First Class. (in English) 247
19. Y. SATÔ, A Note on Tsuboi-Nagata's Method. (in English) ... 259
20. D. SHIMOZURU, Study on the Elasticity near the Melting Point. Part I. Nature of Dilatational Wave. (in English) 271
21. I. YOKOYAMA, Geomagnetic Anomalies related to the Magnetization of the Basalt in the Vicinity of Gembudō. (in English) 281
22. H. TSUYA, R. MORIMOTO and J. OSSAKA, The 1950–1951 Eruptions of Mt. Mihara, Oshima Volcano, Seven Izu Islands, Japan. Part II. The 1951 eruption. A. Activity of the second period. (in English) 289
23. G. NISHIMURA and M. SUZUKI, Anemometer of Inverted Pendulum Type and Wind Construction Studied with It. (in English) 313

Part 4. December, 1954.

24. T. MATUZAWA, Feldtheorie der Erdbeben: Näheres über das Quellengebiet (im Deutschen) 341
25. Y. SATÔ, Study on Surface Waves XII. Non-Dispersive Surface

Waves. (in English) 349
26. K. KANAI, K. OSADA and S. YOSHIZAWA, Observational Study of Earthquake Motion in the Depth of the Ground. V. (The Problem of the Ripple of Earthquake Motion.) (in English)..... 361
27. S. ASANO, On the Accuracy of Hypocentre Determination I. (in English) 371

目　次

第 32 號

第 1 冊　昭和 29 年 3 月

論文及報告　　頁

1. 固体液体の境の面の S-波 (独文) ..... 松沢武雄 1
2. 表面波の研究 X
   流体中の音波と SH-波のつくる表面波の対応性 (英文). 佐藤泰夫 7
3. 三原山の地球磁気学的研究 第 4 報
   (一連の伏角測量と偏角変化の連続観測) (英文) ..... 横山泉 17
4. 伊豆大島三原山昭和 25 年及び 26 年の噴火
   その 1　昭和 25 年の噴火 (英文) ..... 津屋弘逵・森本良平・小坂丈予 35
5. 弾性波の発生機構に関する実験 (第 4 報) (英文) ..... 笠原慶一 67
6. 東北日本における第 4 回爆破地震動観測 (英文) ..... 爆破地震動研究グループ 79
7. エデン平行薄片の理論と地震計への応用 (英文) ..... 西村源六郎・鈴木正治・古川英一 87
8. 自然風及び起振機等による木造二階建住宅の振動 (英文) .. 西村源六郎・鈴木正治 113

第 2 冊　昭和 29 年 6 月

9. Fourier 級数に関する一つの問題 (英文) ..... 高橋健人 147
10. 固体液体の境の面の S波 II (独文) ..... 松沢武雄 155
11. 表面波の研究 XI　表面波の定義及び分類 (英文) ..... 佐藤泰夫 161
12. 三原山の地球磁気学的研究
    第 5 報 (1951 年 5 月から 1953 年 8 月にいたる期間の地
    磁気三成分の変化) (英文) ..... 横山泉 169
13. 東京横浜における加速度地震計記象の解析結果 (英文) ..... 金井清・鈴木正治 189
14. 常時微動の測定 第 1 報 (英文) ..... 金井清・田中貞二・長田甲斐男 199
15. 地震動の振幅と周期との関係 (小引) (英文) ..... 金井清 211
16. 大島新熔岩の粘性の熱履歴について (英文) ..... 佐久間修三 215

第 3 冊　昭和 29 年 9 月

17. 地震の場の論　楕円形の場（独文）……松沢武雄・長谷川博 231
18. 層のある地球の弾性振動（第1種の振動の周期）（英文）……松本利松・佐藤泰夫 247
19. 坪井·永田の方法について（英文）……佐藤泰夫 259
20. 融解点附近の弾性の研究　其の一　縦波の性質（英文）……下鶴大輔 271
21. 玄武洞周辺の磁気異常とその玄武岩の帯磁（英文）……横山泉 281
22. 伊豆大島三原山昭和25年及26年の噴火　その2
昭和26年の噴火
(*A*) 第2期の活動（英文）……津屋弘逵・森本良平・小坂丈予 289
23. 逆立振子型風力計による自然風の観測と解析（英文）……西村源六郎・鈴木正治 313

第 4 冊　昭和 29 年 12 月

24. 地震の場の論　更に精しく力の起る区域に就て（独文）……松沢武雄 341
25. 表面波の研究　XII　分散性のない表面波（英文）……佐藤泰夫 349
26. 地下深所における地震動の観測結果 第5報
（地震動の連の問題）（英文）……金井清・長田甲斐男・吉沢静代 361
27. 震源決定の精度について（第一報）（英文）……浅野周三 371

昭和29年12月25日 印刷
昭和29年12月30日 發行

東京都文京區本富士町一番地
東京大學構内
編纂兼發行者 東京大學地震研究所

東京都千代田區富士見町一丁目十番地
印刷者 笠井康賴

東京都千代田區富士見町一丁目十番地
印刷所 株式會社 國際文献印刷社

賣捌所 東京都千代田區神田一ツ橋通
岩波書店

東京都中央區日本橋通二丁目六番地
丸善株式會社

Sold by
Iwanami Shoten,
Hitotsubashi dôri, Chiyoda-ku, Tôkyô,
and
Maruzen Co., Ltd.,
Nihonbashi dôri, Chûô-ku, Tôkyô.
Price of this copy: 177 Yen. (Postage exclusive.)

BULLETIN OF

THE EARTHQUAKE RESEARCH INSTITUTE

TOKYO UNIVERSITY

Vol. XXXII, Part 4. December, 1954.

Contents.

Papers and Reports.

Page

24. T. MATUZAWA, Feldtheorie der Erdbeben: Näheres über das Quellengebiet. (im Deutschen) 341
25. Y. SATÔ, Study on Surface Waves XII. Non-Dispersive Surface Waves. (in English) 349
26. K. KANAI, K. OSADA and S. YOSHIZAWA, Observational Study of Earthquake Motion in the Depth of the Ground. V. (The Problem of the Ripple of Earthquake Motion.) (in English) 361
27. S. ASANO, On the Accuracy of Hypocentre Determination I. (in English) ... 371

Institute Notes.

Index.

(For the papers written in Japanese or in occidental languages, the abstracts are given in occidental languages or in Japanese respectively.)